The heterologous expression and *in vitro* biochemical characterization of the Hsp70 escort protein 1 and mitochondrial Hsp70 partner proteins of the *Trypanosoma brucei* parasite and humans

A thesis submitted in fulfillment of the requirements for the degree of

DOCTOR OF PHILOSOPHY (BIOTECHNOLOGY)

In the Biotechnology Innovation Centre (BIC)

Faculty of Science

RHODES UNIVERSITY

Maduma Ernest Mahlalela

2023

ABSTRACT

The 70 kDa family of heat shock proteins (Hsp70) plays a central role in the maintenance of cellular proteostasis, with paralogues occurring in all the major compartments of the eukaryotic cell. Hsp70s act in conjunction with proteins known as co-chaperones, as part of the larger molecular chaperone network. In the mitochondrion, Hsp70 (mtHsp70) is responsible for the import of proteins synthesized in the cytosol, protein folding in the matrix and the maintenance of the iron-sulphur cluster. In human cells mtHsp70 (HSPA9) is also referred to as mortalin, as the knockdown of the protein leads to cell mortality. *Trypanosoma brucei* is the causative agent of sleeping sickness in humans and nagana in animals. In the *T. brucei* parasite there are three identical mtHsp70 (TbmtHsp70) proteins that are produced, forming part of the Hsp70 machinery that is essential for parasite survival. In humans, the levels of HSPA9 are often elevated in non-communicable diseases such as cancer and neurodegeneration. Despite their vital cellular roles, mtHsp70s are characteristically prone to self-aggregation. The binding of the Hsp70 escort protein (Hep1) is required to prevent the aggregation of mtHsp70 proteins, enabling the proteins to function. In many non-communicable diseases, mtHsp70 and other molecular chaperones such as heat shock protein 90 (Hsp90) are being investigated as potential drug targets. Existing anti-trypanosomal drugs for treating sleeping sickness are toxic, having adverse side effects that are potentially lethal. Investigations into Hsp70s, and other molecular chaperones, form part of the research into the discovery of novel and efficacious therapeutics.

This is the first study to characterise Hep1 and investigate its partnership with mtHsp70 in *T. brucei.* The overall aim of this study was to comparatively assess the *T. brucei* and human mtHsp70/Hep1 partnerships. The putative *T. brucei* Hep1 (TbHep1) orthologue was analysed *in silico*, and it was found to possess a zinc finger domain consisting of anti-parallel β-sheets that are characteristic of canonical Hep1 proteins, whilst the N-terminal domain was unstructured. Based on sequence analysis, the regions outside of the zinc finger domains lacked conservation. Despite the lack of sequence conservation, the N- and C-terminal regions of TbHep1 shared segments of similarity with Hep1 orthologues of other kinetoplastid and trypanosomal orthologues. The same held true for the N- and C-termini of human Hep1 (HsHep1) when compared to other Hep1 orthologues of mammalian origin.

Biochemical analysis revealed TbmtHsp70 and HSPA9 to be prone to self-aggregation, which was reduced by co-expression with TbHep1 and HsHep1, respectively. Recently Hep1 proteins have been determined to be present in the cytosol. In this study, TbHep1 and HsHep1 also interacted with the cytosolic Hsp70s, HSPA1A and TbHsp70, by preventing their thermally induced aggregation and stimulating their ATPase activities. TbHep1 and HsHep1 also suppressed the thermally induced aggregation of the model substrates malate dehydrogenase and citrate synthase, independently of Hsp70. To date, only two Hep1 orthologues, HsHep1 and LbHep1, have been found to function in a similar manner to a J-protein co-chaperone by stimulating the ATPase activities of their partner

mtHsp70 proteins. In this study, TbHep1 stimulated the ATPase activity of TbmtHsp70. HsHep1 also stimulated the ATPase activity of TbmtHsp70. However, the mechanism of action still needs to be determined. This study also explored the potential of the Hep1 orthologues to be functionally activated by oxidative stress, which is prevalent in mitochondria. The abilities of TbHep1 and HsHep1 to reduce the thermally induced aggregation of malate dehydrogenase were enhanced under oxidative conditions. Disrupting the function of Hep1 has been found to eventually lead to cell death, and given the critical role played by mtHsp70 in the cell, this partnership could be exploited as a potential drug target. In conclusion, this study demonstrated that TbHep1 and HsHep1 functionally interact with mtHsp70s, whilst also possessing independent chaperone activities that are also potentially influenced by the environmental redox state.

DECLARATION

I, Maduma Ernest Mahlalela, hereby declare that this thesis is my own, unaided work. This thesis is being submitted in fulfilment of the requirements for the awarding of the degree of Doctor of Philosophy at Rhodes University, Faculty of Science. This work has not been submitted for any other degree or examination at another university.

MEMahlalela

Maduma Ernest Mahlalela

Dated 13/02/2023 at Sigangeni, Eswatini

DEDICATION

I dedicate this thesis to my mother and father, Virginia, and Justice Mahlalela. I also dedicate this thesis to my late grandparents, Caiphus and Martha Mahlalela, and Lillian Shabangu, not forgetting my grandfather, Daniel Dlamini.

ACKNOWLEDGEMENTS

First and foremost, I wish to express my sincere gratitude to my supervisor, Professor Aileen Boshoff for the mentorship, guidance, encouragement and patience throughout my pursuit of this degree over the years.

I would also like to thank Professor Julio Cesar Borges from the University Sao Paulo for kindly providing the pET28a-HSPA1A, pET28a-HSPA9, pET23a-HsHep1 and pQE2-HsHep1 plasmids.

I would also like to appreciate Professor Dana Reichmann from the Hebrew University of Jerusalem for kindly providing the plasmid vector for the heterologous expression of Hsp33.

I would also like to thank Dr Stephen Bentley and Dr David Nyakundi for their contribution to my journey as a postgraduate student in the research group, especially in the formative years when I was still finding my footing around the university's research community and academia in general. I also appreciate the many colleagues I have had the privilege of encountering during my postgraduate studies in the research group and the department.

I am very grateful for the Pearson-Young Memorial Scholarship and the Rhodes University postgraduate funding office for funding my postgraduate studies.

I also thank my parents and family for supporting me throughout this journey, which has at times seemed impossible to see through.

TABLE OF CONTENTS

LIST OF FIGURES

CHAPTER ONE

CHAPTER TWO

CHAPTER THREE

CHAPTER FOUR

APPENDICES

LIST OF TABLES

LIST OF ABBREVIATIONS

APS	ammonium persulphate
aSEC	analytical size exclusion chromatography
ATP	adenosine triphosphate
Amp^R	ampicillin resistance
AT	African trypanosomiasis
AAT	African animal trypanosomiasis
apoA1	apolipoprotein A1
apoL1	apolipoprotein 1
Ai1	apolipoprotein Ai1
AQP2	aquaglyceroporin
AD	Alzheimer's disease
ALS	amyotrophic lateral sclerosis
AIF	Apoptosis-inducing factor
AIMP2	aminoacyl-transfer RNA synthetase-interacting multifunctional protein 2
BSF	bloodstream forms
BARP	brucei alanine-rich proteins
BLAST	Basic Local Alignment Search Tool
Bp	base pairs
BSA	bovine serum albumin
Cam^R	chloramphenicol resistance
CL	cutaneous leishmaniasis
CNS	central nervous system
CATT	card-agglutination trypanosomiasis test
CHIP	carboxy terminus of Hsc70 interacting protein
CS	citrate synthase
CTD	C-terminal domain
CUPS	chaperone-assisted ubiquitin-proteasome pathway
CR	charged linker region
Cdc2	cyclin-dependent kinase
DRC	Democratic Republic of Congo
DMG	dimyristoylglycerol
DND*i*	Drugs for Neglected Tropical Disease Initiative
DTT	dithiothreitol
EDTA	Ethylenediaminetetraacetic acid disodium salt
ER	Endoplasmic reticulum
ETC	electron transport chain
ERK	extracellular signal-regulated kinase
FAZ	flagellum attachment zone
Fe-S	iron-sulphur clusters
FPLC	fast protein liquid chromatography
gRNA	guide RNAs
***G*-HAT**	*Gambiense* HAT

GPI	glycosylphosphatidylinositol
GIP	glycosylinositolphosphate
HAT	human African trypanosomiais
Hpr	haptoglobin related protein
HpHbr	haptoglobin-haemoglobin receptor
Hsc	heat shock cognate protein
Hsp	heat shock protein
HIP	Hsp70 interacting protein
His-tag	hexahistidine tag
Hep	Hsp70 escort protein
HIF-1α	hypoxia-inducible factor α
HOP	Hsp70/hsp90 organizing protein
ISG	Invariant surface glycoproteins
IDP	intrinsically disordered protein
IPTG	Isopropyl-β-D-thiogalactopyranoside
J-protein	J domain containing protein
JNK	c-Jun N-terminal kinase
JTT	Jones-Taylor-Thornton
Kan^R	kanamycin resistance
Kilo Daltons	kDa
Kbps	kilobase pairs
L	Litre
L. braziliensis	*Leishmania braziliensis*
MBP	maltose binding protein
MCS	multiple cloning site
MD	middle domain
mg	milligrams
ml	millilitres
mM	millimolar
ML	maximum likelihood
MSA	Multiple sequence alignment
MPP	matrix processing peptidase
mAECT	mini anion exchange centrifugation technique
MDH	L-malate dehydrogenase
mtDNA	mitochondrial DNA
mtHsp70	mitochondrial Hsp70
M. musculus	*Mus musculus*
nM	nanomolar
NCBI	National Centre for Biotechnology Information
Ni-NTA	nitrilotriacetic acid-agarose
NTD	neglected tropical disease
NECT	nifurtimox-eflornithine combinatorial therapy
NNI	nearest-neighbor-interchange

NTR	uniquinone nitroreductase
NBD	nucleotide binding domain
NEF	nucleotide exchange factor
NTD	N-terminal domain
NF-κβ	nuclear factor κβ
ORF	open reading frame
ODC	ornithine decarboxylase
OD	optical density
PBS	phosphate buffered saline
PCF	procyclic forms
P. falciparum	*Plasmodium falciparum*
PTRE	post-treatment reactive encephalopathy
PQC	protein quality control
PDB	Protein Data Bank
PEXEL/VTS	*Plasmodium* export element / vacuolar transport signal
PAM	presequence translocase-associated motor
PD	Parkinson's disease
PEG	polyethylene glycol
P_i	inorganic phosphate
pI	isoelectric point
PMSF	phenylmethanesulfonyl fluoride
RDT	Recombinant DNA technology
***R*-HAT**	*Rhodesiense* HAT
RNR	ribonucleotide reductase
S. cerevisiae	*Saccharomyces cerevisiae*
SRA	serum resistance antigen
SIT	sterile insect technique
SBD	substrate binding domain
SDS	sodium dodecyl sulphate
SDS-PAGE	sodium dodecyl sulphate – polyacrylamide gel electrophoresis
SMART	simple modular architecture research tool
STi1	stress-inducible phosphoprotein 1
TAC	tripartite attachment complex
TBS	tris-buffered saline
TBS-T	tris-buffered saline – Tween20
TEMED	tetramethyl ethylenediamine
TLF	trypanolytic factor
TgsGP	*T. b. gambiense* specific glycoprotein
TbENO	*T. brucei* enolase
TPR	tetratricopeptide
TRAP1	tumour necrosis factor receptor-associated protein 1
T. brucei	*Trypanosoma brucei*
T. b. brucei	*Trypanosoma brucei brucei*

T. b. gambiense	*Trypanosoma brucei gambiense*
T. b. rhodesiense	*Trypanosoma brucei rhodesiense*
T. equiperdum	*Trypanosoma equiperdum*
T. cruzi	*Trypanosoma cruzi*
T. evansi	*Trypanosoma evansi*
TIM23	translocase of inner membrane
TOM	translocase of outer membrane
UV	ultraviolet
VSG	variable surface glycoprotein
v/v	volume/volume
WHO	World Health Organisation
w/v	weight/volume
YT	yeast tryptone
ZFLR	zinc-finger like region
α	alpha
β	beta
µ	micro
µg	microgram
µl	microlitre
µM	micromolar
%	percent
°C	Degrees Celsius

CHAPTER ONE
Literature review

1.1 Distinguishing features of kinetoplastids

Kinetoplastid organisms are a class of protozoan unicellular flagellates under the phylum Euglenozoa alongside euglenids and diplonemids (Figure 1.1) (Cavalier-Smith, 1981; Stuart *et al*., 2008; Butenko *et al*., 2020; Kostygov *et al*., 2021). Together with diplonemids, kinetoplastids fall under the Glycomonada clade (or subphylum) and are characterized by possessing sub-cellular structures referred to as glycosomes (Cavalier-Smith, 2016). Organisms of the classs Kinetoplastida are characteristically distinguished by possessing a kinetoplast within a nucleoid, housed inside a single reticular mitochondrion (Stuart *et al*., 2008; Mensa-Wilmot *et al*., 2019). The kinetoplast is an aggregation of high-density circular DNA molecules that conventionally occur within the vicinity of the organism's flagellar basal body (Hoare and Wallace, 1966; Cavalcanti and de Souza, 2018). The circular kinetoplast DNA (kDNA) molecules topologically inter-connect and are categorized according to their sizes into mini- and maxi-circles. Mini-circles are present as several thousand variable DNA molecules (0.5-10 kb) that encode guide RNAs (gRNA). On the other hand, maxi-circles are present as several dozen identical DNA molecules (20-40 kb) that encode a plethora of proteins as well as the 9S and 12S mitochondrial ribosomes, analogous to the mitochondrial DNA of higher eukaryotic organisms (Shapiro and Englund, 1995; Stuart and Panigrahi, 2002; Lukeš *et al*., 2005; Jensen and Englund, 2012; Cavalcanti and de Souza, 2018). The location of kDNA within the mitochondria of kinetoplastids is usually signified by a dilation of the organelle in the region in which the kDNA occurs (de Souza *et al*., 2009).

Glycosomes possess genes that were horizontally inherited from plants and are evolutionarily related to the peroxisomes and glyoxysomes of higher eukaryotes and plants, respectively (Opperdoes and Borst, 1977; Wilson *et al*., 1996; Maldonado and Fairlamb, 2001; Michels *et al*., 2005; Lopes, 2010). These sub-cellular structures impart kinetoplastids with an expeditious glycolytic process, as they possess most of the enzymes that are of relevance to this pathway (Vickerman, 1994). Apart from being glycolytic compartments, glycosomes also play a role in the synthesis of pyrimidines, fatty acids and lipids (Vickerman, 1994; Michels *et al*., 2000; Moyersoen *et al*., 2004). Although glycolysis entails the utilization of glucose for energy production, glycosomes have the ability to generate free energy by utilizing amino acids (Cross *et al*., 1975; Hannaert *et al*., 2003).

In addition to the glycosomes which kinetoplastids share in common with diplonemids, they are also distinguished by their RNA editing feature (Lopes, 2010). RNA editing is carried out using one of two mechanisms: the one being the insertion and deletion of uridine residues within coding regions of maxi

circles in order to yield open reading frames (ORF) that are readable. This process is mediated by gRNAs (Blum *et al*., 1990; Blum and Simpson, 1990; Lopes, 2010). Since tRNA genes are absolutely lacking in the kinetoplastid genome, as with many other groups of organisms, the organisms import their tRNAs from the cytosol. The issue with this is that kinetoplastid tryptophan tRNAs imported from the cytosol are specific for cytosolic UGG codon yet most of the tryptophan codons in the mitochondrion are encoded by UGA (Paris *et al*., 2012). Therefore, in the mitochondrion, the second RNA editing mechanisms entails editing $tRNA^{TRP}$ by substituting cytosine for uridine at the 34^{th} nucleotide residue which forms part of the tryptophan encoding anti-codon. This in order to render the anti-codon compatible with the UGA codon (Alfonzo *et al*., 1999). The C to U modification has been reported to be coupled to the thiolation is of an adjacent uridine residue, which acts as a regulatory machinery for this tRNA editing mechanism (Wohlgamuth-Benedum *et al*., 2009).

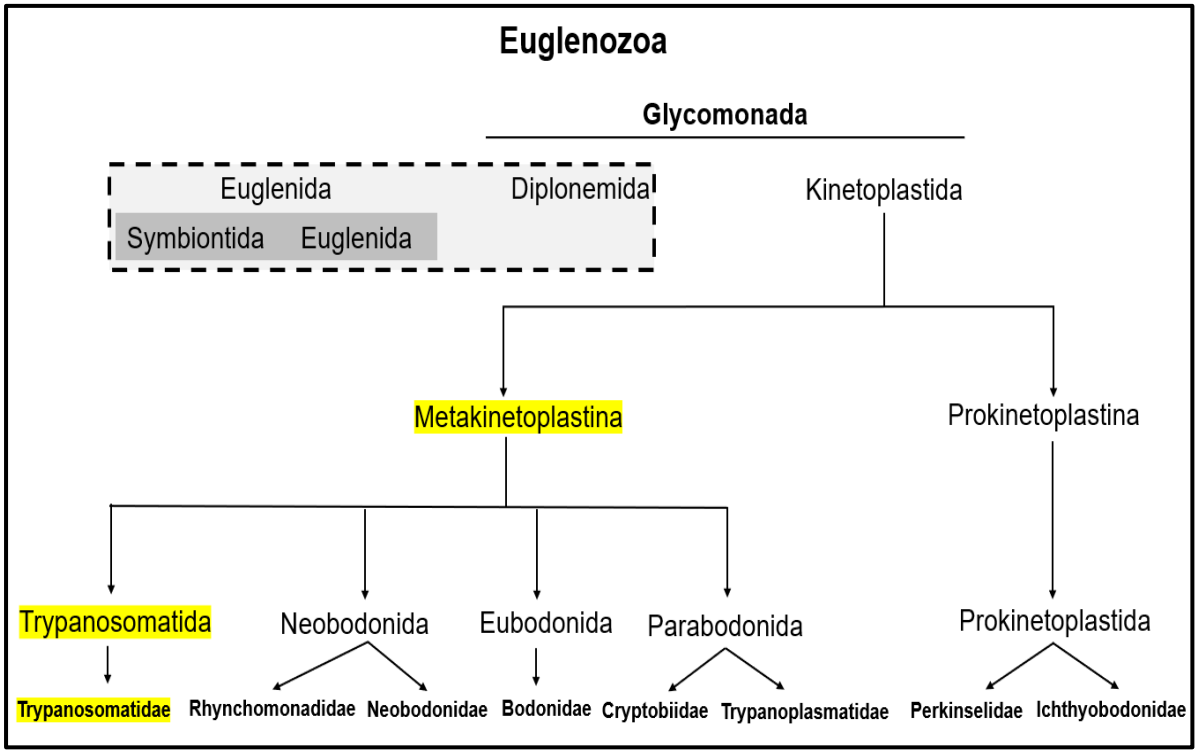

Figure 1.1: Diagram detailing the taxonomy of the class Kinetoplastida. This diagram illustrates the organisation of kinetoplasts under the phylum Euglenozoa. In the dashed box are the other classes of organisms in the phylum. Highlighted in yellow is the lineage of trypanosomatid organisms. *Adapted from* d'Avila-Levy et al. (2015); Kostygov et al. (2021).

Kinetoplastids are either saprozoic or parasitic heterotrophs which are sub-divided into two sub-classes: namely Prokinetoplastina and Metakinetoplastina (Figure 1.1) (Tikhonenkov *et al*., 2021). Within the sub-class Prokinetoplastina is the order Prokinetoplastida whilst the sub-class Metakinetoplastina is constituted of the orders Trypanosomatida, Neobodonida, Eubodonida and Parabodonida (Moreira *et al*., 2004; Cavalier-Smith, 2016). Kinetoplastids are constituted of more than 30 genera of organisms, the bulk of them being under the order Trypanosomatida (d'Avila-Levy *et al*., 2015; Kaufer *et al*., 2017).

1.2 Trypanosomatids

Trypanosomatids are constituted of a single family of organisms, Trypanosomatidae (Figure 1.1) (d'Avila-Levy *et al*., 2015). Trypanosomatids are characterized by a small kinetoplast and a single flagellum (Maslov *et al*., 2001). Trypanosomatids uniquely exhibit mRNA trans-splicing, a rarity amongst eukaryotic organisms (Johnson, 1987; Figueroa-Angulo *et al*., 2003; Martínez-Calvillo *et al*., 2010). Trans-splicing of the mRNA serves to yield monocistronic mRNA molecules that are translatable for ribosomal protein synthesis (Stuart *et al*., 2005; Lopes, 2010). Trypanosomatids are obligately parasitic, parasitizing virtually all vertebrates, some invertebrates, and even plants (Wallace, 1966; Vickerman, 1994; Svobodová *et al*., 2007; Vickerman, 2009).

Table 1.1: Members of the order Trypanosomatida, family Trypanosomatidae. This table presents all the known genera (middle column) of Trypanosomatid organisms many of which fall under several acknowledged sub-families (left column). In the column on the right are the insect hosts/vectors of the various genera of organisms. Dixenous organisms in vertebrates and plants are indicated by the (*****) and (•) symbols, respectively. *Adapted from* Maslov et al. (2019), Frolov et al. (2021), Kostygov et al. (2021).

***Trypanosomatinae**	*Trypanosoma*	Diptera, Hemiptera, Siphonaptera
***Leishmaniiae**	*Leishmania*	Diptera
	Porcisia	Diptera
	Endotrypanum	Diptera
	Leptomonas	Diptera, Hemiptera, Hymenoptera, Siphonaptera
	Crithidia	Diptera, Hemiptera, Hymenoptera
	Lotmaria	Hymenoptera
	Novymonas	Hemiptera
	Zelonia	Diptera, Hemiptera
	Borovskyia	Hemiptera
Blastocrithidiinae	*Obscuromonas*	Hemiptera
	Blastocrithidia	Hemiptera
Herpetomonadinae	*Herpetomonas*	Diptera, Hemiptera, Hymenoptera, Siphonaptera, Blattodea
	Lafontella	Diptera
	•*Phytomonas*	Hemiptera
	Jaenimonas	Diptera
Strigomonadinae	*Angomonas*	Diptera, Hemiptera
	Strigomonas	Diptera, Hemiptera
	Kentomonas	Diptera
	Sergeia	Diptera
	Wallacemonas	Diptera, Hemiptera
	Vickermania	Diptera
Blechomonadinae	*Blechomonas*	Siphonaptera
Paratrypanosomatinae	*Paratrypanosoma*	Diptera

Trypanosomatids date back to some 100 million years ago and are divided into 24 known genera many of which are distributed across 7 recognized subfamilies: *Leptomonas*, *Crithidia*, *Lotmaria*, *Novymonas*, *Zelonia*, *Borovskyia*, *Obscuromonas*, *Blastocrithidia*, *Herpetomonas*, *Lafontella*, *Phytomonas*, *Jaenimonas*, *Angomonas*, *Strigomonas*, *Kentomonas*, *Sergeia*, *Wallacemonas*, *Vickermania*, *Blechomonas*, *Paratrypanosoma*, *Leishmania*, *Porcisia*, *Endotrypanum* and *Trypanosoma* (Table 1.1) (Poinar and Poinar, 2004, 2005; Simpson *et al*., 2006; Kaufer *et al*., 2017). The genera are determined and classified according to cellular morphological traits such as size, shape, and the positioning of the kinetoplast-flagellar pocket complex in relation to nucleus (Hoare and

Wallace, 1966; Svobodová *et al*., 2007). Most genera of trypanosomatids are monoxenous (or monogenetic) parasites of insects, but some exhibit a dixenous (or digenetic) life cycle as they shuttle between their respective invertebrate vectors and vertebrate (or plant) hosts (Kaufer *et al*., 2017).

However, the classification of genera according to cellular morphology and host range remains a contentious subject in the taxonomy of trypanosomatids as this has led to cases of paraphyly and polyphyly (Olsen and Woese, 1993; Merzlyak *et al*., 2001; Kaufer *et al*., 2017). Furthermore, some genera which are classified as monoxenous (e.g., *Leptomonas*) have been reported to be opportunistic parasites of vertebrates in HIV and leishmaniasis patients (Singh *et al*., 2013). On the other hand, some genera (e.g., *Novymonas* and *Zelonia*) which occur within dixenous clades of trypanosomatids alongside *Leishmania* seem to be monoxenous. Molecular evidence of monoxenous trypanosomatids having the ability to infect multiple insect organisms has also been presented (Chicharro and Alvar, 2003; Kaufer *et al*., 2017). It is currently thought that only a fraction of the trypanosomatid genera have been described, and that the discovery of more trypanosomatid organisms will allow for an improved taxonomic system (Kaufer *et al*., 2017). Currently, trypanosomatids are proposed to be divided into 2 superclasses, the juxtaform and liberform (Wheeler *et al*., 2013). The juxtaform superclass is constituted of morphotypes that possess a laterally fixed flagellum: epimastigotes and trypomastigotes such as those found in the genus *Trypanosoma*. The liberform superclass is constituted of morphotypes that possess a free flagellum: opisthomastigotes, choanomastigotes and promastigotes such as those observed in *Leishmania* and *Leptomonas* (Wheeler *et al*., 2013). Other morphotypes, such as amastigotes have also been described. Amastigotes occur in both superclasses and therefore may not be used as a classification or distinguishing factor (Maslov *et al*., 2013). Numerous species of trypanosomatids are responsible for acute and chronic neglected tropical diseases (NTDs) that are of medical, veterinary, and economic pertinence. Three of these species; *Leishmania major*, *Trypanosoma cruzi*, and *Trypanosoma brucei* are collectively known as the Tritryps and are the causative agents of devastating human and animal diseases (Portman and Gull, 2010; Jackson *et al*., 2016). The Tritryps are vector-borne and haemoflagellate parasites that are transmitted to their mammalian hosts by hematophagous organisms of the phylum Arthropoda (Hotez *et al*., 2016).

L. major is an obligate intracellular zoonotic parasite that targets dendritic cells and macrophages (Kaye and Scott, 2011; Walker *et al*., 2014). It is transmitted to humans through the bite of an infected female phlebotomine sandfly (*Phlebotomous papatasi*) (Dobson *et al*., 2010; Paz *et al*., 2013). It forms part of the *Leishmania* organisms that are causative agents of old-world cutaneous leishmaniasis (CL) (Alvar *et al*., 2012). Alongside *L. major*: *L. tropica*, *L. aethipica*, *L. infantum* and *L. donovani* are also causative agents of old-world leishmaniasis. CL is the most geographically widespread form of leishmaniasis and is usually symptomized by a single localized ulcerative skin lesion that often heals without treatment (Kaye and Scott, 2011). CL lesions are characterized by having necrotic tissue at their bases and borders

that exhibit induration (Goto and Lindoso, 2010; Paz *et al*., 2013). *T. cruzi* is an obligate zoonotic intracellular parasite that targets cells such as fibroblasts, macrophages, neurons and myocytes (de Souza *et al*., 2010). *T. cruzi* is the causative agent of Chagas, also referred to as American trypanosomiasis, a globally distributed disease that is mostly prevalent in the Americas, extending from Mexico in the north to Chile in the South. *T. cruzi* is transmitted to humans through the excrement of several dozen species of triatomine insects (the 'kissing bugs') (Lopes, 2010). The kissing bugs derive their name from their behavioural characteristic of biting the human host around the mouth and eyes during their bloodmeal (Klotz *et al*., 2010). Post meal, the infected kissing bugs defecates on or around the host, creating an opportunity for the parasite-infested excrement to come into contact with the mucous membrane or skin openings of the mammalian host (Klotz *et al*., 2014; Lopes, 2010). Chagas occurs in two phases: acute and chronic. The acute phase occurs in the early stages of the disease and is symptomized by a fever, fatigue, skin rashes and nausea (Calvopina *et al*., 2020). The chronic phase of the disease is symptomized by heart disease and intestinal neural deficiency (Bern, 2015; Pérez-Molina and Molina, 2018).

1.3. Aetiology and disease burden of African trypanosomiasis

African trypanosomiasis (AT) is a parasite-borne neuropathic and wasting disease that is endemic to sub-Saharan Africa, affecting humans and animals alike (Raper, 2001; Lopes, 2010; Alsan, 2015). The causative agents of the disease are three subspecies of the extracellular vector-borne *Trypanosoma brucei* parasite (Lopes, 2010). The parasite is transmitted to humans and animals through the bite of an infected tsetse fly (genus: *Glossina*) during a bloodmeal, which usually occurs during the daytime (Cecchi *et al*., 2009). In humans the disease is referred to as human African trypanosomiasis (HAT) or more commonly as African sleeping sickness. It is caused by the phenotypically indistinguishable *T. brucei. gambiense* and *T. brucei. rhodesiense* subspecies (Lopes, 2010). Two types of *T. b. gambiense*, types 1 and 2, have been described by isoenzymatic characterization. *T. b. gambiense* is anthroponotic as humans are the main reservoirs whilst *T. b. rhodesiense* is zoonotic since its transmission also relies on animal reservoirs (Kennedy, 2013). *T. b. gambiense* and *T. b. rhodesiense* are the only trypanosomes in Africa which have been reported to successfully establish an infection in humans (Cayla *et al*., 2019).

All 22 species and subspecies in the genus *Glossina* have the ability to transmit trypanosomes to humans, but specific groups have been particularly adapted for transmission of *T. b. gambiense* and *T. b. rhodesiense*: the *Glossina palpalis* and *Glossina fuscipes* groups for *T. b. gambiense* and the *Glossina morsitans* and *Glossina pallidipes* group for *T. b. rhodesiense* (Maudlin, 2006; Simarro *et al*., 2011). Although parasite transmission is primarily due to the bite of the tsetse fly, other modes of transmission have been reported: mother to child transmission through the placenta (for *T. b. gambiense*), mechanical transmission by other hematophagous insects, mishandling of laboratory samples, and sexual

intercourse involving infected individuals (Gruvel, 1980; Lindner and Priotto, 2010; Simarro *et al*., 2014).

African sleeping sickness is distributed across 36 sub-Saharan African countries, with rural farming communities being the most vulnerable (Figure 1.2) (Kennedy, 2004; Kennedy and Rodgers, 2019). The two causative agents of HAT, *T. b. gambiense* and *T. b. rhodesiense*, are found in different regions of the continent. *T. b. gambiense* occurs in 24 countries in Central and Western Africa whilst *T. b. rhodesiense* occurs in 13 countries in Eastern and Southern Africa (Kennedy, 2004; Torr *et al*., 2012; Kennedy, 2013; Simo *et al*., 2014). Only in Uganda have *T. b. gambiense* and *T. b. rhodesiense* been reported to co-occur, albeit in different regions; *T. b. gambiense* in the northwest and *T. b. rhodesiense* in the central regions (Figure 1.2) (Berrang-Ford *et al*., 2006, 2012). In Central and Western Africa tsetse flies are found in stream side flora and forests whilst in East Africa they occur in woodlands and the savannah. *T. b. rhodesiense* is less prevalent and is responsible for the acute form of HAT (*R*-HAT) (Maudlin, 2006; Simarro *et al*., 2011).

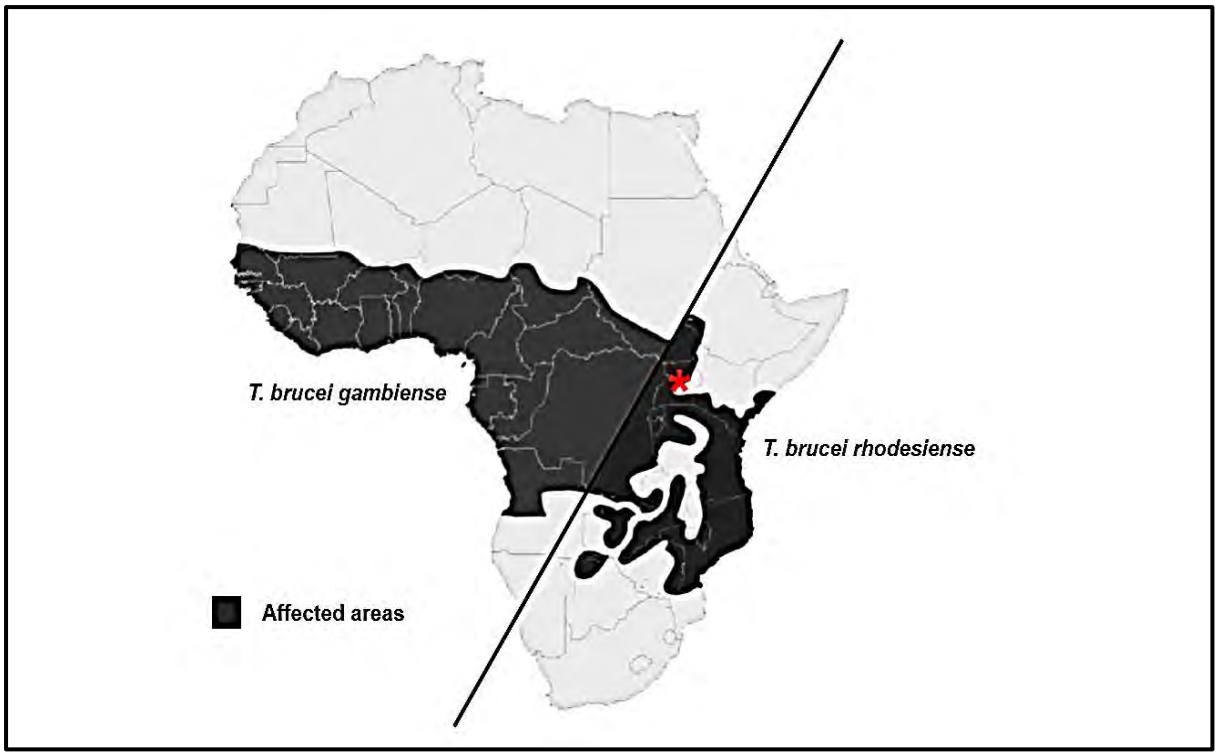

Figure 1.2: Distribution map for African sleeping sickness. The map illustrates the distribution of *R*-HAT and *G*-HAT. The bold line is a demarcation separating the regions in which the *T. b. rhodesiense* and *T.b. gambiense* occur. The red asterisk serves to highlight Uganda, the only country in which the subspecies co-occur (Kennedy, 2004).

T. b. gambiense accounts for 98% of reported cases and is primarily responsible for the chronic form of HAT (*G*-HAT) (Simarro *et al*., 2012). *T. b. gambiense* type 1 is more prevalent, accounting for approximately 90% of those cases, and causes the chronic form of HAT. On the other hand, *T. b. gambiense* type 2 causes the acute form of the disease (Cordon-Obras *et al*., 2010; Wombou Toukam *et al*., 2011). HAT has been an African health challenge since the late 19th century having caused

millions of fatalities in the 20th century due to numerous outbreaks which have led to epidemics. However, due to concerted efforts in the surveillance and management of the disease, reported cases have been dropping significantly over the years; from 40 000 cases in 1998 to 9 878 cases in 2009. In 2019, the number of reported cases had declined to 992, with over 70% of cases reported between 2009 and 2019 having been recorded in the Democratic Republic of Congo (DRC) (WHO, 2022). The World Health Organisation had aimed to have eradicated the transmission of the parasite by the year 2030, with the disease being eliminated from being a public health concern by the year 2020. Despite the strides made in combating the disease, approximately 60 million people are still at risk of HAT contraction, with *R*-HAT accounting for approximately 18 % of that risk (Lopes, 2010; Simarro *et al*., 2012). The disease burden of HAT is compounded by the geographical distribution of the disease with many of the affected communities being remote rural areas with poor access to medical infrastructure. Incidentally, cases of HAT do get reported in non-endemic territories, even outside of Africa. These cases are attributed to infected individuals travelling from endemic countries (Ripamonti *et al*., 2002).

The third subspecies of *T. brucei*, *T. brucei. brucei* infects animals and is a causative agent of African animal trypanosomiasis (AAT). AAT, commonly referred to as nagana in cattle, primarily affects cattle and horses, but can also infect dogs, cats, camels, and pigs. *T. b. brucei* is not the only causative agent of AAT. The other trypanosomal causative agents of AAT include *T. Congolese*, *T. vivax* , *T. equiperdum, T. simiae*, and *T. evansi* (Leak, 1999; Lopes, 2010). According to molecular and parasitological characterization, *T. equiperdum* and *T. evansi* are also considered to be strains or subspecies of *T. brucei. T. equiperdum* and *T. evansi* are thought to have evolved spontaneously, having lost a fraction of (dyskinetoplastidy) or their whole (akinetoplastidy) kDNA complement, respectively (Lai *et al*., 2008). *T. equiperdum* and *T. evansi* are therefore also referred to as *T. brucei equiperdum* and *T. brucei evansi*, respectively (Lai et al., 2008). *T. equiperdum* is sexually transmitted between horses and the resultant disease is referred to as dura whilst the disease caused by *T. evansi* is referred to as surra (Desquesnes *et al*., 2013). Of the causative agents of AAT, *T. vivax* and *T. evansi* can be transmitted mechanically and their epidemiology, along with that of *T. equiperdum*, is not restricted to the African continent (Desquesnes *et al*., 2013; Kasozi *et al*., 2021). AAT, especially in the case of nagana in cattle, is of economic and veterinary importance due to its adverse effects on agricultural outputs such as meat and milk (Raper, 2001; Desquesnes *et al*., 2013). The symptoms of AAT include, but are not limited to, anaemia, weight loss, decreased infertility, and miscarriage (Desquesnes *et al*., 2013). AAT is endemic to 38 African countries covering approximately a third of the continent's total land area (Lopes, 2010; Desquesnes *et al*., 2013).

1.4 HAT: Symptoms and disease progression

The symptoms of HAT vary according to the stage of parasitic infection (Figure 1.3) (Stuart *et al*., 2008; Lopes, 2010). After parasite transmission into the human host's bloodstream, headaches, fatigue, general malaise, and fever occur (Kennedy, 2004). At the site of the insect bite, a lesion also known as a trypanosomal chancre may also occur, more especially in cases of *R*- HAT (MacLean *et al*., 2010). As the infection progresses, the parasites invade the lymph nodes resulting in lymphadenopathy (Kennedy and Rodgers, 2019). The associated symptoms are heightened fever, chills, and hepatosplenomegaly (Kennedy, 2008; Kennedy and Rodgers, 2019).

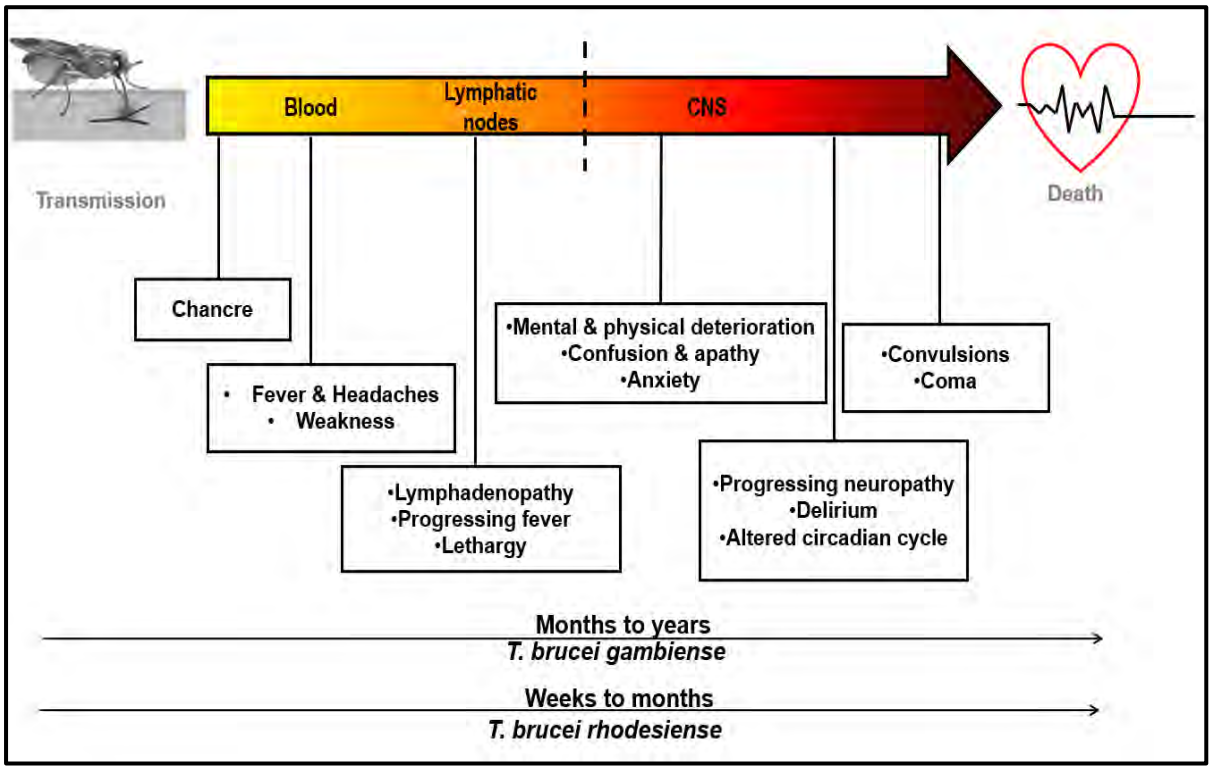

Figure 1.3: An infographic depicting the progression of HAT. The diagram highlights some of the defining symptoms of HAT as they relate to the progression of the *T. brucei* infection. The dashed line demarcates the point at which the parasitic infection infiltrates the CNS. The arrows at the bottom of the infographic indicate the different rates at which *R*-HAT and *G*-HAT progress. Adapted from Ponte-Sucre (2016).

At the phase of bloodstream and lymph node infection, the disease is said to be at the haemolymphatic stage (Brun *et al*., 2010). As the infection advances, the parasites breach the blood-brain barrier to infiltrate the central nervous system (CNS). At this point, the disease is said to be at the meningoencephalitic stage (Figure 1.3) (Brun *et al*., 2010). The meningoencephalitic stage of the disease is characterized by mental, neurological and sensory degeneration. The symptoms include, but are not limited to, delirium, disorientation, apathy, anxiety, emotional instability, abnormal speech, paraesthesia, anaesthesia, convulsions, seizures, and coma (Kennedy, 2004, 2008). The meningoencephalitic phase of the disease also symptomized by a disruption of the circadian cycle, symptomized by daytime somnolence and nocturnal insomnia (Figure 1.3). The common name of the disease, "African sleeping sickness", is a derivative of this symptom (Blum *et al*., 2006). If not treated,

the meningoencephalitic stage of HAT may be lethal (Stuart *et al*., 2008; Kennedy, 2013). In addition to the aforementioned symptoms, more especially in cases of *R*-HAT, cardiac and endocrine maladies such as myocarditis and hypogonadism may also occur (de Raadt and Koten, 1968; Petzke *et al*., 1996). An intermediate stage of the disease has also been suggested; whereby the parasitic infection has breached the blood-brain barrier but has not yet reached or infiltrated the brain parenchyma (Bisser *et al*., 2002; Buguet *et al*., 2005; Bonnet *et al*., 2015). The rate of disease progression differs between *R*-HAT and *G*-HAT (Simarro *et al*., 2012). For *R*-HAT, the haemolymphatic stage symptoms appear 1 to 3 weeks following the bite of the tsetse fly whilst the symptoms manifest much later in the case of *G*-HAT (Kennedy, 2004; MacLean *et al*., 2010). The onset of the meningoencephalitic stage of the disease occurs within 2-60 days of infection in cases of *R*-HAT and death may take place within 3 months (Kennedy and Rodgers, 2019). For *G*-HAT, the onset of the meningoencephalitic stage occurs between 300 and 500 days from infection and the disease may persist for years (Stich, 2002; Brun *et al*., 2010).

1.5 Biology and pathology of *T. brucei*

The cellular structure of *T. brucei* is characterized by polarization as determined by its microtubule cytoskeleton (Matthews, 2005) (Figure 1.4). The posterior and anterior of the cell are the positive and negative ends of the microtubular cytoskeleton, respectively (Robinson *et al*., 1995). The cytoskeleton is anchored to the cell membrane via microtubule associated proteins, and forms a robust, yet pliable corset which is structurally consistent throughout much of the cell (Bramblett *et al*., 1987; Hemphill *et al*., 1991; Ooi and Bastin, 2013). The robustness of the cytoskeleton is thought to be a protective adaptation to shield the cell from erratic environmental elements as it also serves to prevent molecular traversal across much of the cell membrane (Ooi and Bastin, 2013). Only a small area of the cell body's membrane, within an area referred to as the flagellar pocket, is permissive to endo- and exocytosis. The flagellar pocket is an invagination on the cell's surface from which the flagellum, originating from the flagellar basal body, protrudes to the outside of the cell body (Figure 1.4) (Ooi and Bastin, 2013). The membrane in the flagellar pocket is continuous with that of the plasma membrane, and as such it offers a point at which the microtubule cytoskeleton is less restrictive to the passage of molecules (Ooi and Bastin, 2013). Within the flagellar pocket, the flagellar basal body is in turn linked to the kinetoplast through a structural assembly referred to as the tripartite attachment complex (TAC) (Ogbadoyi *et al*., 2003; Matthews, 2005). The TAC structure consists of three components: exclusion zone filaments that connect the basal body of the flagellum to the outer membrane of the mitochondria, the inner and outer mitochondrial membranes, as well as unilateral filaments that connect the inner membrane of the mitochondria to the kinetoplast (Ogbadoyi *et al*., 2003). Since trypanosomes have a single copy of the mitochondrial genome, the TAC serves to mediate the complete segregation of replicated kDNA molecules in order to ensure that each daughter cell receives a full complement of kDNA during cell division (Ogbadoyi *et al*., 2003; Matthews, 2005; Baudouin *et al*., 2020). The TAC also serves as a link to connect the flagellar basal body and kinetoplast to the cell's microtubular cytoskeleton (Gull, 2003;

Matthews, 2005). Additionally, trypanosomal cells are distinctively coated with tightly packed variable surface glycoproteins (VSGs) which are linked to the membrane by glycophosphatidyl inositol (GPI) anchor molecules (Ferguson *et al*., 1988; Magez *et al*., 2002; Horn, 2014). Each GPI molecule consists of two components: glycosylinositolphosphate (GIP) and dimyristoylglycerol (DMG) (Magez *et al*., 2002; Stijlemans *et al*., 2016).

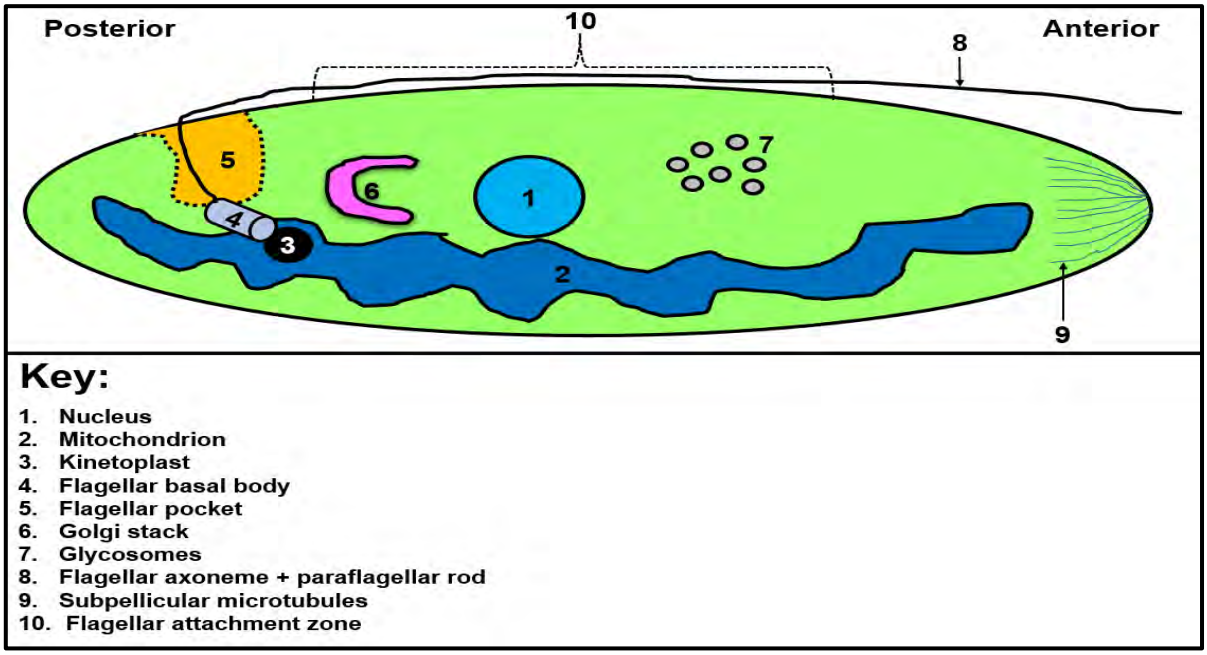

Figure 1.4: A schematic representation of the *T. brucei* cell. The illustration serves to highlight some key and defining subcellular structures of the *T. brucei* parasite. Adapted from Matthews (2005).

The structure of the trypanosomal flagellum is semi-pliable and comprised of a microtubular axoneme that is coupled to a paraflagellar rod (Bastin *et al*., 1998; Vaughan and Gull, 2003). The flagellum plays multiple roles and has been determined to be important for cellular motility and signalling (Langousis and Hill, 2014). For much of its length, the flagellum is laterally attached to the cell body through a complex of structural entities referred to as the flagellum attachment zone (FAZ) (Sherwin, 1989; Ooi and Bastin, 2013). These structures resemble those of cell-to-cell adhesins, such as desmosomes in multicellular organisms, and they from a complex that traverses through both the flagellar and cell membranes (Vickerman, 1969; Sherwin, 1989; Robinson *et al*., 1995; Lacomble *et al*., 2009). An essential component of the FAZ is trypanin. Trypanin is a trypanosomal protein that facilitates the stable binding of the flagellum to the subpellicular microtubules of the cell body, and also facilitates the directional motility of the parasite and, is important in terms of launching an effective infection in the bloodstream of the mammalian host (Hutchings *et al*., 2002; Ralston and Hill, 2006). Within the cytoskeletal corset are single copy organelles, including the nucleus, mitochondrion, and Golgi apparatus, which are predominantly located and assembled at the hub of the cell towards its posterior end (Matthews, 2005) (Figure 1.4). The nucleus is typical of eukaryotic organisms, having a porous membranous envelope that houses a dense chromatin network and nucleolus in the nucleoplasm (De

Souza and Meyer, 1974; Elias *et al*., 2001; Souza, 2009). The nuclear genome is comprised of 11 megabase chromosomes, 5 intermediate chromosomes, and more than a hundred minichromosomes. The total size of the nuclear genome is 35 mbps, comprising of 9068 predicted genes (Donelson, 2003; Kennedy, 2004; Berriman *et al*., 2005). Of the entire genome, 10 % of the genes encode VSGs (Donelson, 2003). The *T. brucei* mitochondrion is large and branched, with its length spanning much of the cell (Matthews, 2005). The main cellular function of the mitochondrion is to produce energy for the cell via oxidative phosphorylation in the ATP generating electron transport chain (ETC). *T. brucei* employs two different terminal oxidases in the ETC: the cyanide-sensitive cytochrome c oxidase (complex IV) and salicylhydroxamic acid-sensitive alternative oxidase (cytochrome independent trypanosome alternative oxidase, abbreviated as TAO) (Moore and Siedow, 1991; Vanlerberghe and McIntosh, 1997; Lukeš *et al*., 2005; Chaudhuri *et al*., 2006). Unlike in higher eukaryotes, the presence of complex I has not been definitively established in *T. brucei* (Guler *et al*., 2008). The mobile redox agents, ubiquinone and cytochrome c, of *T. brucei* are also divergent (Hill, 1976; Lenaz and Genova, 2010). The Golgi apparatus of *T. brucei* is comprised of a single stack which is located between the nucleus and flagellar pocket, tightly packed between the two structures. The positioning of the Golgi stack in the parasite has made *T. brucei* a model organism for the biogenesis of the Golgi apparatus in eukaryotes (Matthews, 2005).

1.6 Life cycle of *T. brucei*

The *T. brucei* mammalian infection commences as the tsetse fly, during a bloodmeal, intradermally inoculates the non-proliferative metacyclic trypomastigote morphotype of the parasite into the bloodstream (Figure 1.5) (Lopes, 2010; Stijlemans *et al*., 2016). The parasites are transmitted as the tsetse fly injects its saliva in order to inhibit blood clotting and vasoconstriction (Cappello *et al*., 1998; Mant and Parker, 2008; Caljon *et al*., 2010; Zhao *et al*., 2015). Inside the host's bloodstream, the short and stumpy metacyclic trypomastigotes differentiate into proliferative long and slender-bodied bloodstream trypomastigotes (Figure 1.5) (Langousis and Hill, 2014). The long and slender-bodied bloodstream trypomastigotes possess the ability to traverse blood vessels and infiltrate perivascular spaces and are therefore disseminated to various sites in the body, including lymph nodes and the cerebrospinal fluid (Langousis and Hill, 2014). The long and slender-bodied bloodstream trypomastigotes are subsequently propagated by binary fission. The proliferation of the long and slender form sets off a quorum sensing pathway which results in a differentiation into the non-proliferative (or quiescent) short and stumpy form (Matthews *et al*., 2004; MacGregor *et al*., 2011). The differentiation into the quiescent short and stumpy form is an adaptation that prepares the parasite for survival in the vector insect's midgut (MacGregor *et al*., 2011). It also prolongs the host's survival to increase chances of the parasite being transmitted back to the vector (Gibson and Bailey, 2003). The parasite is therefore subsequently transmitted to the vector during a blood meal. In the tsetse fly's midgut, the bloodstream trypomastigotes transform into procyclic trypomastigotes which rapidly replicate by binary fission

(Aksoy, 2003) (Figure 1.5). The replication of the procyclic trypomastigotes is subsequently arrested, followed by a migration from the insect's midgut. In the vector's salivary glands, the procyclic trypomastigotes transform into proliferative epimastigotes which attach to the salivary glands via their flagella (Kennedy, 2004). The proliferation of the epimastigotes is subsequently arrested before they transform into the metacyclic epimastigotes which the tsetse fly transmits to the human host during a bloodmeal (Kennedy, 2004). This completes the parasite's life cycle. The parasite morphotypes in the human and tsetse fly are referred to as the bloodstream (BSF) and procyclic (PCF) forms, respectively. An adipocyte tissue form has also been reported. It invades the mammalian fat tissues and can utilize exogenous fatty acids such as myristic acid as a carbon source. This may be a causative factor in the weight loss (wasting) that is observed in HAT sufferers (Trindade *et al*., 2016). It has also been established, that a subpopulation of metacyclic trypomastigotes is retained intradermally, within the vicinity of the tsetse fly's bite (Caljon *et al*., 2016).

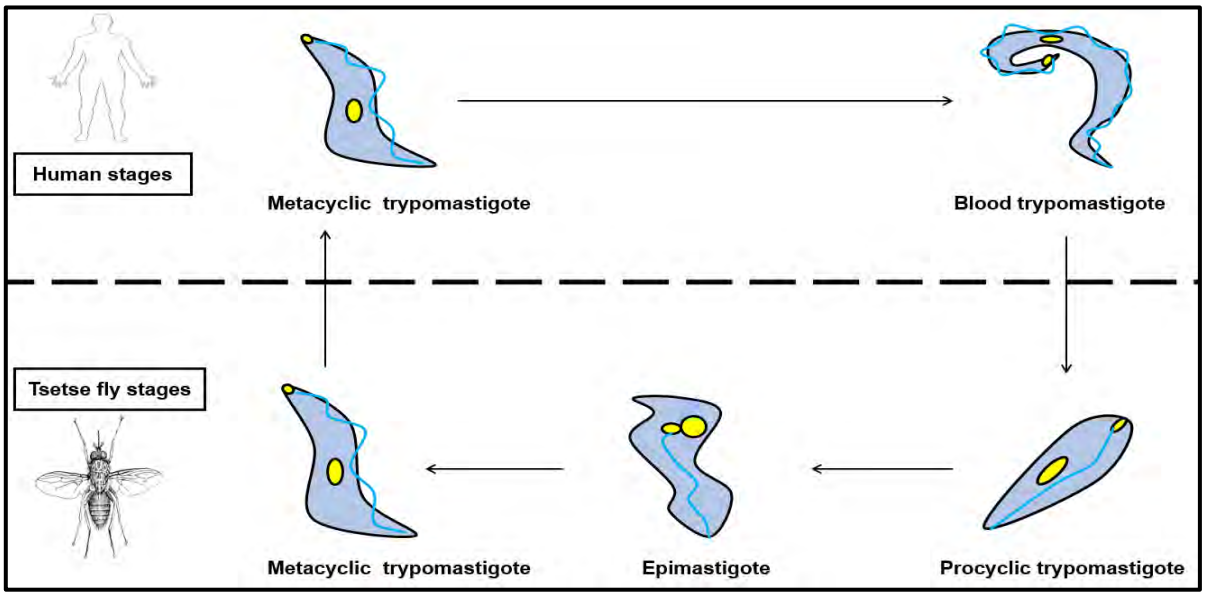

Figure 1.5: Depiction of the *T. brucei* life cycle. The diagram illustrates the various morphotypes of *T. brucei* as well as how the parasite shuttles between the insect vector and human host. The dashed line serves as a demarcation that differentiates between the vector and host stages of the life cycle. Adapted from Matthews (2005).

Notable variations between the BSFs and PCFs are in the functions and structures of the mitochondrion, glycosomes, and the VSG coat (Vickerman, 1965; Richardson *et al*., 1988; Priest and Hajduk, 1994; Lamour *et al*., 2005). The mitochondrion is enlarged and reticulated in the PCFs compared to the BSFs (Priest and Hajduk, 1994; Lopes, 2010). This is due to an increased reliance on oxidative-level phosphorylation in the mitochondria of the PCFs, whereas the mitochondrial functions of the BSF forms are down-regulated in favour of substrate-level phosphorylation (glycolysis) in the glycosomes (Hill, 1976; Hannaert *et al*., 2003; Chaudhuri *et al*., 2006). The structure of the BSF mitochondrion is simple, lacking in cristae, but the glycosomal structures are more elaborate and metabolically activated. These

metabolic alterations are due to glucose and proline being the major carbon sources in the mammalian host and vector, respectively (Priest and Hajduk, 1994; Lamour *et al*., 2005).

Upon uptake by the tsetse fly, the parasite relinquishes its VSG coat for procyclins which are in turn eventually replaced by *brucei* alanine-rich proteins (BARPs) in the salivary glands (Urwyler *et al*., 2007). The procyclins and BARPs also attach to the cell membrane via the GPI anchor (Ziegelbauer *et al*., 1990; Matthews and Gull, 1994; Nolan *et al*., 2000; Urwyler *et al*., 2007). The functions of the procyclins and BARPs in the tsetse vector have not yet been elucidated (Ruepp *et al*., 1997; Acosta-Serrano *et al*., 2001; Vassella *et al*., 2003; Savage *et al*., 2012). However, it is thought that procyclins may be a protective adaptation against the insect vector's midgut proteases (Ruepp *et al*., 1997).

1.7 Host-pathogen interactions

The *T. brucei* parasite is extracellular throughout its lifecycle and is perpetually exposed to the host immune system's elements (Ferrante and Allison, 1983; Lopes, 2010). The VSG coat has been reported to play an important role in the pathology and virulence of *T. brucei* (Morrison *et al*., 2009). At any point of the trypanosomal infection, the parasite population expresses at least 15 variations of the VSG proteins, with each parasite coated by about 10^7 identical VSG molecules of approximately 60 kDa (Cross, 1975; Hall et al., 2013a; Cnops et al., 2015). Despite the variation in the VSG coats in the trypanosome population, the infective trypanosomal population is dominated by cells that express one particular VSG variation at any single point in time. Notwithstanding that trypanosomes possess a complement of 2000 VSG genes (Cnops et al., 2015). The VSG proteins are highly antigenic and elicit a humoral anti-VSG response from the mammalian immune system (Cnops *et al*., 2015). The immune system therefore mounts a response until it reaches a peaking point. Upon peaking of the immune response, a minority of the trypanosome population with a different VSG coat rapidly multiplies and becomes dominant (Horn and McCulloch, 2010). This results in the immune system targeting the newly dominant variation within the population (Horn, 2014). This cycle of the trypanosomes switching the dominant variation within the population is referred to as antigenic variation and is essential for the maintenance of a prolonged infection (Pays, 2006; Taylor and Rudenko, 2006; Savage *et al*., 2012). Recently, VSGs have also been shown to be potentially responsible for drug resistance (Wiedemar *et al*., 2019). Trypanosomes also have a deleterious effect on B cells as they result in the over exertion of the immune cells as a result of antibody over-production. This leads to a condition referred to as hypergammaglobulinimea (Murray *et al*., 1974; Onyilagha and Uzonna, 2019). Antigenic variation further leads to immuno-pathologies such as the expression of autoantibodies, non-specific polyclonal antibodies and a decrease in the populations of selected B cells, resulting in a decreased capacity to launch and maintain an effective anti-trypanosomal secondary response (Diffley, 1983; Magez *et al*., 2020). Antigenic variation ultimately results in a loss of the ability to launch an immune response against other pathogens for which the affected individual may have been vaccinated (immunized)

against (Radwanska *et al*., 2008; Magez *et al*., 2020). Antibody production by B cells is either T cell dependant or independent (Reinitz and Mansfield, 1990). African trypanosomes particularly impair T cell independent antibody expression (Stijlemans *et al*., 2016). The extent of the damage in this regard has also been reported to even result in false positives in patients when administering anti-HIV antibody diagnostic tests (Lejon *et al*., 2010). The loss of immune memory also applies to VSGs, therefore previously prevalent VSG variants in the parasite population may re-emerge (La Greca and Magez, 2011). There are also VSG molecules that present non-specific (cross reactive) epitopes (Hall *et al*., 2013b). Furthermore, anti-VSG antibodies which bind to the VSGs are rapidly endocytosed, along with the bound VSG molecule, for lysosomal degradation in order to decrease the antibody concentration. The VSG molecule is subsequently recycled to the surface of the cell, to bind more antibodies for endocytosis (Field and Carrington, 2009; Horn, 2014). Since the flagellar pocket is the only point at which endocytosis may take place, rapid flagellar beating in the BSFs has been reported to be also essential for an increased rate of endocytosis of VSG-antibody complexes (Engstler *et al*., 2007; Field and Carrington, 2009). The flagellum has also been demonstrated to play a role in the parasites crossing the blood-brain barrier of the mammalian host (Langousis and Hill, 2014). The GPI anchor molecules of the VSG coat also play a role in the pathology of *T. brucei* by interacting with macrophages to bring about the secretion of pro-inflammatory cytokines. The DMG component of the anchor plays a role in the priming of macrophages, whilst the GIP component induces their activation. The GIP component also induces TNF-α subsequent to IFN-γ stimulation (Baral, 2010; Lopes, 2010).

The inability of most trypanosomes to sustain an infection in humans is attributed to trypanolytic factors 1 and 2 (TLF 1 and 2), which are found in the blood serum of healthy individuals (Barrett *et al*., 2003). These factors are released by the innate immune system as part of a mechanism to bring about the lysis of the trypanosomal cells (Raper *et al*., 1999; Thomson *et al*., 2014). The functions of the trypanolytic factors are facilitated by a high-density lipoprotein that is referred to as apolipoprotein 1 (apoL1) (Thomson *et al*., 2014). TLF-1 is part of a complex that is formed in association with apoL1, Haptoglobin related protein (Hpr), apolipoprotein A1 (apoA1) and haptoglobin, whilst TLF-2 is part of a complex that is formed by the association of polyclonal IgM antibodies, apoL1, apolipoprotein Ai1 (Ai1) as well as Hpr (Raper *et al*., 1999; Vanhollebeke *et al*., 2007; Thomson and Finkelstein, 2015; Vanwalleghem *et al*., 2015; Verdi *et al*., 2020). The trypanosomal uptake of TLF-1 is facilitated by the trypanosome haptoglobin-haemoglobin receptor (HpHbr). This receptor is essential for the parasite's supply of haem (Vanhollebeke *et al*., 2008). This receptor, however, cannot distinguish between the haptoglobin-haemoglobin (Hp-Hb) complex and the complex that contains TLF-1 (Cnops et al., 2015). The parasite therefore endocytoses the TLF-L1 containing complex inadvertently. This leads to the formation of pores in the lysosome, causing an osmotic imbalance. The trypanosomal cell subsequently expands uncontrollably and eventually ruptures (Hager *et al*., 1994; Pays *et al*., 2006). TLF-2 is thought

to be the main lytic factor responsible for protecting humans from trypanosomiasis, but its mode of action has not been clearly elucidated (Cnops et al., 2015; Raper et al., 1996).

The resistance of *T. b. gambiense* and *T. b. rhodesiense* to the trypanolytic factors is attributed the *T. b. gambiense* specific glycoprotein (TgsGP) and serum resistance antigen (SRA), respectively (De Greef *et al*., 1989; Van Xong *et al*., 1998; Cnops *et al*., 2015). TgsGP and SRA resemble derivatives of VSG truncations and impart resistance to the human host's trypanolytic factors (Cnops *et al*., 2015). *T. b. gambiense* expresses low levels of HpHbr, and therefore endocytoses low levels of TLF-1 (Kieft *et al*., 2010).

1.8 Diagnosis of HAT

Timely and accurate diagnosis is of paramount importance as early diagnosis is key in ensuring that the patient receives treatment before the onset of the meningoencephalitic stage of the disease, whilst accuracy prevents a misdiagnosis since some of the disease's symptoms mirror that of malaria (Bonnet *et al*., 2015). To prevent misdiagnosis microscopic analysis is carried out on the buffy coat of the blood sample (Chappuis *et al*., 2005). Prior to microscopic analysis, the parasites may also be eluted from the blood sample by means of the mini anion exchange centrifugation technique (mAECT), in cases of low trypanosome concentrations (Chappuis *et al*., 2005; Büscher *et al*., 2009; Camara *et al*., 2010). The above-mentioned diagnostic techniques are not always useful for *G*-HAT diagnosis. Therefore, the card-agglutination trypanosomiasis test (CATT) is also carried out (Truc *et al*., 2002). This diagnostic technique is specific to *T. b. gambiense*, detecting the presence of antibodies specific to VSG variants LiTat 1.3 and LiTat 1.5 (Bonnet *et al*., 2015; Bisser *et al*., 2016). Since treatment for HAT is infection stage specific, lumbar punctures are also administered as a supplementary technique to determine if the infection has infiltrated the CNS (Bonnet *et al*., 2015). In cases of low trypanosome concentrations in the blood, diagnosis may also be carried out using lymphatic fluids drawn from the swollen cervical lymph nodes of patients (Chappuis *et al*., 2005).

1.9 Treatment: drugs and strategies

At present, there is no umbrella treatment drug or strategy for HAT. The anti-trypanosomal chemotherapeutic treatment that is administered needs to be specific to whether the disease is at the haemolymphatic or meningoencephalitic stage and, on whether the patient is infected with *T. b. gambiense* or *T. b. rhodesiense* (Babokhov *et al*., 2013; Brun *et al*., 2010; Lopes, 2010). The haemolymphatic stage of the disease is treated with pentamidine isethionate (or pentamidine) and suramin for *G*-HAT and *R*-HAT, respectively. The meningoencephalitic stage is treated with melarsoprol (or Mel B or Arsobal®) and elfornithine (or alpha-difluoromethylornithine, abbreviated as DFMO). DFMO is used in cases of meningoencephalitic *G*-HAT, whilst melarsoprol is used in cases of both *G*-HAT and *R*-HAT (Lopes, 2010; Babokhov *et al*., 2013). To expedite treatment of

meningoencephalitic *G*-HAT, DFMO is also being used as a combinatorial drug in conjunction with nifurtimox (or Lampit®) in what has been dubbed the nifurtimox-eflornithine combinatorial therapy (NECT). Nifurtimox as an independent drug has not been authorised for the treatment of HAT but is rather used for treating chagas (Bisser *et al*., 2007; Patterson and Wyllie, 2014; Kansiime *et al*., 2018; Munoz-Calderon *et al*., 2019).

Most recently, fexinidazole, has also been sanctioned for the treatment of both stages of *G*-HAT, albeit indicated for non-severe meningoencephalitic HAT (Deeks, 2019; Hidalgo *et al*., 2021; Kande Betu Ku Mesu *et al*., 2021). The drugs used to treat HAT have differing modes of action. Pentamidine, which is administered through intramuscular injections, is an aromatic diamine and its anti-trypanosomal utilisation dates back to the 1930s. This drug hinders DNA replication by influencing topological changes in the parasite's DNA, thereby inhibiting normal topoisomerase functioning. Pentamidine accumulation in trypanosomal cells also hinders mitochondrial activities (Lopes, 2010; Babokhov *et al*., 2013). Suramin, dating back to the 1920s, is a polysulphonated naphthalene dye which inhibits glycosome-based glycolysis by interacting with selected enzymes which include 6-phosphogluconate dehydrogenase. Suramin anti-trypanocidal activity is also thought to be brought about by inhibiting low density lipoprotein uptake, consequently having an adverse effect on the parasite's cholesterol and phospholipid supply. Suramin is administered by means of intravenous injections. Even though suramin is only administered for treating *R*-HAT, it is also effective against *G*-HAT (Lopes, 2010; Babokhov *et al*., 2013).

It is generally accepted that the distinguishing factor between haemolymphatic and meningoencephalitic HAT treatment is whether the drugs are able to cross the blood-brain barrier (Masocha *et al*., 2007; Priotto *et al*., 2008). Melarsoprol is a derivative of a melamine arsenical, melarsen, which has been used as a trypanocidal agent since the 1940s. The melarsoprol mode of action is not clearly understood, but it has been hypothesized that the drug adversely modulates the parasite's glycolytic and redox metabolism pathways. This drug is administered by means of an intravenous injection (Barrett *et al*., 2007; Gehrig and Efferth, 2008; Babokhov *et al*., 2013). DFMO, a trypanocidal agent that was first used as a potential anti-cancer agent, acts by inhibiting ornithine decarboxylase (ODC), with its use dating back to the 1980s. ODC is required for synthesizing polyamines which are essential for mediating trypanosomal proliferation by means of cell division. DFMO is also administered through intravenous infusions (Meyskens and Gerner, 1999; Lopes, 2010; Babokhov *et al*., 2013).

The NECT strategy has been the main treatment of *G*-HAT since 2010. In addition to DFMO's mode of action, nifurtimox places the trypanosomal cells under oxidative stress. This combinatorial therapy is administered orally and intravenously for nifurtimox and DFMO, respectively (Priotto *et al*., 2009; Babokhov *et al*., 2013). Fexinidazole, on the other hand, is a pro drug that emerged from a Drugs for

Neglected Diseases *initiative* (DND*i*) and Swiss Tropical and Public Health Institute (Swiss TPH) collaboration. Subsequent to the collaboration, fexinidazole was further developed by Sanofi. The drug is currently the only HAT treatment that is administered exclusively by oral intake, having efficacy at both stages of the disease (Kande Betu Ku Mesu *et al*., 2021). Fexinidazole, like nifurtimox, is a nitro pro-drug dependent on the putative ubiquinone nitroreductase (NTR) for activation in the mitochondrion. It is however unclear whether the mode of trypanocidal action is mainly due to mitochondrial function hindrance or the targeting of components outside the parasite's mitochondrion (Wilkinson *et al*., 2008; Sokolova *et al*., 2010; Alsford *et al*., 2012; Thomas *et al*., 2018).

Even though African trypanosomes were first described more than a century ago, only a few efficacious drugs have since been approved for treatment. These drugs however present some challenges that include toxicity, administration techniques and even trypanosome resistance. Administering the drugs is also costly and labour intensive in some cases, a disadvantage considering the fact that HAT is endemic to remote and resource lacking regions (Stuart *et al*., 2008; Babokhov *et al*., 2013). Pentamidine has been reported to be nephrotoxic, having side effects that are symptomized by hypoglycaemia and hypotension. In rare cases, pancreatic anomalies, hepatic disorders, and Stevens-Johnson have been reported as side effects. The severity and chance of occurrence of pentamidine's side effects is also dependent on the dosage administered (Bacchi, 2009; Babokhov *et al*., 2013). The most prevalent side effects of suramin when administered at high concentrations are lethargy, neuropathy, renal complications, nausea, anaphylactic shock, and even an allergic reaction (Babokhov *et al*., 2013).

The drugs used to treat the second stage of HAT also have their accompanying disadvantages. Due to being an arsenate, melarsoprol has severe side effects associated with post-treatment reactive encephalopathy (PTRE). Approximately 5-10% of meningoencephalitic HAT sufferers treated with melarsoprol develop PTRE. PTRE is symptomized by convulsions, severe fever, and a coma. More than 50% of the individuals who develop PTRE die within 48 hours of having been initially treated with melarsoprol. Due to the toxicity of melarsoprol, pentamidine is also used in cases of the disease being at the intermediate stage. Trypanosomes are also becoming increasingly resistant to melarsoprol, with reports of the resistance rate being at 30 % (Luscher *et al*., 2007; Priotto *et al*., 2009).

DFMO treatment is complicated by the drug's low affinity for plasma proteins, resulting in a need for prolonged dosing in order to ensure efficacy. DFMO also has a very short half-life and is mostly passed out in urine without having been altered (Babokhov *et al*., 2013). DFMO interacts with mammalian and trypanosomal ODCs, in a similar manner, but is hydrolysed at a lower rate in the trypanosomes (Barrett *et al*., 2007). Furthermore, DFMO is costly to administer as a single kit of the drug contains two treatments costing €554 each (Simarro *et al*., 2012). The kit is also large, with a volume of 190 L and weighing 40 kg, requiring trained medical personnel and extensive labour. The efficiency of DFMO is

also dependant on a healthy immune system, therefore immunocompromised individuals, such as HIV positive individuals, have a lower chance of getting cured (Babokhov *et al*., 2013). The side effects of the NECT include nausea, convulsions, various aches, and insomnia. The NECT is also expensive, providing four treatments which cost €336 by the year 2010. The kit is also large, with a volume of 100 L and weighing 30 kg (Simarro *et al*., 2012; Babokhov *et al*., 2013). Fexinidazole also needs to be taken post meals as bioavailability is considerably compromised in the fasted state (Tarral *et al*., 2014).

Due to the disadvantages of current anti-trypanosomal drugs and their concomitant challenges, more drug development is required to combat HAT. Drug development needs to take safety, efficacy, and cost efficiency into account. In several years, multiple anti-trypanosomal compounds have been taken through to human clinical trials. One such compound is acoziborole (SCYX-7158), a benzoxaborole, which is also a project of the DND*i*. This compound is highly efficacious, curing meningoencephalitic HAT in a single dose of 960 mg (Jacobs *et al*., 2011; Babokhov *et al*., 2013). Investigations into the compound's mechanism of action are ongoing (Steketee *et al*., 2018).

Taking into consideration the adverse effects of anti-trypanosomal drugs and the fact that HAT is endemic in remote areas where poverty and conflict are factors, there is a need for more cost-effective and easier-to-administer drugs (Berrang Ford, 2007; Chappuis *et al*., 2010). Melarsoprol administration for example, is associated with pain, whilst its toxicity is potentially lethal (Robays *et al*., 2008). The drug also causes an adverse reaction at the site of injection, meaning that a different area has to be identified for subsequent doses (World Health Organization, 2019). There is also evidence of resistance against some of the existing drugs, which could possibly worsen overtime as trypanosomes evolve more resistance mechanisms. For example, resistance against pentamidine and melarsoprol is linked to mutations in the aquaglyceroporin (AQP2) transporter that is responsible for their uptake by parasitic cells (Baker *et al*., 2012).

1.10 Vaccine development

As a consequence of the antigenic variation phenomenon, successful vaccine development for HAT is deemed to be unlikely (Kennedy, 2013). This is due to the constant switching of surface antigens which could potentially be targets of the vaccine primed immune response. VSGs also shield potential vaccine antigenic targets such as the antigenic invariant surface glycoproteins (ISGs) from the immune system's components (Ziegelbauer and Overath, 1992, 1993; Salmon *et al*., 1994; Nolan *et al*., 2000; Mehlert *et al*., 2012; Horn, 2014). ISGs are transmembrane proteins that intercalate between the VSGs (Ziegelbauer and Overath, 1993). Additionally, B cell impairment and depletion by trypanosomes means that developing vaccine antigens based on memory B cells could be unlikely (Radwanska *et al*., 2008). Examples of ISGs are ISG65 and ISG75 which present approximately 70000 and 50000 copies of themselves, respectively, on the trypanosome's surface (Chung *et al*., 2008). Both ISG65 and ISG75

have been studied as potential antigenic targets in *T. brucei* vaccine development, with ISG75 having been determined to induce insufficient protection (Ziegelbauer and Overath, 1992, 1993; Lança *et al*., 2011). Interestingly, ISG75 has also been shown to be a target of suramin, implicated in the endocytosis of the drug (Salmon *et al*., 1994). In a recent study by Magez et al. (2021), the immunogenic potential of ISG75 alongside *T. brucei* enolase (TbENO) was reassessed. TbENO, like with enolase in *T. cruzi* and *Leishmania*, forms part of the secretome, and is highly antigenic (Geiger *et al*., 2010; Magez *et al*., 2021). Though proving to be highly immunogenic, both ISG75 and TbENO were ultimately determined to be inadequate as antigenic targets (Magez *et al*., 2021).

1.11 Vector control

In the absence of efficacious vaccines and prophylactic drugs, HAT management is largely limited to diagnosis and treatment, whilst vector control is also increasingly being employed (Solano *et al*., 2013). Recommended prophylactic control measures against HAT include wearing protective clothing that is neutral-coloured, avoiding bushes, and travelling in vehicles that are not harbouring tsetse flies (CDC, 2022). These preventative interventions are aimed at reducing the chances of being bitten by a tsetse fly. In 1997, the potential of vector control was demonstrated in the eradication of the *Glossina austeni* tsetse fly that was responsible for the transmission of AAT on the Unguja Island of Zanzibar (Vreysen *et al*., 2014). The method of vector control deployed on Unguja Island relied on the sterile insect technique (SIT) which essentially entailed releasing competitive sterilised male insects into the environment in order to decrease the fly populations (Molyneux *et al*., 2004; Vreysen *et al*., 2011). The success of vector control in the case of Unguja Island inspired the deployment of this control measure on a continent-wide basis (Vreysen *et al*., 2014).

It is known that the chances of *T. b. rhodesiense* and *T. b. gambiense* transmission from the vector to the mammalian are less than 1 % (Jamonneau *et al*., 2004; Auty *et al*., 2012). It is therefore thought that vector control, even if ineffective in eliminating the tsetse vector, may eliminate transmission. Historically, vector control has been viewed as a necessary tool for managing *R*-HAT, but not so much for *G*-HAT as it was thought to be expensive and unfeasible (Gouteux and Artzrouni, 1996). The restricted application of insecticides on cattle (insecticide treated cattle, abbreviated as ITC) has proven to be an effective control technique for *R*-HAT, however it relies on areas that are densely populated with cattle, whereas *G*-HAT endemic areas usually do not meet the required cattle density threshold (Welburn *et al*., 2006; Torr *et al*., 2007; Solano *et al*., 2013). In low cattle density areas, insecticide treated cloths or cloth traps have been used as a control measure against *R*-HAT (Lancien, 1991). With regard to *G*-HAT, which is specifically targeted for eradication by the WHO, vector control later became to be accepted as essential control tool (Solano *et al*., 2013; Solano, 2021). Whilst treatment and monitoring (diagnostic screening) are effective in reducing disease incidence, it became clear that vector control is required for elimination of *G*-HAT where transmission frequency is increased

(Artzrouni and Gouteux, 1996; Gouteux and Artzrouni, 1996). More especially because *G*-HAT patients and those who are asymptomatic can live long whilst harbouring the parasite, giving vectors an increased opportunity to spread the disease (Bucheton *et al*., 2011; Jamonneau *et al*., 2012).

As such, *G*-HAT targeted vector control is increasingly being employed as a disease management strategy (Rayaisse *et al*., 2010; Esterhuizen *et al*., 2011). The vector control technique in use entails insecticide impregnated blue polyester fabrics with a surface area of 0.375 m^2 (50 cm x 75 cm) bordered by a black propylene net (Rayaisse *et al*., 2011). These targets attract the *T. b. gambiense* transmitting *G. palpalis* and *G. fuscipes* tsetse species with a high affinity, whereby the insects make contact with the insecticide, leading to fatality (Rayaisse *et al*., 2010; Esterhuizen *et al*., 2011). The tiny targets are highly cost effective, estimated to be ranging between 66 and 86 US$ per km^2 for the years 2015 to 2020 (Shaw *et al*., 2015; Rayaisse *et al*., 2020). The efficacy of the tiny targets was further demonstrated to be elevated when mounted on mobile pirogues rather than when stationary along river banks for the *Glossina palplalis gambiense*, *Glossina morsitans submorsitans* and *Glossina tachinoides* tsetse fly groups (Rayaisse *et al*., 2015).

A one health approach has therefore also been adopted in tackling African trypanosomiasis whereby vector control is at the centre of managing both HAT and AAT (Wamwiri and Changasi, 2016). With this approach, suppressing tsetse populations results in a decreases of zoonosis in terms of *R*-HAT, but is also effective with regard to *G*-HAT as it decreases chances of interactions between humans and the tsetse fly vector (Grady *et al*., 2011; Funk *et al*., 2013). With respect to vector control, research into paratransgenesis is also ongoing. Paratransgenesis is the genetic manipulation of the bacterial symbionts of the tsetse fly in order to adversely affect the vector's competence in harbouring the *T. brucei* parasite (De Vooght *et al*., 2018). The tsetse has 4 main symbionts: *Wiggleswothia glossinidus* the primary endosymbiont, *Sodalis glossinidus* the commensal endosymbiont, *Wolbachia pipientis* and *Spiroplasma* (Chen *et al*., 1999; Dale and Maudlin, 1999; Aksoy, 2000; Doudoumis *et al*., 2017).

Forming part of the effort to decipher appropriate cellular targets for anti-trypanosomal drugs is research into molecular chaperones (Bentley *et al*., 2019; Andreassend *et al*., 2020; Burger *et al*., 2021). The molecular chaperone response has been shown to be essential for parasitic survival as they navigate ever changing environmental conditions during their respective life cycles (Shonhai *et al*., 2011; Ludewig *et al*., 2015). Therapeutic drugs induce a heat shock response. It is speculated that administering anti molecular chaperone drugs in combination with current drugs could result in the synergistic enhancement of the already existing anti-trypanosomal chemotherapeutics (Burger *et al*., 2014).

1.12 Molecular chaperones

Molecular chaperones are a super-family of conserved and ubiquitous cytoprotective proteins that are primarily responsible for cellular proteostasis, as part of the protein quality control (PQC) system (Hartl *et al*., 2011; Kim *et al*., 2013). Heat shock proteins (Hsps) constitute part of the molecular chaperone system of the cell. They were first discovered in *Drosophila melanogaster*, being upregulated as a response to heat stress (Ritossa, 1962; Tissiéres *et al*., 1974). However, Hsp regulation has since been demonstrated to also respond to other stresses, including oxidation, hypoxia, toxicity and even nutrient deficiency. Even though Hsps are upregulated under stress, some are constitutively expressed and referred to as heat shock cognate proteins (Hscs) (Garrido *et al*., 2001; Daugaard *et al*., 2007; Zhao *et al*., 2020). Hsps primarily function to facilitate nascent protein homeostasis by way of folding them into their correct tertiary structures (Craig *et al*., 1993). Protein folding is either carried out co-translationally or posttranslationally by Hsps binding to the hydrophobic moieties of misfolded proteins and assisting them to fold without forming a part of the final polypeptide product (Hartl, 1996).

Hsps occur in all the main sub-cellular compartments and are historically named and classified according to their molecular weight. There are five major families of Hsps in the molecular chaperone network: Hsp100 (ClpA, CplB, CplP, CplX), Hsp90 (HtpG), Hsp70 (DnaK), Hsp60 (GroEL), and the small Hsps (IbpA and IbpB) (Walter and Buchner, 2002; Jee, 2016; Fauvet *et al*., 2021). In parentheses are the respective prokaryotic orthologues. The human orthologues also have a unique nomenclature: HSPH (Hsp110), HSPC (Hsp90), HSPA (Hsp70), HSPD (Hsp60), and HSPB (small Hsps) (Kampinga *et al*., 2009). According to Kampinga et al., (2009), the need for a unique naming system arose due to human Hsp families having an increased number of members as a result of gene duplication over the course of evolution. As a consequence, human Hsps were named in a disorderly fashion with different molecules having very similar names. There were also instances of single Hsp genes each having numerous names by which they were referred to (Kampinga *et al*., 2009). Molecular chaperones carry out their functions, in an ATP-dependent or independent manner, in concert with partner proteins referred to as co-chaperones or co-factors. The major ATP-dependent molecular chaperones are constituted of the Hsp100, Hsp90, Hsp70 and Hsp60 families (Clare and Saibil, 2013). Depending on whether they are ATP dependant or independent, molecular chaperones carry out their functions using several modes of action: unfolding, holding, and disaggregation. Protein unfolding entails the active conversion of stably misfolded into natively refoldable species in an ATP-dependent manner. Holding entails holding unfolded proteins in solution until they are spontaneously folded, in an ATP-independent manner. Disaggregation entails the active unfolding of protein aggregates and solubilizing them in their native conformations, in an ATP-dependent manner (Ciechanover and Kwon, 2017). Severe and prolonged stress which goes beyond the capabilities of the Hsp PQC system leads to cell pathology and death (Rao and Bredesen, 2004).

1.12.1 Hsp70: a central role player in the molecular chaperone network

The Hsp70 sub-family of molecular chaperones is the most conserved and ubiquitous cross all domains of life. They play a central role in the molecular chaperone network by mediating protein folding, translocation, assembly formation and degradation. Hsp70 acts as a chaperone at most stages of a protein's lifespan; from the folding of nascent polypeptides as they are released from the ribosome to the repair and degradation of terminally misfolded proteins, as well as transmembrane translocation (Hunt and Morimoto, 1985; Karlin and Brocchieri, 1998; Fernández-Fernández *et al*., 2017; Nitika *et al*., 2020). They are found in most sub-cellular compartments including the nucleus, cytosol, endoplasmic reticulum, and chloroplasts (Craig, 2018). They have the responsibility of folding approximately 20% of nascent polypeptides and account for approximately 0.5 to 2 % of the cellular protein mass under non-stress conditions (Mayer and Bukau, 2005; Finka and Goloubinoff, 2013). Hsp70s, utilising energy derived from ATP hydrolysis, mediate the proper folding of proteins into their native structural conformations (Finka *et al*., 2016). However, Hsp70s also bind to aggregated proteins in an ATP-independent manner, acting as holdases (Rothman, 1989; Slepenkov and Witt, 2002).

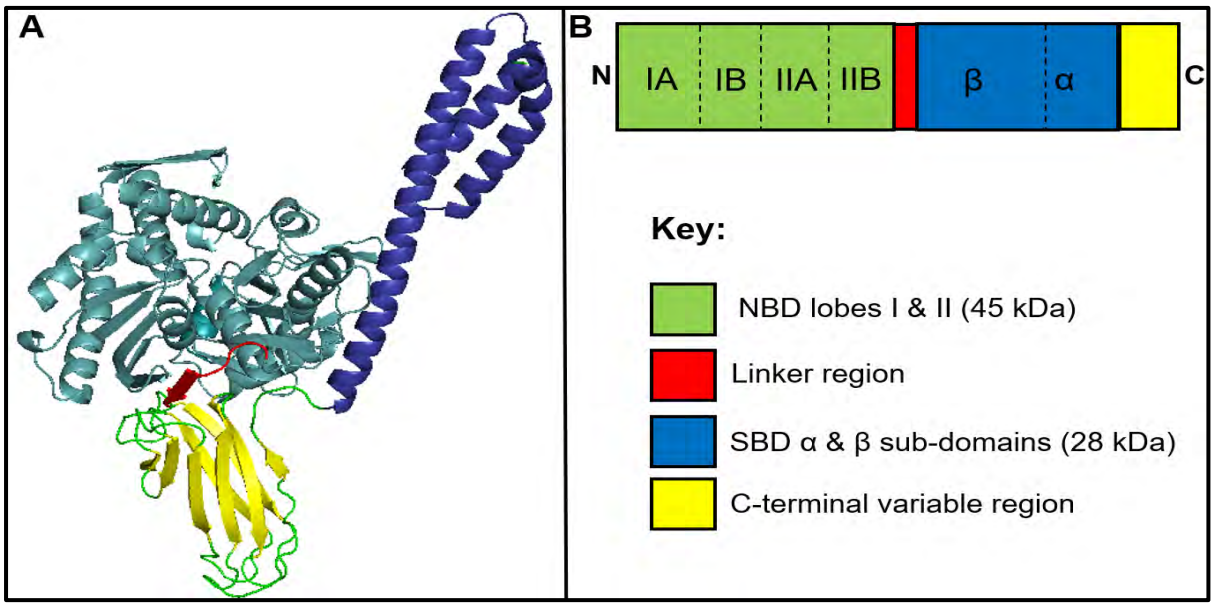

Figure 1.6: Structure of canonical Hsp70. A) Structure of *E. coli* DnaK (PDB accession no: 7ko2) (Wang *et al*., 2021). The structure was rendered in PyMOL (https://sourceforge.net/projects/pymol/; DeLano, 2003). The NBD is depicted in teal whilst the SBD-β sub-domain (containing the substrate binding pocket) is depicted in yellow. The SBD-α subdomain (α-helical lid) is shown in blue. The linker region is shown in red. **B)** The illustration depicts the domain arrangement of canonical Hsp70s, from N- to C-terminal. The dashed lines demarcate the segments of the NBD lobes. This diagram is not to scale and is therefore not necessarily representative of the relative lengths (molecular masses) of the respective domains. The key to the diagram is also provided.

The structure of canonical Hsp70s is constituted of two main domains: the conserved 45 kDa nucleotide binding domain (NBD) and the less conserved 25 kDa substrate binding domain (SBD) (Figure 1.6). In between the NBD and SBD is a conserved, short, flexible, and highly charged linker region (Vogel *et al*., 2006; Swain *et al*., 2007). Hsp70 also possesses an extended, dynamic, and disordered tail region which is situated at the C-terminal. The NBD is structurally similar to hexokinase and actin. It is V-

shaped and constituted of two lobes, I & II, which act as subdomains that form a nucleotide binding cassette cleft to which ATP binds. The lobes are further subdivided into regions A and B (Flaherty *et al*., 1990, 1991; Alderson *et al*., 2016). ATP binding is also dependent upon certain metal ions, including magnesium and potassium (Flaherty *et al*., 1990; Palleros *et al*., 1993). Magnesium has also been determined to be critical for ADP binding (Arakawa *et al*., 2011).

The SBD is subdivided into the 15 kDa SBD-β and 10 kDa SBD-α subdomains. The SBD-β subdomain consists of anti-parallel β-sheets and acts as a hydrophobic substrate binding pocket (Zhu *et al*., 1996). The SBD-α subdomain consists of α-helices and acts as a lid to for the substrate binding pocket (Figure 1.6) (Strub *et al*., 2003). The tail region of cytosolic eukaryotic Hsp70s characteristically contains an EEVD motif at the extreme C-terminal end of the chaperone (Freeman *et al*., 1995; Scheufler *et al*., 2000). The EEVD motif is essential for interaction with tetratricopeptide (TPR) domain containing partner proteins (Odunuga *et al*., 2004). Findings of a recent study suggest that the variability of the tail region results in some functional variation amongst Hsp70 paralogs (Knighton *et al*., 2022). The study by Knighton et al. (2022) utilizing the cytosolic stress seventy subfamily A (Ssa) paralogs 1 to 4 transformed into Ssa 1-4 knockdown (Δ*ssa1-4*) yeast cells, determined that the C-terminal domain is the driver of functional specificity in the maintenance of ribonucleotide reductase (RNR). Ssa1 and Ssa2 were determined to be essential for the maintenance of RNR, whilst Ssa3 and Ssa 4 proved inadequate for this purpose. Additionally, a chimeric protein of the C-terminal end of Ssa2 (SBD-β and SBD-α) fused to the N-terminal of Ssa4 resulted in the successful maintenance of RNR (Knighton *et al*., 2022). Worth noting is that the most divergent regions between the sequences of Ssa2 and Ssa4 are the α-helical lid and unstructured C-terminal domain (Knighton *et al*., 2022).

The substrate binding domain recognizes client proteins by their hydrophobic motifs which occur 30-40 amino acid residues apart. However, Hsp70 does not have a specific recognition site that it binds to and is therefore capable of acting as a chaperone of a plethora of proteins. Hsp70 clients include transducers of signals, cytoskeletal components, and receptors of nuclear hormones (Zhu et al., 1996; Rudiger, 1997; Frydman, 2001; Jason C Young et al., 2003; Gaestel, 2006). The linker region plays a role in the allosteric communication between the NBD and SBD (Kityk *et al*., 2018). The canonical eukaryotic Hsp70 linker is characteristically constituted of three segments: a hydrophilic and variable length section, an extended hydrophobic β-strand segment, and an LDV motif (General *et al*., 2014; English *et al*., 2017).

The nucleotide state of Hsp70 has conformational implications on the interactions between the NBD and SBD-β. In the ATP-bound state, the NBD interacts with SBD-β and SBD-α to form interfaces (Swain *et al*., 2007). In the ADP-bound or nucleotide-free state, the NBD is disengaged from the SBD subdomains, with SBD-α forming a lid over the SBD-β binding pocket, allowing for high affinity substrate-chaperone interactions (Bertelsen *et al*., 2009). The hydrophobic β-strand segment of the

linker region, in the ATP-bound state, binds to the NBD in between the α-helices (Kityk *et al*., 2012; Qi *et al*., 2013). This interaction of the linker and NBD results in a higher turnover of ATP hydrolysis, similar to how substrate binding at the SBD influences ATP hydrolysis. Interestingly, the linker region also has the same effect on ATP hydrolysis even in instances of the SBD having been truncated (Vogel *et al*., 2006; Swain *et al*., 2007). This proves the linker to be an important regulator of the allosteric communication between the NBD and SBD. The flexibility of the linker region also allows the NBD and SBD to exist as structurally independent entities (Mayer and Kityk, 2015; Zhuravleva and Gierasch, 2015; Chakafana *et al*., 2019).

Hsp70 does not act in isolation, but in conjunction with co-chaperones and co-factors, and as a central component of the larger molecular chaperone network (Mayer and Bukau, 2005; Goloubinoff, 2017). Some folded substrates of Hsp70 are transferred to the Hsp60 and Hsp90 systems for further maturation (Wegele *et al*., 2006; Genest *et al*., 2019). In prokaryotes, fungi and plants, Hsp70 also cooperates with Hsp100 in preventing protein aggregation, *reviewed by* Mogk et al. (2015).

1.12.2 Co-chaperones of Hsp70

In carrying out its functions, the Hsp70 molecular chaperone cooperates with co-chaperones. The major driving force of Hsp70 functions are J-proteins, which primarily play the role of delivering client proteins to Hsp70 to promote protein folding. Other important co-chaperones of Hsp70 are comprised of a group of TPR domain containing proteins. One such co-chaperone is the Hsp70 interacting protein (HIP), which primarily functions to prolong the interaction between Hsp70 and its substrate for optimal protein folding (Höfeld *et al*., 1995). In instances of terminal protein damage, another TPR co-chaperone, the carboxy terminus of Hsp70 interacting protein (CHIP), channels terminally damaged client proteins towards degradation. Also, in between the Hsp70 and Hsp90 chaperone systems is a TPR containing co-chaperone, stress inducible phosphoprotein 1 (STi1) which is also referred to as the Hsp70/Hsp90 organizing protein (HOP) in some instances (Odunuga *et al*., 2004). STi1 stabilizes and transfers partially folded polypeptides from Hsp70 to Hsp90 (Johnson *et al*., 1998).

1.12.2.1 J-proteins: the main co-chaperones of Hsp70

J-proteins (or J domain proteins, abbreviated as JDPs) are comprised of a divergent family of proteins that possess a J domain. J-proteins are also referred to as heat shock protein 40 (Hsp40) despite most members of this protein family having a molecular mass that is markedly different from 40 kDa (Kampinga and Craig, 2010). The J domain is usually situated at the N-terminal end and is constituted of four α-helices (helices I-IV). Between helices II and III, in a loop, is a highly conserved HPD motif (Rajan and D'Silva, 2009). The J domain has been determined to be the most important entity within J-proteins in respect to their interactions with Hsp70. Mutations within the HPD motif abrogate the co-chaperone functionality of J-proteins (Liberek *et al*., 1991; Genevaux *et al*., 2001; Wittung-Stafshede

et al., 2003). Furthermore, mutations in helices II and III also result in the loss of function (Hennessy *et al*., 2005a).

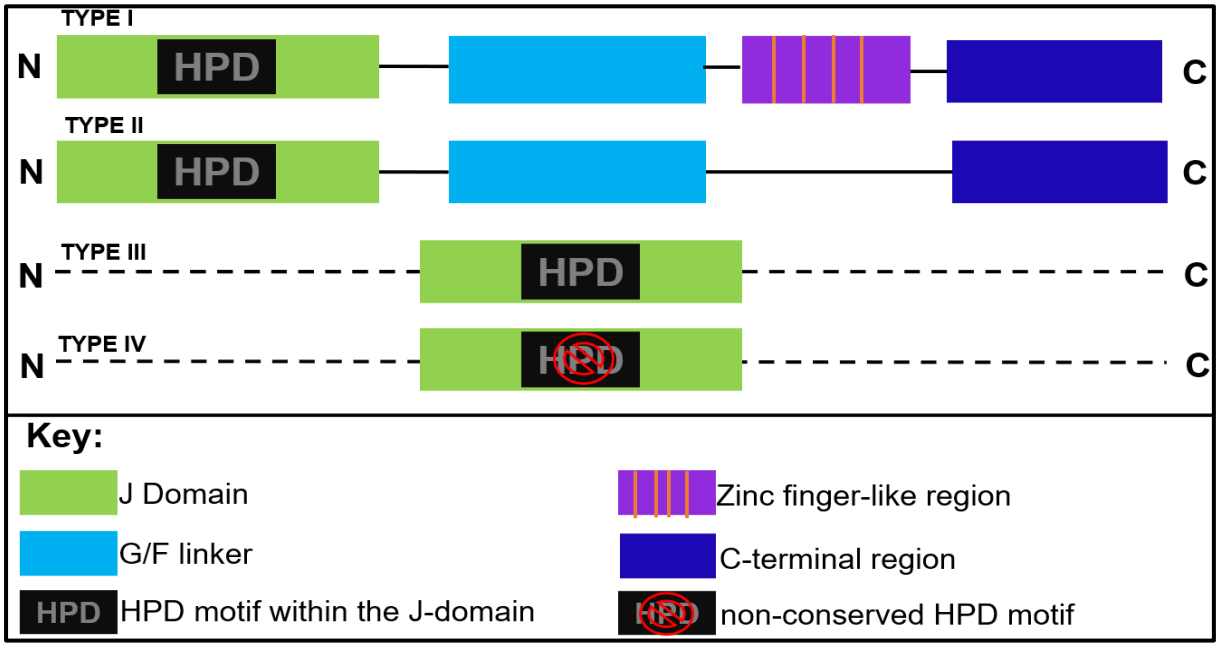

Figure 1.7: Schematic diagram of the domain organization of J-proteins. The illustration depicts the domain arrangement of the different types of J-proteins, from N- to C-terminal. Type I and II J-proteins have similar domain arrangements, with the J domain being at the N-terminal. The only difference is that type II J-proteins do not possess the zinc finger-like region (ZFLR). In type III J-proteins the J domain is the only conserved moiety, and it may occur anywhere along the backbone of the protein. The J domain of type IV J-proteins is non-conserved. This diagram is not to scale and is therefore not necessarily representative of the relative lengths (molecular masses) of the respective domains. The key to the diagram is also provided, *adapted from* Pesce et al. (2015).

J-proteins are classically divided, according to their domain organization, into 3 types (I to III) or classes A to C), whilst a fourth type (type IV) has also been identified (Figure 1.7) (Cheetham and Caplan, 1998; Hennessy *et al*., 2000; Ohtsuka and Hata, 2000; Walsh *et al*., 2004; Hageman and Kampinga, 2009). Type I J-proteins possess the J-domain, a G/F rich region, a signature cysteine rich zinc finger-like region (ZFLR), and a C-terminal region, similar in structure to the *E. coli* orthologue (DnaJ) (Cheetham and Caplan, 1998; V. Rajan and D'Silva, 2009; Kampinga and Craig, 2010). The cysteine rich ZFLR contains two pairs of highly conserved CXXCXGXG motifs, whereby each pair of the motifs has their cysteine residues spatially coordinated around a zinc ion (Banecki *et al*., 1996; Martinez-Yamout *et al*., 2000). The first and second pairs of zinc finger centres are essential for substrate binding and interactions with Hsp70, respectively (Tang and Wang, 2001; Linke *et al*., 2003). Type II J-proteins are similar to type I J-proteins, but they lack the ZFLR (Figure 1.7) (Cheetham and Caplan, 1998). The C-terminal regions of type I and II J-proteins are each comprised of two C-terminal domains (CTD), I and II, of β-barrel topology (Kampinga and Craig, 2010). CTD I possesses a hydrophobic substrate binding pocket, whilst CTD II serves as a dimerization domain. The CTD I of type I J-proteins has the ZFLR protruding from it (Wu *et al*., 2005; Kampinga and Craig, 2010; Kityk *et al*., 2018). Details surrounding the G/F rich region remain obscure, however it has been suggested to play a role in

substrate binding as well as functional specificity (Wall *et al.*, 1995; Yan and Craig, 1999; Kampinga and Craig, 2010; Perales-Calvo *et al*., 2010).

Type III J-proteins only possess a J domain which can occur at any point along the length of the protein (Liu *et al*., 2020). Furthermore, type III J-proteins may possess domains that are not found in type I and II J-proteins (Craig and Marszalek, 2017). Type I and II J-proteins are the main co-chaperones of Hsp70 which function in presenting Hsp70 with misfolded, unfolded, and aggregated substrates (Hennessy *et al*., 2005b). Type III J-proteins are more diverse across species and are thought to be adapted for specific substrate proteins in the cell (Liu *et al*., 2020). They are thought to be responsible for channelling Hsp70 to particular cellular locations (Hennessy *et al*., 2005b). Type IV J-proteins, are also referred to as J-like proteins, possessing a non-conserved or abrogated HPD motif, with the J domain occurring anywhere along the protein's length (Figure 1.7) (Walsh *et al*., 2004). Type IV J-proteins were identified in *P. falciparum* and their function is not clearly defined (Botha et al., 2007). However, it has been inferred that they do have co-chaperone responsibilities since it has been reported that J-proteins without a typical J-domain do perform co-chaperone functions (Ajit Tamadaddi and Sahi, 2016; Solana *et al*., 2022). A unique feature about *P. falciparum* Hsp40s (PfHsp40) is that a number of them possess an N-terminal signal sequence referred to as the *Plasmodium* export element/vacuolar transport signal (PEXEL/VTS) (Pesce *et al*., 2015). The PEXEL/VTS targets plasmodial proteins to the infected host's erythrocytic cytosol (Marti *et al*., 2004; Hiss *et al*., 2008). Worth noting is that 50 % of the PfHsp40s with the PEXEL/VTS signal element are type IV Hsp40s (Pesce *et al*., 2015).

Hsp70 chaperones possess a low intrinsic ATPase activity. Therefore, the primary co-chaperone function of J-proteins is to stimulate the basal ATPase activity of Hsp70 in order to bring about effective substrate protein folding (Lopez-Buesa *et al*., 1998; Sahi and Craig, 2007; Kampinga and Craig, 2010; Kityk *et al*., 2018). The J-domain, through the HPD motif, binds to the linker region and fosters an interaction with the NBD and SBD-β at the interface of the domains (Kityk *et al*., 2018). The J domain binds in between the IA and IIA subdomains of the NBD (Jiang *et al*., 2007). The aspartic and histidine amino residues of the HPD motif interacts with the NBD's catalytic residues through hydrogen bonding and hydrophobic interactions in order to bring about ATP hydrolysis (Kityk *et al*., 2018). In synergy with substrate binding at SBD-β, J-protein binding enhances the ATPase activity of Hsp70 (Mayer, 2013). When the substrate binds to SBD-β, a signal is sent to the interface between SBD-β and the NBD (Zhuravleva and Gierasch, 2011; Kityk *et al*., 2018). The protein folding functions of eukaryotic Hsp70 are further enhanced by another co-chaperone, HIP. HIP is a TPR-domain containing co-chaperone that decreases the rate at which ADP dissociates in the presence of ATP. In this way the Hsp70 chaperone is maintained in a conformation that has an increased affinity for substrate for a prolonged period, resulting in an enhancement of the protein folding process (Höfeld *et al*., 1995; Velten *et al*., 2000; Z. Li *et al*., 2013). The Hsp70/J-protein partnership also extends to the other functions of Hsp70, including

protein translocation and degradation (Kampinga and Craig, 2010). J-proteins, in addition to being Hsp70 co-chaperones, possess the ability to suppress the aggregation of model substrate in an ATP-independent manner (Rudiger, 2001; Burger *et al*., 2014). J-proteins have also been demonstrated to play a role in Hsp70's interactions with other members of the molecular chaperone network, including Hsp100 and Hsp90 (Mayer and Bukau, 2005; Zolkiewski *et al*., 2012).

1.12.2.2 Nucleotide exchange factors

In order to release folded substrates, and re-enter the protein folding cycle, Hsp70s need to substitute bound ADP for ATP. Nucleotide exchange factors (NEFs) facilitate the release of ADP so that ATP may bind (Bracher and Verghese, 2015). There are four evolutionarily unrelated families of Hsp70 NEF co-chaperones: the GrpE family, the Bag-domain family, HspBP1/Sil1 proteins, and the Hsp110/Grp170 family (Hohfeld, 1997; Kabani *et al*., 2002; Steel *et al*., 2004; Dragovic *et al*., 2006; Raviol *et al*., 2006). The GrpE family of NEFs is the only group that occurs in prokaryotes whilst the other families are only found in eukaryotes. In addition to being prokaryotic NEFs, the GrpE family also occurs in the endosymbiotic organelles of eukaryotes (Bracher and Verghese, 2015). The Bag-domain family occurs in the nucleus and cytosol whilst the HspBP1/Sil1 family occurs in the cytosol, nucleus, and the ER (Alberti *et al*., 2003; Bracher and Verghese, 2015). The Hsp110 and Grp170 NEFs localize in the cytosol and ER, respectively (Easton *et al*., 2000).

The NEFs bind to the IIB subdomain of the Hsp70 NBD (Shomura *et al*., 2005; Polier *et al*., 2008; Ung *et al*., 2013; Bracher and Verghese, 2015). GrpE functions as a homodimer that asymmetrically binds to the Hsp70 IIB subdomain at the nucleotide binding cleft. The structure of GrpE consists of a helical dimerization domain at the C-terminus, and a small β-sheet domain (Harrison *et al*., 1997). GrpE inserts its β-sheet domain between subdomains IB and IIB in order to break a salt bridge that traverses the nucleotide binding cleft of ATP-bound Hsp70 (Harrison *et al*., 1997). GrpE does this by twisting open the nucleotide binding cleft (Ung *et al*., 2013; Bracher and Verghese, 2015). The Bag-domain NEFs are a diverse family of proteins that have the Bag domain. The Bag domain consists of a bundle of three helices that are formed by a sequence of approximately eighty amino acid residues (Sondermann *et al*., 2001). The Bag domain interacts with the IB and IIB subdomains of the Hsp70 NBD, resulting in the opening of the nucleotide binding cleft (Brive *et al*., 2001; Gässler *et al*., 2001; Mayer and Gierasch, 2019). HspBP1 and Sil1 are characterized by armadillo repeats, and reside in the cytosol and ER lumen, respectively (Bracher and Verghese, 2015). Through their armadillo repeats, these NEFs bind to the IIB subdomain of the Hsp70 NBD and twist it open (Shomura *et al*., 2005; Bracher and Verghese, 2015).

ATP-bound Hsp110 and Grp170 interact with the Hsp70 IB and IIB subdomains through their NBDs (Polier *et al*., 2008). The Hsp110 and Grp170 paralogs share structural and functional similarities with Hsp70s and are homologous to canonical Hsp70s. As such, they are also referred to as a non-canonical

Hsp70s (Easton *et al*., 2000; Liu and Hendrickson, 2007). They possess sequence insertions in the SBD and an extension of the CTD in comparison to canonical Hsp70s (Oh *et al*., 1999). Hsp110s have also been determined to possess holdase functions which are more efficient than those of canonical Hsp70s. Hsp110s also have the ability to cooperate with canonical Hsp70s and J-proteins as foldase chaperones (Oh *et al*., 1999; Mattoo *et al*., 2013).

1.12.2.3 TPR-containing co-chaperones: STi1 and CHIP

The stress inducible phosphoprotein 1 (STi1) is a co-chaperone of Hsp70 and Hsp90 that acts as a bridge between the two chaperones (Smith *et al*., 1993; Odunuga *et al*., 2004). The protein consists of three TPR domains (TPR1, TRP2A, and TPR2B) that are responsible for binding to the EEVD motifs of Hsp90 and Hsp70 (Odunuga *et al*., 2004). The protein also possesses proline-aspartate repeat linker domains; DP1 and DP2. The DP1 linker occurs in between TPR1 and TPR2A, whilst the DP2 linker occurs at the C-terminus of the protein (Chen and Smith, 1998; Nelson *et al*., 2003; Carrigan *et al*., 2004). The TPR1 domain binds to the EEVD motif of Hsp70 whilst TPR2A binds to the EEVD motif of Hsp90 (Scheufler *et al*., 2000; Brinker *et al*., 2002). STi1 acts as a functional bridge that shuttles client proteins from Hsp70 to Hsp90 (Odunuga *et al*., 2004).

CHIP plays a role in the chaperone-assisted ubiquitin-proteasome pathway (CUPS) (Fernández-Fernández *et al*., 2017). The structure of CHIP comprises of an N-terminal TPR domain, a coiled-coil domain, and a C-terminal U-box domain (Nikolay *et al*., 2004). The TPR domain binds to the EEVD motif of Hsp70 whilst the U-box possesses ubiquitin ligase activity (Ballinger *et al*., 1999; Fernández-Fernández *et al*., 2017). CHIP acts as a homodimer that inhibits the ATP hydrolysis of Hsp70 which consequently inhibits substrate binding and folding (Nikolay *et al*., 2004; Fernández-Fernández *et al*., 2017). The U-box domain associates with the E2 ubiquitin-conjugating enzyme which is responsible for the ubiquitination of the Hsp70 substrate (Zhang *et al*., 2005). Ubiquitinated substrates are subsequently targeted for proteasomal degradation (Connell *et al*., 2001; Qian *et al*., 2006). CHIP also acts as an Hsp90 co-chaperone that targets its substrate proteins for proteasomal degradation in a similar fashion to Hsp70 (Ballinger *et al*., 1999; Connell *et al*., 2001).

1.12.2.4 The co-chaperone assisted protein folding cycle of Hsp70

Briefly, upon client protein delivery by type I or II J-proteins, the ATPase activity of Hsp70 is enhanced (Figure 1.8) (Kampinga and Craig, 2010). Upon ATP hydrolysis at the NBD of Hsp70, the conformation of the chaperone undergoes changes to bring about a higher affinity for substrate at the SBD-β subdomain's substrate binding pocket (Bukau *et al*., 2000). As protein folding takes place, the SBD-α subdomain acts as a lid for the substrate binding pocket (Zhu *et al*., 1996). During protein folding, the HIP co-chaperone prolongs the Hsp70/substrate interaction by momentarily preventing nucleotide exchange at the NBD (Figure 1.8) (Höfeld et al., 1995; Li et al., 2013). Substrate release, post folding,

is facilitated by NEFs as they exchange ADP for ATP at the NBD to bring about the Hsp70 conformation that has decreased affinity for the substrate (Figure 1.8) (Bracher and Verghese, 2015). Improperly or incompletely folded substrate proteins may be subjected to another round of the Hsp70 functional cycle. Since client proteins possess multiple Hsp70 binding sites, they may have to go through a few cycles of protein folding in order to bring about their native states (Rosenzweig *et al*., 2017).

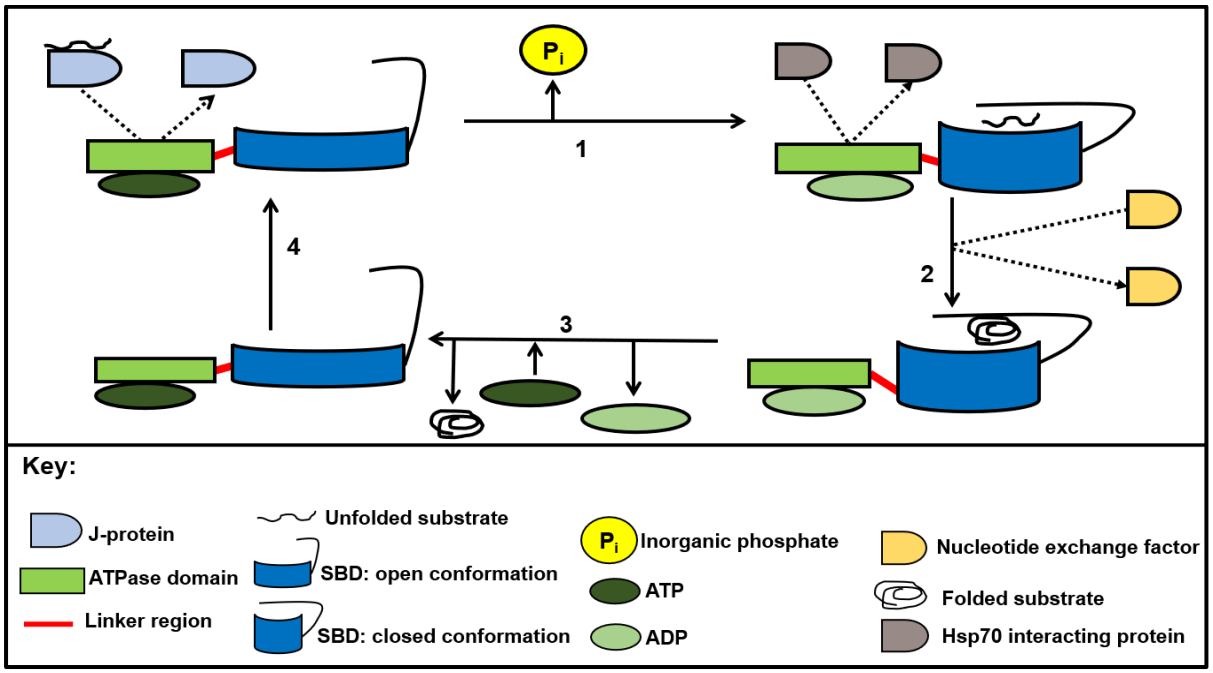

Figure 1.8: Diagram depicting the functional cycle of Hsp70 in protein folding. 1) Client proteins are presented to ATP-bound Hsp70 by J-proteins which also function to stimulate its ATPase activity. Due to the hydrolysis of ATP to ADP, Hsp70 undergoes a conformational change that it increases its affinity for substrate. This results in an efficient protein folding process. The protein folding process is further enhanced by HIP. **2)** NEFs subsequently bind to Hsp70. **3)** NEF binding results in the exchange of ADP for ATP. **4)** ATP binding results in Hsp70's reversion to the conformation with a low affinity for substrate. The folded substrate is therefore released, and Hsp70 is availed for another cycle of protein folding. *Adapted from* Shiber and Ravid (2014).

Alternatively, substrate proteins are channelled towards the CUPS protein degradation pathway if terminally damaged (Esser *et al*., 2004; Fernández-Fernández *et al*., 2017). Some Hsp70 folded client proteins are transferred to Hsp90 for further folding in a process facilitated by STi1 in eukaryotes (Odunuga *et al*., 2004). It is proposed that Hsp70 substrate folding may result in incompletely folded intermediates, especially at physiological protein concentrations, that require the Hsp90 machinery to complete their folding (Morán Luengo *et al*., 2018). In the mitochondria, the Hsp60 molecular chaperone is also important for protein folding, acting downstream of Hsp70 (Manning-Krieg *et al*., 1991; Heyrovská *et al*., 1998).

1.12.3 The Hsp90 chaperone system

Hsp90 is one of the most abundant proteins in the cell, accounting for approximately 2% of the cellular proteome under normal physiological conditions (Whitesell and Lindquist, 2005). Initially, humans

were known to possess 5 isoforms of Hsp90 (HSPC) located in different cellular compartments: HSPC1, HSPC2, HSPC3, HSPC4 and HSPC5. However, HSPC2 is a product of a pseudogene of HSPC1 whereby HSPC2 and HSPC1 are 96 % identical (Gupta, 1995; Langer, 2003; Chen *et al*., 2005; Johnson, 2012; Buchner and Li, 2013). HSPC1 and HSPC3, which are thought to have arisen from a gene duplication event, occur in the cytosol, being inducible and constitutively expressed, respectively. HSPC1 shares 86 % identity with HSPC3 (Lyon and Milligan, 2019). The other two isoforms of the Hsp90 family are HSPC4 [94-kDa glucose regulated protein (GRP94)] and HSPC5 [tumour necrosis factor receptor-associated protein 1 (TRAP1)] and they localize in the endoplasmic reticulum and mitochondria, respectively (Hoter *et al*., 2018). The structure of canonical Hsp90 is comprised of the N-terminal (NTD), middle (MD), and C-terminal dimerization (CTD) domains. In between the NTD and MD is a charged linker region (CR) (Csermely *et al*., 1998; Sreedhar *et al*., 2004; Whitesell and Lindquist, 2005; Jackson, 2012; Tsutsumi *et al*., 2012; Lavery *et al*., 2014). The C-terminal domain contains an MEEVD or KDEL motif at its extreme end, depending on the isoform. Hsp90α and Hsp90β both have the MEEVD motif, whilst GRP94 has the KDEL ER retention motif. TRAP1 does not contain a C-terminal motif, and also lacks the charged linker region (Masgras *et al*., 2017; Hoter *et al*., 2018). The MEEVD motif serves to bind TPR containing co-chaperones, whilst the KDEL motif serves to retain the protein in the ER (Scheufler *et al*., 2000; Jackson, 2012; Garg *et al*., 2016). The NTD serves as a nucleotide binding site that binds ATP whilst the MD has a dual function of modulating the ATPase activity and client protein binding. The CTD is responsible for the dimerization of Hsp90 molecules (Meng *et al*., 1996; Panaretou, 1998; Meyer *et al*., 2003; Huai *et al*., 2005).

Under physiological conditions, dimerization of Hsp90 isoforms serves as an essential process for their effective functioning (Prodromou, 2016). Of the cytosolic human Hsp90s, HSPC1 is more prone to dimerization compared to HSPC3 (Sreedhar *et al*., 2004). Furthermore, the two isoforms differ at very specific regions of their sequences, possibly having implications for their functions (Hoter *et al*., 2018). HSPC1 has also been determined to be located at the extracellular space under various stress conditions, playing a role in cell motility and wound healing (Li et al., 2013). HSPC1 is also an important protein for cancer cell stemness, playing a role in maintaining mutant proteins involved in biochemical pathways of oncogenesis (Tatokoro *et al*., 2015; Lee *et al*., 2017). Additionally, HSPC1 is secreted by cancer cells, even in the absence of stressors (Li et al., 2013). Worth mentioning is that another isoform of Hsp90, referred to as Hsp90N, was thought to exist. However, it was later discovered that Hsp90N has no orthologues amongst eukaryotes, merely being a chimera of HSPC1 and another protein, resulting from cDNA or chromosomal rearrangement (Schweinfest *et al*., 1998; Chen *et al*., 2005; Zurawska *et al*., 2008).

1.13 Hsp70 at the mitochondrion

The majority of mitochondrial proteins are nuclear-encoded and synthesized by ribosomes in the cytosol. Therefore, mitochondrial biogenesis is hinged upon the import of the organelle's proteins from the cytosol, *reviewed by* Chacinska et al. (2009), Zhao and Zhou (2021). Mitochondrial protein import deficiencies have been implicated in diseases such as cancer and neurodegeneration (Nicolas *et al*., 2019). Mitochondrial Hsp70 (mtHsp70) plays a central role in the import of mitochondrial proteins from the cytosol (Rassow *et al*., 1994; Schneider *et al*., 1994; Horst, 1997). For import into the matrix, the positive charge of the mitochondrial targeting sequence (presequence) at the N-terminal of the mitochondrial protein is attracted to the core of the translocase of inner membrane (TIM23) pore by the negative membrane potential at the inner membrane (Martin *et al*., 1991; Matouschek *et al*., 2000; Kulawiak *et al*., 2013). However, this affinity is insufficient for the translocation of the whole protein into the matrix. Therefore, protein import into the matrix is also driven by the presequence translocase-associated motor (PAM) on the matrix side of the inner membrane (Craig, 2018). This membrane-bound multi-component machine, PAM, associates with TIM23 and acts as a motor-assembly that actively pulls the preprotein into the matrix, utilising energy exclusively derived from mtHsp70's ATP hydrolysis (Gambill *et al*., 1993; Wachter *et al*., 1994). The PAM complex is comprised of TIM44, mtHsp70, Pam18 (or Tim14), Pam16 (or Tim16), Mge1, and Pam17 (Craig, 2018). TIM44 is a peripheral membrane protein comprising of an N-terminal and C-terminal domain. TIM44 is the central organiser of the PAM complex serving to foster an association between mtHsp70 and the TIM23 channel. The N-terminal domain of TIM44 binds to both mtHsp70 and Pam16 whilst the C-terminal domain binds to TIM23 (Josyula *et al*., 2006; Schiller *et al*., 2008; Marom *et al*., 2009; Schilke *et al*., 2012; Ting *et al*., 2017). TIM44 is also involved in shuttling the mitochondrial preproteins from TIM23 to mtHsp70.

Once the preprotein binds to mtHsp70, the chaperone hydrolyses ATP in order to provide energy for the import of the preprotein (Glick, 1995; Pfanner and Meijer, 1995). Pam18 and Pam16 are J-like proteins. Pam18 is an integral membrane protein which interacts with Tim17 and Pam16 in the intermembrane space and matrix, respectively. Pam18 plays a role in modulating the ATPase activity of mtHsp70. Pam16 contains a J-like domain that does not have the capability to stimulate the ATPase activity of mtHsp70 but is important for interactions of mtHsp70 with Pam18 and TIM23 (Li *et al*., 2004; Craig, 2018). Pam16 also plays a role in regulating the dual roles of Pam18 in mitochondrial protein import and respiratory chain complex formation. Pam16 influences the functional distribution of Pam18 between protein translocation and the respiratory chain complexes (Priesnitz *et al*., 2022). Mge1 plays the role of an NEF for mtHsp70 (Kulawiak *et al*., 2013). Pam17 serves to promote the interaction of Pam18 and Pam16 with TIM23 (van der Laan *et al*., 2005). Once in the matrix, the presequence is cleaved by the matrix processing peptidase (MPP) (Kulawiak *et al*., 2013). In the matrix, preproteins are further folded by mtHsp70 in a process independent of the PAM complex. However, in

the case of protein folding at the matrix Mdj1, a type-I J-protein, acts as a co-chaperone instead of Pam18/Pam16 complex. For certain substrate proteins, mtHsp70 cooperates with Hsp60 in order to ensure proper folding (Liu *et al*., 2001; Voos, 2013; Böttinger *et al*., 2015).

The functions of mtHsp70 also extend to the formation of iron-sulphur (Fe-S) protein clusters and maintaining the mitochondrial genome. Fe-S clusters are capable of binding to and releasing electrons, and they function in electron transfer, sulphur and nitrate reduction, co-factor biogenesis, and DNA repair (Lill and Mühlenhoff, 2008; Gao, 2020). The central role player in Fe-S cluster proteins if Isu1, which serves as a scaffold for the assembly of the cluster (Maio and Rouault, 2015). Once the Fe-S cluster has been formed on the Isu1 scaffold, the cluster is subsequently released from Isu1 and transferred to their relevant apoproteins (Kleczewska *et al*., 2020). MtHsp70 in conjunction with a specialized J-protein, Jac1, is essential for the transfer of the Fe-S cluster from Isu1 to target proteins (Vickery and Cupp-Vickery, 2007). The NEF for mtHsp70 in Fe-S cluster biogenesis is Mge1 (Schmidt *et al*., 2001). For the maintenance of mitochondrial DNA, mtHsp70 and its co-chaperones, Mdj1 and Mge1 have been determined to be indispensable. MtHsp70 has been reported to localize in the mitochondrial nucleoid whilst Mdj1 has been reported to bind to mitochondrial DNA (mtDNA) (Týč *et al*., 2015).

In mammalian organisms, mtHsp70 is also referred to as mortalin due to being essential for cellular survival (Wadhwa *et al*., 1996). Human mortalin (HSPA9) has been shown to cooperate with various co-chaperones and partner proteins in carrying out its functions (Goswami *et al*., 2010). One such co-chaperone is DnaJA3 (commonly referred to as tumorous imaginal disc, abbreviated as Tid1), which is represented by two isoforms in humans, Tid1L (L for long) and Tid1S (S for short) (Syken *et al*., 1999). Tid1L and Tid1S are type I J-proteins which differ at the carboxy terminal; whereby Tid1L possesses 33 amino residues and Tid1S 6 (Syken *et al*., 1999). Additionally, Tid1L and Tid1S primarily reside in the cytosol and mitochondria, respectively, and have been shown to be functionally equivalent to Mdj1 as they complemented the co-chaperone in yeast (Lu *et al*., 2006). Tid1 cooperates with Hsp70, playing a role in cell signalling pathways such as promoting apoptosis (Syken *et al*., 1999). Tid1L on the other hand plays a role in maintaining the integrity of mtDNA and maintaining the membrane potential of the organelle and has also been reported to have an inhibitory effect on apoptosis (Syken *et al*., 1999; Ng *et al*., 2014). In an *in vitro* study, Tid1L and Tid1S, were shown to cooperate with HSPA9 in holdase function. Additionally, they modulated the ATPase activity of HSPA9 by way of stimulation, with Tid1S having a greater effect (Goswami *et al*., 2010).

Independently of each other and HSPA9, Tid1L and Tid1S were also demonstrated to possess holdase functionality, with Tid1S exhibiting a greater suppression of aggregation activity (Goswami *et al*., 2010). Tid1S has also been shown to have a greater synergistic effect on HSPA9 in terms of substrate protein reactivation *vitro* (Iosefson *et al*., 2012). Interestingly, the synergistic effect of Tid1L and Tid1S,

was greater on DnaK than on HSPA9 when it came to substrate reactivation (Iosefson *et al*., 2012). More recently, HSPA9 in addition to Tid1, has also been reported to functionally and synergistically interact with LONP1, a protease protein which has been determined to possess intrinsic chaperone activity as well as the ability to bind mtDNA (Bota and Davies, 2016; Shin *et al*., 2021). In the study by Shin et al., (2021), Tid1 and LONP1 were shown to be essential for HSPA9 protein folding in numerous cell lines. Knocking down Tid1 lead to the insolubility of OXA1L (an inner mitochondrial membrane protein) and NDUFA9 (a subunit of the ETC). Furthermore, LONP1 lead to the insolubility of HSPA9 and Tid1 (Shin *et al*., 2021). Under conditions of NEF (GrpE1) deletion and ATP depletion, the interaction of HSPA9 with either Tid1 or LONP1 proved to be with greater affinity, and LONP1 mutations associated with numerous human diseases proved to be adverse for LONP1/HSPA9 interactions. Additionally, the HSPA9 chaperone machinery proved to be unable to rescue OXA1L aggregates in the absence of LONP1, and LONP1 alone led to the degradation of OXA1L (Shin *et al*., 2021).

Worth noting is that mitochondrial Hsp70, in protein folding, also functions in concert with the group I chaperonin system which is constituted of Hsp60 and its partner protein Hsp10 (Manning-Krieg *et al*., 1991). MtHsp70 client proteins may be transferred to Hsp60 for further folding (Manning-Krieg *et al*., 1991; Heyrovská *et al*., 1998). Structurally, the group I chaperonin forms a barrel consisting of two stacked rings (*cis* and *trans* rings) which are each formed by 7 Hsp60 monomers (heptamer), with an Hsp10 heptamer acting as a dome shaped lid (Braig *et al*., 1994; Hunt *et al*., 1996). Inside the barrel is a closed environment in which client proteins may be folded in an ATP dependant manner (Weissman *et al*., 1995; Ishida *et al*., 2018). The Hsp60 monomer comprises of a substrate binding domain and ATP hydrolysing domain, an equatorial domain that facilitates the assembly of Hsp60 monomers in a heptameric domain, and the intermediate domain that acts as an interface between the apical and equatorial domains (Braig *et al*., 1994; Ishida *et al*., 2018). It is reported that the formation of the mature chaperonin complex is also dependent upon mtHsp70 initially interacting with Hsp10 in order to recruit Hsp60 to the complex (Böttinger *et al*., 2015).

1.13.1 The Hsp70 escort protein and the mtHsp70 paradox

Despite the essential mtHsp70 functions in mitochondrial proteostasis, the chaperone itself is predisposed to forming self-aggregates, in a seemingly concentration-dependant manner (Dores-Silva *et al*., 2017; Nyakundi *et al*., 2018; Kiraly *et al*., 2020). The self-aggregation property of mtHsp70 has previously presented challenges for the biochemical characterization of mtHsp70. MtHsp70 is therefore dependent on the Hsp70 escort protein 1 (Hep1), a mitochondrial tetra-cysteine zinc finger protein, for structural and functional stability. Hep1 is an mtHsp70 partner protein that was initially referred to as Zim17 or Tim15 in yeast (Burri *et al*., 2004; Sanjuán Szklarz *et al*., 2005; Sichting *et al*., 2005; Yamamoto *et al*., 2005). Hep1 is a nuclear encoded protein that was also initially thought to be an

integral constituent of the mitochondrial protein import machinery (Burri *et al*., 2004; Sanjuán Szklarz *et al*., 2005). No known Hep1 orthologues have been identified in prokaryotes (Sichting *et al*., 2005). The escort protein transiently interacts with mtHsp70 in order to promote solubility and therefore functionality.

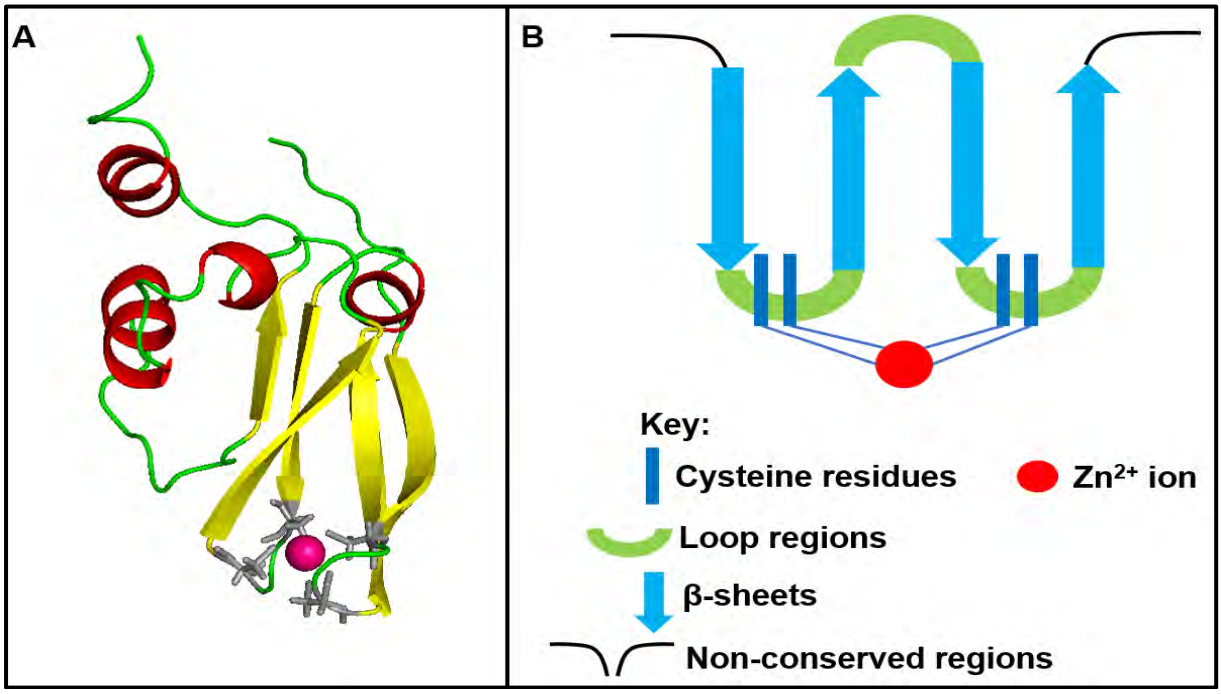

Figure 1.9: Diagram describing the structural properties of Hep1. A) Structure of yeast Hep1 (PDB accession no: 2E2Z) (Momose *et al*., 2007). The α-helices, β-sheets and loop regions are shown in red, yellow and green, respectively. The cysteine residues of the CXXC motifs are depicted as grey sticks, and the coordinated zinc ion is depicted as a magenta sphere. The structure was rendered in PyMOL (https://sourceforge.net/projects/pymol/; DeLano, 2003). **B)** An illustrative schematic diagram of the structure of canonical Hep1, laid out on a single plain.

Structurally, Hep1 is a small L-shaped protein that contains a conserved C-terminal zinc-finger domain, and an unfolded N-terminal region (Figure 1.9). The oligomeric state of Hep1 is usually asymmetric monomers, but concentration-dependant oligomerization has also been observed and reported (Dores-Silva *et al*., 2013). The zinc-finger domain is made up of anti-parallel β-sheets consisting of one pair of zinc coordinating CXXC motifs at their loop structures whereby the cysteine residues chelate the zinc ion (Figure 1.9) (Momose *et al*., 2007; Dores-Silva *et al*., 2013). The zinc-finger domain is the only conserved moiety amongst Hep1 orthologues. Outside of the zinc finger domain, the secondary structure consists of α-helices, β-sheets, and random coil structures (Nyakundi *et al*., 2018). The structure of monomeric Hep1 has been established to be elongated, probably due to the unordered structure of the N-terminal portion of the protein (Dores-Silva et al., 2013; Dores-Silva et al., 2015). The zinc-finger domain is essential for the functions of Hep1. Furthermore, the cysteine residues and their coordination around a zinc ion is required for the function and structure of the protein (Yamamoto et al., 2005; Momose et al., 2007; Dores-Silva et al., 2013; Dores-Silva et al., 2015; Nyakundi et al., 2016). The residues that occur within the loop structures that link the CXXC motifs have also been reported to be important for Hep1 function (Momose *et al*., 2007).

The self-aggregation of mtHsp70 is due to the ATPase and linker domains as it has been determined that these entities serve as the only moieties that Hep1 requires to bind and solubilize the chaperone (Zhai *et al*., 2008). Furthermore, truncations of mtHsp70 have revealed that the ATPase and SBD moieties are soluble when expressed separately. Chimeric proteins whereby the ATPase domain and SBD of *E. coli* HSCA and mtHsp70, respectively, were fused, and vice versa, revealed that the presence of the mtHsp70 ATPase domain results in aggregation. Also, the expression of the mtHsp70 ATPase domain in isolation results in a self-aggregating protein entity (Zhai *et al*., 2008). Hep1 preferentially binds to a transient nucleotide-free conformation of mtHsp70 resulting in a conformational change that promotes ATP binding (Zhai *et al*., 2008). Hep1 is subsequently released to make way for ATP binding, resulting in a conformational change that renders mtHsp70 soluble and functional (Blamowska *et al*., 2012).

1.14 The functional relevance of the CXXC motif

In proteins with sulphur containing amino acid residues, methionine and cysteine, oxidative stress results in adverse structural modifications that may lead to inactivation and aggregation (Serebryany *et al*., 2016; Karri *et al*., 2019). To directly deal with oxidative toxins, cells deploy cysteine containing antioxidant enzymes such as catalase, superoxide dismutase, and glutathione peroxidase to hydrolyse them, as the first line of defence (Guttmann and Powell, 2012; Ighodaro and Akinloye, 2018). However, there are other groups of proteins that indirectly combat oxidative stress by preventing the misfolding and aggregation of proteins that face damage due to oxidant exposure (Dahl *et al*., 2015; Seco-Cervera *et al*., 2020). These proteins are also characterized by having cysteine residues which allow for their reversible activation in response to oxidation and as such they are referred to as redox-regulated proteins (Klomsiri *et al*., 2011; Radzinski *et al*., 2021).

Cysteine is one of the least frequent amino acid residues present in the sequence of proteins (UniProt Consortium, 2013; Krick *et al*., 2014; Pham *et al*., 2021). However, where it does occur, it is highly conserved and often indispensable for function and structure (Marino and Gladyshev, 2010). Cysteines contain a highly reactive thiol group which enables them to reversibly form covalent (disulphide) bonds with other cysteines or a sulphenic acid (Gupta and Carroll, 2014). The CXXC motif is a common, and essential, feature among redox-regulated proteins. It serves as the active site of redox-regulated proteins, acting as a switch that reversibly modulates them (Conway and Lee, 2015). The cysteines in the CXXC motif are involved in the reversible formation of disulphide bonds, allowing for the cycling of redox-regulated proteins between their active and inactive forms. The CXXC motif occurs within a structural feature referred to as the thioredoxin fold (Conway and Lee, 2015). The XX dipeptide flanked by the cysteines of the CXXC motif also serves an important role in the functions of the proteins. The regulatory importance of the XX dipeptide within the CXXC motif has led to it being dubbed a redox rheostat (Chivers *et al*., 1997; Huber-Wunderlich and Glockshuber, 1998; Mössner *et al*., 1998). Redox-

regulated proteins include metabolic oxidoreductases and some ATP-independent molecular chaperones. Since oxidative stress results in damaging modifications of proteins, by formation of disulphide bonds at their sulphur-containing amino acid residues, a group of proteins known as oxidoreductases function to reduce (break) the disulphide bonds. Oxidoreductases are upregulated under oxidative conditions as they play an essential role in the maintenance of the redox state of cells.

Two of the most well characterized oxidoreducatase systems are thioredoxins and glutaredoxins (Berndt *et al*., 2008; Conway and Lee, 2015). The reduction of the disulphide bonds by thioredoxins in particular serves to prevent the misfolding and aggregation of proteins as a result of the structural alterations caused by inappropriate disulphide bonding (Dahl *et al*., 2015). Oxidoreductases function by reversibly regulating the formation of intramolecular, intermolecular, and mixed disulphide bonds in oxidized proteins. One damaging effect of oxidation on cells is the inactivation or aggregation of proteins as a result of misfolding. Misfolding and aggregation occur due to the modification of protein side chains, leading to adverse structural and functional modulation, particularly on the sulphur containing amino acids (Dahl *et al*., 2015).

Within the context of molecular chaperones, cells also possess a mechanism by which oxidative stress related protein misfolding and aggregation is prevented. A prime example of such a molecular chaperone system is Hsp33, a prokaryotic redox-regulated molecular chaperone, that has also been identified in certain eukaryotic organisms, including green algae (*Chlamydomonas*) and trypanosomatids (Segal and Shapira, 2015). The structure of Hsp33 is comprised of a tightly folded N-terminal domain, and a C-terminal domain that contains CXC and CXXC motifs. In between the N- and C-terminal domains of Hsp33 is a highly charged linker region which is implicated in the mechanistic regulation of the molecular chaperone (Graf *et al*., 2004; Ulrich *et al*., 2021). Under normal reducing conditions, the CXC and CXXC motifs of Hsp33 coordinate a zinc ion in the inactive and monomeric state of the chaperone (Jakob *et al*., 2000).

Upon oxidation, the cysteines in the respective CXC and CXXC motifs form disulphide bonds, triggering the release of the coordinated zinc ion. This results in the formation of an active Hsp33 dimer which is able to bind substrate proteins. The conformational changes emanating from the formation of the disulphide bonds and the zinc ion release, result in the unfolding of the linker region to activate Hsp33 as a molecular chaperone (Barbirz *et al*., 2000; Graumann *et al*., 2001; Graf *et al*., 2004). In the presence of slow acting oxidants such as H_2O_2, only the cysteines of the CXXC motif form a disulphide bond. The zinc ion is subsequently released, but the linker region is only partially unfolded with the chaperone remaining a monomer (Ulrich *et al*., 2021). Only upon the application of heat shock do the cysteines of the CXC form a disulphide bond in order to result in the complete unfolding of the linker region and dimerization (Cremers *et al*., 2010; Graf *et al*., 2004). This implicates the linker region as a key regulator of the Hsp33's activation, as it is also thought to act as a thermolabile sensor that regulates

the formation of the second disulphide bond (Ilbert *et al*., 2007; Cremers *et al*., 2014). Furthermore, mutations in the linker region render Hsp33 constitutively active with an increased sensitivity towards oxidants (Rimon *et al*., 2017). The linker region has also been implicated in substrate release upon the return of normal reducing cellular conditions. The exposure of Hsp33 to fast acting oxidants such as HOCl results in the complete activation of the chaperone as they result in more widespread unfolding of the protein (Winter *et al*., 2008). Interestingly, the Hsp33 orthologue of the green algae, *C. reinhardtii* lacks the CXC motif, and coordinates zinc in a loose interaction. This structural deviation of the *C. reinhardtii* Hsp33 (CrHsp33) has resulted in a different mechanism of activation. CrHsp33 can be activated by heat shock, in the absence of oxidants (Segal and Shapira, 2015).

Upon the return of normal reducing conditions, Hsp33 is reduced by oxidoreductases (Hoffmann *et al*., 2004). However, substrate release, also requires the normalization of cellular ATP levels so that the client proteins may be released to be folded by ATP-dependent chaperones (Hoffmann *et al*., 2004; Winter *et al*., 2005). Hsp33 also promotes client protein folding by channelling them into partially folded conformations which may easily be folded by the ATP-dependent foldases (Moayed *et al*., 2020).

1.15 Hsp70 in human disease and health

The role of Hsp70 in various human pathologies has been extensively documented (Albakova *et al*., 2022). Hsp70s are involved in a myriad of pathways relevant to human health and have been associated with a number of diseases (Edkins *et al*., 2018). In neurodegeneration and cancer, Hsp70 is widely implicated in disease formation (Murphy, 2013; Albakova *et al*., 2022). As such, research into Hsp70s as targets for therapeutic drugs is also ongoing (Hendriks and Dingemans, 2017). There are 13 paralogs of Hsp70 in humans, localized in different compartments including the cytosol, ER and the mitochondria (Kampinga *et al*., 2009; Rosenzweig *et al*., 2019). The involvement of Hsp70 in disease involves a myriad of biochemical pathways with Hsp90 also implicated in many of them (Albakova *et al*., 2020, 2022). In parasitic diseases such as malaria and African trypanosomiasis, Hsp70s are implicated in aiding the parasites' survival throughout their erratic lifecycles (Louw *et al*., 2010; Przyborski *et al*., 2015).

1.15.1 Hsp70 in neurodegeneration and oncogenicity

Neurodegenerative disorders arise from conditions whereby there is an accumulation of misfolded proteins to an extent that the cellular PCQ machinery is overburdened (Rutledge *et al*., 2022). In numerous cases these proteins form amyloid fibrils that are constituted of highly ordered cross β-sheets, however they can also form aggregates or be found in inclusions. In particular, intrinsically disordered proteins (IDPs) such as tau, α-synuclein, Tar DNA binding protein 43 (TDP-43) can be found in neuronal cell aggregates of Alzheimer's disease (AD), Parkinson's disease (PD) and amyotrophic lateral sclerosis (ALS) sufferers (Chiti and Dobson, 2017; Gupta *et al*., 2020). The IDPs do not have a

proper native conformation and are therefore prone to forming non-functional and toxic aggregates (Brundin *et al*., 2010; Uversky, 2010; Rutledge *et al*., 2022). Hsp70, along with Hsp90, has been implicated in neurodegenerative diseases in that it has been demonstrated to interact with tau, α-synuclein, and TDP-43 (Rutledge *et al*., 2022). When the IDPs misfold, it is thought that they expose their hydrophobic moieties to which the molecular chaperones may bind. However, another mechanism has been proposed. It is hypothesized that there is a competition between the molecular chaperones and the intramolecular interactions of the native IDPs. This competition consequently promotes IDPs transitioning into seed-competent conformations. The seed-competent conformations are prone to self-aggregation (Karagöz *et al*., 2014; Gu *et al*., 2021; Rutledge *et al*., 2022).

In cancer cells, Hsp70 participates in the inhibition of cell death and senescence whilst also promoting the metastasis and aggression of tumours (Murphy, 2013). The heat inducible cytosolic Hsp70, HSPA1A, hinders apoptosis by partaking in inhibitory interactions with c-Jun N-terminal kinase (JNK), p38 and apoptosis-inducing factor (AIF) (Tournier *et al*., 2000; Garrido *et al*., 2001; Gao *et al*., 2010). The inhibition of JNK, accompanied by the maintenance of the lysosome's membrane, also extends to blocking necrosis. HSPA1A also inhibits the assembly of the death-inducing signalling complex (DISC) (Guo *et al*., 2005). In inhibiting senescence, HSPA1A modulates the activities of tumour suppressor protein p53 and cyclin-dependent kinase (Cdc2) (Yaglom *et al*., 2007). In promoting metastasis and tumour aggression, HSPA1A forms interactions with hypoxia-inducible factor α (HIF-1α) and the aminoacyl-transfer RNA synthetase-interacting multifunctional protein 2 (AIMP2) which is devoid of the second exon. HIF- 1α and AIMP2 also promote tumour angiogenesis (Huang and Bunn, 2003; Zhou *et al*., 2004; Han *et al*., 2008; Lim *et al*., 2020). HSPA8, the constitutively expressed cytosolic Hsp70, has also been suggested to promote cancer cell survival, by interacting with and stabilizing Rab1A (Tanaka *et al*., 2014).

HSPA9, also referred to as mortalin in mammals due to its essentiality for cell survival, plays multiple roles in oncogenicity. HSPA9 participates in various other pathways in cancer cells (Wadhwa *et al*., 2006; Albakova *et al*., 2022). HSPA9 expression is increased in tumours, resulting in the promotion of metastasis, tumour expansion and angiogenesis (Wadhwa *et al*., 2006; Yun *et al*., 2017). HSPA9 also prevents apoptosis through interactions with HIF-1α, under hypoxic conditions. HSPA9 facilitates the process by which HIF-1α is targeted to the outer membrane of the mitochondrion (Mylonis *et al*., 2016). The targeting of HIF-1α to the mitochondria hinders apoptosis when the extracellular signal-regulated kinase (ERK) is in its inactive form (Mylonis *et al*., 2016). In ovarian cancer cells, the upregulation of HSPA9, as a consequence of nuclear factor κB (NF-κB) binding to its promoter, promotes the replication of ovarian cancer (Li *et al*., 2019). HSPA9 has also been associated with the survival of medullary thyroid carcinoma cells (Li *et al*., 2019). Due to its involvement in neurodegeneration and cancer, Hsp70 has been the subject of much research into its targeting for chemotherapeutic purposes.

Compounds targeting Hsp70 and Hsp90 for anti-cancer chemotherapeutics have also reached clinical trials (Miyata *et al*., 2013; Murphy, 2013; Albakova *et al*., 2021).

1.15.2 Hsp70 in *T. brucei*

It is thought that Hsp70s may play a key cytoprotective role in the *T. brucei* parasite as it contends with the numerous environmental stresses associated with its life cycle, *reviewed by* Louw et al. (2010). Hsp70s may also be important for the parasite's differentiation (Van der Ploeg *et al*., 1985). In *T. brucei*, it has been established that Hsp70s are expressed in both the PCFs and BSFs of the parasite (Jones *et al*., 2006; Vertommen *et al*., 2008). As such, biochemical characterization and *in silico* identification of *T. brucei* Hsp70s has also been carried out in various studies. It has been predicted that the *T. brucei* family of Hsp70s is comprised of 12 members, with 4 of them being Hsp110s. There are 3 cytosolic paralogs of the canonical Hsp70s: TbHsp70, TbHsp70.4 and TbHsp70.c. TbHsp70 possesses the typical C-terminal EEVD motif. In TbHsp70.4 and TbHsp70.c, as in other kinetoplast organisms, the EEVD motif is divergent (DDVD motif) or absent, respectively (Bentley *et al*., 2019). Generally, GGMP repeats are associated with cytosolic Hsp70s of parasitic origin, in a loop region within the vicinity of the α-helical lid (Chakafana *et al*., 2019). Interestingly, human Hsc70 (HSPA8) also possesses a GGMP motif (Chakafana *et al*., 2019). Although GGMP repeats were thought to be a characteristic of constitutively expressed Hsp70s, stress inducible Hsp70s of numerous species also possess it, *Argopecten irradians* and *Pinctada futada* being examples (Song *et al*., 2006; Wang *et al*., 2009). The GGMP motif is important for facilitating Hsp70 partner protein binding by forming a functional association with the EEVD motif (Demand *et al*., 1998).

In the parasitic organism cytosolic *P. falciparum* Hsp70, PfHsp70-1, the GGMP repeats have been determined to be of functional significance (Makumire *et al*., 2021). In the study, *in vitro* assessments using chimeric proteins demonstrated that the GGMP motifs are essential for PfHsp70-1 in substrate binding as well as in interactions with the Hsp70/Hsp90 organising protein (HOP), PfHop (Makumire *et al*., 2021). Of the cytosolic Hsp70s, only TbHsp70 possesses the GGMP motif (Burger *et al*., 2021). To this end, both TbHsp70 and TbHsp70.4 are capable of interacting with STi1, whilst it has been experimentally demonstrated that TbHsp70.c is incapable of interacting with STi1. However, TbHsp70.4 binding to STi1 is with reduced affinity compared to TbHsp70 binding (Bentley *et al*., 2019; Burger *et al*., 2021). In the ER there are two Hsp70 paralogs, TbGRP78A and TbGRP78B, whilst the mitochondrion has 3 identical paralogs, TbmtHsp70A, TbmtHsp70B and TbmtHsp70C. Of the cytosolic Hsp70s, TbHsp70 and TbHsp70.4 are also located in nucleus and the cell surface, whilst TbHsp70.c can also be found in the nucleus. TbmtHsp70 have also been shown to locate on the cell surface (Bentley *et al*., 2019). The Hsp110 complement is comprised of TbHsp110 found in the cytosol, TbGrp170 and TbHsp70.a in the ER as well as the mitochondrial TbHsp70.b.

The Hsp70 proteins of the *T. brucei* parasite play a pivotal role in ensuring that the parasite copes with ever-changing environmental parameters as dictated by the life cycle (Bentley *et al*., 2019). TbHsp70, TbHsp110, TbHsp70.a and TbHsp70.c were determined to be downregulated whilst TbmtHsp70A and TbHsp70.4 were observed to be upregulated in the PCFs. The converse seems to be true for the BSFs as TbHsp110 and TbHsp70.a were shown to be upregulated whilst the levels of TbmtHsp70s A-C and TbHsp70 were relatively low (Butter *et al*., 2013; Urbaniak *et al*., 2012). It has also been reported that TbHsp70 and TbHsp70.c are upregulated as a consequence of heat stress (Burger *et al*., 2014; Bentley and Boshoff, 2019). In addition, the cytosolic TbHsp70s are subject to posttranslational modification by way of phosphorylation (Nett *et al*., 2009; Urbaniak *et al*., 2013). In vitro studies have also confirmed that the cytosolic TbHsp70s exhibit holdase and foldase capabilities towards denatured model substrates (Burger *et al*., 2014; Bentley and Boshoff, 2019). TbmtHsp70 has been determined to be indispensable for the maintenance of the parasite's kDNA, and in extension viability (Týč *et al*., 2015).

The *T. brucei* J-protein complement is comprised of 67 proteins that are found across all the major subcellular compartments (Louw *et al*., 2010; Bentley *et al*., 2019). Of the type I J-proteins, it has been determined that Tbj2 is essential for the parasite's viability at all the stages of its lifecycle (Alsford *et al*., 2011; Ludewig *et al*., 2015). Tbj2 has also been shown to interact with the cytosolic TbHsp70s, stimulating their basal ATPase activities. Tbj2 also has a stimulatory effect on the holdase and foldase functions of TbHsp70 and TbHsp70.4 (Burger *et al*., 2014; Bentley and Boshoff, 2019). In addition, Tbj2 like various other type I J-proteins, has also been shown to exhibit holdase activity. The mitochondrial type I J-protein, Tbj50, has been shown to co-localize with TbmtHsp70 in the mitochondrion, playing a role in maintaining the mitochondrial genome (kDNA) (Týč *et al*., 2015).

A better understanding of the *T. brucei* chaperone network could therefore contribute to the development of safe and efficacious therapeutics against the parasite (Bentley *et al*., 2019). To that end, a recent study carried out to determine the effects of alcyomarian coral-derived molecules shows that the cytosolic TbHsp70s are subject to modulation (Andreassend *et al*., 2020). The molecules, malonganenones and nuttingins, inhibited the holdase functions of TbHsp70 and TbHsp70.4. The compounds were also screened on the basal and Tbj2 stimulated ATPase activities of TbHsp70 and TbHsp70.4. The compounds had an inhibitory effect. The effect of the compounds on the ATPase activity of human HSPA8 were also determined to be inhibitory, but to a much lesser extent. Therefore, the compounds proved to differentially affect the human and parasitic chaperone systems (Andreassend *et al*., 2020).

1.16 Knowledge gap and motivation

Mitochondrial Hsp70 plays a central role in the import and maintenance of the compartment's proteome. However, despite being a molecular chaperone, mtHsp70 is itself susceptible to self-

aggregation, and requires the Hsp70 escort protein 1 (Hep1) for stability. Hep1 is a cys_4 zinc-finger protein that is primarily responsible for maintaining mtHsp70 in a soluble and functional state. Numerous studies to characterize Hep1 have been carried out using orthologues from various species, and their findings suggest that the different Hep1 orthologues display functional diversity. In this regard, the characterization of Hep1 from *Trypanosoma brucei* will contribute to elucidating the functional relevance and biochemical mechanisms of the Hep1 protein in the trypanosomal cell. The novelty of this study lies in the fact that TbHep1 characterisation has not been carried out thus far and it is not known if TbHep1 is functionally similar to other Hep1 proteins. The characterization of TbHep1 alongside HsHep1 will also be beneficial in that HsHep1 has already been the subject of numerous investigations. This approach may also provide insights into differences, if any, between the *T. brucei* and human Hep1 networks that may potentially be exploited for anti-trypanosomal drug discovery purposes. This study will include the effects of co-expression of TbmtHsp70 and TbHep1 on the function of TbmtHsp70. In *T. brucei* as with other protozoan parasites, Hsp70s have been demonstrated to be essential for survival in the erratic environmental conditions the organisms experience throughout their respective lifecycles. TbmtHsp70, in particular, has been demonstrated to be essential in maintaining the mitochondrial genome, and in extension on the viability of the parasite. Human Hsp70s on the other hand, have been widely implicated in neurodegenerative diseases and are biomarkers for various cancer cell lines. The independent holdase functions of TbHep1 alongside that of HsHep1 will also be assessed with Tbj2 as a control. This will form part of assessing TbHep1's intrinsic chaperone capabilities as the novel protein in this study.

Canonical Hep1 is structurally constituted of a highly conserved zinc finger domain with two CXXC motifs. The CXXC motif has been shown to be important for the function of various redox-regulated proteins under oxidative stress conditions. This study will incorporate Hsp33 as a control in attempting to characterize, on a preliminary basis, the effects of H_2O_2 induced oxidative stress on the holdase functions and structures of TbHep1 and HsHep1. The rationale behind studying Hep1 in this regard is due to the mitochondria being a major source of oxidants in the cell due to processes such as the electron transport chain. Oxidative stress is associated with various human diseases, including neurodegeneration and cancer. Therefore, characterizing Hep1 on this front will potentially lead to a better understanding of disease formation resulting from oxidative stress conditions. It may also be beneficial in bettering the current understanding of the *T. brucei* parasite's redox related pathways since the parasite is also subject to the oxidative elements of the host's immune system. This is also a novel approach in as far as Hep1 characterization is concerned.

1.17 Hypothesis

TbHep1 is a canonical Hep1 orthologue with the ability to interact with TbmtHsp70 in order to enhance its functionality.

1.18 Aims and objectives

1.18.1 Overall aim

The aim of this study is to biochemically characterize putative TbHep1 as a potential co-chaperone of TbmtHsp70. This study will also incorporate cytosolic TbHsp70 in order to determine if it also functionally interacts with TbHep1. The independent chaperone capabilities of TbHep1 will also be investigated. Furthermore, this study will also include HSPA9 and human Hep1. Additionally, this study will preliminarily explore the potential capabilities of the Hep1 orthologues in combating cellular oxidative stress as could possibly be imparted by their CXXC motifs.

1.18.2 Specific objectives

I) *In silico* analyses of putative TbHep1, TbmtHsp70, HsHep1 and HSPA9

The *in silico* analyses were used to predict the various characteristics of the subject. This was to provide insights into the physical properties of the proteins so that could be taken into consideration when heterologously expressing the proteins and characterizing them *in vitro*. The *in silico* analyses were also conducted to predict properties such as 3D structure and domain organization which are important in drug discovery and design. Orthology and similarity was also assessed by means of multiple sequence alignments and syntenic analysis. In addition to orthology and similarity, evolutionary relationships were assessed by phylogenetic analyses.

II) Expression and purification TbHep1, TbmtHsp70, HsHep1, HSPA9 and the other molecular chaperones used in this study

Plasmids encoding the subject proteins were cloned and transformed into genetically engineered *E. coli* strains for heterologous protein expression. Protein expression in the *E. coli* and their subsequent purification were optimized so as to ensure appropriate yields for downstream biochemical characterization. The optimization also took into account the conditions required for the optimal stability and functionality of the proteins.

III) Biochemical characterization of TbHep1, TbmtHsp70, HsHep1 and HSPA9

The aim of this study was to biochemically characterize the Hep1-mtHsp70 utilizing orthologues from the *T. brucei* parasite and humans. The ability of Hep1 to suppress the aggregation of mtHsp70 was assessed, furthermore determining the chaperone abilities of Hep1 on model substrate proteins. The holdase chaperone functions of mtHsp70 co-expressed with Hep1 were also assessed. This study also preliminarily investigated the ability of heat and oxidation stressed Hep1 to suppress the aggregation model substrate proteins. This study also assessed the basal and Hep1 modulated ATPase activity of mtHsp70. In this study, the Hep1 orthologues were also assessed against the heat-inducible cytosolic Hsp70 orthologues of *T. brucei* and humans.

CHAPTER TWO
The *in silico* analysis of the Hep1/mtHsp70 partnership of the *T. brucei* parasite and humans

2.1 Introduction

Hsp70 is central to the molecular chaperone network, playing a critical role in cellular protein maintenance. The Hsp70 molecular chaperone occurs in all the major sub-cellular compartments, including the endoplasmic reticulum (ER) and mitochondria (Craig, 2018). Hsp70 in the mitochondria (mtHsp70) is important for the organelle's protein complement, all the way from import to refolding in the matrix (Craig, 2018).

In mammalian cells mtHsp70 is also referred to as mortalin due to its knockdown having detrimental effects on cellular viability (Wadhwa et al., 1993; Kaul and Wadhwa, 2012). The protein was first identified in mouse fibroblasts and classified as an Hsp70 due to its high sequence homology with other Hsp70s (Wadhwa et al., 1993). Mice possess 2 isoforms of mortalin, MOT-1 and MOT-2, whose amino acid sequences only differs at 2 amino acid residues within the substrate binding domain (SBD) (Wadhwa *et al*., 1996). In terms of function, MOT-1 and MOT-2 are reported to be divergent. MOT-1 was found to be primarily localised in the cytosol, having no interaction with tumour suppressor protein p53, whilst MOT-2 was predominantly found in the perinuclear space interacting with p53. The interaction of MOT-2 with p53 resulted in the immortality of the cells, and therefore malignancy of the mouse fibroblasts (Wadhwa *et al*., 1998; Deocaris, 2006). In humans, there is only one copy of mortalin, and it shares greater similarity with MOT-2 in comparison to MOT-1. Human mortalin (HSPA9) also possesses the ability to interact with p53 in order to promote malignancy, by preventing the binding of p53 to the centrosome (Wadhwa *et al*., 2006; Ryu *et al*., 2014). Though predominantly localized in the mitochondria, HSPA9 is also found in other cellular compartments. HSPA9, when localised outside of the mitochondria, results in increased malignancy, and the protection of cancer cells from oxidative stress (Ryu *et al*., 2014). HSPA9 has been shown to cooperate with various co-chaperones and partner proteins, including the Hsp70 escort protein 1 (Hep1), in carrying out its functions (Goswami *et al*., 2010). In *T. brucei*, mtHsp70 (TbmtHsp70) and the other components of the protein import machinery, have been shown to play a role in the import of tRNA molecules from the cytosol, since the parasite lacks mitochondrial tRNA molecules (Tan *et al*., 2002; Tschopp *et al*., 2011). The *T. brucei* parasite possesses three identical genes of mtHsp70, all of them occurring on the same chromosome (Bentley *et al*., 2019).

The self-aggregation of mtHsp70s has been determined to be remedied by Hep1, a eukaryotic cys_4 zinc finger protein (Sichting *et al*., 2005). Besides the conserved cysteine residues at the zinc finger domain, a number of other highly conserved residues within the zinc finger domain have also been reported to

be indispensable for interactions with mtHsp70. These residues are arginine, histidine, and aspartic acid which have been determined to be essential for suppressing the aggregation of mtHsp70 as well as cell viability (Momose *et al*., 2007; Zhai *et al*., 2011; Vu *et al*., 2012). It has been uncovered that the mutations of these residues decreases the affinity of Hep1 for mtHsp70. Additionally, the mutation of the histidine results in Hep1 being incapable of stimulating the ATPase activity of mtHsp70 (Zhai et al., 2011). These residues have also been confirmed to be conserved across all the Hep1 orthologues that have been biochemically characterised, however PfHep1 was uncovered to be divergent in this regard, with lysine replacing the arginine (Nyakundi *et al*., 2018). The sequence of PfHep1, in a study by Nyakundi et al, (2016) was also found to share greater similarities with the *Chlamydomonas reinhardtii* Hep2 (CrHep2) homologue compared to its fellow Hep1 orthologues. PfHep1 is also much larger in terms of amino acid residue composition due to having asparagine repeats that constitute approximately one fourth of its amino acid complement, a property that is consistent with the proteome of *P. falciparum* (Singh *et al*., 2004; Nyakundi *et al*., 2016). In human Hep1 (HsHep1), tryptophan 115 within the zinc finger domain has been reported to be essential for oligomerization (Dores-Silva *et al*., 2013). Phosphorylation was determined to occur at five amino acid residues of HsHep1, three of them being in the mitochondrial targeting sequence (Havalová *et al*., 2021). The phosphorylation sites that occur within the sequence of HsHep1 protein, serine 51 and 171, have been reported in cancer cell lines. Mass spectrometry data revealed that the Ser 51 phosphorylation occurs in Jurkat T-lymphocytes, whilst the Ser 171 phosphorylation was identified in breast and lung cancer cell lines (Hornbeck *et al*., 2015; Tsai *et al*., 2015; NCI CPTAC *et al*., 2016).

HsHep1 is the most extensively studied, whilst yeast (ScHep1) and the parasitic orthologues of *P. falciparum* (PfHep1) and *L. braziliensis* (LbHep1) have also been characterized (Sichting et al., 2005; Dores-Silva et al., 2013; Dores-Silva et al., 2015; Nyakundi et al., 2016). An interesting observation amongst the characterised Hep1 orthologues is that they exhibit functional variation. HsHep1 possesses the unique ability to suppress the induced aggregation of model substrate proteins (Goswami *et al*., 2010; Dores-Silva *et al*., 2021). Furthermore, HsHep1 and LbHep1 have been demonstrated to stimulate the ATPase activities of their respective mtHsp70 partners, a property that ScHep1 lacks (Sichting *et al*., 2005; Goswami *et al*., 2010; Dores-Silva *et al*., 2017). Recent research in respect of HsHep1, has also reported emerging properties of Hep1. HsHep1 was determined to be potentially be able to bind the inner and outer mitochondrial membranes (Dores-Silva *et al*., 2021). In the study by Dores-Silva et al. (2021), HsHep1 was reported to be able to interact with the human stress-inducible Hsp70, HSPA1A, in a similar manner as with HSPA9.

In this regard, the aim of this study was to comparatively analyse the *T. brucei* and human Hep1/mtHsp70 machinery *in silico*. With the advent of the genomic sequencing of *T. brucei* and other kinetoplastid organisms, as well as the TriTrypDB project, *in silico* research into kinetoplastid genes

and their products is possible. Therefore, this study will uncover more information with regard to the putative TbHep1 (Berriman *et al*., 2005; Aslett *et al*., 2010).

Since only a handful of Hep1 orthologues have been characterised, this study was also expanded to include a range of other groups of Hep1 orthologues from organisms such as kinetoplastids, plants, mammals, *Plasmodium* and flies. This was due to Hep1 orthologues being known to be highly divergent in regions outside of the zinc finger domains. Using a bigger range of Hep1 orthologues could also shed more light on the properties of the Hep1 escort protein in general. The Hep1 orthologues were also compared to type I J-proteins and Hsp33 in order to gain more insights into the significance of the Hep1 zinc finger protein, more especially because some Hep1 orthologues possess the type I J-protein ability of stimulating Hsp70 ATPase hydrolysis and independently preventing the aggregation of substrate proteins (Goswami et al., 2010; Dores-Silva et al., 2015). Hsp33 was also included for comparative analysis with regard to the zinc finger motif of Hep1 in order to shed more light in terms of other potential cellular roles of the escort protein. Hsp33 also possesses substrate binding abilities (Jakob *et al*., 1999). Type I J-proteins and Hsp33 possess zinc finger domains which are essential for their interactions with substrate proteins (Graumann *et al*., 2001; Tang and Wang, 2001; Linke *et al*., 2003). The study also sought to structurally confirm HSPA9 and TbmtHsp70, *in silico*, since the research that has been conducted on them is mostly biochemical or biophysical. The significance of the mtHsp70s is that they are implicated in diseases whereby HSPA9 is at the forefront of oncogenesis and TbmtHsp70 aids in parasitic survival (Týč *et al*., 2015; Na *et al*., 2016). Since Hep1 is crucial for mtHsp70 function and structure, studying the escort protein is significant in that it could be a drug target to indirectly inhibit mtHsp70.

2.2 Specific objectives

- Analyse the primary structure of the *T. brucei* and human Hep1 orthologues by conducting multiple sequence alignments that include numerous Hep1 orthologues and homologues from other organisms. Also analyse the primary sequences of TbmtHsp70 and HSPA9 by means of multiples sequence alignments that include their cytosolic and ER *T. brucei* and human paralogues, as well as orthologues from other organisms.
- Comparatively analyse the zinc finger domain of TbHep1, HsHep1 and other Hep1 orthologues by conducting alignments that include other zinc finger molecular chaperones: type I J-proteins and Hsp33 orthologues from various organisms.
- Computationally predict the physio- and bio-chemical properties the *T. brucei* and human Hep1 orthologues and compare with their counterparts from other organisms. Also compute the physio- and bio-chemical properties of the Hsp70s being used in this study.
- Analyse the relationships of the Hep1 orthologues by conducting phylogenetic and distance analyses. Also conduct the phylogenetic and distance assessments of TbmtHsp70 and HSPA9

in relation to other Hsp70s including their cytosolic *T. brucei* and human paralogues, as well as orthologues from other organisms.

- Retrieve the predicted tertiary structures of *T. brucei* and human Hep1 from the EMBL-EBI Alpha Fold repository and analyse comparatively. Also retrieve the predicted tertiary structures of TbmtHsp70 and HSPA9 and analyse accordingly.

2.3 Approach and methodology

2.3.1 Database mining and sequence analyses

To retrieve the amino acid sequences of TbHep1 and the other Hep1 orthologues used in this study, LbrHep1, ScHep1 and HsHep1 were used as queries in BLASTP searches on TriTrypDB (version 61; https://tritrypdb.org/tritrypdb/app), PlasmoDB (version 61; https://plasmodb.org/plasmo/app), ToxoDB (version 61; https://toxodb.org/toxo/app), FlyBase (version FB2022_06; https://flybase.org/), Saccharomyces Genome Database (SGD, https://www.yeastgenome.org/) and NCBI (https://ncbi.nlm.nih.gov/) (Gajria *et al*., 2008; Aurrecoechea *et al*., 2009; Aslett *et al*., 2010; Engel *et al*., 2014; Gramates *et al*., 2022). From the BLASTP searches, sequences with an e-value of 1e-20 or less were selected. For the kinetoplastid, Hep1 orthologues, the orthology and synteny function on the VEuPathDB (https://veupathdb.org/veupathdb/app) databases was also applied in the sequence searches (Amos *et al*., 2022). Subsequent to retrieving the sequences from TritrypDB, PlasmoDB, ToxoDB, FlyBase and Saccharomyces Genome Database, reciprocal BLASTP searches were conducted on NCBI as an additional measure to confirm the sequences. The Hsp70, type I J-protein and Hsp33 sequences were retrieved from TritrypDB, PlasmoDB, ToxoDB, and NCBI using accession IDs listed in published research, as well as conducting BLASTP searches.

For primary sequences analyses, Clustal Omega multiple sequence alignments (MSA) were conducted on the JalView (version 2.11.2.5) web service and annotated by selecting the Clustal colour option (Waterhouse *et al*., 2009; Sievers and Higgins, 2014). Clustal Omega MSAs were also conducted on the EMBL-EBI (https://www.ebi.ac.uk/Tools/msa/clustalo/) web server and annotated manually.

2.3.2 Domain mapping, cellular localisation prediction, physical property prediction, posttranslational modification prediction and syntenic analysis

Physiochemical properties were predicted using the Expasy ProtParam (https://web.expasy.org/protparam/) tool in order to predict molecular weight, pI, extinction co-efficients, instability and aliphatic indices (Gasteiger *et al*., 2005). Conserved regions and domains were predicted using the simple modular architecture research tool (SMART, version 9; http://smart.embl-heidelberg.de/) and Prosite Expasy (https://prosite.expasy.org/) (Sigrist *et al*., 2013; Letunic *et al*., 2021). Cellular localisation was predicted by entering the amino acid sequences as queries on the NucPred (https://nucpred.bioinfo.se/cgi-bin/multi.cgi), SignalP (version 5.0; https://services.healthtech.dtu.dk/service.php?SignalP-6.0), WoLF PSORT (https://wolfpsort.hgc.jp/)

and MitoPROT (https://ihg.helmholtz-muenchen.de/ihg/mitoprot.html) web servers (Claros and Vincens, 1996; Brameier *et al*., 2007; Horton *et al*., 2007; Almagro Armenteros *et al*., 2019). To map the mitochondrial targeting sequence cleavage sites, MitoPROT and MitoFates (https://mitf.cbrc.pj.aist.go.jp/MitoFates/cgi-bin/top.cgi) were used. The posttranslational modifications were predicted using MusiteDeep (https://www.musite.net/) with the probability of modification set at the default of 0.5 (Wang *et al*., 2017, 2019, 2020). Phosphorylation, N-linked glycosylation, O-linked glycosylation, N6-acetylation and methylation posttranslational modifications were predicted. To highlight the predicted posttranslational modifications, the relevant sequences were first aligned on JalView (version 2.11.2.5) using the Clustal Omega tool on the web service and then annotated accordingly.

Syntenic analysis was conducted using the Hep1 sequences retrieved from the VEuPathDB, FlyBase and Saccharomyces Genome databases. The genes adjacent to the Hep1 gene were identified using the orthology and synteny function.

2.3.3 Phylogenetic analyses and determination of pairwise distances

The Maximum Likelihood (ML) phylogenetic trees were constructed in MEGA X (https://www.megasoftware.net/) to determine the relationships amongst orthologues (Kumar *et al*., 2018). In MEGA X, ClustalW multiple sequence alignments (MSA) were conducted using default parameters and exported as MEGA files (Larkin *et al*., 2007). The MEGA files were subsequently used to construct unrooted phylogenetic trees with test of phylogeny consisting of 1 000 bootstrap replicates. The Jones-Taylor-Thornton (JTT) amino acid substitution matrix model was applied with Gamma distribution G (Jones *et al*., 1992). The nearest-neighbour-interchange (NNI) was used as the ML heuristic method (Collienne and Gavryushkin, 2021). To gain numerical insights into the relationships of the proteins of interest, pairwise distances were also computed using the JTT amino acid substitution matrix model with Gamma distribution G.

2.3.4 Tertiary structure prediction

The tertiary structures of TbHep1, HsHep1, TbmtHsp70 and HSPA9 were retrieved from the AlphaFold/EMBL-EBI (https://alphafold.ebi.ac.uk/) platform and rendered using PyMol (version 1.7.4.5; https://pymol.org/2/) (Schrodinger and De Lano, 2020; Jumper *et al*., 2021; Varadi *et al*., 2022). Manual annotations were also conducted in order to highlight and emphasize the important features of the proteins of interest.

2.4 Results and discussion

2.4.1 Sequences analyses of the Hep1 orthologues

The TbHep1 and HsHep1 were analysed in comparison to PfHep1, LbrHep1 and ScHep1. For the purposes of this study TbHep1 refers to the Hep1 orthologues from *T. b. brucei* (TbbHep1), whilst TbgHep1 refers to the Hep1 orthologue from *T.b. gambiense*. TbgHep1, TevHep1 and TeqHep1share 99 % identity to each other. TbbHep1 also represents TeqHep1 as they are 100 % identical; ScHep1 and *S. pastorianus* Hep1 (SpasHep1) are also 100% identical. *S. pastorianus* is defined as being a "domesticated hybrid of *S. cerevisiae* and *S. eubayanus*" (Libkind *et al*., 2011) (Figure 2.1, Appendix A, Figure A1). The details regarding the Hep1 orthologues used in this study are provided in Appendix A, Table A1. The zinc finger domain of the putative TbHep1 orthologue is similar to the previously characterised HsHep1, PfHep1, ScHep1 and LbrHep1 orthologues (Figure 2.1) (Sichting et al., 2005; Dores-Silva et al., 2015; Nyakundi et al., 2016). A few amino acid residues are conserved across all the Hep1 orthologues, the cysteine residues that form part of the 2 CXXC motifs that are responsible for zinc ion binding are highly conserved. On the MSA, the cysteine residues occur at sites 238, 241, 263 and 266 as labelled at the top of the MSA (Figure 2.1). Relative to TbbHep1, TbgHep1 and TevHep1, the 100 % conserved cysteine residues occur at amino acid residues 119, 122, 144 and 147. Mutations of these cysteine residues has been shown to be detrimental for cellular viability (Yamamoto *et al*., 2005). The other 100% conserved residues were occurring at sites 237 (T), 251 (K), 253 (A), 254 (Y), 259 (V), 264 (P), 270 (H), 274 (D), 281 (D), 289 (E) and 296 (G) of the multiple sequence alignment (Figure 2.1). Relative to TbHep1, the residues are 118 (T), 132 (K), 134 (A), 135 (Y), 140 (V), 145 (V), 145 (P), 151 (H), 155 (D), 162 (D), 167 (E) and 174 (G). When comparing amongst Hep1 orthologues from a wider range of organisms, these residues are highly conserved (Appendix A, Figure A1).

Some of these residues have previously been determined to be highly conserved, with some determined to be indispensable for function. In yeast and human Hep1, the arginine and aspartic acid have been determined to be essential for the suppression of mtHsp70 aggregation (Momose *et al*., 2007; Zhai *et al*., 2011; Vu *et al*., 2012). The mutation of the histidine at residue number 107 in HsHep1 resulted in HsHep1 being unable to stimulate the ATPase activity of HSPA9. The highly conserved R residue at position 125 in the alignment is substituted for K in PfHep1, which has also been previously determined by Nyakundi et al. (2016 & 2018). When carrying out the sequence analysis with a wider range of Hep1 orthologues, including various plasmodial organisms, it can be observed that the R to K substitution is a characteristic of plasmodial Hep1 orthologues (Appendix A, Figure A1).

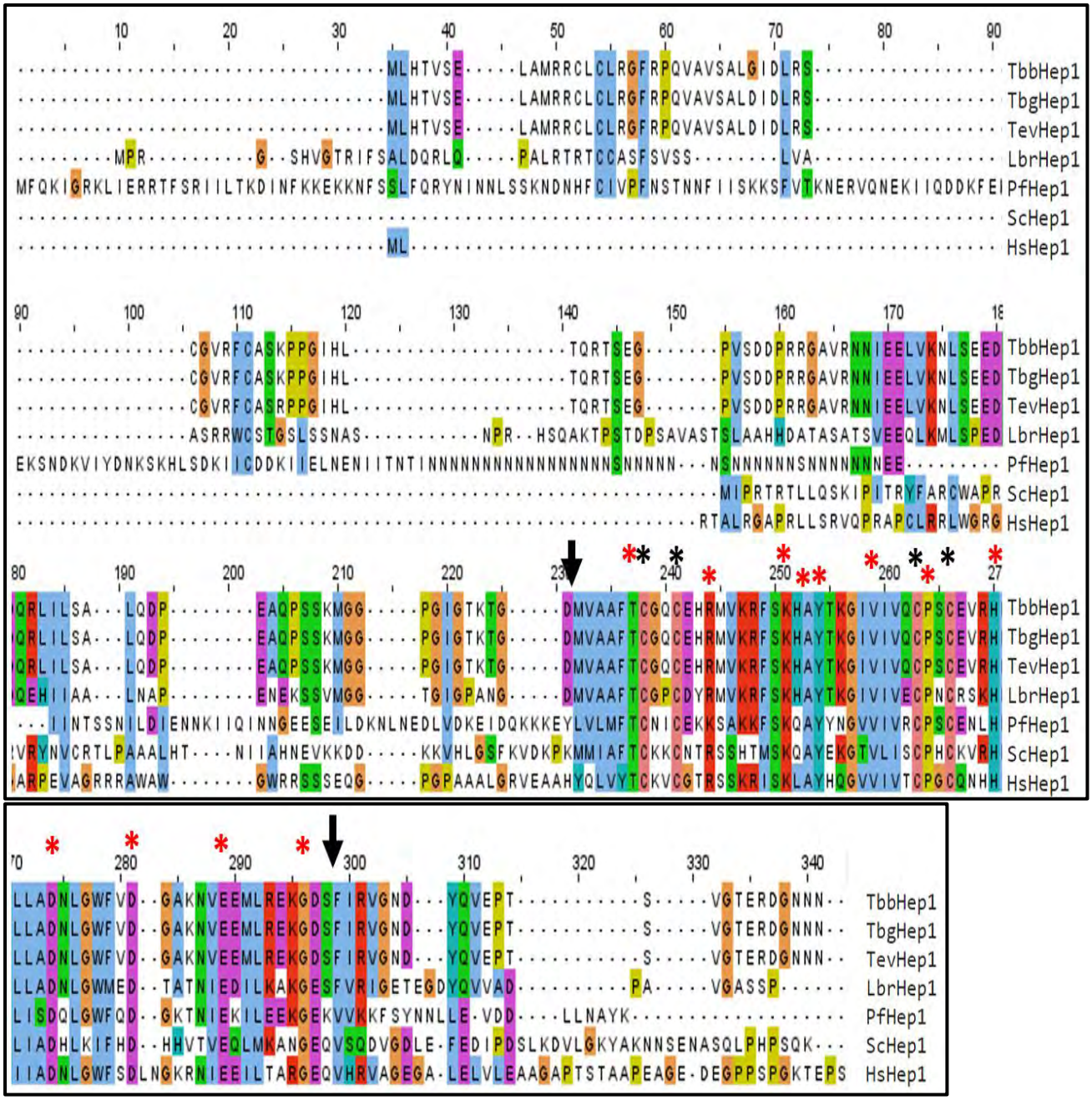

Figure 2.1. The Clustal Omega multiple sequence alignment (MSA) of the Hep1 orthologues and homologues. The sequences were aligned using the built in Clustal Omega MSA platform on the JalView web service. The annotation is based on the JalView Clustal colour option. The Hep1 sequences aligned were from: *T. b. gambiense* TbgHep1 (Tb972.3.2280), *T. b. brucei* TbbHep1 **(**Tb927.3.2300), *T. evansi* TevHep1 (TevSTIB805.3.2330), *L. braziliensis* LbrHep1 (LbrM.25.0680), *P. falciparum* PfHep1 (PF3D7_1420300), *Saccharomyces cerevisiae* ScHep1 (NP_014089.2) and HsHep1 (NP_001074318.1) The arrows demarcate the zinc finger domain. The black asterisks point to the cysteine residues of the CXXC motifs whilst the red asterisks point to the other conserved residues within the zinc finger motif.

The X residues of the upstream CXXC motifs in trypanosomes are GQ or GR, whereas in the *Leishmania* they are GP. With the exception of PfHep1, the plasmodial residues represented by the Xs in the upstream CXXC motif are KI (Appendix A, Figure A1). In PfHep1 the Xs represent NI. The *Saccharomyces* orthologues possess KK in place of the Xs, whilst the mammals possess KV. The Xs of the downstream CXXC motifs represent, PS and PN in *Trypanosoma* and *Leishmania*, respectively.

The mammalian orthologues possess PG, and in *Saccharomyces* they are PH. With CneoHep1 and CalbHep1 and the plasmodial orthologues the residues are PS. In this regard, PberHep1 varies by possessing a PQ motif (Appendix A, Figure A1). In *E. coli* thioredoxin which also possesses the CXXC motif, it was reported that substitutions in the residues represented by the X abrogates function (Chivers *et al*., 1997). The conservation of the X residues of the Hep1 orthologues according to closely related species implies that they are functionally relevant within those groups of organisms. The putative TbHep1 orthologue and HsHep1, in terms of their primary sequences displayed characteristics of canonical Hep1 orthologues, possessing zinc finger domains that are characteristic of Hep1 orthologues.

The identical TbbHep1 and TeqHep1 orthologues, at their zinc finger domains, share a 100 % sequence identity with TbgHep1 and TevHep1. TbgHep1 only differs from TbbHep1 and TeqHep1 by one residue at the N-terminal region, whereas TevHep1 differs by two amino acid residues. These variations can be observed at site 68 and 114 on the MSA (Figure 2.1 & Appendix A, Figure A1). Relative to TbbHep1, these variations occur at amino acid residues 29 and 43. The similarity of the Hep1 orthologues of TbbHep1, TbgHep1, TeqHep1 and TevHep1 are not unexpected as they are all subspecies of *T. brucei*.

No other amino acids were 100% conserved across all species examined in the regions outside of the zinc finger domains (Figure 2.1). In this study, it is revealed that the N- and C-terminal regions of Hep1 orthologues originating from closely related organisms share sequence similarities (Appendix A, Figure A2). These similarities are in the form of signature sequences or motifs which are unique to those groups of organisms and are specifically unique to Hep1 orthologues. Using the signature sequences as queries in BLASTP searches only returned Hep1 orthologues from the organisms of very close relations. TbbHep1, TbgHep1, TeqHep1 and TevHep1 only share similarities with Hep1 orthologues from *Trypanosoma Congolese*, *Trypanosoma cruzi* and *Trypanosoma vivax* at the C-terminal region. Amongst the trypanosomal Hep1 orthologues, there were no shared similarities at the N-terminal region.

Apart from the trypanosomal Hep1 orthologues, the *Leishmania* Hep1 orthologues LbrHep1, LmjHep1, LdoHep1 and LmxHep1 exhibited high sequence similarity at the N-terminal region. The LdoHep1, LmjHep1 and LmxHep1 orthologues, possessed a shared C-terminal extension which LbrHep1 lacks. (Appendix A, Figure A2). HsHep1 also shares great similarities with Hep1 orthologues from other mammalian organisms, *Mus musculus* Hep1 (MsmHep1-iso1) and *Bos taurus* Hep1 (BtauHep1) at the N-terminal region, seemingly sharing greater similarity with MsmHep1-iso1 (Appendix A, Figure A2). At the C-terminal region, the mammalian orthologues share two separate moieties of high similarity. With regard to *Mus musculus*, it was also discovered that there are 3 isoforms of Hep1, with only isoform 1 (MsmHep1-iso1) possessing the zinc finger domain. Through performing BLASTP searches, it was further revealed that various other mammalian organisms, murine and primate, possess multiple

Hep1 isoforms (Appendix A, Tables A3 & A4). Due to the mammalian Hep1 orthologues possessing great similarities when compared to HsHep1, they are discussed in more detail later in this study.

2.4.2 Phylogenetic and distance analyses of the Hep1 orthologues

The relationships amongst the TbbHep1, TbgHep1, TevHep1, LbrHep1, PfHep1, ScHep1 and HsHep1 were also analysed alongside many other various Hep1 orthologues. Details regarding the Hep1 orthologues are provided in Appendix A, Table A1. Generally, the Hep1 orthologues that were closely related originate from closely related organisms (Figure 2.2). When analysed according to the full-length sequences, the kinetoplastid Hep1 orthologues were demonstrated to be closely related, however the trypanosomal orthologues occupied a different clade in relation to the *Leishmania* orthologues (Figure 2.2A). *Crithidia fasciculata* Hep1 (CfHep1) fell into the *Leishmania* clade, whilst BsalHep1 was observed to be closer to the trypanosomal orthologues. TbbHep1, TbgHep1, TeqHep1 and TevHep1 were in the same clade whilst TcoHep1, TcrHep1 and TviHep1 occupied a separate clade. TviHep1 and TcrHep1 are more closely related to each other than they are to TcoHep1 (Figure 2.2A).

HsHep1 fell into the same clade as the other mammalian orthologues, being more closely related to *Mus musculus* Hep1 isoform 1 (MsmHep1-iso1) as also suggested in section 2.4.1. The *Drosophila* Hep1 orthologues, *D. melanogaster* Hep1 (DmelHep1) and *D. simulans* Hep1 (DsimHep1), fell into a clade that suggested close relations with the mammalian Hep1 orthologues. This observation could be due to mammals and flies falling under the Kingdom Animalia. The other fly Hep1 orthologue from *Musca domestica* (MdomHep1), albeit in a different clade to the *Drosophila* Hep1 orthologues, is also closely related to the mammalian Hep1 orthologues (Figure 2.2A). The other isoforms of *Mus musculus* Hep1, MsmHep1-iso2 (isoform 2) and MsmHep1-iso3 (isoform 3), were also closely related to HsHep1, MsmHep1 iso-1 and BtauHep1. The MsmHep1-iso2 (isoform 2) and MsmHep1-iso3 (isoform 3) are discussed in detail later in this study together with other Hep1 isoforms of murine and primate organisms. The plasmodial orthologues also fell into the same clade, with TgoHep1 being closely related to them. This could be due to *Plasmodium* and *Toxoplasma* being apicomplexan organisms. The *Saccharomyces* Hep1 orthologues, ScHep1, SpasHep1 and SparHep1 proved to be closely related to the plant Hep1 homologues, AtZR3, AtHep1 and CrHep2. Some unexpected relations were also observed whereby *Cryptococcus neoformans* Hep1 (CneoHep1) proved to be closely related to the mammalian and fly orthologues whilst *Candida albicans* Hep1 (CalbHep1) is closely related to PfHep1. This is unexpected because *C. neoformans* and *C. albicans* are also yeast organisms. LmxHep1 was in an isolated clade, whereby CfHep1 which is from a different genus fell into the same clade as the other *Leishmania* orthologues (Figure 2.2A).

When analysing the relationships of the Hep1 orthologues with respect to the N-terminal regions, the trypanosomal orthologues fell into the same clade and were arranged in the same way as when analysed

according to the full-length sequences (Figure 2.2B). The *Saccharomyces* orthologues occupied a sub-clade that was adjacent to the sub-clade of the mammalian orthologues. The *Leishmania* orthologues fell into the same clade, which included CfHep1 and BsalHep1. The plasmodial orthologues, PfHep1, PmalHep1 and PberHep1 fell into the same sub-clade, which was adjacent to the clade occupied by AtHep1, AtZR3 and CneoHep1. PviHep1 fell into a separate clade together with MdomHep1, whilst TgoHep1 and CalbHep1 were in the same clade as the *Drosophila* orthologues (Figure 2.2B).

The phylogenetic analyses were also carried out with respect to the sequences of the zinc finger domains. The trypanosomal orthologues were arranged as they were when analysed according to their full-length and N-terminal sequences (Figure 2.2 A & B). The *Leishmania* orthologues fell into the same clade, which was also occupied by BsalHep1 and CfHep1. LdoHep1 and LmxHep1 proved to be very closely related according to their zinc finger domains, with LmjHep1 being adjacent to them. LbrHep1 was more closely related to CfHep1 and BsalHep1. Interestingly, the CneoHep1 and CalbHep1 yeast orthologues occupied the same clade as the *Saccharomyces* orthologues whilst MdomHep1 also fell into the same clade as the *Drosophila* orthologues. The sub-clade occupied by the fly Hep1 orthologues was in the same clade as the sub-clade occupied by the mammalian orthologues (Figure 2.2C).

The findings of the phylogenetic analyses demonstrate that both the divergent N-terminal region and the conserved zinc finger domain possess primary sequence properties that are unique to specific groups of organisms. This is despite the zinc finger domain being highly conserved across Hep1 orthologues of eukaryotic organisms. For the N-terminal regions, signature sequences were identified, as displayed in Appendix A, Figure A2, which were specific to orthologues of closely related organisms. The residues between the cysteines in the CXXC motifs in the zinc finger domains were observed to be conserved in closely related species (Appendix A, Figure A1). The zinc finger domain of Hep1 is also commonly referred to as the zf-DNL because of a DNL motif that is conserved amongst certain Hep1 orthologues (Nyakundi *et al*., 2016, 2018). For HsHep1 and the kinetoplastid Hep1 orthologues, this motif is DNL, whilst in PfHep1 and ScHep1 respectively, it is DQL and DHL (Figure 2.1). The observation made in this regard is that this motif is divergent, whereby it is only identical amongst Hep1 orthologues from closely related organisms (Appendix A, Figure A2).

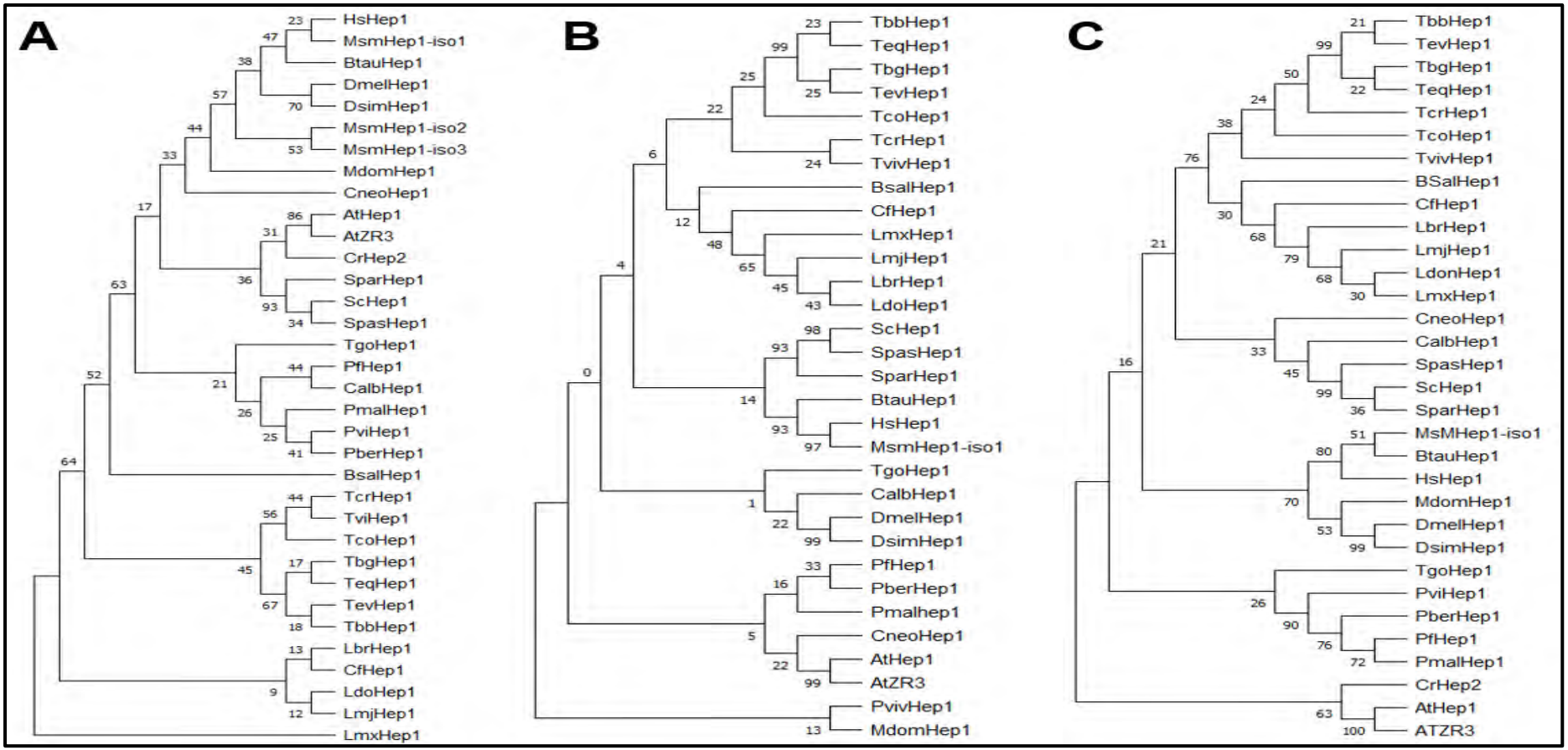

Figure 2.2. Phylogenetic analyses of the A) full-length, B) N-terminal region and C) zinc-finger domain of the Hep1 orthologues. The maximum-likelihood tree was constructed using MEGAX with the Jones-Taylor (JTT) amino acid substitution matrix-model, Gamma distribution (G) from the built in ClustalW platform. The bootstrap analysis consisted of 100 replicates. The Hep1 sequences used were from: TbgHep1 (Tb972.3.2280), TbbHep1 (Tb927.3.2300), TeqHep1 (TEOVI_000221600), TevHep1 (TevSTIB805.3.2330), TcrHep1 (TcCLB.508479.274), TviHep1 (TvY486_0301660), TcoHep1 (TcIL3000_0_42310), LbrHep1 (LbrM.25.0680), LdoHep1 (LdBPK_250830.1), LmjHep1 (LmjF.25.0800), LmxHep1 (LmxM.25.0800), BsalHep1 (BSAL_79370), CfHep1 (CFAC1_220016500), PfHep1 (PF3D7_1420300), PmalHep1 (PmUG01_13038600), PviHep1 (PVP01_1328600), PberHep1 (PBANKA_1022900), TgoHep1 (TGME49_260340), AtHep1 (NP_974434.2), ScHep1 (NP_014089.2), SpasHep1 (QID81845.1), SparHep1 (XP_033768657.1), CneoHep1 (XP_024514386.1), CalbHep1 (KHC45981.1), HsHep1 (NP_001074318.1), MsmHep1-iso1 (NP_081104.1), BtauHep1 (XP_003586730.1), DmelHep1 (AAS15675.1), DsimHep1 (XP_016039443.1), MdomHep1 (XP_00518472.3), CrHep2 C-term (XP_001700157.1) and ATZR3 (AAO64784.1).

Distances matrices were also constructed to numerically analyse the relationship amongst the various Hep1 orthologues. The distance matrices give numerical insights into the relationships amongst the Hep1 orthologues, whereby an orthologue's relationship towards itself is zero. According to the full-length sequences, TbbHep1, TbgHep1, TeqHep1 and TevHep1 are identical, having very minimal sequence variation compared to TcrHep1, TcoHep1 and TviHep1 (Appendix A, Figure A3). This was also the case for all the other orthologues originating from the other groups of organisms. When analysing the distances according to the N-terminal regions in the absence of the zinc finger domain, there was a remarkable increase in variation (Appendix A, Figure A4). When the same analyses were carried out using the zinc finger domain sequences, the variation was considerably decreased (Appendix A, Figure A5). In Figure 2.2 B & C, the N-terminal region and the zinc finger domain were shown to specify the relationships of the Hep1 orthologues according to organism of origin. The distance analysis however demonstrated the N-terminal region to be the primary driver of diversity of Hep1 orthologues, due to being non-conserved, whereas the zinc finger region is more of a unifying factor. However, there are distinguishing factors in the zinc finger domains as they still resulted in the orthologues being segregated according to the types of organisms they originate from (Figure 2.2C & Appendix A, Figures A1 & A2).

2.4.3 Computational characterisation of the Hep1 orthologues

The Expasy ProtParam tool web server was used to compute various parameters of the Hep1 orthologues. There is variation in terms of the sizes of the proteins, both in terms of the lengths of the amino acid sequences, and the molecular weights (Appendix A, Table A6). The pI values also varied greatly. The computed extinction co-efficients also varied amongst the orthologues. The extinction co-efficients were also computed according to whether the cysteine residues were oxidised (forming disulphide bonds, cystines) or they were reduced. The potential formation of the disulphide bonds between cysteine residues is shown to cause an increase in extinction co-efficients. The instability and aliphatic indices were also computed. According to the Expasy ProtParam documentation, the value of 40 in the instability indices is a benchmark, whereby an instability index above 40 indicates instability, and values below indicate stability (Gasteiger *et al*., 2005). Most of the Hep1 orthologues, including TbbHep1 and its orthologues, were predicted to be unstable. The only stable orthologues were from *Saccharomyces* and the flies. PfHep1 and PberHep1 were also determined to be stable (Appendix A, Table A6). The aliphatic indices indicate the volume, in proportion, occupied by the aliphatic (non-polar/hydrophobic amino acids) side chains of the proteins. A high aliphatic index indicates stability over an increased range of temperatures. GRAVY scores less than zero, indicate potential hydrophilicity whilst GRAVY scores above zero indicate hydrophobicity (Gasteiger *et al*., 2005). All the orthologues had a GRAVY score less than zero. The aliphatic indices were in the 70-80 range for most of the orthologues. The fly orthologues, PfHep1 and CalbHep1 had increased aliphatic indices whilst PviHep1

had a lower aliphatic index, whilst LbrHep1 and PviHep1 had decreased aliphatic indices (Appendix A, Table A6). The high aliphatic index of PfHep1 could also have been a contributing factor to its insolubility as reported by Nyakundi et al. (2016), besides the presence of the plasmodial asparagine repeats. TbbHep1 and TeqHep1, which are 100 % identical, had a different pI from TbgHep1 and TevHep1 which differ from them by 1 and 2 amino acid substitutions, respectively. All the Hep1 orthologues were predicted to localise in the mitochondria, whilst the CrHep2 and AtZR3 homologues were predicted to reside in the chloroplasts.

The properties of the N-terminal regions and the zinc finger domains were also computed separately. The sizes of the zinc finger regions were determined to be very similar, with molecular weights in the region of about 7 000 Da, constituted of 63-64 amino acid residues (Appendix A, Table A7). This is despite the full-length orthologues having been determined to be highly divergent in this regard. The N-terminal regions exhibited vast differences in the number of amino acid residues and in their molecular weights (Appendix A, Table A7), pointing to this moiety of the Hep1 orthologues being the primary driver of divergence in terms of the characteristics of the Hep1 orthologues.

2.4.4 Computational prediction of the Hep1 posttranslational modifications

The posttranslational modifications were predicted using the MusiteDeep web server and highlighted on the Hep1 orthologues after they were aligned by Clustal Omega on the JalView web server (Appendix A, Figure A6). The predominant posttranslational modifications were phosphorylation and glycosylation. Most posttranslational modifications occurred at the non-conserved N- and C-terminal regions (Appendix A, Figure A6). Many of the posttranslational modifications predicted to be outside of the zinc finger domain were conserved according to the species from which the orthologues originate. TbbHep1 has previously been reported to be phosphorylated, at threonine 4 and serine 6, and methylated at arginine 196 (Fisk *et al*., 2013; Urbaniak *et al*., 2013). None of these posttranslational modifications were predicted in this study. The stringency level was set at a probability of 0.5, reducing it could have probably also revealed the posttranslational modifications. The mammalian orthologues had minimal posttranslational modifications. The phosphorylation of serines 51 and 171 was reported to occur in cancer cell lines (Hornbeck *et al*., 2015; Tsai *et al*., 2015; NCI CPTAC *et al*., 2016). In this study, these posttranslational modifications were predicted (Appendix A, Figure A6). Phosphorylated residues were also identified by Havalova et al. (2021) at the MTS of HsHep1 serines 14 and 49, which were also predicted in this study (Appendix A, Figure A6).

Some amino acid residues were shown to be subject to either both phosphorylation and glycosylation or both methylation and acetylation. A limited number of acetylated and methylated amino acid residues were predicted. Although the residues at the zinc finger domain are highly conserved, only the acetylation of lysine at site 281 was shown to have some conservation (Appendix A, Figure A6). An

interesting observation is the prevalence of posttranslational modifications outside of the conserved zinc finger regions, some of which are conserved between some groups of Hep1 orthologues. Posttranslational modifications in eukaryote proteins are of relevance as they may dictate whether a protein is functionally activated or not in some respects. This points to the non-conserved N- and C-terminal regions of Hep1 orthologues as being functionally important. As observed in Appendix A, Figure A1, certain groups of Hep1 orthologues possess conserved sequences at the N- and C-terminal regions, suggesting that they could be of evolutionary importance within the organisms in which they occur.

2.4.5 Syntenic analyses of the Hep1 gene across various species of organisms

Syntenic analyses were carried out in order to predict orthology amongst selected Hep1 orthologues. Synteny of the Hep1 genes is conserved amongst closely related organisms. TbbHep1 and TcrHep1 displayed conservation in the arrangement of genes that are adjacent to the Hep1 gene (Figure 2.3). The only difference was that in *T. cruzi* there is an insertion of the MBAP2 gene between the CSPs2 and KKP genes. The synteny of the trypanosomal Hep1 genes was also shared by the BsalHep1 gene, whereby the MBAP2 gene was also inserted between the CSPs2 and KKP genes (Figure 2.3). The synteny between the LbrHep1 and LmjHep1 genes was also conserved. The LbrHep1 and LmjHep1 genes shared synteny with the CfHep1 gene. However, the CfHep1 gene had 3 isoforms of the gene denoted as Ukp2 (abbreviation for unknown/hypothetical protein 2) (Figure 2.3). The synteny amongst the plasmodial Hep1 genes also proved to be conserved. The TgoHep1, DmelHep1 and ScHep1 genes each displayed unique synteny when compared to the kinetoplastid orthologues (Figure 2.3).

The syntenic arrangement amongst the kinteoplastid Hep1 genes is not unexpected. The phylogenetic analysis revealed that the trypanosomal and *Leishmania* Hep1 orthologues occupied separate clades (Figure 2.2). CfHep1 and BsalHep1 also shared a clade with the *Leishmania* orthologues, despite the synteny of the BsalHep1 gene being shared with the trypanosomal orthologues. A closer look at the phylogenetic trees in Figure 2.2 does, however, reveal that BsalHep1 is the most distant relative within the *Leishmania* Hep1 clade, and closer to the trypanosomal Hep1 clade. Another observation that was made in terms of the genes adjacent to Hep1 amongst the kinetoplastids is that some of the genes whose accession numbers are listed in Appendix A, Figure A7, possess cysteine rich motifs such as CXXC, CXC and CXXXC. The CXXC motifs are also contained by Hep1. This suggests that the expression of these genes is under the control of one element, whereby they could be induced under identical cellular conditions whereby the cysteine rich motifs are essential.

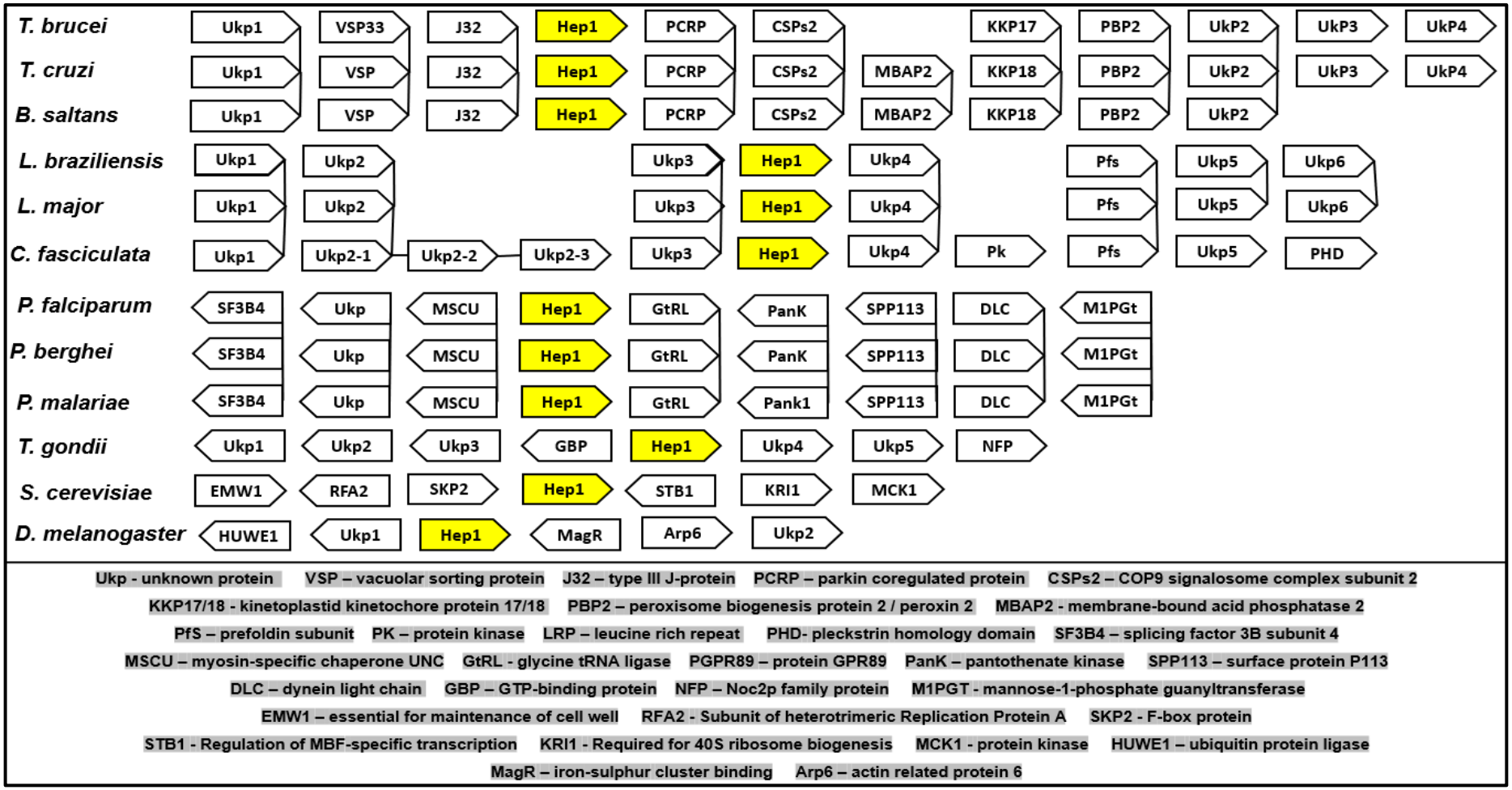

Figure 2.3. The syntenic analysis of selected Hep1 orthologue genes. The Hep1 orthologues used for this assessment were: TbbHep1 **(**Tb927.3.2300), TcrHep1 (TcCLB.508479.274), LbrHep1 (LbrM.25.0680), LmjHep1 (LmjF.25.0800), BsalHep1 (BSAL_79370), CfHep1 (CFAC1_220016500), PfHep1 (PF3D7_1420300), PmalHep1 (PmUG01_13038600), PberHep1 (PBANKA_1022900), TgoHep1 (TGME49_260340), ScHep1/Zim17/YNL310C (SGD accession ID: S000005254) and DmelHep1 (FlyBase accession ID: FBpp0271786). The gene arrangement is schematically presented displaying genes that are adjacent to Hep1 with directionality also taken into consideration. The lines joining the boxes representing the various genes across species indicate orthology. The bottom panel is a key that provides the full names for the genes presented in shorthand in the figure. The database accession numbers of the genes adjacent to Hep1 are provided in Appendix A, Figure A7.

Some Hep1 orthologues have been determined to possess type I and type II J-protein characteristics of stimulating the ATPase activity of Hsp70 and binding to substrate protein. Besides having a zinc finger domain, in this study, the TbHep1, TcrHep1 and BsalHep1 genes were found to be adjacent to the J32 gene. However, J32 is a type III J-protein without a zinc finger domain, but does possess a single CXXC motif, much like the other proteins encoded by genes adjacent to the Hep1 genes. To be noted is that the J32 gene in *L. braziliensis* and *L. major* is also in the same chromosome as the Hep1 gene, but they are quite a distance apart.

2.4.6 Analysis of the structural models of TbHep1 and HsHep1

The zinc finger domain of ScHep1(PDB ID: 2e2z) has been experimentally resolved by nuclear magnetic resonance (Momose *et al*., 2007). The report by Momose et al. (2007) revealed that the ScHep1 zinc finger domain consists of 4 anti-parallel β-sheets with two CXXC motifs occurring at the loops. The cysteine residues of the CXXC motifs were reported to be bound to a single zinc ion. The TbHep1 model analysed in this study also possesses the 4 antiparallel β-sheets which are shown in yellow (Figure 2.4A). The N-terminal region ends immediately upstream of the anti-parallel β-sheets. The N-terminal region is constituted of an unstructured stretch and 2 α-helices. A signature sequence that is shared by the kinetoplastid Hep1 orthologues at their N-termini is also highlighted in teal (Figure 2.4B). It begins near the beginning of the second α-helix of the N-terminal region and ends at the very beginning of the first β-sheet of the zinc finger domain (Figure 2.4B). The C-terminal region begins after the α-helix that is at the C-terminal border of the zinc finger domain. At the C-terminal region, the signature sequence begins where the α-helix at the C-terminal border of the zinc finger region ends, and it ends at C-terminal end of the protein (Figure 2.4C).

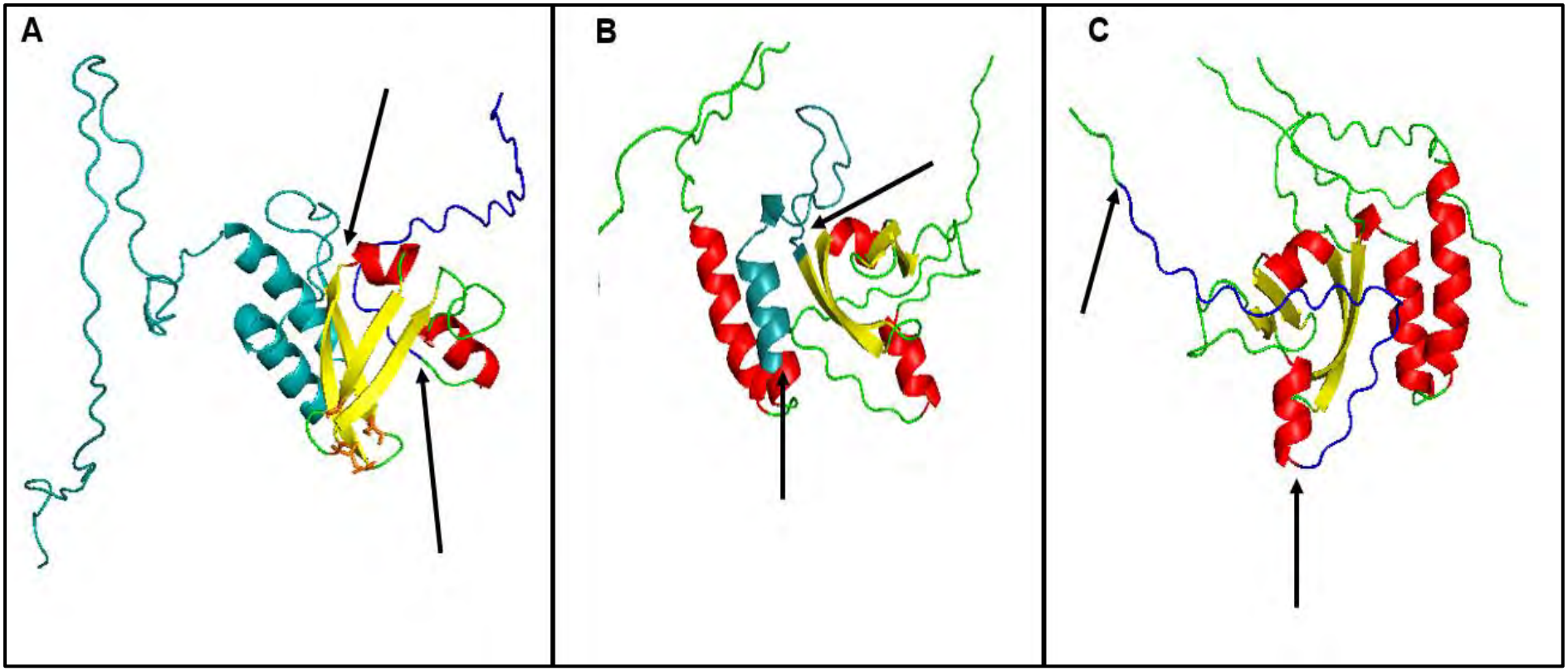

Figure 2.4. AlphaFold2 predicted 3D structure of TbHep1. The 3D structure was rendered in PyMol and manually annotated. **A)** The full perspective of the predicted 3D structure. In teal is the N-terminal, whilst the zf-DNL is represented by the yellow β-sheets, red α-helices and green loop regions. In blue is the region downstream of the zf-DNL. The arrows indicate the beginning and the end of the zf-DNL on the structure. The cysteine residues within the CXXC motifs of the zf-DNL are displayed as orange sticks. **B)** The 3D structure with emphasis on the signature moiety (QRLILSALQDPEAQPSSKMGGPGIGTKTGD) of the N-terminal region. The signature moiety is shown in teal, with the arrows demarcating its beginning and end. **C)** The 3D structure with emphasis on the signature moiety (FIRVGNDYQVEPTSVGTERD) of the region downstream of the zf-DNL. The arrows indicate the beginning and end of the C-terminal signature moiety which is shown in blue.

HsHep1 exhibited structural similarities when compared to TbHep1. HsHep1 also has a long unstructured N-terminal region (Figure 2.5A). However, the N-terminal region of HsHep1 does not possess the α-helices that are observed in TbHep1 (Figure 2.4 A & B). Instead, the long unstructured region of the N-terminal region in HsHep1 leads straight into the first β-sheet of the zinc finger region (Figure 2.5A). The zinc finger region also consists of 4 antiparallel β-sheets with the cysteine residues of the CXXC motif occurring at the loops. The C-terminal region occurs shortly after the end of the α-helix that is at the C-terminal border of the zinc finger domain (Figure 2.5B). The entire N-terminal region of HsHep1 shares high similarity with the other mammalian Hep1 orthologues used in this study but was very different from all the other Hep1 orthologues (Appendix A, Figure A2). It was therefore deemed not to be necessary to highlight the N-terminal signature sequence in the structure, but to show the two signature sequences that occur at the C-terminal region. The C-terminal signature sequences of HsHep1 are shared with BtauHep1 and MsmHep1-iso1 (Figure 2.5B).

The structural differences outside of the zinc finger domains between TbHep1 and HsHep1 point to a possible functional divergence between the two proteins. The N-terminal region in this study was shown to be the primary determinant of diversity of the Hep1 orthologues. The pairwise distances of the Hep1 orthologues were shown to be markedly higher when they were compared according to their N-terminal regions (Appendix A, Figure A4). TbHep1 structure displayed two α-helices and an unstructured stretch, whereas the entire N-terminal region of HsHep1 was unstructured (Figures 2.4 & 2.5).

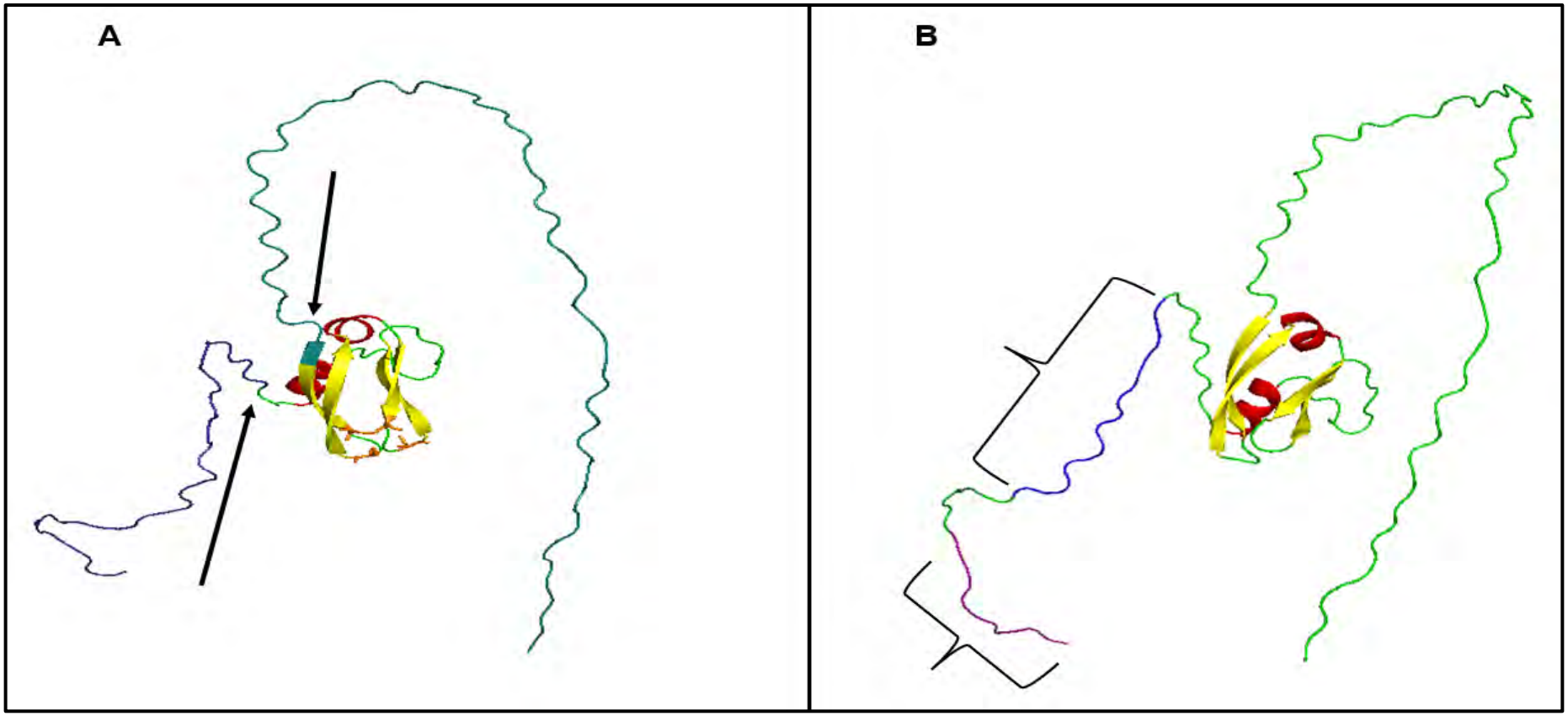

Figure 2.5. AlphaFold2 predicted 3D structure of HsHep1. The 3D structure was rendered in PyMol and manually annotated. **A)** The full perspective of the predicted 3D structure. In teal is the N-terminal, whilst the zf-DNL is represented by the yellow β-sheets, red α-helices and green loop regions. In blue is the region downstream of the zf-DNL. The arrows indicate the beginning and the end of the zf-DNL on the structure. The cysteine residues within the CXXC motifs of the zf-DNL are displayed as orange sticks. **B)** The 3D structure with emphasis on the signature moieties of the region downstream of the zf-DNL at the C-terminal region. In blue is the GALELVLEEAGAPTST signature sequence and in purple is the DEGPPSPGKTEPS sequence. The curly braces serve to highlight the respective signature sequences at the C-terminal region.

2.4.7 Phylogenetic and structural comparison between the Hep1 orthologues and type I J-proteins and Hsp33.

The rationale for comparing the Hep1 orthologues to type I J-proteins and Hsp33 is 2-fold. Firstly, type I J-proteins and Hsp33 also possess zinc coordinating cysteine rich motifs which have been determined to be essential for substrate protein binding (Banecki *et al*., 1996; Jakob *et al*., 1999; Martinez-Yamout *et al*., 2000). Secondly, in this study in section 2.4.5, the genes encoding Hep1 in kinetoplastids were shown to be in close proximity to genes encoding proteins possessing similar cysteine rich motifs such as CXC, CXXC and CXXXC. These genes were also determined to be unique to the kinetoplastids. Therefore, it was important to compare the Hep1 orthologues to the other members of the molecular chaperone family that possess cysteine rich motifs. Details regarding the type I J-proteins and Hsp33 orthologues employed in this analysis are provided in Appendix A, Table A2. The phylogenetic analysis shows that the Hep1 orthologues form a separate clade from the type I J-proteins and Hsp33 orthologues. TbHep1 and the rest of the kinetoplastid Hep1 orthologues were the most distantly related to the J-proteins and Hsp33 orthologues (Figure 2.6). From this analysis, it was difficult to reach a conclusion with regard to making inferences about the function of Hep1 with regard to what is known about type I J-proteins and Hsp33.

Clustal Omega MSA analyses were also conducted to determine if zinc finger domains of the Hep1 orthologues resemble those of the type I J-proteins and/or Hsp33 orthologues. When aligned with selected type I J-proteins, the cysteine residues of the CXXC motifs of the Hep1 orthologues aligned with the cysteine residues of the first and third CXXC motifs of the J-proteins (Appendix A, Figure A8). This is a finding that has previously been reported (Burri *et al*., 2004). The glycine residue at site 397 of the MSA was also conserved between the Hep1 orthologues and the type I J-proteins (Appendix A, Figure A8). Relative to TbHep1, this highly conserved glycine residue occurs at amino acid residue 174 (Appendix A. Figure A2). The MSA of the Hep1 orthologues with the Hsp33 orthologues shows that the downstream CXXC motif of Hep1 has the cysteine residues aligns to those of Hsp33 at the CXXC motif as well. The first cysteine residue of the upstream CXXC motif of Hep1 aligns with the first cysteine residue of the CXC motif of Hsp33 (Appendix A, Figure A9).

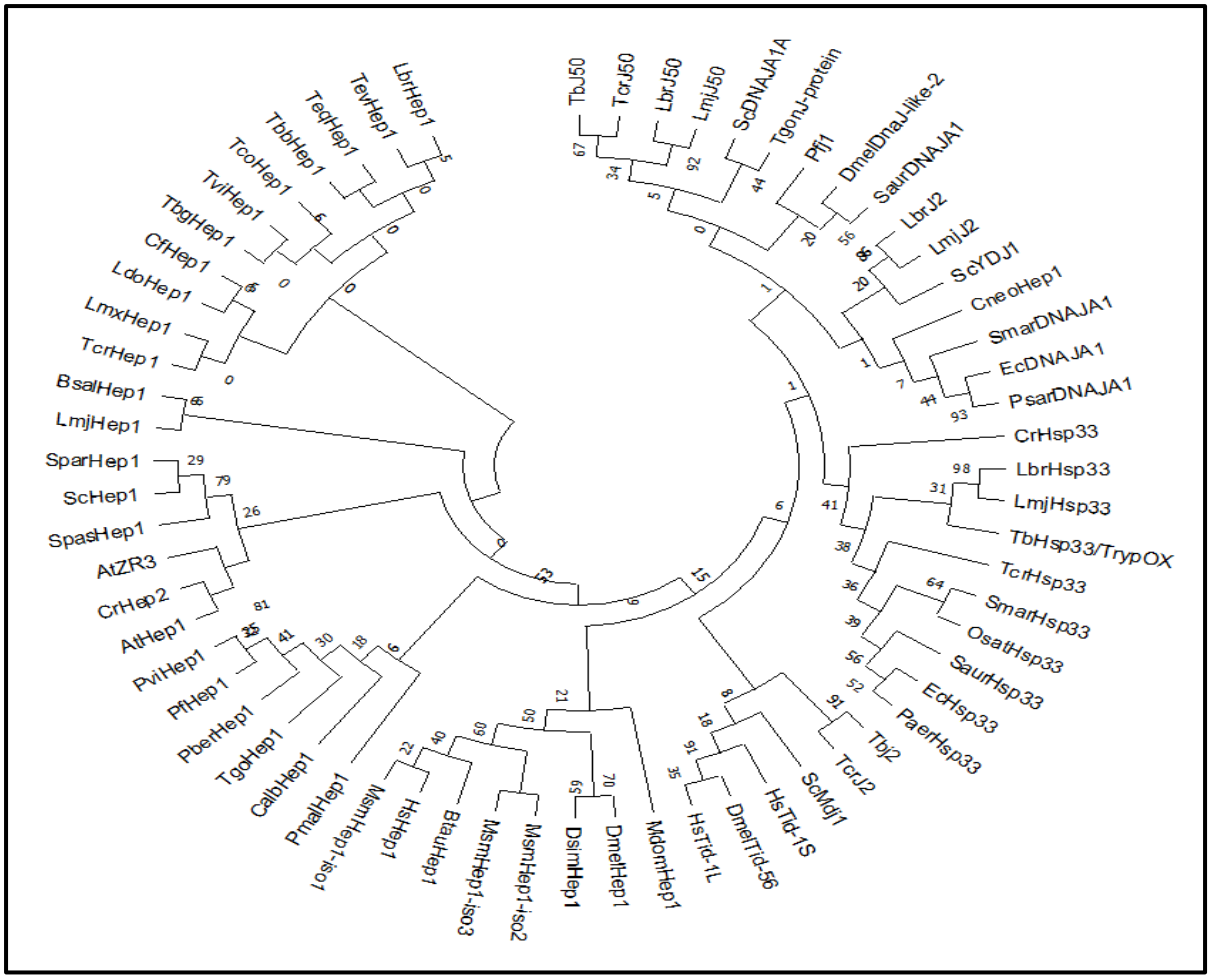

Figure 2.6. Phylogenetic analysis of the Hep1 orthologues in relation to other zinc finger proteins of the molecular chaperone family. The maximum-likelihood tree was constructed using MEGAX with the Jones-Taylor (JTT) amino acid substitution matrix-model, Gamma distribution (G) from the built in ClustalW platform. A bootstrap analysis consisting of 1000 replicates applied. The Hep1 sequences used for this assessment were from: TbgHep1 (Tb972.3.2280), TbbHep1 **(**Tb927.3.2300), TeqHep1 (TEOVI_000221600), TevHep1 (TevSTIB805.3.2330), TcrHep1 (TcCLB.508479.274), TviHep1 (TvY486_0301660), TcoHep1 (TcIL3000_0_42310), LbrHep1 (LbrM.25.0680), LdoHep1 (LdBPK_250830.1), LmjHep1 (LmjF.25.0800), LmxHep1 (LmxM.25.0800), BsalHep1 (BSAL_79370), CfHep1 (CFAC1_220016500), PfHep1 (PF3D7_1420300), PmalHep1 (PmUG01_13038600), PviHep1 (PVP01_1328600), PberHep1 (PBANKA_1022900), TgoHep1 (TGME49_260340), AtHep1 (NP_974434.2), ScHep1 (NP_014089.2), SpasHep1 (QID81845.1), SparHep1 (XP_033768657.1), CneoHep1 (XP_024514386.1), CalbHep1 (KHC45981.1), HsHep1 (NP_001074318.1), MsmHep1-iso1 (NP_081104.1), MsmHep1-iso2 (NP_001132975.1), MsmHep1-iso3 (NP_001132976.1), BtauHep1 (XP_003586730.1), DmelHep1 (AAS15675.1), DsimHep1 (XP_016039443.1), MdomHep1 (XP_00518472.3), CrHep2 C-term (XP_001700157.1) and ATZR3 (AAO64784.1). The cytosolic and mitochondrial and prokaryotic type I J-protein sequences used for this assessment were from: Tbj2 (Tb927.2.5160), Tcrj2 (TcCLB.511627.110), Lbrj2 (LbrM.27.2610), Lmjj2 (LmjF.27.2400), ScYdj1 (NP_014335.1), DmelDnaJ-like-2 (NP_650283.1), HsDNAJA1 (NP_001530.1), Tbj50 (Tb927.9.12730), Tcrj50 (TcCLB.510743.100), Lbrj50 (LbrM.34.2890), Lmjj50 (LmjF.35.2980), Pfj1 (PF3D7_1437900), TgonJ-protein (TGME49_311240), ScMdj1 (QHB08320.1), DmelTid-56 (CAA64531.1), HsTid-1L (NP_005138.3), HsTid-1S (NP_001128582.1), EcDNAJA1 (MRF42610.1), SmarDNAJA1 (MBH2573448), PsarDNAJA1 (WP_009685335.1) and SaurDNAJA1 (MCR0757594.1). The Hsp33 sequences used for this assessment were from: EcHsp33 (EDV67745.1), SmarHsp33 (WP_060448467.1), PaerHsp33 (MXH37999.1), SaurHsp33 (HAY6579316.1), TbHsp33/TrypOX (Tb927.6.2630), LbrHsp33 (LBRM2903_300022900), LmjHsp33 (LmjF.30.1670), TcrHsp33 (TcCLB.509965.120), OsatHsp33 (EEC84194.1) and CrHsp33 (PNW70318.1). Tbb/TeqHep1 refers to the identical TbbHep1 and TeqHep1 orthologues, whilst Sc/SpasHep1 refers to the identical ScHep1 and SpasHep1 orthologues.

The distance analyses comparing relations between Hep1 and the J-proteins or Hsp33 orthologues shows that Hep1 is more closely related to the type I J-proteins (Appendix A, Figure A10). Therefore, the J-protein qualities that some Hep1 orthologues have been determined to possess could be attributed, in part, to their shared similarities at their zinc finger domains. Type I and type II J-proteins possess a protein binding domain with which they bind substrate proteins (Kampinga and Craig, 2010). It still needs to be determined how Hep1 orthologues bind to substrate proteins. The ability of J-proteins to stimulate the ATPase activity of Hsp70 is attributed to the HPD motif at their J domains (Liberek *et al*., 1991; Genevaux *et al*., 2001; Wittung-Stafshede *et al*., 2003). In HsHep1, the zinc finger domain histidine residue that is 100 % conserved across all the Hep1 orthologues has been determined to be indispensable for the ability to stimulate the ATPase activity of mtHsp70 (Zhai *et al*., 2011).

2.4.8 Sequence and phylogenetic analyses of the murine and primate Hep1 isoforms

In section 2.4.1, *Mus musculus* Hep1 sequence retrieval using the NCBI BLASTP platform resulted in the discovery of multiple Hep1 orthologues or isoforms in some murine and primate organisms (Appendix A, Tables A3 & A4). The isoforms were analysed by means of MSAs, phylogenetics and predictive computation. As a starting point, the murine and primate/ape Hep1 isoforms were phylogenetically analysed. The clades formed were each occupied only by isoforms from the same organism (Figure 2.7). This means that each organism possesses isoforms that share greater similarity with each other when compared to Hep1 orthologues or isoforms of the other mammalian organisms. The isoforms of Hep1 within each organism have an identical gene ID (Appendix A, Table A3).

Domain mapping revealed that some of the isoforms do not possess a canonical zinc finger domain and were much smaller in size in terms of their molecular weights and number of amino acid residues. These isoforms were also predicted to localise in the mitochondria (Appendix A, Table A3). With the murine and primate Hep1 orthologues that possessed the zinc finger domain, it was determined that they share complete conservation with the zinc fingers of HsHep1 and BtauHep1. Only a handful of sequence variations were observed (Figure 2.8). Computing the parameters of the zinc finger domains of the murine and primate isoforms also revealed that they are constituted of 66 amino acid residues, with a molecular weight of approximately 7 300 Da. The only exception was CjacHep1-iso2, which has a zinc finger consisting of 60 amino acid residues with a molecular weight of 6674.6 Da. CjacHep1-iso2 was also non-conserved compared to the other orthologues that possess a zinc finger domain, varying at the C-terminal end (Figure 2.8). The zinc finger domains of the murine and primate Hep1 orthologues are structurally similar to those of the rest of the orthologues used in this study (Appendix A, Table A3).

The murine Hep1 orthologue lacking the zinc finger, that is canonical of Hep1 orthologues, fell into 2 categories. One category, whose sequences terminate at site 147 of the MSA is shorter than the isoforms of the other category of the Hep1 isoforms lacking a zinc finger domain (Figure 2.8). Relative to

HsHep1, this termination occurs at amino acid residue 79. The second category is much longer, terminating at site 203 of the multiple sequence alignment. Relative to HsHep1, this termination occurs at amino acid residue 130. When comparing the isoforms within each of the 2 categories of the primate Hep1 orthologues lacking zinc finger domains, it can be observed that they are highly conserved. The zinc finger lacking isoforms all possess a cysteine residue that is conserved with the first cysteine residue of the CXXC residue of the isoforms possessing a typical zinc finger domain. Within the primate organisms, none of the Hep1 isoforms lacked the zinc finger domain (Figure 2.8). Using the zinc finger lacking MsmHep1-iso2 and MsmHep1-iso3 isoforms as queries on BLASTP revealed that there are more murine organisms that possess isoforms that lack the zinc finger domain (Appendix A, Table A4).

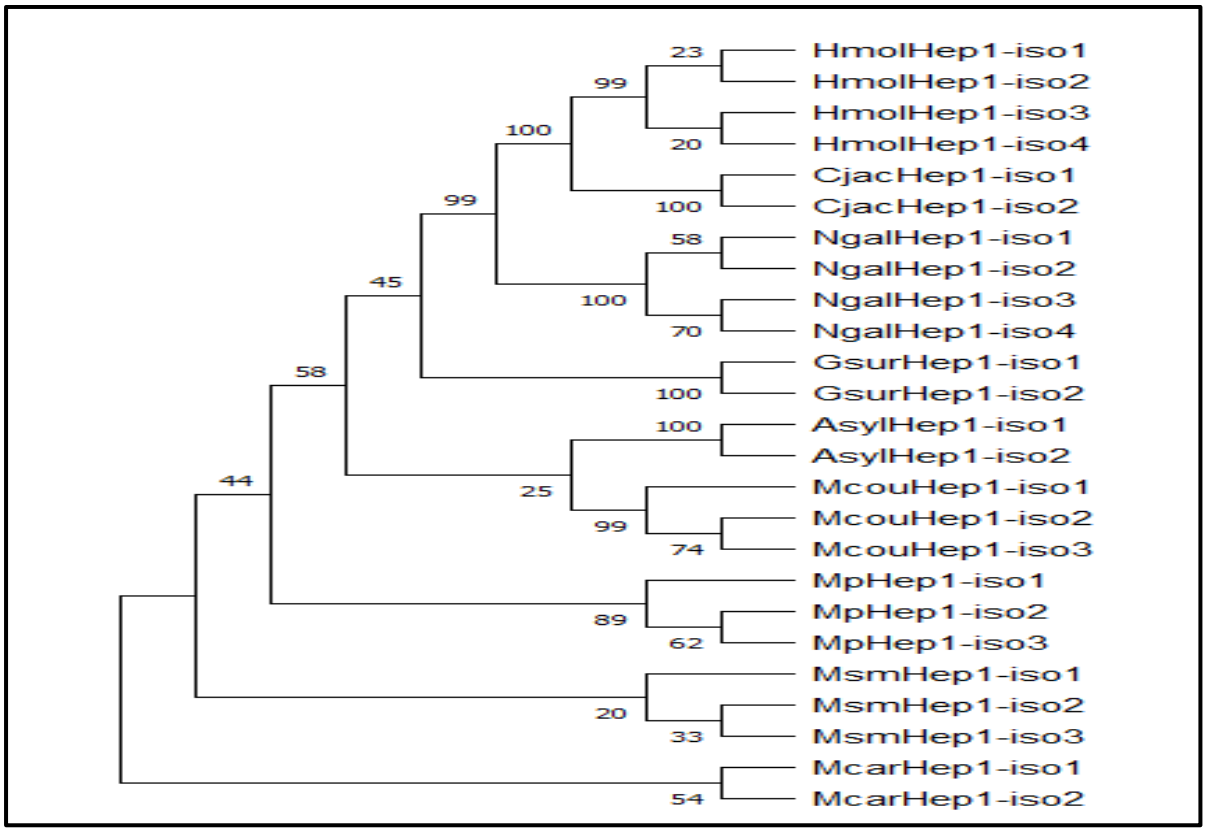

Figure 2.7. Phylogenetic analysis of the murine Hep1 orthologues/isoforms. The maximum-likelihood tree was constructed using MEGAX with the Jones-Taylor (JTT) amino acid substitution matrix-model with Gamma distribution (G) from the built in ClustalW platform. The murine and primate Hep1 sequences used in this assessment were from: MsmHep1-iso1 (NP_081104.1), MsmHep1-iso2 (NP_001132975.1), MsmHep1-iso3 (NP_001132976.1), MpHep1-iso1 (XP_021050144.1), MpHep1-iso2 (XP_021050145.1), MpHep1-iso3 (XP_021050146.1), McarHep1-iso1 (XP_021011688.1), McarHep1-iso2 (XP_021011689.1), McouHep1-iso1 (XP_031225303.1), McouHep1-iso2 (XP_031225305.1), McouHep1-iso3 (XP_031225306.1), GsurHep1-iso1 (XP_028628786.1), GsurHep1-iso2 (XP_028628787.1), AsylHep1-iso1 (XP_052037841.1), AsylHep1-iso2 (XP_052037846.1), NgalHep1-iso1 (XP_029423617.1), NgalHep1-iso2 (XP_017655799.2), NgalHep1-iso3 (XP_017655800.1), NgalHep1-iso4 (XP_029423618.1), HmolHep1-iso1 (XP_032021543.1), HmolHep1-iso2 (XP_032021544.1), HmolHep1-iso3 (XP_032021545.1), HmolHep1-iso4 (XP_032021546.1), CjacHep1-iso1 (XP_035119009.1) and CjacHep1-iso2 (XP_035119020.1).

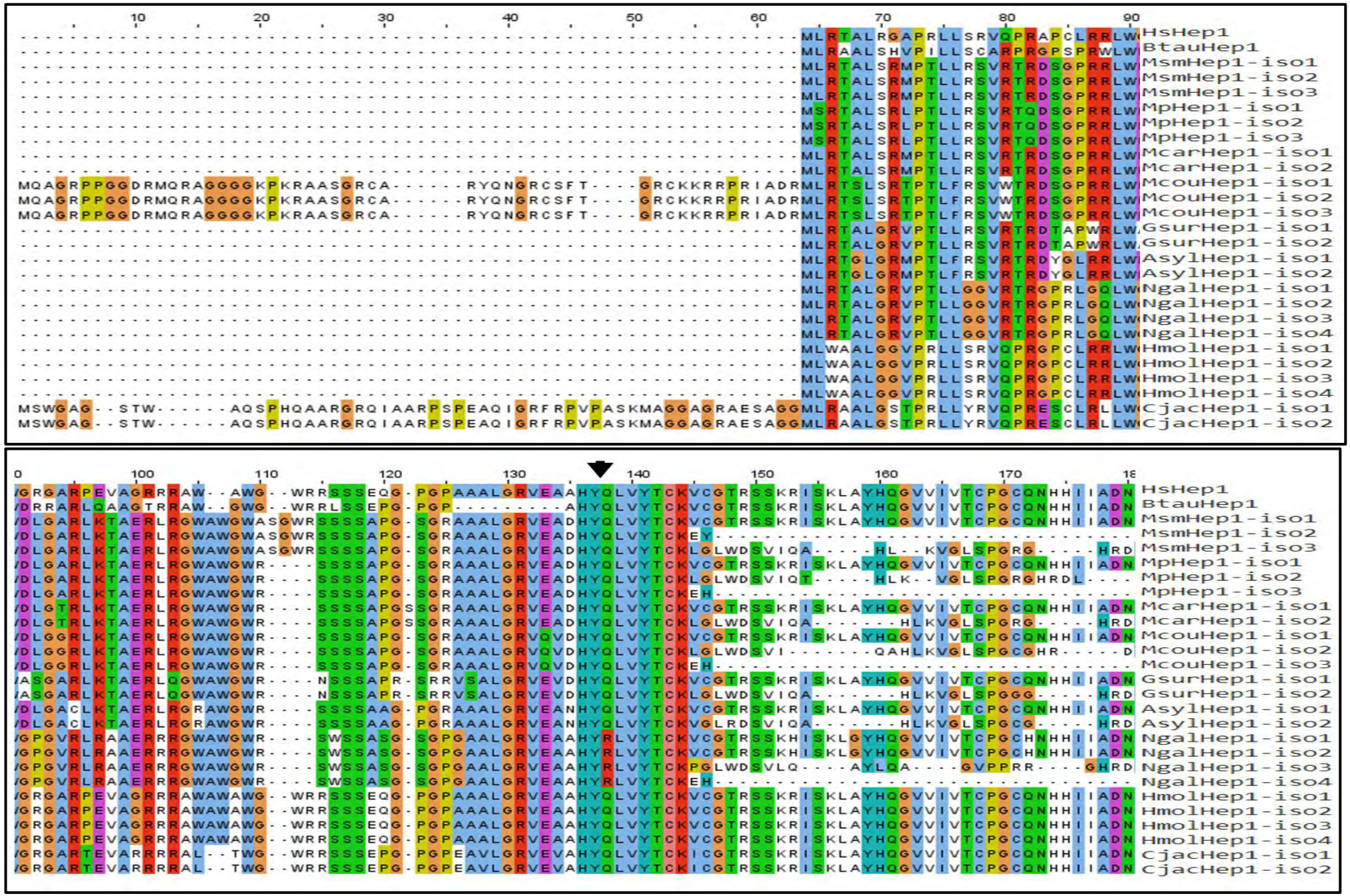
10 20 30 40 50 60 70 80 90
HsHep1
BtauHep1
MsmHep1-iso1
MsmHep1-iso2
MsmHep1-iso3
MpHep1-iso1
MpHep1-iso2
MpHep1-iso3
McarHep1-iso1
McarHep1-iso2
McouHep1-iso1
McouHep1-iso2
McouHep1-iso3
GsurHep1-iso1
GsurHep1-iso2
AsylHep1-iso1
AsylHep1-iso2
NgalHep1-iso1
NgalHep1-iso2
NgalHep1-iso3
NgalHep1-iso4
HmolHep1-iso1
HmolHep1-iso2
HmolHep1-iso3
HmolHep1-iso4
CjacHep1-iso1
CjacHep1-iso2
0 100 110 120 130 140 150 160 170 18
HsHep1
BtauHep1
MsmHep1-iso1
MsmHep1-iso2
MsmHep1-iso3
MpHep1-iso1
MpHep1-iso2
MpHep1-iso3
McarHep1-iso1
McarHep1-iso2
McouHep1-iso1
McouHep1-iso2
McouHep1-iso3
GsurHep1-iso1
GsurHep1-iso2
AsylHep1-iso1
AsylHep1-iso2
NgalHep1-iso1
NgalHep1-iso2
NgalHep1-iso3
NgalHep1-iso4
HmolHep1-iso1
HmolHep1-iso2
HmolHep1-iso3
HmolHep1-iso4
CjacHep1-iso1
CjacHep1-iso2

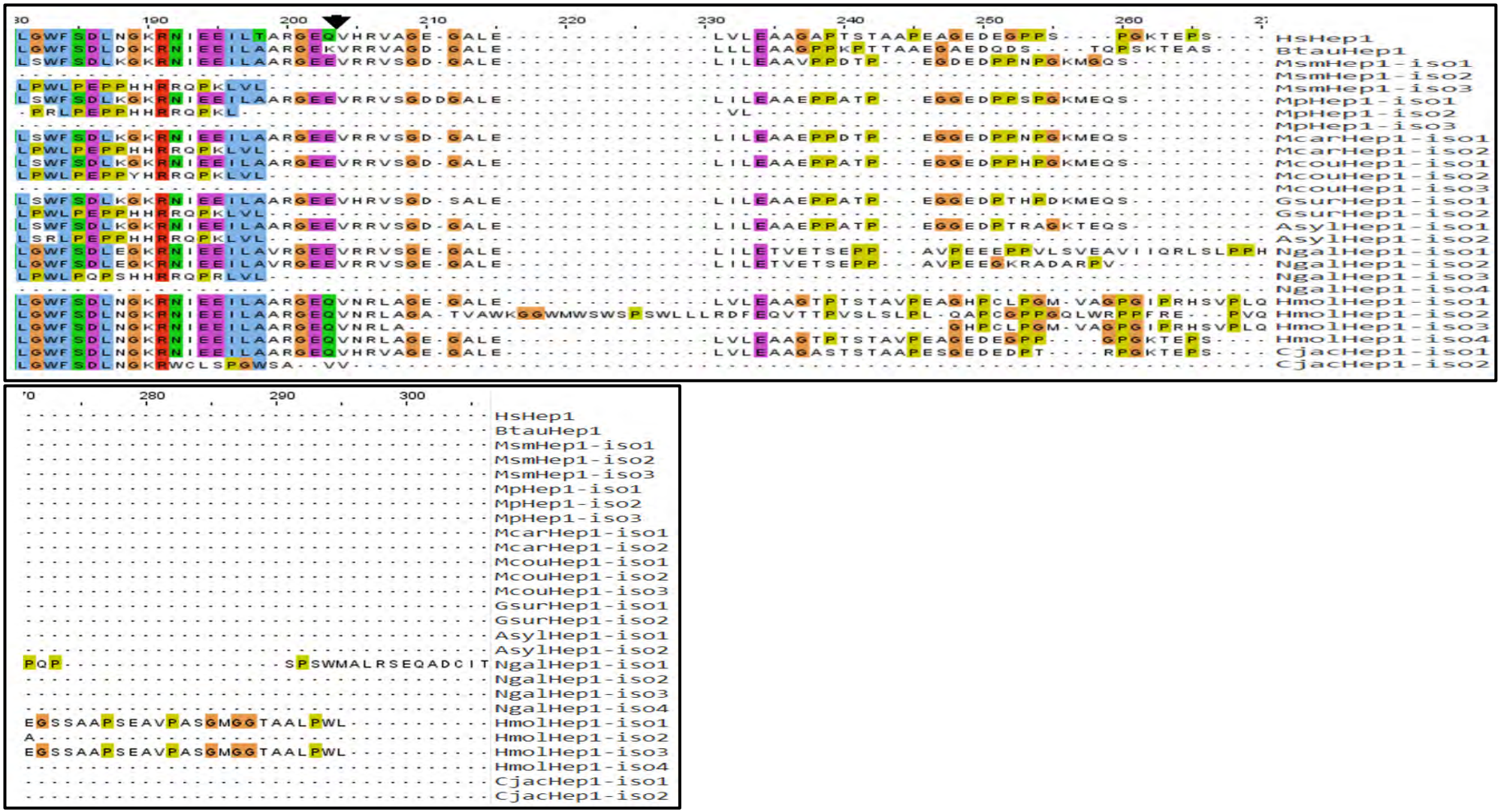

Figure 2.8. The Clustal Omega multiple sequence alignment of the murine and primate Hep1 orthologues/isoforms alongside the bovine and human Hep1 orthologues. The sequences were aligned using the built in Clustal Omega platform on the JalView web service with default settings. The annotation is based on the JalView Clustal colour option. The sequences aligned were from: MsmHep1-iso1 (NP_081104.1), MsmHep1-iso2 (NP_001132975.1), MsmHep1-iso3 (NP_001132976.1), MpHep1-iso1 (XP_021050144.1), MpHep1-iso2 (XP_021050145.1), MpHep1-iso3 (XP_021050146.1), McarHep1-iso1 (XP_021011688.1), McarHep1-iso2 (XP_021011689.1), McouHep1-iso1 (XP_031225303.1), McouHep1-iso2 (XP_031225305.1), McouHep1-iso3 (XP_031225306.1), GsurHep1-iso1 (XP_028628786.1), GsurHep1-iso2 (XP_028628787.1), AsylHep1-iso1 (XP_052037841.1), AsylHep1-iso2 (XP_052037846.1), NgalHep1-iso1 (XP_029423617.1), NgalHep1-iso2 (XP_017655799.2), NgalHep1-iso3 (XP_017655800.1), NgalHep1-iso4 (XP_029423618.1), HmolHep1-iso1 (XP_032021543.1), HmolHep1-iso2 (XP_032021544.1), HmolHep1-iso3 (XP_032021545.1), HmolHep1-iso4 (XP_032021546.1), CjacHep1-iso1 (XP_035119009.1), CjacHep1-iso2 (XP_035119020.1), HsHep1 (NP_001074318.1) and BtauHep1 (XP_003586730.1).

The conservation of the non-canonical Hep1 isoforms indicates a potential evolutionary adaptation within the murine organisms. The zinc finger domain of the CjacHep1-iso2 is non-conserved at the C-terminal end when compared to all the other mammalian Hep1 orthologues possessing a zinc finger domain (Figure 2.8). Phylogenetic analysis, inclusive of all the murine and Hep1 isoforms as well as all the other Hep1 orthologues used in this study, was also conducted. In the phylogenetic tree, the zinc finger domain lacking murine isoforms falling into the shorter category occupying a sub-clade that was in the same clade occupied by the MdomHep1, CjacHep1-iso1 and CjacHep1-ios2 Hep1 orthologues (Figure 2.9). The zinc finger domain lacking murine isoforms falling into the longer category occupied a separate clade. The clades within which the zinc finger domain lacking murine isoforms were within the clades occupied by all the other mammalian Hep1 isoforms. Hep1 orthologues from the flies fell into clades that was within the mammalian Hep1 orthologues. HsHep1 was most closely related to HmolHep1-iso3 (Figure 2.9). This is not unexpected as humans and apes are very closely related in terms of evolution. HsHep1 shares high sequence identity with the other Hep1 orthologues within the class Mammalia. The fly Hep1 orthologues also proved to be closely related to the mammalian Hep1 orthologues.

Distance analyses were also carried out separately for the mammalian orthologues/isoforms possessing a zinc finger domain and the zinc finger lacking Hep1 orthologues and isoforms from the same organism are most closely related (Appendix A, Figure A11). In the distance analysis, the closest relative of HsHep1 is HmolHep1-iso4 (Appendix A, Figure A11). In the phylogenetic analysis, HsHep1 was in the same clade as HmolHep1-iso3, whereas HmolHep1-iso4 was in the adjacent clade together with BtauHep1. These findings further point to the *Hylobates moloch* as a good model organism for studying HsHep1 in human disease.

Proteomic evidence has not been produced of the different isoforms of Hep1 in murine and primate organisms. The isoforms from a single organism share the same gene ID, meaning that they are potential transcript variants (Appendix A, Table A3). It needs to be ascertained if the observed isoforms do exist as proteins and are not just transcript variants which may or may not be translated into protein. Transcript variants are a result of alternative splicing events of a single gene which result in multiple, divergent products (Tress *et al*., 2007). Alternative splicing is a phenomenon by which higher eukaryotes are thought to increase their complexity by increasing the number of different proteins from a limited set of genes (Dhamija and Menon, 2018). In mice and humans, most genes undergo alternative splicing (Johnson *et al*., 2003). In humans, genes that undergo more frequent alternative splicing events have been determined to be constitutively expressed (Ryu *et al*., 2015). It has been reported that not all transcript variants get to be translated into protein (Szempruch and Guttman, 2017).

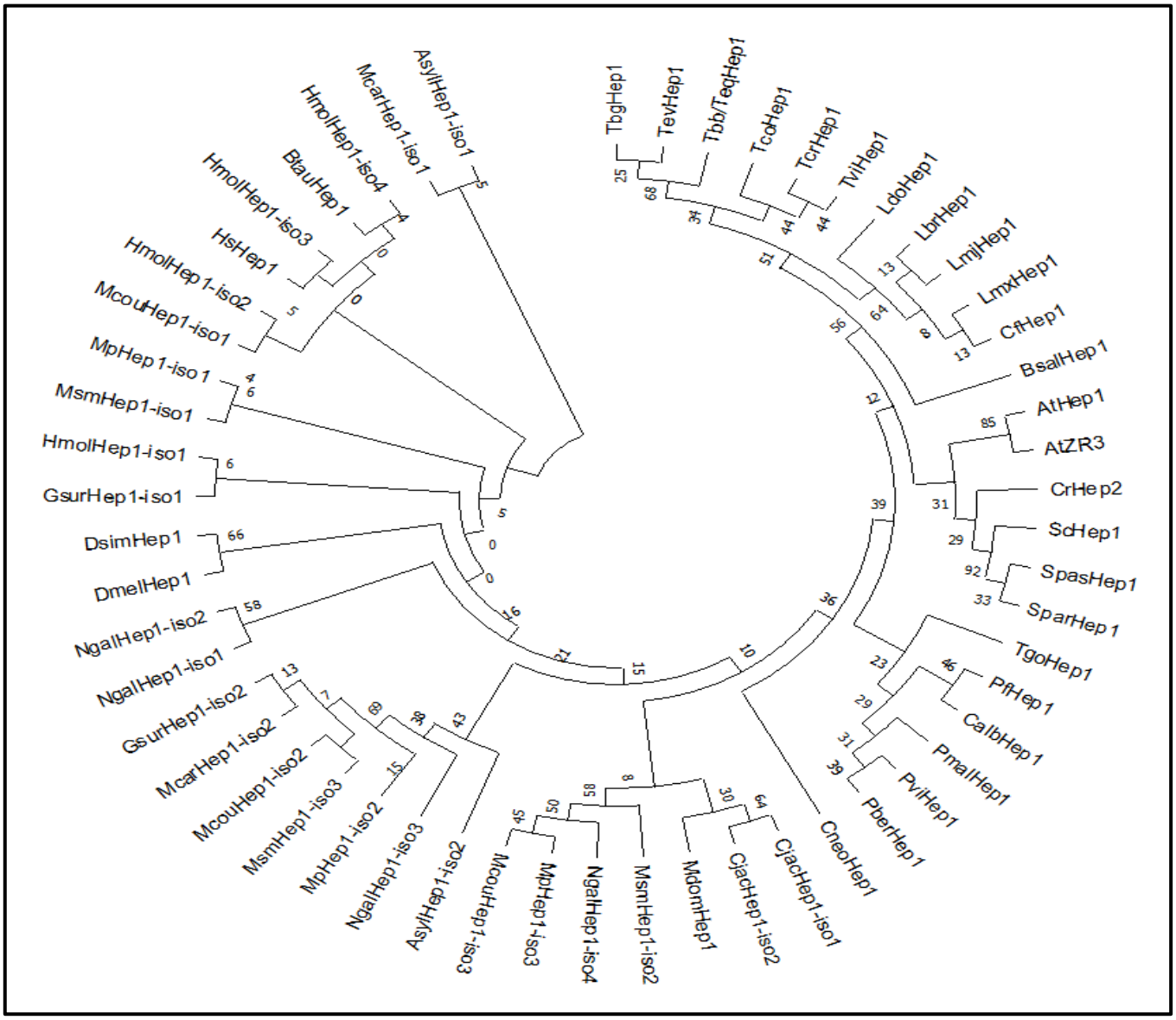

Figure 2.9. Phylogenetic analysis of the murine Hep1 orthologues/isoforms within the broader context of the rest of the Hep1 orthologues used in this study. The maximum-likelihood tree was constructed using MEGAX with the Jones-Taylor (JTT) amino acid substitution model with Gamma distribution (G) from the built in ClustalW platform. The murine and primate sequences used from this assessment were from: MsmHep1-iso1 (NP_081104.1), MsmHep1-iso2 (NP_001132975.1), MsmHep1-iso3 (NP_001132976.1), MpHep1-iso1 (XP_021050144.1), MpHep1-iso2 (XP_021050145.1), MpHep1-iso3 (XP_021050146.1), McarHep1-iso1 (XP_021011688.1), McarHep1-iso2 (XP_021011689.1), McouHep1-iso1 (XP_031225303.1), McouHep1-iso2 (XP_031225305.1), McouHep1-iso3 (XP_031225306.1), GsurHep1-iso1 (XP_028628786.1), GsurHep1-iso2 (XP_028628787.1), AsylHep1-iso1 (XP_052037841.1), AsylHep1-iso2 (XP_052037846.1), NgalHep1-iso1 (XP_029423617.1), NgalHep1-iso2 (XP_017655799.2), NgalHep1-iso3 (XP_017655800.1), NgalHep1-iso4 (XP_029423618.1), HmolHep1-iso1 (XP_032021543.1), HmolHep1-iso2 (XP_032021544.1), HmolHep1-iso3 (XP_032021545.1), HmolHep1-iso4 (XP_032021546.1), CjacHep1-iso1 (XP_035119009.1) and CjacHep1-iso2 (XP_035119020.1). The other sequences used were from: TbgHep1 (Tb972.3.2280), TbbHep1 (Tb927.3.2300), TeqHep1 (TEOVI_000221600), TevHep1 (TevSTIB805.3.2330), TcrHep1 (TcCLB.508479.274), TviHep1 (TvY486_0301660), TcoHep1 (TcIL3000_0_42310), LbrHep1 (LbrM.25.0680), LdoHep1 (LdBPK_250830.1), LmjHep1 (LmjF.25.0800), LmxHep1 (LmxM.25.0800), BsalHep1 (BSAL_79370), CfHep1 (CFAC1_220016500), PfHep1 (PF3D7_1420300), PmalHep1 (PmUG01_13038600), PviHep1 (PVP01_1328600), PberHep1 (PBANKA_1022900), TgoHep1 (TGME49_260340), AtHep1 (NP_974434.2), ScHep1 (NP_014089.2), SpasHep1 (QID81845.1), SparHep1 (XP_033768657.1), CneoHep1 (XP_024514386.1), CalbHep1 (KHC45981.1), HsHep1 (NP_001074318.1), BtauHep1 (XP_003586730.1), DmelHep1 (AAS15675.1), DsimHep1 (XP_016039443.1), MdomHep1 (XP_00518472.3), CrHep2 (XP_001700157.1) and ATZR3 (AAO64784.1). Tbb/TeqHep1 refers to the identical TbbHep1 and TeqHep1 orthologues, whilst Sc/SpasHep1 refers to the identical ScHep1 and SpasHep1 orthologues.

2.4.9 Phylogenetic, distance and sequence analyses of TbmtHsp70 and HSPA9

The mtHsp70 partners of TbHep1 and HsHep1, TbmtHsp70 and HSPA9 respectively, were also analysed in this *in silico* study. Phylogenetic analyses revealed that the mtHsp70 orthologues share a clade with the *E. coli* DnaK. The cytosolic and BiP Hsp70 orthologues also formed their own separate clades (Figure 2.10A). Details regarding the Hsp70 sequences used for this study are provided in Appendix A, Table A5. Deeper analysis of the constructed phylogenetic trees reveals that the parasitic mtHsp70 orthologues formed a separate sub-clade from HSPA9 and the yeast orthologues, ScSsc1, ScEcm10 and ScSsq1. The yeast orthologues ScSsc1, ScEcm10 and ScSsq1 banded together separate from HSPA9 within the sub-clade. The yeast mtHsp70 orthologues have all been determined to be prone to self-aggregation, but the aggregates of ScEcm10 cannot be rescued by Hep1. ScSsq1 is divergent in that it is specialised for the maintenance the iron-sulphur cluster (Lutz *et al*., 2001). ScSsc1 is the main yeast mtHsp70 paralogue, whilst ScEcm10 has also been shown to functionally overlap with ScSsc1 (Craig *et al*., 1989; Kang *et al*., 1990; Pareek *et al*., 2011). TbmtHsp70 was most closely related to TcrmtHsp70, and LbrmtHsp70 was closely related to LmjmtHsp70. The computed parameters of the Hsp70s also showed that they are highly similar in terms of molecular weight, the number of amino acid residues and pI (Appendix A, Table A5). The distance analysis confirmed the conclusions reached in the phylogenetic tree with regard to the mtHsp70 orthologues (Figure 2.10B). TbmtHsp70 is most closely related to TcrmtHsp70. Between LbrmtHsp70 and LmjmtHs70, TbmtHsp70 is most closely related to LbrmtHsp70. HSPA9 is most closely related to ScSsc1 and most distantly related to ScSsq1. Of the parasitic orthologues, HSPA9 is closely related to PfHsp70-3 (Figure 2.10B).

MtHsp70 orthologues are known to be different at the linker region, when compared to their cytosolic counterparts. Cytosolic Hsp70s of eukaryotes, in comparison to prokaryotic DnaK, possess an insertion of either one of three motifs: KSEN, ESSK and QSNA (Chakafana *et al*., 2019). In this study these insertions at the linker regions of the cytosolic Hsp70s were observed between sites 470 and 480 of the MSA (Figure 2.11). The BiP orthologues also exhibited insertions in the linker region (Figure 2.11 & Appendix A, Figure A12). MtHsp70s lack the insertion and their linker regions are most similar to the *E. coli* DnaK linker, GDVKDVLLLLDVT (Vogel *et al*., 2006; Swain *et al*., 2007). In this study, the mtHsp70s possessed linker regions that aligned with EcDnaK (Figure 2.11 & Appendix A, Figure A12).

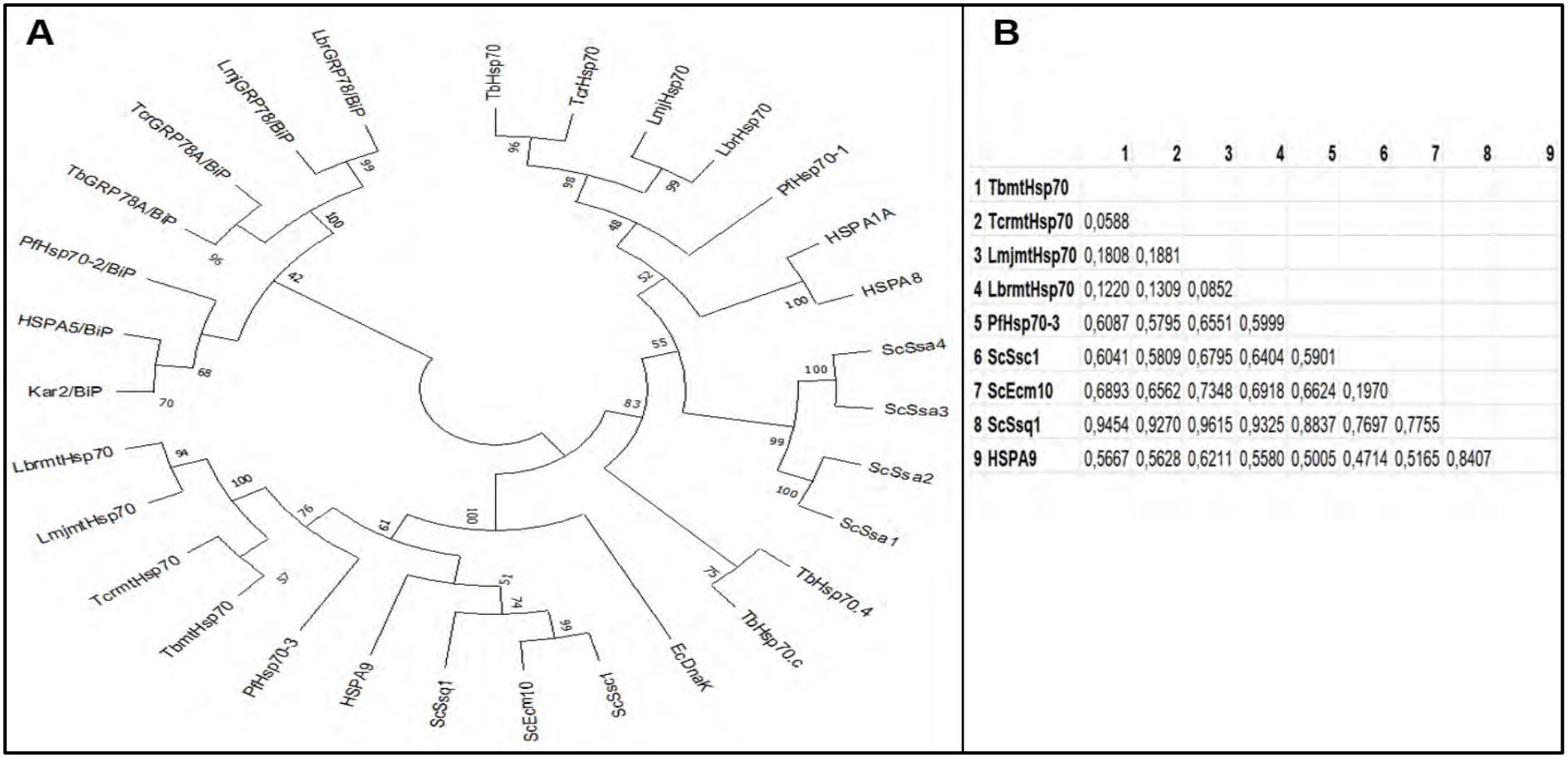

Figure 2.10. Phylogenetic and distance analyses of the mtHsp70 orthologues and their cytosolic and ER counterparts. The **A)** phylogenetic analysis was performed on all the Hsp70s whilst the **B)** distance analysis was only performed on the mtHsp70 orthologues. The maximum-likelihood tree and distance matrix were constructed using MEGAX with the Jones-Taylor (JTT) amino acid substitution model with Gamma distribution (G) from the built in ClustalW platform. The sequences used were from: TbHsp70 (Tb927.11.11330), TbHsp70.4 (Tb927.7.710), TbHsp70.c (Tb927.11.11290), TbmtHsp70 (Tb927.6.3740), TbGRP78A/BiP (Tb927.11.7460), TcrHsp70 (TcCLB.511211.170), TcrmtHsp70 (TcCLB.507029.30), TcrGRP78A/BiP (TcCLB.506585.40), LmjHsp70 (LmjF.28.2770), LmjmtHsp70 (LmjF.30.2460), LmjGRP78/BiP (LmjF.28.1200), LbrHsp70 (LbrM.28.2990), LbrmtHsp70 (LbrM.30.2420), LbGRP78/BiP (LbrM.30.2420), PfHsp70-1 (PF3D7_0818900), PfHsp70-3 (PF3D7_1134000), PfHsp70-2/BiP (PF3D7_0917900), ScSsa4 (AJU50241.1), ScSsa3 (AJQ13321.1), ScSsa2 (AJV59097.1), ScSsa1 (AJO96864.1), ScSsc1 (AJV44330.1), ScEcm10 (AJU50104.1), ScSsq1 (AJV59432.1), ScKar2 (AJR59823.1), HSPA1A (NP_005336.3), HSPA8 (NP_006588.1), HSPA9 (AAH00478.1), HsHSPA5/BiP (AAI12964.1) and EcDnaK (WP_097477514.1).

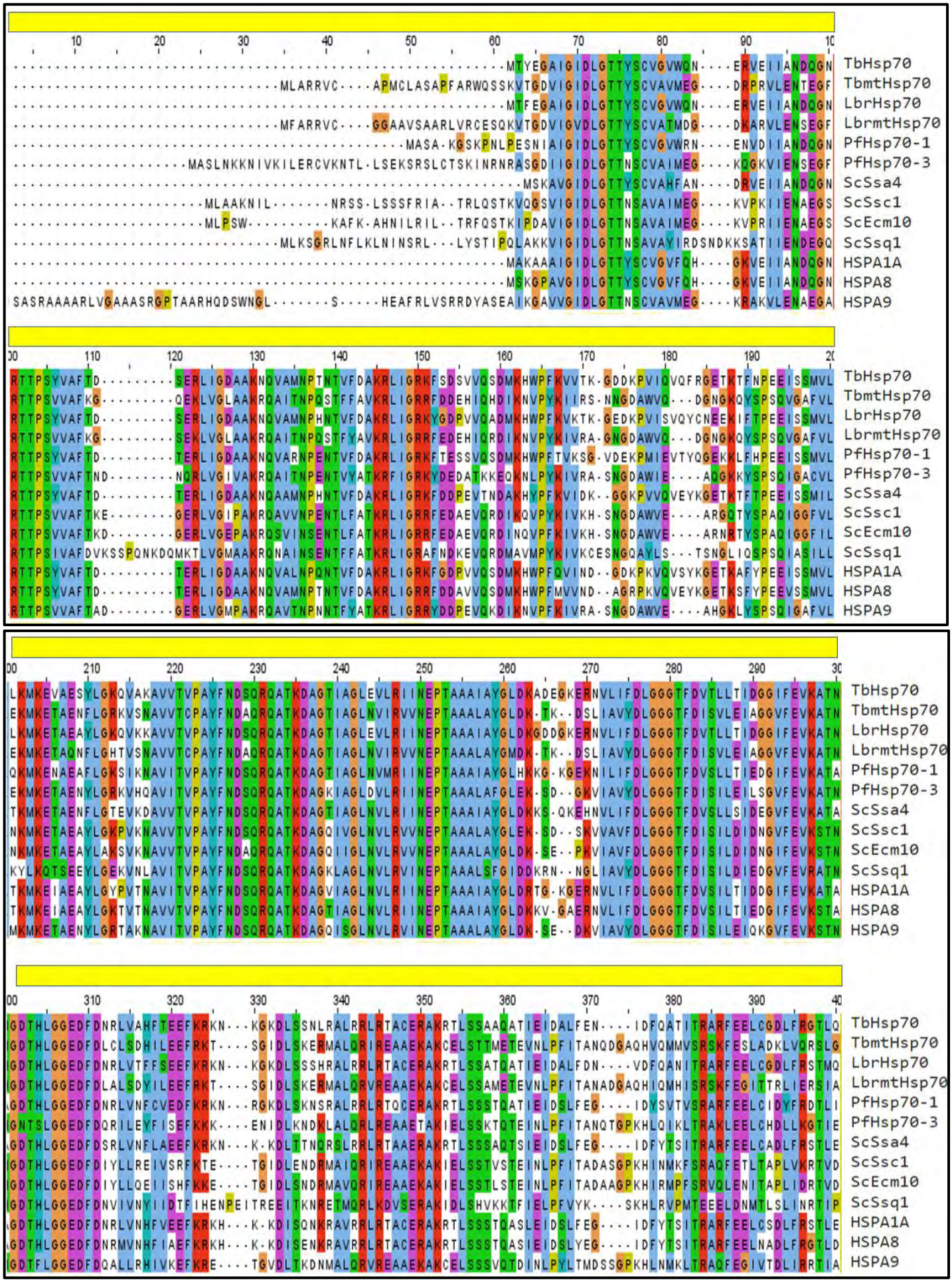
TbHsp70
TbmtHsp70
LbrHsp70
LbrmtHsp70
PfHsp70-1
PfHsp70-3
ScSsa4
ScSsc1
ScEcm10
ScSsq1
HSPA1A
HSPA8
HSPA9

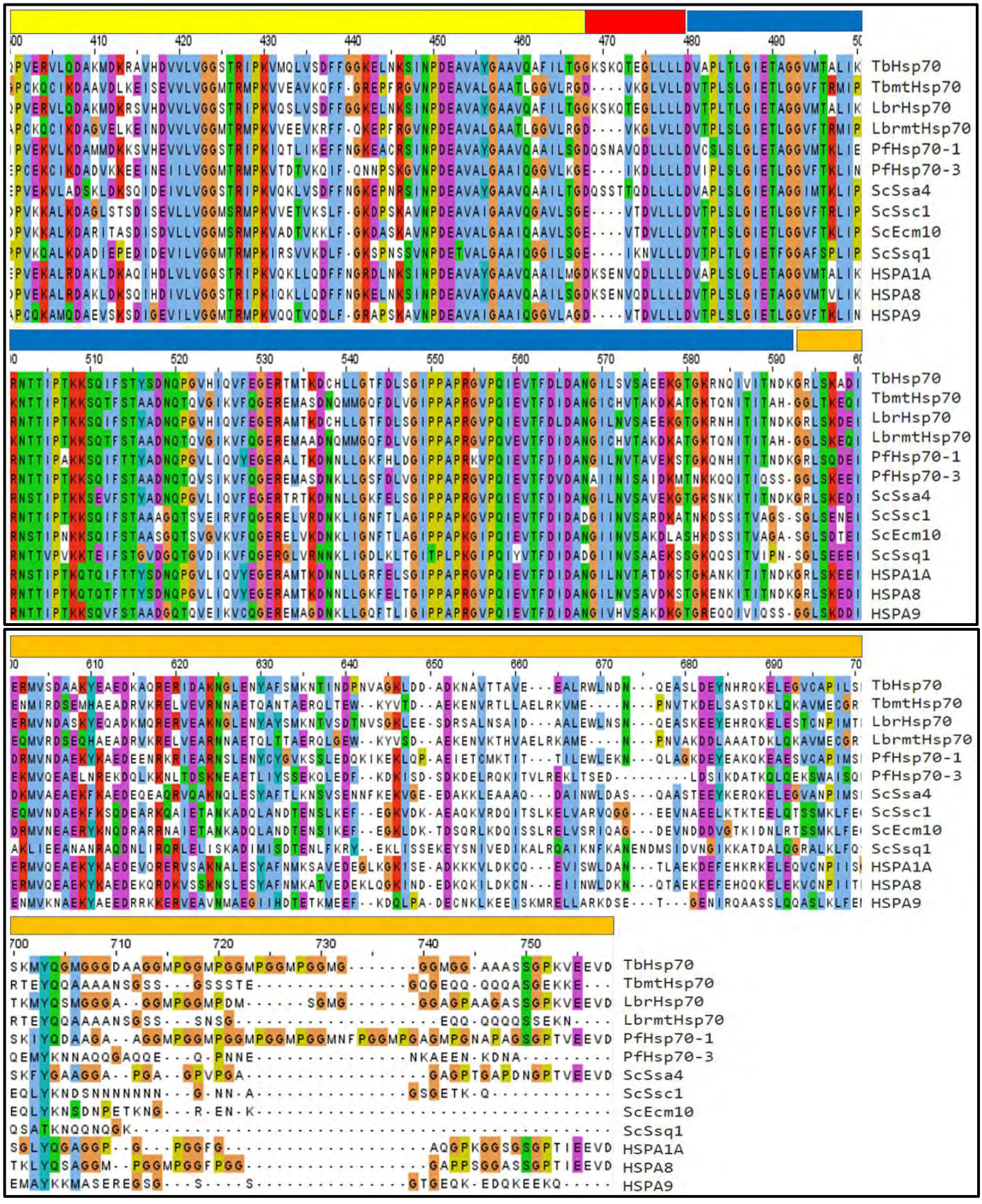

Figure 2.11. The Clustal Omega multiple sequence alignment of the Hsp70 orthologues. The sequences were aligned using the built in Clustal Omega platform on the JalView web service. The annotation is based on the JalView Clustal colour option. The sequences aligned were from: TbHsp70 (Tb927.11.11330), TbmtHsp70 (Tb927.6.3740), LbrHsp70 (LbrM.28.2990), LbrmtHsp70 (LbrM.30.2420), PfHsp70-1 (PF3D7_0818900), PfHsp70-3 (PF3D7_1134000), ScSsa4 (AJU50241.1), ScSsc1 (AJV44330.1), ScEcm10 (AJU50104.1), ScSsq1 (AJV59432.1), HSPA1A (NP_005336.3), HSPA8 (NP_006588.1) and HSPA9 (AAH00478.1). The bars above the multiple sequence alignment serve to indicate the various domains of the Hsp70s: yellow (ATPase domain), red (linker region), blue (SBD-β) and orange (SBD-α). The domain annotation is relative to HSPA1A (Vostakolaei *et al*., 2021).

A known property of mtHsp70 orthologues is that they are prone to self-aggregation. The HSPA9, PfHsp70-3, LbrmtHsp70 and ScSsc1 orthologues used in this study have been determined to form self-aggregates that are rescued by their respective Hep1 orthologues (Sichting et al., 2005; Goswami et al., 2010; Dores-Silva et al., 2015; Nyakundi et al., 2016). The linker region together with the ATPase domain have been implicated in the self-aggregation of mtHsp70 (Zhai *et al*., 2008). TbmtHsp70 exhibits the properties of the rest of the mtHsp70s at the linker region and was determined to be closely related to them (Figures 2.10 & 2.11). Therefore, by inference, it would be expected that TbmtHsp70 also forms self-aggregates. EcDnaK has been determined to not aggregate when directed to the mitochondria, despite the mtHsp70 linker region being derived from EcDnaK (Blamowska *et al*., 2010). As suggested by Zhai et al. (2008), the ATPase domain of mtHsp70 is also responsible for self-aggregation. On the MSA, it can be observed that there are some differences between the mtHsp70 and cytosolic Hsp70s at the ATPase domain (Figure 2.11). At site 180-190 of the ATPase domain of the MSA the mtHsp70 orthologues are lacking some amino acid residues, as well as at around site 270. Relative to TbmtHsp70 these sites are 129 and 213-215. At site 375-380 of the alignment, the mtHsp70 orthologues and EcDnaK exhibit an insertion, but ScSsq1 lacks it (Appendix A, Figure A12). Relative to TbmtHsp70, this insertion occurs between amino acid residues 310 and 315. Since EcDnaK does not aggregate in the mitochondria, there are other factors that lead to mtHsp70 being prone to self-aggregation. EcDnaK possesses an insertion between site 290 and 300, which is the most notable difference compared to the mtHsp70s (Appendix A, Figure A12). This could be the reason for EcDnaK being soluble in the mitochondria as it is the only unique property when compared to the mtHsp70 orthologues at the ATPase domain. The mtHsp70 orthologues differ at the C-terminal end, whereas EcDnaK shares similarities with the cytosolic Hsp70s in this regard (Appendix A, Figure A12).

C-terminal domain of the eukaryotic cytosolic Hsp70s, have GGMP repeat motifs. The cytosolic Hsp70s lacking GGMP repeats were the yeast orthologues as well as the human stress inducible orthologue HSPA1A. The EEVD motifs are only present in the cytosolic Hsp70s (Figure 2.11). The C-terminal motifs of all the mtHsp70s were non-conserved. The BiP ER orthologues of Hsp70 terminated with motifs similar to the human ER retention motif KDEL.

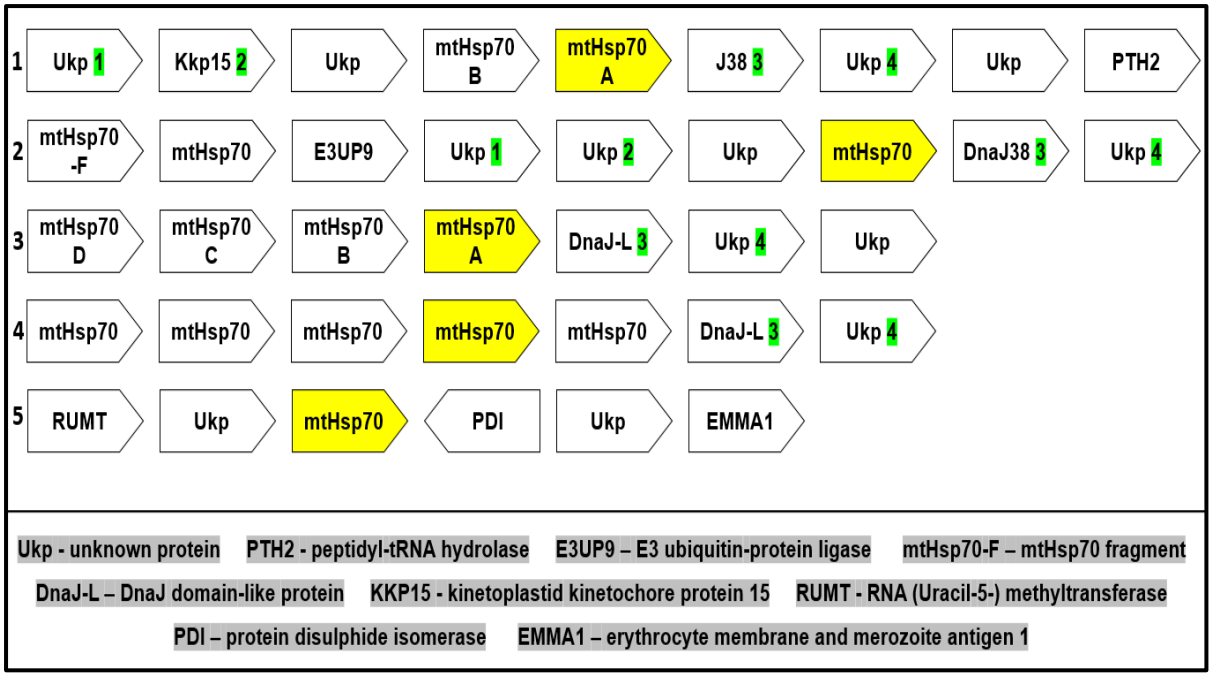

Figure 2.12. The syntenic analysis of selected mtHsp70 orthologues. The genes used for this analysis were from: **1)** TbmtHsp70 (Tb927.6.3740), **2)** TcrmtHsp70 (TcCLB.507029.30), **3)** LmjmtHsp70 (LmjF.30.2460), **4)** LbrmtHsp70 (LbrM.30.2420) and **5)** PfHsp70-3 (PF3D7_1134000). The gene arrangement is schematically presented displaying genes that are adjacent to mtHsp70 with directionality also taken into consideration. The numbers (1 to 4) highlighted in green signify orthology whereby each number indicates a group of orthologs. The bottom panel is a key that provides the full names for the genes presented in shorthand in the figure. The accession numbers of the genes adjacent to mtHsp70 are provided in Appendix A, Figure A14.

2.4.10 Computational prediction of the mtHsp70 posttranslational modifications

The posttranslational modifications of the mtHsp70 were predicted on the MusiteDeep web server and highlighted on a Clustal Omega MSA. Some of the predicted posttranslational modifications are conserved throughout, with some only being conserved in separate groups of orthologues (Appendix A, Figure A13). TbmtHsp70 shares numerous acetylation posttranslational modifications with the other kinetoplastid mtHsp70s, they occur at site 110, 122, 331, 381 and 631. At sites 325 and 575, respectively. HSPA9 has a unique posttranslational modification profile. At amino acid sites 103 and 684, HSPA9 shares glycosylation posttranslational modification sites with the yeast mtHsp70 orthologues (Appendix A, Figure A13). The posttranslational modifications sites that are conserved within the kinetoplastid suggest that they are important for the functions of the orthologues in those organisms. The conserved sites of posttranslational modifications point to those residues being essential for the functions of the mtHsp70 orthologues. No posttranslational modification sites were predicted for the linker regions, at sites 461-472 (Appendix A, Figure A13).

2.4.11 Analysis of mtHsp70 orthology

Syntenic analysis revealed that TbmtHsp70 and the other kinetoplast parasitic mtHsp70s are orthologous. The kinetoplastid mtHsp70s were also observed to possess numerous isoforms as has previously been determine by Bentley et al. (2019) and Louw et al. (2010). TbmtHsp70 possesses 3

identical copies. TbmtHsp70 A-C, all occurring on the same chromosome. The TbmtHsp70A and TbmtHsp70B genes are adjacent, whilst there are 4 genes occurring between TbmtHs70B and TbmtHsp70C (Figure 2.12) (Bentley et al., 2019). On the other hand, *L. braziliensis* has 5 non-identical mtHsp70 genes. This points to an evolutionary adaptation by kinetoplastid organisms whereby multiple mtHsp70 genes are required, albeit identical in *T. brucei*. Within the kinetoplastid organisms, the genes adjacent to the mtHsp70 genes were orthologous, even thought they were not arranged in the same order (Figure 2.12). The synteny of the PfHsp70-3 gene was unique in this regard. PfHsp70-3 does not possess any isoforms.

2.4.12 Analysis of the structural models of TbmtHsp70 and HSPA9

The structural models of TbmtHsp70 and HSPA9 were retrieved from the Alpha Fold/EMB-EBI repository. They both possess structural features that are characteristic of Hsp70 proteins (Figure 2.13). The substrate binding domain sub-domains alpha and beta can clearly be observed, constituted of α-helices and anti-parallel β-sheets, respectively. The beta subdomains possess a hydrophobic substrate binding domain, and in this study it they have been predicted to be hydrophobic as antiparallel β-sheets are known to be hydrophobic. The alpha subdomains are in an open conformation, linked to the beta subdomains by loop regions (Figure 2.13 A & B). The linker region can also be observed, occurring between the ATPase domains and the substrate binding domains.

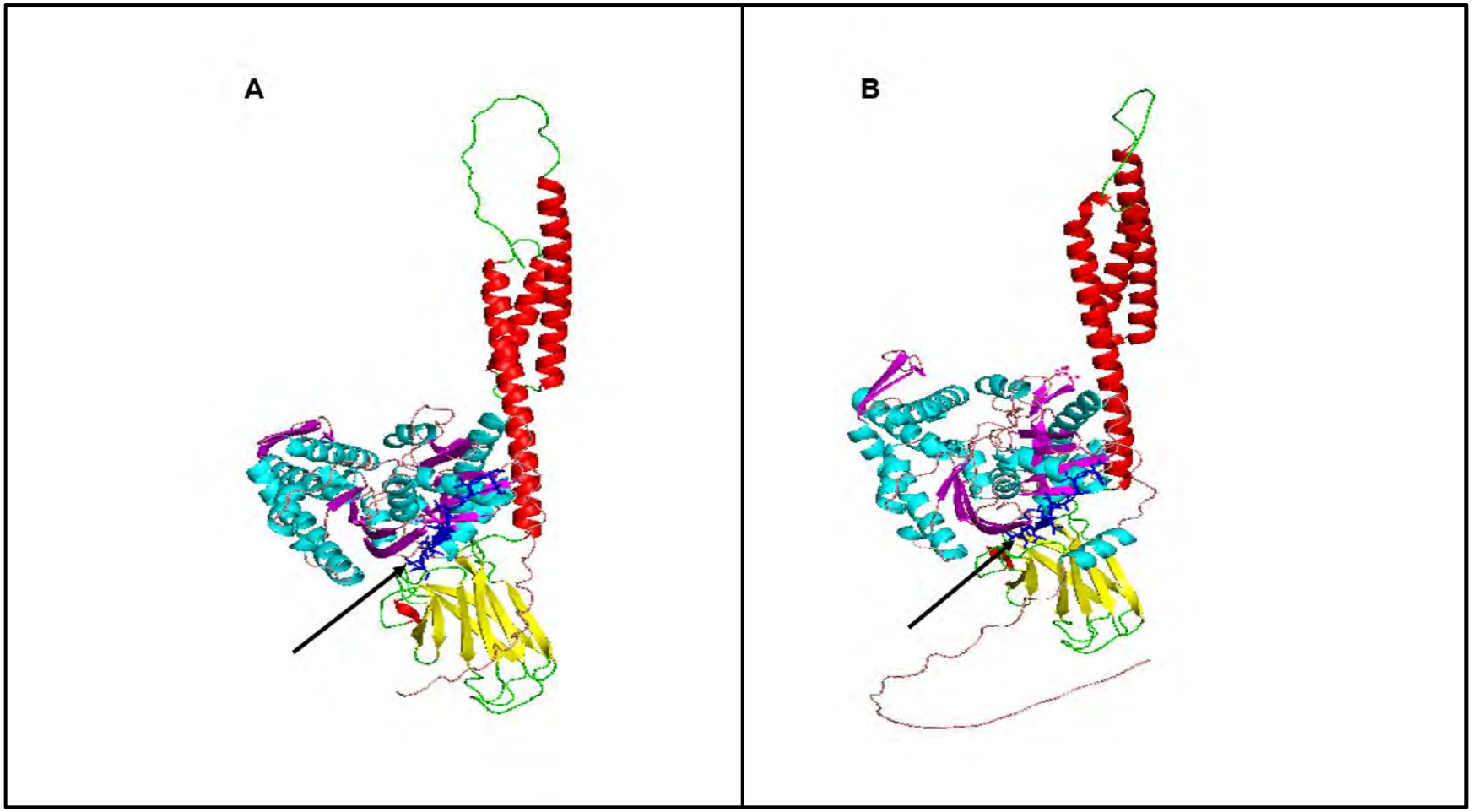

Figure 2.13. The AlphaFold2 predicted 3D structures of A) TbmtHsp70 and B) HSPA9. The 3D structures were rendered in PyMol and annotated manually. The teal α-helices, purple/pinkish β-sheets and loop regions represent the ATPase domain. The red α-helices, yellow β-sheets and green loop regions represent the α and β subdomains of the substrate binding domain. The arrow points to the interdomain linker which is shown as blue sticks.

2.5 Conclusions

The zinc finger domain is indispensable for Hep1 function. Several Hep1 orthologues have been biochemically assessed and determined to be essential for the solubility and functionality of mtHsp70 (Sichting et al., 2005; Dores-Silva et al., 2013; Dores-Silva et al., 2015; Nyakundi et al., 2016). HsHep1 and LbrHep1 are unique in that they stimulate the ATPase activity of mtHsp70, whilst ScHep1 does not stimulate the ATPase of yeast mtHsp70 (Sichting et al., 2005; Goswami et al., 2010; Dores-Silva et al., 2015; Dores-Silva et al., 2021). HsHep1 has also been reported to possess the ability to suppress the aggregation of substrate proteins, independently of mtHsp70 (Goswami et al., 2010; Dores-Silva et al., 2021). Recently, with HsHep1 as a model, new potential roles of Hep1 have emerged. These include the ability to interact with mitochondrial membranes and cytosolic Hsp70 (Dores-Silva *et al*., 2021). The aim of this study was to characterise, *in silico*, the putative TbHep1 orthologue alongside HsHep1. This study included numerous putative Hep1 in order to gain a better understanding of Hep1 as a protein.

Sequence analysis and domain mapping revealed that TbHep1 and HsHep1 indeed possess the highly conserved zinc finger domain and are canonical Hep1 orthologues. This is the first study to characterise TbHep1. Biochemical characterisation of HsHep1 has revealed that the orthologue possesses the ability to suppress the aggregation of mtHsp70, which has also been reported for PfHsp70-3, LbrHep1 and HsHep1 (Sichting et al., 2005; Dores-Silva et al., 2013; Dores-Silva et al., 2015; Nyakundi et al., 2016). It can be hypothesised that TbHep1 possesses the ability to interact with TbmtHsp70 and enhance its solubility and function since it displays the structural hallmarks of Hep1 orthologues. The sequence analysis also revealed that the Hep1 orthologues vary widely outside of the zinc finger domain. The orthologues also varied widely in terms of their computed molecular weights as a result of being constituted of widely varying numbers of amino acid residues. When the parameters of the zinc finger domains were computed, it was revealed that the variation in size was due to regions outside of the zinc finger domain, more specifically the N-terminal region. The zinc finger domains were found to be very similar in terms of the number of amino acids.

Despite the divergence observed in the sequences of the regions outside of the zinc finger domain, some Hep1 orthologues exhibited similarities. TbHep1, at the N- and C-terminal regions, shares some sequence similarities with other trypanosomal and kinetoplastid Hep1 orthologues. HsHep1 proved to share high sequence similarity with the other mammalian orthologues used in this study. The predicted structures of TbHep1 and HsHep1 also revealed that their divergence at the N-terminal region also applied to their secondary structures. TbHep1 possesses an unstructured stretch and two α-helices at the N-terminal domain, whereas the entire N-terminal domain of HsHep1 is unstructured. In terms of predicted posttranslational modifications, they were abundant outside of the zinc finger domain,

meaning that the N- and C-termini could be important for function. Some of these posttranslational modifications were conserved along the lines of the relatedness of the organisms of origin. The analysis of orthology by means of synteny also fell along the lines of species of origin, whereby the trypanosomal Hep1 genes had unique synteny compared to the *Leishmania* Hep1 genes. Phylogenetic analysis of the Hep1 orthologues also revealed that they are mostly related according to their species of origin. This was the case when they were phylogenetically analysed using the full-length sequences, the N-terminal region sequences and the zinc finger domain sequences.

This is the first report of the presence of multiple Hep1 isoforms in mice and apes, as 3 isoforms were found for *Mus musculus*. Further investigations revealed that some murine organisms and apes possess numerous Hep1 isoforms with identical gene IDs. With the murine Hep1 isoforms, some lacked the canonical zinc finger domain, falling into two categories. At the N-terminal regions, these non-canonical isoforms shared high conservation with the rest of the mammalian Hep1 isoforms. Of interest was the category of murine isoforms whose sequence terminates a few amino acids into the zinc finger domain. It would be worthwhile determining whether they are essential within the organisms from which they originate, and if they play any other role. Within all the mammalian Hep1 orthologues, HsHep1 was most closely related to the isoforms 3 and 4 of the *Hylobates moloch* Hep1 orthologues. Proteomic validation of the murine and primate Hep1 isoforms needs to be conducted in order to determine if all the potential alternative splicing products do get translated into proteins. This is because not all transcript variants get to be translated into proteins (Szempruch and Guttman, 2017). It would also be interesting to determine the conditions under which expression occurs. In *vivo* complementation assays or genetic knockdown could also be used to determine if the transcript variants/isoforms are indeed essential in the mice and primate organisms. Alternative splicing is a mechanism by which higher eukaryotes increase the proteomic diversity from a limited number of genes. It is therefore interesting to observe that the supposed transcript variants of the primate Hep1 orthologues produce highly similar isoforms that also possess zinc finger domains.

Due to some Hep1 orthologues being functionally similar to type I proteins, which also possess a zinc finger domain, the Hep1 orthologues were comparatively analysed against selected type I J-protein orthologues. Additionally, syntenic analysis revealed that some of the genes adjacent to Hep1 in the kinetoplastid organisms possess cysteine rich motifs such as CXC, CXXC and CXXXC. Hsp33 orthologues were also included as they also possess these cysteine rich motifs. Distance analysis revealed that the Hep1 orthologues were more closely related to the type I J-proteins, providing a possible scientific explanation for the holdase activity of HsHep1, and the ability of HsHep1 and LbrHep1 to stimulate Hsp70 ATPase activity.

Phylogenetic analysis showed that TbmtHsp70 and HSPA9 are related to the other mtHsp70 orthologues, and the MSA revealed that they aligned with the other mtHsp70s. In this study, the linker

regions of the mtHsp70s were shown to align with the linker of EcDnaK. The ATPase domains of the mtHsp70s were also very similar to that of EcDnaK, despite EcDnaK having been determined to be soluble in the mitochondrial matrix (Blamowska *et al*., 2010). Posttranslational modification predictions revealed that the mtHsp70 orthologues are most likely to be acetylated or phosphorylated, with no modifications predicted for the linker region. Syntenic analysis confirmed orthology for the TbmtHsp70 and the other kinetoplastid mtHsp70s, whereby they all possess multiple isoforms of the mtHsp70 gene. In terms of structure, the models revealed that TbmtHsp70 and HSPA9 share a similar structure.

CHAPTER THREE
Optimization and analysis of the heterologous expression and purification of the heat shock proteins

3.1 Introduction

Recombinant DNA technology (RDT) entails a set of molecular techniques that allow for the efficient synthesis of recombinant proteins in selected host organisms. It involves the genetic manipulation of the host organism such that it acquires genes that enable it to effectively produce the desired protein (Sørensen and Mortensen, 2005; Khan *et al*., 2016). This technique has revolutionized molecular biology as it permits for the expression of proteins in large amounts as opposed to directly sourcing them from large volumes of their natural host tissues or fluids in minute quantities (Rohou *et al*., 2007; Rosano and Ceccarelli, 2014). This technique could also be viewed as a safe alternative to extracting and isolating proteins from virulent pathogenic agents such as bacteria, viruses and protozoans as well as other potentially toxic sources (Burnett *et al*., 2009; Rosano and Ceccarelli, 2014; Rivera-de-Torre *et al*., 2022). Recombinant protein expression is useful for the biochemical characterization of proteins as well as the development of therapeutic and commercial proteins, reviewed by Rosano and Ceccralli (2014) and Puetz and Wurm (2019). Recombinant protein expression can either be homologous or heterologous. In homologous protein expression, the gene being expressed is also found in the host organism whilst heterologous protein expression entails expressing a gene that is foreign to the host organism (Martínez-Espinosa, 2019). *E. coli* is the organism of choice with regard to recombinant protein expression (Snustad and Simmons, 2016). This bacterium is well characterized, having high growth rates, inexpensive growth media and can easily have foreign DNA introduced into it by transformation (Lee, 1996; Pope and Kent, 1996; Shiloach and Fass, 2005; Sezonov *et al*., 2007).

Plasmid vectors are typically constituted of numerous elements that enable for the efficient expression of recombinant proteins. These include a multiple cloning site (MCS), promoter, selection marker, origin of replication (replicon) and an affinity tag, reviewed by (Ahmad *et al*., 2018; Kaur *et al*., 2018). The selection marker further ensures that cells do not dispose of the vector plasmid as it is a survival requirement, reviewed by Rosano et al. (2014). However, the co-expression of recombinant proteins encoded in vectors with identical replicons has been demonstrated to be feasible (Yang *et al.*, 2001). Also important for the co-expression of recombinant proteins is that they must be encoded in vector plasmids with different selection markers (Kholod and Mustelin, 2001).

Protein over expression in *E. coli* cells also presents some challenges which can be alleviated or circumvented by altering the expression system or modifying growth conditions. These include the formation of inclusion bodies, codon bias, recombinant protein toxicity and posttranslational modifications (Kaur *et al*., 2018). Though inclusion body formation may protect proteins from

proteolytic degradation, it obstructs the retrieval of the correctly folded recombinant protein in adequate amounts (Burgess, 2009). Lowering the temperature of incubation and inducer concentration is a solution to avert inclusion bodies (García-Fraga *et al*., 2015). Co-expressing the protein in the presence of molecular chaperones could block the formation of aggregates (de Marco *et al*., 2007). The natural bacterial chaperone response may also be induced to solubilize the protein of interest by adding alcohols to the growth media (de Marco *et al*., 2005). Solubilization reagents such as Triton X-100 and sarkosyl may also be used to retrieve the protein of interest from inclusion bodies (Tao *et al*., 2010). The solubility of proteins that form inclusion bodies is also enhanced by expressing them as fusion proteins using a fusion tag such as the maltose binding protein (MBP) and glutathione S-transferase (Bedouelle and Duplay, 1988; Smith and Johnson, 1988; Sachdev and Chirgwin, 1999). Codon bias is the phenomenon of organisms having divergent codons for same amino acid (Gouy and Gautier, 1982). Heterologous protein expression in *E. coli* from a gene containing exogenous codons may result in incomplete protein synthesis (Kaur *et al*., 2018). To prevent this, codon optimization is carried out in order to express a gene that comprises codons that are compatible with the *E. coli* tRNA complement. Alternatively, *E. coli* Rosetta 2 (DE3) pLysS, and BL21-codon Plus series of strains may be used to express genes made up of rare codons.

The affinity tag is important for downstream isolation and purification of the recombinant protein, after expression has been concluded (Kaur *et al*., 2018). Purification relies on the use of peptide affinity tags occurring at the N- or C-terminus of the protein of interest (Bornhorst and Falke, 2000). An advantage of using affinity tags is that specific antibodies are available for protein detection, even in cases whereby the proteins cannot be detected by SDS-PAGE (Rosano and Ceccarelli, 2014). A commonly used affinity tag is the hexahistidine (his) tag, a peptide tag, which is applicable for nickel affinity chromatography (Bornhorst and Falke, 2000). Nickel ions are attached to nitrilotriacetic acid-agarose (Ni-NTA) resins, allowing for the specific binding of proteins containing the his tag (Crowe *et al*., 1994). In this way, non-bound proteins from the *E. coli* cell extract can be washed away, and the protein of interest eluted using histidine or imidazole (Janknecht and Nordheim, 1992; Terpe, 2003). Imidazole may have adverse structural or functional influence on protein structure (Hefti *et al*., 2001), necessitating buffer exchange for its removal.

The heterologous expression and purification of Hsp70 chaperones of parasitic origin has been carried out in various biochemical and biophysical studies (Shonhai *et al*., 2008; Burger *et al*., 2014). For *T. brucei*, the cytosolic Hsp70, TbHsp70, has been determined to be upregulated under heat shock, with its co-chaperone J-protein (Tbj2) being essential for cell survival (Ludewig *et al*., 2015; Bentley and Boshoff, 2019). Heterologous protein expression and purification has been carried out in several studies whereby important biochemical parameters of the cytosolic Hsp70s of *T. brucei* have been determined *in vitro* (Burger *et al*., 2014; Bentley and Boshoff, 2019; Burger *et al*., 2021). This characterization has

also extended to the screening of potential inhibitors of the *T. brucei* Hsp70s (Andreassend *et al*., 2020; Burger *et al*., 2021). The mitochondrial paralogue of TbHsp70 has been determined to play a key role in mitochondrial DNA maintenance *in vivo* (Týč *et al*., 2015). MtHsp70s are usually challenging to purify from *E. coli* expression systems due to their insoluble nature (Sichting *et al*., 2005). For *in vitro* characterization, mtHsp70s are co-expressed with Hep1 in order to extract them natively, in a soluble and functional state (Nyakundi *et al*., 2016; Dores-Silva *et al*., 2017, 2021). Hep1 is a partner/co-chaperone protein of mtHsp70, which has been characterized in the *P. falciparum* and *L. braziliensis* parasites, having the ability to enhance the solubility of mtHsp70 (Nyakundi et al., 2016; Dores-Silva et al., 2015). Evidence of Hep1 possessing intrinsic holdase capabilities, like type I and type II J-proteins, has also been presented for the human Hep1 orthologue (Goswami *et al*., 2010; Dores-Silva *et al*., 2021).

The aim of this study was to determine the sets of parameters required for the optimal heterologous expression and subsequent purification of TbHep1 and TbmtHsp70 as well as the previously characterized HsHep1, HSPA9, TbHsp70, Tbj2, HSPA1A and Hsp33 recombinant proteins (Dores-Silva *et al*., 2013; Burger *et al*., 2014; Dores-Silva *et al*., 2015; Bentley *et al*., 2019). TbHep1 characterization has not been carried out prior to this study and TbmtHsp70 is expected to be insoluble as has widely been reported for mtHsp70s (Nyakundi *et al*., 2018). Therefore, this study also sought to investigate the ability of TbHep1 to enhance the solubility and functionality of TbmtHsp70, in comparison to the human counterparts HsHep1 and HSPA9, when co-expressed in *E. coli* cells (Dores-Silva *et al*., 2013).

3.2 Specific objectives

- Determination of the integrity of the pQE30-TbHep1, pQE30-TbmtHsp70, pQE2-HsHep1, pET28a-HSPA9, pQE2-TbHsp70 and pET28a-Tbj2 plasmid constructs by means of diagnostic restriction enzyme digestions.
- Insert the TbHep1 gene from the pQE30 vector into pACYCDuet-1 for co-expression studies and confirm the pACYCDuet-1-TbHep1 plasmid construct by means of diagnostic restriction enzyme digestion.
- Heterologous expression of TbHep1, HsHep1, TbHsp70, Tbj2, HSPA1A and Hsp33 in *E. coli* cells.
- Heterologous co-expression of TbmtHsp70 and HSPA9 with TbHep1 and HsHep1, respectively, and determine the ability of the Hep1 orthologues to enhance the solubility of the mtHsp70s.
- Purify TbHep1, TbmtHsp70, HsHep1, HSPA9, TbHsp70, Tbj2, HSPA1A and Hsp33 by means of nickel affinity chromatography.

3.3 Materials and methods

3.3.1 Materials

The expression plasmids pQE30-TbHep1, pQE30-TbmtHsp70, pQE2-HsHep1, pET28a-HSPA9, pET23a-HsHep1, pQE2-TbHsp70, pET28a-Tbj2, pET28a-HSPA1A and pET11a-Hsp33 were obtained from different sources and are listed in Table 3.1. Details about the *E. coli* strains used in this study are provided in Table 3.2. The reagents used were sourced or obtained from different suppliers. Ampicillin sodium salt, tryptone, yeast extract, bacteriological agar, sodium chloride and adenosine 5` - triphosphate disodium salt were purchased from Sigma-Aldrich (U.S.A.). Kanamycin sulphate and chloramphenicol were sourced from ThermoFisher Scientific (U.S.A.) and Calbiochem (U.S.A.), respectively. Sodium phosphate dibasic, potassium dihydrogen phosphate and potassium chloride were obtained from Merck (Germany). Sodium dodecyl sulphate, β-mercaptoethanol, bromophenol blue, ethidium bromide, ethylenediaminetetraacetic acid disodium salt dihydrate (EDTA sodium salt), tris (hydroxymethyl) aminomethane (Tris base) and N-(2-hydroxyethyl) piperazine-N`-(2-ethanesulphonic acid) (HEPES) were sourced from Sigma-Aldrich (U.S.A.). SeaKem® LE agarose was obtained from Lonza (Switzerland). Hydrochloric acid, methanol, Coomassie brilliant blue G 250, glycerol, glacial acetic acid, Tween® 20, polyethylene glycol 20 000 (PEG), glycine and dithiothreitol were obtained from Merck (Germany). Ammonium persulphate (APS), N-lauroylsarcosine (sarkosyl), lysozyme from chicken egg white, phenylmethanesulphonyl fluoride (PMSF) and Bradford reagent were obtained from Sigma-Aldrich (U.S.A.). The restriction enzymes were purchased from either ThermoFisher Scientific (U.S.A.) or New England Biolabs (U.S.A.). The 1kb DNA ladder and the T4 DNA ligase were purchased from New England Biolabs (U.S.A.) and ThermoFisher Scientific (U.S.A.), respectively. 30 % arylamide/bis solution 29:1, nitrocellulose membrane 0.45 µM, *N,N,N`,N`* - tetramethylethylenediamine (TEMED), the Clarity™ western ECL substrate and the Precision plus protein™ all blue standards were sourced from BIO-RAD (U.S.A.). Isopropyl-β-D-1-thiogalactopyranoside (IPTG) dioxane free, SnakeSkin™ dialysis tubing 10 kDa MWCO and the GeneJet gel extraction kit were obtained from ThermoFisher Scientific (U.S.A.). The Bovine serum albumin and the cOmplete™ his-tag purification resin were sourced from Roche (Switzerland). The Zyppy™ plasmid miniprep kit was sourced from ZymoResearch (U.S.A.). The anti-his-tag antibody (H-3) and m-IgGκ BP-HRP were sourced from Santa Cruz Biotechnology (U.S.A.). Plastic ware (lab consumables) and 96-well plates were procured from Quality Scientific Plastics (U.S.A.), Nest Scientific (U.S.A.), Corning (U.S.A.) and Greiner Bio-One (Germany).

Table 3.1: Description of the plasmids used in this study.

Plasmid	Description	Source or Reference
pQE30-TbHep1	pQE30 encoding TbHep1, Amp^R	This study
pQE30-TbmtHsp70	pQE30 encoding TbmtHsp70, Amp^R	This study
pACYCDuet-1-TbHep1	pACYC-Duet-1 encoding TbHep1, Cam^R	This study
pQE2-TbHsp70	pQE2 encoding TbHsp70, Amp^R	Dr Stephen Bentley, (Bentley and Boshoff, 2019)
pET28a-Tbj2	pET28a encoding Tbj2, Kan^R	Dr MHL Ludewig, (Burger *et al*., 2014)
pQE2-HsHep1	pQE2 encoding HsHep1, Amp^R	Prof. J-C Borges, (Dores-Silva *et al*., 2013)
pET28a-HSPA9	pET28a encoding HSPA9, Kan^R	Prof. J-C Borges, (Dores-Silva et al., 2013, p. 70)
pET23a-HsHep1	pET23a encoding HsHep1, Amp^R	Prof. J-C Borges, (Dores-Silva et al., 2015, p. 70)
pET28a-HSPA1A	pET28a encoding HSPA1A, Kan^R	Prof. J-C Borges, (Borges and Ramos, 2006)
pET11a-Hsp33	pET11a encoding *E. coli* Hsp33, Amp^R	Prof. D Reichmann

The *E. coli* strains used for propagating the plasmids or expressing the proteins encoded in the gene inserts were selected on the basis of various factors, including origin of replication, the promoter system and selection markers. In Table 3.2, the genotypic characteristics of the *E. coli* strains are listed, whilst in Table 3.1, the selection markers of the plasmids are also listed.

Table 3.2: Description of the *E. coli* strains used in this study.

Cloning		
Strain	**Genotype**	**Source or Reference**
E. coli DH5α	*end*A1, *rec*A1, *gyr*A96, *thi*, *hsd*R17, *rel*A1, *sup*E44, Δ*lac*U169, Φ80 *lac*ZΔM15	(Meselson and Yuan, 1968)
E. coli JM109	*rec*A1, *end*A1, *sup*E44, *hsd*R17, *gyr*A96, *thi*, *rel*A1, λ^{-1} Δ*(lac-pro*AB) F *tra*D36 *pro*AB *lac*IqZ ΔM15	(Yanisch-Perron *et al*., 1985)
Expression		
Strain	**Genotype**	**Source or Reference**
E. coli M15 (pREP4)	*lac*, *ara*, *gal*, *mtl*, *rec*A, *uvr*, pREP4, *lac*I, Kan^R	(Villarejo and Zabin, 1974)
E. coli XL1 Blue	F, *Tn10*, *proA*$^+$*B*$^+$, *lacI*^{q}, *lacZΔM15, recA1, endA1, gyrA96,* (Nal^R), *thi, hsdR17, rK*$^-$ *mK*$^+$, *glnV44, relA1, lac*	(Bullock *et al*., 1987)
E. coli BL21 (DE3)	F^-, *omp*T, *hsd*S_B, (r_B^-, m_B^-), *gal*, *dcm*, (DE3)	(Studier and Moffatt, 1986)

3.3.2 Methods

3.3.2.1 Construction and confirmation of the pQE30-TbHep1, pQE30-TbmtHsp70 and pACYCDuet-1-TbHep1 recombinant plasmids

The pQE30 plasmids encoding full length codon optimized TbHep1 (TriTrypDB accession: Tb927.3.2300) and codon optimized TbmtHsp70 (TriTrypDB accession: Tb927.6.3740) were synthesized by Genscript (Piscataway, New Jersey, U.S.A.), ligated at the *Bam*HI and *Hind*III restriction sites of the multiple cloning site (MCS). The plasmids were confirmed by means of restriction digestions (Appendix B1.5). The pQE30-TbHep1 plasmid was restricted with *Bam*HI and *Hind*III and the TbHep1 coding region was cut out from the agarose gel purified and then ligated into *Bam*HI and *Hind*III double digested pACYCDuet-1 (Appendix B1.8). The pACYCDuet-1-TbHep1 vector was confirmed by agarose gel electrophoresis (Appendix B1.6), following diagnostic restriction enzyme digestions (Appendix B1.5).

3.3.2.2 Confirmation of the pQE2-HsHep1, pET28a-HSPA9, pET28a-Tbj2 and pQE2-TbHsp70 recombinant plasmids

The integrity of the plasmid constructs (Table 3.1) was confirmed by restriction enzyme digestions (Appendix B1.5) and agarose gel electrophoresis (Appendix B1.6).

3.3.2.3 Induction studies to assess the expression profiles of the proteins in *E. coli*

The *E. coli* expression strains were transformed with DNA plasmids encoding the heat shock proteins (Table 3.3 & Appendix B1.3). Single colonies from the transformation were then inoculated into sterile 10 mL of 2x YT broth (Appendix B1.1) supplemented with the appropriate antibiotics, and incubated

overnight at 37 °C, with agitation, to make the starter culture. After overnight incubation, the 10 mL starter culture was transferred to 90 mL of sterile 2x YT broth supplemented with the appropriate antibiotics. The cultures were allowed to grow at 37 °C with agitation until the mid-log phase of growth as determined by measuring absorbance (turbidity) at 600 nm. At this point, a 1 mL cell sample was taken before protein expression was induced by adding IPTG to a final concentration of 1 mM. Thereafter the cells were incubated at 37 °C with agitation, with 1 mL samples being taken at hourly intervals up to the fifth hour. An overnight 1 mL sample of the culture was also taken. The cell samples taken from the culture were centrifuged at 10 000 *g* for 2 minutes. The supernatant was discarded and the cells were resuspended in PBS buffer (10 mM Na_2HPO_4, 2 mM KH_2PO_4, 137 mM NaCl, 2.7 mM KCl) of different volumes in order to ensure that all the samples had the same cell concentration, using the following equation:

$$\text{PBS buffer volume (µl)} = \text{O.D.}_{600} \text{ x 2 x 150 x dilution factor}$$

The resuspended cells were then analyzed by SDS-PAGE (Appendix B1.9). The protein of interest was also detected by means of western blotting (Appendix B1.10). For SDS-PAGE the Bio-Rad Precision-Plus™ All Blue standards was used as the molecular weight marker (Bio-Rad, U.S.A.). For western blotting the anti-his-tag primary antibody (H-3) (1: 2500 dilution) (Santa Cruz Biotechnology, U.S.A) and m-IgGκ BP-HRP (1: 3000 dilution) (Santa Cruz Biotechnology, U.S.A.) were used as primary and secondary antibodies, respectively.

Table 3.3: Details of the *E. coli* strains that were used for each plasmid.

Protein	Expression plasmid	Expression strain used
TbHep1	pQE30-TbHep1	*E. coli* M15 (pREP4)
TbmtHsp70	pQE30-TbmtHsp70	*E. coli* M15 (pREP4)
TbHsp70	pQE2-TbHsp70	*E. coli* XL1 Blue
Tbj2	pET28a-Tbj2	*E. coli* BL21 (DE3)
HsHep1	pQE2-HsHep1	*E. coli* XL1 Blue
HSPA9	pET28a-HSPA9	*E. coli* BL21 (DE3)
HSPA1A	pET28a-HSPA1A	*E. coli* BL21 (DE3)
Hsp33	pET11a-Hsp33	*E. coli* BL21 (DE3)

3.3.2.4 Co-expressing TbmtHsp70 and HSPA9 with TbHep1 and HsHep1 respectively.

The co-expression of TbmtHsp70 with TbHep1 was adapted from Nyakundi et al. (2016). The proteins were co-expressed in *E. coli* BL21 (DE3) cells co-transformed with pQE30-TbmtHsp70 and pACYCDuet-1-TbHep1. The co-expression of HSPA9 and HsHep1 was adapted from Dores-Silva et al. (2013). The proteins were co-expressed in *E. coli* BL21 (DE3) cells co-transformed with pET28a-

HSPA9 and pQE2-HsHep1. Protein expression was carried out as detailed in Section 3.3.2.3. SDS-PAGE and western blotting analysis were also conducted (Appendices B1.9 & B1.10).

3.3.2.5 Solubility studies of TbmtHsp70 and HSPA9

Solubility studies were carried out on TbmtHsp70 and HSPA9 expressed alone or in combination with TbHep1 and HsHep1, respectively. The transformed *E. coli* cells were grown until optimal protein production was achieved (Sections 3.3.2.3 & 3.3.2.4). Thereafter the cultures were centrifuged at 7 500 *g* for 15 minutes to harvest the cells. The pelleted cells were then resuspended in lysis buffer (100 mM Tris-HCl pH 7.5, 300 mM NaCl) supplemented with lysozyme and PMSF. The resultant lysate was frozen at -80 °C overnight. The frozen lysate was thawed on ice before being sonicated (Appendix B1.14). After sonication, an aliquot of the whole cell lysate was kept for SDS-PAGE and western blotting analysis (Appendices B1.9 & B1.10). The sonicated lysate was then centrifuged at 15 000 *g* for 45 minutes at 4 °C. After centrifugation, an aliquot of the supernatant was kept for SDS-PAGE and western blotting analysis (Appendices B1.9 & B1.110). The rest of the supernatant was removed, and the cells resuspended in PBS buffer up to the volume of the removed supernatant. A sample of the resuspended pellet was then analysed by SDS-PAGE and western analysis (Appendices B1.9 & B1.10).

3.3.2.6 Purification of recombinant proteins by nickel affinity chromatography

The protein purification procedures applied in this study were adapted from Burger et al. (2014), Nyakundi et al. (2016), and Bentley and Boshoff. (2019). After IPTG induction, protein expression was carried out for an optimal period as determined by the induction study. Thereafter, the culture was centrifuged at 7 500 *g* at 4 °C for 15 minutes. The pelleted cells were then resuspended in lysis buffer (100 mM Tris-HCl pH 7.5, 300 mM NaCl) supplemented with lysozyme and PMSF. The resultant cell lysate was then frozen at -80 °C overnight. The frozen lysate was then thawed on ice, before being sonicated (Appendix B1.14). The sonicated lysate was then centrifuged at 15 000 *g* for 45 minutes at 4 °C, and the supernatant containing the cell extract was mixed with the cOmplete his-tag purification resin (Roche, Switzerland) acclimatized in lysis buffer (100 mM Tris-HCl pH 7.5, 300 mM NaCl). The resin and cell extract were then incubated overnight at 4 °C with agitation. To purify the protein of interest, the resin was washed 4 times with wash buffer (100 mM Tris-HCl pH 7.5, 300 mM NaCl) containing 5 mM imidazole, each wash being 10 minutes. For the purification of TbHep1, HsHep1, and Tbj2, the wash buffer contained 2 mM of ATP to eliminate the possibility of *E. coli* DnaK contamination (Burger *et al*., 2014). For the purification of TbmtHsp70 and HSPA9 co-expressed with TbHep1 and HsHep1, respectively, 2 mM ATP was also used to ensure that the mtHsp70s are purified free of the Hep1 orthologues. Between the washes, the unbound proteins and the his-tag resin were separated by centrifugation at 7 000 *g* at 4 °C for 4 minutes, with most of the supernatant being discarded. After the washes, the protein of interest was eluted with buffer (100 mM Tris-HCl pH 7.5, 300 mM NaCl, 250 mM imidazole) 4 times, each elution being 30 minutes. Between the elutions, the purified protein and

the his-tag resin were separated by centrifugation at 7 000 *g* at 4 °C for 4 minutes. The protein of interest was obtained by keeping the supernatant after centrifugation. Small aliquots from each step of the purification were subjected to SDS-PAGE and western analysis (Appendices B1.9 & B1.10). Subsequent to elution, buffer exchange was carried out on the eluted proteins by extensive dialysis to remove imidazole (10 mM Tris-HCl pH 7.5, 100 mM NaCl, 0.5 mM DTT, 50 mM KCl, 10 % glycerol [v/v]) using SnakeSkin™ dialysis tubing 10 kDa MWCO (ThermoFisher Scientific, U.S.A.) (Appendix A.11). The proteins were then concentrated using PEG 20 000. Protein concentration was determined using the Bradford assay (Appendix B1.12).

3.4 Results and discussion

3.4.1 Heterologous expression and the subsequent purification of the proteins

Herein the expression and purification of the proteins of interest are reported and discussed.

3.4.1.1 TbHep1

The pQE30-TbHep1 plasmid was synthesized by GenScript (U.S.A.), with the TbHep1 encoding sequence ligated at the *Bam*HI and *Hind*III restriction sites of the vector's MCS (Figure 3.1A). The structural integrity of the plasmid was confirmed by means of restriction digestions with *Bam*HI and *Hind*III and agarose gel electrophoresis (Appendices B1.5 & B1.6). Digestion with either of the restriction enzymes resulted in the linear conformation of the plasmid (3959 bp) (Figure 3.1B, lanes B & H). The double digestion with *Bam*HI and *Hind*III yielded fragments of approximately 3461 bp and 498 bp, corresponding to the sizes of the pQE30 vector and the TbHep1 gene, respectively (Figure 3.1B, lane B/H). The pQE30-TbHep1 plasmid was successfully confirmed by diagnostic restriction enzyme digestion.

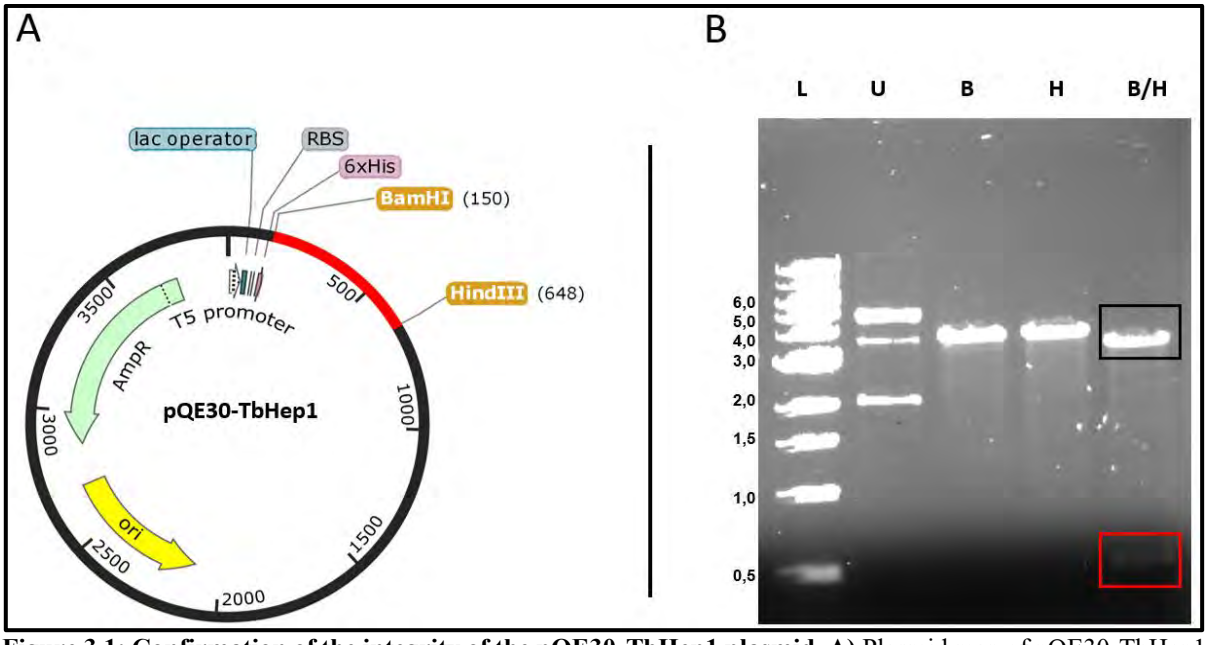

Figure 3.1: Confirmation of the integrity of the pQE30-TbHep1 plasmid. A) Plasmid map of pQE30-TbHep1 was generated using the SnapGene 5.0.7 software. The *Bam*HI and *Hind*III restriction sites occur immediately upstream and downstream of the TbHep1 insert (in red), respectively. **B)** Restriction enzyme digestion of pQE30-TbHep1 separated at 100 V on a 0.8 % agarose gel. In lane L is the DNA ladder (1 kb DNA ladder, New England

Biolabs). In lane U is the uncut plasmid. In lanes B and H are the *Bam*HI and *Hind*III single cuts of the plasmid, respectively. In lane B/H is the double digestion of the plasmid, with the larger and smaller fragments representing the pQE30 vector (3419 when *Bam*HI/*Hind*III double digested bp, inside black box) and TbHep1 insert (498 bp, inside red box), respectively.

The plasmid was transformed into *E. coli* M15 (pREP4) cells for purposes of protein expression analysis by SDS-PAGE and western blotting (Figure 3.2) (Appendices B1.9 & B1.10). Following IPTG induced expression, there is an increased visibility of protein bands of approximately 25 kDa and 20 kDa over time (Figure 3.2A, lanes 1-5 & 18). The protein was not observed in lane U before induction with IPTG. The optimal time point for TbHep1 induction was determined to be 3 hours, and the cell culture was harvested 3 hours post induction for lysing and subsequent nickel affinity chromatography for protein purification. Since there are two bands that seemed to increase in visibility due to IPTG induced protein expression, the band representing TbHep1 was confirmed to be the one occurring at approximately 20 kDa after nickel affinity chromatography (Figure 3.2B, lanes E1-E3 & B). The molecular weight of TbHep1 is predicted to be 22.08 kDa. The presence of TbHep1 was further confirmed by western analysis that is specific to TbHep1's N-terminal his-tag (Figure 3.2, lower panels).

The *P. falciparum* counterpart of TbHep1 was also successfully purified using the same expression system under similar conditions (Nyakundi *et al*., 2016). However, PfHep1 proved to be insoluble, requiring the sarkosyl detergent for solubilization (Nyakundi *et al*., 2016). *P. falciparum* proteins are generally challenging to purify, even when codon optimized for expression in *E. coli* cells (Muralidharan and Goldberg, 2013). TbHep1 was purified with high levels of purity as can be visually observed, routinely yielding concentrations greater than 1 mg/mL as determined by Bradford assay analysis (Appendix B1.12). No protein was lost with the unbound protein and washes (Figure 3.2B, lanes U, W1 & W4), however a considerable amount of the protein was still bound to the beads post elution (Figure 3.2B, lane B). Important in the purification of TbHep1 was the elimination of the possibility of DnaK contamination by introducing ATP to the wash buffers, as has been reported for J-proteins (Burger *et al*., 2014).

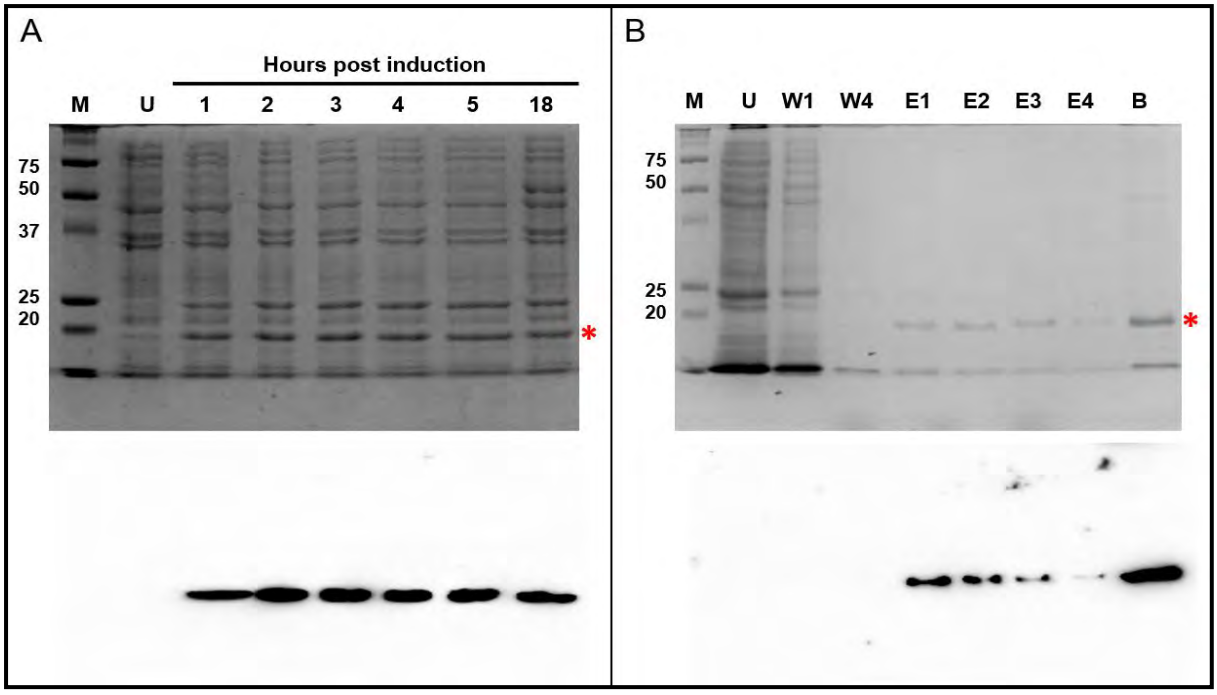

Figure 3.2: SDS-PAGE analysis of the expression and purification of TbHep1 heterologously expressed in *E. coli* M15 (pREP4/pQE30-TbHep1). A) Induction study of TbHep1 in a Coomassie-stained 15 % acrylamide gel. In lane M is the protein molecular weight marker (Bio-Rad Precision-Plus™ All Blue standards) and in lane U is the un-induced whole cells. 1-5: Hourly samples one to five hours post IPTG induction (whole cell extract), 18: Overnight induction sample (whole cell extract). **B)** Purification of TbHep1 in a Coomassie-stained 15 % acrylamide gel. In lane M is the protein molecular weight and in lane U is the unbound protein (flow-through) sample. In lanes W1 and W4 are the first and fourth (final) wash samples, respectively. In lanes E1 to E4 are the elution samples, and in lane B is the bead sample post elution. The red asterisks indicate the points at which bands representing TbHep1 occur on the acrylamide gels. **Lower panels)** Corresponding Western blot images generated using mouse anti-his-tag (H-3) monoclonal antibodies (Santa Cruz).

3.4.1.2 TbmtHsp70

The structural integrity of the plasmid was confirmed by means of restriction digestions with *Bam*HI and *Hind*III and agarose gel electrophoresis (Figure 3.3) (Appendices B1.5 & B1.6). Digestion with either of the restriction enzymes resulted in the linear conformation of the plasmid (5372 bp) (Figure 3.3B, lanes B & H). The double digestion with *Bam*HI and *Hind*III yielded fragments of approximately 3461 bp and 1911 bp, corresponding to the sizes of the pQE30 vector and the TbmtHsp70 gene, respectively (Figure 3.3B, lane B/H).

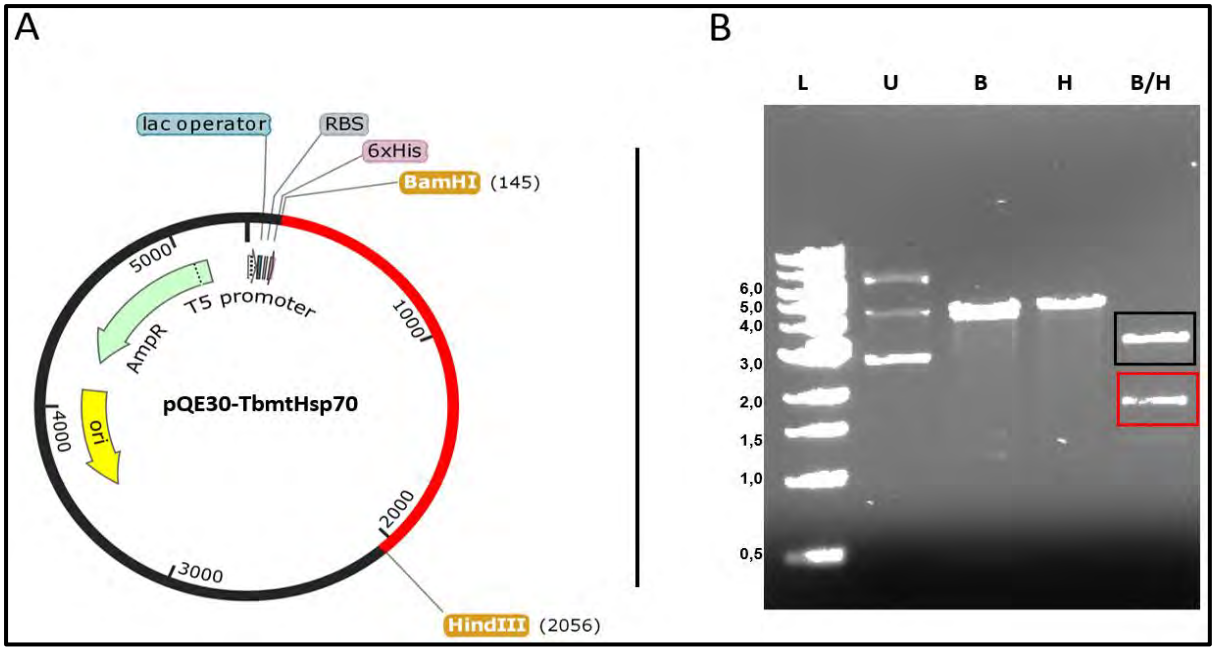

Figure 3.3: Confirmation of the integrity of the pQE30-TbmtHsp70 plasmid DNA. A) Plasmid map of pQE30-TbmtHsp70 generated using the SnapGene 5.0.7 software. The *Bam*HI and *Hind*III restriction sites occur immediately upstream and downstream of the TbmtHsp70 insert (in red), respectively. **B)** Restriction enzyme digestion of pQE30-TbmtHsp70 separated at 100 V on a 0.8% agarose gel. In lane L is the DNA ladder (1 kb DNA ladder, New England Biolabs). In lane U is the uncut plasmid. In lanes B and H are the *Bam*HI and *Hind*III single cuts of the plasmid, respectively. In lane B/H is the double digestion of the plasmid, with the larger and smaller fragments representing the pQE30 vector (3419 bp when *Bam*HI/*Hind*III double digested, inside black box) and TbmtHsp70 insert (1911 bp, inside red box), respectively.

The plasmid was transformed into *E. coli* M15 (pREP4) cells for purposes of protein expression analysis by SDS-PAGE and western blotting (Figure 3.4) (Appendices B1.9 & B1.10). Following IPTG induced protein expression, there is an increased visibility of a protein band of approximately 70 kDa over time (Figure 3.4A, lanes 1-5 & 18). The band cannot be observed in the uninduced sample (Figure 3.4A, lane U). The molecular weight of TbmtHsp70 is predicted to be 71,48 kDa. The presence of TbmtHsp70 was further confirmed by western analysis using the N-terminal his-tag on the protein (Figure 3.4, lower panels). Optimal protein over expression was determined to be achieved 5 hours post IPTG induction and cells were harvested and lysed for subsequent solubility studies and nickel affinity chromatography. TbmtHsp70 was determined to be insoluble (Figure 3.4B), a trait that is synonymous with mtHsp70 proteins (lane P, Figure 3.4B) (Sichting *et al*., 2005). No TbmtHsp70 was detected in the supernatant (soluble) fraction (Figure 3.4B). The study by Nyakundi et al. (2016) whereby mitochondrial PfHsp70-3 was also found to be insoluble also utilised the same expression system under similar conditions. TbmtHsp70 could only be solubilized in the presence of sarkosyl, a detergent (Figure 3.4C). Treatment of the whole cell extract with sarkosyl resulted in TbmtHsp70 being present in both the supernatant (soluble) and pellet (insoluble) fractions. Sarkosyl is a known detergent that is used to extract proteins from inclusion bodies and self-aggregates (Frankel *et al*., 1991). The use of sarkosyl in the study could

serve as a good comparative control in validating the ability of TbHep1 to solubilize TbmtHsp70 when co-expressed in *E. coli*.

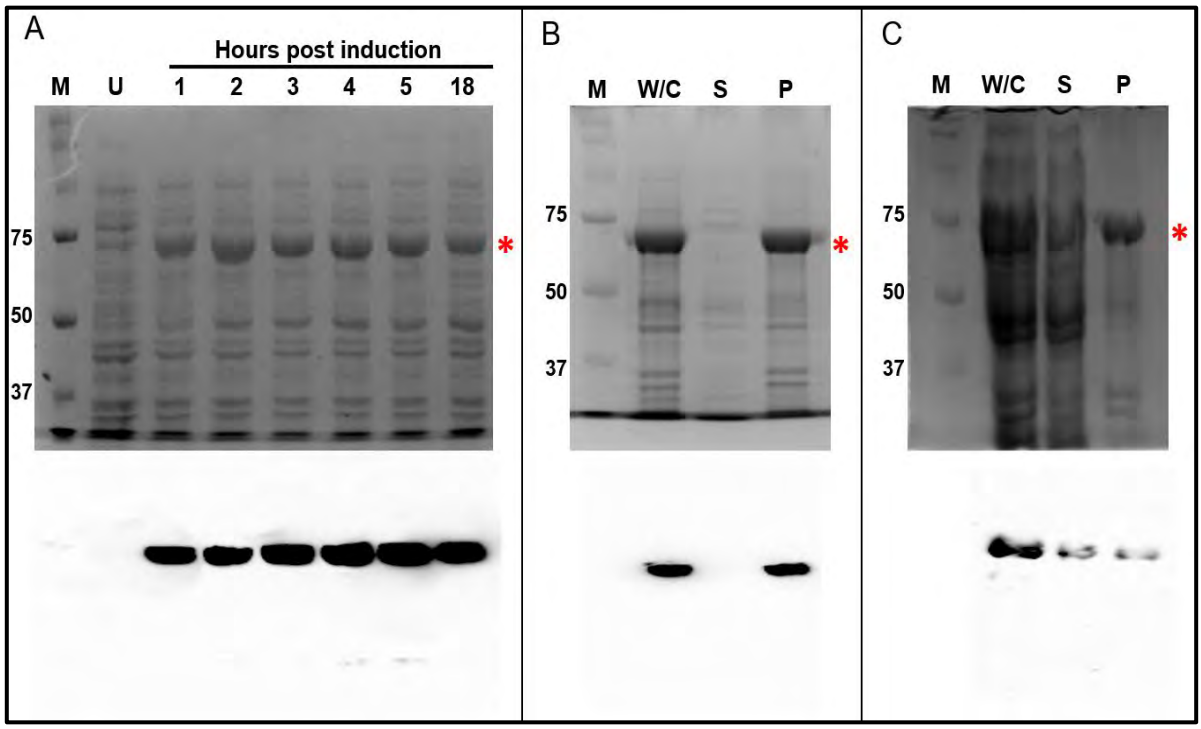

Figure 3.4: SDS-PAGE analysis of the expression and solubility of TbmtHsp70 heterologously expressed in *E. coli* M15 (pREP4/pQE30-TbmtHsp70). A) The induction study of TbmtHsp70 in a Coomassie-stained 10 % acrylamide gel. In lane M is the protein molecular weight marker (Bio-Rad Precision-Plus™ All Blue standards) and in lane U is the un-induced whole cell sample. Lanes 1-5: Hourly samples one to five hours post IPTG induction (whole cell extract), lane 18: Overnight induction sample (whole cell extract). **B)** The solubility study samples of TbmtHsp70 in a Coomassie-stained 10 % acrylamide gel. In lane M is the protein molecular weight marker. In lane W.C. is the whole cell extract of *E. coli* M15 (pREP4/pQE30-TbmtHsp70). In lane S is the supernatant (soluble fraction) of the cell lysate and in lane P is the pellet (insoluble fraction). **C)** The solubility study samples of sarkosyl-treated TbmtHsp70 in a Coomassie-stained 10 % acrylamide gel. In lane M is the protein molecular weight marker. In lane W.C. is the whole cell extract of sarkosyl-treated *E. coli* M15 (pREP4/pQE30-TbmtHsp70). In lane S is the supernatant (soluble fraction) of the cell lysate and in lane P is the pellet (insoluble fraction). The red asterisks indicate the points at which bands representing TbmtHsp70 occur on the acrylamide gels. **Lower panels)** Corresponding Western blot images generated using mouse anti-his-tag (H-3) monoclonal antibodies (Santa Cruz).

3.4.1.3 Co-expression of TbmtHsp70 and TbHep1

Co-expressing mtHsp70 with Hep1 is a strategy that is utilized to obtain the protein in a soluble and functional state (Dores-Silva *et al*., 2013; Nyakundi *et al*., 2016). The TbHep1 coding region was ligated into the pACYCDuet-1 vector to allow for the co-expression of TbmtHsp70 and TbHep1 in *E. coli* BL21 (DE3) cells (Figure 3.5). After the ligation of the TbHep1 gene into the pACYCDuet-1 vector, the structural integrity of the pACYCDuet-1-TbHep1 plasmid was confirmed by restriction digestions with *Bam*HI and *Hind*III and agarose gel electrophoresis (Figure 3.5) (Appendices B1.5 & B1.6). Digestion with either of the restriction enzymes resulted in the linear conformation of the plasmid (4506 bp) (Figure 3.5B, lanes B & H). The double digestion with *Bam*HI and *Hind*III yielded a fragment of

approximately 4008 bp and 498 bp, corresponding to the sizes of the pACYCDuet-1 vector and the TbHep1 coding region, respectively (Figure 3.5B, lane B/H). The pACYC-TbHep1 plasmid was therefore successfully confirmed by restriction enzyme digestion.

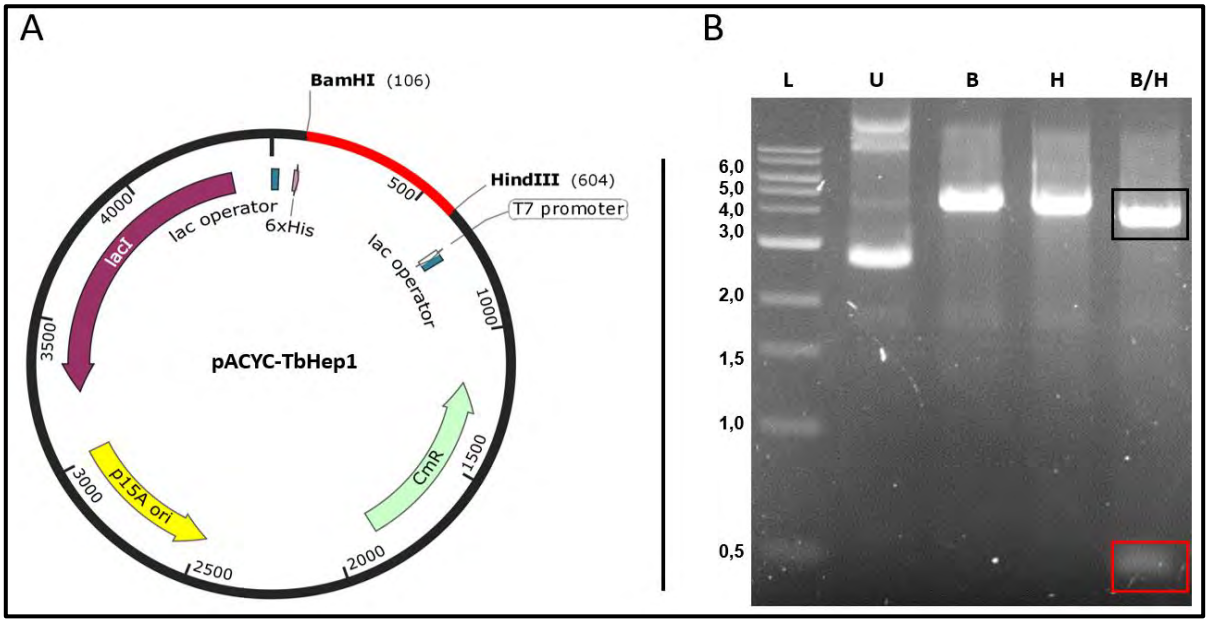

Figure 3.5: Confirmation of the integrity of the pACYC-TbHep1 plasmid. A) Plasmid map of pACYC-TbHep1 generated using the SnapGene 5.0.7 software. The *Bam*HI and *Hind*III restriction sites occur immediately upstream and downstream of the TbHep1 insert (in red), respectively. **B)** Restriction enzyme digestion of pACYC-TbHep1 separated at 80 V on a 1.0 % agarose gel. In lane L is the DNA ladder (1 kb DNA ladder, New England Biolabs) and in lane U is the uncut plasmid. In lanes B and H are the *Bam*HI and *Hind*III single cuts of the plasmid, respectively. In lane B/H is the *Bam*HI and *Hind*III double digestion of the plasmid with the larger and smaller fragments representing the pACYC-Duet1 vector (3971 bp when *Bam*HI/*Hind*III double digested, in black box) and the TbHep1 insert (498 bp, inside red box), respectively.

The co-expression of TbmtHsp70 with TbHep1 was analysed by SDS-PAGE and western blotting (Appendices B1.9 & B1.10). Following IPTG induced expression, there is an increased visibility of a protein band of approximately 70 kDa over time (Figure 3.6A, lanes 1-5 & 18). The presence of TbmtHsp70 was further confirmed by western analysis that is specific to TbmtHsp70's N-terminal his-tag (Figure 3.6, lower panels). Optimal protein expression was determined to be achieved 5 hours post IPTG induction, and the cells were harvested at this time point for lysis and subsequent solubility studies and nickel affinity chromatography.

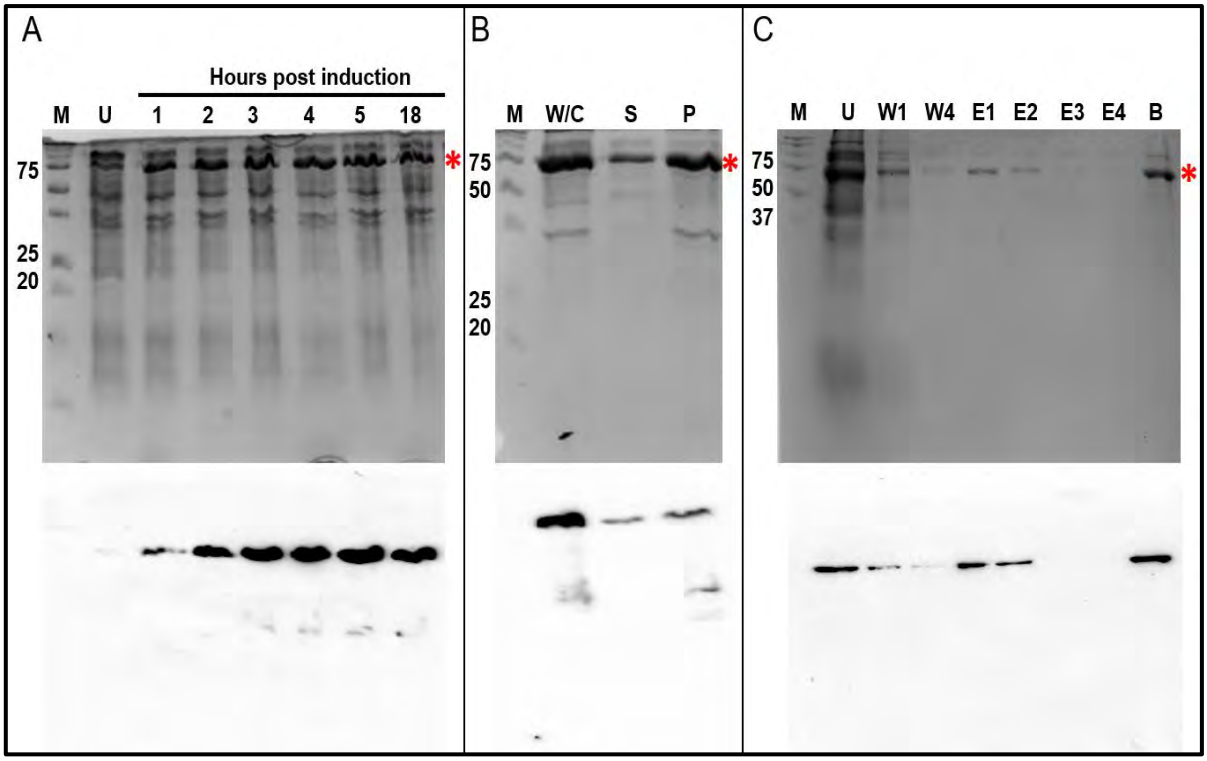

Figure 3.6: SDS-PAGE analysis of the expression, solubility and purification of TbmtHsp70 heterologously co-expressed with TbHep1 in *E. coli* BL21 DE3 (pQE30-TbmtHsp70/pACYC-TbHep1). A) The induction study of TbmtHsp70 co-expressed with TbHep1 in a Coomassie-stained 13.5 % acrylamide gel. In lane M is the protein molecular weight marker (Bio-Rad Precision-Plus™ All Blue standards) and in lane U is the un-induced cell sample. Lanes 1-5: Hourly samples one to five hours post IPTG induction (whole cell extract), lane 18: Overnight induction sample (whole cell extract). **B)** The solubility study samples of TbmtHsp70 co-expressed with TbHep1 in a Coomassie-stained 13.5 % acrylamide gel. In lane M is the protein molecular weight marker. In lane W.C. is the whole cell lysate of *E. coli* BL21 (pQE30-TbmtHsp70/pACYC-TbHep1), in lane S is the supernatant (soluble fraction) of the cell lysate and in lane P is the pellet (insoluble fraction). **C)** Purification of TbmtHsp70 after co-expression with TbHep1 in a Coomassie-stained 13.5 % acrylamide gel. In lane M is the protein molecular weight marker. In lane U is the unbound protein (flowthrough) sample, whilst in lanes W1 and W4 are the first and fourth (final) wash samples, respectively. In lanes E1 to E4 are the elution samples, and in lane B is the bead sample after post-elution. The red asterisks indicate the points at which bands representing TbmtHsp70 occur on the acrylamide gels. **Lower panels)** Corresponding Western blot generated using mouse anti-his-tag (H-3) monoclonal antibodies (Santa Cruz).

TbmtHsp70 was partially soluble when co-expressed with TbHep1 in this expression system (Figure 3.6B) as the chaperone was detected in both the supernatant (soluble) fraction and the pellet (insoluble) fraction. This observation mirrors the findings of (Dores-Silva *et al*., 2013; Nyakundi *et al*., 2016). TbHep1 was not detectable in this expression system by western analysis. This is in contrast to (Nyakundi *et al*., 2016) whereby the *P. falciparum* Hep1 was detectable when co-expressed from the pACYCDuet-1 vector with PfHsp70-3 Despite TbHep1 being undetected, soluble TbmtHsp70 was produced. This is similar to a finding by (Dores-Silva et al., 2015) whereby HsHep1 co-expressed with HSPA9 using pET23a-HsHep1 and pET28a-HSPA9 plasmids, respectively, resulted in the enhanced solubility of HSPA9, yet the HsHep1 was undetectable. Insoluble proteins have been reported to become soluble when co-expressed with molecular chaperones in *E. coli* (Yoshimune *et al*., 2004), also

comprehensively reviewed by (Martínez-Alonso *et al*., 2010). The findings that co-expression with TbHep1 renders TbmtHsp70 soluble suggests that TbHep1 is a specific chaperone of TbmtHsp70. The solubility of TbmtHsp70 when co-expressed with TbHep1 was similar to how TbmtHsp70 was solubilized by treating with sarkosyl (Figure 3.4), confirming that Hep1 in *T. brucei* also has the ability to interact with aggregated mtHsp70 in order to bring about its solubility. Consequently, TbmtHsp70 was successfully purified by nickel affinity chromatography under native conditions (Figure 3.6C). Some of the protein was lost in the unbound protein sample and the washes (Figure 3.6C, lanes U, W1 & W4). Some of the protein also remained in the beads post elution (Figure 3.6C, lane B). However, the amount of protein was sufficient for downstream biochemical characterization in the form of protein activity assays. Concentrations of purified TbmtHsp70 after co-expression with TbHep1 were usually determined to be 0.8-1 mg/mL using the Bradford assay (Appendix B1.12). The TbmtHsp70 lost in the flowthrough and washes could have been due to amount of protein extracted from the *E. coli* BL21 DE3 (pQE30-TbmtHsp70/pACYC-TbHep1) lysate exceeding the resin's binding capacity. Alternatively, the low concentration of imidazole used to reverse non-specific binding could have resulted in the loss of TbmtHsp70 in the washes. The cOmplete™ his-tag purification resin has an increased sensitivity for imidazole as it was designed for protein elution using low imidazole concentrations (Roche Diagnostics, 2020).

3.4.1.4 Human Hep1

The structural integrity of the pQE2-HsHep1 plasmid was confirmed by means of restriction digestions with *Nde*I and *Kpn*I and agarose gel electrophoresis (Figure 3.7) (Appendices B1.5 & B1.6). Digestion with either of the restriction enzymes resulted in the linear conformation of the plasmid (5301 bp) (Figure 3.7B, lanes N & K). The double digestion with *Nde*I and *Kpn*I yielded fragments of approximately 4758 bp and 543, corresponding to the sizes of the pQE2 vector and the HsHep1 gene, respectively (Figure 3.7B, lane N/K). The pQE2-HsHep1 plasmid was successfully confirmed by restriction enzyme digestions.

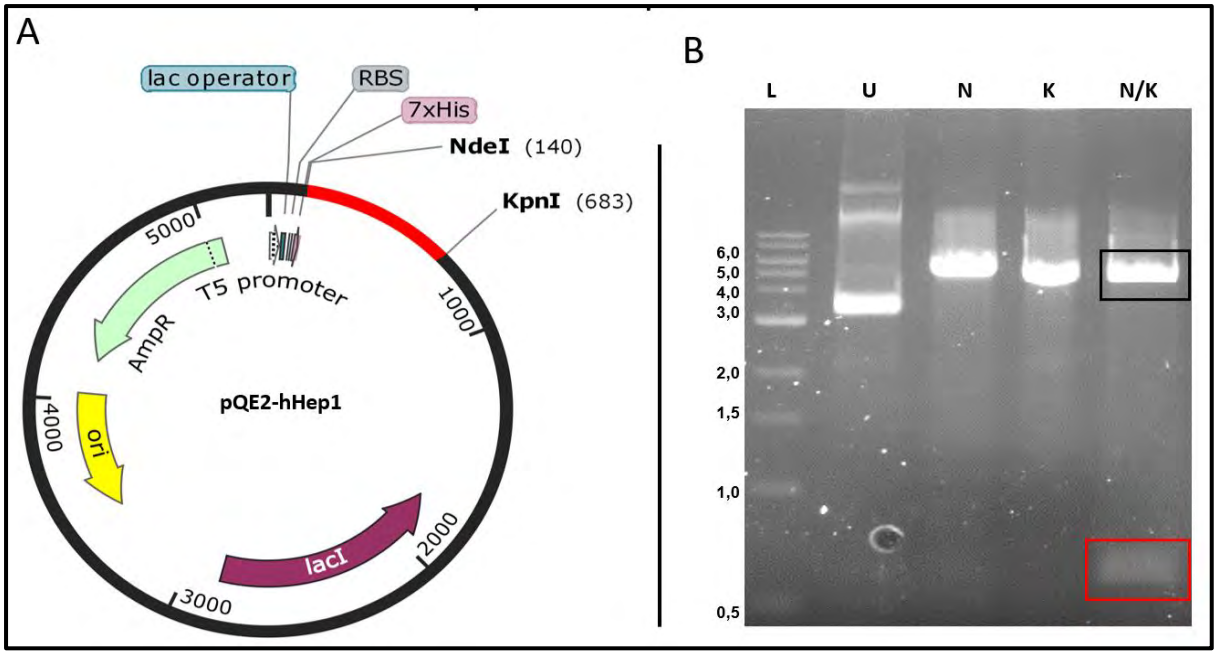

Figure 3.7: Confirmation of the integrity of the pQE2-HsHep1 vector. A) Plasmid map of pQE2-HsHep1 generated using the SnapGene 5.0.7 software. The *Nde*I and *Kpn*I restriction sites occur immediately upstream and downstream of the HsHep1 insert (in red), respectively. **B)** Restriction enzyme digestion of pQE2-HsHep1 separated at 100 V on a 0.8 % agarose gel. In lane L is the DNA ladder (1 kb DNA ladder, New England Biolabs) and in lane U is the uncut plasmid. In lanes N and K are the *Nde*I and *Kpn*I single cuts of the plasmid, respectively. In lane N/K is the *Nde*I and *Kpn*I double digestion of the plasmid, with the larger and smaller fragments representing the pQE2 vector (4725 bp when *Nde*I/*Kpn*I double digested, inside black box) and HsHep1 insert (543 bp, inside red box), respectively.

The plasmid was transformed into *E. coli* XL1 Blue cells for purposes of protein expression analysis. HsHep1 expression was analysed by SDS-PAGE and western blotting (Appendices B1.9 & B1.10). Following IPTG induced expression, there is an increased visibility of protein bands of less than 20 kDa in size over time (Figure 3.8A, lanes 1-5 & 18). The molecular weight of HsHep1 was estimated to be approximately 17 kDa. However, Hep1 has been determined to be monomeric with a molecular weight of 14.8 kDa (Dores-Silva *et al*., 2013). The optimal time required for HsHep1 expression was determined to be 4 hours, therefore the *E. coli* XL1 Blue (pQE2-HsHep1) cultures were harvested 4 hours post induction for lysing and subsequent nickel affinity chromatography. Human Hep1 was purified with high levels of purity as can be visually observed. Some of the protein was lost as unbound protein and in the washes (Figure 3.8B, lanes U, W1 & W4). Some of the protein was also bound to the beads post elution (Figure 3.8, lane B). This observation mirrors the findings of Dores-Silva et al. (2013) where HsHep1 expressed in *E. coli* BL21 (DE3) cells from the pQE2 vector yielded high concentrations and purity. The presence of HsHep1 was further confirmed by western analysis that is specific to HsHep1's N-terminal his-tag (Figure 3.8B, lower panel).

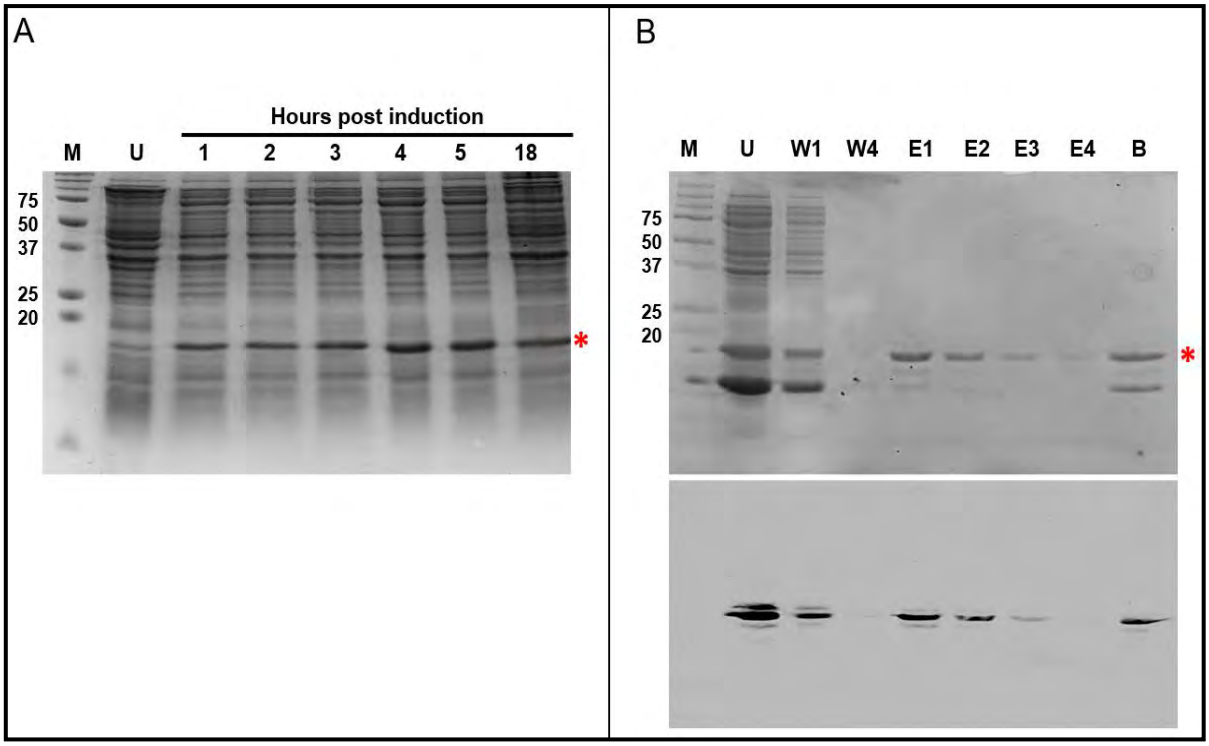

Figure 3.8: SDS-PAGE analysis of the expression and purification of HsHep1 heterologously expressed in *E. coli* XL1-Blue (pQE2-HsHep1). A) Induction study of HsHep1 in a Coomassie-stained 15 % acrylamide gel. In lane M is the protein molecular weight marker (Bio-Rad Precision-Plus™ All Blue standards) and in lane U is the un-induced cell sample. Lanes 1-5: Hourly samples one to five hours post IPTG induction (whole cell extract), lane 18: Overnight induction sample (whole cell extract). **B)** Purification of HsHep1 in a Coomassie-stained 13.5 % acrylamide gel. In lane M is the protein molecular weight marker and in lane U is the unbound protein (flowthrough) sample. In lanes W1 and W4 are the first and fourth (final) wash samples, respectively. In lanes E1 to E4 are the elution samples, and in lane B is the bead sample post-elution. The red asterisks indicate the points at which bands representing HsHep1 occur on the acrylamide gels. **Lower panel of B)** Corresponding Western blot image generated using mouse anti-his-tag (H-3) monoclonal antibodies (Santa Cruz).

Despite losing some of the protein in the washes and beads, concentrations of HsHep1 were approximately 1.5 mg/mL as determined by Bradford assay quantification (Appendix B1.12). Excess HsHep1 remained bound to the resin post purification. Increasing the concentration of imidazole in the elution buffers from 250 mM to 500 mM or 1 mM did not result in improved extraction.

3.4.1.5 HSPA9

The structural integrity of the pET28a-HSPA9 plasmid was confirmed by means of restriction digestions with *Bam*HI and *Nde*I and agarose gel electrophoresis (Figure 3.9 A & B) (Appendices B1.5 & A.6). Restriction with either of the restriction enzymes resulted in linear bands of the plasmid construct (Figure 3.9B, lanes B & N). The double digestion with *Bam*HI and *Nde*I yielded fragments of approximately 5369 bp and 2065 bp, corresponding to the sizes of the pET28a vector and the HSPA9 gene, respectively (Figure 3.9B, lane B/H). The pET28-HSPA9 plasmid was successfully verified by restriction enzyme digestion. The plasmid was transformed into *E. coli* BL21 (DE3) cells for purposes of protein expression analysis by SDS-PAGE (Figure 3.9C) (Appendices B1.9). Following IPTG

induced expression, there is an increased visibility of a protein band of approximately 70 kDa over time (Figure 3.9C, lanes 1-5 & 18). Optimal protein expression was determined to be achieved 5 hours post IPTG induction.

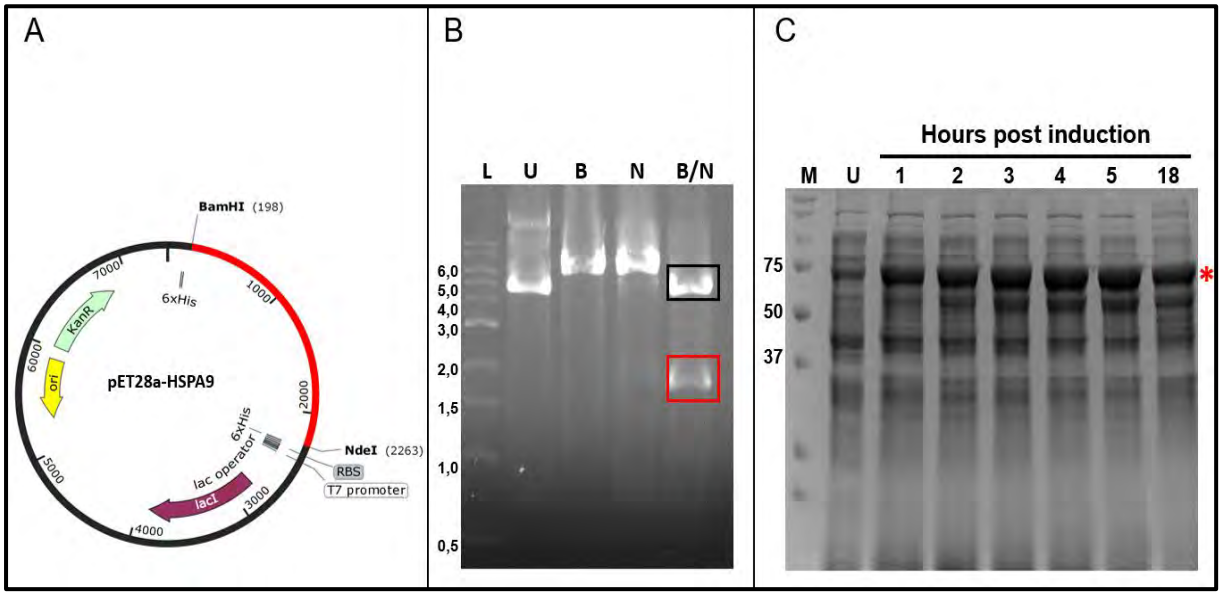

Figure 3.9: Confirmation of the integrity of the pET28a-HSPA9 vector and the expression of HSPA9 in *E. coli* BL21 (DE3) (pET28-HSPA9) cells. A) Plasmid map of pET28a-HSPA9 generated using the SnapGene 5.0.7 software. The *Bam*HI and *Nde*I restriction sites occur immediately upstream and downstream of the HSPA9 insert (in red), respectively. **B)** Restriction enzyme digestion of pET28a-HSPA9 separated at 100 V on a 0.8 % agarose gel. In lane L is the DNA ladder (1 kb DNA ladder, New England Biolabs) and in lane U is the uncut plasmid. In lanes B and N are the *Bam*HI and *Nde*I single cuts of the plasmid, respectively. In lane B/N is the *Bam*HI and *Nde*I double digestion of the plasmid, with the larger and smaller fragments representing the pET28a vector (5329 bp when *Bam*HI/*Nde*I double digested, inside black box) and HSPA9 insert (2065 bp, inside red box), respectively. **C)** The induction study of HSPA9 in a Coomassie-stained 10 % acrylamide gel. In lane M is the protein molecular mass marker (Bio-Rad Precision-Plus™ All Blue standards) and in lane U is the un-induced whole cell sample. Lanes 1-5: Hourly samples one to five hours post IPTG induction (whole cell extract), lane 18: Overnight induction sample (whole cell extract). The red asterisk indicates the point at which bands representing HSPA9 occur on the acrylamide gel.

3.4.1.6 Co-expression of HSPA9 with HsHep1

Since HSPA9 is known to be insoluble, a trait that is synonymous with mtHsp70 proteins, the protein was co-expressed with HsHep1. The *E. coli* BL21 (DE3) (pET28a-HSPA9/pQE2-HsHep1) cells were treated with IPTG to induce protein expression. Protein expression was analysed by SDS-PAGE and western blotting (Appendices B1.9 & B1.10). Following IPTG induced expression, there is an increased visibility of a protein band of approximately 70 kDa over time (Figure 3.10A, lanes 1-5 & 18). The band cannot be observed in the uninduced sample (Figure 3.10A, lane U). The presence of HSPA9 was further confirmed by western analysis that is specific to the N-terminal tag of HSPA9 (Figure 3.10 A & C, lower panels). Optimal protein expression was determined to be achieved 5 hours post IPTG induction.

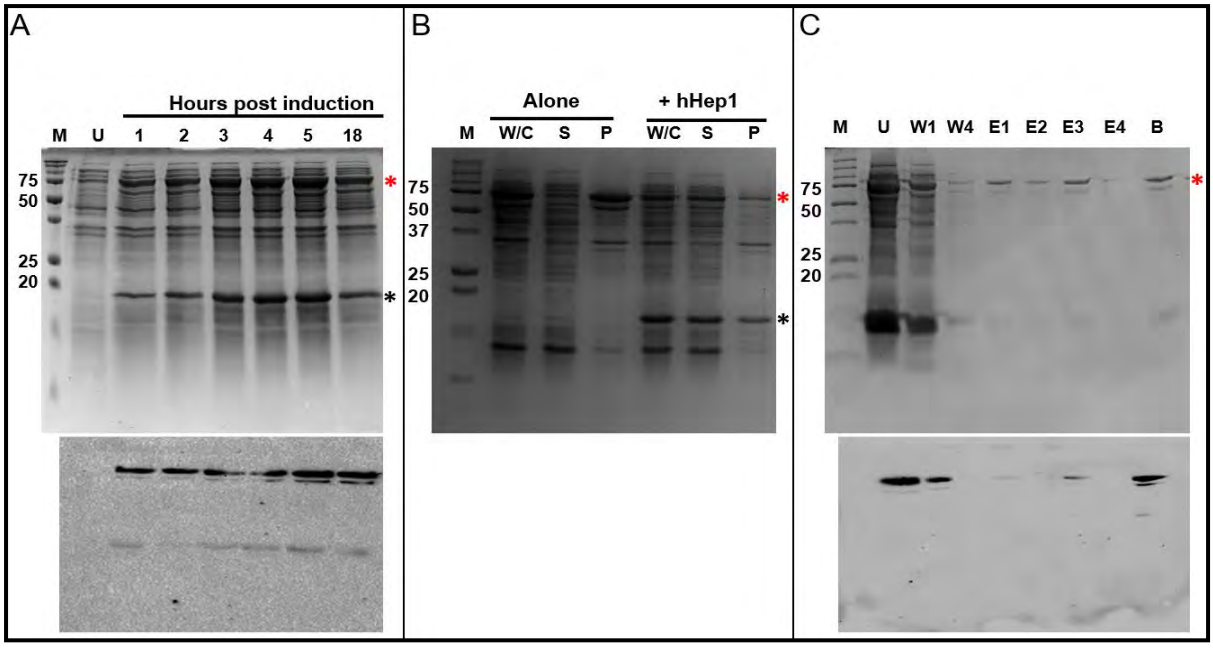

Figure 3.10: SDS-PAGE analysis of the expression, solubility and purification profiles of human HSPA9 heterologously co-expressed with HsHep1 in BL21 DE3 (pET28a-HSPA9/pQE2-HsHep1). A) The induction study samples of HSPA9 co-expressed with HsHep1 in a Coomassie-stained 13.5% acrylamide gel. In lane M is the protein molecular weight marker (Bio-Rad Precision-Plus™ All Blue standards) and in lane U is the un-induced whole cell extract. Lanes 1-5: Hourly samples one to five hours post IPTG induction (whole cell extract), lane 18: Overnight induction sample (whole cell extract). **B)** The solubility study samples of HSPA9 expressed alone or co-expressed HsHep1 in a Coomassie-stained 13.5% acrylamide gel. In lane M is the protein molecular weight marker. In the lanes labelled W.C. are the whole cell lysates of *E. coli* BL21 DE3 (pET28a-HSPA9) or *E. coli* BL21 DE3 (pET28a-HSPA9/pQE2-HsHep1). in the lanes labelled S are the supernatants (soluble fractions) of the cell lysates and in the lanes labelled P are the pellets (insoluble fractions). **C)** Purification of HSPA9 after co-expression with HsHep1 in *E. coli* BL21 DE3 (pET28a-HSPA9/pET23a-HsHep1) cells in a Coomassie-stained 13.5% acrylamide gel. In lane M is the protein molecular weight marker. In lane U is the unbound protein (flowthrough) sample, whilst in lanes W1 and W4 are the first and fourth (final) wash samples, respectively. In lanes E1 to E4 are the elution samples, and in lane B is the bead sample post-elution. The red and black asterisks indicate the points at which bands representing HSPA9 and HsHep1 occur, respectively, on the acrylamide gels. **Lower panels)** Corresponding Western blot images generated using mouse anti-his-tag (H-3) monoclonal antibodies (Santa Cruz).

HSPA9 was determined to be partly soluble when co-expressed with HsHep1 in this expression system as the chaperone was detectable in both the supernatant (soluble) fraction and the pellet (insoluble) fraction (Figure 3.10B). This observation mirrors the findings of Dores-Silva et al. (2013) using the same protein expression system. This has also led to HsHep1 being described as a "chaperone of a chaperone" due to its functions in relations to HSPA9 (Dores-Silva *et al*., 2021). With this system of co-expression, HsHep1 was also detected as has also been reported by Dores-Silva et al. (2013) (Figure 3.10, A & B). The co-expression of HSPA9 and HsHep1 was carried out using the pET28a-HSPA9 and pET23a- HsHep1 transformed into *E. coli* BL21 (DE3) cell. HSPA9 was purified with high levels of purity as can be visually observed (Figure 3.10 C). This observation was also made by Dores-Silva et al. (2015) using the same expression system. Some of the protein was lost with the unbound protein and washes (Figure 3.10C, lanes U, W1 & W4). Some of the protein was also bound to the beads post

elution (Figure 3.10C, lane B). However, the HSPA9 yield was still sufficient for downstream biochemical characterization in the form of protein activity assays. HSPA9 concentrations yielded were usually determined to be above 1 mg/mL as determined by the Bradford assay (Appendix B1.12). Some of the HSPA9 was lost in the washes and the flowthrough. The excess HSPA9 bound to the beads was not eluted by increasing the concentration of imidazole from 250 mM to 500 mM or 1 M.

3.4.1.7 TbHsp70

The structural integrity of the pQE2-TbHsp70 plasmid was confirmed by means of restriction digestions with *Nde*I and *Hind*III and agarose gel electrophoresis (Figure 3.11) (Appendices B1.5 & B1.6). Digestion with either of the plasmids restriction enzymes resulted in the linear conformation of the plasmid (Figure 3.11B, lanes N & H). The double digestion with *Nde*I and *Hind*III yielded fragments of approximately 4758 bp and 1988 bp, corresponding to the sizes of the pQE2 vector and the TbHsp70 gene, respectively (Figure 3.11B, lane N/H). This restriction enzyme digestion successfully verified the pQE2-TbHsp70 plasmid.

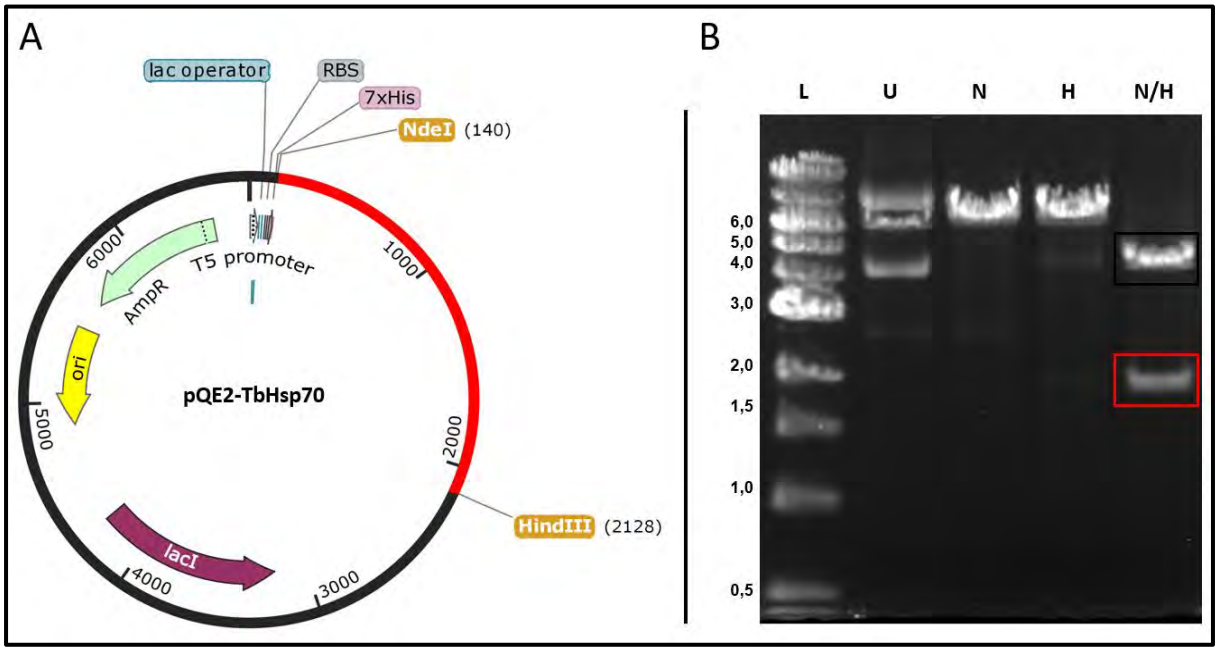

Figure 3.11: Confirmation of the integrity of the pQE2-TbHsp70 vector. A) Plasmid map of pQE2-TbHsp70 generated using the SnapGene 5.0.7 software. The *Nde*I and *Hind*III restriction sites occur immediately upstream and downstream of the TbHsp70 insert (in red), respectively. **B)** Restriction enzyme digestion of pQE2-TbHsp70 separated at 100 V on a 0.8 % agarose gel. In lane L is the DNA ladder (1 kb DNA ladder, New England Biolabs) and in lane U is the uncut plasmid. In lanes N and H are the *Nde*I and *Hind*III single cuts of the plasmid, respectively. In lane N/H is the *Nde*I and *Hind*III double digestion of the plasmid, with the larger and smaller fragments representing the pQE2 vector (4704 bp when *Nde*I/*Hind*III double digested, inside black box) and TbHsp70 insert (1988 bp, inside red box) respectively.

The plasmid was transformed into *E. coli* XL1 Blue cells for purposes of protein expression analysis by SDS-PAGE and western blotting (Figure 3.12) (Appendices B1.9 & B1.10). Following IPTG induced expression, there is an increased visibility of a protein band of approximately 70 kDa over time (Figure 3.12A, lanes 1-5 & 18). The presence of TbHsp70 was further confirmed by western analysis

that is specific to TbHsp70's N-terminal his-tag (Figure 3.12, lower panels) (Bentley and Boshoff, 2019). Optimal protein expression was determined to be achieved 5 hours post IPTG induction, TbHsp70 was purified with high levels of purity as can be visually observed. Also, to be noted is that some protein was lost with the unbound protein and washes (Figure 3.12B, lanes U, W1 & W4). The concentration of TbHsp70 was approximately 0.8-0.9 mg/mL as determined by the Bradford assay (Appendix B1.12). Successful expression and purification of TbHsp70 using this expression system has been reported previously (Bentley and Boshoff, 2019).

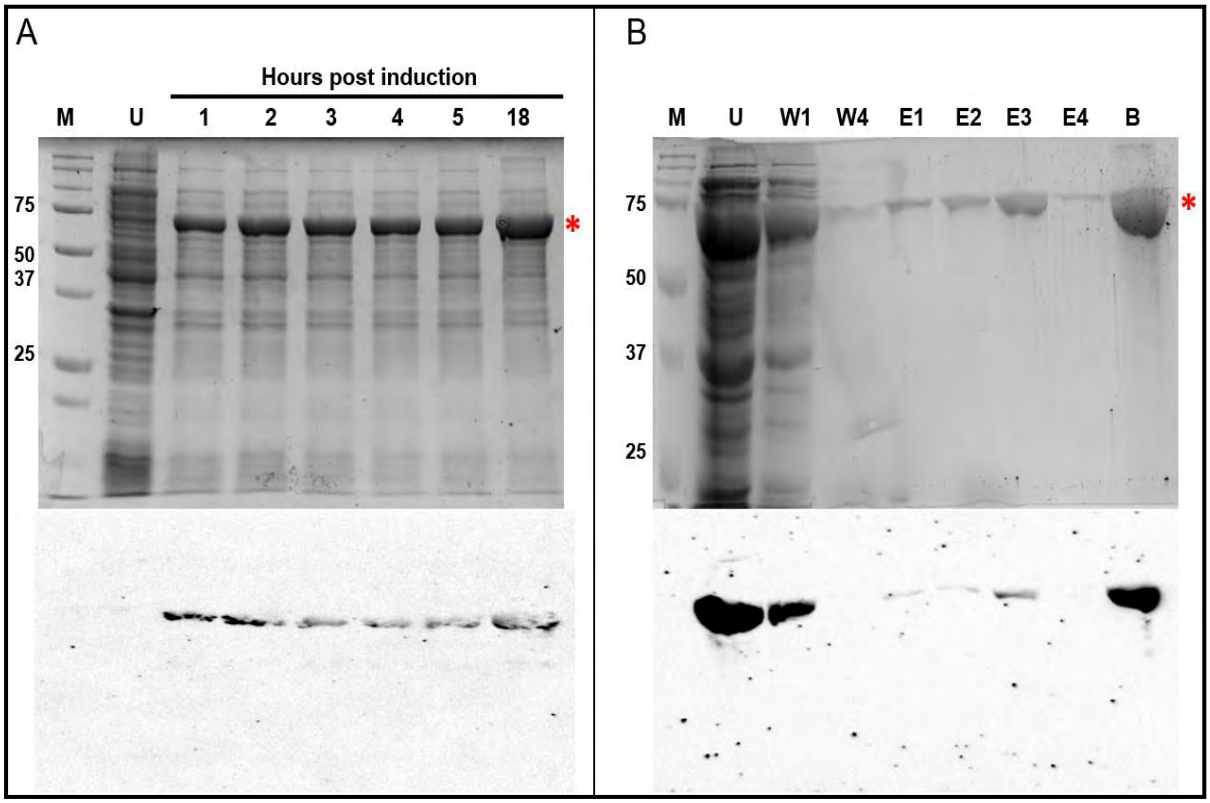

Figure 3.12: SDS-PAGE analysis of the expression and purification profiles of TbHsp70 heterologously expressed in *E. coli* XL1-Blue (pQE2-TbHsp70). A) The induction study samples of TbHsp70 in a Coomassie-stained 10 % acrylamide gel. In lane M is the protein molecular weight marker (Bio-Rad Precision-Plus™ All Blue standards) and in lane U is the un-induced whole cell extract. Lanes 1-5: Hourly samples one to five hours post IPTG induction (whole cell extract), lane 18: Overnight induction sample (whole cell extract). **B)** Purification of TbHsp70 in a Coomassie-stained 10 % acrylamide gel. In lane M is the protein molecular weight marker. In lane U is the unbound protein (flowthrough) sample, whilst in lanes W1 and W4 are the first and fourth (final) wash samples, respectively. In lanes E1 to E4 are the elution samples, and in lane B is the bead sample post-elution. The red asterisks indicate the points at which bands representing TbHsp70 occur on the acrylamide gels. **Lower panels)** Corresponding Western blot images generated using mouse anti-his-tag (H-3) monoclonal antibodies (Santa Cruz).

Protein was lost in the flowthrough and washes, with some of it remaining in the beads. Worth observing is that no truncation products of the protein were present. Increasing the concentration of imidazole in the elution buffer to 500 mM and 1 M did not result in improved elution of TbHsp70.

3.4.1.8 Tbj2

The structural integrity of the pET28a-Tbj2 plasmid was confirmed by means of restriction digestions with *Sal*I and *Nde*I and agarose gel electrophoresis (Figure 3.13 & Appendices B1.5 & B1.6). Digestion

with *Sal*I resulted in the linear conformation of the plasmid (Figure 3.13B, lane S). The double digestion with *Sal*I and *Nde*I yielded fragments of approximately 5369 bp and 1209 bp, corresponding to the sizes of the pET28a vector and the Tbj2 gene, respectively (Figure 3.13B, lane S/N). The pET28a-Tbj2 plasmid was successfully confirmed by diagnostic restriction enzyme digestion.

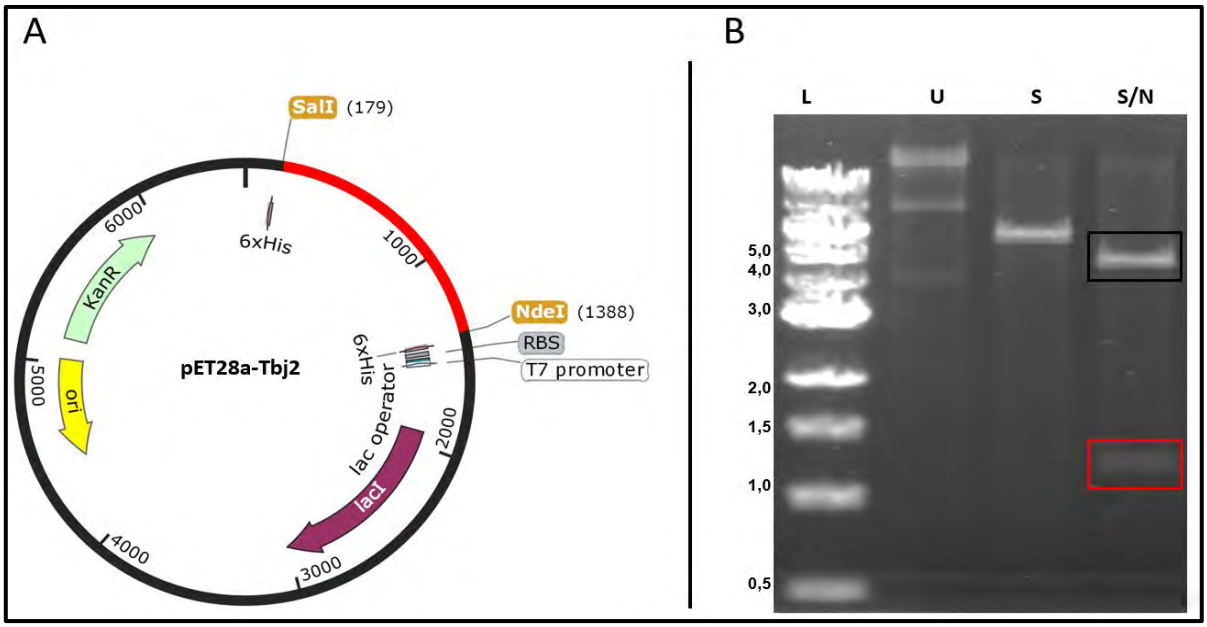

Figure 3.13: Confirmation of the integrity of the pET28a-Tbj2 vector. A) Plasmid map of pET28a-Tbj2 generated using the SnapGene 5.0.7 software. The *Sal*I and *Nde*I restriction sites occur immediately upstream and downstream of the Tbj2 insert (in red), respectively. **B)** Restriction enzyme digestion of pET28a-Tbj2 separated at 100 V on a 0.8 % agarose gel. In lane L is the DNA ladder (1 kb DNA ladder, New England Biolabs) and in lane U is the uncut plasmid. In lane S is the *Sal*I single cut of the plasmid. In lane S/N is the *Sal*I and *Nde*I double digestion of the plasmid, with the larger and smaller fragments representing the pET28a vector (5310 bp when *Sal*I/*Nde*I double digested, inside black box) and Tbj2 insert (1209 bp, inside red box), respectively.

The plasmid was transformed into *E. coli* BL21 (DE3) cells for purposes of protein expression analysis by SDS-PAGE and western blotting (Figure 3.14) (Appendices B1.9 & B1.10). Following IPTG induced expression, there is an increased visibility of a protein band of approximately 50 kDa over time (Figure 3.14A, lanes 1-5 & 18). The presence of Tbj2 was further confirmed by western analysis that is specific to Tbj2's N-terminal his-tag (Figure 3.14, lower panels) (Bentley and Boshoff, 2019). Optimal protein expression was determined to be achieved 5 hours post IPTG induction,

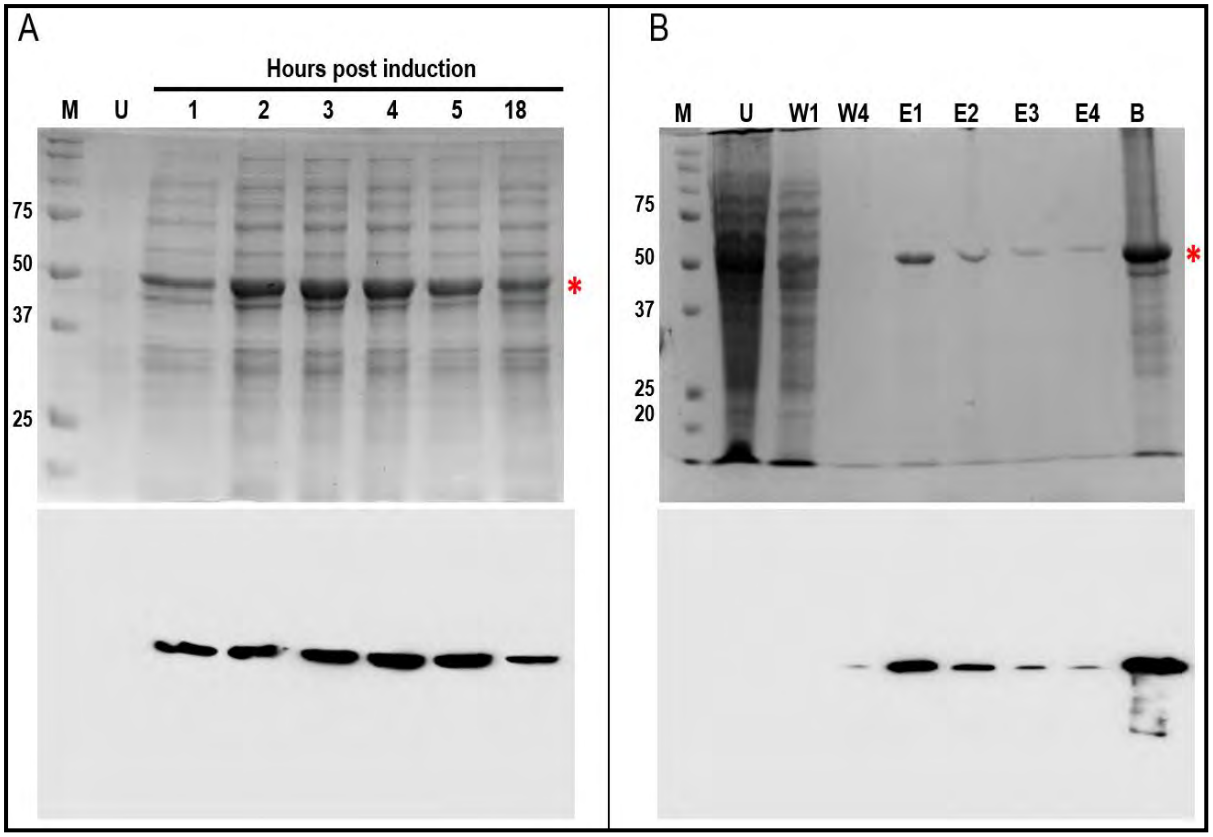

Figure 3.14: SDS-PAGE analysis of the expression and purification profiles of Tbj2 heterologously expressed in *E. coli* BL21 DE3 (pET28a-Tbj2). A) The induction study samples of Tbj2 in a Coomassie-stained 10 % acrylamide gel. In lane M is the protein molecular weight marker (Bio-Rad Precision-Plus™ All Blue standards) and in lane U is the un-induced whole cell extract. Lanes 1-5: Hourly samples one to five hours post IPTG induction (whole cell extract), lane 18: Overnight induction sample (whole cell extract). **B)** Purification of Tbj2 in Coomassie-stained 10 % acrylamide gel. In lane M is the protein molecular weight marker. In lane U is the unbound protein (flowthrough) sample, whilst in lanes W1 and W4 are the first and fourth (final) wash samples, respectively. In lanes E1 to E4 are the elution samples, and in lane B is the bead sample post-elution. The red asterisks indicate the points at which bands representing Tbj2 occur on the acrylamide gels. **Lower panels)** Corresponding Western blot images generated using mouse anti-his-tag (H-3) monoclonal antibodies (Santa Cruz).

The successful expression and purification of Tbj2 using this expression system has been reported previously (Burger *et al*., 2014; Bentley and Boshoff, 2019). A considerable amount of the protein was also bound to the beads post elution (Figure 3.14, lane B). Furthermore, increasing imidazole concentrations in the elution buffer from 250 mM to 500 mM to 1 M did not result in the extraction of the protein remaining in the beads. Concentrations of Tbj2 were usually determined to be 0.6 mg/mL by the Bradford assay (Appendix B1.12). Important in the purification of J-proteins is the removal of possibly bound DnaK by introducing ATP in the wash procedures of the purification process (Burger *et al*., 2014).

3.4.1.9 HSPA1A

The pET28a-HSPA1A vector was expressed in *E. coli* BL21 (DE3) cells (Figure 3.15). Protein expression was analysed by SDS-PAGE and western blotting (Appendices B1.9 & B1.10). Following

IPTG induced expression, there is an increased visibility of a protein band of approximately 70 kDa over time (Figure 3.15A, lanes 1-5). The presence of HSPA1A was further confirmed by western analysis that is specific to the N-terminal his-tag of HSPA1A (Figure 3.15A, lower panel). Optimal protein expression was determined to be achieved 4-5 hours post IPTG induction, The chaperone protein has previously been reported to be successfully purified using the same expression system, under similar conditions (Borges and Ramos, 2006; Dores-Silva *et al*., 2021). A considerable amount of the protein was also bound to the beads post elution (Figure 3.15, lane B). There also appeared to be some contaminating protein bands in the elutions, which are smaller than HSPA1A in size. Similar bands which can be observed on the western blot his-tag specific of the induction study (Figure 3.15A, lower panel). This observation suggests that there could be some truncation products of HSPA1A or incomplete synthesis of the proteins. Concentrations of HSPA1A were usually above 2 mg/mL as determined by the Bradford assay (Appendix B1.12).

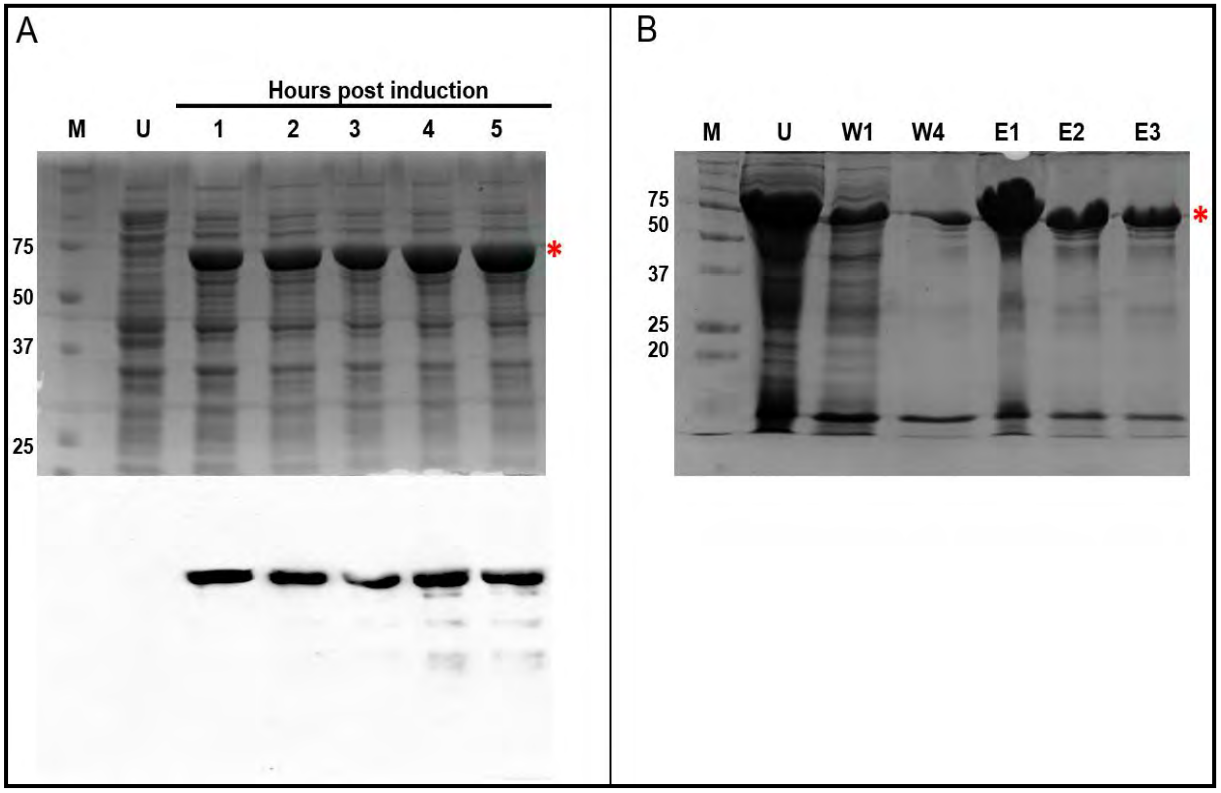

Figure 3.15: SDS-PAGE analysis of the expression and purification profiles of human HSPA1A heterologously expressed in *E. coli* BL21 DE3 (pET28a-HSPA1A). A) Induction study samples of HSPA1A in a Coomassie-stained 10 % acrylamide gel. In lane M is the protein molecular weight marker (Bio-Rad Precision-Plus™ All Blue standards) and in lane U is the un-induced whole cell extract. Lanes 1-5: Hourly samples one to five hours post IPTG induction (whole cell extract), lane 18: Overnight induction sample (whole cell extract). **B)** Purification of HSPA1A in a Coomassie-stained 10 % acrylamide gel. In lane M is the protein molecular weight marker and in lane U is the unbound protein (flowthrough) sample. In lanes W1 and W4 are the first and fourth (final) wash samples, respectively. In lanes E1 to E3 are the elution samples. The red asterisks indicate the points at which bands representing HSPA1A occur on the acrylamide gels. **Lower panel of A)** Corresponding Western blot image generated using mouse anti-his-tag (H-3) monoclonal antibodies (Santa Cruz).

3.4.1.10 Hsp33

Hsp33 was expressed in *E. coli* BL21 (DE3) cells (Figure 3.16). Protein expression was analysed by SDS-PAGE and western blotting (Appendices B1.9 & B1.10). Following IPTG induced expression, there is an increased visibility of a protein band of approximately 35 kDa over time (Figure 3.16, lanes 1-5). The presence of Hsp33 was further confirmed by western analysis that is specific to Hsp33's N-terminal his-tag (Figure 3.16B, lower panel). Optimal protein expression was determined to be achieved 4-5 hours post IPTG induction. The Hsp33 purification resulted in concentrations above 2 mg/mL as determined using the Bradford assay (Appendix B1.12). Some protein was lost with the unbound protein, washes or beads (Figure 3.16B, lanes U, W1, W4 & B). Two bands of the Hsp33 protein were observed after elution (Figure 3.16B), which may be attributed to having incomplete protein synthesis or degradation during the cell lysis process since these stacked bands are not present in the induction study (Figure 3.16A). The doublet could also point the presence of a posttranslationally modified species of Hsp33 that results in an electromobility shift, which has been reported in cases of glycosylation and oxidation (Kim *et al*., 1985; Joseph *et al*., 1997). A known posttranslational modification of Hsp33 is the formation of disulphide bonds as a result of oxidative stress (Jakob et al., 1999). Since the *E. coli* cytosol is a reducing environment, the possible disulphide bonding could be a result of the purification process which employs buffers that do not contain reducing nor oxidizing agents.

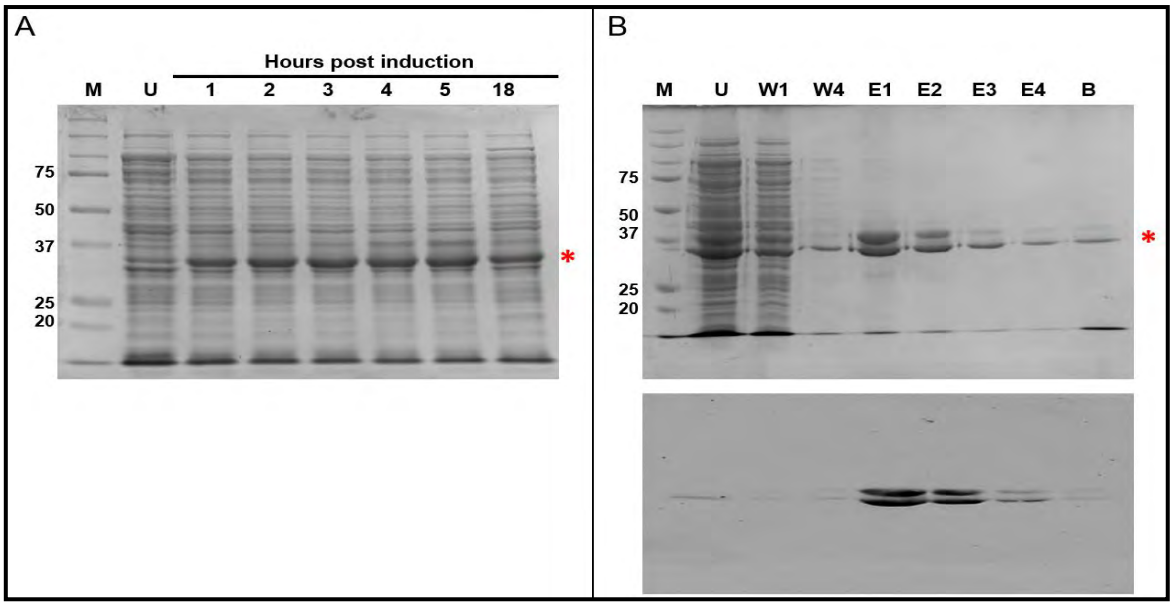

Figure 3.16: SDS-PAGE analysis of the expression and purification profiles of *E. coli* Hsp33 homologously expressed *E. coli* BL21 (DE3) (pET11a-Hsp33). A) Induction study samples of Hsp33 in a Coomassie-stained 10 % acrylamide gel. In lane M is the protein molecular weight marker (Bio-Rad Precision-Plus™ All Blue standards) and in lane U is the un-induced whole cell extract. Lanes 1-5: Hourly samples one to five hours post IPTG induction (whole cell extract), lane 18: Overnight induction sample (whole cell extract). **B)** Purification of Hsp33 in a Coomassie-stained 10 % acrylamide gel. In lane M is the protein molecular weight marker and in lane U is the unbound protein (flowthrough) sample. In lanes W1 and W4 are the first and fourth (final) wash samples, respectively. In lanes E1 to E4 are the elution samples, and in lane B is the bead sample post-elution. The red

asterisks indicate the points at which bands representing Hsp33 occur on the acrylamide gels. **Lower panel of B)** Corresponding Western blot image generated using mouse anti-his-tag (H-3) monoclonal antibodies (Santa Cruz).

Alternatively, it could be due to the expression system not being reducing enough to result in the complete reduction of Hsp33. In the study by Jakob et al. (1999), purified Hsp33 was shown to be constituted of 55 % oxidized and active species and 45 % reduced and inactive species.

3.5 Conclusions

The heterologous expression and purification of *T. brucei* Hsp70 has been carried out in previous *in vitro* studies, including *in vitro* molecular inhibition studies (Burger *et al*., 2014; Bentley and Boshoff, 2019; Andreassend *et al*., 2020). In order to enable the *in vitro* biochemical characterization of the proteins of interest, the proteins had to be expressed and then purified. TbHep1, TbmtHsp70, HsHep1, HSPA9, TbHsp70, Tbj2, HSPA1A and Hsp33 were all successfully expressed in the various *E. coli* protein expression strains. The proteins were further successfully purified by nickel affinity chromatography, with satisfactory yields. The proteins were all confirmed by SDS-PAGE and western analysis using anti-His antibodies. Prior to expression, the vectors housing the genes that encode TbHep1, TbmtHsp70, HsHep1, HSPA9, TbHsp70 and Tbj2 were all successfully constructed and confirmed by means of diagnostic restriction enzyme digestions.

Central to this study was assessing the interaction between mtHsp70 and Hep1 in *T. brucei* and humans. Co-expressing TbmtHsp70 and HSPA9 with TbHep1 and HsHep1, respectively, resulted in the solubilization of the mtHsp70s. This finding has previously been reported for HSPA9 and HsHep1 and numerous other mtHsp70/Hep1 systems of other organisms (Dores-Silva *et al*., 2013; Nyakundi *et al*., 2016; Dores-Silva *et al*., 2017, 2021). This study reports for the first time that the mtHsp70 in *T. brucei* is insoluble and requires Hep1 to rescue it aggregation.

CHAPTER FOUR
Comparative biochemical analysis of the Hep1/mtHsp70 functional partnerships of the *T. brucei* parasite and humans

4.1 Introduction

A very small fraction of the mitochondrial proteome is encoded and synthesized within the organelle. A vast majority of mitochondrial proteins is imported from the cytosol as they are nuclear encoded (Fox, 2012). At the outer membrane, the preprotein utilizes the translocase of outer membrane (TOM) complex, consisting of TOM40, TOM70/71 and TOM20, to initiate entry into the organelle. TOM40 acts as the pore of the translocation complex (Hill *et al*., 1998; Araiso *et al*., 2019). The TOM70/71 component is a tetratricopeptide (TPR) domain containing protein that binds to cytosolic Hsp70 and Hsp90 at their EEVD motifs. The molecular chaperones are prerequisites for the translocation of preproteins at the TOM complex. (Young et al., 2003; Li et al., 2009). Since preproteins must be linearized when entering the mitochondria, Hsp70 in the cytosol, by binding to the TPR domain of TOM70/71 also prevents preprotein aggregation (Beddoe and Lithgow, 2002). On the matrix side of the mitochondrial membrane, mitochondrial Hsp70 (mtHsp70), as a component of the PAM complex, is the primary driving force for preprotein import (Craig, 2018).

Independent of the PAM complex in the matrix, Hsp70 also ensures correct protein folding together with its J-protein and NEF co-chaperones Mdj1 and Mge1, respectively (Voos and Röttgers, 2002). MtHsp70 folding activity also extends to proteins that are encoded and synthesized in the mitochondria (Herrmann *et al*., 1994). Even though the exact details of how mtHsp70 effects protein import into the matrix are unclear, two hypotheses have been proposed: the Brownian-ratchet model and the pulling model (or power stroke model) (Voos, 2013; Craig, 2018). The Brownian model hypothesizes that the preprotein is imported by a chain of mtHsp70 molecules and shuttled into the matrix. As the preprotein emerges from TIM23 it is bound to mtHsp70 molecule and is transferred to another mtHsp70 molecule further into the matrix which in turn transfers it to another mtHsp70 molecule. In this way the protein is pulled deeper and deeper into the matrix until it has fully traversed the TIM23 channel (Craig, 2018). The pulling model is similar to the Brownian model in that it proposes that a chain of mtHsp70 molecules is involved in protein import. As the preprotein emerges from TIM23 and binds to mtHsp70, it is thought that the ATP hydrolysis induced conformational changes result in a pulling force being exerted on the preprotein. The preprotein is then shuttled to more mtHsp70 molecules, which act upon it in an identical manner as the first mtHsp70 until full importation is achieved (Craig, 2018). The functions of mtHsp70 and Mdj1 also have implications on mitochondrial morphology, as well as oxidative phosphorylation activities (Lee *et al*., 2015). The role of Hsp70 in the mitochondria has also

been demonstrated to extend to the biogenesis of complex IV (cytochrome *c* oxidase) of the electron transport chain. MtHsp70 and Mge1 have been shown to interact with subunit 4 of cytochrome *c* oxidase (*Cox4*) (Böttinger *et al*., 2013). MtHsp70 also interacts with *Ms551*, the translation regulator of the mRNA encoding subunit one of cytochrome *c* oxidase (*Cox1*) (Fontanesi et al., 2010).

Despite their critical cellular functions, mtHsp70s are characteristically predisposed to forming self-aggregates, with the linker region and NBD being primarily implicated (Zhai *et al*., 2008; Blamowska *et al*., 2010). A recent study, utilising human mtHsp70 (HSPA9) has elucidated the structural properties of mtHsp70 aggregates (Kiraly *et al*., 2020). It was determined that HSPA9 can form supramolecular assemblies that can reach up to 26 megaDaltons and 50 nm in molecular weight and average radius, respectively (Kiraly *et al*., 2020). As such, mtHsp70 requires a partner protein, the Hsp70 escort protein 1 (Hep1), to prevent its aggregation and ensure functionality. Hep1 is a zinc finger protein, possessing two CXXC motifs coordinating a zinc ion (Sichting *et al*., 2005). The escort protein is essential for mtHsp70 functionality, interacting with the molecular chaperone at the linker region (Zhai *et al*., 2008; Blamowska *et al*., 2010). Cells lacking Hep1 display a petite morphology and deficient mitochondria with diminished DNA, having anomalies that are associated with mtHsp70 knockdown (Sanjuán Szklarz *et al*., 2005; Sichting *et al*., 2005). Furthermore, the deletion of Hep1 also has implications on ribosome biogenesis, and even the nuclear genome, linked to defects in the formation of the iron-sulphur cluster (de la Loza *et al*., 2011). Interestingly, Hsp70 of cytosolic origin was found to be soluble in the matrices of mitochondria lacking Hep1, serving as evidence that self-aggregation is a distinguishing factor of mtHsp70 (Blamowska *et al*., 2010). Hep1 functions as the central stabilizing agent against the self-aggregation of mtHsp70 as it has been determined that other components of the mitochondrial chaperone network are not required for its folding (Blamowska *et al*., 2012).

The CXXC motifs of Hep1 have been determined to be essential for structural integrity and function as relates to interactions with mtHsp70 (Dores-Silva et al., 2015; Nyakundi et al., 2016). The CXXC motif and other similar motifs have been identified in other members of the molecular chaperone family, including in chaperones that are regulated according to the cellular redox state. A well characterized redox-regulated molecular chaperone is the ATP-independent Hsp33. The functional dynamics of Hsp33 are centred around its zinc finger domain whereby there are 4 cysteines that coordinate a zinc ion (Jakob *et al*., 1999). Oxidative conditions result in a formation of 2 disulphide bonds by the cysteine residues, whereby the zinc ion is released, and the chaperone is active in suppressing the aggregation of substrate proteins (Graumann *et al*., 2001). Despite ATP-dependent chaperones being known to be deactivated, due to a lack of ATP, under oxidative stress, the Hsp70/J-protein system has been reported to be responsive to oxidative stress. Bacterial DnaJ has been shown to possess weak oxidoreductase activity due to its zinc finger domain containing four CXXC motifs. Using mature insulin as a substrate protein, DnaJ has been reported to reduce insulin, thus inducing the aggregation of insulin (Mattoo *et al*., 2014). Mature insulin is sensitive to reduction, rapidly forming aggregates in the presence of

reducing agents. DnaJ was determined to cause the insulin to aggregate in a similar fashion as thioredoxin or the dithiothreitol (DTT) reducing agent (Mattoo *et al*., 2014). Furthermore, DnaJ is determined to synergistically enhance the refolding of slightly oxidized protein substrates, in a similar manner as thioredoxin (Mattoo *et al*., 2014). Additionally, in yeast cells, the ER paralog of Hsp70, immunoglobulin heavy chain binding protein (BiP) has been reported to switch from being an ATP-dependent foldase to being an ATP-independent holdase under oxidative conditions (Wang *et al*., 2014). Upon the return of normal reducing conditions, BiP switches back to being an ATP-dependent foldase. BiP possesses a single cysteine residue which forms a sulphenic acid upon oxidation (Wang *et al*., 2014; Wang and Sevier, 2016).

The overall aim of this study was to comparatively assess the potential biochemical interaction of putative *T. brucei* Hep1 and TbmtHsp70 with that of HsHep1 and HSPA9, further determining the potential effects of oxidative stress on the functionality of the Hep1 orthologues. The study further aims to determine the TbmtHsp70 independent chaperone functionalities of the putative TbHep1 orthologue in comparison to HsHep1. The holdase chaperone capable *T. brucei* stress inducible type I JDP, Tbj2, will be used as a positive control for the Hep1 orthologues' Hsp70 independent holdase activity determination (Ludewig *et al*., 2015; Bentley and Boshoff, 2019). The holdase chaperone and ATP hydrolysis capabilities of TbmtHsp70 alongside TbHsp70, HSPA9 and HSPA1A will also be assessed. The ability of TbHep1 to interact with the stress inducible cytosolic TbHsp70 will also be investigated alongside HsHep1 and HSPA1A. HsHep1 having the ability to interact with HSPA1A has been demonstrated, with HsHep1 being shown to also reside in the nucleoplasm (Dores-Silva *et al*., 2021). Therefore, it is also fitting to investigate whether this is also the case for the *T. brucei* orthologues of HsHep1 and HSPA1A. HSPA9 is also known to localise in the cytosol, possibly with HsHep1 by affinity, co-localising with HSPA9 outside the mitochondria (Ran *et al*., 2000). The benefit of characterizing the parasitic chaperones parallel to those of humans is that it will make it possible to decipher if the Hep1 and Hsp70 interaction is conserved between the two species. This will be investigated by determining if the Hep1 orthologue of one species can functionally interact with the Hsp70s of the other species.

HSPA9 is implicated in cancer and neurodegeneration (Wadhwa *et al*., 2006; Londono *et al*., 2012), whilst TbmtHsp70 is essential for the *T. brucei* parasite's viability (Týč *et al*., 2015). Oxidative stress in humans is linked to diseases such as neurodegeneration and cancer, *reviewed by* Milkovic et al. (2014) and Bozzo et al. (2017). The *T. brucei* parasite may also be subjected to oxidative stresses induced by the mammalian host's immune system or anti trypanosomal compounds (He *et al*., 2012; Greene and Hajduk, 2016). The mitochondrion, whereby Hep1 localizes, is the main source of cellular reactive oxygen species because of the electron transport chain, *reviewed by* Murphy (2009). In common with Hsp33, Hep1 also possesses 2 cysteine rich motifs whereby the cysteine residues coordinate a zinc ion. However, Hsp33 is only found in prokaryotes, algae and kinetoplastids, whereas

Hep1 is found in the mitochondria of eukaryotic organisms (Jakob *et al*., 1999; Sichting *et al*., 2005; Segal and Shapira, 2015). Therefore, it would be interesting to determine if Hep1 plays a similar role as Hsp33 in mitochondria, especially since the mitochondrion is an endosymbiotic organelle. A better understanding of the influences of the cell's redox state on Hep1 functionality could possibly open up new avenues for drug discovery relevant to neurodegenerative diseases, cancer and HAT. HSPA9 is known to be involved in oncogenesis and is being investigated as a target for anti-cancer drugs, whilst exploring new targets for HAT is important due to the many disadvantages associated with current drugs (Wadhwa *et al*., 2006; Babokhov *et al*., 2013).

4.2 Specific objectives

i. Determine the ability of the TbHep1 and HsHep1 to suppress the thermally induced aggregation of the TbmtHsp70, HSPA9, TbHsp70 and HSPA1A in *vitro*.
ii. Determine the ability of the Hep1 and Hsp70 proteins to suppress the thermally induced aggregation of MDH in *vitro*.
iii. Subject the Hep1 orthologues and Hsp33 to H_2O_2 induced oxidative stress coupled with heat shock.
iv. Determine the ability of the oxidized Hep1 orthologues and Hsp33 to suppress the thermally induced aggregation of MDH in *vitro*.
v. Ascertain if there are any structural modifications that the Hep1 orthologues and Hsp33 undergo as a result of oxidative stress couple with heat shock.
vi. Investigate the basal and Hep1 modulated ATPase activities of the mitochondrial and cytosolic Hsp70s in *vitro*.

4.3 Materials and methods

4.3.1 Materials

L-malate dehydrogenase (MDH) was sourced from Roche (Switzerland). Triton X-100, citrate synthase (CS), magnesium chloride, sodium citrate, malachite green, and sodium molybdate were obtained from Sigma-Aldrich (U.S.A.). Other materials that were used for the study are listed in detail in section 3.3.1.

4.3.2 Methods

4.3.2.1 Hep1 suppression of thermal aggregation of Hsp70s

The assay to assess the ability of the Hep1 orthologues to suppress the thermally induced aggregation of the Hsp70s was adapted from Dores-Silva et al. (2015; 2021) and Nyakundi et al. (2016). Briefly, in UV-vis 96 well plates, TbmtHsp70 (2 μM) and HSPA9 (2 μM), separately, were incubated with either TbHep1 (2-8 μM) or HsHep1 (2-8 μM) at 48 °C for 1 hour in assay buffer (50 mM Tris-HCl pH 7.4, 100 mM NaCl). Light scattering was measured by taking end-point absorbance readings at 360 nm before and after incubation. The suppression of aggregation activities of TbHep1 (4 μM) and HsHep1 (4 μM) were also determined using the cytosolic paralogs of TbmtHsp70 and HSPA1A, TbHsp70 (1

μM) and HSPA1A (1 μM) at 48 °C for 1 hour. The assays were conducted in triplicate using independently expressed and purified batches of proteins. Separate assays of each of the Hsp70s were also conducted under the same conditions. The absorbance readings recorded from the Hsp70s alone were benchmarked as 100 % aggregation.

4.3.2.2 Suppression of MDH thermal aggregation by the molecular chaperones

The assay to evaluate the holdase activity of TbHep1 (2-8 μM), TbmtHsp70 (0.25-0.75 μM), HsHep1 (2-8 μM), HSPA9 (0.25-0.75 μM), TbHsp70 (0.25-0.75 μM), Tbj2 (0.25-0.5 μM) and HSPA1A (0.25-0.75 μM) on the thermolabile protein substrate MDH (1 μM) was adapted from Dores-Silva et al. (2015; 2021) and Nyakundi et al. (2016). Briefly, in UV-vis 96 well plates, the chaperones were mixed with MDH in assay buffer (50 mM Tris-HCl pH 7.4, 100 mM NaCl) and then incubated at 48 °C for 1 hour. Light scattering was measured by taking end-point absorbance readings at 360 nm before and after incubation. The assays were conducted in triplicate using independently expressed and purified batches of proteins. The absorbance reading recorded from incubated MDH alone was benchmarked as 100 % aggregation. A negative control assay included was also conducted MDH (1 μM) incubated with BSA (0.8 μM) to demonstrate that the suppression of aggregation observed is strictly due to the presence of a molecular chaperone. Since all proteins scatter light at the wavelength of 360 nm, background aggregate formation by the molecular chaperones was also taken into account.

4.3.2.3 Densitometric verification of the aggregation suppression of the molecular chaperones

This assay was adapted from Zininga et al. (2017). Briefly, TbHep1 (1.5-2 μM), HsHep1 (0.1-1 μM), TbmtHsp70 (0.1-1 μM) and HSPA9 (0.1-1 μM) were each incubated with MDH (0.72 μM) in assay buffer (50 mM Tris-HCl pH 7.4, 100 mM NaCl) at 50 °C for 1 hour. After incubation, the reactions were centrifuged at 15 000 *g* for 10 minutes. Thereafter, a sample of the supernatant (soluble fraction) was removed, and the pellet (aggregate fraction) resuspended in the assay buffer (50 mM Tris-HCl pH 7.4, 100 mM NaCl) to the initial volume of the assay. The fractionation of MDH alone and in the presence of the chaperones was analyzed by densitometry using Image Lab 6.1 software (Bio-Rad, U.S.A.), subsequent to SDS-PAGE (Appendix B1.9) of the pellet and supernatant fractions. A negative control assay included MDH (0.72 μM) incubated with BSA (0.8 μM) to demonstrate that the suppression of aggregation observed is due to the presence of a molecular chaperone. The assays were conducted in triplicate using independently expressed and purified proteins.

The assay, under identical conditions, was also carried out with citrate synthase (1 μM) as a substrate of TbHep1 (1 μM), HsHep1 (1 μM) and TbmtHsp70 (1 μM).

4.3.2.4 Oxidation of Hep1 orthologues and Hsp33

The protocol for the oxidation of TbHep1, HsHep1 and Hsp33 was adapted from Fassler et al. (2018). TbHep1, HsHep1 and Hsp33 were expressed and purified as outlined in sections 3.3.2.3 and 3.3.2.6 and

then extensively dialyzed in buffer [10 mM Tris-HCl pH 7.5, 100 mM NaCl, 50 µM $ZnCl_2$, 5 mM DTT, 50 mM KCl, 10 % (v/v) glycerol] (Appendix B1.11). After dialysis, the proteins were incubated at 37 °C for 90 minutes in order to ensure the complete reduction of all cysteine disulphide bonds. Thereafter, the proteins were dialyzed in buffer [10 mM Tris-HCl pH 7.5, 100 mM NaCl, 50 mM KCl, 10 % (v/v) glycerol] without DTT or $ZnCl_2$ (Appendix B1.11). H_2O_2 was then added to each of the proteins to a final concentration of 5 mM before incubation at 45 °C for 90 minutes. The proteins were then extensively dialyzed to remove the H_2O_2 [10 mM Tris-HCl pH 7.5, 100 mM NaCl, 50 µM $ZnCl_2$, 5 mM DTT, 50 mM KCl, 10 % (v/v) glycerol], and then concentrated using PEG 20000 (Appendix B1.11). Protein concentration was determined using the Bradford assay (Appendix B1.12).

4.3.2.5 Determining the suppression of aggregation activities of the oxidized Hep1 orthologues and Hsp33

The ability of oxidized TbHep1 (2-8 µM), HsHep1 (2-8 µM) and Hsp33 (0.1-0.4 µM) to suppress the thermally induced aggregation of MDH (1 µM) was assessed as outlined in section 4.3.2.2. The assays were carried out in the presence of 5 mM DTT in order to determine the effects of reducing the cysteine disulphide bonds on the oxidized proteins.

4.3.2.6 Assessing disulphide bond formation in the oxidized TbHep1, HsHep1 and Hsp33

Disulphide bond formation was assessed by carrying out reducing and non-reducing SDS-PAGE on the oxidized protein samples. The SDS-PAGE procedure used is outline in Appendix B1.9. Briefly, SDS-PAGE was carried out in duplicate on the oxidized proteins. However, one of the replicates of each of the proteins was ran using sample buffer void of β-mercaptoethanol. Native PAGE (Appendix B1.13) was also carried out to determine if there were any structural differences between TbHep1, HsHep1 and Hsp33 purified under the respective reducing and oxidizing conditions. The native PAGE protocol was adapted from Segal & Shapira (2015). In both the non-reducing/reducing SDS-PAGE and native PAGE, BSA was used as a control. For both the SDS-PAGE and native PAGE, the Bio-Rad Precision-Plus™ All Blue standards was used as the molecular weight marker (Bio-Rad, U.S.A.).

4.3.2.7 Assessment of the basal and Hep1 modulated ATPase activity of the Hsp70s

The malachite green colorimetric ATPase assay was modified from Hoenig et al. (1989). The colourimetric development in this assay is derived from the complex formed by phosphate, molybdate and malachite green (Hoenig *et al*., 1989). Briefly, stock solutions of the proteins were prepared in assay buffer [20 mM Tris-HCl pH 7.5, 24 mM NaCl, 0.001 % (v/v) Triton X-100, (v/v) 0.5 % glycerol, 6 % (v/v) $MgCl_2$]. The proteins were then mixed with ATP to a final ATP concentration of 125 µM. The assay was conducted with the Hsp70s alone (0.1 µM) or in combination with the Hep1 orthologues (0.5 µM). Assays with Hep1 (0.5 µM) alone were also conducted. To determine if the ATPase activities of the Hsp70s are concentration dependant, the assay was also carried out with varying concentrations (0.1-0.2 µM) of the Hsp70s. The steady-state kinetics of the Hsp70s (0.2 µM) were assessed by

incubating them with varying concentrations of ATP (7.8 – 125 µM). All the assays were incubated at 37 °C for 1 hour. Thereafter, colourimetric assessment of P_i generated was carried out by mixing the reactions with malachite green buffer [0.126 % (w/v) malachite green: 2.6 % (w/v) sodium molybdate: 2.5 N HCl mixed in a 1: 18; 18 ratio]. Sodium citrate (0.1 M, pH 6.6) was then added to stop colour development prior to measuring absorbance at 620 nm. P_i standards (1.25 – 40 µM of Na_2HPO_4) were also prepared to generate a standard curve from which to calculate the P_i concentrations in the assays. The assays were conducted in triplicate using independently expressed and purified proteins.

4.4 Results and discussion

4.4.1 TbHep1 and HsHep1 suppressed the thermally induced aggregation of TbmtHsp70, HSPA9, TbHsp70 and HSPA1A

TbHep1 suppressed the aggregation of TbmtHsp70 *in vitro*. The addition of TbHep1 resulted in a 60 % decrease in aggregation of TbmtHsp70 (Figure 4.1A). Increasing the TbHep1 to TbmtHsp70 ratio from 1:1 to 4:1 did not significantly decrease the aggregation of TbmtHsp70.

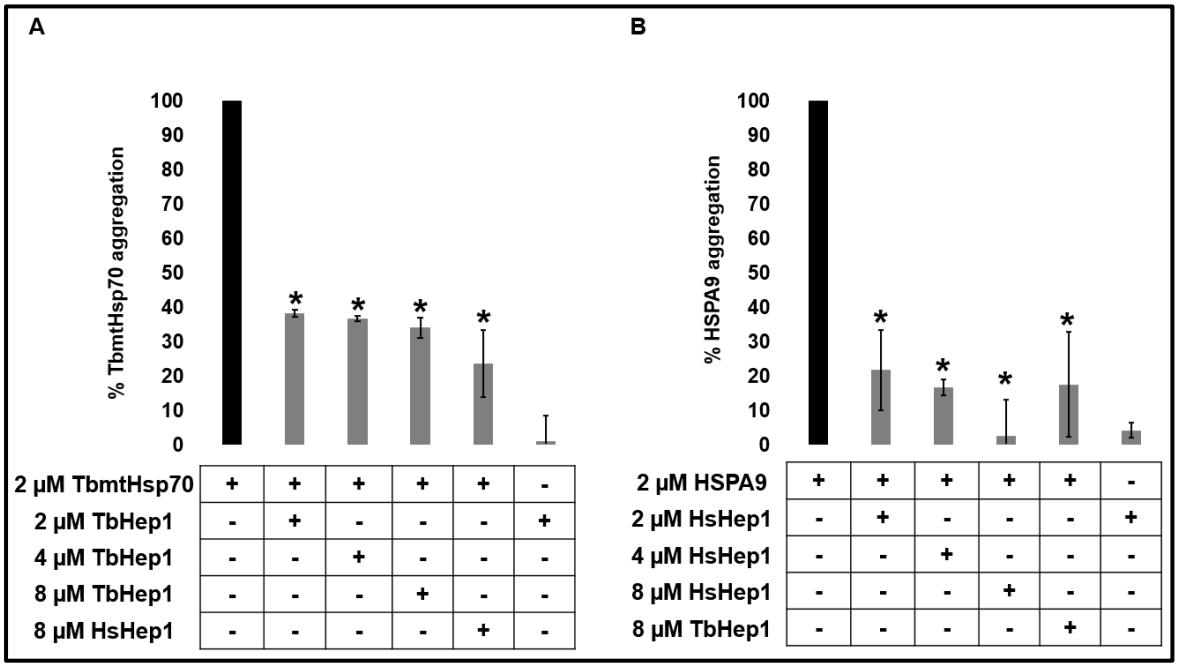

Figure 4.1: TbHep1 and HsHep1 suppressed the thermally induced aggregation of TbmtHsp70 and HSPA9. When incubated at 48 °C with increasing concentrations (2-8 µM) of TbHep1 or HsHep1, the presence of **A)** TbmtHsp70 (2 µM) and **B)** HSPA9 (2 µM) aggregates was considerably reduced. The % aggregation was determined with the aggregation of the mtHsp70s alone set at 100 %. The assays were conducted in triplicate using independently expressed and purified batches of proteins. The error bars represent standard deviation, with the asterisks indicating a significant difference between reactions with the mtHsp70s alone and those containing either TbHep1 or HsHep1. Statistical significance was benchmarked at $P < 0.05$ using a student's T-test.

HsHep1 was also shown to suppress the aggregation TbmtHsp70 to an even greater extent than TbHep1, however the difference between the effects of HsHep1 and TbHep1 on TbmtHsp70 aggregation was insignificant (Figure 4.1A). With regard to the aggregation of HSPA9, HsHep1 reduced the HSPA9 aggregates, in a concentration dependant manner (Figure 4.1B). HsHep1 was previously demonstrated to suppress HSPA9 aggregation under similar experimental conditions (Dores-Silva *et al*., 2021).

HsHep1 had a greater effect on suppressing the aggregation of HSPA9 as it decreased aggregation to below 10 %, whereas TbHep1 decreased it to approximately 25 %. TbHep1 also decreased the aggregation of HSPA9, to a greater extent than it did on TbmtHsp70 (Figure 4.1B). However, the suppression of aggregation activity of TbHep1 on TbmtHsp70 and HSPA9 was not significantly different. The results suggest that HsHep1 may be more effective at suppressing mtHsp70 aggregation compared to TbHep1. The findings of TbHep1 and HsHep1 possessing the ability to suppress mtHsp70 aggregation are in line with previous studies whereby yeast Hep1, LbrHep1, HsHep1 and PfHep1 suppressed the aggregation of their respective mtHsp70 partners *in vitro* (Sichting et al., 2005; Goswami et al., 2010; Dores-Silva et al., 2015; Nyakundi et al., 2016; Dores-Silva et al., 2021). The TbHep1 orthologues also enhanced the solubility of their mtHsp70 partners when co-expressed in *E. coli* as reported in previous studies (Sichting *et al*., 2005; Dores-Silva *et al*., 2013; Dores-Silva *et al*., 2015; Nyakundi *et al*., 2016). Dores-Silva et al. (2015) further showed that the zinc finger containing C-terminal region of LbrHep1 resulted in the enhancement of LbmtHsp70's solubility in a similar manner as the full-length protein, and its orthologues. This points to the zinc finger domain as being the central role player in the suppression of the aggregation of mtHsp70, since it is the only conserved moiety of Hep1 (Nyakundi *et al*., 2018). The ability of TbHep1 and HsHep1 to suppress the aggregation of HSPA9 and TbmtHsp70, respectively, suggest that the Hep1/mtHsp70 mode of interaction is conserved between the *T. brucei* parasite and humans.

It has been reported that HsHep1 may also be found in the nucleoplasm, whilst HSPA9 is also known to be found outside of the mitochondria, including in the cytosol (Dores-Silva *et al*., 2021). Therefore, Hep1 as an essential partner protein of mtHsp70 could also co-localise in the cytosol. HsHep1 was recently reported to suppress the aggregation of HSPA1A. This therefore begs the question of whether TbHep1 may also functionally interact with cytosolic TbHsp70. In this study, TbHep1 suppressed the aggregation of TbHsp70 by more than 50 % at a 4:1 ratio in *vitro* (Figure 4.2A). HsHep1 was also shown to suppress the aggregation of TbHsp70 at the same ratio, resulting in a decrease of TbHsp70 aggregation by more than 50 %. HsHep1 suppressed the aggregation of HSPA1A by more than 70 % at a 4:1 ratio. TbHep1 was also shown to be active on HSPA1A at the same ratio, (Figure 4.2B). These findings further cement the idea that HsHep1 may be a more effective Hsp70 partner protein when compared to TbHep1. The interaction of TbHep1 and HsHep1 with HSPA1A and TbHsp70, respectively, suggests that the Hep1/cytosolic Hsp70 interaction is also conserved between humans and the parasite. Even though self-aggregation is associated with mtHsp70s, the study by Kiraly et al. (2021) showed that HSPA1A also aggregated in a temperature and concentration dependant manner. However, in the same study, the aggregation of HSPA1A was shown to be less than that of HSPA9. What can also be observed in this study by comparison, is that the Hep1 orthologues performed with greater efficacy in suppressing the aggregation of the mitochondrial Hsp70 compared to the aggregates of the cytosolic Hsp70s. This suggests that Hep1 has a greater specificity/affinity for mitochondrial Hsp70. In

the study by Dores-Silva et al. (2021), HsHep1 was shown to suppress HSPA9 aggregation to a greater extent when compared to the aggregation of HSPA1A. In terms of HsHep1 being highly efficacious against aggregates of HSPA9 and HSPA1A, more especially HSPA9, is that defects in mtHsp70 in mammals has implications on cell survival. Therefore, a highly effective HsHep1/HSPA9 interaction could be a physiological adaptation to prevent cell mortality.

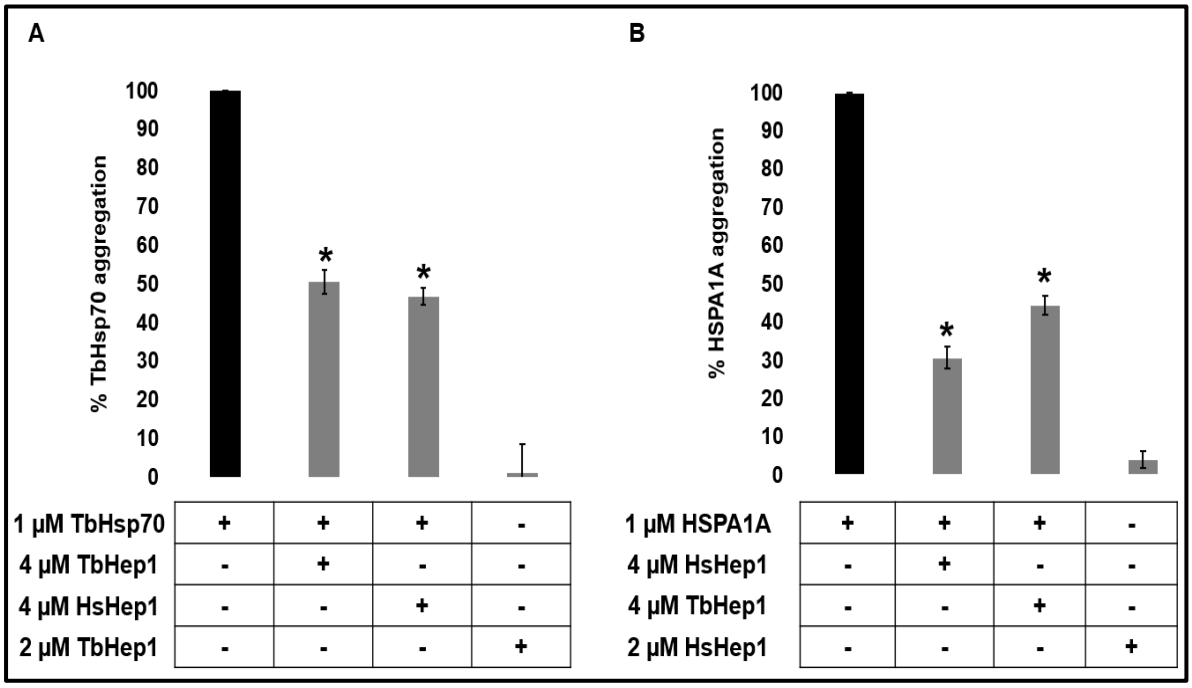

Figure 4.2: TbHep1 and HsHep1 suppressed the thermally induced aggregation of TbHsp70 and HSPA1A. When incubated at 48 °C with TbHep1 (4 µM) or HsHep1 (4 µM), the presence of **A)** TbHsp70 (1 µM) and **B)** HSPA1A (1 µM) aggregates was considerably reduced. The % aggregation was determined with the aggregation of the cytosolic Hsp70s alone set at 100 %. The assays were conducted in triplicate using independently expressed and purified batches of proteins. The error bars represent standard deviation, with the asterisks indicating a significant difference between reactions with the cytosolic Hsp70s alone and those containing either TbHep1 or HsHep1. Statistical significance was benchmarked at $P < 0.05$ using a student's T-test.

4.4.2 TbHep1 and HsHep1 suppressed the thermally induced aggregation of MDH

In suppression of aggregation assays, chemically or heat denatured model substrate are routinely used to assess the ability of molecular chaperones to act as holdase proteins (Gong, 2009; Burger *et al*., 2014). In this study, the holdase activity of TbHep1 was tested on heat denatured thermolabile L-MDH as a substrate *in vitro*, by means of the spectrophotometric quantification of aggregates. At a TbHep1 to MDH ratio of 2:1 to 8:1, TbHep1 prevented the aggregation of MDH (Figure 4.3A). TbHep1 was capable of decreasing the aggregation of MDH by approximately 90 % at excess molar concentrations. HsHep1 also suppressed the aggregation of MDH (Figure 4.3B). In previous studies, HsHep1 was demonstrated to suppress the aggregation of chemically denatured rhodanese as well as heat denatured MDH and luciferase (Goswami *et al*., 2010; Dores-Silva *et al*., 2021). PfHep1 was demonstrated to be incapable of suppressing the thermally induced aggregation of MDH and citrate synthase, whilst

LbrHep1 had no effect on the thermally induced aggregation of MDH (Dores-Silva *et al*., 2015; Nyakundi *et al*., 2016). Hep1 orthologues are poorly conserved outside of their characteristic zinc finger domains, *reviewed by* Nyakundi et al. (2018). The study by Dores-Silva et al. (2015) showed that the zinc finger domain of LbrHep1 was able to suppress the thermally induced aggregation of *L. braziliensis* Hep1 (LbmtHsp70) in a similar manner as the full-length protein. Therefore, the inconsistencies with regard to suppressing the aggregation of model substrates could partly be attributed to the non-conserved regions of Hep1. The suppression of aggregation observed in this study was confirmed to be specifically due to the presence of TbHep1 and HsHep1 rather than the presence of another protein in solution. Using BSA as a negative control, the thermally induced aggregation of MDH was not suppressed (Appendix C, Figure C1). Incubating TbHep1 or HsHep1 under these experimental conditions did not result in aggregation (Figure 4.3).

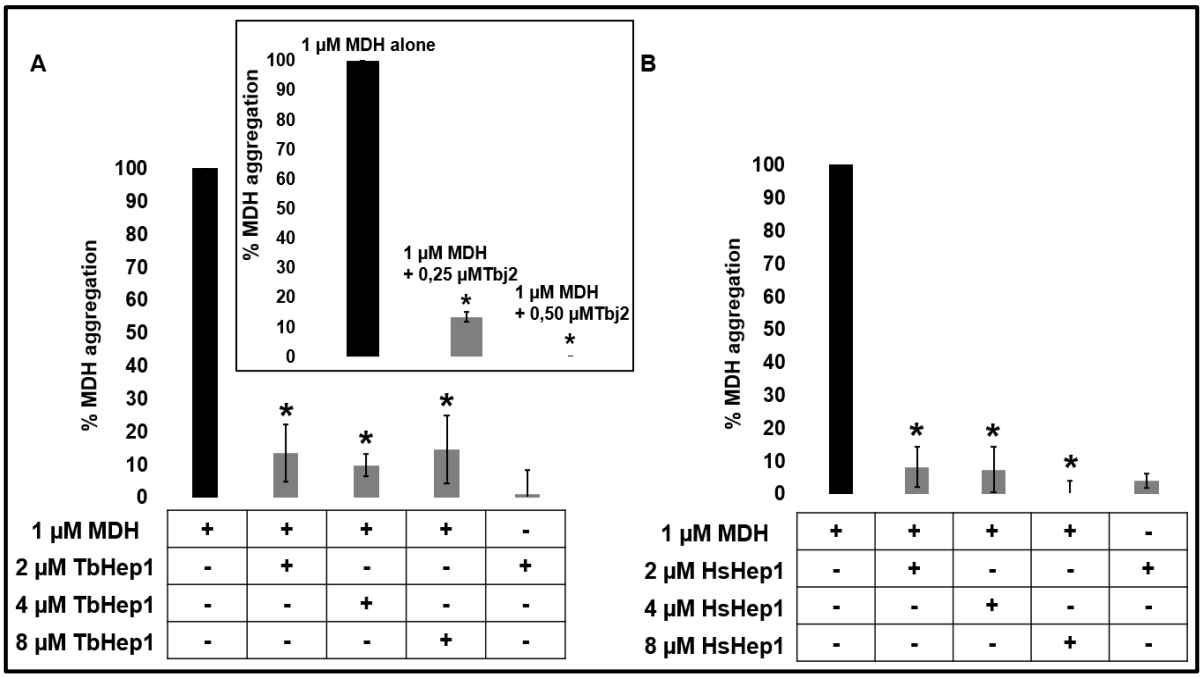

Figure 4.3: TbHep1 and HsHep1 suppressed the thermally induced aggregation of L-malate dehydrogenase (MDH). When incubated at 48 °C with increasing concentrations of **A)** TbHep1 (2-8 µM) or **B)** HsHep1 (2-8 µM), the presence of MDH (1 µM) aggregates was considerably reduced. **(Inset)** The comparative control, Tbj2 (0.25-0.5 µM), also suppressed the thermally induced aggregation of MDH. The % aggregation was determined with the aggregation of the MDH alone set at 100 %. The assays were conducted in triplicate using independently expressed and purified batches of proteins. The error bars represent standard deviation, with the asterisks indicating a significant difference between reactions with MDH alone and those containing either TbHep1 or HsHep1. Statistical significance was benchmarked at $P < 0.05$ using a student's T-test.

The holdase activities of TbHep1 and HsHep1 are reflective of those of J-proteins (Goswami *et al*., 2010; Kuo *et al*., 2013). In this study, the cytosolic *T. brucei* type I J-protein, Tbj2 had been employed as a comparative control. Under identical experimental conditions as those of TbHep1 and HsHep1, Tbj2 suppressed the thermally induced aggregation of MDH as has previously been determined (Burger *et al*., 2014; Bentley and Boshoff, 2019). Tbj2, under these experimental conditions, at sub molar

concentrations of MDH, suppressed aggregation by more than 90 % (Figure 4.3, inset). To be noted is that Tbj2 has also been reported to suppress the chemically induced aggregation of rhodanese (Burger *et al*., 2014), a capability that has also been confirmed for HsHep1 (Goswami *et al*., 2010).

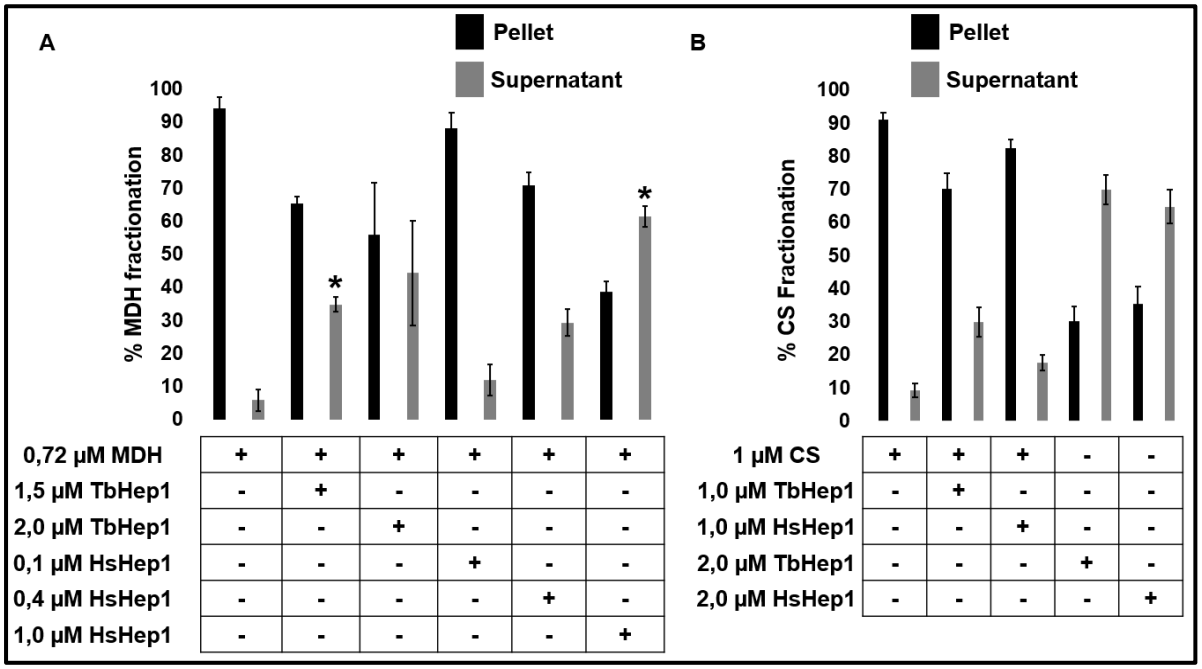

Figure 4.4: TbHep1 and HsHep1 increased the solubility of L-malate dehydrogenase (MDH) and citrate synthase (CS). The fractionation of thermally aggregated **A)** MDH (0.72 µM) and **B)** CS (1 µM) was considerably altered by incubation with TbHep1or HsHep1, resulting in an increase and decrease of substrate protein in the supernatant (grey bars) and pellet (black bars) fractions, respectively. The concentrations of TbHep1 and HsHep1 used on MDH were 1.5-2 µM and 0.1-1 µM, respectively. The concentration of TbHep1 and HsHep1 used on CS was 1 µM. The assays were conducted in triplicate using independently expressed and purified batches of proteins. The error bars represent standard deviation, with the asterisks indicating a significant difference between the soluble fractions of reactions with MDH or CS alone and those containing either TbHep1 or HsHep1. Statistical significance was benchmarked at $P < 0.05$ using a student's T-test.

Another technique to measure protein aggregation is by determining the relative proportions of soluble and aggregated protein by separating the aggregates from the soluble protein using centrifugation. The aggregates are subject to sedimentation under centrifugal force, and may therefore be fractionally separated from soluble proteins (Sultana *et al*., 2021). The technique applied in this study was adapted from Zininga et al. (2017), whereby aggregated and soluble protein proportions were determined by densitometric quantification. Using this method, TbHep1 and HsHep1 were still determined to possess the ability to suppress the thermally induced aggregation of MDH *in vitro*, and also in a concentration dependant manner (Figure 4.4A). Increasing concentrations of TbHep1 or HsHep1 resulted in an increased and decreased prevalence of MDH in the supernatant and pellet fractions, respectively. HsHep1 was shown to be possessing greater activity using this technique with MDH as a substrate, still suggesting the human orthologue to be a more effective chaperone. With HsHep1, MDH predominantly featured in the soluble fraction at excess molar concentrations, whereas with TbHep1 excess molar concentrations still resulted in MDH being more prevalent in the insoluble fraction. Using this method, TbHep1 and HsHep1 were also tested on thermally aggregated citrate synthase (Figure 4.4B). HsHep1

(2 μM) was shown to have decreased efficacy in reducing the aggregation of citrate synthase than HsHep1 (1 μM) on MDH. These findings mirror the findings of a previous study whereby HsHep1 suppressed the aggregation of MDH and luciferase, but not citrate synthase (Dores-Silva *et al*., 2021). These findings point to a possible substrate preference/specificity as the proteins proved to be less effective in preventing the aggregation of citrate synthase compared to MDH. To also be noted is that TbHep1 performed slightly better as a chaperone using citrate synthase as a substrate compared to HsHep1. This raises the question of whether HsHep1 is actually a more effective chaperone, or is it a matter of substrate specificity between TbHep1 and HsHep1. Molecular chaperones are known to bind to aggregated proteins at exposed hydrophobic regions. MDH could be possessing more Hep1 specific hydrophobic binding sites. By means of densitometric quantification of MDH fractionation, Tbj2 was previously confirmed to be active against the thermal aggregates of MDH, suppressing the aggregates in a concentration dependant manner (Bentley and Boshoff, 2019). The suppression of aggregation observed in this study was confirmed to be specifically due to the presence of TbHep1 and HsHep1 rather than having another protein in solution. Using BSA as a negative control, the thermally induced aggregation of MDH and citrate synthase was not suppressed (Appendix C, Figure C2). Worth observing is that TbHep1 and HsHep1 aggregated by approximately 25 % and 35 %, respectively, under these experimental conditions (Figure 4.4B). TbHep1 suppressed the aggregation of MDH and citrate synthase by 40 % and 20 %, respectively. HsHep1 suppressed the aggregation of MDH and citrate synthase by approximately 50 % and 10 %, respectively. Even though HsHep1 incubated alone aggregated slightly more compared to TbHep1, HsHep1 at lower concentrations resulted in a more remarkable suppression of MDH aggregation.

4.4.3 TbmtHsp70 and HSPA9 co-expressed with TbHep1 and HsHep1, respectively, suppressed the thermally induced aggregation of MDH

PfHsp70-3 has been demonstrated to suppress the thermally induced aggregation of citrate synthase and MDH (Nyakundi *et al*., 2016). In this study, TbmtHsp70 (Figure 4.5A) and HSPA9 (Figure 4.5B) were shown to suppress the aggregation of MDH *in vitro*, at sub molar concentrations. The chaperones suppressed the aggregation of MDH by approximately 90 %. MtHsp70s are prone to self-aggregation, which may be exacerbated by increased temperature (Dores-Silva *et al*., 2017; Kiraly *et al*., 2020), but have been shown to still manage to prevent the thermal aggregation of model substrate proteins (Nyakundi *et al*., 2016). A study by Kiraly et al. (2020) determined that aggregates formed by HSPA9 and HSPA1A exhibited ATPase activity that was half of the monomeric HSPA9 and HSPA1A, respectively. The partial ATPase activity exhibited by the HSPA9 and HSPA1A aggregates could still apply to holdase functionality, which could be the reason for TbmtHsp70 and HSPA9 in this study managing to suppress the thermally induced aggregation of MDH.

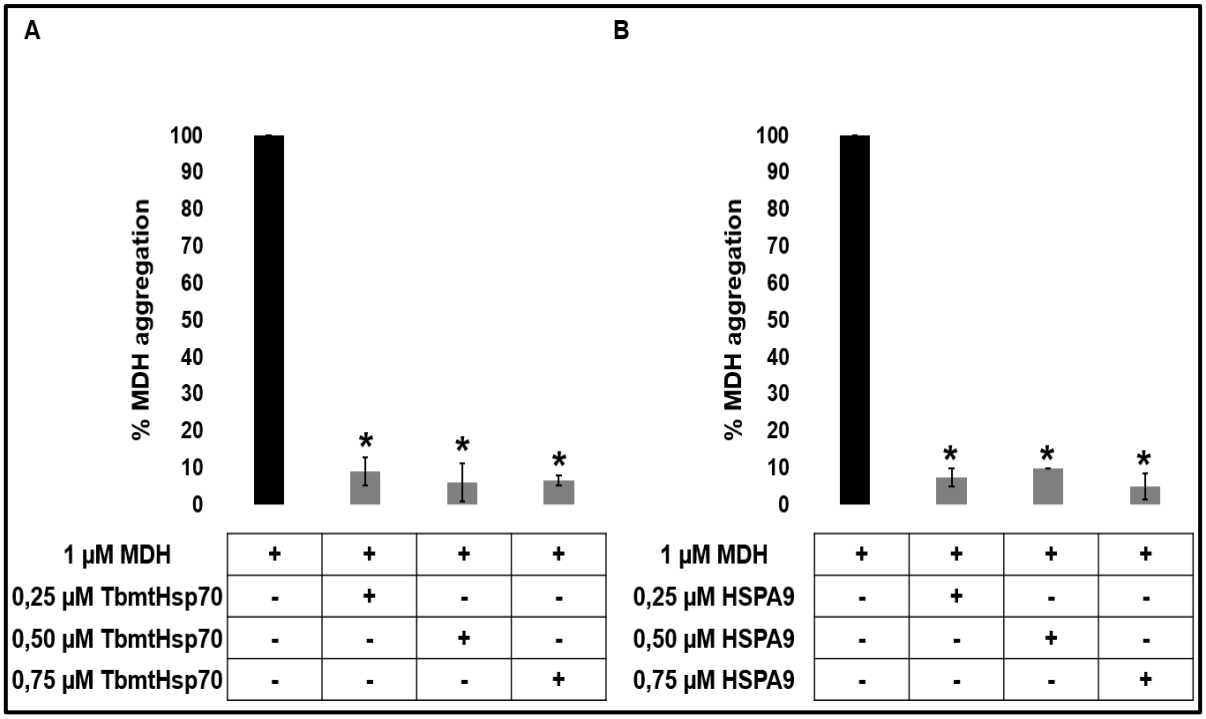

Figure 4.5: TbmtHsp70 and HSPA9 suppressed the thermally induced aggregation of L-malate dehydrogenase (MDH). When incubated at 48 °C with increasing concentrations (0.25-0.75 µM) of **A)** TbmtHsp70 or **B)** HSPA9, the presence of MDH (1 µM) aggregates was considerably reduced. The % aggregation was determined with the aggregation of the MDH alone set at 100 %. The assays were conducted in triplicate using independently expressed and purified batches of proteins. The error bars represent standard deviation, with the asterisks indicating a significant difference between reactions with MDH alone and those containing either TbmtHsp70 or HSPA9. Statistical significance was benchmarked at $P < 0.05$ using a student's T-test.

The holdase activities of TbmtHsp70 and HSPA9 on MDH were also confirmed by the fractionation method adopted from Zininga et al. (2017). At excess molar concentrations, TbmtHsp70 and HSPA9 resulted in MDH being more prevalent in the soluble fraction (Figure 4.6A). Furthermore, using this method TbmtHsp70 was also determined to be capable of preventing the thermally induced aggregation of citrate synthase (Figure 4.6B), a capability that was previously reported for PfHsp70-3 and HSPA9 (Nyakundi *et al*., 2016; Khan *et al*., 2017). Using this method, the suppression of aggregation activity of TbmtHsp70 and HSPA9 proved to be concentration dependant with MDH as a substrate. With increasing concentrations of TbmtHsp70 or HSPA9, MDH increasingly fractionated in the supernatant. TbmtHsp70 was more effective in preventing MDH aggregation compared to the aggregation of citrate synthase. This could be due to MDH possessing more Hsp70 specific binding sites compared to citrate synthase. The cytosolic *T. brucei* Hsp70, TbHsp70.c, was also reported to have greater specificity for MDH compared to rhodanese (Burger *et al*., 2014). The holdase activity of the cytosolic counterparts of TbmtHsp70, TbHsp70 and TbHsp70.4, on thermally aggregated MDH has also been confirmed using this technique (Bentley and Boshoff, 2019).

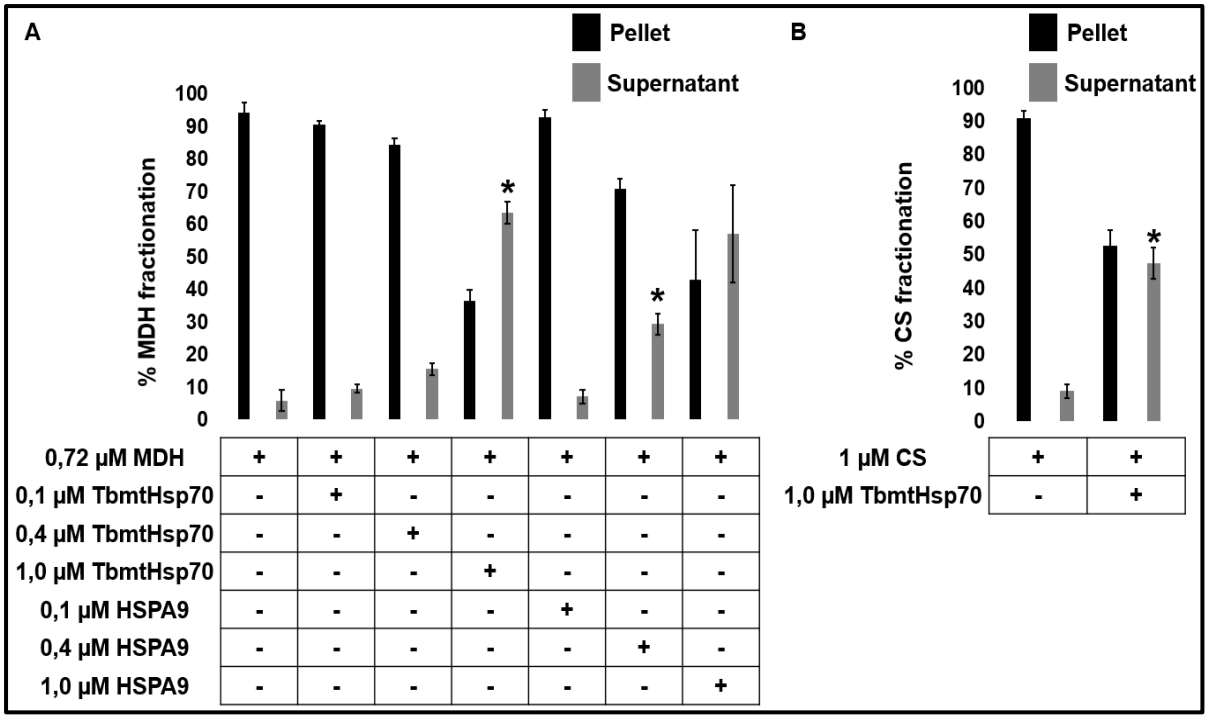

Figure 4.6: The chaperone capabilities of TbmtHsp70 and HSPA9 were also confirmed by means of fractionation. The fractionation of thermally aggregated **A) L-malate dehydrogenase (**MDH) (0.72 µM) and citrate synthase (CS) **B)** (1 µM) was considerably altered by incubation with TbmtHsp70 or HsHsHep1, resulting in an increase and decrease of substrate protein in the supernatant (grey bars) and pellet (black bars) fractions, respectively. The concentrations of TbmtHsp70 or HSPA9 used on MDH was 0.1-1.0 µM. The assays were conducted in triplicate using independently expressed and purified batches of proteins. The error bars represent standard deviation, with the asterisks indicating a significant difference between the soluble fractions of reactions with MDH or CS alone and those containing either TbmtHsp70 or HSPA9. Statistical significance was benchmarked at $P < 0.05$ using a student's T-test.

4.4.4 TbHep1 did not modulate the suppression of aggregation activity of TbmtHsp70

Having determined that TbmtHsp70 suppresses the aggregation of MDH, this study further investigated if TbmtHsp70 and TbHep1 can functionally cooperate in suppressing the thermally induced aggregation of MDH. The addition of TbHep1 did not enhance the holdase activity of TbmtHsp70 (Figure 4.7). These results are in line with what was previously observed for PfHep1. Combining PfHep1 with the *P. falciparum* mtHsp70 (PfHsp70-3) did not result in an improvement of the holdase activity of PfHsp70-3 on thermally aggregated MDH and citrate synthase (Nyakundi *et al*., 2016). These observations, however, contrast findings whereby HsHep1 and HSPA9 synergistically suppressed the chemically induced aggregation of rhodanese (Goswami *et al*., 2010). The cytosolic counterparts of Tbmthsp70, TbHsp70 and TbHsp70.4, cooperated with Tbj2 in suppressing the thermal aggregation of MDH (Bentley and Boshoff, 2019). A common feature between Tbj2 and HsHep1 is that they also possess intrinsic holdase capabilities (Goswami *et al*., 2010; Burger *et al*., 2014; Bentley and Boshoff, 2019; Dores-Silva *et al*., 2021). In this study (Section 4.4.2), TbHep1 was shown to be capable of suppressing aggregation, similar to HsHep1 and Tbj2. PfHep1 was determined to not possess intrinsic holdase activity (Nyakundi *et al*., 2016).

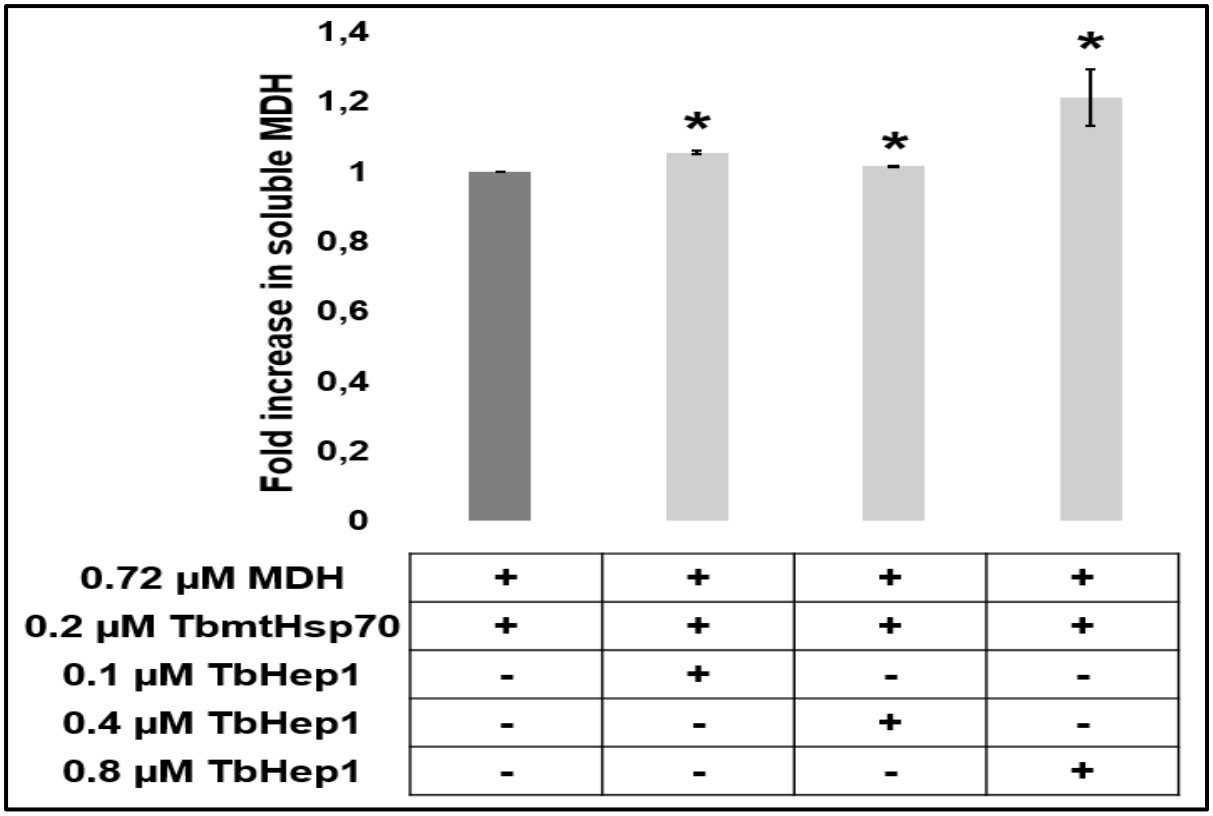

Figure 4.7: TbHep1 and TbmtHsp70 did not cooperate in the suppression of the thermally induced aggregation of L-malate dehydrogenase (MDH). Incrementally adding TbHep1 (0.1-0.8 µM) to TbmtHsp70 (0.2 µM) did not result in an improvement of the suppression of aggregation activity of TbmtHsp70. The MDH in the soluble fraction with TbmtHsp70 alone was set at 1-fold. The assays were conducted in triplicate using independently expressed and purified batches of proteins. The error bars represent standard deviation, with the asterisk indicating a significant difference between the soluble fractions of reactions with TbmtHsp70 and MDH alone and those containing TbHep1. Statistical significance was benchmarked at $P < 0.05$ using a student's T-test.

4.4.5 TbHsp70 and HSPA1A suppressed the thermally induced aggregation of MDH

TbHsp70 which has been determined to suppress aggregation had been employed as a control in this study (Bentley and Boshoff, 2019). TbHsp70 and HSPA1A suppressed the thermally induced aggregation of MDH (Figure 4.8, A & B). These findings are also in line with previous studies whereby the cytosolic *T. brucei* Hsp70s, TbHsp70.4 and TbHsp70.c were determined to suppress the thermally induced aggregation of model substrates (Burger *et al*., 2014; Bentley and Boshoff, 2019). The *T. cruzi* cytosolic Hsp70, TcHsp70B, which is homologous to TbHsp70 was also demonstrated to be active against the thermally and chemically induced aggregation, respectively, of MDH and rhodanese (Burger *et al*., 2014). Suppression of thermally aggregated MDH and luciferase was also reported for *P. falciparum* cytosolic Hsp70, PfHsp70-1 (Shonhai *et al*., 2008; Zininga *et al*., 2016). The constitutively expressed cytosolic counterpart of HSPA1A, HSPA8 was unexpectedly observed to be susceptible to aggregation under heat stress conditions (Andreassend *et al*., 2020).

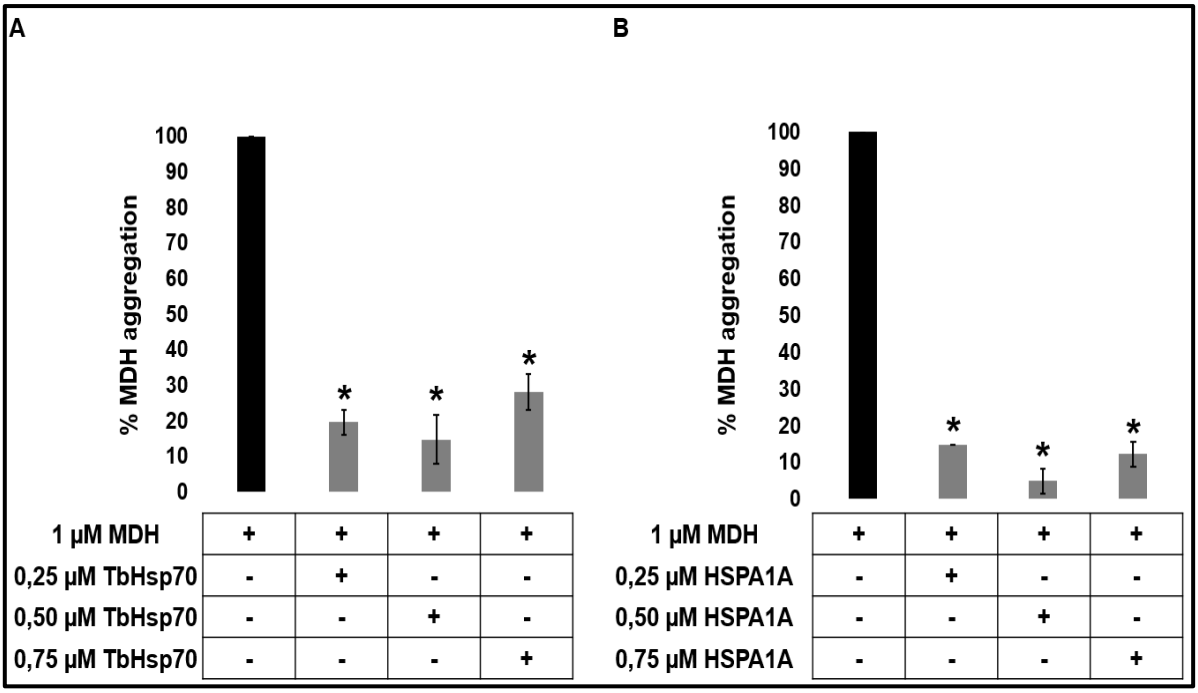

Figure 4.8: TbHsp70 and HSPA1A suppressed the thermally induced aggregation of L-malate dehydrogenase (MDH). When incubated at 48 °C with increasing concentrations (0.25-0.75 µM) of **A)** TbHsp70 or **B)** HSPA1A, the presence of MDH (1 µM) aggregates was considerably reduced. The % aggregation was determined with the aggregation of the MDH alone set at 100 %. The assays were conducted in triplicate using independently expressed and purified batches of proteins. The error bars represent standard deviation, with the asterisks indicating a significant difference between reactions with MDH alone and those containing either TbHsp70 or HSPA1A. Statistical significance was benchmarked at $P < 0.05$ using a student's T-test.

4.4.6 TbHep1 and HsHep1, subjected to H_2O_2, induced oxidative stress, suppressed the thermally induced aggregation of MDH

Hep1 orthologues have been determined to possess two CXXC tetra motifs which occur within the zinc finger domain, *reviewed by* Nyakundi et al. (2018). In the redox regulated molecular chaperone, Hsp33, the CXXC motif plays a central role in regulating the functionality whereby oxidative stress leads to the molecular chaperone's activation primarily due to the formation of disulphide bonds (Graumann *et al*., 2001). In this preliminary study, TbHep1 and HsHep1 were subjected to H_2O_2 induced oxidative stress coupled to heat shock prior to being assessed for holdase function under conditions identical to those outlined in section 4.4.2 (Figure 4.3). TbHep1 (Figure 4.9A) and HsHep1 (Figure 4.10A) were determined to be active after having been exposed to oxidative stress conditions. The assay was also carried out on the oxidized TbHep1 and HsHep1 orthologues in the presence of 5 mM DTT, under identical conditions. The presence of DTT in high concentrations resulted in a slight reversal of the suppression of aggregation activities of TbHep1 (Figure 4.9B) and HsHep1 (Figure 4.10B). The comparative control, H_2O_2 oxidized Hsp33 also followed the same trend as TbHep1 and HsHep1 in the absence (Figure 4.11A) and presence of (Figure 4.11B) 5 mM DTT. Numerous investigations have been carried out on Hsp33 in this regard in previous studies, *comprehensively reviewed by* Ulrich et al.

(2021). The oxidative activation of Hsp33 has previously been shown to be reversible in the presence of DTT, in a time dependant manner (Jakob *et al*., 1999).

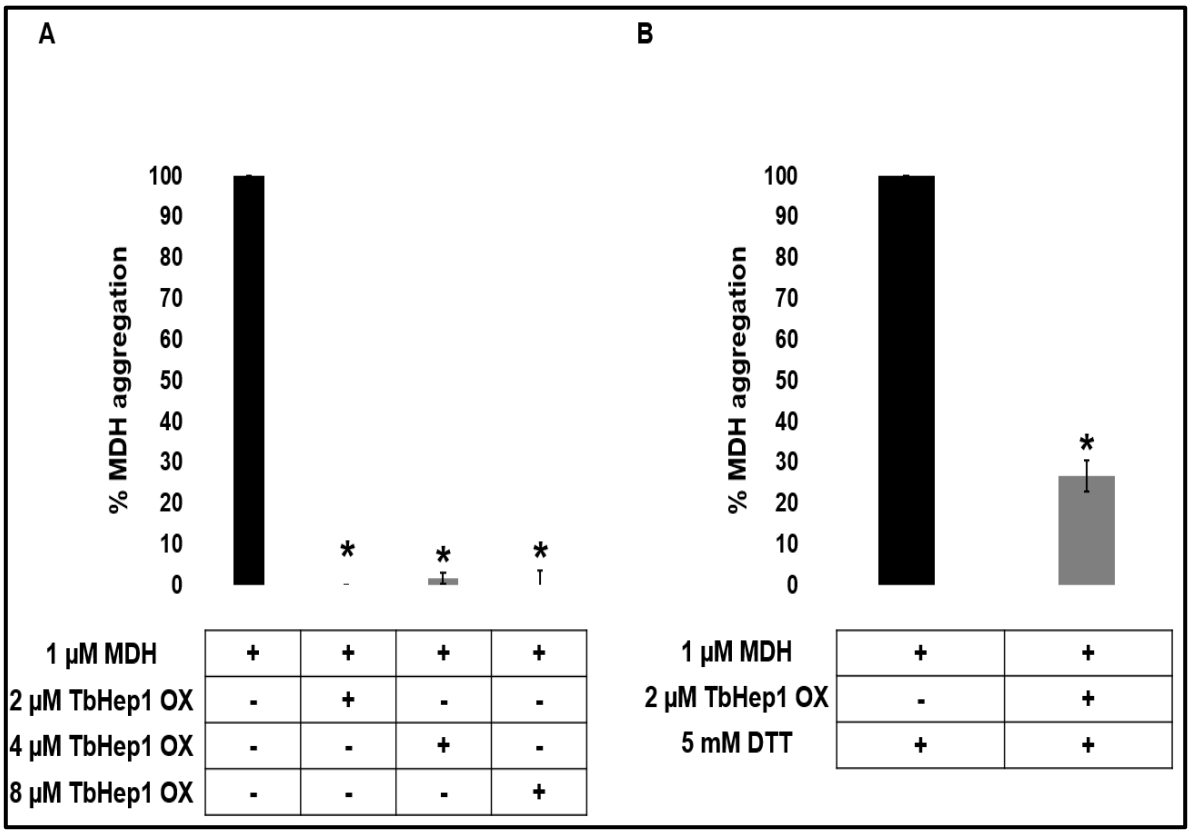

Figure 4.9: Oxidized TbHep1 exhibits holdase activity towards thermally aggregated L-malate dehydrogenase (MDH). When incubated at 48 °C with increasing concentrations of oxidized **A)** TbHep1 (2-8 µM) the presence of MDH (1 µM) aggregates was considerably reduced. **B)** In the presence of 5 mM DTT, the suppression of aggregation activity of oxidized TbHep1 (2 µM) was considerably reduced. The % aggregation was determined with the aggregation of the MDH alone set at 100 %. The assays were conducted in triplicate using independently expressed and purified batches of proteins. The error bars represent standard deviation, with the asterisks indicating a significant difference between reactions with MDH alone and those containing TbHep1. Statistical significance was benchmarked at $P < 0.05$ using a student's T-test.

In this study, oxidized TbHep1 (Figure 4.9B) and HsHep1 (Figure 4.10B) displayed DTT reversible activity in a similar manner as Hsp33 (Figure 4.11B), under identical experimental conditions. TbHep1 reduced the aggregation of MDH at excess molar concentrations by more than 90 % (Figure 4.9A), with 5 mM DTT partially reversing that activity (Figure 4.9B). HsHep1 also suppressed the aggregation of MDH by more than 90 % (Figure 4.10A), with 5 mM DTT partially reversing activity (Figure 4.10B).

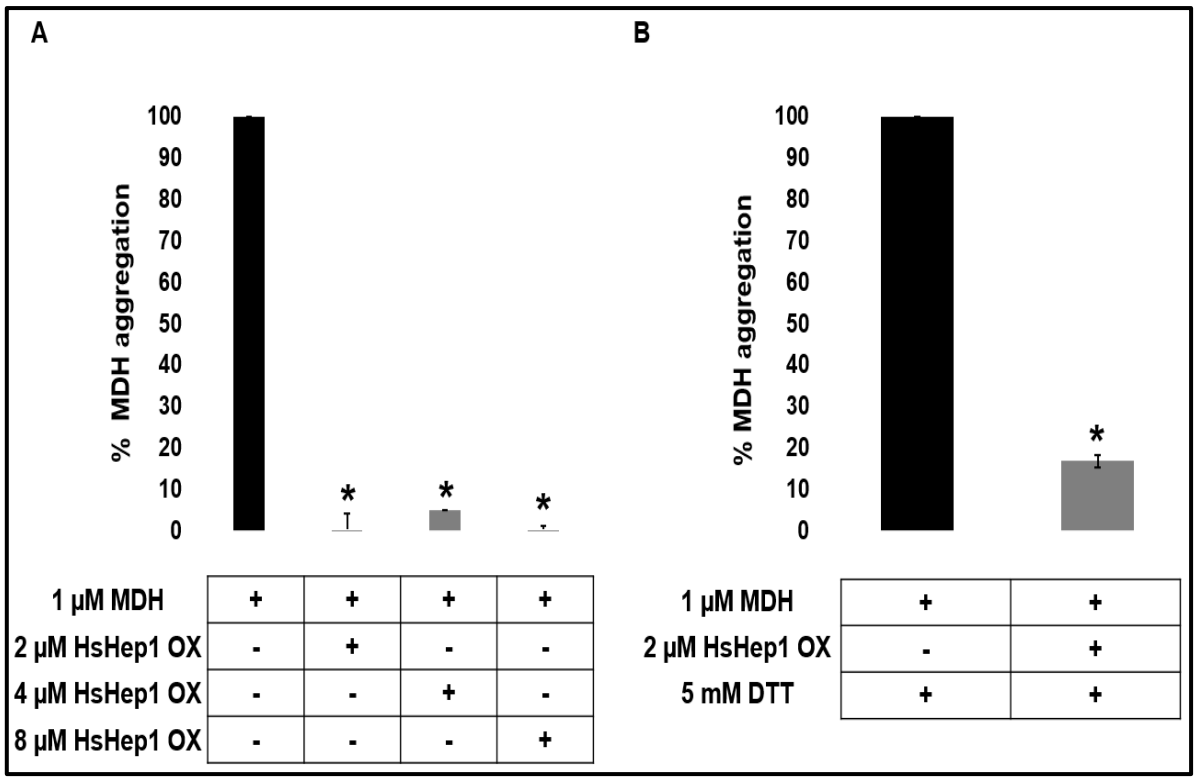

Figure 4.10: Oxidized HsHep1 exhibits holdase activity towards thermally aggregated L-malate dehydrogenase (MDH). When incubated at 48 °C with increasing concentrations of oxidized **A)** HsHep1 (2-8 µM) the presence of MDH (1 µM) aggregates was considerably reduced. **B)** In the presence of 5 mM DTT, the suppression of aggregation activity of oxidized HsHep1 (2 µM) was considerably reduced. The % aggregation was determined with the aggregation of the MDH alone set at 100 %. The assays were conducted in triplicate using independently expressed and purified batches of proteins. The error bars represent standard deviation, with the asterisks indicating a significant difference between reactions with MDH alone and those containing HsHep1. Statistical significance was benchmarked at $P < 0.05$ using a student's T-test.

The findings of this preliminary study suggest that TbHep1 and HsHep1, similar to Hsp33, possess holdase activity that is amenable to influences of the cells redox state. Hsp33 is active under oxidative stress, and inactive under reducing conditions (Jakob *et al*., 1999). Without having treated TbHep1 and HsHep1 with an oxidizing agent they exhibited potent holdase activity (Figure 4.3), having been purified under mildly reducing conditions (dialysed in buffer containing 0.5 mM DTT). Also, in previous studies whereby there was no oxidative stress exerted, HsHep1 was shown to be a potent holdase independently of mtHsp70 (Goswami *et al*., 2010; Dores-Silva *et al*., 2021). Hep1 suppression of mtHsp70 aggregation in this study and previous studies has been determined under conditions whereby oxidative stress was not a factor (Dores-Silva *et al*., 2015; Nyakundi *et al*., 2016; Dores-Silva *et al*., 2021). The co-expression of mtHsp70 with Hep1 in order to enhance the solubility of mtHsp70 in *E. coli* can also be said to occur under reducing conditions since the prokaryotic cytosol is known to be a reducing environment (Sichting *et al*., 2005; Dores-Silva *et al*., 2013; Dores-Silva *et al*., 2015; Nyakundi *et al*., 2016). Therefore, more investigations are required to elucidate the underlying redox-related mechanisms of the Hep1 chaperone activities. In the study by Dores-Silva et al. (2021) HsHep1

was prepared in TKP buffer containing 2 mM β-mercaptoethanol, whilst in this study all the proteins were prepared in buffer containing 0.5 mM DTT. Interestingly, in the study by Jakob et al. (1999), it was reported that Hsp33 not having been treated with oxidizing or reducing agent possesses activity that is on par with that of oxidized Hsp33. Furthermore, in the same study, substantial Hsp33 inhibition was observed in the presence of 3 mM DTT.

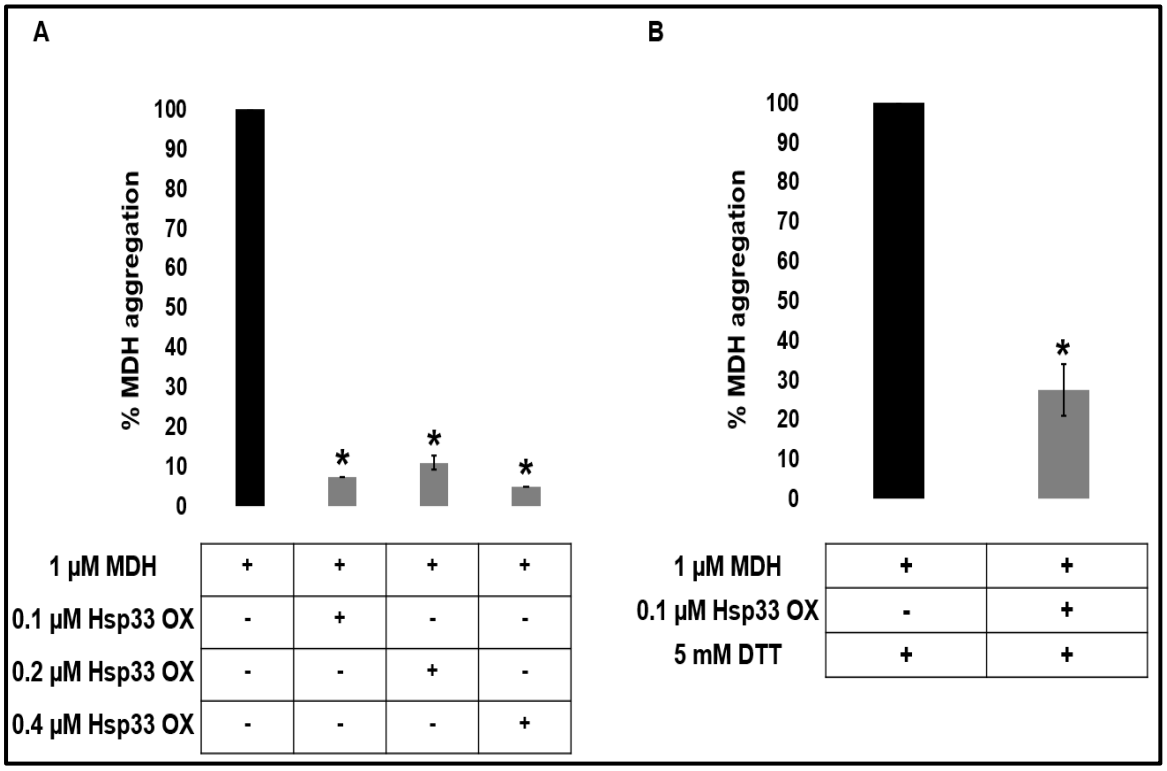

Figure 4.11: Oxidized Hsp33 exhibits holdase activity towards thermally aggregated L-malate dehydrogenase (MDH). When incubated at 48 °C with increasing concentrations of oxidized **A)** Hsp33 (0.1-0.4 µM) the presence of MDH (1 µM) aggregates was considerably reduced. **B)** In the presence of 5 mM DTT, the suppression of aggregation activity of oxidized Hsp33 (0.1 µM) was considerably reduced. The % aggregation was determined with the aggregation of the MDH alone set at 100 %. The assays were conducted in triplicate using independently expressed and purified batches of proteins. The error bars represent standard deviation, with the asterisks indicating a significant difference between reactions with MDH alone and those containing Hsp33. Statistical significance was benchmarked at $P < 0.05$ using a student's T-test.

4.4.7 TbHep1, HsHep1 and Hsp33 treated with H_2O_2 and heat shock exhibited structural modifications

Hsp33 has been previously reported to form two intramolecular disulphide bonds by iodoacetamide/AMS thiol trapping (Jakob *et al*., 1999) at the CXC and CXXC motifs (Graumann *et al*., 2001). In this study, with Hsp33 as a comparative control, oxidized TbHep1 and HsHep1 were subjected to reducing and non-reducing SDS-PAGE in order to decipher whether there may have been disulphide bond formation. Oxidized TbHep1, HsHep1 and Hsp33 were shown to migrate slightly further when not treated with β-mercaptoethanol (Figure 4.12). This suggests that the proteins had formed disulphide bonds at their CXXC motifs, resulting in more compact conformations which in turn resulted in further

migration in the SDS-PAGE gels. The disulphide bonds were amenable to reduction by β-mercaptoethanol, resulting in less compact conformations that migrated slightly less (Figure 4.12). The importance of including BSA in this structural assessment is that the mammalian serum albumin is known to possess multiple cysteine residues which can result in the formation of 17 disulphide bonds (Carter and Ho, 1994). As can clearly be observed, oxidized BSA migrated to a much greater extent when compared to the reduced sample (Figure 4.12), serving as an indication of what should be expected of the migration of non-reduced and reduced protein samples of the same protein on an SDS-PAGE gel.

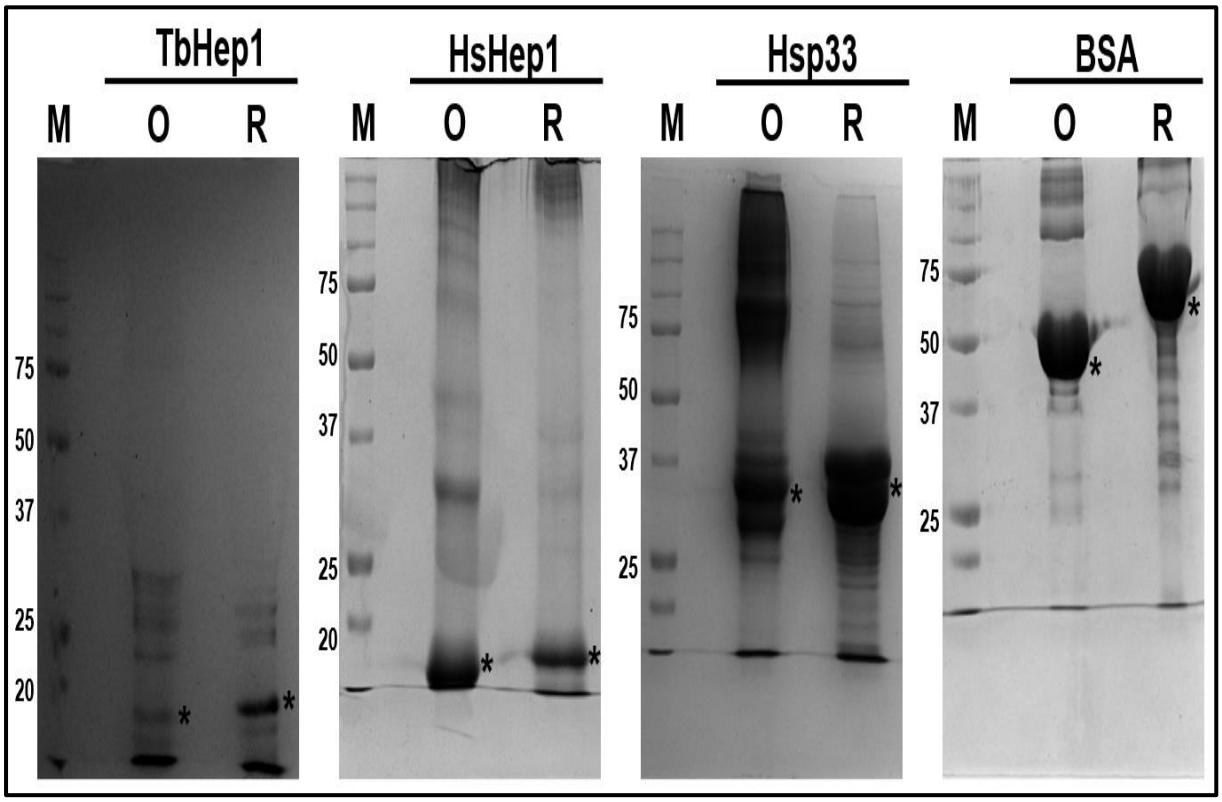

Figure 4.12: Reducing and non-reducing SDS-PAGE resulted in the electromobility shifts of the oxidized proteins. The oxidized proteins were separated on 10 % acrylamide gels using sample buffer with (lanes labelled R) or without (lanes labelled O) 5 % β-mercaptoethanol. In the lanes labelled M is the protein molecular mass marker (Bio-Rad Precision-Plus™ All Blue standards). The black asterisks indicate the point at which the bands representing the proteins of interest occur.

The Hsp33 doublet can also be observed in Figure 4.12 as in Figure 3.16 in Section 3.4.1.9. In Section 3.4.1.9 it appeared as though the doublet could have been due to the presence of both oxidized and reduced Hsp33 species in the same sample. However, in this section, one sample was loaded using buffer containing β-mercaptoethanol, whereas the other sample was subjected to non-reducing SDS-PAGE. In the sample loaded with buffer void of β-mercaptoethanol resulted in the doublet migrating even further, therefore eliminating the possibility that the stacked bands are due to the presence of both reduced and oxidized Hsp33 species. As such, it could be a possibility that the doublet was due to the

overloading of a highly concentrated Hsp33 sample. Incorporating western blot detection could have served as further confirmation of the apparent electromobility shift observed between the samples subjected to reducing or non-reducing SDS-PAGE.

Treating Hsp33 with oxidizing agents under heat stress not only leads to the formation of disulphide bonds, but further results in dimerization (Graumann *et al*., 2001). In a technique adapted from Segal and Shapira et al. (2015), oxidized and reduced independent samples of each of the proteins were analysed by native PAGE. Oxidized Hsp33 was shown to dimerize (Figure 4.13) as has previously been reported (Segal and Shapira, 2015). Oxidized and reduced TbHep1 appeared as monomeric species. Reduced HsHep1 appeared to be monomeric, whilst the oxidized sample of the protein showed no bands in the lane (Figure 4.13).

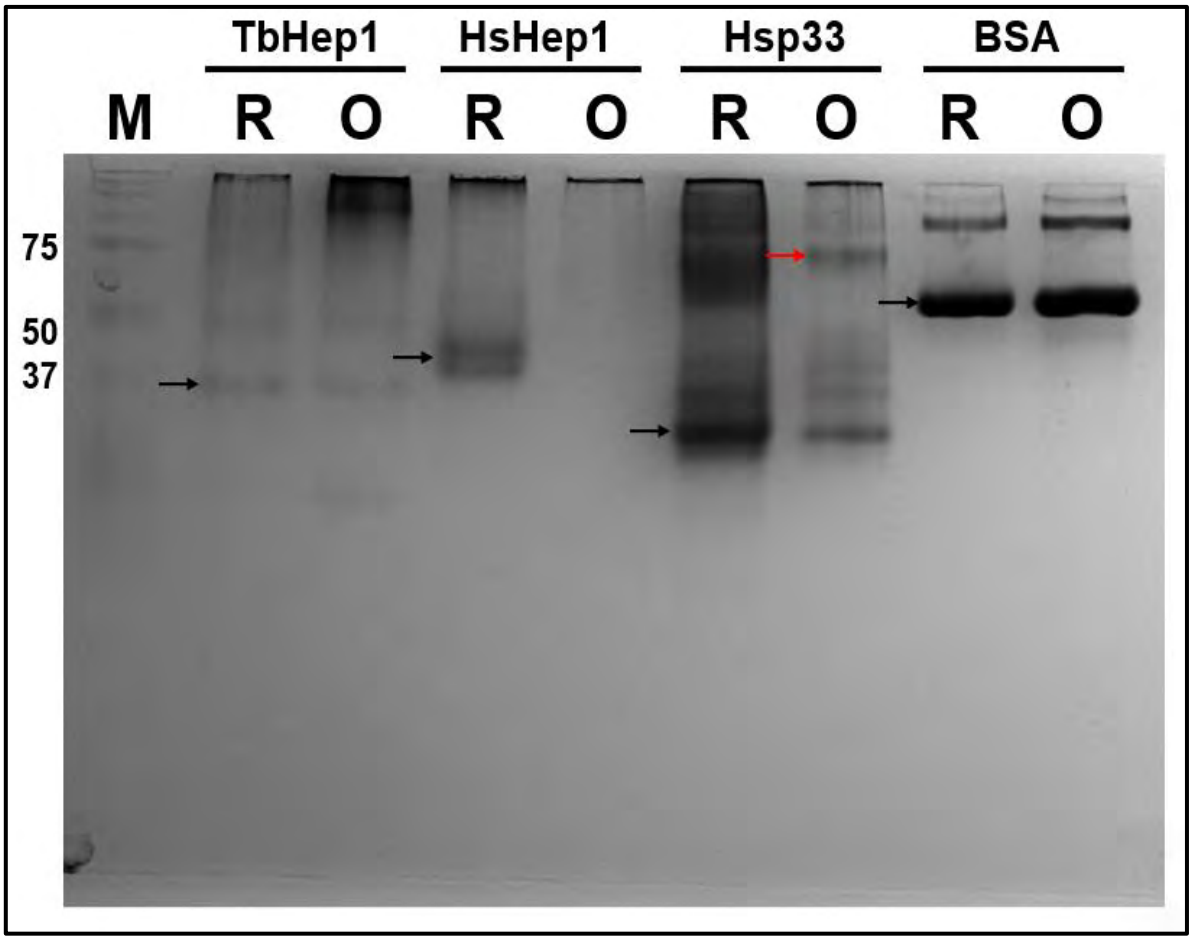

Figure 4.13: Reduced and oxidized samples of TbHep1, HsHep1 and Hsp33 on a 12 % acrylamide gel. The samples were separated under native PAGE conditions at 60 V for 3 hours. In the lanes labelled R are the samples purified under strictly reducing conditions. In the lanes labelled O are the samples that were oxidized. In the lanes labelled M is the protein molecular mass marker (Bio-Rad Precision-Plus™ All Blue standards). The black arrows point to the bands representing the proteins of interest. The red arrow points to the Hsp33 dimer.

This could mean that oxidized HsHep1 resulted in a higher order of oligomerization which could not migrate into the gel. Interestingly, the apparent TbHep1 and HsHep1 monomers migrated less than

Hsp33. This could be due to HsHep1 having been determined to be a slightly elongated monomer (Dores-Silva *et al*., 2013), therefore it could be inferred TbHep1 is also structurally elongated. Moreover, LbrHep1 has also been determined to be an extensively elongated monomer, which was suggested to be due to the extended N-terminal region (Dores-Silva et al., 2015). In place of native PAGE, oligomeric differences between the reduced and oxidized protein samples could have been observed using fast protein liquid chromatography (FPLC) whereby oligomeric species would elute before monomeric species.

4.4.8 Assessment of the steady-state kinetics of TbmtHsp70, HSPA9, TbHsp70 and HSPA1A

Hsp70s are ATP-dependant, possessing the ability to hydrolyze ATP. Thus, Hsp70s are regulated between different functional states by whether they are ATP or ADP bound (Kityk *et al*., 2018). The Michaelis-Menten curves obtained from this study show that there is a positive correlation between ATPase activity rate and ATP concentration of TbmtHsp70, HSPA9, TbHsp70 and HSPA1A (Figure 4.14). The K_m and V_{max} values are shown in Table 4.1. The outcomes from this study imply that TbmtHsp70 has a lower affinity for ATP compared to its cytosolic counterpart, TbHsp70. The V_{max} values imply the inverse, with TbmtHsp70 exhibiting a higher ATPase activity rate than TbHsp70. In a previous study with the cytosolic TbHsp70s, under differing experimental conditions, Bentley and Boshoff (2019) found that TbHsp70 had a higher basal activity than that of TbHsp70.4. Compared to HSPA9, TbmtHsp70 has a lower affinity for ATP, but still exhibited a higher ATPase activity rate. When comparing the human Hsp70s, HSPA9 had a slightly elevated ATPase activity rate and higher affinity for ATP.

Table 4.1: The K_m and V_{max} values of the Hsp70s as they relate to their ATP hydrolysis activities.

Hsp70 homologue	K_m (µM)	V_{max} (µM P_i/min)
TbmtHsp70	641.2	0.4906
TbHsp70	50.52	0.2476
HSPA9	125.1	0.3002
HSPA1A	159.4	0.2683

The K_m of HSPA9 and HSPA1A were previously reported to be 190 and 270 µM, respectively. The V_{max}, on the other hand, was determined to be 0.38 and 0.21 µM P_i/min for HSPA9 and HSPA9, respectively (Dores-Silva *et al*., 2015). The V_{max} values obtained in this study for HSPA9 and HSPA1A are similar to those reported previously by Dores-Silva et al. (2015), whilst the K_m values are different. The divergence in the K_m values could be due to differences in methodology, nonetheless, the results obtained in this study still imply that HSPA9 has a higher affinity for ATP than HSPA1A. The increased ATP hydrolysis rates of TbmtHsp70 and HSPA9 point to a potential physiological adaptation of the

mitochondrial Hsp70s. The import of proteins into the mitochondrion is driven by energy derived from ATP hydrolysis by mtHsp70. Therefore, it could be hypothesized that for an expeditious protein import process, mtHsp70s may be required to hydrolyse ATP at increased rates.

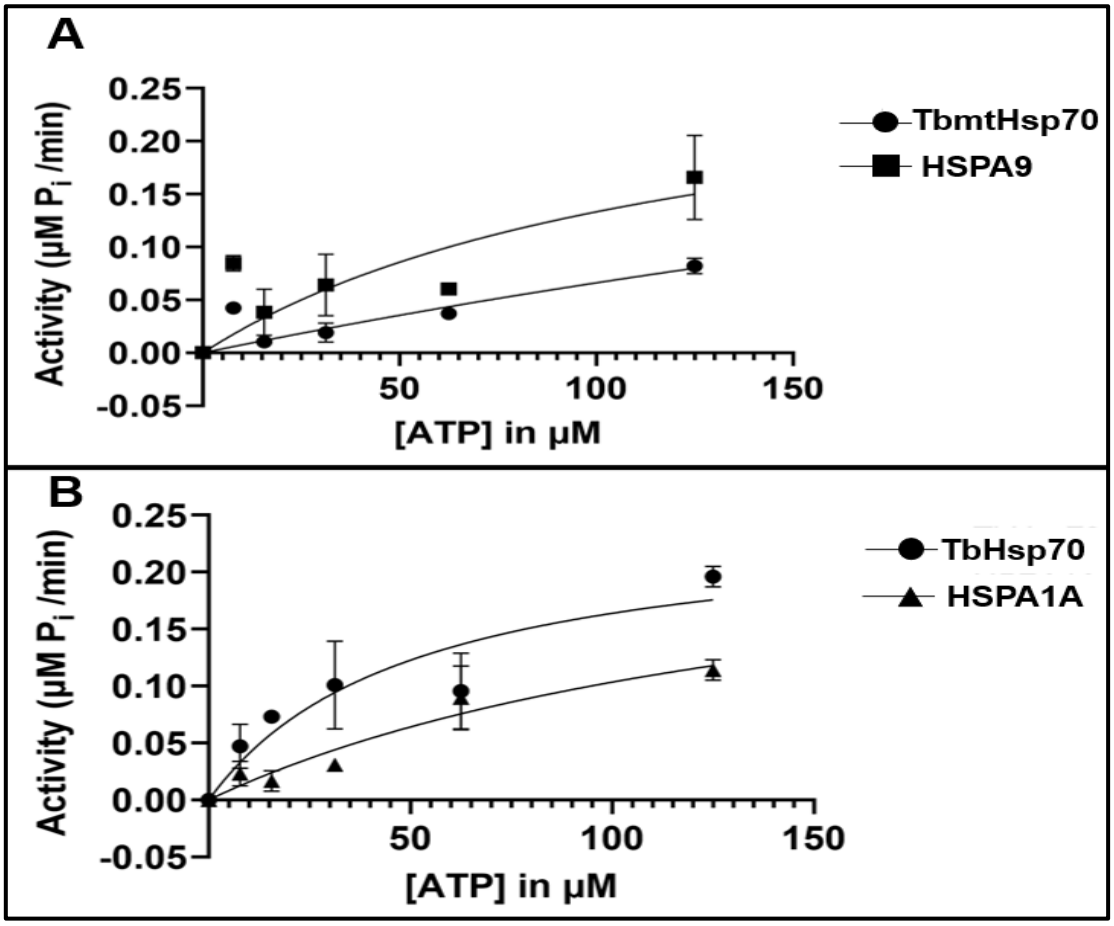

Figure 4.14: Characterization of the steady-state kinetics of the Hsp70s with ATP as a substrate. The Michaelis-Menten curves of the **A)** mitochondrial Hsp70s (0.2 μM) and **B)** cytosolic Hsp70s (0.1 μM) generated by plotting the ATPase activities (expressed as μM P_i generated per min) of the Hsp70s as a function of ATP concentration (μM) using GraphPad Prism 9.2.0 (332) software. Non-linear regression was used. The assays were conducted in triplicate using independently expressed and purified batches of proteins.

4.4.9 TbHep1 and HsHep1 stimulated the basal ATPase activity of TbmtHsp70, HSPA9, TbHsp70 and HSPA1A

When evaluating the basal ATPase activities of the Hsp70s, they exhibited concentration dependant ATPase activity, except for HSPA1A (Figure 4.15). HSPA1A appeared to have a slightly lower ATPase activity than the *T. brucei* cytosolic Hsp70 (Figure 4.15). The reason for HSPA1A apparently having lower ATPase activity rate between 0.1 and 0.2 μM could be due to being saturated by ATP at low concentrations. In a study by Dores-Silva et al. (2015), HSPA1A has an ATPase activity rate that is approximately half that of HSPA9. These reports are also reflected in this study. The increase in ATPase activity as protein concentration increases indicates that more ATP was being hydrolysed as a result of

increased enzyme concentration, validating the Hsp70s as enzymes that hydrolyse ATP as their substrate.

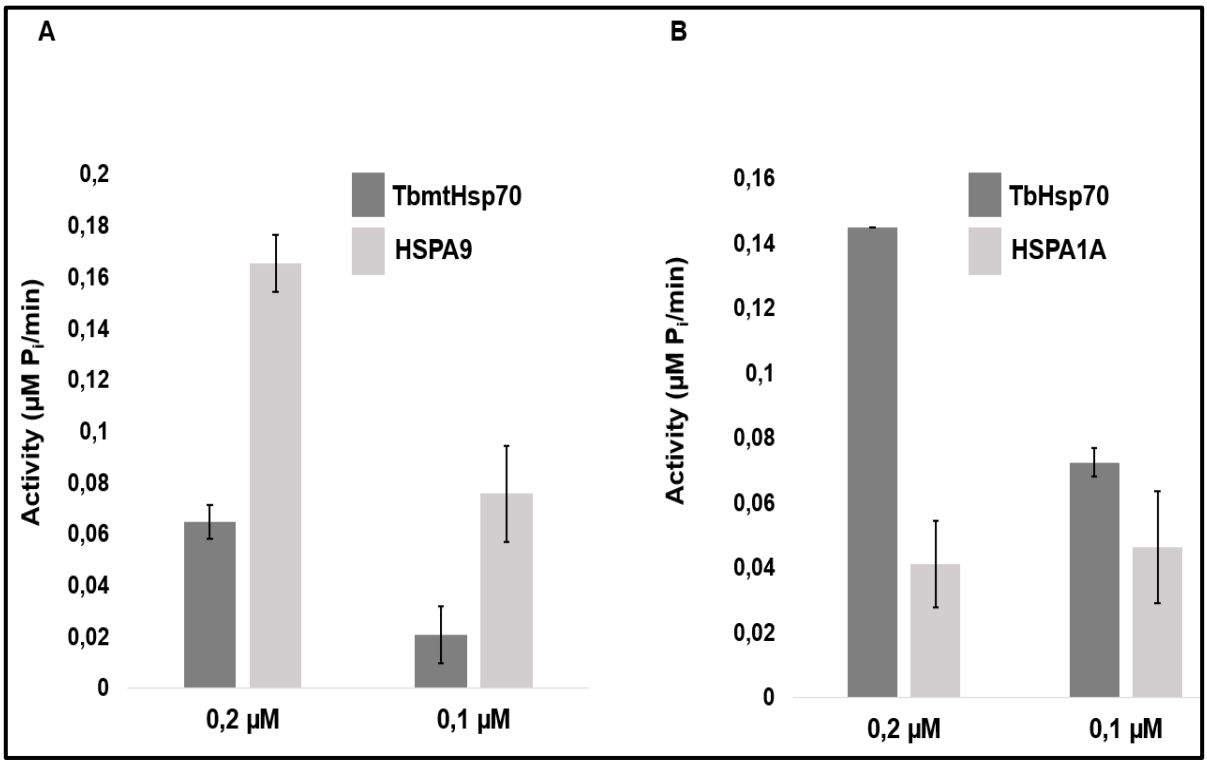

Figure 4.15: The basal ATPase activities of the Hsp70s expressed as µM P_i generated per min. The assay on the **A)** mitochondrial (0.1-0.2 µM) and the **B)** cytosolic Hsp70 (0.1-0.2 µM) was conducted at 37 °C in the presence of 125 µM ATP for 1 hour. The assays were conducted in triplicate using independently expressed and purified batched of proteins.

The modulatory effects of the Hep1 orthologues on the ATPase activity rates of the Hsp70s was also assessed, using excess molar concentrations of Hep1 (Figure 4.16). TbHep1 had a notable stimulatory effect on the ATPase activity of TbmtHsp70 but had little effect on the activities of the other Hsp70s. HsHep1, on the other hand, stimulated the ATPase activities of all the Hsp70s, except TbHsp70 (Figure 4.16). The stimulatory effects of TbHep1 and HsHep1 were lower on TbHsp70 and HSPA1A, respectively, than on the cytosolic Hsp70s from the same species (Figure 4.16). These results indicate that the Hep1 orthologues have greater specificity for their respective mtHsp70 orthologues, compared to the cytosolic Hsp70s. These results also point to HsHep1 being a more effective co-chaperone than TbHep1 since HsHep1 also stimulated the ATPase activity of HSPA1A. The study by Dores-Silva et al. (2021) also reported that HsHep1 had a greater stimulatory effect on the ATPase activity of monomeric HSPA9 than HSPA1A. In the same study, the same also held true for the modulatory effects of HsHep1 on aggregates of HSPA9 and HSPA1A basal ATPase activities. The stimulatory effect of HsHep1 on the ATPase activity of HSPA9 was also reported by Goswami et al. (2010). HSPA9 was also previously shown to be more amenable to ATPase activity stimulation by the NR peptide (sequence: NRLLLTG) compared to HSPA1A (Dores-Silva *et al*., 2015). The NR peptide is a substrate

peptide that is known to bind to *E. coli* DnaK with high affinity (Gragerov *et al*., 1994). The ability of Hep1 to stimulate the ATPase activity of mtHsp70 was also reported with the *L. braziliensis* orthologues whereby LbrHep1 stimulated the ATPase activity of LbmtHsp70 (Dores-Silva *et al*., 2015). Yeast Hep1 was shown not to have an effect on the ATPase activity of mtHsp70 (Sichting *et al*., 2005).

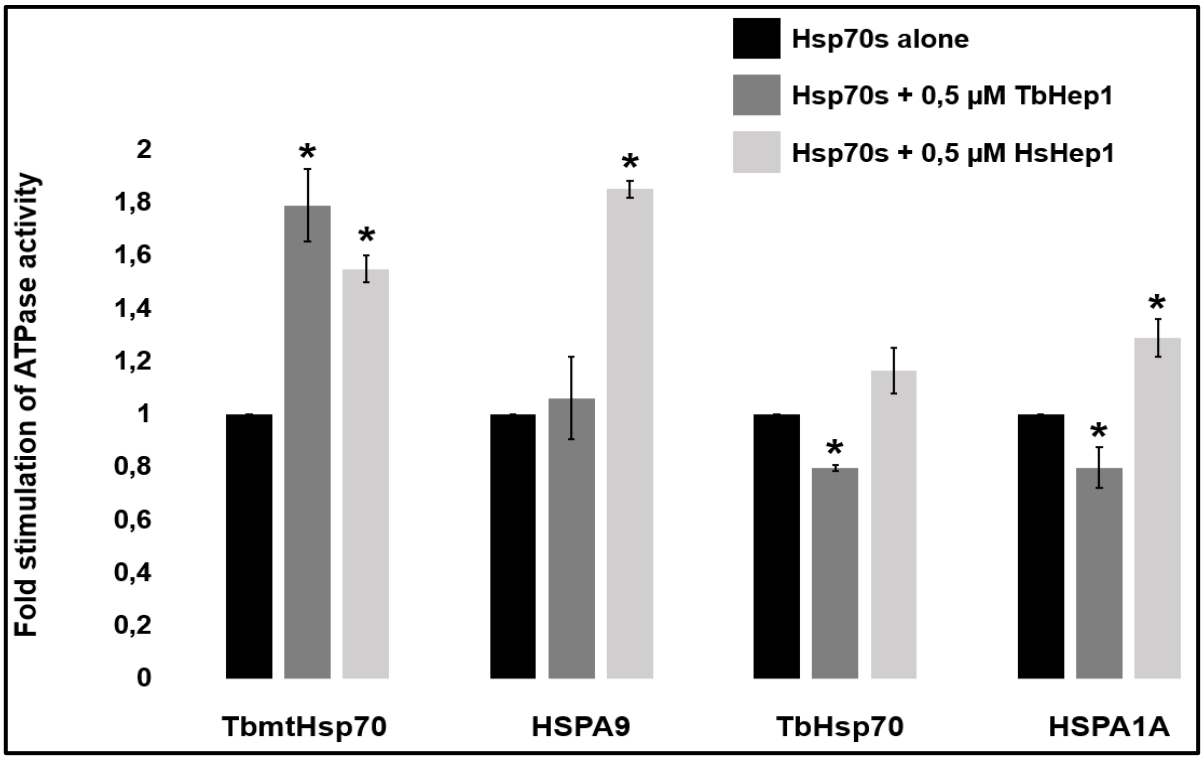

Figure 4.16: TbHep1 and HsHep1 enhanced the basal ATPase activities of Hsp70s. Excess molar concentrations of TbHep1 (0.5 µM) and HsHep1 (0.5 µM) were used to assess the ability of the Hep1 orthologues to modulate the intrinsic ATPase activities of the Hsp70s (0.1 µM). The Hsp70s alone were benchmarked at 1-fold. The black asterisks indicate a significant difference between assays with the Hsp70s alone and those in combination with either TbHep1 or HsHep1. Background noise from the ATPase assay with Hep1 orthologues alone was also taken into account. The assays were conducted in triplicate using independently expressed and purified batches of protein. Statistical significance was benchmarked at $P < 0.05$ using a student's T-test.

4.5 Conclusions

The aim of this study was to biochemically characterize the TbHep1 and TbmtHsp70 partnership. Also incorporated into this study were the stress inducible cytosolic Hsp70s from the *T. brucei* parasite and humans. The type I JDP Tbj2 was also used as a control in relation to some biochemical properties of the Hep1 orthologues that were being investigated. Tbj2 has previously been determined to suppress the thermally induced aggregation of model substrate MDH. In this study, TbHep1 was determined to be a TbmtHsp70 partner protein, as it suppressed the thermally induced aggregation of the mtHsp70. The characterization of the Hep1/mtHsp70 system in *T. brucei* was carried out in parallel to that of the previously characterized human system (Goswami *et al*., 2010; Dores-Silva *et al*., 2021). Indeed, HsHep1 suppressed the thermally induced aggregation of HSPA9. In this study, TbHep1 was also tested for the ability to interact with the cytosolic Hsp70, TbHsp70. TbHep1 was shown to interact with

TbHsp70 by preventing the formation of thermal aggregates of TbHsp70. Parallel to the characterization of the interaction of TbHep1 with TbHsp70, was the determination of the effect of HsHep1 on HSPA1A thermally induced aggregation, as has recently been reported by Dores-Silva et al. (2021). Indeed, in this study, HsHep1 also prevented the thermally induced aggregation of HSPA1A. HsHep1 has been reported to localise in the nucleoplasm, whilst HSPA9 also occurs in the cytosol (Dores-Silva *et al*., 2021). Therefore, there could be a possibility that HsHep1 co-localises with HSPA9 in the cytosol, having the opportunity to also interact with cytosolic Hsp70. The findings of this study suggest that a partnership between Hep1 and cytosolic Hsp70 is possible. TbHep1 and HsHep1 also suppressed the thermally induced aggregation of HSPA1A and TbHsp70, respectively.

TbHep1 and HsHep1 were further shown to possess the ability to suppress the thermally induced aggregation of MDH by means of both spectrophotometric and densitometric analysis. By densitometric analysis, they were further shown to possess holdase activity using citrate synthase as a substrate. HsHep1 appeared to be a more effective at suppressing the aggregation of MDH than TbHep1. TbHep1 seemed to be slightly more effective at suppressing the aggregation of citrate synthase than HsHep1. Therefore, the activity of TbHep1 and HsHep1 could also be substrate dependant, rather than HsHep1 just being a more efficacious chaperone. In this regard, it would be worthwhile to determine the holdase activity of other Hep1 orthologues, TbHep1 and HsHep1 included, using a wide array of aggregated proteins as substrate. Incorporating PfHep1 and LbrHep1, which were reported to not possess holdase activity against MDH and citrate synthase, would be useful in determining the substrate specificity/affinity parameters and holdase capabilities of Hep1. The suppression of MDH aggregation activity of TbHep1 and HsHep1 mirrored that of Tbj2. HsHep1 in this study was also shown to be more effective against HSPA9 aggregation compared to TbHep1 on TbmtHsp70 aggregates. The potential physiological relevance thereof being that mtHsp70 defects are fatal for mammalian cells (Wadhwa et al., 1993). To validate this hypothesis, the effects of TbmtHsp70 deletion in *T. brucei* could be assessed. The mitochondrial Hsp70s, TbmtHsp70 and HSPA9, were both determined to be active on thermally induced aggregates of MDH by means of spectrophotometric and densitometric analysis. By densitometric analysis, TbmtHsp70 was also shown to suppress the thermally induced aggregation of citrate synthase, albeit with less efficiency. Substrate preference has previously been demonstrated with TbHsp70.c being less effective on chemically denatured rhodanese compared to thermally aggregated MDH. The suppression of aggregation activity of PfHsp70-3 on thermally aggregated MDH or citrate synthase was demonstrated to be similar (Nyakundi *et al*., 2016). HSPA9 has previously been shown to be effective against citrate synthase and DTT-treated insulin aggregates (Khan *et al*., 2017). In addition to determining whether Hep1 proteins interact with cytosolic Hsp70s, TbHsp70 and HSPA1A were also included for the comparative validation of the suppression aggregation activity of TbmtHsp70 and HSPA9. The suppression of aggregation activity of TbmtHsp70 and HSPA9 was determined to be similar to that of TbHsp70 and HSPA1A by means of spectrophotometric analysis. TbHsp70 and MDH

have previously been determined to suppress aggregation, with TbHsp70 having been shown to suppress the thermally induced aggregation of MDH (Bentley and Boshoff, 2019; Serlidaki *et al*., 2020).

This is the first study to analyse the functional and structural effects of oxidative stress on Hep1 proteins. Both TbHep1 and HsHep1 demonstrated to be potent holdase chaperones as they suppressed the thermally induced aggregation of MDH under the same conditions as with the reduced samples (0.5 mM DTT) of the same proteins. The holdase activity of the oxidized Hep1 orthologues was partially reversed when the assay was carried out in the presence of 5 mM DTT. The comparative control, Hsp33 followed the same trend as the test proteins in this study, similar to the reports of previous studies (Jakob *et al*., 1999), *comprehensively reviewed by* Ulrich et al. (2021). Hsp33 is absent in higher eukaryotes, making it tempting to speculate that Hep1 could be a descendant or evolutionary replacement of Hsp33 in a functional continuum since the mitochondrion is a symbiotic organelle (Nyakundi *et al*., 2018). The eukaryotic Hsp33 in algae, *Chlamydomonas reinhardtii*, unlike prokaryotic Hsp33, is activated by H_2O_2 induced oxidative stress, even in the absence of heat (Segal and Shapira, 2015). TbHep1 and HsHep1 should further be studied to determine the specific effects of oxidative stress, in the absence of heat shock. It is assumed that oxidative stress would result in disulphide bond formation between the cysteine residues at the CXXC motifs of the Hep1 orthologues. By means of reducing and non-reducing SDS-PAGE, it was observed that the oxidized Hep1 orthologues migrated further through the polyacrylamide gel, suggesting that the oxidized forms of the proteins were more compact as a result of disulphide bond formation. The same was also observed for the comparative control, Hsp33, which has previously been shown to form to disulphide bonds at its CXC and CXXC motifs by means of thiol trapping (Graumann *et al*., 2001). Thiol trapping would provide additional validation of the results obtained in this study that indeed the migration differences were due to disulphide bond formation. A known consequence of disulphide bond formation is the release of the zinc ion coordinated by the cysteine residues of Hsp33 (Graf *et al*., 2004). Analysing zinc binding by reduced or oxidized TbHep1 and HsHep1 samples could also assist in deciphering if any disulphide bonds occur. The comparative control, Hsp33, is known to dimerize as a result of the disulphide bond formation (Graumann *et al*., 2001), and this was confirmed in this study by means of native PAGE. Reduced and oxidized TbHep1 was shown to be monomeric, with the same holding true for reduced HsHep1. Oxidized HsHep1 did not show any bands in the native PAGE gel, probably due to a higher order of oligomerization which could not migrate into the gel. Previous studies whereby Hep1 is not oxidized have reported oligomerisation (Dores-Silva *et al*., 2013). Hsp33 dimerization has previously been demonstrated by native PAGE (Segal and Shapira, 2015). The reducing and non-reducing SDS-PAGE was confirmed using BSA as a control. Mammalian serum albumins form 17 disulphide bonds (Carter and Ho, 1994). BSA served as a good positive control as a it served as a template of what differences in migration should be expected from reduced and oxidized forms of the same protein. In the native PAGE, the HsHep1 monomers appeared to have migrated less than Hsp33. HsHep1 has previously been shown to be an elongated monomer (Dores-Silva *et al*., 2013),

as well as LbrHep1 (Dores-Silva *et al*., 2015). Analytical size exclusion chromatography (aSEC) was used in determining the structural elongation of HsHep1 and LbrHep1. The structural elongation can also be inferred for TbHep1. Fast protein liquid chromatography (FPLC) could also be useful for determining oligomerisation.

With regard to the ATPase activities of the Hsp70s, they were all shown to possess the ability to hydrolyse ATP. Deriving from the K_m values, TbHsp70 was shown to have the highest affinity for ATP, followed by HSPA9, HSPA1A and then TbmtHsp70. With the parasitic Hsp70s, the cytosolic Hsp70 had a higher affinity for ATP compared to the mitochondrial paralog, whilst the inverse was true for the human Hsp70s. The mitochondrial Hsp70s exhibited higher ATPase activity rates compared to the cytosolic paralogs, and this applied to both the parasitic and human orthologues. When determining if increased Hsp70 concentration resulted in increased ATP hydrolysis it was found that increasing the concentrations of all the Hsp70s, except HSPA1A, resulted in an increase in P_i generation. This pointed to the Hsp70s being enzymes that hydrolyze ATP as their substrate. TbHep1 was shown to have a stimulatory effect on the ATPase activity of TbmtHsp70, and not on TbHsp70. HsHep1 stimulated the basal ATPase activities of HSPA9 and HSPA1A, HSPA9 to a greater extent. This was in line with the findings of a previous study (Dores-Silva *et al*., 2021). These findings indicate that the Hep1 orthologues have a greater interaction specificity for the mitochondrial Hsp70, and this is affirmed by findings of previous studies (Dores-Silva *et al*., 2015; Dores-Silva *et al*., 2021). The ability to enhance the ATPase activity of Hsp70 is associated with type I and II J-proteins. In this study, TbHep1 and HsHep1 also exhibited the J-protein property of possessing holdase function. This raises the question of whether Hep1 also serves the function of presenting Hsp70 with client protein for folding.

The benefit of characterizing the *T. brucei* Hep/mtHsp70 partnership parallel to that of humans is that it could preliminarily be assessed if this system's interaction mechanisms are conserved between the two species. TbHep1 was shown to be capable of suppressing HSPA9 and HSPA1A aggregation, and this was found to be also the case for HsHep1 on TbmtHsp70 and TbHsp70 aggregates. HsHep1 also stimulated the basal ATPase activity of TbmtHsp70. These findings imply that the Hep1 mode of action on mtHsp70 is conserved between *T. brucei* and humans.

CHAPTER FIVE
Conclusions and future perspectives

This study focussed on the mitochondrial Hsp70 (mtHsp70) and Hsp70 escort protein 1 (Hep1) of the African trypanosome, with the foresight that it could potentially be relevant for anti-trypanosomal drug discovery. The human orthologues of mtHsp70 and Hep1 were included for the benefit of comparative analysis since numerous studies have characterised the human mtHsp70 (HSPA9) and Hep1 (HsHep1) partnership. Furthermore, they were included in order to determine if there are any differential aspects between the human and parasitic mtHsp70/Hep1 systems that could potentially be exploited in the interest of anti-trypanosomal drugs, such that only the parasitic proteins are inhibited. Due to possessing zinc finger domains in common, the Hep1 orthologues were also comparatively analysed together with type I J-proteins and Hsp33 orthologues.

In *silico* analysis of TbHep1 and HsHep1, including many other putative Hep1 orthologues was carried out. In terms of primary structure, TbHep1 and HsHep1, along with all the Hep1 orthologues, were determined to possess a highly conserved zinc finger domain. Outside of the zinc finger domain, there was divergence. However, for the first time in this study, it was uncovered that the N- and C-terminal regions are actually very similar when compared amongst orthologues from closely related organisms. This observation was also made in terms of predicted posttranslational modifications. The posttranslational modifications were prevalent in the N- and C-terminal regions, whereby some of them were common amongst orthologues of closely related organisms. This led to the conclusion that the N- and C-terminal regions may be functionally relevant within the context of the organisms in which they occur. Future studies should explore this hypothesis, whereby complementation assays are carried out in cells of organisms using Hep1 chimeras possessing N- and C-terminal regions from Hep1 orthologues of distant organisms. This could be a first step in determining if the N- and C-terminal regions are essential according to species of origin. For example, with human cells with the Hep1 gene knocked down, a chimera constituted of the HsHep1 zinc finger, linked to the N- and C-terminal regions of TbHep1 could be used in complementation assays.

HsHep1 in the study by Dores-Silva et al., (2021) was reported to potentially bind the mitochondrial membranes, localise in the nucleoplasm and interact with cytosolic Hsp70. With regard to the potential of HsHep1 to localise in the nucleoplasm it should be kept in mind that HSPA9 has also been shown to localise in the nucleus under stress conditions (Wadhwa et al., 2006). In the case of parasitic diseases such as HAT, the differences between the HsHep1 and TbHep1 orthologues should be explored to form a foundation from which anti parasitic drugs may be developed, such that they have no detrimental effects in human cells. In comparing the predicted tertiary structures of TbHep1 and HsHep1, a structural variation was observed at their N-terminal regions. The regions outside of the zinc finger

domains are known to be divergent in terms of primary structure, but in this case they were also different in terms of secondary structure at the N-termini. The N-terminal region signature sequence that TbHep1 shares with the other kinetoplastid organisms occurred within an α-helix, which HsHep1 lacks. In terms of drug discovery, docking *in silico* analysis could be carried out using a library of compounds to predict those that preferentially bind to the TbHep1 signature sequence before laboratory experiments are carried out.

Phylogenetic and distance analysis proved that in general, Hep1 orthologues from related organisms are similar. This was observed when the Hep1 orthologues were analysed according to their full-length sequences, the N-terminal region and the zinc finger domain. However, with analysis using the full-length sequences and N-terminal region, there were some discrepancies whereby some orthologues from distantly related organisms occupied the same clades. Also, with the yeast and flies, orthologues from different genera were segregated when analysed according to the full-length sequences and the N-terminal regions. Surprisingly, though highly conserved across all the orthologues, the zinc finger domain phylogenetic analysis strictly segregated the orthologues according to which type of organism they originate from. Therefore, all the fly Hep1 orthologues converged, regardless of genera, the same held true for the yeast Hep1 orthologues of different genera. This led to the conclusion that even though the zinc finger domain is highly conserved throughout nature, there are some residues or motifs within this domain that can only be found in the orthologues of certain organisms. Also, regarding the zinc finger domain of the Hep1 orthologues, they possess almost the same number of amino acid residues, and have similar molecular weights. Syntenic analysis revealed that synteny is conserved amongst orthologues of close relations.

In terms of the mammalian Hep1 orthologues, some murine and primate organisms were discovered to possess multiple isoforms of Hep1. It seemed as if there could have been Hep1 gene duplication events in these organisms, but the isoforms within a single organism were determined to possess the same gene IDs. This suggests that the Hep1 gene in these organisms is subject to alternative splicing whereby multiple products may be obtained from the same gene. These isoforms need to be confirmed at the proteomic level, and complementation assays carried out on knock down cells to determine the physiological significance of these isoforms. What is intriguing about the murine Hep1 isoforms is that some of them lack the zinc finger domain, falling into two categories of sequence conservation. Since alternative splicing is accepted to be a mechanism by which higher eukaryotes achieve complexity from a limited gene set, it should be investigated why the primate Hep1 isoforms all possess the zinc finger domain and are highly identical within the same organism (Tress et al., 2007).

TbHep1 and HsHep1 were also analysed comparatively with type I J-proteins and Hsp33 orthologues. Primary sequence analyses revealed that Hep1 conservation with the zinc fingers of the J-proteins and Hsp33 orthologues was at the cysteine rich motifs that bind zinc. Distance analyses revealed the Hep1

orthologues to be slightly more similar to type I J-proteins compared to the Hsp33 orthologues. The substrate binding mechanisms of Hsp33 and type I and type II J-proteins have been described. Moreover, the ability of type I and II J-proteins have been described in terms of how they stimulate the ATPase activity of Hsp70s. With Hep1, these mechanisms still need to be uncovered. With regard to the cysteine rich motifs of TbHep1 and the other kinetoplastid Hep1 orthologues used in this study, the kinetoplastid Hep1 genes are in close proximity with genes possessing CXC, CXXC and CXXXC motifs. This points to the cysteine motifs in the kinetoplastid Hep1 orthologues as being essential for function. Proteomic studies of the kinetoplastid Hep1 orthologues together with the other cysteine rich motif proteins could also shed some more light into their range of functions. Due to the proximity of the genes, kinetoplastid Hep1 could be under the same transcriptional control as the other cysteine rich motif proteins. For example, heat or oxidative stress could be applied onto the trypanosomatid organisms, and then analysed to determine if Hep1 is upregulated along with the other cysteine rich motif proteins. In this regard, it is plausible that Hep1 may be upregulated under heat stress, as a potential protective mechanism against the self-aggregation of mtHsp70.

Adjacent to the Hep1 gene in trypanosomatids is the gene encoding J32, which is a type III J-protein that is thought to reside in the ER. Previously, an association between Hep1 and type III J-proteins has been hypothesized. The hypothesis, dubbed the fractured J hypothesis, postulates that Hep1 may also function to supplement type III J-proteins in presenting substrate proteins to Hsp70 (Burri et al., 2004). In the hypothesis, Hep1 is said to act as a zinc finger domain for the J domain of Pam18 which is a type III J-protein. In this regard, confirming the localisation of J32 in the mitochondria would be worthwhile, followed by experimental confirmation of whether the trypanosomatid Hep1 orthologues and J32 combination acts a type I J-protein. In these confirmatory experimental studies, it should be kept in mind that TbHep1 in this study, exhibited some functional properties of type I J-proteins.

TbmtHsp70 and HSPA9 were also observed in this study, in comparison to orthologues from various organisms. In terms of primary structure, TbmtHsp70 and HSPA9 were determined to be canonical mtHsp70 orthologues. At the ATPase domain and linker region, TbmtHsp70 and HSPA9 proved to be highly identical to the other mtHsp70 orthologues used in this study. Previously characterised orthologues used in this study included PfHsp70-3 and LbrmtHsp70. Therefore, it can be predicted that TbmtHsp70 is prone to self-aggregation. TbmtHsp70 has been determined to be essential for the import of mitochondrial tRNA and the maintenance of kDNA but has not been studied in terms of the self-aggregation property of mtHsp70s (Tan et al., 2002; Tschopp et al., 2011; Týč et al., 2015). Posttranslational modifications carried out revealed that there is minimal conservation amongst the mtHsp70 orthologues in this regard. More investigations need to be conducted in order to determine the entity of mtHsp70s that result in self-aggregation in the mitochondria. The *E. coli* DnaK orthologue

when directed to the mitochondria does not aggregate, despite being highly identical to mtHsp70s (Blamowska et al., 2010). In terms of tertiary structure, HSPA9 and TbmtHsp70 proved to be similar.

Experimental data from this study indeed showed that TbmtHsp70 is prone to aggregation, which is remedied by TbHep1. Previous studies with HSPA9 and HsHep1 have shown that HsHep1 prevents the aggregation of HSPA9 (Goswami et al., 2010; Dores-Silva et al., 2013). This study further went on to show that the mtHsp70/Hep1 systems between humans and *T. brucei* are conserved as HsHep1 and TbHep1 prevented the aggregation of TbmtHsp70 and HSPA9, respectively. The only shared similarity between TbHep1 and HsHep1 is at the zinc finger, therefore implicating the domain in the suppression of mtHsp70 aggregation activity of the orthologues. The same held true for ATPase activity whereby TbHep1 stimulated TbmtHsp70 and cytosolic TbHsp70 ATPase activity. The ATPase activity stimulation capability of HsHep1 has previously been confirmed for HSPA9 and the cytosolic Hsp70, HSPA1A (Dores-Silva et al., 2021). TbHep1 also stimulated the ATPase activity of the human Hsp70 orthologues, just as HsHep1 stimulated the ATPase activity of the *T. brucei* Hsp70 orthologues. TbHep1 is the third Hep1 orthologue that has been confirmed to stimulate the ATPase activity of its partner Hsp70. Far westerns or surface plasmon resonance (SPR) could be used to confirm the species-specific and cross-species interaction of the Hsp70/Hep1 system. In this regard, truncation studies of TbHep1 and HsHep1 could also be conducted with the aim of determining the functional regions of these proteins in stimulating the ATPase activities of the Hsp70s, and in suppressing the aggregation of model substrate proteins. This is especially in light of the levels of conservation determined for TbHep1 and HsHep1 when comparing them to their fellow kinetoplastid and mammalian Hep1 orthologues, respectively, at their N- and C-termini.

For the first time, this study has demonstrated that Hep1 may also be more active under oxidative stress conditions. With Hsp33 employed as a control in this regard, TbHep1 and HsHep1, subjected to simultaneous heat and oxidative stress proved to be able to suppress the thermally induced aggregation of model substrate protein MDH. Using reducing and non-reducing PAGE, the Hep1 orthologues were shown to potentially form cysteine disulphide bonds (cystines) which resulted in more compact conformations which migrate further during electrophoresis. In this regard, more downstream confirmative procedures need to be carried out, such as thiol trapping which has been applied to Hsp33 (Jakob et al., 1999). It was not conclusively determined whether the oxidised Hep1 orthologues also dimerise like Hsp33. Methods such as FPLC could be applied for that purpose. Hsp33 has been demonstrated to dimerize subsequent to the formation of the disulphide bonds. Complementation assays could also be carried out to determine the potential of the Hep1 orthologues to functionally replace Hsp33 under conditions of cellular oxidative stress. In the context of determining the physiological relevance of Hep1 as a chaperone of oxidative stress. Assays, *in vivo*, could be carried out to determine the effects of Hep1 knockdown under oxidative stress. For example, drugs that are known to exert

oxidative pressure on the mitochondrion could be tested on wild type and Hep1 knockdown cell lines to potentially determine the physiological significance of Hep1 in alleviating the effects of oxidative stress. Of the existing drugs, nifurtimox which is used in combination with DFMO is known to place trypanosomal cells under oxidative stress. The effects of Hep1 knockdown on nifurtimox induced oxidative stress could also be investigated in order to determine if drugs that targets Hep1 could synergistically cooperate with nifurtimox in killing trypanosomes.

Hep1 deletions and mutations have been reported to have similar effects to the deletion of mtHsp70 and may eventually lead to cell death. Therefore, given the essential role of mtHsp70 in the cell, the mtHsp70/Hep1 partnership could be exploited as a potential drug target. The mtHsp70 independent roles of Hep1, some of which have been explored and determined in this study, place a further importance on the potential of Hep1 as a drug target. The cellular roles of Hep1 still need to be further explored in order to determine the physiological reach of the protein, and validation studies carried out in order to determine if Hep1 is indeed essential for cell survival.

References

Acosta-Serrano, A., Vassella, E., Liniger, M., Renggli, C.K., Brun, R., Roditi, I., Englund, P.T., 2001. The surface coat of procyclic *Trypanosoma brucei:* Programmed expression and proteolytic cleavage of procyclin in the tsetse fly. Proc. Natl. Acad. Sci. 98, 1513–1518. https://doi.org/10.1073/pnas.98.4.1513

Ahmad, I., Nawaz, N., Darwesh, N.M., ur Rahman, S., Mustafa, M.Z., Khan, S.B., Patching, S.G., 2018. Overcoming challenges for amplified expression of recombinant proteins using Escherichia coli. Protein Expr. Purif. 144, 12–18. https://doi.org/10.1016/j.pep.2017.11.005

Ajit Tamadaddi, C., Sahi, C., 2016. J domain independent functions of J proteins. Cell Stress Chaperones 21, 563–570. https://doi.org/10.1007/s12192-016-0697-1

Aksoy, S., 2003. Control of tsetse flies and trypanosomes using molecular genetics. Vet. Parasitol. 115, 125–145. https://doi.org/10.1016/S0304-4017(03)00203-6

Aksoy, S., 2000. Tsetse--A haven for microorganisms. Parasitol. Today Pers. Ed 16, 114–118. https://doi.org/10.1016/s0169-4758(99)01606-3

Albakova, Z., Armeev, G.A., Kanevskiy, L.M., Kovalenko, E.I., Sapozhnikov, A.M., 2020. HSP70 Multi-Functionality in Cancer. Cells 9, E587. https://doi.org/10.3390/cells9030587

Albakova, Z., Mangasarova, Y., Albakov, A., Gorenkova, L., 2022. HSP70 and HSP90 in Cancer: Cytosolic, Endoplasmic Reticulum and Mitochondrial Chaperones of Tumorigenesis. Front. Oncol. 12, 829520. https://doi.org/10.3389/fonc.2022.829520

Albakova, Z., Siam, M.K.S., Sacitharan, P.K., Ziganshin, R.H., Ryazantsev, D.Y., Sapozhnikov, A.M., 2021. Extracellular heat shock proteins and cancer: New perspectives. Transl. Oncol. 14, 100995. https://doi.org/10.1016/j.tranon.2020.100995

Alberti, S., Esser, C., Höhfeld, J., 2003. BAG-1—a nucleotide exchange factor of Hsc70 with multiple cellular functions. Cell Stress Chaperones 8, 225. https://doi.org/10.1379/1466-1268(2003)008<0225:BNEFOH>2.0.CO;2

Alderson, T.R., Kim, J.H., Markley, J.L., 2016. Dynamical Structures of Hsp70 and Hsp70-Hsp40 Complexes. Structure 24, 1014–1030. https://doi.org/10.1016/j.str.2016.05.011

Alfonzo, J.D., Blanc, V., Estévez, A.M., Rubio, M.A., Simpson, L., 1999. C to U editing of the anticodon of imported mitochondrial tRNA(Trp) allows decoding of the UGA stop codon in Leishmania tarentolae. EMBO J. 18, 7056–7062. https://doi.org/10.1093/emboj/18.24.7056

Almagro Armenteros, J.J., Tsirigos, K.D., Sønderby, C.K., Petersen, T.N., Winther, O., Brunak, S., von Heijne, G., Nielsen, H., 2019. SignalP 5.0 improves signal peptide predictions using deep neural networks. Nat. Biotechnol. 37, 420–423. https://doi.org/10.1038/s41587-019-0036-z

Alsan, M., 2015. The Effect of the TseTse Fly on African Development. Am. Econ. Rev. 105, 382–410. https://doi.org/10.1257/aer.20130604

Alsford, S., Eckert, S., Baker, N., Glover, L., Sanchez-Flores, A., Leung, K.F., Turner, D.J., Field, M.C., Berriman, M., Horn, D., 2012. High-throughput decoding of antitrypanosomal drug efficacy and resistance. Nature 482, 232–236. https://doi.org/10.1038/nature10771

Alsford, S., Turner, D.J., Obado, S.O., Sanchez-Flores, A., Glover, L., Berriman, M., Hertz-Fowler, C., Horn, D., 2011. High-throughput phenotyping using parallel sequencing of RNA interference targets in the African trypanosome. Genome Res. 21, 915–924. https://doi.org/10.1101/gr.115089.110

Alvar, J., Vélez, I.D., Bern, C., Herrero, M., Desjeux, P., Cano, J., Jannin, J., Boer, M. den, the WHO Leishmaniasis Control Team, 2012. Leishmaniasis Worldwide and Global Estimates of Its Incidence. PLoS ONE 7, e35671. https://doi.org/10.1371/journal.pone.0035671

Amos, B., Aurrecoechea, C., Barba, M., Barreto, A., Basenko, E.Y., Bażant, W., Belnap, R., Blevins, A.S., Böhme, U., Brestelli, J., Brunk, B.P., Caddick, M., Callan, D., Campbell, L., Christensen, M.B., Christophides, G.K., Crouch, K., Davis, K., DeBarry, J., Doherty, R., Duan, Y., Dunn, M., Falke, D., Fisher, S., Flicek, P., Fox, B., Gajria, B., Giraldo-Calderón, G.I., Harb, O.S., Harper, E., Hertz-Fowler, C., Hickman, M.J., Howington, C., Hu, S., Humphrey, J., Iodice, J., Jones, A., Judkins, J., Kelly, S.A., Kissinger, J.C., Kwon, D.K., Lamoureux, K., Lawson, D., Li, W., Lies, K., Lodha, D., Long, J., MacCallum, R.M., Maslen, G., McDowell, M.A., Nabrzyski, J., Roos, D.S., Rund, S.S.C., Schulman, S.W., Shanmugasundram, A., Sitnik, V., Spruill, D., Starns, D., Stoeckert, C.J., Tomko, S.S., Wang, H., Warrenfeltz, S., Wieck, R., Wilkinson, P.A., Xu, L., Zheng, J., 2022. VEuPathDB: the eukaryotic pathogen, vector and host bioinformatics resource center. Nucleic Acids Res. 50, D898–D911. https://doi.org/10.1093/nar/gkab929

Andreassend, S.K., Bentley, S.J., Blatch, G.L., Boshoff, A., Keyzers, R.A., 2020. Screening for Small Molecule Modulators of Trypanosoma brucei Hsp70 Chaperone Activity Based upon Alcyonarian Coral-Derived Natural Products. Mar. Drugs 18, E81. https://doi.org/10.3390/md18020081

Araiso, Y., Tsutsumi, A., Qiu, J., Imai, K., Shiota, T., Song, J., Lindau, C., Wenz, L.-S., Sakaue, H., Yunoki, K., Kawano, S., Suzuki, J., Wischnewski, M., Schütze, C., Ariyama, H., Ando, T., Becker, T., Lithgow, T., Wiedemann, N., Pfanner, N., Kikkawa, M., Endo, T., 2019. Structure of the mitochondrial import gate reveals distinct preprotein paths. Nature 575, 395–401. https://doi.org/10.1038/s41586-019-1680-7

Arakawa, A., Handa, N., Shirouzu, M., Yokoyama, S., 2011. Biochemical and structural studies on the high affinity of Hsp70 for ADP. Protein Sci. Publ. Protein Soc. 20, 1367–1379. https://doi.org/10.1002/pro.663

Artzrouni, M., Gouteux, J.-P., 1996. Control strategies for sleeping sickness in Central Africa: a model-based approach. Trop. Med. Int. Health 1, 753–764. https://doi.org/10.1111/j.1365-3156.1996.tb00107.x

Aslett, M., Aurrecoechea, C., Berriman, M., Brestelli, J., Brunk, B.P., Carrington, M., Depledge, D.P., Fischer, S., Gajria, B., Gao, X., Gardner, M.J., Gingle, A., Grant, G., Harb, O.S., Heiges, M., Hertz-Fowler, C., Houston, R., Innamorato, F., Iodice, J., Kissinger, J.C., Kraemer, E., Li, W., Logan, F.J., Miller, J.A., Mitra, S., Myler, P.J., Nayak, V., Pennington, C., Phan, I., Pinney, D.F., Ramasamy, G., Rogers, M.B., Roos, D.S., Ross, C., Sivam, D., Smith, D.F., Srinivasamoorthy, G., Stoeckert, C.J., Subramanian, S., Thibodeau, R., Tivey, A., Treatman, C., Velarde, G., Wang, H., 2010. TriTrypDB: a functional genomic resource for the Trypanosomatidae. Nucleic Acids Res. 38, D457-462. https://doi.org/10.1093/nar/gkp851

Aurrecoechea, C., Brestelli, J., Brunk, B.P., Dommer, J., Fischer, S., Gajria, B., Gao, X., Gingle, A., Grant, G., Harb, O.S., Heiges, M., Innamorato, F., Iodice, J., Kissinger, J.C., Kraemer, E., Li, W., Miller, J.A., Nayak, V., Pennington, C., Pinney, D.F., Roos, D.S., Ross, C., Stoeckert, C.J.,

Treatman, C., Wang, H., 2009. PlasmoDB: a functional genomic database for malaria parasites. Nucleic Acids Res. 37, D539–D543. https://doi.org/10.1093/nar/gkn814

Auty, H.K., Picozzi, K., Malele, I., Torr, S.J., Cleaveland, S., Welburn, S., 2012. Using Molecular Data for Epidemiological Inference: Assessing the Prevalence of Trypanosoma brucei rhodesiense in Tsetse in Serengeti, Tanzania. PLoS Negl. Trop. Dis. 6, e1501. https://doi.org/10.1371/journal.pntd.0001501

Babokhov, P., Sanyaolu, A.O., Oyibo, W.A., Fagbenro-Beyioku, A.F., Iriemenam, N.C., 2013. A current analysis of chemotherapy strategies for the treatment of human African trypanosomiasis. Pathog. Glob. Health 107, 242–252. https://doi.org/10.1179/2047773213Y.0000000105

Bacchi, C.J., 2009. Chemotherapy of Human African Trypanosomiasis. Interdiscip. Perspect. Infect. Dis. 2009, 1–5. https://doi.org/10.1155/2009/195040

Baker, N., Glover, L., Munday, J.C., Aguinaga Andrés, D., Barrett, M.P., de Koning, H.P., Horn, D., 2012. Aquaglyceroporin 2 controls susceptibility to melarsoprol and pentamidine in African trypanosomes. Proc. Natl. Acad. Sci. U. S. A. 109, 10996–11001. https://doi.org/10.1073/pnas.1202885109

Ballinger, C.A., Connell, P., Wu, Y., Hu, Z., Thompson, L.J., Yin, L.-Y., Patterson, C., 1999. Identification of CHIP, a Novel Tetratricopeptide Repeat-Containing Protein That Interacts with Heat Shock Proteins and Negatively Regulates Chaperone Functions. Mol. Cell. Biol. 19, 4535–4545. https://doi.org/10.1128/MCB.19.6.4535

Banecki, B., Liberek, K., Wall, D., Wawrzynów, A., Georgopoulos, C., Bertoli, E., Tanfani, F., Zylicz, M., 1996. Structure-Function Analysis of the Zinc Finger Region of the DnaJ Molecular Chaperone. J. Biol. Chem. 271, 14840–14848. https://doi.org/10.1074/jbc.271.25.14840

Baral, T.N., 2010. Immunobiology of African Trypanosomes: Need of Alternative Interventions. J. Biomed. Biotechnol. 2010, 1–24. https://doi.org/10.1155/2010/389153

Barbirz, S., Jakob, U., Glocker, M.O., 2000. Mass Spectrometry Unravels Disulfide Bond Formation as the Mechanism That Activates a Molecular Chaperone. J. Biol. Chem. 275, 18759–18766. https://doi.org/10.1074/jbc.M001089200

Barrett, M.P., Boykin, D.W., Brun, R., Tidwell, R.R., 2007. Human African trypanosomiasis: pharmacological re-engagement with a neglected disease: Drugs for human African trypanosomiasis. Br. J. Pharmacol. 152, 1155–1171. https://doi.org/10.1038/sj.bjp.0707354

Barrett, M.P., Burchmore, R.J., Stich, A., Lazzari, J.O., Frasch, A.C., Cazzulo, J.J., Krishna, S., 2003. The trypanosomiases. The Lancet 362, 1469–1480. https://doi.org/10.1016/S0140-6736(03)14694-6

Bastin, P., Sherwin, T., Gull, K., 1998. Paraflagellar rod is vital for trypanosome motility. Nature 391, 548–548. https://doi.org/10.1038/35300

Baudouin, H.C.M., Pfeiffer, L., Ochsenreiter, T., 2020. A comparison of three approaches for the discovery of novel tripartite attachment complex proteins in Trypanosoma brucei. PLoS Negl. Trop. Dis. 14, e0008568. https://doi.org/10.1371/journal.pntd.0008568

Beddoe, T., Lithgow, T., 2002. Delivery of nascent polypeptides to the mitochondrial surface. Biochim. Biophys. Acta BBA - Mol. Cell Res. 1592, 35–39. https://doi.org/10.1016/S0167-4889(02)00262-8

Bedouelle, H., Duplay, P., 1988. Production in Escherichia coli and one-step purification of bifunctional hybrid proteins which bind maltose. Export of the Klenow polymerase into the periplasmic space. Eur. J. Biochem. 171, 541–549. https://doi.org/10.1111/j.1432-1033.1988.tb13823.x

Bentley, S.J., Boshoff, A., 2019. Trypanosoma brucei J-Protein 2 Functionally Co-Operates with the Cytosolic Hsp70 and Hsp70.4 Proteins. Int. J. Mol. Sci. 20, 5843. https://doi.org/10.3390/ijms20235843

Bentley, S.J., Jamabo, M., Boshoff, A., 2019. The Hsp70/J-protein machinery of the African trypanosome, Trypanosoma brucei. Cell Stress Chaperones 24, 125–148. https://doi.org/10.1007/s12192-018-0950-x

Bern, C., 2015. Chagas' Disease. N. Engl. J. Med. 373, 456–466. https://doi.org/10.1056/NEJMra1410150

Berndt, C., Lillig, C.H., Holmgren, A., 2008. Thioredoxins and glutaredoxins as facilitators of protein folding. Biochim. Biophys. Acta BBA - Mol. Cell Res. 1783, 641–650. https://doi.org/10.1016/j.bbamcr.2008.02.003

Berrang Ford, L., 2007. Civil conflict and sleeping sickness in Africa in general and Uganda in particular. Confl. Health 1, 6. https://doi.org/10.1186/1752-1505-1-6

Berrang-Ford, L., Odiit, M., Maiso, F., Waltner-Toews, D., McDermott, J., 2006. Sleeping sickness in Uganda: revisiting current and historical distributions. Afr. Health Sci. 6, 223–231. https://doi.org/10.5555/afhs.2006.6.4.223

Berrang-Ford, L., Wamboga, C., Kakembo, A.S.L., 2012. *Trypanososma brucei rhodesiense* Sleeping Sickness, Uganda. Emerg. Infect. Dis. 18, 1686–1687. https://doi.org/10.3201/eid1810.111213

Berriman, M., Ghedin, E., Hertz-Fowler, C., Blandin, G., Renauld, H., Bartholomeu, D.C., Lennard, N.J., Caler, E., Hamlin, N.E., Haas, B., Böhme, U., Hannick, L., Aslett, M.A., Shallom, J., Marcello, L., Hou, L., Wickstead, B., Alsmark, U.C.M., Arrowsmith, C., Atkin, R.J., Barron, A.J., Bringaud, F., Brooks, K., Carrington, M., Cherevach, I., Chillingworth, T.-J., Churcher, C., Clark, L.N., Corton, C.H., Cronin, A., Davies, R.M., Doggett, J., Djikeng, A., Feldblyum, T., Field, M.C., Fraser, A., Goodhead, I., Hance, Z., Harper, D., Harris, B.R., Hauser, H., Hostetler, J., Ivens, A., Jagels, K., Johnson, D., Johnson, J., Jones, K., Kerhornou, A.X., Koo, H., Larke, N., Landfear, S., Larkin, C., Leech, V., Line, A., Lord, A., MacLeod, A., Mooney, P.J., Moule, S., Martin, D.M.A., Morgan, G.W., Mungall, K., Norbertczak, H., Ormond, D., Pai, G., Peacock, C.S., Peterson, J., Quail, M.A., Rabbinowitsch, E., Rajandream, M.-A., Reitter, C., Salzberg, S.L., Sanders, M., Schobel, S., Sharp, S., Simmonds, M., Simpson, A.J., Tallon, L., Turner, C.M.R., Tait, A., Tivey, A.R., Van Aken, S., Walker, D., Wanless, D., Wang, S., White, B., White, O., Whitehead, S., Woodward, J., Wortman, J., Adams, M.D., Embley, T.M., Gull, K., Ullu, E., Barry, J.D., Fairlamb, A.H., Opperdoes, F., Barrell, B.G., Donelson, J.E., Hall, N., Fraser, C.M., Melville, S.E., El-Sayed, N.M., 2005. The Genome of the African Trypanosome *Trypanosoma brucei*. Science 309, 416–422. https://doi.org/10.1126/science.1112642

Bertelsen, E.B., Chang, L., Gestwicki, J.E., Zuiderweg, E.R.P., 2009. Solution conformation of wild-type E. coli Hsp70 (DnaK) chaperone complexed with ADP and substrate. Proc. Natl. Acad. Sci. U. S. A. 106, 8471–8476. https://doi.org/10.1073/pnas.0903503106

Bisser, S., Lejon, V., Preux, P.M., Bouteille, B., Stanghellini, A., Jauberteau, M.O., Büscher, P., Dumas, M., 2002. Blood–cerebrospinal fluid barrier and intrathecal immunoglobulins compared to field diagnosis of central nervous system involvement in sleeping sickness. J. Neurol. Sci. 193, 127–135. https://doi.org/10.1016/S0022-510X(01)00655-4

Bisser, S., Lumbala, C., Nguertoum, E., Kande, V., Flevaud, L., Vatunga, G., Boelaert, M., Büscher, P., Josenando, T., Bessell, P.R., Biéler, S., Ndung'u, J.M., 2016. Sensitivity and Specificity of a Prototype Rapid Diagnostic Test for the Detection of Trypanosoma brucei gambiense Infection: A Multi-centric Prospective Study. PLoS Negl. Trop. Dis. 10, e0004608. https://doi.org/10.1371/journal.pntd.0004608

Bisser, S., N'Siesi, F., Lejon, V., Preux, P., Van Nieuwenhove, S., Miaka Mia Bilenge, C., Büscher, P., 2007. Equivalence Trial of Melarsoprol and Nifurtimox Monotherapy and Combination Therapy for the Treatment of Second-Stage *Trypanosoma brucei gambiense* Sleeping Sickness. J. Infect. Dis. 195, 322–329. https://doi.org/10.1086/510534

Blamowska, M., Neupert, W., Hell, K., 2012. Biogenesis of the mitochondrial Hsp70 chaperone. J. Cell Biol. 199, 125–135. https://doi.org/10.1083/jcb.201205012

Blamowska, M., Sichting, M., Mapa, K., Mokranjac, D., Neupert, W., Hell, K., 2010. ATPase Domain and Interdomain Linker Play a Key Role in Aggregation of Mitochondrial Hsp70 Chaperone Ssc1. J. Biol. Chem. 285, 4423–4431. https://doi.org/10.1074/jbc.M109.061697

Blum, B., Bakalara, N., Simpson, L., 1990. A model for RNA editing in kinetoplastid mitochondria: RNA molecules transcribed from maxicircle DNA provide the edited information. Cell 60, 189–198. https://doi.org/10.1016/0092-8674(90)90735-W

Blum, B., Simpson, L., 1990. Guide RNAs in kinetoplastid mitochondria have a nonencoded 3' oligo(U) tail involved in recognition of the preedited region. Cell 62, 391–397. https://doi.org/10.1016/0092-8674(90)90375-O

Blum, J., Schmid, C., Burri, C., 2006. Clinical aspects of 2541 patients with second stage human African trypanosomiasis. Acta Trop. 97, 55–64. https://doi.org/10.1016/j.actatropica.2005.08.001

Bonnet, J., Boudot, C., Courtioux, B., 2015. Overview of the Diagnostic Methods Used in the Field for Human African Trypanosomiasis: What Could Change in the Next Years? BioMed Res. Int. 2015, 1–10. https://doi.org/10.1155/2015/583262

Borges, J.C., Ramos, C.H.I., 2006. Spectroscopic and thermodynamic measurements of nucleotide-induced changes in the human 70-kDa heat shock cognate protein. Arch. Biochem. Biophys. 452, 46–54. https://doi.org/10.1016/j.abb.2006.05.006

Bornhorst, J.A., Falke, J.J., 2000. [16] Purification of proteins using polyhistidine affinity tags, in: Methods in Enzymology. Elsevier, pp. 245–254. https://doi.org/10.1016/S0076-6879(00)26058-8

Bota, D.A., Davies, K.J.A., 2016. Mitochondrial Lon protease in human disease and aging: Including an etiologic classification of Lon-related diseases and disorders. Free Radic. Biol. Med. 100, 188–198. https://doi.org/10.1016/j.freeradbiomed.2016.06.031

Botha, M., Pesce, E.-R., Blatch, G.L., 2007. The Hsp40 proteins of Plasmodium falciparum and other apicomplexa: regulating chaperone power in the parasite and the host. Int. J. Biochem. Cell Biol. 39, 1781–1803. https://doi.org/10.1016/j.biocel.2007.02.011

Böttinger, L., Guiard, B., Oeljeklaus, S., Kulawiak, B., Zufall, N., Wiedemann, N., Warscheid, B., van der Laan, M., Becker, T., 2013. A complex of Cox4 and mitochondrial Hsp70 plays an important role in the assembly of the cytochrome c oxidase. Mol. Biol. Cell 24, 2609–2619. https://doi.org/10.1091/mbc.E13-02-0106

Böttinger, L., Oeljeklaus, S., Guiard, B., Rospert, S., Warscheid, B., Becker, T., 2015. Mitochondrial Heat Shock Protein (Hsp) 70 and Hsp10 Cooperate in the Formation of Hsp60 Complexes. J. Biol. Chem. 290, 11611–11622. https://doi.org/10.1074/jbc.M115.642017

Bracher, A., Verghese, J., 2015. The nucleotide exchange factors of Hsp70 molecular chaperones. Front. Mol. Biosci. 2. https://doi.org/10.3389/fmolb.2015.00010

Braig, K., Otwinowski, Z., Hegde, R., Boisvert, D.C., Joachimiak, A., Horwich, A.L., Sigler, P.B., 1994. The crystal structure of the bacterial chaperonin GroEL at 2.8 A. Nature 371, 578–586. https://doi.org/10.1038/371578a0

Bramblett, G.T., Chang, S.L., Flavin, M., 1987. Periodic crosslinking of microtubules by cytoplasmic microtubule-associated and microtubule-corset proteins from a trypanosomatid. Proc. Natl. Acad. Sci. 84, 3259–3263. https://doi.org/10.1073/pnas.84.10.3259

Brameier, M., Krings, A., MacCallum, R.M., 2007. NucPred--predicting nuclear localization of proteins. Bioinforma. Oxf. Engl. 23, 1159–1160. https://doi.org/10.1093/bioinformatics/btm066

Brinker, A., Scheufler, C., von der Mülbe, F., Fleckenstein, B., Herrmann, C., Jung, G., Moarefi, I., Hartl, F.U., 2002. Ligand Discrimination by TPR Domains. J. Biol. Chem. 277, 19265–19275. https://doi.org/10.1074/jbc.M109002200

Brive, L., Takayama, S., Briknarová, K., Homma, S., Ishida, S.K., Reed, J.C., Ely, K.R., 2001. The Carboxyl-Terminal Lobe of Hsc70 ATPase Domain Is Sufficient for Binding to BAG1. Biochem. Biophys. Res. Commun. 289, 1099–1105. https://doi.org/10.1006/bbrc.2001.6087

Brun, R., Blum, J., Chappuis, F., Burri, C., 2010. Human African trypanosomiasis. The Lancet 375, 148–159. https://doi.org/10.1016/S0140-6736(09)60829-1

Brundin, P., Melki, R., Kopito, R., 2010. Prion-like transmission of protein aggregates in neurodegenerative diseases. Nat. Rev. Mol. Cell Biol. 11, 301–307. https://doi.org/10.1038/nrm2873

Bucheton, B., MacLEOD, A., Jamonneau, V., 2011. Human host determinants influencing the outcome of *Trypanosoma brucei gambiense* infections. Parasite Immunol. 33, 438–447. https://doi.org/10.1111/j.1365-3024.2011.01287.x

Buchner, J., Li, J., 2013. Structure, Function and Regulation of the Hsp90 Machinery. Biomed. J. 36, 106. https://doi.org/10.4103/2319-4170.113230

Buguet, A., Bisser, S., Josenando, T., Chapotot, F., Cespuglio, R., 2005. Sleep structure: a new diagnostic tool for stage determination in sleeping sickness. Acta Trop. 93, 107–117. https://doi.org/10.1016/j.actatropica.2004.10.001

Bukau, B., Mayer, M.P., Schröder, H., Rüdiger, S., Paal, K., Laufen, T., 2000. Multistep mechanism of substrate binding determines chaperone activity of Hsp70. Nat. Struct. Biol. 7, 586–593. https://doi.org/10.1038/76819

Bullock, W., Fernandez, J., Short, J., 1987. XL1-Blue: a high efficiency plasmid transforming recA Escherichia coli strain with beta-galactosidase selection. Biotechniques 5, 376–379.

Burger, A., Ludewig, M.H., Boshoff, A., 2014. Investigating the Chaperone Properties of a Novel Heat Shock Protein, Hsp70.c, from *Trypanosoma brucei*. J. Parasitol. Res. 2014, 1–12. https://doi.org/10.1155/2014/172582

Burger, A., Macucule-Tinga, P., Bentley, S.J., Ludewig, M.H., Mhlongo, N.N., Shonhai, A., Boshoff, A., 2021. Characterization of an Atypical Trypanosoma brucei Hsp70 Demonstrates Its Cytosolic-Nuclear Localization and Modulation by Quercetin and Methylene Blue. Int. J. Mol. Sci. 22, 6776. https://doi.org/10.3390/ijms22136776

Burgess, R.R., 2009. Chapter 17 Refolding Solubilized Inclusion Body Proteins, in: Methods in Enzymology. Elsevier, pp. 259–282. https://doi.org/10.1016/S0076-6879(09)63017-2

Burnett, L.C., Lunn, G., Coico, R., 2009. Biosafety: Guidelines for Working with Pathogenic and Infectious Microorganisms. Curr. Protoc. Microbiol. 13. https://doi.org/10.1002/9780471729259.mc01a01s13

Burri, L., Vascotto, K., Fredersdorf, S., Tiedt, R., Hall, M.N., Lithgow, T., 2004. Zim17, a Novel Zinc Finger Protein Essential for Protein Import into Mitochondria. J. Biol. Chem. 279, 50243–50249. https://doi.org/10.1074/jbc.M409194200

Büscher, P., Mumba Ngoyi, D., Kaboré, J., Lejon, V., Robays, J., Jamonneau, V., Bebronne, N., Van der Veken, W., Biéler, S., 2009. Improved Models of Mini Anion Exchange Centrifugation Technique (mAECT) and Modified Single Centrifugation (MSC) for Sleeping Sickness Diagnosis and Staging. PLoS Negl. Trop. Dis. 3, e471. https://doi.org/10.1371/journal.pntd.0000471

Butenko, A., Opperdoes, F.R., Flegontova, O., Horák, A., Hampl, V., Keeling, P., Gawryluk, R.M.R., Tikhonenkov, D., Flegontov, P., Lukeš, J., 2020. Evolution of metabolic capabilities and molecular features of diplonemids, kinetoplastids, and euglenids. BMC Biol. 18, 23. https://doi.org/10.1186/s12915-020-0754-1

Butter, F., Bucerius, F., Michel, M., Cicova, Z., Mann, M., Janzen, C.J., 2013. Comparative Proteomics of Two Life Cycle Stages of Stable Isotope-labeled Trypanosoma brucei Reveals Novel Components of the Parasite's Host Adaptation Machinery. Mol. Cell. Proteomics 12, 172–179. https://doi.org/10.1074/mcp.M112.019224

Caljon, G., De Ridder, K., De Baetselier, P., Coosemans, M., Van Den Abbeele, J., 2010. Identification of a Tsetse Fly Salivary Protein with Dual Inhibitory Action on Human Platelet Aggregation. PLoS ONE 5, e9671. https://doi.org/10.1371/journal.pone.0009671

Caljon, G., Van Reet, N., De Trez, C., Vermeersch, M., Pérez-Morga, D., Van Den Abbeele, J., 2016. The Dermis as a Delivery Site of Trypanosoma brucei for Tsetse Flies. PLOS Pathog. 12, e1005744. https://doi.org/10.1371/journal.ppat.1005744

Calvopina, M., Segovia, G., Cevallos, W., Vicuña, Y., Costales, J.A., Guevara, A., 2020. Fatal acute Chagas disease by Trypanosoma cruzi DTU TcI, Ecuador. BMC Infect. Dis. 20, 143. https://doi.org/10.1186/s12879-020-4851-0

Camara, M., Camara, O., Ilboudo, H., Sakande, H., Kaboré, J., N'Dri, L., Jamonneau, V., Bucheton, B., 2010. Sleeping sickness diagnosis: use of buffy coats improves the sensitivity of the mini anion exchange centrifugation test: **mAECT-bc and sleeping sickness diagnostic**. Trop. Med. Int. Health 15, 796–799. https://doi.org/10.1111/j.1365-3156.2010.02546.x

Cappello, M., Li, S., Chen, X., Li, C.-B., Harrison, L., Narashimhan, S., Beard, C.B., Aksoy, S., 1998. Tsetse thrombin inhibitor: Bloodmeal-induced expression of an anticoagulant in salivary glands and gut tissue of *Glossina morsitans morsitans*. Proc. Natl. Acad. Sci. 95, 14290–14295. https://doi.org/10.1073/pnas.95.24.14290

Carrigan, P.E., Nelson, G.M., Roberts, P.J., Stoffer, J., Riggs, D.L., Smith, D.F., 2004. Multiple Domains of the Co-chaperone Hop Are Important for Hsp70 Binding. J. Biol. Chem. 279, 16185–16193. https://doi.org/10.1074/jbc.M314130200

Carter, D.C., Ho, J.X., 1994. Structure of Serum Albumin, in: Advances in Protein Chemistry. Elsevier, pp. 153–203. https://doi.org/10.1016/S0065-3233(08)60640-3

Cavalcanti, D.P., de Souza, W., 2018. The Kinetoplast of Trypanosomatids: From Early Studies of Electron Microscopy to Recent Advances in Atomic Force Microscopy. Scanning 2018, 1–10. https://doi.org/10.1155/2018/9603051

Cavalier-Smith, T., 2016. Higher classification and phylogeny of Euglenozoa. Eur. J. Protistol. 56, 250–276. https://doi.org/10.1016/j.ejop.2016.09.003

Cavalier-Smith, T., 1981. Eukaryote kingdoms: Seven or nine? Biosystems 14, 461–481. https://doi.org/10.1016/0303-2647(81)90050-2

Cayla, M., Rojas, F., Silvester, E., Venter, F., Matthews, K.R., 2019. African trypanosomes. Parasit. Vectors 12, 190. https://doi.org/10.1186/s13071-019-3355-5

CDC, 2022. Parasites - African Trypanosomiasis (also known as Sleeping Sickness).

Cecchi, G., Courtin, F., Paone, M., Diarra, A., Franco, J.R., Mattioli, R.C., Simarro, P.P., 2009. Mapping sleeping sickness in Western Africa in a context of demographic transition and climate change. Parasite 16, 99–106. https://doi.org/10.1051/parasite/2009162099

Chakafana, G., Zininga, T., Shonhai, A., 2019. Comparative structure-function features of Hsp70s of Plasmodium falciparum and human origins. Biophys. Rev. 11, 591–602. https://doi.org/10.1007/s12551-019-00563-w

Chakafana, Zininga, Shonhai, 2019. The Link That Binds: The Linker of Hsp70 as a Helm of the Protein's Function. Biomolecules 9, 543. https://doi.org/10.3390/biom9100543

Chappuis, F., Lima, M.A., Flevaud, L., Ritmeijer, K., 2010. Human African trypanosomiasis in areas without surveillance. Emerg. Infect. Dis. 16, 354–356. https://doi.org/10.3201/eid1602.090967

Chappuis, F., Loutan, L., Simarro, P., Lejon, V., Büscher, P., 2005. Options for Field Diagnosis of Human African Trypanosomiasis. Clin. Microbiol. Rev. 18, 133–146. https://doi.org/10.1128/CMR.18.1.133-146.2005

Chaudhuri, M., Ott, R.D., Hill, G.C., 2006. Trypanosome alternative oxidase: from molecule to function. Trends Parasitol. 22, 484–491. https://doi.org/10.1016/j.pt.2006.08.007

Cheetham, M.E., Caplan, A.J., 1998. Structure, function and evolution of DnaJ: conservation and adaptation of chaperone function. Cell Stress Chaperones 3, 28. https://doi.org/10.1379/1466-1268(1998)003<0028:SFAEOD>2.3.CO;2

Chen, B., Piel, W.H., Gui, L., Bruford, E., Monteiro, A., 2005. The HSP90 family of genes in the human genome: Insights into their divergence and evolution. Genomics 86, 627–637. https://doi.org/10.1016/j.ygeno.2005.08.012

Chen, S., Smith, D.F., 1998. Hop as an Adaptor in the Heat Shock Protein 70 (Hsp70) and Hsp90 Chaperone Machinery. J. Biol. Chem. 273, 35194–35200. https://doi.org/10.1074/jbc.273.52.35194

Chen, X., Li, S., Aksoy, S., 1999. Concordant Evolution of a Symbiont with Its Host Insect Species: Molecular Phylogeny of Genus Glossina and Its Bacteriome-Associated Endosymbiont, Wigglesworthia glossinidia. J. Mol. Evol. 48, 49–58. https://doi.org/10.1007/PL00006444

Chicharro, C., Alvar, J., 2003. Lower trypanosomatids in HIV/AIDS patients. Ann. Trop. Med. Parasitol. 97, 75–78. https://doi.org/10.1179/000349803225002552

Chiti, F., Dobson, C.M., 2017. Protein Misfolding, Amyloid Formation, and Human Disease: A Summary of Progress Over the Last Decade. Annu. Rev. Biochem. 86, 27–68. https://doi.org/10.1146/annurev-biochem-061516-045115

Chivers, P.T., Prehoda, K.E., Raines, R.T., 1997. The CXXC Motif: A Rheostat in the Active Site. Biochemistry 36, 4061–4066. https://doi.org/10.1021/bi9628580

Chung, W.-L., Leung, K.F., Carrington, M., Field, M.C., 2008. Ubiquitylation is Required for Degradation of Transmembrane Surface Proteins in Trypanosomes. Traffic 9, 1681–1697. https://doi.org/10.1111/j.1600-0854.2008.00785.x

Ciechanover, A., Kwon, Y.T., 2017. Protein Quality Control by Molecular Chaperones in Neurodegeneration. Front. Neurosci. 11. https://doi.org/10.3389/fnins.2017.00185

Clare, D.K., Saibil, H.R., 2013. ATP-driven molecular chaperone machines. Biopolymers 99, 846–859. https://doi.org/10.1002/bip.22361

Claros, M.G., Vincens, P., 1996. Computational Method to Predict Mitochondrially Imported Proteins and their Targeting Sequences. Eur. J. Biochem. 241, 779–786. https://doi.org/10.1111/j.1432-1033.1996.00779.x

Cnops, J., De Trez, C., Bulte, D., Radwanska, M., Ryffel, B., Magez, S., 2015. IFN-γ mediates early B-cell loss in experimental African trypanosomosis. Parasite Immunol. 37, 479–484. https://doi.org/10.1111/pim.12208

Cnops, J, Magez, S., De Trez, C., 2015. Escape mechanisms of African trypanosomes: why trypanosomosis is keeping us awake. Parasitology 142, 417–427. https://doi.org/10.1017/S0031182014001838

Collienne, L., Gavryushkin, A., 2021. Computing nearest neighbour interchange distances between ranked phylogenetic trees. J. Math. Biol. 82, 8. https://doi.org/10.1007/s00285-021-01567-5

Connell, P., Ballinger, C.A., Jiang, J., Wu, Y., Thompson, L.J., Höhfeld, J., Patterson, C., 2001. The co-chaperone CHIP regulates protein triage decisions mediated by heat-shock proteins. Nat. Cell Biol. 3, 93–96. https://doi.org/10.1038/35050618

Conway, M.E., Lee, C., 2015. The redox switch that regulates molecular chaperones. Biomol. Concepts 6, 269–284. https://doi.org/10.1515/bmc-2015-0015

Cordon-Obras, C., García-Estébanez, C., Ndong-Mabale, N., Abaga, S., Ndongo-Asumu, P., Benito, A., Cano, J., 2010. Screening of Trypanosoma brucei gambiense in Domestic Livestock and Tsetse Flies from an Insular Endemic Focus (Luba, Equatorial Guinea). PLoS Negl. Trop. Dis. 4, e704. https://doi.org/10.1371/journal.pntd.0000704

Craig, E.A., 2018. Hsp70 at the membrane: driving protein translocation. BMC Biol. 16, 11. https://doi.org/10.1186/s12915-017-0474-3

Craig, E.A., Gambill, B.D., Nelson, R.J., 1993. Heat shock proteins: molecular chaperones of protein biogenesis. Microbiol. Rev. 57, 402–414. https://doi.org/10.1128/mr.57.2.402-414.1993

Craig, E.A., Kramer, J., Shilling, J., Werner-Washburne, M., Holmes, S., Kosic-Smithers, J., Nicolet, C.M., 1989. SSC1, an essential member of the yeast HSP70 multigene family, encodes a mitochondrial protein. Mol. Cell. Biol. 9, 3000–3008. https://doi.org/10.1128/mcb.9.7.3000-3008.1989

Craig, E.A., Marszalek, J., 2017. How Do J-Proteins Get Hsp70 to Do So Many Different Things? Trends Biochem. Sci. 42, 355–368. https://doi.org/10.1016/j.tibs.2017.02.007

Cremers, C.M., Knoefler, D., Vitvitsky, V., Banerjee, R., Jakob, U., 2014. Bile salts act as effective protein-unfolding agents and instigators of disulfide stress in vivo. Proc. Natl. Acad. Sci. 111. https://doi.org/10.1073/pnas.1401941111

Cremers, C.M., Reichmann, D., Hausmann, J., Ilbert, M., Jakob, U., 2010. Unfolding of Metastable Linker Region Is at the Core of Hsp33 Activation as a Redox-regulated Chaperone. J. Biol. Chem. 285, 11243–11251. https://doi.org/10.1074/jbc.M109.084350

Cross, G.A.M., 1975. Identification, purification and properties of clone-specific glycoprotein antigens constituting the surface coat of *Trypanosoma brucei*. Parasitology 71, 393–417. https://doi.org/10.1017/S003118200004717X

Cross, G.A.M., Klein, R.A., Linstead, D.J., 1975. Utilization of amino acids by *Trypanosoma brucei* in culture: L-threonine as a precursor for acetate. Parasitology 71, 311–326. https://doi.org/10.1017/S0031182000046758

Crowe, J., Döbeli, H., Gentz, R., Hochuli, E., Stüber, D., Henco, K., 1994. 6xHis-Ni-NTA Chromatography as a Superior Technique in Recombinant Protein Expressiod/Purification, in: Protocols for Gene Analysis. Humana Press, New Jersey, pp. 371–388. https://doi.org/10.1385/0-89603-258-2:371

Csermely, P., Schnaider, T., So"ti, C., Prohászka, Z., Nardai, G., 1998. The 90-kDa Molecular Chaperone Family. Pharmacol. Ther. 79, 129–168. https://doi.org/10.1016/S0163-7258(98)00013-8

Dahl, J.-U., Gray, M.J., Jakob, U., 2015. Protein Quality Control under Oxidative Stress Conditions. J. Mol. Biol. 427, 1549–1563. https://doi.org/10.1016/j.jmb.2015.02.014

Dale, C., Maudlin, I., 1999. Sodalis gen. nov. and Sodalis glossinidius sp. nov., a microaerophilic secondary endosymbiont of the tsetse fly Glossina morsitans morsitans. Int. J. Syst. Bacteriol. 49 Pt 1, 267–275. https://doi.org/10.1099/00207713-49-1-267

Daugaard, M., Rohde, M., Jäättelä, M., 2007. The heat shock protein 70 family: Highly homologous proteins with overlapping and distinct functions. FEBS Lett. 581, 3702–3710. https://doi.org/10.1016/j.febslet.2007.05.039

d'Avila-Levy, C.M., Boucinha, C., Kostygov, A., Santos, H.L.C., Morelli, K.A., Grybchuk-Ieremenko, A., Duval, L., Votýpka, J., Yurchenko, V., Grellier, P., Lukeš, J., 2015. Exploring the environmental diversity of kinetoplastid flagellates in the high-throughput DNA sequencing era. Mem. Inst. Oswaldo Cruz 110, 956–965. https://doi.org/10.1590/0074-02760150253

De Greef, C., Imberechts, H., Matthyssens, G., Van Meirvenne, N., Hamers, R., 1989. A gene expressed only in serum-resistant variants of Trypanosoma brucei rhodesiense. Mol. Biochem. Parasitol. 36, 169–176. https://doi.org/10.1016/0166-6851(89)90189-8

de Marco, A., Deuerling, E., Mogk, A., Tomoyasu, T., Bukau, B., 2007. Chaperone-based procedure to increase yields of soluble recombinant proteins produced in E. coli. BMC Biotechnol. 7, 32. https://doi.org/10.1186/1472-6750-7-32

de Marco, A., Vigh, L., Diamant, S., Goloubinoff, P., 2005. Native folding of aggregation-prone recombinant proteins in Escherichia coli by osmolytes, plasmid- or benzyl alcohol-overexpressed molecular chaperones. Cell Stress Chaperones 10, 329–339. https://doi.org/10.1379/csc-139r.1

de Raadt, P., Koten, J.W., 1968. Myocarditis in Rhodesiense trypanosomiasis. East Afr. Med. J. 45, 128–132.

de Souza, W., Attias, M., Rodrigues, J.C.F., 2009. Particularities of mitochondrial structure in parasitic protists (Apicomplexa and Kinetoplastida). Int. J. Biochem. Cell Biol. 41, 2069–2080. https://doi.org/10.1016/j.biocel.2009.04.007

de Souza, W., de Carvalho, T.M.U., Barrias, E.S., 2010. Review on *Trypanosoma cruzi* : Host Cell Interaction. Int. J. Cell Biol. 2010, 1–18. https://doi.org/10.1155/2010/295394

De Souza, W., Meyer, H., 1974. On the Fine Structure of the Nucleus in *Trypanosoma cruzi* in Tissue Culture Forms. Spindle Fibers in the Dividing Nucleus*. J. Protozool. 21, 48–52. https://doi.org/10.1111/j.1550-7408.1974.tb03615.x

De Vooght, L., Van Keer, S., Van Den Abbeele, J., 2018. Towards improving tsetse fly paratransgenesis: stable colonization of Glossina morsitans morsitans with genetically modified Sodalis. BMC Microbiol. 18, 165. https://doi.org/10.1186/s12866-018-1282-9

Deeks, E.D., 2019. Fexinidazole: First Global Approval. Drugs 79, 215–220. https://doi.org/10.1007/s40265-019-1051-6

Demand, J., Lüders, J., Höhfeld, J., 1998. The carboxy-terminal domain of Hsc70 provides binding sites for a distinct set of chaperone cofactors. Mol. Cell. Biol. 18, 2023–2028. https://doi.org/10.1128/MCB.18.4.2023

Deocaris, C.C., 2006. Structural and Functional Differences between Mouse Mot-1 and Mot-2 Proteins That Differ in Two Amino Acids. Ann. N. Y. Acad. Sci. 1067, 220–223. https://doi.org/10.1196/annals.1354.027

Desquesnes, M., Holzmuller, P., Lai, D.-H., Dargantes, A., Lun, Z.-R., Jittaplapong, S., 2013. *Trypanosoma evansi* and Surra: A Review and Perspectives on Origin, History, Distribution, Taxonomy, Morphology, Hosts, and Pathogenic Effects. BioMed Res. Int. 2013, 1–22. https://doi.org/10.1155/2013/194176

Dhamija, S., Menon, M.B., 2018. Non-coding transcript variants of protein-coding genes – what are they good for? RNA Biol. 1–7. https://doi.org/10.1080/15476286.2018.1511675

Díaz de la Loza, M. del C., Gallardo, M., García-Rubio, M.L., Izquierdo, A., Herrero, E., Aguilera, A., Wellinger, R.E., 2011. Zim17/Tim15 links mitochondrial iron–sulfur cluster biosynthesis to nuclear genome stability. Nucleic Acids Res. 39, 6002–6015. https://doi.org/10.1093/nar/gkr193

Diffley, P., 1983. Trypanosomal surface coat variant antigen causes polyclonal lymphocyte activation. J. Immunol. Baltim. Md 1950 131, 1983–1986.

Dobson, D.E., Kamhawi, S., Lawyer, P., Turco, S.J., Beverley, S.M., Sacks, D.L., 2010. Leishmania major Survival in Selective Phlebotomus papatasi Sand Fly Vector Requires a Specific SCG-Encoded Lipophosphoglycan Galactosylation Pattern. PLoS Pathog. 6, e1001185. https://doi.org/10.1371/journal.ppat.1001185

Donelson, J.E., 2003. Antigenic variation and the African trypanosome genome. Acta Trop. 85, 391–404. https://doi.org/10.1016/S0001-706X(02)00237-1

Dores-Silva, P., Beloti, L., Minari, K., Silva, S., Barbosa, L., Borges, J., 2015. Structural and functional studies of Hsp70-escort protein – Hep1 – of Leishmania braziliensis. Int. J. Biol. Macromol. 79, 903–912. https://doi.org/10.1016/j.ijbiomac.2015.05.042

Dores-Silva, P.R., Barbosa, L.R.S., Ramos, C.H.I., Borges, J.C., 2015. Human Mitochondrial Hsp70 (Mortalin): Shedding Light on ATPase Activity, Interaction with Adenosine Nucleotides, Solution Structure and Domain Organization. PLOS ONE 10, e0117170. https://doi.org/10.1371/journal.pone.0117170

Dores-Silva, P.R., Kiraly, V.T.R., Moritz, M.N. de O., Serrão, V.H.B., dos Passos, P.M.S., Spagnol, V., Teixeira, F.R., Gava, L.M., Cauvi, D.M., Ramos, C.H.I., De Maio, A., Borges, J.C., 2021. New insights on human Hsp70-escort protein 1: Chaperone activity, interaction with liposomes, cellular localizations and HSPA's self-assemblies remodeling. Int. J. Biol. Macromol. 182, 772–784. https://doi.org/10.1016/j.ijbiomac.2021.04.048

Dores-Silva, P.R., Minari, K., Ramos, C.H.I., Barbosa, L.R.S., Borges, J.C., 2013. Structural and stability studies of the human mtHsp70-escort protein 1: An essential mortalin co-chaperone. Int. J. Biol. Macromol. 56, 140–148. https://doi.org/10.1016/j.ijbiomac.2013.02.009

Dores-Silva, P.R., Nishimura, L.S., Kiraly, V.T.R., Borges, J.C., 2017. Structural and functional studies of the Leishmania braziliensis mitochondrial Hsp70: Similarities and dissimilarities to human orthologues. Arch. Biochem. Biophys. 613, 43–52. https://doi.org/10.1016/j.abb.2016.11.004

Doudoumis, V., Blow, F., Saridaki, A., Augustinos, A., Dyer, N.A., Goodhead, I., Solano, P., Rayaisse, J.-B., Takac, P., Mekonnen, S., Parker, A.G., Abd-Alla, A.M.M., Darby, A., Bourtzis, K., Tsiamis, G., 2017. Challenging the Wigglesworthia, Sodalis, Wolbachia symbiosis dogma in tsetse flies: Spiroplasma is present in both laboratory and natural populations. Sci. Rep. 7, 4699. https://doi.org/10.1038/s41598-017-04740-3

Dragovic, Z., Broadley, S.A., Shomura, Y., Bracher, A., Hartl, F.U., 2006. Molecular chaperones of the Hsp110 family act as nucleotide exchange factors of Hsp70s. EMBO J. 25, 2519–2528. https://doi.org/10.1038/sj.emboj.7601138

Easton, D.P., Kaneko, Y., Subjeck, J.R., 2000. The Hsp110 and Grp170 stress proteins: newly recognized relatives of the Hsp70s. Cell Stress Chaperones 5, 276. https://doi.org/10.1379/1466-1268(2000)005<0276:THAGSP>2.0.CO;2

Edkins, A.L., Price, J.T., Pockley, A.G., Blatch, G.L., 2018. Heat shock proteins as modulators and therapeutic targets of chronic disease: an integrated perspective. Philos. Trans. R. Soc. B Biol. Sci. 373, 20160521. https://doi.org/10.1098/rstb.2016.0521

Elias, M.C.Q.B., Marques-Porto, R., Freymüller, E., Schenkman, S., 2001. Transcription rate modulation through the Trypanosoma cruzi life cycle occurs in parallel with changes in nuclear organisation. Mol. Biochem. Parasitol. 112, 79–90. https://doi.org/10.1016/S0166-6851(00)00349-2

Engel, S.R., Dietrich, F.S., Fisk, D.G., Binkley, G., Balakrishnan, R., Costanzo, M.C., Dwight, S.S., Hitz, B.C., Karra, K., Nash, R.S., Weng, S., Wong, E.D., Lloyd, P., Skrzypek, M.S., Miyasato, S.R., Simison, M., Cherry, J.M., 2014. The Reference Genome Sequence of *Saccharomyces cerevisiae* : Then and Now. G3 GenesGenomesGenetics 4, 389–398. https://doi.org/10.1534/g3.113.008995

English, C.A., Sherman, W., Meng, W., Gierasch, L.M., 2017. The Hsp70 interdomain linker is a dynamic switch that enables allosteric communication between two structured domains. J. Biol. Chem. 292, 14765–14774. https://doi.org/10.1074/jbc.M117.789313

Engstler, M., Pfohl, T., Herminghaus, S., Boshart, M., Wiegertjes, G., Heddergott, N., Overath, P., 2007. Hydrodynamic Flow-Mediated Protein Sorting on the Cell Surface of Trypanosomes. Cell 131, 505–515. https://doi.org/10.1016/j.cell.2007.08.046

Esser, C., Alberti, S., Höhfeld, J., 2004. Cooperation of molecular chaperones with the ubiquitin/proteasome system. Biochim. Biophys. Acta 1695, 171–188. https://doi.org/10.1016/j.bbamcr.2004.09.020

Esterhuizen, J., Rayaisse, J.B., Tirados, I., Mpiana, S., Solano, P., Vale, G.A., Lehane, M.J., Torr, S.J., 2011. Improving the cost-effectiveness of visual devices for the control of riverine tsetse

flies, the major vectors of human African trypanosomiasis. PLoS Negl. Trop. Dis. 5, e1257. https://doi.org/10.1371/journal.pntd.0001257

Fauvet, B., Finka, A., Castanié-Cornet, M.-P., Cirinesi, A.-M., Genevaux, P., Quadroni, M., Goloubinoff, P., 2021. Bacterial Hsp90 Facilitates the Degradation of Aggregation-Prone Hsp70–Hsp40 Substrates. Front. Mol. Biosci. 8, 653073. https://doi.org/10.3389/fmolb.2021.653073

Ferguson, M.A.J., Homans, S.W., Dwek, R.A., Rademacher, T.W., 1988. Glycosyl-Phosphatidylinositol Moiety That Anchors *Trypanosoma brucei* Variant Surface Glycoprotein to the Membrane. Science 239, 753–759. https://doi.org/10.1126/science.3340856

Fernández-Fernández, M.R., Gragera, M., Ochoa-Ibarrola, L., Quintana-Gallardo, L., Valpuesta, J.M., 2017. Hsp70 - a master regulator in protein degradation. FEBS Lett. 591, 2648–2660. https://doi.org/10.1002/1873-3468.12751

Ferrante, A., Allison, A.C., 1983. Alternative pathway activation of complement by African trypanosomes lacking a glycoprotein coat. Parasite Immunol. 5, 491–498. https://doi.org/10.1111/j.1365-3024.1983.tb00763.x

Field, M.C., Carrington, M., 2009. The trypanosome flagellar pocket. Nat. Rev. Microbiol. 7, 775–786. https://doi.org/10.1038/nrmicro2221

Figueroa-Angulo, E., MartÄ±Ì‍nez-Calvillo, S., LÃ³pez-VillaseÃ±or, I., HernÃ¡ndez, R., 2003. Evidence supporting a major promoter in the *Trypanosoma cruzi* rRNA gene. FEMS Microbiol. Lett. 225, 221–225. https://doi.org/10.1016/S0378-1097(03)00516-0

Finka, A., Goloubinoff, P., 2013. Proteomic data from human cell cultures refine mechanisms of chaperone-mediated protein homeostasis. Cell Stress Chaperones 18, 591–605. https://doi.org/10.1007/s12192-013-0413-3

Finka, A., Mattoo, R.U.H., Goloubinoff, P., 2016. Experimental Milestones in the Discovery of Molecular Chaperones as Polypeptide Unfolding Enzymes. Annu. Rev. Biochem. 85, 715–742. https://doi.org/10.1146/annurev-biochem-060815-014124

Fisk, J.C., Li, J., Wang, H., Aletta, J.M., Qu, J., Read, L.K., 2013. Proteomic Analysis Reveals Diverse Classes of Arginine Methylproteins in Mitochondria of Trypanosomes. Mol. Cell. Proteomics 12, 302–311. https://doi.org/10.1074/mcp.M112.022533

Flaherty, K.M., DeLuca-Flaherty, C., McKay, D.B., 1990. Three-dimensional structure of the ATPase fragment of a 70K heat-shock cognate protein. Nature 346, 623–628. https://doi.org/10.1038/346623a0

Flaherty, K.M., McKay, D.B., Kabsch, W., Holmes, K.C., 1991. Similarity of the three-dimensional structures of actin and the ATPase fragment of a 70-kDa heat shock cognate protein. Proc. Natl. Acad. Sci. 88, 5041–5045. https://doi.org/10.1073/pnas.88.11.5041

Fontanesi, F., Soto, I.C., Horn, D., Barrientos, A., 2010. Mss51 and Ssc1 facilitate translational regulation of cytochrome c oxidase biogenesis. Mol. Cell. Biol. 30, 245–259. https://doi.org/10.1128/MCB.00983-09

Fox, T.D., 2012. Mitochondrial protein synthesis, import, and assembly. Genetics 192, 1203–1234. https://doi.org/10.1534/genetics.112.141267

Frankel, S., Sohn, R., Leinwand, L., 1991. The use of sarkosyl in generating soluble protein after bacterial expression. Proc. Natl. Acad. Sci. U. S. A. 88, 1192–1196. https://doi.org/10.1073/pnas.88.4.1192

Freeman, B.C., Myers, M.P., Schumacher, R., Morimoto, R.I., 1995. Identification of a regulatory motif in Hsp70 that affects ATPase activity, substrate binding and interaction with HDJ-1. EMBO J. 14, 2281–2292. https://doi.org/10.1002/j.1460-2075.1995.tb07222.x

Frydman, J., 2001. Folding of Newly Translated Proteins In Vivo: The Role of Molecular Chaperones. Annu. Rev. Biochem. 70, 603–647. https://doi.org/10.1146/annurev.biochem.70.1.603

Funk, S., Nishiura, H., Heesterbeek, H., Edmunds, W.J., Checchi, F., 2013. Identifying transmission cycles at the human-animal interface: the role of animal reservoirs in maintaining gambiense human african trypanosomiasis. PLoS Comput. Biol. 9, e1002855. https://doi.org/10.1371/journal.pcbi.1002855

Gaestel, M., 2006. Molecular Chaperones in Signal Transduction, in: Starke, K., Gaestel, Matthias (Eds.), Molecular Chaperones in Health and Disease, Handbook of Experimental Pharmacology. Springer-Verlag, Berlin/Heidelberg, pp. 93–109. https://doi.org/10.1007/3-540-29717-0_4

Gajria, B., Bahl, A., Brestelli, J., Dommer, J., Fischer, S., Gao, X., Heiges, M., Iodice, J., Kissinger, J.C., Mackey, A.J., Pinney, D.F., Roos, D.S., Stoeckert, C.J., Wang, H., Brunk, B.P., 2008. ToxoDB: an integrated Toxoplasma gondii database resource. Nucleic Acids Res. 36, D553-556. https://doi.org/10.1093/nar/gkm981

Gambill, B.D., Voos, W., Kang, P.J., Miao, B., Langer, T., Craig, E.A., Pfanner, N., 1993. A dual role for mitochondrial heat shock protein 70 in membrane translocation of preproteins. J. Cell Biol. 123, 109–117. https://doi.org/10.1083/jcb.123.1.109

Gao, F., 2020. Iron–Sulfur Cluster Biogenesis and Iron Homeostasis in Cyanobacteria. Front. Microbiol. 11, 165. https://doi.org/10.3389/fmicb.2020.00165

Gao, Y., Han, C., Huang, H., Xin, Y., Xu, Y., Luo, L., Yin, Z., 2010. Heat shock protein 70 together with its co-chaperone CHIP inhibits TNF-α induced apoptosis by promoting proteasomal degradation of apoptosis signal-regulating kinase1. Apoptosis 15, 822–833. https://doi.org/10.1007/s10495-010-0495-7

García-Fraga, B., da Silva, A.F., López-Seijas, J., Sieiro, C., 2015. Optimized expression conditions for enhancing production of two recombinant chitinolytic enzymes from different prokaryote domains. Bioprocess Biosyst. Eng. 38, 2477–2486. https://doi.org/10.1007/s00449-015-1485-5

Garg, G., Khandelwal, A., Blagg, B.S.J., 2016. Anticancer Inhibitors of Hsp90 Function, in: Advances in Cancer Research. Elsevier, pp. 51–88. https://doi.org/10.1016/bs.acr.2015.12.001

Garrido, C., Gurbuxani, S., Ravagnan, L., Kroemer, G., 2001. Heat Shock Proteins: Endogenous Modulators of Apoptotic Cell Death. Biochem. Biophys. Res. Commun. 286, 433–442. https://doi.org/10.1006/bbrc.2001.5427

Gässler, C.S., Wiederkehr, T., Brehmer, D., Bukau, B., Mayer, M.P., 2001. Bag-1M Accelerates Nucleotide Release for Human Hsc70 and Hsp70 and Can Act Concentration-dependent as

Positive and Negative Cofactor. J. Biol. Chem. 276, 32538–32544. https://doi.org/10.1074/jbc.M105328200

Gasteiger, E., Hoogland, C., Gattiker, A., Duvaud, S., Wilkins, M.R., Appel, R.D., Bairoch, A., 2005. Protein Identification and Analysis Tools on the ExPASy Server, in: Walker, J.M. (Ed.), The Proteomics Protocols Handbook. Humana Press, Totowa, NJ, pp. 571–607. https://doi.org/10.1385/1-59259-890-0:571

Gehrig, S., Efferth, T., 2008. Development of drug resistance in Trypanosoma brucei rhodesiense and Trypanosoma brucei gambiense. Treatment of human African trypanosomiasis with natural products (Review). Int. J. Mol. Med. 22, 411–419.

Geiger, A., Hirtz, C., Bécue, T., Bellard, E., Centeno, D., Gargani, D., Rossignol, M., Cuny, G., Peltier, J.-B., 2010. Exocytosis and protein secretion in Trypanosoma. BMC Microbiol. 10, 20. https://doi.org/10.1186/1471-2180-10-20

General, I.J., Liu, Y., Blackburn, M.E., Mao, W., Gierasch, L.M., Bahar, I., 2014. ATPase Subdomain IA Is a Mediator of Interdomain Allostery in Hsp70 Molecular Chaperones. PLoS Comput. Biol. 10, e1003624. https://doi.org/10.1371/journal.pcbi.1003624

Genest, O., Wickner, S., Doyle, S.M., 2019. Hsp90 and Hsp70 chaperones: Collaborators in protein remodeling. J. Biol. Chem. 294, 2109–2120. https://doi.org/10.1074/jbc.REV118.002806

Genevaux, P., Wawrzynow, A., Zylicz, M., Georgopoulos, C., Kelley, W.L., 2001. DjlA Is a Third DnaK Co-chaperone of Escherichia coli, and DjlA-mediated Induction of Colanic Acid Capsule Requires DjlA-DnaK Interaction. J. Biol. Chem. 276, 7906–7912. https://doi.org/10.1074/jbc.M003855200

Gibson, W., Bailey, M., 2003. The development of Trypanosoma brucei within the tsetse fly midgut observed using green fluorescent Trypanosomes. Kinetoplastid Biol. Dis. 2, 1. https://doi.org/10.1186/1475-9292-2-1

Glick, B.S., 1995. Can Hsp70 proteins act as force-generating motors? Cell 80, 11–14. https://doi.org/10.1016/0092-8674(95)90444-1

Goloubinoff, P., 2017. Editorial: The HSP70 Molecular Chaperone Machines. Front. Mol. Biosci. 4. https://doi.org/10.3389/fmolb.2017.00001

Gong, W., 2009. Inhibition of Citrate Synthase Thermal Aggregation In Vitro by Recombinant Small Heat Shock Proteins. J. Microbiol. Biotechnol. 19, 1628–1634. https://doi.org/10.4014/jmb.0901.0046

Goswami, A.V., Chittoor, B., D'Silva, P., 2010. Understanding the Functional Interplay between Mammalian Mitochondrial Hsp70 Chaperone Machine Components. J. Biol. Chem. 285, 19472–19482. https://doi.org/10.1074/jbc.M110.105957

Goto, H., Lindoso, J.A.L., 2010. Current diagnosis and treatment of cutaneous and mucocutaneous leishmaniasis. Expert Rev. Anti Infect. Ther. 8, 419–433. https://doi.org/10.1586/eri.10.19

Gouteux, P.J., Artzrouni, M., 1996. [Is vector control needed in the fight against sleeping sickness? A biomathematical approach]. Bull. Soc. Pathol. Exot. 1990 89, 299–305.

Gouy, M., Gautier, C., 1982. Codon usage in bacteria: correlation with gene expressivity. Nucleic Acids Res. 10, 7055–7074. https://doi.org/10.1093/nar/10.22.7055

Grady, S.C., Messina, J.P., McCord, P.F., 2011. Population vulnerability and disability in Kenya's tsetse fly habitats. PLoS Negl. Trop. Dis. 5, e957. https://doi.org/10.1371/journal.pntd.0000957

Graf, P.C.F., Martinez-Yamout, M., VanHaerents, S., Lilie, H., Dyson, H.J., Jakob, U., 2004. Activation of the Redox-regulated Chaperone Hsp33 by Domain Unfolding. J. Biol. Chem. 279, 20529–20538. https://doi.org/10.1074/jbc.M401764200

Gragerov, A., Zeng, L., Zhao, X., Burkholder, W., Gottesman, M.E., 1994. Specificity of DnaK-peptide Binding. J. Mol. Biol. 235, 848–854. https://doi.org/10.1006/jmbi.1994.1043

Gramates, L.S., Agapite, J., Attrill, H., Calvi, B.R., Crosby, M.A., Dos Santos, G., Goodman, J.L., Goutte-Gattat, D., Jenkins, V.K., Kaufman, T., Larkin, A., Matthews, B.B., Millburn, G., Strelets, V.B., the FlyBase Consortium, 2022. Fly Base: a guided tour of highlighted features. Genetics 220, iyac035. https://doi.org/10.1093/genetics/iyac035

Graumann, J., Lilie, H., Tang, X., Tucker, K.A., Hoffmann, J.H., Vijayalakshmi, J., Saper, M., Bardwell, J.C.A., Jakob, U., 2001. Activation of the Redox-Regulated Molecular Chaperone Hsp33—A Two-Step Mechanism. Structure 9, 377–387. https://doi.org/10.1016/S0969-2126(01)00599-8

Greene, A.S., Hajduk, S.L., 2016. Trypanosome Lytic Factor-1 Initiates Oxidation-stimulated Osmotic Lysis of Trypanosoma brucei brucei. J. Biol. Chem. 291, 3063–3075. https://doi.org/10.1074/jbc.M115.680371

Gruvel, J., 1980. Considérations générales sur la signification de la transmission mécanique des trypanosomoses chez le bétail. Int. J. Trop. Insect Sci. 1, 55–57. https://doi.org/10.1017/S1742758400000138

Gu, J., Wang, C., Hu, R., Li, Y., Zhang, S., Sun, Y., Wang, Q., Li, D., Fang, Y., Liu, C., 2021. Hsp70 chaperones TDP-43 in dynamic, liquid-like phase and prevents it from amyloid aggregation. Cell Res. 31, 1024–1027. https://doi.org/10.1038/s41422-021-00526-5

Guler, J.L., Kriegova, E., Smith, T.K., Lukeš, J., Englund, P.T., 2008. Mitochondrial fatty acid synthesis is required for normal mitochondrial morphology and function in Trypanosoma brucei. Mol. Microbiol. 67, 1125–1142. https://doi.org/10.1111/j.1365-2958.2008.06112.x

Gull, K., 2003. Host–parasite interactions and trypanosome morphogenesis: a flagellar pocketful of goodies. Curr. Opin. Microbiol. 6, 365–370. https://doi.org/10.1016/S1369-5274(03)00092-4

Guo, F., Sigua, C., Bali, P., George, P., Fiskus, W., Scuto, A., Annavarapu, S., Mouttaki, A., Sondarva, G., Wei, S., Wu, J., Djeu, J., Bhalla, K., 2005. Mechanistic role of heat shock protein 70 in Bcr-Abl-mediated resistance to apoptosis in human acute leukemia cells. Blood 105, 1246–1255. https://doi.org/10.1182/blood-2004-05-2041

Gupta, A., Bansal, A., Hashimoto-Torii, K., 2020. HSP70 and HSP90 in neurodegenerative diseases. Neurosci. Lett. 716, 134678. https://doi.org/10.1016/j.neulet.2019.134678

Gupta, R., 1995. Phylogenetic analysis of the 90 kD heat shock family of protein sequences and an examination of the relationship among animals, plants, and fungi species. Mol. Biol. Evol. https://doi.org/10.1093/oxfordjournals.molbev.a040281

Gupta, V., Carroll, K.S., 2014. Sulfenic acid chemistry, detection and cellular lifetime. Biochim. Biophys. Acta 1840, 847–875. https://doi.org/10.1016/j.bbagen.2013.05.040

Guttmann, R.P., Powell, T.J., 2012. Redox Regulation of Cysteine-Dependent Enzymes in Neurodegeneration. Int. J. Cell Biol. 2012, 1–8. https://doi.org/10.1155/2012/703164

Hageman, J., Kampinga, H.H., 2009. Computational analysis of the human HSPH/HSPA/DNAJ family and cloning of a human HSPH/HSPA/DNAJ expression library. Cell Stress Chaperones 14, 1–21. https://doi.org/10.1007/s12192-008-0060-2

Hager, K.M., Pierce, M.A., Moore, D.R., Tytler, E.M., Esko, J.D., Hajduk, S.L., 1994. Endocytosis of a cytotoxic human high density lipoprotein results in disruption of acidic intracellular vesicles and subsequent killing of African trypanosomes. J. Cell Biol. 126, 155–167. https://doi.org/10.1083/jcb.126.1.155

Hall, J.P.J., Wang, H., Barry, J.D., 2013a. Mosaic VSGs and the Scale of Trypanosoma brucei Antigenic Variation. PLoS Pathog. 9, e1003502. https://doi.org/10.1371/journal.ppat.1003502

Hall, J.P.J., Wang, H., Barry, J.D., 2013b. Mosaic VSGs and the Scale of Trypanosoma brucei Antigenic Variation. PLoS Pathog. 9, e1003502. https://doi.org/10.1371/journal.ppat.1003502

Han, J.M., Park, B.-J., Park, S.G., Oh, Y.S., Choi, S.J., Lee, S.W., Hwang, S.-K., Chang, S.-H., Cho, M.-H., Kim, S., 2008. AIMP2/p38, the scaffold for the multi-tRNA synthetase complex, responds to genotoxic stresses via p53. Proc. Natl. Acad. Sci. 105, 11206–11211. https://doi.org/10.1073/pnas.0800297105

Hannaert, V., Bringaud, F., Opperdoes, F.R., Michels, P.A., 2003. Evolution of energy metabolism and its compartmentation in Kinetoplastida. Kinetoplastid Biol. Dis. 2, 11. https://doi.org/10.1186/1475-9292-2-11

Harrison, C.J., Hayer-Hartl, M., Liberto, M.D., Hartl, F.-U., Kuriyan, J., 1997. Crystal Structure of the Nucleotide Exchange Factor GrpE Bound to the ATPase Domain of the Molecular Chaperone DnaK. Science 276, 431–435. https://doi.org/10.1126/science.276.5311.431

Hartl, F.U., 1996. Molecular chaperones in cellular protein folding. Nature 381, 571–580. https://doi.org/10.1038/381571a0

Hartl, F.U., Bracher, A., Hayer-Hartl, M., 2011. Molecular chaperones in protein folding and proteostasis. Nature 475, 324–332. https://doi.org/10.1038/nature10317

Havalová, H., Ondrovičová, G., Keresztesová, B., Bauer, J.A., Pevala, V., Kutejová, E., Kunová, N., 2021. Mitochondrial HSP70 Chaperone System—The Influence of Post-Translational Modifications and Involvement in Human Diseases. Int. J. Mol. Sci. 22, 8077. https://doi.org/10.3390/ijms22158077

He, S., Dayton, A., Kuppusamy, P., Werbovetz, K.A., Drew, M.E., 2012. Induction of Oxidative Stress in Trypanosoma brucei by the Antitrypanosomal Dihydroquinoline OSU-40. Antimicrob. Agents Chemother. 56, 2428–2434. https://doi.org/10.1128/AAC.06386-11

Hefti, M.H., Van Vugt-Van der Toorn, C.J.G., Dixon, R., Vervoort, J., 2001. A Novel Purification Method for Histidine-Tagged Proteins Containing a Thrombin Cleavage Site. Anal. Biochem. 295, 180–185. https://doi.org/10.1006/abio.2001.5214

Hemphill, A., Lawson, D., Seebeck, T., 1991. The Cytoskeletal Architecture of Trypanosoma brucei. J. Parasitol. 77, 603. https://doi.org/10.2307/3283167

Hendriks, L.E.L., Dingemans, A.-M.C., 2017. Heat shock protein antagonists in early stage clinical trials for NSCLC. Expert Opin. Investig. Drugs 26, 541–550. https://doi.org/10.1080/13543784.2017.1302428

Hennessy, F., Boshoff, A., Blatch, G.L., 2005a. Rational mutagenesis of a 40 kDa heat shock protein from Agrobacterium tumefaciens identifies amino acid residues critical to its in vivo function. Int. J. Biochem. Cell Biol. 37, 177–191. https://doi.org/10.1016/j.biocel.2004.06.009

Hennessy, F., Cheetham, M.E., Dirr, H.W., Blatch, G.L., 2000. Analysis of the levels of conservation of the J domain among the various types of DnaJ-like proteins. Cell Stress Chaperones 5, 347. https://doi.org/10.1379/1466-1268(2000)005<0347:AOTLOC>2.0.CO;2

Hennessy, F., Nicoll, W.S., Zimmermann, R., Cheetham, M.E., Blatch, G.L., 2005b. Not all J domains are created equal: Implications for the specificity of Hsp40-Hsp70 interactions. Protein Sci. 14, 1697–1709. https://doi.org/10.1110/ps.051406805

Herrmann, J.M., Stuart, R.A., Craig, E.A., Neupert, W., 1994. Mitochondrial heat shock protein 70, a molecular chaperone for proteins encoded by mitochondrial DNA. J. Cell Biol. 127, 893–902. https://doi.org/10.1083/jcb.127.4.893

Heyrovská, N., Frydman, J., Höhfeld, J., Hartl, F.U., 1998. Directionality of polypeptide transfer in the mitochondrial pathway of chaperone-mediated protein folding. Biol. Chem. 379, 301–309. https://doi.org/10.1515/bchm.1998.379.3.301

Hidalgo, J., Ortiz, J.F., Fabara, S.P., Eissa-Garcés, A., Reddy, D., Collins, K.D., Tirupathi, R., 2021. Efficacy and Toxicity of Fexinidazole and Nifurtimox Plus Eflornithine in the Treatment of African Trypanosomiasis: A Systematic Review. Cureus 13, e16881. https://doi.org/10.7759/cureus.16881

Hill, G.C., 1976. Electron transport systems in kinetoplastida. Biochim. Biophys. Acta BBA - Rev. Bioenerg. 456, 149–193. https://doi.org/10.1016/0304-4173(76)90011-2

Hill, K., Model, K., Ryan, M.T., Dietmeier, K., Martin, F., Wagner, R., Pfanner, N., 1998. Tom40 forms the hydrophilic channel of the mitochondrial import pore for preproteins. Nature 395, 516–521. https://doi.org/10.1038/26780

Hiss, J.A., Przyborski, J.M., Schwarte, F., Lingelbach, K., Schneider, G., 2008. The Plasmodium Export Element Revisited. PLoS ONE 3, e1560. https://doi.org/10.1371/journal.pone.0001560

Hoare, C.A., Wallace, F.G., 1966. Developmental Stages of Trypanosomatid Flagellates: a New Terminology. Nature 212, 1385–1386. https://doi.org/10.1038/2121385a0

Hoenig, M., Lee, R.J., Ferguson, D.C., 1989. A microtiter plate assay for inorganic phosphate. J. Biochem. Biophys. Methods 19, 249–251. https://doi.org/10.1016/0165-022X(89)90031-6

Höfeld, J., Minami, Y., Hartl, F.-U., 1995. Hip, a novel cochaperone involved in the eukaryotic hsc70/hsp40 reaction cycle. Cell 83, 589–598. https://doi.org/10.1016/0092-8674(95)90099-3

Hoffmann, J.H., Linke, K., Graf, P.C., Lilie, H., Jakob, U., 2004. Identification of a redox-regulated chaperone network. EMBO J. 23, 160–168. https://doi.org/10.1038/sj.emboj.7600016

Hohfeld, J., 1997. GrpE-like regulation of the Hsc70 chaperone by the anti-apoptotic protein BAG-1. EMBO J. 16, 6209–6216. https://doi.org/10.1093/emboj/16.20.6209

Horn, D., 2014. Antigenic variation in African trypanosomes. Mol. Biochem. Parasitol. 195, 123–129. https://doi.org/10.1016/j.molbiopara.2014.05.001

Horn, D., McCulloch, R., 2010. Molecular mechanisms underlying the control of antigenic variation in African trypanosomes. Curr. Opin. Microbiol. 13, 700–705. https://doi.org/10.1016/j.mib.2010.08.009

Hornbeck, P.V., Zhang, B., Murray, B., Kornhauser, J.M., Latham, V., Skrzypek, E., 2015. PhosphoSitePlus, 2014: mutations, PTMs and recalibrations. Nucleic Acids Res. 43, D512–D520. https://doi.org/10.1093/nar/gku1267

Horst, M., 1997. Sequential action of two hsp70 complexes during protein import into mitochondria. EMBO J. 16, 1842–1849. https://doi.org/10.1093/emboj/16.8.1842

Horton, P., Park, K.-J., Obayashi, T., Fujita, N., Harada, H., Adams-Collier, C.J., Nakai, K., 2007. WoLF PSORT: protein localization predictor. Nucleic Acids Res. 35, W585–W587. https://doi.org/10.1093/nar/gkm259

Hoter, A., El-Sabban, M., Naim, H., 2018. The HSP90 Family: Structure, Regulation, Function, and Implications in Health and Disease. Int. J. Mol. Sci. 19, 2560. https://doi.org/10.3390/ijms19092560

Hotez, P.J., Pecoul, B., Rijal, S., Boehme, C., Aksoy, S., Malecela, M., Tapia-Conyer, R., Reeder, J.C., 2016. Eliminating the Neglected Tropical Diseases: Translational Science and New Technologies. PLoS Negl. Trop. Dis. 10, e0003895. https://doi.org/10.1371/journal.pntd.0003895

Huai, Q., Wang, H., Liu, Y., Kim, H.-Y., Toft, D., Ke, H., 2005. Structures of the N-Terminal and Middle Domains of E. coli Hsp90 and Conformation Changes upon ADP Binding. Structure 13, 579–590. https://doi.org/10.1016/j.str.2004.12.018

Huang, L.E., Bunn, H.F., 2003. Hypoxia-inducible Factor and Its Biomedical Relevance. J. Biol. Chem. 278, 19575–19578. https://doi.org/10.1074/jbc.R200030200

Huber-Wunderlich, M., Glockshuber, R., 1998. A single dipeptide sequence modulates the redox properties of a whole enzyme family. Fold. Des. 3, 161–171. https://doi.org/10.1016/S1359-0278(98)00024-8

Hunt, C., Morimoto, R.I., 1985. Conserved features of eukaryotic hsp70 genes revealed by comparison with the nucleotide sequence of human hsp70. Proc. Natl. Acad. Sci. 82, 6455–6459. https://doi.org/10.1073/pnas.82.19.6455

Hunt, J.F., Weaver, A.J., Landry, S.J., Gierasch, L., Deisenhofer, J., 1996. The crystal structure of the GroES co-chaperonin at 2.8 A resolution. Nature 379, 37–45. https://doi.org/10.1038/379037a0

Hutchings, N.R., Donelson, J.E., Hill, K.L., 2002. Trypanin is a cytoskeletal linker protein and is required for cell motility in African trypanosomes. J. Cell Biol. 156, 867–877. https://doi.org/10.1083/jcb.200201036

Ighodaro, O.M., Akinloye, O.A., 2018. First line defence antioxidants-superoxide dismutase (SOD), catalase (CAT) and glutathione peroxidase (GPX): Their fundamental role in the entire antioxidant defence grid. Alex. J. Med. 54, 287–293. https://doi.org/10.1016/j.ajme.2017.09.001

Ilbert, M., Horst, J., Ahrens, S., Winter, J., Graf, P.C.F., Lilie, H., Jakob, U., 2007. The redox-switch domain of Hsp33 functions as dual stress sensor. Nat. Struct. Mol. Biol. 14, 556–563. https://doi.org/10.1038/nsmb1244

Iosefson, O., Sharon, S., Goloubinoff, P., Azem, A., 2012. Reactivation of protein aggregates by mortalin and Tid1--the human mitochondrial Hsp70 chaperone system. Cell Stress Chaperones 17, 57–66. https://doi.org/10.1007/s12192-011-0285-3

Ishida, R., Okamoto, T., Motojima, F., Kubota, H., Takahashi, H., Tanabe, M., Oka, T., Kitamura, A., Kinjo, M., Yoshida, M., Otaka, M., Grave, E., Itoh, H., 2018. Physicochemical Properties of the Mammalian Molecular Chaperone HSP60. Int. J. Mol. Sci. 19, E489. https://doi.org/10.3390/ijms19020489

Jackson, A.P., Otto, T.D., Aslett, M., Armstrong, S.D., Bringaud, F., Schlacht, A., Hartley, C., Sanders, M., Wastling, J.M., Dacks, J.B., Acosta-Serrano, A., Field, M.C., Ginger, M.L., Berriman, M., 2016. Kinetoplastid Phylogenomics Reveals the Evolutionary Innovations Associated with the Origins of Parasitism. Curr. Biol. 26, 161–172. https://doi.org/10.1016/j.cub.2015.11.055

Jackson, S.E., 2012. Hsp90: Structure and Function, in: Jackson, S. (Ed.), Molecular Chaperones, Topics in Current Chemistry. Springer Berlin Heidelberg, Berlin, Heidelberg, pp. 155–240. https://doi.org/10.1007/128_2012_356

Jacobs, R.T., Plattner, J.J., Nare, B., Wring, S.A., Chen, D., Freund, Y., Gaukel, E.G., Orr, M.D., Perales, J.B., Jenks, M., Noe, R.A., Sligar, J.M., Zhang, Y.-K., Bacchi, C.J., Yarlett, N., Don, R., 2011. Benzoxaboroles: a new class of potential drugs for human African trypanosomiasis. Future Med. Chem. 3, 1259–1278. https://doi.org/10.4155/fmc.11.80

Jakob, U., Eser, M., Bardwell, J.C.A., 2000. Redox Switch of Hsp33 Has a Novel Zinc-binding Motif. J. Biol. Chem. 275, 38302–38310. https://doi.org/10.1074/jbc.M005957200

Jakob, U., Muse, W., Eser, M., Bardwell, J.C.A., 1999. Chaperone Activity with a Redox Switch. Cell 96, 341–352. https://doi.org/10.1016/S0092-8674(00)80547-4

Jamonneau, V., Ilboudo, H., Kaboré, J., Kaba, D., Koffi, M., Solano, P., Garcia, A., Courtin, D., Laveissière, C., Lingue, K., Büscher, P., Bucheton, B., 2012. Untreated Human Infections by Trypanosoma brucei gambiense Are Not 100% Fatal. PLoS Negl. Trop. Dis. 6, e1691. https://doi.org/10.1371/journal.pntd.0001691

Jamonneau, V., Ravel, S., Koffi, M., Kaba, D., Zeze, D.G., Ndri, L., Sane, B., Coulibaly, B., Cuny, G., Solano, P., 2004. Mixed infections of trypanosomes in tsetse and pigs and their epidemiological significance in a sleeping sickness focus of Côte d'Ivoire. Parasitology 129, 693–702. https://doi.org/10.1017/s0031182004005876

Janknecht, R., Nordheim, A., 1992. Affinity purification of histidine-tagged proteins transiently produced in HeLa cells. Gene 121, 321–324. https://doi.org/10.1016/0378-1119(92)90137-E

Jee, H., 2016. Size dependent classification of heat shock proteins: a mini-review. J. Exerc. Rehabil. 12, 255–259. https://doi.org/10.12965/jer.1632642.321

Jensen, R.E., Englund, P.T., 2012. Network News: The Replication of Kinetoplast DNA. Annu. Rev. Microbiol. 66, 473–491. https://doi.org/10.1146/annurev-micro-092611-150057

Jiang, J., Maes, E.G., Taylor, A.B., Wang, L., Hinck, A.P., Lafer, E.M., Sousa, R., 2007. Structural Basis of J Cochaperone Binding and Regulation of Hsp70. Mol. Cell 28, 422–433. https://doi.org/10.1016/j.molcel.2007.08.022

Johnson, B.D., Schumacher, R.J., Ross, E.D., Toft, D.O., 1998. Hop modulates Hsp70/Hsp90 interactions in protein folding. J. Biol. Chem. 273, 3679–3686. https://doi.org/10.1074/jbc.273.6.3679

Johnson, J.L., 2012. Evolution and function of diverse Hsp90 homologs and cochaperone proteins. Biochim. Biophys. Acta BBA - Mol. Cell Res. 1823, 607–613. https://doi.org/10.1016/j.bbamcr.2011.09.020

Johnson, J.M., Castle, J., Garrett-Engele, P., Kan, Z., Loerch, P.M., Armour, C.D., Santos, R., Schadt, E.E., Stoughton, R., Shoemaker, D.D., 2003. Genome-Wide Survey of Human Alternative Pre-mRNA Splicing with Exon Junction Microarrays. Science 302, 2141–2144. https://doi.org/10.1126/science.1090100

Johnson, P., 1987. Inactivation of transcription by UV irradiation of T. brucei provides evidence for a multicistronic transcription unit including a VSG gene. Cell 51, 273–281. https://doi.org/10.1016/0092-8674(87)90154-1

Jones, A., Faldas, A., Foucher, A., Hunt, E., Tait, A., Wastling, J.M., Turner, C.M., 2006. Visualisation and analysis of proteomic data from the procyclic form ofTrypanosoma brucei. PROTEOMICS 6, 259–267. https://doi.org/10.1002/pmic.200500119

Jones, D.T., Taylor, W.R., Thornton, J.M., 1992. The rapid generation of mutation data matrices from protein sequences. Comput. Appl. Biosci. CABIOS 8, 275–282. https://doi.org/10.1093/bioinformatics/8.3.275

Joseph, S.K., Boehning, D., Pierson, S., Nicchitta, C.V., 1997. Membrane Insertion, Glycosylation, and Oligomerization of Inositol Trisphosphate Receptors in a Cell-free Translation System. J. Biol. Chem. 272, 1579–1588. https://doi.org/10.1074/jbc.272.3.1579

Josyula, R., Jin, Z., Fu, Z., Sha, B., 2006. Crystal structure of yeast mitochondrial peripheral membrane protein Tim44p C-terminal domain. J. Mol. Biol. 359, 798–804. https://doi.org/10.1016/j.jmb.2006.04.020

Jumper, J., Evans, R., Pritzel, A., Green, T., Figurnov, M., Ronneberger, O., Tunyasuvunakool, K., Bates, R., Žídek, A., Potapenko, A., Bridgland, A., Meyer, C., Kohl, S.A.A., Ballard, A.J., Cowie, A., Romera-Paredes, B., Nikolov, S., Jain, R., Adler, J., Back, T., Petersen, S., Reiman, D., Clancy, E., Zielinski, M., Steinegger, M., Pacholska, M., Berghammer, T., Bodenstein, S., Silver, D., Vinyals, O., Senior, A.W., Kavukcuoglu, K., Kohli, P., Hassabis, D., 2021. Highly accurate protein structure prediction with AlphaFold. Nature 596, 583–589. https://doi.org/10.1038/s41586-021-03819-2

Kabani, M., Beckerich, J.-M., Brodsky, J.L., 2002. Nucleotide Exchange Factor for the Yeast Hsp70 Molecular Chaperone Ssa1p. Mol. Cell. Biol. 22, 4677–4689. https://doi.org/10.1128/MCB.22.13.4677-4689.2002

Kampinga, H.H., Craig, E.A., 2010. The HSP70 chaperone machinery: J proteins as drivers of functional specificity. Nat. Rev. Mol. Cell Biol. 11, 579–592. https://doi.org/10.1038/nrm2941

Kampinga, H.H., Hageman, J., Vos, M.J., Kubota, H., Tanguay, R.M., Bruford, E.A., Cheetham, M.E., Chen, B., Hightower, L.E., 2009. Guidelines for the nomenclature of the human heat shock proteins. Cell Stress Chaperones 14, 105–111. https://doi.org/10.1007/s12192-008-0068-7

Kande Betu Ku Mesu, V., Mutombo Kalonji, W., Bardonneau, C., Valverde Mordt, O., Ngolo Tete, D., Blesson, S., Simon, F., Delhomme, S., Bernhard, S., Mahenzi Mbembo, H., Mpia Moke, C., Lumeya Vuvu, S., Mudji E'kitiak, J., Akwaso Masa, F., Mukendi Ilunga, M., Mpoyi Muamba Nzambi, D., Mayala Malu, T., Kapongo Tshilumbwa, S., Botalema Bolengi, F., Nkieri Matsho, M., Lumbala, C., Scherrer, B., Strub-Wourgaft, N., Tarral, A., 2021. Oral fexinidazole for stage 1 or early stage 2 African Trypanosoma brucei gambiense trypanosomiasis: a prospective, multicentre, open-label, cohort study. Lancet Glob. Health 9, e999–e1008. https://doi.org/10.1016/S2214-109X(21)00208-4

Kang, P.-J., Ostermann, J., Shilling, J., Neupert, W., Craig, E.A., Pfanner, N., 1990. Requirement for hsp70 in the mitochondrial matrix for translocation and folding of precursor proteins. Nature 348, 137–143. https://doi.org/10.1038/348137a0

Kansiime, F., Adibaku, S., Wamboga, C., Idi, F., Kato, C.D., Yamuah, L., Vaillant, M., Kioy, D., Olliaro, P., Matovu, E., 2018. A multicentre, randomised, non-inferiority clinical trial comparing a nifurtimox-eflornithine combination to standard eflornithine monotherapy for late stage Trypanosoma brucei gambiense human African trypanosomiasis in Uganda. Parasit. Vectors 11, 105. https://doi.org/10.1186/s13071-018-2634-x

Karagöz, G.E., Duarte, A.M.S., Akoury, E., Ippel, H., Biernat, J., Morán Luengo, T., Radli, M., Didenko, T., Nordhues, B.A., Veprintsev, D.B., Dickey, C.A., Mandelkow, E., Zweckstetter, M., Boelens, R., Madl, T., Rüdiger, S.G.D., 2014. Hsp90-Tau complex reveals molecular basis for specificity in chaperone action. Cell 156, 963–974. https://doi.org/10.1016/j.cell.2014.01.037

Karlin, S., Brocchieri, L., 1998. Heat Shock Protein 70 Family: Multiple Sequence Comparisons, Function, and Evolution. J. Mol. Evol. 47, 565–577. https://doi.org/10.1007/PL00006413

Karri, S., Singh, S., Paripati, A.K., Marada, A., Krishnamoorthy, T., Guruprasad, L., Balasubramanian, D., Sepuri, N.B.V., 2019. Adaptation of Mge1 to oxidative stress by local unfolding and altered Interaction with mitochondrial Hsp70 and Mxr2. Mitochondrion 46, 140–148. https://doi.org/10.1016/j.mito.2018.04.003

Kasozi, K.I., Zirintunda, G., Ssempijja, F., Buyinza, B., Alzahrani, K.J., Matama, K., Nakimbugwe, H.N., Alkazmi, L., Onanyang, D., Bogere, P., Ochieng, J.J., Islam, S., Matovu, W., Nalumenya, D.P., Batiha, G.E.-S., Osuwat, L.O., Abdelhamid, M., Shen, T., Omadang, L., Welburn, S.C., 2021. Epidemiology of Trypanosomiasis in Wildlife—Implications for Humans at the Wildlife Interface in Africa. Front. Vet. Sci. 8, 621699. https://doi.org/10.3389/fvets.2021.621699

Kaufer, A., Ellis, J., Stark, D., Barratt, J., 2017. The evolution of trypanosomatid taxonomy. Parasit. Vectors 10, 287. https://doi.org/10.1186/s13071-017-2204-7

Kaul, S.C., Wadhwa, R. (Eds.), 2012. Mortalin Biology: Life, Stress and Death. Springer Netherlands, Dordrecht. https://doi.org/10.1007/978-94-007-3027-4

Kaur, Jashandeep, Kumar, A., Kaur, Jagdeep, 2018. Strategies for optimization of heterologous protein expression in E. coli: Roadblocks and reinforcements. Int. J. Biol. Macromol. 106, 803–822. https://doi.org/10.1016/j.ijbiomac.2017.08.080

Kaye, P., Scott, P., 2011. Leishmaniasis: complexity at the host–pathogen interface. Nat. Rev. Microbiol. 9, 604–615. https://doi.org/10.1038/nrmicro2608

Kennedy, P.G., 2013. Clinical features, diagnosis, and treatment of human African trypanosomiasis (sleeping sickness). Lancet Neurol. 12, 186–194. https://doi.org/10.1016/S1474-4422(12)70296-X

Kennedy, P.G.E., 2008. The continuing problem of human African trypanosomiasis (sleeping sickness). Ann. Neurol. 64, 116–126. https://doi.org/10.1002/ana.21429

Kennedy, P.G.E., 2004. Human African trypanosomiasis of the CNS: current issues and challenges. J. Clin. Invest. 113, 496–504. https://doi.org/10.1172/JCI200421052

Kennedy, P.G.E., Rodgers, J., 2019. Clinical and Neuropathogenetic Aspects of Human African Trypanosomiasis. Front. Immunol. 10, 39. https://doi.org/10.3389/fimmu.2019.00039

Khan, M.S., Ahmed, A., Tabrez, S., Islam, B.U., Rabbani, N., Malik, A., Ismael, M.A., Alsenaidy, M.A., Alsenaidy, A.M., 2017. Optimization of expression and purification of human mortalin (Hsp70): Folding/unfolding analysis. Spectrochim. Acta. A. Mol. Biomol. Spectrosc. 187, 98–103. https://doi.org/10.1016/j.saa.2017.06.015

Khan, S., Ullah, M.W., Siddique, R., Nabi, G., Manan, S., Yousaf, M., Hou, H., 2016. Role of Recombinant DNA Technology to Improve Life. Int. J. Genomics 2016, 2405954. https://doi.org/10.1155/2016/2405954

Kholod, N., Mustelin, T., 2001. Novel Vectors for Co-Expression of Two Proteins in *E. coli*. BioTechniques 31, 322–328. https://doi.org/10.2144/01312st03

Kieft, R., Capewell, P., Turner, C.M.R., Veitch, N.J., MacLeod, A., Hajduk, S., 2010. Mechanism of *Trypanosoma brucei gambiense* (group 1) resistance to human trypanosome lytic factor. Proc. Natl. Acad. Sci. 107, 16137–16141. https://doi.org/10.1073/pnas.1007074107

Kim, K., Rhee, S.G., Stadtman, E.R., 1985. Nonenzymatic cleavage of proteins by reactive oxygen species generated by dithiothreitol and iron. J. Biol. Chem. 260, 15394–15397.

Kim, Y.E., Hipp, M.S., Bracher, A., Hayer-Hartl, M., Ulrich Hartl, F., 2013. Molecular Chaperone Functions in Protein Folding and Proteostasis. Annu. Rev. Biochem. 82, 323–355. https://doi.org/10.1146/annurev-biochem-060208-092442

Kiraly, V.T.R., Dores-Silva, P.R., Serrão, V.H.B., Cauvi, D.M., De Maio, A., Borges, J.C., 2020. Thermal aggregates of human mortalin and Hsp70-1A behave as supramolecular assemblies. Int. J. Biol. Macromol. 146, 320–331. https://doi.org/10.1016/j.ijbiomac.2019.12.236

Kityk, R., Kopp, J., Mayer, M.P., 2018. Molecular Mechanism of J-Domain-Triggered ATP Hydrolysis by Hsp70 Chaperones. Mol. Cell 69, 227-237.e4. https://doi.org/10.1016/j.molcel.2017.12.003

Kityk, R., Kopp, J., Sinning, I., Mayer, M.P., 2012. Structure and dynamics of the ATP-bound open conformation of Hsp70 chaperones. Mol. Cell 48, 863–874. https://doi.org/10.1016/j.molcel.2012.09.023

Kleczewska, M., Grabinska, A., Jelen, M., Stolarska, M., Schilke, B., Marszalek, J., Craig, E.A., Dutkiewicz, R., 2020. Biochemical Convergence of Mitochondrial Hsp70 System Specialized in Iron–Sulfur Cluster Biogenesis. Int. J. Mol. Sci. 21, 3326. https://doi.org/10.3390/ijms21093326

Klomsiri, C., Karplus, P.A., Poole, L.B., 2011. Cysteine-based redox switches in enzymes. Antioxid. Redox Signal. 14, 1065–1077. https://doi.org/10.1089/ars.2010.3376

Klotz, J.H., Dorn, P.L., Logan, J.L., Stevens, L., Pinnas, J.L., Schmidt, J.O., Klotz, S.A., 2010. "Kissing Bugs": Potential Disease Vectors and Cause of Anaphylaxis. Clin. Infect. Dis. 50, 1629–1634. https://doi.org/10.1086/652769

Klotz, S.A., Dorn, P.L., Mosbacher, M., Schmidt, J.O., 2014. Kissing Bugs in the United States: Risk for Vector-Borne Disease in Humans. Environ. Health Insights 8s2, EHI.S16003. https://doi.org/10.4137/EHI.S16003

Knighton, L.E., Nitika, Omkar, S., Truman, A.W., 2022. The C-terminal domain of Hsp70 is responsible for paralog-specific regulation of ribonucleotide reductase. PLOS Genet. 18, e1010079. https://doi.org/10.1371/journal.pgen.1010079

Kostygov, A.Y., Karnkowska, A., Votýpka, J., Tashyreva, D., Maciszewski, K., Yurchenko, V., Lukeš, J., 2021. Euglenozoa: taxonomy, diversity and ecology, symbioses and viruses. Open Biol. 11, rsob.200407, 200407. https://doi.org/10.1098/rsob.200407

Krick, T., Verstraete, N., Alonso, L.G., Shub, D.A., Ferreiro, D.U., Shub, M., Sánchez, I.E., 2014. Amino Acid Metabolism Conflicts with Protein Diversity. Mol. Biol. Evol. 31, 2905–2912. https://doi.org/10.1093/molbev/msu228

Kulawiak, B., Höpker, J., Gebert, M., Guiard, B., Wiedemann, N., Gebert, N., 2013. The mitochondrial protein import machinery has multiple connections to the respiratory chain. Biochim. Biophys. Acta BBA - Bioenerg. 1827, 612–626. https://doi.org/10.1016/j.bbabio.2012.12.004

Kumar, S., Stecher, G., Li, M., Knyaz, C., Tamura, K., 2018. MEGA X: Molecular Evolutionary Genetics Analysis across Computing Platforms. Mol. Biol. Evol. 35, 1547–1549. https://doi.org/10.1093/molbev/msy096

Kuo, Y., Ren, S., Lao, U., Edgar, B.A., Wang, T., 2013. Suppression of polyglutamine protein toxicity by co-expression of a heat-shock protein 40 and a heat-shock protein 110. Cell Death Dis. 4, e833–e833. https://doi.org/10.1038/cddis.2013.351

La Greca, F., Magez, S., 2011. Vaccination against trypanosomiasis: Can it be done or is the trypanosome truly the ultimate immune destroyer and escape artist? Hum. Vaccin. 7, 1225–1233. https://doi.org/10.4161/hv.7.11.18203

Lacomble, S., Vaughan, S., Gadelha, C., Morphew, M.K., Shaw, M.K., McIntosh, J.R., Gull, K., 2009. Three-dimensional cellular architecture of the flagellar pocket and associated cytoskeleton in trypanosomes revealed by electron microscope tomography. J. Cell Sci. 122, 1081–1090. https://doi.org/10.1242/jcs.045740

Lai, D.-H., Hashimi, H., Lun, Z.-R., Ayala, F.J., Lukeš, J., 2008. Adaptations of *Trypanosoma brucei* to gradual loss of kinetoplast DNA: *Trypanosoma equiperdum* and *Trypanosoma evansi* are *petite* mutants of *T. brucei*. Proc. Natl. Acad. Sci. 105, 1999–2004. https://doi.org/10.1073/pnas.0711799105

Lamour, N., Rivière, L., Coustou, V., Coombs, G.H., Barrett, M.P., Bringaud, F., 2005. Proline Metabolism in Procyclic Trypanosoma brucei Is Down-regulated in the Presence of Glucose. J. Biol. Chem. 280, 11902–11910. https://doi.org/10.1074/jbc.M414274200

Lança, A.S.C., de Sousa, K.P., Atouguia, J., Prazeres, D.M.F., Monteiro, G.A., Silva, M.S., 2011. Trypanosoma brucei: Immunisation with plasmid DNA encoding invariant surface glycoprotein gene is able to induce partial protection in experimental African trypanosomiasis. Exp. Parasitol. 127, 18–24. https://doi.org/10.1016/j.exppara.2010.06.017

Lancien, J., 1991. [Campaign against sleeping sickness in South-West Uganda by trapping tsetse flies]. Ann. Soc. Belg. Med. Trop. 71 Suppl 1, 35–47.

Langer, T., 2003. Intracellular localization of the 90 kDA heat shock protein (HSP90α) determined by expression of a EGFP–HSP90α-fusion protein in unstressed and heat stressed 3T3 cells. Cell Biol. Int. 27, 47–52. https://doi.org/10.1016/S1065-6995(02)00256-1

Langousis, G., Hill, K.L., 2014. Motility and more: the flagellum of Trypanosoma brucei. Nat. Rev. Microbiol. 12, 505–518. https://doi.org/10.1038/nrmicro3274

Larkin, M.A., Blackshields, G., Brown, N.P., Chenna, R., McGettigan, P.A., McWilliam, H., Valentin, F., Wallace, I.M., Wilm, A., Lopez, R., Thompson, J.D., Gibson, T.J., Higgins, D.G., 2007. Clustal W and Clustal X version 2.0. Bioinformatics 23, 2947–2948. https://doi.org/10.1093/bioinformatics/btm404

Lavery, L.A., Partridge, J.R., Ramelot, T.A., Elnatan, D., Kennedy, M.A., Agard, D.A., 2014. Structural Asymmetry in the Closed State of Mitochondrial Hsp90 (TRAP1) Supports a Two-Step ATP Hydrolysis Mechanism. Mol. Cell 53, 330–343. https://doi.org/10.1016/j.molcel.2013.12.023

Leak, S.G.A., 1999. Tsetse biology and ecology: their role in the epidemiology and control of trypanosomosis. CABI Publishing in association with International Livestock Research Institute, Oxon ; New York.

Lee, B., Ahn, Y., Kang, S.-M., Park, Y., Jeon, Y.-J., Rho, J.M., Kim, S.-W., 2015. Stoichiometric expression of mtHsp40 and mtHsp70 modulates mitochondrial morphology and cristae structure via Opa1L cleavage. Mol. Biol. Cell 26, 2156–2167. https://doi.org/10.1091/mbc.E14-02-0762

Lee, S.L., Dempsey-Hibbert, N.C., Vimalachandran, D., Wardle, T.D., Sutton, P.A., Williams, J.H.H., 2017. Re-examining HSPC1 inhibitors. Cell Stress Chaperones 22, 293–306. https://doi.org/10.1007/s12192-017-0774-0

Lee, S.Y., 1996. High cell-density culture of Escherichia coli. Trends Biotechnol. 14, 98–105. https://doi.org/10.1016/0167-7799(96)80930-9

Lejon, V., Ngoyi, D.M., Ilunga, M., Beelaert, G., Maes, I., Büscher, P., Fransen, K., 2010. Low Specificities of HIV Diagnostic Tests Caused by *Trypanosoma brucei gambiense* Sleeping Sickness. J. Clin. Microbiol. 48, 2836–2839. https://doi.org/10.1128/JCM.00456-10

Lenaz, G., Genova, M.L., 2010. Structure and Organization of Mitochondrial Respiratory Complexes: A New Understanding of an Old Subject. Antioxid. Redox Signal. 12, 961–1008. https://doi.org/10.1089/ars.2009.2704

Letunic, I., Khedkar, S., Bork, P., 2021. SMART: recent updates, new developments and status in 2020. Nucleic Acids Res. 49, D458–D460. https://doi.org/10.1093/nar/gkaa937

Li, J., Qian, X., Hu, J., Sha, B., 2009. Molecular chaperone Hsp70/Hsp90 prepares the mitochondrial outer membrane translocon receptor Tom71 for preprotein loading. J. Biol. Chem. 284, 23852–23859. https://doi.org/10.1074/jbc.M109.023986

Li, S., Lv, M., Qiu, S., Meng, J., Liu, W., Zuo, J., Yang, L., 2019. NF-κB p65 promotes ovarian cancer cell proliferation and migration via regulating mortalin. J. Cell. Mol. Med. 23, 4338–4348. https://doi.org/10.1111/jcmm.14325

Li, W., Tsen, F., Sahu, D., Bhatia, A., Chen, M., Multhoff, G., Woodley, D.T., 2013. Extracellular Hsp90 (eHsp90) as the actual target in clinical trials: intentionally or unintentionally. Int. Rev. Cell Mol. Biol. 303, 203–235. https://doi.org/10.1016/B978-0-12-407697-6.00005-2

Li, Y., Dudek, J., Guiard, B., Pfanner, N., Rehling, P., Voos, W., 2004. The Presequence Translocase-associated Protein Import Motor of Mitochondria. J. Biol. Chem. 279, 38047–38054. https://doi.org/10.1074/jbc.M404319200

Li, Z., Hartl, F.U., Bracher, A., 2013. Structure and function of Hip, an attenuator of the Hsp70 chaperone cycle. Nat. Struct. Mol. Biol. 20, 929–935. https://doi.org/10.1038/nsmb.2608

Liberek, K., Marszalek, J., Ang, D., Georgopoulos, C., Zylicz, M., 1991. Escherichia coli DnaJ and GrpE heat shock proteins jointly stimulate ATPase activity of DnaK. Proc. Natl. Acad. Sci. 88, 2874–2878. https://doi.org/10.1073/pnas.88.7.2874

Libkind, D., Hittinger, C.T., Valério, E., Gonçalves, C., Dover, J., Johnston, M., Gonçalves, P., Sampaio, J.P., 2011. Microbe domestication and the identification of the wild genetic stock of lager-brewing yeast. Proc. Natl. Acad. Sci. 108, 14539–14544. https://doi.org/10.1073/pnas.1105430108

Lill, R., Mühlenhoff, U., 2008. Maturation of iron-sulfur proteins in eukaryotes: mechanisms, connected processes, and diseases. Annu. Rev. Biochem. 77, 669–700. https://doi.org/10.1146/annurev.biochem.76.052705.162653

Lim, S., Cho, H.Y., Kim, D.G., Roh, Y., Son, S.-Y., Mushtaq, A.U., Kim, M., Bhattarai, D., Sivaraman, A., Lee, Y., Lee, J., Yang, W.S., Kim, H.K., Kim, M.H., Lee, K., Jeon, Y.H., Kim, S., 2020. Targeting the interaction of AIMP2-DX2 with HSP70 suppresses cancer development. Nat. Chem. Biol. 16, 31–41. https://doi.org/10.1038/s41589-019-0415-2

Lindner, A.K., Priotto, G., 2010. The Unknown Risk of Vertical Transmission in Sleeping Sickness—A Literature Review. PLoS Negl. Trop. Dis. 4, e783. https://doi.org/10.1371/journal.pntd.0000783

Linke, K., Wolfram, T., Bussemer, J., Jakob, U., 2003. The Roles of the Two Zinc Binding Sites in DnaJ. J. Biol. Chem. 278, 44457–44466. https://doi.org/10.1074/jbc.M307491200

Liu, Q., Hendrickson, W.A., 2007. Insights into Hsp70 Chaperone Activity from a Crystal Structure of the Yeast Hsp110 Sse1. Cell 131, 106–120. https://doi.org/10.1016/j.cell.2007.08.039

Liu, Q., Krzewska, J., Liberek, K., Craig, E.A., 2001. Mitochondrial Hsp70 Ssc1: role in protein folding. J. Biol. Chem. 276, 6112–6118. https://doi.org/10.1074/jbc.M009519200

Liu, Q., Liang, C., Zhou, L., 2020. Structural and functional analysis of the Hsp70/Hsp40 chaperone system. Protein Sci. 29, 378–390. https://doi.org/10.1002/pro.3725

Londono, C., Osorio, C., Gama, V., Alzate, O., 2012. Mortalin, Apoptosis, and Neurodegeneration. Biomolecules 2, 143–164. https://doi.org/10.3390/biom2010143

Lopes, A., 2010. Trypanosomatids: Odd Organisms, Devastating Diseases. Open Parasitol. J. 4, 30–59. https://doi.org/10.2174/1874421401004010030

Lopez-Buesa, P., Pfund, C., Craig, E.A., 1998. The biochemical properties of the ATPase activity of a 70-kDa heat shock protein (Hsp70) are governed by the C-terminal domains. Proc. Natl. Acad. Sci. 95, 15253–15258. https://doi.org/10.1073/pnas.95.26.15253

Louw, C.A., Ludewig, M.H., Mayer, J., Blatch, G.L., 2010. The Hsp70 chaperones of the Tritryps are characterized by unusual features and novel members. Parasitol. Int. 59, 497–505. https://doi.org/10.1016/j.parint.2010.08.008

Lu, B., Garrido, N., Spelbrink, J.N., Suzuki, C.K., 2006. Tid1 Isoforms Are Mitochondrial DnaJ-like Chaperones with Unique Carboxyl Termini That Determine Cytosolic Fate. J. Biol. Chem. 281, 13150–13158. https://doi.org/10.1074/jbc.M509179200

Ludewig, M.H., Boshoff, A., Horn, D., Blatch, G.L., 2015. Trypanosoma brucei J protein 2 is a stress inducible and essential Hsp40. Int. J. Biochem. Cell Biol. 60, 93–98. https://doi.org/10.1016/j.biocel.2014.12.016

Lukeš, J., Hashimi, H., Zíková, A., 2005. Unexplained complexity of the mitochondrial genome and transcriptome in kinetoplastid flagellates. Curr. Genet. 48, 277–299. https://doi.org/10.1007/s00294-005-0027-0

Luscher, A., de Koning, H., Maser, P., 2007. Chemotherapeutic Strategies Against Trypanosoma brucei: Drug Targets vs. Drug Targeting. Curr. Pharm. Des. 13, 555–567. https://doi.org/10.2174/138161207780162809

Lutz, T., Westermann, B., Neupert, W., Herrmann, J.M., 2001. The mitochondrial proteins Ssq1 and Jac1 are required for the assembly of iron sulfur clusters in mitochondria11Edited by B. Holland. J. Mol. Biol. 307, 815–825. https://doi.org/10.1006/jmbi.2001.4527

Lyon, M.S., Milligan, C., 2019. Extracellular heat shock proteins in neurodegenerative diseases: New perspectives. Neurosci. Lett. 711, 134462. https://doi.org/10.1016/j.neulet.2019.134462

MacGregor, P., Savill, N.J., Hall, D., Matthews, K.R., 2011. Transmission Stages Dominate Trypanosome Within-Host Dynamics during Chronic Infections. Cell Host Microbe 9, 310–318. https://doi.org/10.1016/j.chom.2011.03.013

MacLean, L.M., Odiit, M., Chisi, J.E., Kennedy, P.G.E., Sternberg, J.M., 2010. Focus–Specific Clinical Profiles in Human African Trypanosomiasis Caused by Trypanosoma brucei rhodesiense. PLoS Negl. Trop. Dis. 4, e906. https://doi.org/10.1371/journal.pntd.0000906

Magez, S., Li, Z., Nguyen, H.T.T., Pinto Torres, J.E., Van Wielendaele, P., Radwanska, M., Began, J., Zoll, S., Sterckx, Y.G.-J., 2021. The History of Anti-Trypanosome Vaccine Development Shows

That Highly Immunogenic and Exposed Pathogen-Derived Antigens Are Not Necessarily Good Target Candidates: Enolase and ISG75 as Examples. Pathog. Basel Switz. 10, 1050. https://doi.org/10.3390/pathogens10081050

Magez, S., Pinto Torres, J.E., Obishakin, E., Radwanska, M., 2020. Infections With Extracellular Trypanosomes Require Control by Efficient Innate Immune Mechanisms and Can Result in the Destruction of the Mammalian Humoral Immune System. Front. Immunol. 11, 382. https://doi.org/10.3389/fimmu.2020.00382

Magez, S., Stijlemans, B., Baral, T., De Baetselier, P., 2002. VSG-GPI anchors of African trypanosomes: their role in macrophage activation and induction of infection-associated immunopathology. Microbes Infect. 4, 999–1006. https://doi.org/10.1016/S1286-4579(02)01617-9

Maio, N., Rouault, T.A., 2015. Iron –sulfur cluster biogenesis in mammalian cells: New insights into the molecular mechanisms of cluster delivery. Biochim. Biophys. Acta BBA - Mol. Cell Res. 1853, 1493–1512. https://doi.org/10.1016/j.bbamcr.2014.09.009

Makumire, S., Dongola, T.H., Chakafana, G., Tshikonwane, L., Chauke, C.T., Maharaj, T., Zininga, T., Shonhai, A., 2021. Mutation of GGMP Repeat Segments of Plasmodium falciparum Hsp70-1 Compromises Chaperone Function and Hop Co-Chaperone Binding. Int. J. Mol. Sci. 22, 2226. https://doi.org/10.3390/ijms22042226

Maldonado, R.A., Fairlamb, A.H., 2001. Cloning of a pyruvate phosphate dikinase from Trypanosoma cruzi. Mol. Biochem. Parasitol. 112, 183–191. https://doi.org/10.1016/S0166-6851(00)00362-5

Manning-Krieg, U.C., Scherer, P.E., Schatz, G., 1991. Sequential action of mitochondrial chaperones in protein import into the matrix. EMBO J. 10, 3273–3280. https://doi.org/10.1002/j.1460-2075.1991.tb04891.x

Mant, M.J., Parker, K.R., 2008. Two Platelet Aggregation Inhibitors in Tsetse (Glossina) Saliva with Studies of Roles of Thrombin and Citrate in in Vitro Platelet Aggregation. Br. J. Haematol. 48, 601–608. https://doi.org/10.1111/j.1365-2141.1981.00601.x

Marino, S.M., Gladyshev, V.N., 2010. Cysteine Function Governs Its Conservation and Degeneration and Restricts Its Utilization on Protein Surfaces. J. Mol. Biol. 404, 902–916. https://doi.org/10.1016/j.jmb.2010.09.027

Marom, M., Safonov, R., Amram, S., Avneon, Y., Nachliel, E., Gutman, M., Zohary, K., Azem, A., Tsfadia, Y., 2009. Interaction of the Tim44 C-terminal domain with negatively charged phospholipids. Biochemistry 48, 11185–11195. https://doi.org/10.1021/bi900998v

Marti, M., Good, R.T., Rug, M., Knuepfer, E., Cowman, A.F., 2004. Targeting malaria virulence and remodeling proteins to the host erythrocyte. Science 306, 1930–1933. https://doi.org/10.1126/science.1102452

Martin, J., Mahlke, K., Pfanner, N., 1991. Role of an energized inner membrane in mitochondrial protein import. Delta psi drives the movement of presequences. J. Biol. Chem. 266, 18051–18057.

Martínez-Alonso, M., García-Fruitós, E., Ferrer-Miralles, N., Rinas, U., Villaverde, A., 2010. Side effects of chaperone gene co-expression in recombinant protein production. Microb. Cell Factories 9, 64. https://doi.org/10.1186/1475-2859-9-64

Martínez-Calvillo, S., Vizuet-de-Rueda, J.C., Florencio-Martínez, L.E., Manning-Cela, R.G., Figueroa-Angulo, E.E., 2010. Gene Expression in Trypanosomatid Parasites. J. Biomed. Biotechnol. 2010, 1–15. https://doi.org/10.1155/2010/525241

Martínez-Espinosa, R.M., 2019. Heterologous and Homologous Expression of Proteins from Haloarchaea: Denitrification as Case of Study. Int. J. Mol. Sci. 21, 82. https://doi.org/10.3390/ijms21010082

Martinez-Yamout, M., Legge, G.B., Zhang, O., Wright, P.E., Dyson, H.J., 2000. Solution Structure of the Cysteine-rich Domain of the Escherichia coli Chaperone Protein DnaJ. J. Mol. Biol. 300, 805–818. https://doi.org/10.1006/jmbi.2000.3923

Masgras, I., Sanchez-Martin, C., Colombo, G., Rasola, A., 2017. The Chaperone TRAP1 As a Modulator of the Mitochondrial Adaptations in Cancer Cells. Front. Oncol. 7. https://doi.org/10.3389/fonc.2017.00058

Maslov, D.A., Podlipaev, S.A., Lukes, J., 2001. Phylogeny of the kinetoplastida: taxonomic problems and insights into the evolution of parasitism. Mem. Inst. Oswaldo Cruz 96, 397–402. https://doi.org/10.1590/S0074-02762001000300021

Maslov, D.A., Votýpka, J., Yurchenko, V., Lukeš, J., 2013. Diversity and phylogeny of insect trypanosomatids: all that is hidden shall be revealed. Trends Parasitol. 29, 43–52. https://doi.org/10.1016/j.pt.2012.11.001

Masocha, W., Rottenberg, M.E., Kristensson, K., 2007. Migration of African trypanosomes across the blood–brain barrier. Physiol. Behav. 92, 110–114. https://doi.org/10.1016/j.physbeh.2007.05.045

Matouschek, A., Pfanner, N., Voos, W., 2000. Protein unfolding by mitochondria: The Hsp70 import motor. EMBO Rep. 1, 404–410. https://doi.org/10.1093/embo-reports/kvd093

Matthews, K.R., 2005. The developmental cell biology of *Trypanosoma brucei*. J. Cell Sci. 118, 283–290. https://doi.org/10.1242/jcs.01649

Matthews, K.R., Ellis, J.R., Paterou, A., 2004. Molecular regulation of the life cycle of African trypanosomes. Trends Parasitol. 20, 40–47. https://doi.org/10.1016/j.pt.2003.10.016

Matthews, K.R., Gull, K., 1994. Evidence for an interplay between cell cycle progression and the initiation of differentiation between life cycle forms of African trypanosomes. J. Cell Biol. 125, 1147–1156. https://doi.org/10.1083/jcb.125.5.1147

Mattoo, R.U.H., Farina Henriquez Cuendet, A., Subanna, S., Finka, A., Priya, S., Sharma, S.K., Goloubinoff, P., 2014. Synergism between a foldase and an unfoldase: reciprocal dependence between the thioredoxin-like activity of DnaJ and the polypeptide-unfolding activity of DnaK. Front. Mol. Biosci. 1. https://doi.org/10.3389/fmolb.2014.00007

Mattoo, R.U.H., Sharma, S.K., Priya, S., Finka, A., Goloubinoff, P., 2013. Hsp110 is a bona fide chaperone using ATP to unfold stable misfolded polypeptides and reciprocally collaborate with Hsp70 to solubilize protein aggregates. J. Biol. Chem. 288, 21399–21411. https://doi.org/10.1074/jbc.M113.479253

Maudlin, I., 2006. African trypanosomiasis. Ann. Trop. Med. Parasitol. 100, 679–701. https://doi.org/10.1179/136485906X112211

Mayer, M.P., 2013. Hsp70 chaperone dynamics and molecular mechanism. Trends Biochem. Sci. 38, 507–514. https://doi.org/10.1016/j.tibs.2013.08.001

Mayer, M.P., Bukau, B., 2005. Hsp70 chaperones: Cellular functions and molecular mechanism. Cell. Mol. Life Sci. 62, 670–684. https://doi.org/10.1007/s00018-004-4464-6

Mayer, M.P., Gierasch, L.M., 2019. Recent advances in the structural and mechanistic aspects of Hsp70 molecular chaperones. J. Biol. Chem. 294, 2085–2097. https://doi.org/10.1074/jbc.REV118.002810

Mayer, M.P., Kityk, R., 2015. Insights into the molecular mechanism of allostery in Hsp70s. Front. Mol. Biosci. 2, 58. https://doi.org/10.3389/fmolb.2015.00058

Mehlert, A., Wormald, M.R., Ferguson, M.A.J., 2012. Modeling of the N-Glycosylated Transferrin Receptor Suggests How Transferrin Binding Can Occur within the Surface Coat of Trypanosoma brucei. PLoS Pathog. 8, e1002618. https://doi.org/10.1371/journal.ppat.1002618

Meng, X., Devin, J., Sullivan, W.P., Toft, D., Baulieu, E.E., Catelli, M.G., 1996. Mutational analysis of Hsp90 alpha dimerization and subcellular localization: dimer disruption does not impede “in vivo’ interaction with estrogen receptor. J. Cell Sci. 109, 1677–1687. https://doi.org/10.1242/jcs.109.7.1677

Mensa-Wilmot, K., Hoffman, B., Wiedeman, J., Sullenberger, C., Sharma, A., 2019. Kinetoplast Division Factors in a Trypanosome. Trends Parasitol. 35, 119–128. https://doi.org/10.1016/j.pt.2018.11.002

Merzlyak, E., Yurchenko, V., Kolesnikov, A.A., Alexandrov, K., Podlipaev, S.A., Maslov, D.A., 2001. Diversity and Phylogeny of Insect Trypanosomatids Based on Small Subunit rRNA Genes: Polyphyly of Leptomonas and Blastocrithidia. J. Eukaryot. Microbiol. 48, 161–169. https://doi.org/10.1111/j.1550-7408.2001.tb00298.x

Meselson, M., Yuan, R., 1968. DNA restriction enzyme from E. coli. Nature 217, 1110–1114. https://doi.org/10.1038/2171110a0

Meyer, P., Prodromou, C., Hu, B., Vaughan, C., Roe, S.M., Panaretou, B., Piper, P.W., Pearl, L.H., 2003. Structural and Functional Analysis of the Middle Segment of Hsp90: Implications for ATP Hydrolysis and Client Protein and Cochaperone Interactions. Mol. Cell 11, 647–658. https://doi.org/10.1016/S1097-2765(03)00065-0

Meyskens, F.L., Gerner, E.W., 1999. Development of difluoromethylornithine (DFMO) as a chemoprevention agent. Clin. Cancer Res. Off. J. Am. Assoc. Cancer Res. 5, 945–951.

Michels, P.A.M., Hannaert, V., Bringaud, F., 2000. Metabolic Aspects of Glycosomes in Trypanosomatidae – New Data and Views. Parasitol. Today 16, 482–489. https://doi.org/10.1016/S0169-4758(00)01810-X

Michels, P.A.M., Moyersoen, J., Krazy, H., Galland, N., Herman, M., Hannaert, V., 2005. Peroxisomes, glyoxysomes and glycosomes (Review). Mol. Membr. Biol. 22, 133–145. https://doi.org/10.1080/09687860400024186

Miyata, Y., Nakamoto, H., Neckers, L., 2013. The Therapeutic Target Hsp90 and Cancer Hallmarks. Curr. Pharm. Des. 19, 347–365. https://doi.org/10.2174/138161213804143725

Moayed, F., Bezrukavnikov, S., Naqvi, M.M., Groitl, B., Cremers, C.M., Kramer, G., Ghosh, K., Jakob, U., Tans, S.J., 2020. The Anti-Aggregation Holdase Hsp33 Promotes the Formation of Folded Protein Structures. Biophys. J. 118, 85–95. https://doi.org/10.1016/j.bpj.2019.10.040

Molyneux, D.H., Hopkins, D.R., Zagaria, N., 2004. Disease eradication, elimination and control: the need for accurate and consistent usage. Trends Parasitol. 20, 347–351. https://doi.org/10.1016/j.pt.2004.06.004

Momose, T., Ohshima, C., Maeda, M., Endo, T., 2007. Structural basis of functional cooperation of Tim15/Zim17 with yeast mitochondrial Hsp70. EMBO Rep. 8, 664–670. https://doi.org/10.1038/sj.embor.7400990

Moore, A.L., Siedow, J.N., 1991. The regulation and nature of the cyanide-resistant alternative oxidase of plant mitochondria. Biochim. Biophys. Acta BBA - Bioenerg. 1059, 121–140. https://doi.org/10.1016/S0005-2728(05)80197-5

Morán Luengo, T., Kityk, R., Mayer, M.P., Rüdiger, S.G.D., 2018. Hsp90 Breaks the Deadlock of the Hsp70 Chaperone System. Mol. Cell 70, 545-552.e9. https://doi.org/10.1016/j.molcel.2018.03.028

Moreira, D., López-García, P., Vickerman, K., 2004. An updated view of kinetoplastid phylogeny using environmental sequences and a closer outgroup: proposal for a new classification of the class Kinetoplastea. Int. J. Syst. Evol. Microbiol. 54, 1861–1875. https://doi.org/10.1099/ijs.0.63081-0

Morrison, L.J., Marcello, L., McCulloch, R., 2009. Antigenic variation in the African trypanosome: molecular mechanisms and phenotypic complexity. Cell. Microbiol. 11, 1724–1734. https://doi.org/10.1111/j.1462-5822.2009.01383.x

Mössner, E., Huber-Wunderlich, M., Glockshuber, R., 1998. Characterization of *Escherichia coli* thioredoxin variants mimicking the active-sites of other thiol/disulfide oxidoreductases. Protein Sci. 7, 1233–1244. https://doi.org/10.1002/pro.5560070519

Moyersoen, J., Choe, J., Fan, E., Hol, W.G.J., Michels, P.A.M., 2004. Biogenesis of peroxisomes and glycosomes: trypanosomatid glycosome assembly is a promising new drug target. FEMS Microbiol. Rev. 28, 603–643. https://doi.org/10.1016/j.femsre.2004.06.004

Munoz-Calderon, A., Díaz-Bello, Z., Ramírez, J., Noya, O., de Noya, B., 2019. Nifurtimox response of Trypanosoma cruzi isolates from an outbreak of Chagas disease in Caracas, Venezuela. J. Vector Borne Dis. 56, 237. https://doi.org/10.4103/0972-9062.289397

Muralidharan, V., Goldberg, D.E., 2013. Asparagine Repeats in Plasmodium falciparum Proteins: Good for Nothing? PLoS Pathog. 9, e1003488. https://doi.org/10.1371/journal.ppat.1003488

Murphy, M.E., 2013. The HSP70 family and cancer. Carcinogenesis 34, 1181–1188. https://doi.org/10.1093/carcin/bgt111

Murray, M., Murray, P.K., Jennings, F.W., Fisher, E.W., Urquhart, G.M., 1974. The Pathology of Trypanosoma brucei Infection in the Rat. Res. Vet. Sci. 16, 77–84. https://doi.org/10.1016/S0034-5288(18)33777-9

Mylonis, I., Kourti, M., Samiotaki, M., Panayotou, G., Simos, G., 2016. Mortalin-mediated and ERK-controlled targeting of HIF-1α to mitochondria confers resistance to apoptosis under hypoxia. J. Cell Sci. jcs.195339. https://doi.org/10.1242/jcs.195339

Na, Y., Kaul, S.C., Ryu, J., Lee, J.-S., Ahn, H.M., Kaul, Z., Kalra, R.S., Li, L., Widodo, N., Yun, C.-O., Wadhwa, R., 2016. Stress chaperone mortalin contributes to epithelial-mesenchymal transition and cancer metastasis. Cancer Res. 76, 2754–2765. https://doi.org/10.1158/0008-5472.CAN-15-2704

NCI CPTAC, Mertins, P., Mani, D.R., Ruggles, K.V., Gillette, M.A., Clauser, K.R., Wang, P., Wang, X., Qiao, J.W., Cao, S., Petralia, F., Kawaler, E., Mundt, F., Krug, K., Tu, Z., Lei, J.T., Gatza, M.L., Wilkerson, M., Perou, C.M., Yellapantula, V., Huang, K., Lin, C., McLellan, M.D., Yan, P., Davies, S.R., Townsend, R.R., Skates, S.J., Wang, J., Zhang, B., Kinsinger, C.R., Mesri, M., Rodriguez, H., Ding, L., Paulovich, A.G., Fenyö, D., Ellis, M.J., Carr, S.A., 2016. Proteogenomics connects somatic mutations to signalling in breast cancer. Nature 534, 55–62. https://doi.org/10.1038/nature18003

Nelson, G.M., Huffman, H., Smith, D.F., 2003. Comparison of the carboxy-terminal DP-repeat region in the co-chaperones Hop and Hip. Cell Stress Chaperones 8, 125. https://doi.org/10.1379/1466-1268(2003)008<0125:COTCDR>2.0.CO;2

Nett, I.R.E., Martin, D.M.A., Miranda-Saavedra, D., Lamont, D., Barber, J.D., Mehlert, A., Ferguson, M.A.J., 2009. The Phosphoproteome of Bloodstream Form Trypanosoma brucei, Causative Agent of African Sleeping Sickness. Mol. Cell. Proteomics 8, 1527–1538. https://doi.org/10.1074/mcp.M800556-MCP200

Ng, A.C.-H., Baird, S.D., Screaton, R.A., 2014. Essential role of TID1 in maintaining mitochondrial membrane potential homogeneity and mitochondrial DNA integrity. Mol. Cell. Biol. 34, 1427–1437. https://doi.org/10.1128/MCB.01021-13

Nicolas, E., Tricarico, R., Savage, M., Golemis, E.A., Hall, M.J., 2019. Disease-Associated Genetic Variation in Human Mitochondrial Protein Import. Am. J. Hum. Genet. 104, 784–801. https://doi.org/10.1016/j.ajhg.2019.03.019

Nikolay, R., Wiederkehr, T., Rist, W., Kramer, G., Mayer, M.P., Bukau, B., 2004. Dimerization of the Human E3 Ligase CHIP via a Coiled-coil Domain Is Essential for Its Activity. J. Biol. Chem. 279, 2673–2678. https://doi.org/10.1074/jbc.M311112200

Nitika, Porter, C.M., Truman, A.W., Truttmann, M.C., 2020. Post-translational modifications of Hsp70 family proteins: Expanding the chaperone code. J. Biol. Chem. 295, 10689–10708. https://doi.org/10.1074/jbc.REV120.011666

Nolan, D.P., Jackson, D.G., Biggs, M.J., Brabazon, E.D., Pays, A., Van Laethem, F., Paturiaux-Hanocq, F., Elliot, J.F., Voorheis, H.P., Pays, E., 2000. Characterization of a Novel Alanine-rich Protein Located in Surface Microdomains in Trypanosoma brucei. J. Biol. Chem. 275, 4072–4080. https://doi.org/10.1074/jbc.275.6.4072

Nyakundi, D.O., Bentley, S.J., Boshoff, A., 2018. Hsp70 Escort Protein: More Than a Regulator of Mitochondrial Hsp70. Curr. Proteomics 16, 64–73. https://doi.org/10.2174/1570164615666180713104919

Nyakundi, D.O., Vuko, L.A.M., Bentley, S.J., Hoppe, H., Blatch, G.L., Boshoff, A., 2016. Plasmodium falciparum Hep1 Is Required to Prevent the Self Aggregation of PfHsp70-3. PLOS ONE 11, e0156446. https://doi.org/10.1371/journal.pone.0156446

Odunuga, O.O., Longshaw, V.M., Blatch, G.L., 2004. Hop: more than an Hsp70/Hsp90 adaptor protein. BioEssays 26, 1058–1068. https://doi.org/10.1002/bies.20107

Ogbadoyi, E.O., Robinson, D.R., Gull, K., 2003. A High-Order *Trans* -Membrane Structural Linkage Is Responsible for Mitochondrial Genome Positioning and Segregation by Flagellar Basal Bodies in Trypanosomes. Mol. Biol. Cell 14, 1769–1779. https://doi.org/10.1091/mbc.e02-08-0525

Oh, H.J., Easton, D., Murawski, M., Kaneko, Y., Subjeck, J.R., 1999. The Chaperoning Activity of hsp110. J. Biol. Chem. 274, 15712–15718. https://doi.org/10.1074/jbc.274.22.15712

Ohtsuka, K., Hata, M., 2000. Mammalian HSP40/DNAJ homologs: cloning of novel cDNAs and a proposal for their classification and nomenclature. Cell Stress Chaperones 5, 98. https://doi.org/10.1379/1466-1268(2000)005<0098:MHDHCO>2.0.CO;2

Olsen, G.J., Woese, C.R., 1993. Ribosomal RNA: a key to phylogeny. FASEB J. 7, 113–123. https://doi.org/10.1096/fasebj.7.1.8422957

Onyilagha, C., Uzonna, J.E., 2019. Host Immune Responses and Immune Evasion Strategies in African Trypanosomiasis. Front. Immunol. 10, 2738. https://doi.org/10.3389/fimmu.2019.02738

Ooi, C.-P., Bastin, P., 2013. More than meets the eye: understanding Trypanosoma brucei morphology in the tsetse. Front. Cell. Infect. Microbiol. 3. https://doi.org/10.3389/fcimb.2013.00071

Opperdoes, F.R., Borst, P., 1977. Localization of nine glycolytic enzymes in a microbody-like organelle in *Trypanosoma brucei* : The glycosome. FEBS Lett. 80, 360–364. https://doi.org/10.1016/0014-5793(77)80476-6

Palleros, D.R., Raid, K.L., Shi, L., Welch, W.J., Fink, A.L., 1993. ATP-induced protein Hsp70 complex dissociation requires K+ but not ATP hydrolysis. Nature 365, 664–666. https://doi.org/10.1038/365664a0

Panaretou, B., 1998. ATP binding and hydrolysis are essential to the function of the Hsp90 molecular chaperone invivo. EMBO J. 17, 4829–4836. https://doi.org/10.1093/emboj/17.16.4829

Pareek, G., Samaddar, M., D'Silva, P., 2011. Primary sequence that determines the functional overlap between mitochondrial heat shock protein 70 Ssc1 and Ssc3 of Saccharomyces cerevisiae. J. Biol. Chem. 286, 19001–19013. https://doi.org/10.1074/jbc.M110.197434

Paris, Z., Fleming, I.M.C., Alfonzo, J.D., 2012. Determinants of tRNA editing and modification: avoiding conundrums, affecting function. Semin. Cell Dev. Biol. 23, 269–274. https://doi.org/10.1016/j.semcdb.2011.10.009

Patterson, S., Wyllie, S., 2014. Nitro drugs for the treatment of trypanosomatid diseases: past, present, and future prospects. Trends Parasitol. 30, 289–298. https://doi.org/10.1016/j.pt.2014.04.003

Pays, E., 2006. The variant surface glycoprotein as a tool for adaptation in African trypanosomes. Microbes Infect. 8, 930–937. https://doi.org/10.1016/j.micinf.2005.10.002

Pays, E., Vanhollebeke, B., Vanhamme, L., Paturiaux-Hanocq, F., Nolan, D.P., Pérez-Morga, D., 2006. The trypanolytic factor of human serum. Nat. Rev. Microbiol. 4, 477–486. https://doi.org/10.1038/nrmicro1428

Paz, C., Samake, S., Anderson, J.M., Faye, O., Traore, P., Tall, K., Cisse, M., Keita, S., Valenzuela, J.G., Doumbia, S., 2013. Leishmania major, the predominant Leishmania species responsible for cutaneous leishmaniasis in Mali. Am. J. Trop. Med. Hyg. 88, 583–585. https://doi.org/10.4269/ajtmh.12-0434

Perales-Calvo, J., Muga, A., Moro, F., 2010. Role of DnaJ G/F-rich Domain in Conformational Recognition and Binding of Protein Substrates*. J. Biol. Chem. 285, 34231–34239. https://doi.org/10.1074/jbc.M110.144642

Pérez-Molina, J.A., Molina, I., 2018. Chagas disease. The Lancet 391, 82–94. https://doi.org/10.1016/S0140-6736(17)31612-4

Pesce, E.-R., Blatch, G.L., Edkins, Adrienne L., 2015. Hsp40 Co-chaperones as Drug Targets: Towards the Development of Specific Inhibitors, in: McAlpine, S.R., Edkins, Adrienne Lesley (Eds.), Heat Shock Protein Inhibitors, Topics in Medicinal Chemistry. Springer International Publishing, Cham, pp. 163–195. https://doi.org/10.1007/7355_2015_92

Petzke, F., Heppner, C., Mbulamberi, D., Winkelmann, W., Chrousos, G.P., Allolio, B., Reincke, M., 1996. Hypogonadism in Rhodesian sleeping sickness: evidence for acute and chronic dysfunction of the hypothalamic-pituitary-gonadal axis**Supported in part by a grant of the Deutsche Forschungsgemeinschaft (Re 752/2–1) and the Gesellschaft für Technische Zusammenarbeit. Fertil. Steril. 65, 68–75. https://doi.org/10.1016/S0015-0282(16)58029-7

Pfanner, N., Meijer, M., 1995. Protein sorting. Pulling in the proteins. Curr. Biol. CB 5, 132–135. https://doi.org/10.1016/s0960-9822(95)00033-9

Pham, T.K., Buczek, W.A., Mead, R.J., Shaw, P.J., Collins, M.O., 2021. Proteomic Approaches to Study Cysteine Oxidation: Applications in Neurodegenerative Diseases. Front. Mol. Neurosci. 14, 678837. https://doi.org/10.3389/fnmol.2021.678837

Poinar, G., Poinar, R., 2005. Fossil evidence of insect pathogens. J. Invertebr. Pathol. 89, 243–250. https://doi.org/10.1016/j.jip.2005.05.007

Poinar, G., Poinar, R., 2004. Evidence of Vector-Borne Disease of Early Cretaceous Reptiles. Vector-Borne Zoonotic Dis. 4, 281–284. https://doi.org/10.1089/vbz.2004.4.281

Polier, S., Dragovic, Z., Hartl, F.U., Bracher, A., 2008. Structural Basis for the Cooperation of Hsp70 and Hsp110 Chaperones in Protein Folding. Cell 133, 1068–1079. https://doi.org/10.1016/j.cell.2008.05.022

Pope, B., Kent, H.M., 1996. High Efficiency 5 Min Transformation of Escherichia Coli. Nucleic Acids Res. 24, 536–537. https://doi.org/10.1093/nar/24.3.536

Portman, N., Gull, K., 2010. The paraflagellar rod of kinetoplastid parasites: From structure to components and function. Int. J. Parasitol. 40, 135–148. https://doi.org/10.1016/j.ijpara.2009.10.005

Priesnitz, C., Böttinger, L., Zufall, N., Gebert, M., Guiard, B., van der Laan, M., Becker, T., 2022. Coupling to Pam16 differentially controls the dual role of Pam18 in protein import and

respiratory chain formation. Cell Rep. 39, 110619. https://doi.org/10.1016/j.celrep.2022.110619

Priest, J.W., Hajduk, S.L., 1994. Developmental regulation of mitochondrial biogenesis inTrypanosoma brucei. J. Bioenerg. Biomembr. 26, 179–191. https://doi.org/10.1007/BF00763067

Priotto, G., Kasparian, S., Mutombo, W., Ngouama, D., Ghorashian, S., Arnold, U., Ghabri, S., Baudin, E., Buard, V., Kazadi-Kyanza, S., Ilunga, M., Mutangala, W., Pohlig, G., Schmid, C., Karunakara, U., Torreele, E., Kande, V., 2009. Nifurtimox-eflornithine combination therapy for second-stage African Trypanosoma brucei gambiense trypanosomiasis: a multicentre, randomised, phase III, non-inferiority trial. The Lancet 374, 56–64. https://doi.org/10.1016/S0140-6736(09)61117-X

Priotto, G., Pinoges, L., Fursa, I.B., Burke, B., Nicolay, N., Grillet, G., Hewison, C., Balasegaram, M., 2008. Safety and effectiveness of first line eflornithine for *Trypanosoma brucei gambiense* sleeping sickness in Sudan: cohort study. BMJ 336, 705–708. https://doi.org/10.1136/bmj.39485.592674.BE

Prodromou, C., 2016. Mechanisms of Hsp90 regulation. Biochem. J. 473, 2439–2452. https://doi.org/10.1042/BCJ20160005

Przyborski, J.M., Diehl, M., Blatch, G.L., 2015. Plasmodial HSP70s are functionally adapted to the malaria parasite life cycle. Front. Mol. Biosci. 2. https://doi.org/10.3389/fmolb.2015.00034

Qi, R., Sarbeng, E.B., Liu, Qun, Le, K.Q., Xu, X., Xu, H., Yang, J., Wong, J.L., Vorvis, C., Hendrickson, W.A., Zhou, L., Liu, Qinglian, 2013. Allosteric opening of the polypeptide-binding site when an Hsp70 binds ATP. Nat. Struct. Mol. Biol. 20, 900–907. https://doi.org/10.1038/nsmb.2583

Qian, S.-B., McDonough, H., Boellmann, F., Cyr, D.M., Patterson, C., 2006. CHIP-mediated stress recovery by sequential ubiquitination of substrates and Hsp70. Nature 440, 551–555. https://doi.org/10.1038/nature04600

Radwanska, M., Guirnalda, P., De Trez, C., Ryffel, B., Black, S., Magez, S., 2008. Trypanosomiasis-Induced B Cell Apoptosis Results in Loss of Protective Anti-Parasite Antibody Responses and Abolishment of Vaccine-Induced Memory Responses. PLoS Pathog. 4, e1000078. https://doi.org/10.1371/journal.ppat.1000078

Radzinski, M., Oppenheim, T., Metanis, N., Reichmann, D., 2021. The Cys Sense: Thiol Redox Switches Mediate Life Cycles of Cellular Proteins. Biomolecules 11, 469. https://doi.org/10.3390/biom11030469

Ralston, K.S., Hill, K.L., 2006. Trypanin, a Component of the Flagellar Dynein Regulatory Complex, Is Essential in Bloodstream Form African Trypanosomes. PLoS Pathog. 2, e101. https://doi.org/10.1371/journal.ppat.0020101

Ran, Q., Wadhwa, R., Kawai, R., Kaul, S.C., Sifers, R.N., Bick, R.J., Smith, J.R., Pereira-Smith, O.M., 2000. Extramitochondrial Localization of Mortalin/mthsp70/PBP74/GRP75. Biochem. Biophys. Res. Commun. 275, 174–179. https://doi.org/10.1006/bbrc.2000.3237

Rao, R.V., Bredesen, D.E., 2004. Misfolded proteins, endoplasmic reticulum stress and neurodegeneration. Curr. Opin. Cell Biol. 16, 653–662. https://doi.org/10.1016/j.ceb.2004.09.012

Raper, J., 2001. Trypanosome lytic factors: novel mediators of human innate immunity. Curr. Opin. Microbiol. 4, 402–408. https://doi.org/10.1016/S1369-5274(00)00226-5

Raper, J., Fung, R., Ghiso, J., Nussenzweig, V., Tomlinson, S., 1999. Characterization of a Novel Trypanosome Lytic Factor from Human Serum. Infect. Immun. 67, 1910–1916. https://doi.org/10.1128/IAI.67.4.1910-1916.1999

Raper, J., Nussenzweig, V., Tomlinson, S., 1996. The main lytic factor of Trypanosoma brucei brucei in normal human serum is not high density lipoprotein. J. Exp. Med. 183, 1023–1029. https://doi.org/10.1084/jem.183.3.1023

Rassow, J., Maarse, A.C., Krainer, E., Kübrich, M., Müller, H., Meijer, M., Craig, E.A., Pfanner, N., 1994. Mitochondrial protein import: biochemical and genetic evidence for interaction of matrix hsp70 and the inner membrane protein MIM44. J. Cell Biol. 127, 1547–1556. https://doi.org/10.1083/jcb.127.6.1547

Raviol, H., Sadlish, H., Rodriguez, F., Mayer, M.P., Bukau, B., 2006. Chaperone network in the yeast cytosol: Hsp110 is revealed as an Hsp70 nucleotide exchange factor. EMBO J. 25, 2510–2518. https://doi.org/10.1038/sj.emboj.7601139

Rayaisse, J.-B., Courtin, F., Mahamat, M.H., Chérif, M., Yoni, W., Gadjibet, N.M.O., Peka, M., Solano, P., Torr, S.J., Shaw, A.P.M., 2020. Delivering 'tiny targets' in a remote region of southern Chad: a cost analysis of tsetse control in the Mandoul sleeping sickness focus. Parasit. Vectors 13, 419. https://doi.org/10.1186/s13071-020-04286-w

Rayaisse, J.B., Esterhuizen, J., Tirados, I., Kaba, D., Salou, E., Diarrassouba, A., Vale, G.A., Lehane, M.J., Torr, S.J., Solano, P., 2011. Towards an optimal design of target for tsetse control: comparisons of novel targets for the control of Palpalis group tsetse in West Africa. PLoS Negl. Trop. Dis. 5, e1332. https://doi.org/10.1371/journal.pntd.0001332

Rayaisse, J.-B., Salou, E., Courtin, F., Yoni, W., Barry, I., Dofini, F., Kagbadouno, M., Camara, M., Torr, S.J., Solano, P., 2015. Baited-boats: an innovative way to control riverine tsetse, vectors of sleeping sickness in West Africa. Parasit. Vectors 8, 236. https://doi.org/10.1186/s13071-015-0851-0

Rayaisse, J.B., Tirados, I., Kaba, D., Dewhirst, S.Y., Logan, J.G., Diarrassouba, A., Salou, E., Omolo, M.O., Solano, P., Lehane, M.J., Pickett, J.A., Vale, G.A., Torr, S.J., Esterhuizen, J., 2010. Prospects for the Development of Odour Baits to Control the Tsetse Flies Glossina tachinoides and G. palpalis s.l. PLoS Negl. Trop. Dis. 4, e632. https://doi.org/10.1371/journal.pntd.0000632

Reinitz, D.M., Mansfield, J.M., 1990. T-cell-independent and T-cell-dependent B-cell responses to exposed variant surface glycoprotein epitopes in trypanosome-infected mice. Infect. Immun. 58, 2337–2342. https://doi.org/10.1128/iai.58.7.2337-2342.1990

Richardson, J.P., Beecroft, R.P., Tolson, D.L., Liu, M.K., Pearson, T.W., 1988. Procyclin: an unusual immunodominant glycoprotein surface antigen from the procyclic stage of African trypanosomes. Mol. Biochem. Parasitol. 31, 203–216. https://doi.org/10.1016/0166-6851(88)90150-8

Rimon, O., Suss, O., Goldenberg, M., Fassler, R., Yogev, O., Amartely, H., Propper, G., Friedler, A., Reichmann, D., 2017. A Role of Metastable Regions and Their Connectivity in the Inactivation

of a Redox-Regulated Chaperone and Its Inter-Chaperone Crosstalk. Antioxid. Redox Signal. 27, 1252–1267. https://doi.org/10.1089/ars.2016.6900

Ripamonti, D., Massari, M., Claudio, A., Ermanno, G., Claudio, F., Brini, M., Capatti, C., Suter, F., 2002. African Sleeping Sickness in Tourists Returning from Tanzania: The First 2 Italian Cases from a Small Outbreak among European Travelers. Clin. Infect. Dis. 34, e18–e22. https://doi.org/10.1086/338157

Ritossa, F., 1962. A new puffing pattern induced by temperature shock and DNP in drosophila. Experientia 18, 571–573. https://doi.org/10.1007/BF02172188

Rivera-de-Torre, E., Rimbault, C., Jenkins, T.P., Sørensen, C.V., Damsbo, A., Saez, N.J., Duhoo, Y., Hackney, C.M., Ellgaard, L., Laustsen, A.H., 2022. Strategies for Heterologous Expression, Synthesis, and Purification of Animal Venom Toxins. Front. Bioeng. Biotechnol. 9, 811905. https://doi.org/10.3389/fbioe.2021.811905

Robays, J., Nyamowala, G., Sese, C., Betu Ku Mesu Kande, V., Lutumba, P., Van der Veken, W., Boelaert, M., 2008. High failure rates of melarsoprol for sleeping sickness, Democratic Republic of Congo. Emerg. Infect. Dis. 14, 966–967. https://doi.org/10.3201/eid1406.071266

Robinson, D.R., Sherwin, T., Ploubidou, A., Byard, E.H., Gull, K., 1995. Microtubule polarity and dynamics in the control of organelle positioning, segregation, and cytokinesis in the trypanosome cell cycle. J. Cell Biol. 128, 1163–1172. https://doi.org/10.1083/jcb.128.6.1163

Roche Diagnostics, 2020. cOmplete his-tag purification resin (No. 4). Roche Diagnostics Gmbh.

Rohou, A., Nield, J., Ushkaryov, Y.A., 2007. Insecticidal toxins from black widow spider venom. Toxicon 49, 531–549. https://doi.org/10.1016/j.toxicon.2006.11.021

Rosano, G.L., Ceccarelli, E.A., 2014. Recombinant protein expression in Escherichia coli: advances and challenges. Front. Microbiol. 5. https://doi.org/10.3389/fmicb.2014.00172

Rosenzweig, R., Nillegoda, N.B., Mayer, M.P., Bukau, B., 2019. The Hsp70 chaperone network. Nat. Rev. Mol. Cell Biol. 20, 665–680. https://doi.org/10.1038/s41580-019-0133-3

Rosenzweig, R., Sekhar, A., Nagesh, J., Kay, L.E., 2017. Promiscuous binding by Hsp70 results in conformational heterogeneity and fuzzy chaperone-substrate ensembles. eLife 6, e28030. https://doi.org/10.7554/eLife.28030

Rothman, J.E., 1989. Polypeptide chain binding proteins: Catalysts of protein folding and related processes in cells. Cell 59, 591–601. https://doi.org/10.1016/0092-8674(89)90005-6

Rudiger, S., 2001. Its substrate specificity characterizes the DnaJ co-chaperone as a scanning factor for the DnaK chaperone. EMBO J. 20, 1042–1050. https://doi.org/10.1093/emboj/20.5.1042

Rudiger, S., 1997. Substrate specificity of the DnaK chaperone determined by screening cellulose-bound peptide libraries. EMBO J. 16, 1501–1507. https://doi.org/10.1093/emboj/16.7.1501

Ruepp, S., Furger, A., Kurath, U., Renggli, C.K., Hemphill, A., Brun, R., Roditi, I., 1997. Survival of Trypanosoma brucei in the Tsetse Fly Is Enhanced by the Expression of Specific Forms of Procyclin. J. Cell Biol. 137, 1369–1379. https://doi.org/10.1083/jcb.137.6.1369

Rutledge, B.S., Choy, W.-Y., Duennwald, M.L., 2022. Folding or holding?—Hsp70 and Hsp90 chaperoning of misfolded proteins in neurodegenerative disease. J. Biol. Chem. 298, 101905. https://doi.org/10.1016/j.jbc.2022.101905

Ryu, J., Kaul, Z., Yoon, A.-R., Liu, Y., Yaguchi, T., Na, Y., Ahn, H.M., Gao, R., Choi, I.-K., Yun, C.-O., Kaul, S.C., Wadhwa, R., 2014. Identification and Functional Characterization of Nuclear Mortalin in Human Carcinogenesis. J. Biol. Chem. 289, 24832–24844. https://doi.org/10.1074/jbc.M114.565929

Ryu, J.Y., Kim, H.U., Lee, S.Y., 2015. Human genes with a greater number of transcript variants tend to show biological features of housekeeping and essential genes. Mol. Biosyst. 11, 2798–2807. https://doi.org/10.1039/C5MB00322A

Sachdev, D., Chirgwin, J.M., 1999. Properties of soluble fusions between mammalian aspartic proteinases and bacterial maltose-binding protein. J. Protein Chem. 18, 127–136. https://doi.org/10.1023/A:1020663903669

Sahi, C., Craig, E.A., 2007. Network of general and specialty J protein chaperones of the yeast cytosol. Proc. Natl. Acad. Sci. 104, 7163–7168. https://doi.org/10.1073/pnas.0702357104

Salmon, D., Geuskens, M., Hanocq, F., Hanocq-Quertier, J., Nolan, D., Ruben, L., Pays, E., 1994. A novel heterodimeric transferrin receptor encoded by a pair of VSG expression site-associated genes in T. brucei. Cell 78, 75–86. https://doi.org/10.1016/0092-8674(94)90574-6

Sanjuán Szklarz, L.K., Guiard, B., Rissler, M., Wiedemann, N., Kozjak, V., van der Laan, M., Lohaus, C., Marcus, K., Meyer, H.E., Chacinska, A., Pfanner, N., Meisinger, C., 2005. Inactivation of the Mitochondrial Heat Shock Protein Zim17 Leads to Aggregation of Matrix Hsp70s Followed by Pleiotropic Effects on Morphology and Protein Biogenesis. J. Mol. Biol. 351, 206–218. https://doi.org/10.1016/j.jmb.2005.05.068

Savage, A.F., Cerqueira, G.C., Regmi, S., Wu, Y., El Sayed, N.M., Aksoy, S., 2012. Transcript Expression Analysis of Putative Trypanosoma brucei GPI-Anchored Surface Proteins during Development in the Tsetse and Mammalian Hosts. PLoS Negl. Trop. Dis. 6, e1708. https://doi.org/10.1371/journal.pntd.0001708

Scheufler, C., Brinker, A., Bourenkov, G., Pegoraro, S., Moroder, L., Bartunik, H., Hartl, F.U., Moarefi, I., 2000. Structure of TPR Domain–Peptide Complexes. Cell 101, 199–210. https://doi.org/10.1016/S0092-8674(00)80830-2

Schilke, B.A., Hayashi, M., Craig, E.A., 2012. Genetic analysis of complex interactions among components of the mitochondrial import motor and translocon in Saccharomyces cerevisiae. Genetics 190, 1341–1353. https://doi.org/10.1534/genetics.112.138743

Schiller, D., Cheng, Y.C., Liu, Q., Walter, W., Craig, E.A., 2008. Residues of Tim44 involved in both association with the translocon of the inner mitochondrial membrane and regulation of mitochondrial Hsp70 tethering. Mol. Cell. Biol. 28, 4424–4433. https://doi.org/10.1128/MCB.00007-08

Schmidt, S., Strub, A., Röttgers, K., Zufall, N., Voos, W., 2001. The two mitochondrial heat shock proteins 70, Ssc1 and Ssq1, compete for the cochaperone Mge1. J. Mol. Biol. 313, 13–26. https://doi.org/10.1006/jmbi.2001.5013

Schneider, H.C., Berthold, J., Bauer, M.F., Dietmeier, K., Guiard, B., Brunner, M., Neupert, W., 1994. Mitochondrial Hsp70/MIM44 complex facilitates protein import. Nature 371, 768–774. https://doi.org/10.1038/371768a0

Schrodinger, L., De Lano, W., 2020. PyMOL.

Schweinfest, C.W., Graber, M.W., Henderson, K.W., Papas, T.S., Baron, P.L., Watson, D.K., 1998. Cloning and sequence analysis of Hsp89αΔN, a new member of the Hsp90 gene family. Biochim. Biophys. Acta BBA - Gene Struct. Expr. 1398, 18–24. https://doi.org/10.1016/S0167-4781(98)00031-1

Seco-Cervera, M., González-Cabo, P., Pallardó, F., Romá-Mateo, C., García-Giménez, J., 2020. Thioredoxin and Glutaredoxin Systems as Potential Targets for the Development of New Treatments in Friedreich's Ataxia. Antioxidants 9, 1257. https://doi.org/10.3390/antiox9121257

Segal, N., Shapira, M., 2015. HSP33 in eukaryotes - an evolutionary tale of a chaperone adapted to photosynthetic organisms. Plant J. 82, 850–860. https://doi.org/10.1111/tpj.12855

Serebryany, E., Woodard, J.C., Adkar, B.V., Shabab, M., King, J.A., Shakhnovich, E.I., 2016. An Internal Disulfide Locks a Misfolded Aggregation-prone Intermediate in Cataract-linked Mutants of Human γD-Crystallin. J. Biol. Chem. 291, 19172–19183. https://doi.org/10.1074/jbc.M116.735977

Serlidaki, D., van Waarde, M.A.W.H., Rohland, L., Wentink, A.S., Dekker, S.L., Kamphuis, M.J., Boertien, J.M., Brunsting, J.F., Nillegoda, N.B., Bukau, B., Mayer, M.P., Kampinga, H.H., Bergink, S., 2020. Functional diversity between HSP70 paralogs caused by variable interactions with specific co-chaperones. J. Biol. Chem. 295, 7301–7316. https://doi.org/10.1074/jbc.RA119.012449

Sezonov, G., Joseleau-Petit, D., D'Ari, R., 2007. *Escherichia coli* Physiology in Luria-Bertani Broth. J. Bacteriol. 189, 8746–8749. https://doi.org/10.1128/JB.01368-07

Shapiro, T.A., Englund, P.T., 1995. THE STRUCTURE AND REPLICATION OF KINETOPLAST DNA. Annu. Rev. Microbiol. 49, 117–143. https://doi.org/10.1146/annurev.mi.49.100195.001001

Shaw, A.P.M., Tirados, I., Mangwiro, C.T.N., Esterhuizen, J., Lehane, M.J., Torr, S.J., Kovacic, V., 2015. Costs Of Using "Tiny Targets" to Control Glossina fuscipes fuscipes, a Vector of Gambiense Sleeping Sickness in Arua District of Uganda. PLoS Negl. Trop. Dis. 9, e0003624. https://doi.org/10.1371/journal.pntd.0003624

Sherwin, T., 1989. The cell division cycle of *Trypanosoma brucei brucei* : timing of event markers and cytoskeletal modulations. Philos. Trans. R. Soc. Lond. B Biol. Sci. 323, 573–588. https://doi.org/10.1098/rstb.1989.0037

Shiloach, J., Fass, R., 2005. Growing E. coli to high cell density—A historical perspective on method development. Biotechnol. Adv. 23, 345–357. https://doi.org/10.1016/j.biotechadv.2005.04.004

Shin, C.-S., Meng, S., Garbis, S.D., Moradian, A., Taylor, R.W., Sweredoski, M.J., Lomenick, B., Chan, D.C., 2021. LONP1 and mtHSP70 cooperate to promote mitochondrial protein folding. Nat. Commun. 12, 265. https://doi.org/10.1038/s41467-020-20597-z

Shomura, Y., Dragovic, Z., Chang, H.-C., Tzvetkov, N., Young, J.C., Brodsky, J.L., Guerriero, V., Hartl, F.U., Bracher, A., 2005. Regulation of Hsp70 Function by HspBP1. Mol. Cell 17, 367–379. https://doi.org/10.1016/j.molcel.2004.12.023

Shonhai, A., Botha, M., de Beer, T., Boshoff, A., Blatch, G., 2008. Structure-Function Study of a Plasmodium falciparum Hsp70 Using Three Dimensional Modelling and in Vitro Analyses. Protein Pept. Lett. 15, 1117–1125. https://doi.org/10.2174/092986608786071067

Shonhai, A., Maier, A.G., Przyborski, J.M., Blatch, G.L., 2011. Intracellular protozoan parasites of humans: the role of molecular chaperones in development and pathogenesis. Protein Pept. Lett. 18, 143–157. https://doi.org/10.2174/092986611794475002

Sichting, M., Mokranjac, D., Azem, A., Neupert, W., Hell, K., 2005. Maintenance of structure and function of mitochondrial Hsp70 chaperones requires the chaperone Hep1. EMBO J. 24, 1046–1056. https://doi.org/10.1038/sj.emboj.7600580

Sievers, F., Higgins, D.G., 2014. Clustal Omega, accurate alignment of very large numbers of sequences. Methods Mol. Biol. Clifton NJ 1079, 105–116. https://doi.org/10.1007/978-1-62703-646-7_6

Sigrist, C.J.A., de Castro, E., Cerutti, L., Cuche, B.A., Hulo, N., Bridge, A., Bougueleret, L., Xenarios, I., 2013. New and continuing developments at PROSITE. Nucleic Acids Res. 41, D344-347. https://doi.org/10.1093/nar/gks1067

Simarro, Pere, Cecchi, G., Franco, J., Paone, M., Diarra, A., Ruiz-Postigo, J., Fèvre, E., Mattioli, R., Jannin, M., Ndung'u, J., 2012. Estimating and Mapping the Population at Risk of Sleeping Sickness. PLoS Negl. Trop. Dis. 6, e1859. https://doi.org/10.1371/journal.pntd.0001859

Simarro, P., Diarra, A., Ruiz Postigo, J.A., Franco, J.R., Jannin, J.G., 2011. The Human African Trypanosomiasis Control and Surveillance Programme of the World Health Organization 2000–2009: The Way Forward. PLoS Negl. Trop. Dis. 5, e1007. https://doi.org/10.1371/journal.pntd.0001007

Simarro, P., Franco, J., Diarra, A., Jannin, J., 2014. Epidemiology of human African trypanosomiasis. Clin. Epidemiol. 257. https://doi.org/10.2147/CLEP.S39728

Simarro, P, Franco, P., Diarra, P., Postigo, Jannin, 2012. Update on field use of the available drugs for the chemotherapy of human African trypanosomiasis. Parasitology 139, 842–846. https://doi.org/10.1017/S0031182012000169

Simo, G., Mbida, J., Eyenga, V., Asonganyi, T., Njiokou, F., Grébaut, P., 2014. Challenges towards the elimination of Human African Trypanosomiasis in the sleeping sickness focus of Campo in southern Cameroon. Parasit. Vectors 7, 374. https://doi.org/10.1186/1756-3305-7-374

Simpson, A.G.B., Stevens, J.R., Lukeš, J., 2006. The evolution and diversity of kinetoplastid flagellates. Trends Parasitol. 22, 168–174. https://doi.org/10.1016/j.pt.2006.02.006

Singh, G.P., Chandra, B.R., Bhattacharya, A., Akhouri, R.R., Singh, S.K., Sharma, A., 2004. Hyper-expansion of asparagines correlates with an abundance of proteins with prion-like domains in Plasmodium falciparum. Mol. Biochem. Parasitol. 137, 307–319. https://doi.org/10.1016/j.molbiopara.2004.05.016

Singh, N., Chikara, S., Sundar, S., 2013. SOLiD™ Sequencing of Genomes of Clinical Isolates of Leishmania donovani from India Confirm Leptomonas Co-Infection and Raise Some Key Questions. PLoS ONE 8, e55738. https://doi.org/10.1371/journal.pone.0055738

Slepenkov, S.V., Witt, S.N., 2002. The unfolding story of the Escherichia coli Hsp70 DnaK: is DnaK a holdase or an unfoldase?: DnaK protein chaperone. Mol. Microbiol. 45, 1197–1206. https://doi.org/10.1046/j.1365-2958.2002.03093.x

Smith, D.B., Johnson, K.S., 1988. Single-step purification of polypeptides expressed in Escherichia coli as fusions with glutathione S-transferase. Gene 67, 31–40. https://doi.org/10.1016/0378-1119(88)90005-4

Smith, D.F., Sullivan, W.P., Marion, T.N., Zaitsu, K., Madden, B., McCormick, D.J., Toft, D.O., 1993. Identification of a 60-kilodalton stress-related protein, p60, which interacts with hsp90 and hsp70. Mol. Cell. Biol. 13, 869–876. https://doi.org/10.1128/mcb.13.2.869-876.1993

Snustad, D.P., Simmons, M.J., 2016. Principles of genetics, Seventh edition. ed. John Wiley & Sons, Inc, Hoboken, NJ.

Sokolova, A.Y., Wyllie, S., Patterson, S., Oza, S.L., Read, K.D., Fairlamb, A.H., 2010. Cross-resistance to nitro drugs and implications for treatment of human African trypanosomiasis. Antimicrob. Agents Chemother. 54, 2893–2900. https://doi.org/10.1128/AAC.00332-10

Solana, J.C., Bernardo, L., Moreno, J., Aguado, B., Requena, J.M., 2022. The Astonishing Large Family of HSP40/DnaJ Proteins Existing in Leishmania. Genes 13, 742. https://doi.org/10.3390/genes13050742

Solano, P., 2021. Need of entomological criteria to assess zero transmission of gambiense HAT. PLoS Negl. Trop. Dis. 15, e0009235. https://doi.org/10.1371/journal.pntd.0009235

Solano, P., Torr, S.J., Lehane, M.J., 2013. Is vector control needed to eliminate gambiense human African trypanosomiasis? Front. Cell. Infect. Microbiol. 3, 33. https://doi.org/10.3389/fcimb.2013.00033

Sondermann, H., Scheufler, C., Schneider, C., Höhfeld, J., Hartl, F.-U., Moarefi, I., 2001. Structure of a Bag/Hsc70 Complex: Convergent Functional Evolution of Hsp70 Nucleotide Exchange Factors. Science 291, 1553–1557. https://doi.org/10.1126/science.1057268

Song, L., Xu, W., Li, C., Li, H., Wu, L., Xiang, J., Guo, X., 2006. Development of expressed sequence tags from the bay scallop, Argopecten irradians irradians. Mar. Biotechnol. N. Y. N 8, 161–169. https://doi.org/10.1007/s10126-005-0126-4

Sørensen, H.P., Mortensen, K.K., 2005. Advanced genetic strategies for recombinant protein expression in Escherichia coli. J. Biotechnol. 115, 113–128. https://doi.org/10.1016/j.jbiotec.2004.08.004

Souza, W. de, 2009. Structural organization of Trypanosoma cruzi. Mem. Inst. Oswaldo Cruz 104, 89–100. https://doi.org/10.1590/S0074-02762009000900014

Sreedhar, S., Kalmár, É., Csermely, P., Shen, Y.-F., 2004. Hsp90 isoforms: functions, expression and clinical importance. FEBS Lett. 562, 11–15. https://doi.org/10.1016/S0014-5793(04)00229-7

Steel, G.J., Fullerton, D.M., Tyson, J.R., Stirling, C.J., 2004. Coordinated Activation of Hsp70 Chaperones. Science 303, 98–101. https://doi.org/10.1126/science.1092287

Steketee, P.C., Vincent, I.M., Achcar, F., Giordani, F., Kim, D.-H., Creek, D.J., Freund, Y., Jacobs, R., Rattigan, K., Horn, D., Field, M.C., MacLeod, A., Barrett, M.P., 2018. Benzoxaborole treatment perturbs S-adenosyl-L-methionine metabolism in Trypanosoma brucei. PLoS Negl. Trop. Dis. 12, e0006450. https://doi.org/10.1371/journal.pntd.0006450

Stich, A., 2002. Human African trypanosomiasis. BMJ 325, 203–206. https://doi.org/10.1136/bmj.325.7357.203

Stijlemans, B., Caljon, G., Van Den Abbeele, J., Van Ginderachter, J.A., Magez, S., De Trez, C., 2016. Immune Evasion Strategies of Trypanosoma brucei within the Mammalian Host: Progression to Pathogenicity. Front. Immunol. 7. https://doi.org/10.3389/fimmu.2016.00233

Strub, A., Zufall, N., Voos, W., 2003. The putative helical lid of the Hsp70 peptide-binding domain is required for efficient preprotein translocation into mitochondria. J. Mol. Biol. 334, 1087–1099. https://doi.org/10.1016/j.jmb.2003.10.023

Stuart, K., Brun, R., Croft, S., Fairlamb, A., Gürtler, R.E., McKerrow, J., Reed, S., Tarleton, R., 2008. Kinetoplastids: related protozoan pathogens, different diseases. J. Clin. Invest. 118, 1301–1310. https://doi.org/10.1172/JCI33945

Stuart, K., Panigrahi, A.K., 2002. RNA editing: complexity and complications: RNA editing: complexity and complications. Mol. Microbiol. 45, 591–596. https://doi.org/10.1046/j.1365-2958.2002.03028.x

Stuart, K.D., Schnaufer, A., Ernst, N.L., Panigrahi, A.K., 2005. Complex management: RNA editing in trypanosomes. Trends Biochem. Sci. 30, 97–105. https://doi.org/10.1016/j.tibs.2004.12.006

Studier, F.W., Moffatt, B.A., 1986. Use of bacteriophage T7 RNA polymerase to direct selective high-level expression of cloned genes. J. Mol. Biol. 189, 113–130. https://doi.org/10.1016/0022-2836(86)90385-2

Sultana, S., Anderson, G.M., Hoffmann, K.P., Dahl, J.-U., 2021. Extraction and Visualization of Protein Aggregates after Treatment of Escherichia coli with a Proteotoxic Stressor. J. Vis. Exp. 62628. https://doi.org/10.3791/62628

Svobodová, M., Zídková, L., Čepička, I., Oborník, M., Lukeš, J., Votýpka, J., 2007. Sergeia podlipaevi gen. nov., sp. nov. (Trypanosomatidae, Kinetoplastida), a parasite of biting midges (Ceratopogonidae, Diptera). Int. J. Syst. Evol. Microbiol. 57, 423–432. https://doi.org/10.1099/ijs.0.64557-0

Swain, J.F., Dinler, G., Sivendran, R., Montgomery, D.L., Stotz, M., Gierasch, L.M., 2007. Hsp70 Chaperone Ligands Control Domain Association via an Allosteric Mechanism Mediated by the Interdomain Linker. Mol. Cell 26, 27–39. https://doi.org/10.1016/j.molcel.2007.02.020

Syken, J., De-Medina, T., Münger, K., 1999. TID1, a human homolog of the Drosophila tumor suppressor l(2)tid, encodes two mitochondrial modulators of apoptosis with opposing functions. Proc. Natl. Acad. Sci. U. S. A. 96, 8499–8504. https://doi.org/10.1073/pnas.96.15.8499

Szempruch, A., Guttman, M., 2017. Linking Protein and RNA Function within the Same Gene. Cell 168, 753–755. https://doi.org/10.1016/j.cell.2017.02.014

Tan, T.H.P., Bochud-Allemann, N., Horn, E.K., Schneider, A., 2002. Eukaryotic-type elongator tRNA ^{Met} of *Trypanosoma brucei* becomes formylated after import into mitochondria. Proc. Natl. Acad. Sci. 99, 1152–1157. https://doi.org/10.1073/pnas.022522299

Tanaka, M., Mun, S., Harada, A., Ohkawa, Y., Inagaki, A., Sano, S., Takahashi, K., Izumi, Y., Osada-Oka, M., Wanibuchi, H., Yamagata, M., Yukimura, T., Miura, K., Shiota, M., Iwao, H., 2014. Hsc70 Contributes to Cancer Cell Survival by Preventing Rab1A Degradation under Stress Conditions. PLoS ONE 9, e96785. https://doi.org/10.1371/journal.pone.0096785

Tang, W., Wang, C., 2001. Zinc Fingers and Thiol−Disulfide Oxidoreductase Activities of Chaperone DnaJ. Biochemistry 40, 14985–14994. https://doi.org/10.1021/bi0107593

Tao, H., Liu, W., Simmons, B.N., Harris, H.K., Cox, T.C., Massiah, M.A., 2010. Purifying natively folded proteins from inclusion bodies using sarkosyl, Triton X-100, and CHAPS. BioTechniques 48, 61–64. https://doi.org/10.2144/000113304

Tarral, A., Blesson, S., Mordt, O.V., Torreele, E., Sassella, D., Bray, M.A., Hovsepian, L., Evène, E., Gualano, V., Felices, M., Strub-Wourgaft, N., 2014. Determination of an Optimal Dosing Regimen for Fexinidazole, a Novel Oral Drug for the Treatment of Human African Trypanosomiasis: First-in-Human Studies. Clin. Pharmacokinet. 53, 565–580. https://doi.org/10.1007/s40262-014-0136-3

Tatokoro, M., Koga, F., Yoshida, S., Kihara, K., 2015. Heat shock protein 90 targeting therapy: state of the art and future perspective. EXCLI J. 14, 48–58. https://doi.org/10.17179/excli2015-586

Taylor, J., Rudenko, G., 2006. Switching trypanosome coats: what's in the wardrobe? Trends Genet. 22, 614–620. https://doi.org/10.1016/j.tig.2006.08.003

Terpe, K., 2003. Overview of tag protein fusions: from molecular and biochemical fundamentals to commercial systems. Appl. Microbiol. Biotechnol. 60, 523–533. https://doi.org/10.1007/s00253-002-1158-6

Thomas, J.A., Baker, N., Hutchinson, S., Dominicus, C., Trenaman, A., Glover, L., Alsford, S., Horn, D., 2018. Insights into antitrypanosomal drug mode-of-action from cytology-based profiling. PLoS Negl. Trop. Dis. 12, e0006980. https://doi.org/10.1371/journal.pntd.0006980

Thomson, R., Finkelstein, A., 2015. Human trypanolytic factor APOL1 forms pH-gated cation-selective channels in planar lipid bilayers: Relevance to trypanosome lysis. Proc. Natl. Acad. Sci. 112, 2894–2899. https://doi.org/10.1073/pnas.1421953112

Thomson, R., Genovese, G., Canon, C., Kovacsics, D., Higgins, M.K., Carrington, M., Winkler, C.A., Kopp, J., Rotimi, C., Adeyemo, A., Doumatey, A., Ayodo, G., Alper, S.L., Pollak, M.R., Friedman, D.J., Raper, J., 2014. Evolution of the primate trypanolytic factor APOL1. Proc. Natl. Acad. Sci. 111. https://doi.org/10.1073/pnas.1400699111

Tikhonenkov, D.V., Gawryluk, R.M.R., Mylnikov, A.P., Keeling, P.J., 2021. First finding of free-living representatives of Prokinetoplastina and their nuclear and mitochondrial genomes. Sci. Rep. 11, 2946. https://doi.org/10.1038/s41598-021-82369-z

Ting, S.-Y., Yan, N.L., Schilke, B.A., Craig, E.A., 2017. Dual interaction of scaffold protein Tim44 of mitochondrial import motor with channel-forming translocase subunit Tim23. eLife 6, e23609. https://doi.org/10.7554/eLife.23609

Tissiéres, A., Mitchell, H.K., Tracy, U.M., 1974. Protein synthesis in salivary glands of Drosophila melanogaster: Relation to chromosome puffs. J. Mol. Biol. 84, 389–398. https://doi.org/10.1016/0022-2836(74)90447-1

Torr, S.J., Chamisa, A., Mangwiro, T.N.C., Vale, G.A., 2012. Where, When and Why Do Tsetse Contact Humans? Answers from Studies in a National Park of Zimbabwe. PLoS Negl. Trop. Dis. 6, e1791. https://doi.org/10.1371/journal.pntd.0001791

Torr, S.J., Maudlin, I., Vale, G.A., 2007. Less is more: restricted application of insecticide to cattle to improve the cost and efficacy of tsetse control. Med. Vet. Entomol. 21, 53–64. https://doi.org/10.1111/j.1365-2915.2006.00657.x

Tournier, C., Hess, P., Yang, D.D., Xu, J., Turner, T.K., Nimnual, A., Bar-Sagi, D., Jones, S.N., Flavell, R.A., Davis, R.J., 2000. Requirement of JNK for Stress- Induced Activation of the Cytochrome c-Mediated Death Pathway. Science 288, 870–874. https://doi.org/10.1126/science.288.5467.870

Tress, M.L., Martelli, P.L., Frankish, A., Reeves, G.A., Wesselink, J.J., Yeats, C., Ólason, P. Ísólfur, Albrecht, M., Hegyi, H., Giorgetti, A., Raimondo, D., Lagarde, J., Laskowski, R.A., López, G., Sadowski, M.I., Watson, J.D., Fariselli, P., Rossi, I., Nagy, A., Kai, W., Størling, Z., Orsini, M., Assenov, Y., Blankenburg, H., Huthmacher, C., Ramírez, F., Schlicker, A., Denoeud, F., Jones, P., Kerrien, S., Orchard, S., Antonarakis, S.E., Reymond, A., Birney, E., Brunak, S., Casadio, R., Guigo, R., Harrow, J., Hermjakob, H., Jones, D.T., Lengauer, T., A. Orengo, C., Patthy, L., Thornton, J.M., Tramontano, A., Valencia, A., 2007. The implications of alternative splicing in the ENCODE protein complement. Proc. Natl. Acad. Sci. 104, 5495–5500. https://doi.org/10.1073/pnas.0700800104

Trindade, S., Rijo-Ferreira, F., Carvalho, T., Pinto-Neves, D., Guegan, F., Aresta-Branco, F., Bento, F., Young, S.A., Pinto, A., Van Den Abbeele, J., Ribeiro, R.M., Dias, S., Smith, T.K., Figueiredo, L.M., 2016. Trypanosoma brucei Parasites Occupy and Functionally Adapt to the Adipose Tissue in Mice. Cell Host Microbe 19, 837–848. https://doi.org/10.1016/j.chom.2016.05.002

Truc, P., Lejon, V., Magnus, E., Jamonneau, V., Nangouma, A., Verloo, D., Penchenier, L., Büscher, P., 2002. Evaluation of the micro-CATT, CATT/Trypanosoma brucei gambiense, and LATEX/T b gambiense methods for serodiagnosis and surveillance of human African trypanosomiasis in West and Central Africa. Bull. World Health Organ. 80, 882–886.

Tsai, C.-F., Wang, Y.-T., Yen, H.-Y., Tsou, C.-C., Ku, W.-C., Lin, P.-Y., Chen, H.-Y., Nesvizhskii, A.I., Ishihama, Y., Chen, Y.-J., 2015. Large-scale determination of absolute phosphorylation stoichiometries in human cells by motif-targeting quantitative proteomics. Nat. Commun. 6, 6622. https://doi.org/10.1038/ncomms7622

Tschopp, F., Charrière, F., Schneider, A., 2011. *In vivo* study in *Trypanosoma brucei* links mitochondrial transfer RNA import to mitochondrial protein import. EMBO Rep. 12, 825–832. https://doi.org/10.1038/embor.2011.111

Tsutsumi, S., Mollapour, M., Prodromou, C., Lee, C.-T., Panaretou, B., Yoshida, S., Mayer, M.P., Neckers, L.M., 2012. Charged linker sequence modulates eukaryotic heat shock protein 90

(Hsp90) chaperone activity. Proc. Natl. Acad. Sci. 109, 2937–2942. https://doi.org/10.1073/pnas.1114414109

Týč, J., Klingbeil, M.M., Lukeš, J., 2015. Mitochondrial heat shock protein machinery hsp70/hsp40 is indispensable for proper mitochondrial DNA maintenance and replication. mBio 6, e02425-14. https://doi.org/10.1128/mBio.02425-14

Ulrich, K., Schwappach, B., Jakob, U., 2021. Thiol-based switching mechanisms of stress-sensing chaperones. Biol. Chem. 402, 239–252. https://doi.org/10.1515/hsz-2020-0262

Ung, P.M.-U., Thompson, A.D., Chang, L., Gestwicki, J.E., Carlson, H.A., 2013. Identification of Key Hinge Residues Important for Nucleotide-Dependent Allostery in E. coli Hsp70/DnaK. PLoS Comput. Biol. 9, e1003279. https://doi.org/10.1371/journal.pcbi.1003279

UniProt Consortium, 2013. Update on activities at the Universal Protein Resource (UniProt) in 2013. Nucleic Acids Res. 41, D43-47. https://doi.org/10.1093/nar/gks1068

Urbaniak, M.D., Guther, M.L.S., Ferguson, M.A.J., 2012. Comparative SILAC Proteomic Analysis of Trypanosoma brucei Bloodstream and Procyclic Lifecycle Stages. PLoS ONE 7, e36619. https://doi.org/10.1371/journal.pone.0036619

Urbaniak, M.D., Martin, D.M.A., Ferguson, M.A.J., 2013. Global Quantitative SILAC Phosphoproteomics Reveals Differential Phosphorylation Is Widespread between the Procyclic and Bloodstream Form Lifecycle Stages of *Trypanosoma brucei*. J. Proteome Res. 12, 2233–2244. https://doi.org/10.1021/pr400086y

Urwyler, S., Studer, E., Renggli, C.K., Roditi, I., 2007. A family of stage-specific alanine-rich proteins on the surface of epimastigote forms of Trypanosoma brucei. Mol. Microbiol. 63, 218–228. https://doi.org/10.1111/j.1365-2958.2006.05492.x

Uversky, V.N., 2010. Targeting intrinsically disordered proteins in neurodegenerative and protein dysfunction diseases: another illustration of the D(2) concept. Expert Rev. Proteomics 7, 543–564. https://doi.org/10.1586/epr.10.36

V. Rajan, V.B., D'Silva, P., 2009. Arabidopsis thaliana J-class heat shock proteins: cellular stress sensors. Funct. Integr. Genomics 9, 433–446. https://doi.org/10.1007/s10142-009-0132-0

van der Laan, M., Chacinska, A., Lind, M., Perschil, I., Sickmann, A., Meyer, H.E., Guiard, B., Meisinger, C., Pfanner, N., Rehling, P., 2005. Pam17 is required for architecture and translocation activity of the mitochondrial protein import motor. Mol. Cell. Biol. 25, 7449–7458. https://doi.org/10.1128/MCB.25.17.7449-7458.2005

Van der Ploeg, L.H.T., Giannini, S.H., Cantor, C.R., 1985. Heat Shock Genes: Regulatory Role for Differentiation in Parasitic Protozoa. Science 228, 1443–1446. https://doi.org/10.1126/science.4012301

Van Xong, H., Vanhamme, L., Chamekh, M., Chimfwembe, C.E., Van Den Abbeele, J., Pays, A., Van Meirvenne, N., Hamers, R., De Baetselier, P., Pays, E., 1998. A VSG Expression Site–Associated Gene Confers Resistance to Human Serum in Trypanosoma rhodesiense. Cell 95, 839–846. https://doi.org/10.1016/S0092-8674(00)81706-7

Vanhollebeke, B., De Muylder, G., Nielsen, M.J., Pays, A., Tebabi, P., Dieu, M., Raes, M., Moestrup, S.K., Pays, E., 2008. A Haptoglobin-Hemoglobin Receptor Conveys Innate Immunity to

Trypanosoma brucei in Humans. Science 320, 677–681. https://doi.org/10.1126/science.1156296

Vanhollebeke, B., Nielsen, M.J., Watanabe, Y., Truc, P., Vanhamme, L., Nakajima, K., Moestrup, S.K., Pays, E., 2007. Distinct roles of haptoglobin-related protein and apolipoprotein L-I in trypanolysis by human serum. Proc. Natl. Acad. Sci. 104, 4118–4123. https://doi.org/10.1073/pnas.0609902104

Vanlerberghe, G.C., McIntosh, L., 1997. ALTERNATIVE OXIDASE: From Gene to Function. Annu. Rev. Plant Physiol. Plant Mol. Biol. 48, 703–734. https://doi.org/10.1146/annurev.arplant.48.1.703

Vanwalleghem, G., Fontaine, F., Lecordier, L., Tebabi, P., Klewe, K., Nolan, D.P., Yamaryo-Botté, Y., Botté, C., Kremer, A., Burkard, G.S., Rassow, J., Roditi, I., Pérez-Morga, D., Pays, E., 2015. Coupling of lysosomal and mitochondrial membrane permeabilization in trypanolysis by APOL1. Nat. Commun. 6, 8078. https://doi.org/10.1038/ncomms9078

Varadi, M., Anyango, S., Deshpande, M., Nair, S., Natassia, C., Yordanova, G., Yuan, D., Stroe, O., Wood, G., Laydon, A., Žídek, A., Green, T., Tunyasuvunakool, K., Petersen, S., Jumper, J., Clancy, E., Green, R., Vora, A., Lutfi, M., Figurnov, M., Cowie, A., Hobbs, N., Kohli, P., Kleywegt, G., Birney, E., Hassabis, D., Velankar, S., 2022. AlphaFold Protein Structure Database: massively expanding the structural coverage of protein-sequence space with high-accuracy models. Nucleic Acids Res. 50, D439–D444. https://doi.org/10.1093/nar/gkab1061

Vassella, E., Bütikofer, P., Engstler, M., Jelk, J., Roditi, I., 2003. Procyclin Null Mutants of *Trypanosoma brucei* Express Free Glycosylphosphatidylinositols on Their Surface. Mol. Biol. Cell 14, 1308–1318. https://doi.org/10.1091/mbc.e02-10-0694

Vaughan, S., Gull, K., 2003. The trypanosome flagellum. J. Cell Sci. 116, 757–759. https://doi.org/10.1242/jcs.00287

Velten, M., Villoutreix, B.O., Ladjimi, M.M., 2000. Quaternary Structure of the HSC70 Cochaperone HIP. Biochemistry 39, 307–315. https://doi.org/10.1021/bi9917535

Verdi, J., Zipkin, R., Hillman, E., Gertsch, R.A., Pangburn, S.J., Thomson, R., Papavasiliou, N., Sternberg, J., Raper, J., 2020. Inducible Germline IgMs Bridge Trypanosome Lytic Factor Assembly and Parasite Recognition. Cell Host Microbe 28, 79-88.e4. https://doi.org/10.1016/j.chom.2020.04.012

Vertommen, D., Van Roy, J., Szikora, J.-P., Rider, M.H., Michels, P.A.M., Opperdoes, F.R., 2008. Differential expression of glycosomal and mitochondrial proteins in the two major life-cycle stages of Trypanosoma brucei. Mol. Biochem. Parasitol. 158, 189–201. https://doi.org/10.1016/j.molbiopara.2007.12.008

Vickerman, K., 2009. “Not a very nice subject.” Changing views of parasites and parasitology in the twentieth century. Parasitology 136, 1395–1402. https://doi.org/10.1017/S0031182009990825

Vickerman, K., 1994. The evolutionary expansion of the trypanosomatid flagellates. Int. J. Parasitol. 24, 1317–1331. https://doi.org/10.1016/0020-7519(94)90198-8

Vickerman, K., 1969. On The Surface Coat and Flagellar Adhesion in Trypanosomes. J. Cell Sci. 5, 163–193. https://doi.org/10.1242/jcs.5.1.163

Vickerman, K., 1965. Polymorphism and Mitochondrial Activity In Sleeping Sickness Trypanosomes. Nature 208, 762–766. https://doi.org/10.1038/208762a0

Vickery, L.E., Cupp-Vickery, J.R., 2007. Molecular Chaperones HscA/Ssq1 and HscB/Jac1 and Their Roles in Iron-Sulfur Protein Maturation. Crit. Rev. Biochem. Mol. Biol. 42, 95–111. https://doi.org/10.1080/10409230701322298

Villarejo, M.R., Zabin, I., 1974. Beta-galactosidase from termination and deletion mutant strains. J. Bacteriol. 120, 466–474. https://doi.org/10.1128/jb.120.1.466-474.1974

Vogel, M., Mayer, M.P., Bukau, B., 2006. Allosteric Regulation of Hsp70 Chaperones Involves a Conserved Interdomain Linker. J. Biol. Chem. 281, 38705–38711. https://doi.org/10.1074/jbc.M609020200

Voos, W., 2013. Chaperone–protease networks in mitochondrial protein homeostasis. Biochim. Biophys. Acta BBA - Mol. Cell Res. 1833, 388–399. https://doi.org/10.1016/j.bbamcr.2012.06.005

Voos, W., Röttgers, K., 2002. Molecular chaperones as essential mediators of mitochondrial biogenesis. Biochim. Biophys. Acta BBA - Mol. Cell Res. 1592, 51–62. https://doi.org/10.1016/S0167-4889(02)00264-1

Vostakolaei, M.A., Hatami-Baroogh, L., Babaei, G., Molavi, O., Kordi, S., Abdolalizadeh, J., 2021. Hsp70 in cancer: A double agent in the battle between survival and death. J. Cell. Physiol. 236, 3420–3444. https://doi.org/10.1002/jcp.30132

Vreysen, M.J.B., Saleh, K., Mramba, F., Parker, A., Feldmann, U., Dyck, V.A., Msangi, A., Bouyer, J., 2014. Sterile insects to enhance agricultural development: the case of sustainable tsetse eradication on Unguja Island, Zanzibar, using an area-wide integrated pest management approach. PLoS Negl. Trop. Dis. 8, e2857. https://doi.org/10.1371/journal.pntd.0002857

Vreysen, M.J.B., Saleh, K.M., Lancelot, R., Bouyer, J., 2011. Factory tsetse flies must behave like wild flies: a prerequisite for the sterile insect technique. PLoS Negl. Trop. Dis. 5, e907. https://doi.org/10.1371/journal.pntd.0000907

Vu, M.T., Zhai, P., Lee, J., Guerra, C., Liu, S., Gustin, M.C., Silberg, J.J., 2012. The DNLZ/HEP zinc-binding subdomain is critical for regulation of the mitochondrial chaperone HSPA9: Structure-Function Analysis of DNLZ. Protein Sci. 21, 258–267. https://doi.org/10.1002/pro.2012

Wachter, C., Schatz, G., Glick, B.S., 1994. Protein import into mitochondria: the requirement for external ATP is precursor-specific whereas intramitochondrial ATP is universally needed for translocation into the matrix. Mol. Biol. Cell 5, 465–474. https://doi.org/10.1091/mbc.5.4.465

Wadhwa, R., Akiyama, S., Sugihara, T., Reddel, R.R., Mitsui, Y., Kaul, S.C., 1996. Genetic differences between the pancytosolic and perinuclear forms of murine mortalin. Exp. Cell Res. 226, 381–386. https://doi.org/10.1006/excr.1996.0239

Wadhwa, R., Kaul, S.C., Ikawa, Y., Sugimoto, Y., 1993. Identification of a novel member of mouse hsp70 family. Its association with cellular mortal phenotype. J. Biol. Chem. 268, 6615–6621. https://doi.org/10.1016/S0021-9258(18)53295-6

Wadhwa, R, Kaul, S.C., Sugimoto, Y., Mitsui, Y., 1993. Induction of cellular senescence by transfection of cytosolic mortalin cDNA in NIH 3T3 cells. J. Biol. Chem. 268, 22239–22242. https://doi.org/10.1016/S0021-9258(18)41515-3

Wadhwa, R., Takano, S., Kaur, K., Deocaris, C.C., Pereira-Smith, O.M., Reddel, R.R., Kaul, S.C., 2006. Upregulation of mortalin/mthsp70/Grp75 contributes to human carcinogenesis. Int. J. Cancer 118, 2973–2980. https://doi.org/10.1002/ijc.21773

Wadhwa, R., Takano, S., Robert, M., Yoshida, A., Nomura, H., Reddel, R.R., Mitsui, Y., Kaul, S.C., 1998. Inactivation of Tumor Suppressor p53 by Mot-2, a hsp70 Family Member. J. Biol. Chem. 273, 29586–29591. https://doi.org/10.1074/jbc.273.45.29586

Walker, D.M., Oghumu, S., Gupta, G., McGwire, B.S., Drew, M.E., Satoskar, A.R., 2014. Mechanisms of cellular invasion by intracellular parasites. Cell. Mol. Life Sci. 71, 1245–1263. https://doi.org/10.1007/s00018-013-1491-1

Wall, D., Zylicz, M., Georgopoulos, C., 1995. The Conserved G/F Motif of the DnaJ Chaperone Is Necessary for the Activation of the Substrate Binding Properties of the DnaK Chaperone. J. Biol. Chem. 270, 2139–2144. https://doi.org/10.1074/jbc.270.5.2139

Wallace, F.G., 1966. The trypanosomatid parasites of insects and arachnids. Exp. Parasitol. 18, 124–193. https://doi.org/10.1016/0014-4894(66)90015-4

Walsh, P., Bursać, D., Law, Y.C., Cyr, D., Lithgow, T., 2004. The J-protein family: modulating protein assembly, disassembly and translocation. EMBO Rep. 5, 567–571. https://doi.org/10.1038/sj.embor.7400172

Walter, S., Buchner, J., 2002. Molecular Chaperones—Cellular Machines for Protein Folding. Angew. Chem. Int. Ed. 41, 1098–1113. https://doi.org/10.1002/1521-3773(20020402)41:7<1098::AID-ANIE1098>3.0.CO;2-9

Wamwiri, F.N., Changasi, R.E., 2016. Tsetse Flies (*Glossina*) as Vectors of Human African Trypanosomiasis: A Review. BioMed Res. Int. 2016, 1–8. https://doi.org/10.1155/2016/6201350

Wang, D., Liang, Y., Xu, D., 2019. Capsule network for protein post-translational modification site prediction. Bioinforma. Oxf. Engl. 35, 2386–2394. https://doi.org/10.1093/bioinformatics/bty977

Wang, D., Liu, D., Yuchi, J., He, F., Jiang, Y., Cai, S., Li, J., Xu, D., 2020. MusiteDeep: a deep-learning based webserver for protein post-translational modification site prediction and visualization. Nucleic Acids Res. 48, W140–W146. https://doi.org/10.1093/nar/gkaa275

Wang, D., Zeng, S., Xu, C., Qiu, W., Liang, Y., Joshi, T., Xu, D., 2017. MusiteDeep: a deep-learning framework for general and kinase-specific phosphorylation site prediction. Bioinforma. Oxf. Engl. 33, 3909–3916. https://doi.org/10.1093/bioinformatics/btx496

Wang, J., Pareja, K.A., Kaiser, C.A., Sevier, C.S., 2014. Redox signaling via the molecular chaperone BiP protects cells against endoplasmic reticulum-derived oxidative stress. eLife 3, e03496. https://doi.org/10.7554/eLife.03496

Wang, J., Sevier, C.S., 2016. Formation and Reversibility of BiP Protein Cysteine Oxidation Facilitate Cell Survival during and post Oxidative Stress. J. Biol. Chem. 291, 7541–7557. https://doi.org/10.1074/jbc.M115.694810

Wang, W., Liu, Qinglian, Liu, Qun, Hendrickson, W.A., 2021. Conformational equilibria in allosteric control of Hsp70 chaperones. Mol. Cell 81, 3919-3933.e7. https://doi.org/10.1016/j.molcel.2021.07.039

Wang, Z., Wu, Z., Jian, J., Lu, Y., 2009. Cloning and expression of heat shock protein 70 gene in the haemocytes of pearl oyster (Pinctada fucata, Gould 1850) responding to bacterial challenge. Fish Shellfish Immunol. 26, 639–645. https://doi.org/10.1016/j.fsi.2008.10.011

Waterhouse, A.M., Procter, J.B., Martin, D.M.A., Clamp, M., Barton, G.J., 2009. Jalview Version 2--a multiple sequence alignment editor and analysis workbench. Bioinforma. Oxf. Engl. 25, 1189–1191. https://doi.org/10.1093/bioinformatics/btp033

Wegele, H., Wandinger, S.K., Schmid, A.B., Reinstein, J., Buchner, J., 2006. Substrate Transfer from the Chaperone Hsp70 to Hsp90. J. Mol. Biol. 356, 802–811. https://doi.org/10.1016/j.jmb.2005.12.008

Weissman, J.S., Hohl, C.M., Kovalenko, O., Kashi, Y., Chen, S., Braig, K., Saibil, H.R., Fenton, W.A., Horwich, A.L., 1995. Mechanism of GroEL action: productive release of polypeptide from a sequestered position under GroES. Cell 83, 577–587. https://doi.org/10.1016/0092-8674(95)90098-5

Welburn, S.C., Coleman, P.G., Maudlin, I., Fèvre, E.M., Odiit, M., Eisler, M.C., 2006. Crisis, what crisis? Control of Rhodesian sleeping sickness. Trends Parasitol. 22, 123–128. https://doi.org/10.1016/j.pt.2006.01.011

Wheeler, R.J., Gluenz, E., Gull, K., 2013. The Limits on Trypanosomatid Morphological Diversity. PLoS ONE 8, e79581. https://doi.org/10.1371/journal.pone.0079581

Whitesell, L., Lindquist, S.L., 2005. HSP90 and the chaperoning of cancer. Nat. Rev. Cancer 5, 761–772. https://doi.org/10.1038/nrc1716

WHO, 2022. Trypanosomiasis, human African (sleeping sickness).

Wiedemar, N., Zwyer, M., Zoltner, M., Cal, M., Field, M.C., Mäser, P., 2019. Expression of a specific variant surface glycoprotein has a major impact on suramin sensitivity and endocytosis in Trypanosoma brucei. FASEB BioAdvances 1, 595–608. https://doi.org/10.1096/fba.2019-00033

Wilkinson, S.R., Taylor, M.C., Horn, D., Kelly, J.M., Cheeseman, I., 2008. A mechanism for cross-resistance to nifurtimox and benznidazole in trypanosomes. Proc. Natl. Acad. Sci. U. S. A. 105, 5022–5027. https://doi.org/10.1073/pnas.0711014105

Wilson, (Iain) R.J.M., Denny, P.W., Preiser, P.R., Rangachari, K., Roberts, K., Roy, A., Whyte, A., Strath, M., Moore, D.J., Moore, P.W., Williamson, D.H., 1996. Complete Gene Map of the Plastid-like DNA of the Malaria ParasitePlasmodium falciparum. J. Mol. Biol. 261, 155–172. https://doi.org/10.1006/jmbi.1996.0449

Winter, J., Ilbert, M., Graf, P.C.F., Özcelik, D., Jakob, U., 2008. Bleach Activates a Redox-Regulated Chaperone by Oxidative Protein Unfolding. Cell 135, 691–701. https://doi.org/10.1016/j.cell.2008.09.024

Winter, J., Linke, K., Jatzek, A., Jakob, U., 2005. Severe Oxidative Stress Causes Inactivation of DnaK and Activation of the Redox-Regulated Chaperone Hsp33. Mol. Cell 17, 381–392. https://doi.org/10.1016/j.molcel.2004.12.027

Wittung-Stafshede, P., Guidry, J., Horne, B.E., Landry, S.J., 2003. The J-Domain of Hsp40 Couples ATP Hydrolysis to Substrate Capture in Hsp70. Biochemistry 42, 4937–4944. https://doi.org/10.1021/bi027333o

Wohlgamuth-Benedum, J.M., Rubio, M.A.T., Paris, Z., Long, S., Poliak, P., Lukes, J., Alfonzo, J.D., 2009. Thiolation controls cytoplasmic tRNA stability and acts as a negative determinant for tRNA editing in mitochondria. J. Biol. Chem. 284, 23947–23953. https://doi.org/10.1074/jbc.M109.029421

Wombou Toukam, C.M., Solano, P., Bengaly, Z., Jamonneau, V., Bucheton, B., 2011. Experimental evaluation of xenodiagnosis to detect trypanosomes at low parasitaemia levels in infected hosts. Parasite 18, 295–302. https://doi.org/10.1051/parasite/2011184295

World Health Organization, 2019. WHO interim guidelines for the treatment of gambiense human African trypanosomiasis. World Health Organization, Geneva.

Wu, Y., Li, J., Jin, Z., Fu, Z., Sha, B., 2005. The Crystal Structure of the C-terminal Fragment of Yeast Hsp40 Ydj1 Reveals Novel Dimerization Motif for Hsp40. J. Mol. Biol. 346, 1005–1011. https://doi.org/10.1016/j.jmb.2004.12.040

Yaglom, J.A., Gabai, V.L., Sherman, M.Y., 2007. High Levels of Heat Shock Protein Hsp72 in Cancer Cells Suppress Default Senescence Pathways. Cancer Res. 67, 2373–2381. https://doi.org/10.1158/0008-5472.CAN-06-3796

Yamamoto, H., Momose, T., Yatsukawa, Y., Ohshima, C., Ishikawa, D., Sato, T., Tamura, Y., Ohwa, Y., Endo, T., 2005. Identification of a novel member of yeast mitochondrial Hsp70-associated motor and chaperone proteins that facilitates protein translocation across the inner membrane. FEBS Lett. 579, 507–511. https://doi.org/10.1016/j.febslet.2004.12.018

Yan, W., Craig, E.A., 1999. The glycine-phenylalanine-rich region determines the specificity of the yeast Hsp40 Sis1. Mol. Cell. Biol. 19, 7751–7758. https://doi.org/10.1128/MCB.19.11.7751

Yang, W., Zhang, L., Lu, Z., Tao, W., Zhai, Z., 2001. A New Method for Protein Coexpression in Escherichia coli Using Two Incompatible Plasmids. Protein Expr. Purif. 22, 472–478. https://doi.org/10.1006/prep.2001.1453

Yanisch-Perron, C., Vieira, J., Messing, J., 1985. Improved M13 phage cloning vectors and host strains: nucleotide sequences of the M13mpl8 and pUC19 vectors. Gene 33, 103–119. https://doi.org/10.1016/0378-1119(85)90120-9

Yoshimune, K., Ninomiya, Y., Wakayama, M., Moriguchi, M., 2004. Molecular chaperones facilitate the soluble expression of N-acyl-d-amino acid amidohydrolases in Escherichia coli. J. Ind. Microbiol. Biotechnol. 31, 421–426. https://doi.org/10.1007/s10295-004-0163-4

Young, Jason C, Barral, J.M., Ulrich Hartl, F., 2003. More than folding: localized functions of cytosolic chaperones. Trends Biochem. Sci. 28, 541–547. https://doi.org/10.1016/j.tibs.2003.08.009

Young, Jason C., Hoogenraad, N.J., Hartl, F.U., 2003. Molecular chaperones Hsp90 and Hsp70 deliver preproteins to the mitochondrial import receptor Tom70. Cell 112, 41–50. https://doi.org/10.1016/s0092-8674(02)01250-3

Yun, C.-O., Bhargava, P., Na, Y., Lee, J.-S., Ryu, J., Kaul, S.C., Wadhwa, R., 2017. Relevance of mortalin to cancer cell stemness and cancer therapy. Sci. Rep. 7, 42016. https://doi.org/10.1038/srep42016

Zhai, P., Stanworth, C., Liu, S., Silberg, J.J., 2008. The Human Escort Protein Hep Binds to the ATPase Domain of Mitochondrial Hsp70 and Regulates ATP Hydrolysis. J. Biol. Chem. 283, 26098–26106. https://doi.org/10.1074/jbc.M803475200

Zhai, P., Vu, M.T., Hoff, K.G., Silberg, J.J., 2011. A conserved histidine in human DNLZ/HEP is required for stimulation of HSPA9 ATPase activity. Biochem. Biophys. Res. Commun. 408, 589–594. https://doi.org/10.1016/j.bbrc.2011.04.066

Zhang, M., Windheim, M., Roe, S.M., Peggie, M., Cohen, P., Prodromou, C., Pearl, L.H., 2005. Chaperoned Ubiquitylation—Crystal Structures of the CHIP U Box E3 Ubiquitin Ligase and a CHIP-Ubc13-Uev1a Complex. Mol. Cell 20, 525–538. https://doi.org/10.1016/j.molcel.2005.09.023

Zhao, H., Raines, L.N., Huang, S.C.-C., 2020. Molecular Chaperones: Molecular Assembly Line Brings Metabolism and Immunity in Shape. Metabolites 10, 394. https://doi.org/10.3390/metabo10100394

Zhao, X., Silva, T.L.A. e, Cronin, L., Savage, A.F., O'Neill, M., Nerima, B., Okedi, L.M., Aksoy, S., 2015. Immunogenicity and Serological Cross-Reactivity of Saliva Proteins among Different Tsetse Species. PLoS Negl. Trop. Dis. 9, e0004038. https://doi.org/10.1371/journal.pntd.0004038

Zhou, J., Schmid, T., Frank, R., Brüne, B., 2004. PI3K/Akt Is Required for Heat Shock Proteins to Protect Hypoxia-inducible Factor 1α from pVHL-independent Degradation. J. Biol. Chem. 279, 13506–13513. https://doi.org/10.1074/jbc.M310164200

Zhu, X., Zhao, X., Burkholder, W.F., Gragerov, A., Ogata, C.M., Gottesman, M.E., Hendrickson, W.A., 1996. Structural Analysis of Substrate Binding by the Molecular Chaperone DnaK. Science 272, 1606–1614. https://doi.org/10.1126/science.272.5268.1606

Zhuravleva, A., Gierasch, L.M., 2015. Substrate-binding domain conformational dynamics mediate Hsp70 allostery. Proc. Natl. Acad. Sci. U. S. A. 112, E2865-2873. https://doi.org/10.1073/pnas.1506692112

Zhuravleva, A., Gierasch, L.M., 2011. Allosteric signal transmission in the nucleotide-binding domain of 70-kDa heat shock protein (Hsp70) molecular chaperones. Proc. Natl. Acad. Sci. 108, 6987–6992. https://doi.org/10.1073/pnas.1014448108

Ziegelbauer, K., Overath, P., 1993. Organization of two invariant surface glycoproteins in the surface coat of Trypanosoma brucei. Infect. Immun. 61, 4540–4545. https://doi.org/10.1128/iai.61.11.4540-4545.1993

Ziegelbauer, K., Overath, P., 1992. Identification of invariant surface glycoproteins in the bloodstream stage of Trypanosoma brucei. J. Biol. Chem. 267, 10791–10796.

Ziegelbauer, K., Quinten, M., Schwarz, H., Pearson, T.W., Overath, P., 1990. Synchronous differentiation of Trypanosoma brucei from bloodstream to procyclic forms in vitro. Eur. J. Biochem. 192, 373–378. https://doi.org/10.1111/j.1432-1033.1990.tb19237.x

Zininga, T., Achilonu, I., Hoppe, H., Prinsloo, E., Dirr, H.W., Shonhai, A., 2016. Plasmodium falciparum Hsp70-z, an Hsp110 homologue, exhibits independent chaperone activity and interacts with Hsp70-1 in a nucleotide-dependent fashion. Cell Stress Chaperones 21, 499–513. https://doi.org/10.1007/s12192-016-0678-4

Zolkiewski, M., Zhang, T., Nagy, M., 2012. Aggregate reactivation mediated by the Hsp100 chaperones. Arch. Biochem. Biophys. 520, 1–6. https://doi.org/10.1016/j.abb.2012.01.012

Zurawska, A., Urbanski, J., Bieganowski, P., 2008. Hsp90n — An accidental product of a fortuitous chromosomal translocation rather than a regular Hsp90 family member of human proteome. Biochim. Biophys. Acta BBA - Proteins Proteomics 1784, 1844–1846. https://doi.org/10.1016/j.bbapap.2008.06.013

Appendices
Supplementary data and information

Appendix A

Table A1: Details regarding the Hep1 orthologues and homologues utilised in this study. These include the species/strain of origin and database accession numbers.

Orthologue	Database	Organism / Species	Strain / NCBI Taxa id	Database accession id
TbbHep1	TriTrypDB	*Trypanosoma brucei brucei*	TREU927	Tb927.3.2300
TbgHep1		*Trypanosoma brucei gambiense*	DAL972	Tb972.3.2280
TeqHep1		*Trypanosoma equiperdum*	OV1	TEOVI_000221600
TevHep1		*Trypanosoma evansi*	STIB805	TevSTIB805.3.2330
TcrHep1		*Trypanosoma cruzi*	CL Brener non-Esmeraldo-like	TcCLB.508479.274
TviHep1		*Trypanosoma vivax*	Y486	TvY486_0301660
TcoHep1		*Trypanosoma congolese*	IL3000	TcIL3000_0_42310
LbrHep1		*Leishmania braziliensis*	MHOM/BR/75/M2904	LbrM.25.0680
LdoHep1		*Leishmania donovani*	BPK282A1	LdBPK_250830.1
LmjHep1		*Leishmania major*	Friedlin	LmjF.25.0800
LmxHep1		*Leishmania Mexicana*	MHOM/GT/2001/U1103	LmxM.25.0800
BsalHep1		*Bodo saltans*	Lake Konstanz	BSAL_79370
CfHep1		*Crithidia fasciculata*	CF-CL	CFAC1_220016500
PfHep1	PlasmoDB	*Plasmodium falciparum*	3D7	PF3D7_1420300
PmalHep1		*Plasmodium malariae*	UG01	PmUG01_13038600
PviHep1		*Plasmodium vivax*	P01	PVP01_1328600
PberHep1		*Plasmodium berghei*	ANKA	PBANKA_1022900
TgoHep1	ToxoDB	*Toxoplasma gondii*	ME49	TGME49_260340
AtHep1	NCBI	*Arabidopsis thaliana*	3702	NP_974434.2
ScHep1		*Saccharomyces cerevisiae*	4932	NP_014089.2
SpasHep1		*Saccharomyces pastorianus*	27292	QID81845.1
SparHep1		*Saccharomyces paradoxus*	27291	XP_033768657.1
CneoHep1		*Cryptococcus neoformans*	5207	XP_024514386.1
CalbHep1		*Candida albicans*	5476	KHC45981.1
HsHep1		*Homo sapiens*	9606	NP_001074318.1
MsmHep1-iso1		*Mus musculus*	10090	NP_081104.1
BtauHep1		*Bos taurus*	9913	XP_003586730.1
DmelHep1		*Drosophila melanogaster*	7227	NP_573061.2
DsimHep1		*Drosophila simulans*	7240	XP_016039443.1
MdomHep1		*Musca domestica*	7370	XP_00518472.3
CrHep2 C-term		*Chlamydomonas reinhardtii*	3055	XP_001700157.1
ATZR3		*Arabidopsis thailiana*	3702	AAO64784.1

Table A2: Details regarding the J-proteins and Hsp33 orthologues utilised in this study. These include the species/strain of origin and database accession numbers.

	Organism/Species	Strain / Taxa ID	Database	Accession ID
Tbj2	*Trypanosoma brucei brucei*	TREU927	TriTrypDB	Tb927.2.5160
Tcrj2	*Trypanosoma cruzi*	CL Brener non-Esmeraldo-like		TcCLB.511627.110
Lbrj2	*Leishmania braziliensis*	MHOM/BR/75/M2904		LbrM.27.2610
Lmjj2	*Leishmania major*	Friedlin		LmjF.27.2400
Tbj50	*Trypanosoma brucei brucei*	TREU927		Tb927.9.12730
Tcrj50	*Trypanosoma cruzi*	CL Brener non-Esmeraldo-like		TcCLB.510743.100
Lbrj50	*Leishmania braziliensis*	MHOM/BR/75/M2904		LbrM.34.2890
Lmjj50	*Leishmania major*	Friedlin		LmjF.35.2980
TbHsp33/TrypOX	*Trypanosoma brucei brucei*	TREU927		Tb927.6.2630
LbrHsp33	*Leishmania braziliensis*	MHOM/BR/75/M2904		LbrM.30.1710
LmjHsp33	*Leishmania major*	Friedlin		LmjF.30.1670
TcrHsp33	*Trypanosoma cruzi*	CL Brener non-Esmeraldo-like		TcCLB.509965.120
Pfj1	*Plasmodium falciparum*	3D7	PlasmoDB	PF3D7_1437900
TgonJ-proein	*Toxoplasma gondii*	MR49	ToxoDB	TGME49_311240
ScYdj1	*Saccharomyces cerevisiae*	4932	NCBI	NP_014335.1
DmelDnaJ-like-2	*Drosophila melanogaster*	7227		NP_650283.1
HsDNAJA1	*Homo sapiens*	9606		NP_001530.1
ScMdj1	*Saccharomyces cerevisiae*	4932		QHB08320.1
DmelTid-56	*Drosophila melanogaster*	7227		CAA64531.1
HsTid-1L	*Homo sapiens*	9606		NP_005138.3
HsTid-1S	*Homo sapiens*	9606		NP_001128582.1
EcDNAJA1	*Escherichia coli*	562		MRF42610.1
SmarDNAJA1	*Serratia marcecens*	615		MBH2573448.1
PaerDNAJA1	*Pseudomonas aeruginosa*	286/287		WP_009685335.1
SaurDNAJA1	*Staphylococcus aureus*	1280		MCR0757594.1
EcHsp33	*Escherichia coli*	562		EDV67745.1
SmarHsp33	*Serratia marcecens*	615		WP_060448467.1
PaerHsp33	*Pseudomonas aeruginosa*	286/287		MXH37999.1
SaurHsp33	*Staphylococcus aureus*	1280		HAY6579316.1
OsatHsp33	*Oryza sativa*	4530		EEC84194.1
CrHsp33	*Chlamydomonas reinhardtii*	3055		PNW70318.1

Table A3: Details regarding the murine and primate Hep1 orthologues/isoforms investigated in this study. Details include the species of origin, computationally predicted physical properties and NCBI accession numbers.

	NCBI Accession ID	Murine or Primate?	Species (Taxa ID / Gene ID)	# AA residues	MW (Da)	pI	Localisation	zf-DNL? (Y/N)	AA residues (zf-DXL)	MW (zf-DNL)
MsmHep1-iso1	NP_081104.1	Murine	*Mus musculus* (10090 / 52838)	177	19403.05	9.58	Mitochondria	Y	66	7386.51
MsmHep1-iso2	NP_001132975.1			82	9265.58	11.32	Mitochondria	N	-	-
MsmHep1-iso3	NP_001132976.1			122	13762.90	11.64	Mitochondria	N	-	-
MpHep1-iso1	XP_021050144.1		*Mus pahari* (10093 / 110319072)	174	19017.52	9.23	Mitochondria	Y	66	7386.51
MpHep1-iso2	XP_021050145.1			118	13298.31	11.64	Mitochondria	N	-	-
MpHep1-iso3	XP_021050146.1			78	8765.92	11.35	Mitochondria	N	-	-
McarHep1-iso1	XP_021011688.1		*Mus caroli* (10089 / 110289692)	174	19162.74	9.42	Mitochondria	Y	66	7386.51
McarHep1-iso2	XP_021011689.1			119	13478.59	11.64	Mitochondria	N	-	-
McouHep1-iso1	XP_031225303.1		*Mastomys coucha* (35358 / 116089854)	226	24859.32	10.60	Mitochondria	Y	66	7386.51
McouHep1-iso2	XP_031225305.1			171	19169.12	11.65	Mitochondria	N	-	-
McouHep1-iso3	XP_031225306.1			131	14672.77	11.79	Mitochondria	N	-	-
GsurHep1-iso1	XP_028628786.1		*Grammomys surdaster* (491861 / 114625609)	173	19292.92	9.42	Mitochondria	Y	66	7386.51
GsurHep1-iso2	XP_028628787.1			118	13457.60	11.67	Mitochondria	N	-	-
AsylHep1-iso1	XP_052037841.1		*Apodemus sylvaticus* (10129 / 127685086)	173	18973.62	9.71	Mitochondria	Y	66	7386.51
AsylHep1-iso2	XP_052037846.1			118	13206.36	11.49	Mitochondria	N	-	-
NgalHep1-iso1	XP_029423617.1		*Nannospalax galili* (1026970 / 103741206)	202	22088.31	8.97	Mitochondria	Y	66	7389.48
NgalHep1-iso2	XP_017655799.2			172	18763.45	9.86	Mitochondria	Y	66	7389.48
NgalHep1-iso3	XP_017655800.1			118	13199.29	12.05	Mitochondria	N	-	-
NgalHep1-iso4	XP_029423618.1			78	8581	11.94	Mitochondria	N	-	-
HmolHep1-iso1	XP_032021543.1	Primate	*Hylobates moloch* (81572 / 116475863)	212	22428.73	9.80	Mitochondria	Y	66	7341.43
HmolHep1-iso2	XP_032021544.1			200	22263.71	10.79	Mitochondria	Y	66	7341.43
HmolHep1-iso3	XP_032021545.1			189	20263.35	10.56	Mitochondria	Y	66	7341.43
HmolHep1-iso4	XP_032021546.1			180	19365.04	9.54	Mitochondria	Y	66	7341.43
CjacHep1-iso1	XP_035119009.1		*Callithrix jacchus* (9483 / 100399618)	233	25036.32	10.03	Mitochondria	Y	66	7355.46
CjacHep1-iso2	XP_035119020.1			189	20625.70	11.26	Mitochondria	Y	60	6674.76

Table A4: Details regarding the murine Hep1 orthologues returned when *Mus musculus* Hep1 isoforms 1 and 2 without zinc finger domains were used as BLASTP search queries.

	Isoform	NCBI accession ID	
Meriones unguiculatus	**3**	XP_021496788.1	Short
Ascomys russatus	**3**	XP_051022554.1	
Arvicanthis niloticus	**2**	XP_034360666.1	Long
Acomys russatus	**2**	XP_05102255.3	
Onychomys torridus	**2**	XP_036039773.1	
Peromyscus californicus insignis	**2**	XP_05251065.1	
Peromyscus maniculatus bairdii	**2**	XP_006981044.1	
Meriones unguiculatus	**2**	XP_021496787.1	
Peromyscus leocopus	**2**	XP_028724670.1	
Jaculus Jaculus	**2**	XP_004654135.2	

Table A5: Details regarding the Hsp70 orthologues used in this study.

Orthologue	Database	Organism/Species (Strain/Taxa ID)	Database accession id	MW (Da)	pI	# AA residues
TbHsp70	TriTrypDB	*Trypanosoma brucei brucei* (TREU927)	Tb927.11.11330	71408.78	5.29	661
TbHsp70.4			Tb927.7.710	70211.83	4.95	639
TbHsp70.c			Tb927.11.11290	73630.82	5.11	676
TbmtHsp70			Tb927.6.3740	71475.05	5.76	657
TbGRP78A/BiP			Tb927.11.7460	71435.18	5.34	653
TcrHsp70		*Trypanosoma cruzi* (CL Brener non-Esmeraldo-like & CL Brener Esmeraldo-like)	TcCLB.511211.170	73298.06	5.42	677
TcrmtHsp70			TcCLB.507029.30	70990.26	5.75	655
TcrGRP78A/BiP			TcCLB.506585.40	71315.87	5.09	651
LmjHsp70		*Leishmania major* (Friedlin)	LmjF.28.2770	71652.76	5.30	658
LmjmtHsp70			LmjF.30.2460	68948.27	5.81	635
LmjGRP78/BiP			LmjF.28.1200	71940.59	5.05	658
LbrHsp70		*Leishmania braziliensis* (MHOM/BR/75/M2904)	LbrM.28.2990	71276.37	5.40	654
LbrmtHsp70			LbrM.30.2420	70528.76	5.90	651
LbGRP78/BiP			LbrM.30.2420	71910.67	5.06	658
PfHsp70-1	PlasmoDB	*Plasmodium falciparum* (3D7)	PF3D7_0818900	73914.90	5.50	677
PfHsp70-3			PF3D7_1134000	73297.45	6.51	663
PfHsp70-2/BiP			PF3D7_0917900	72387.2	5.18	652
ScSsa4	NCBI	*Saccharomyces cerevisiae* (4932)	AJU50241.1	69623.07	5.02	642
ScSsa3			AJQ13321.1	70606.89	5.05	649
ScSsa2			AJV59097.1	69498.10	4.97	639
ScSsa1			AJO96864.1	69657.25	4.99	642
ScSsc1			AJV44330.1	70555.77	5.55	654
ScEcm10			AJU50104.1	70050.52	6.07	644
ScSsq1			AJV59432.1	72363.65	6.09	657
ScKar2			AJR59823.1	74451.99	4.79	682
HSPA1A		*Homo sapiens* (9606)	NP_005336.3	70052.23	5.47	641
HSPA8			NP_006588.1	70898.09	5.37	646
HSPA9			AAH00478.1	73727.60	6.03	679
HsHSPA5/BiP			AAI12964.1	72422.06	5.07	655
EcDnaK		*Escherichia coli* (562)	WP_097477514.1	69086.90	4.83	638

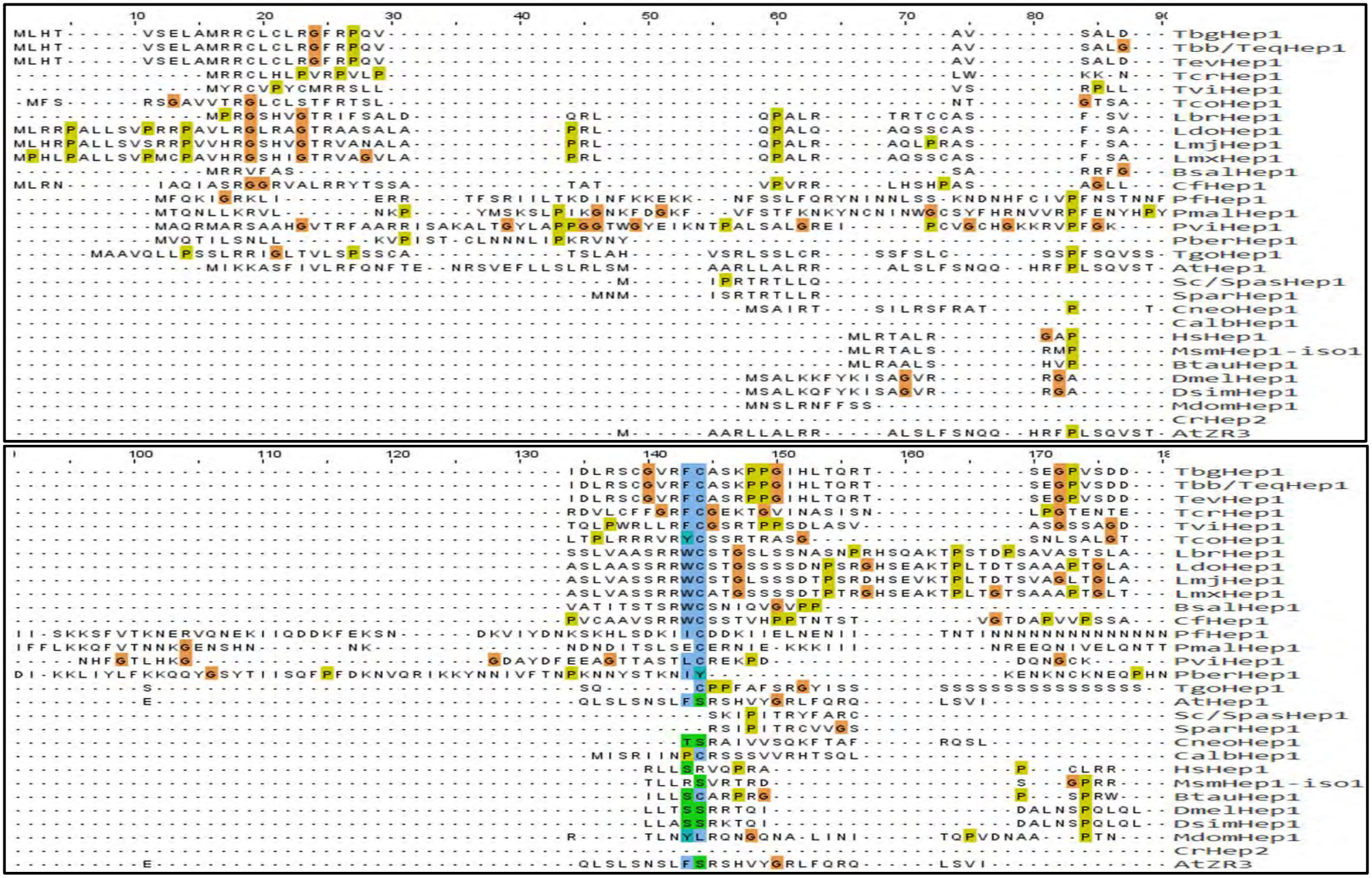
TbgHep1
Tbb/TeqHep1
TevHep1
TcrHep1
TviHep1
TcoHep1
LbrHep1
LdoHep1
LmjHep1
LmxHep1
BsalHep1
CfHep1
PfHep1
PmalHep1
PviHep1
PberHep1
TgoHep1
AtHep1
Sc/SpasHep1
SparHep1
CneoHep1
CalbHep1
HsHep1
MsmHep1-iso1
BtauHep1
DmelHep1
DsimHep1
MdomHep1
CrHep2
AtZR3

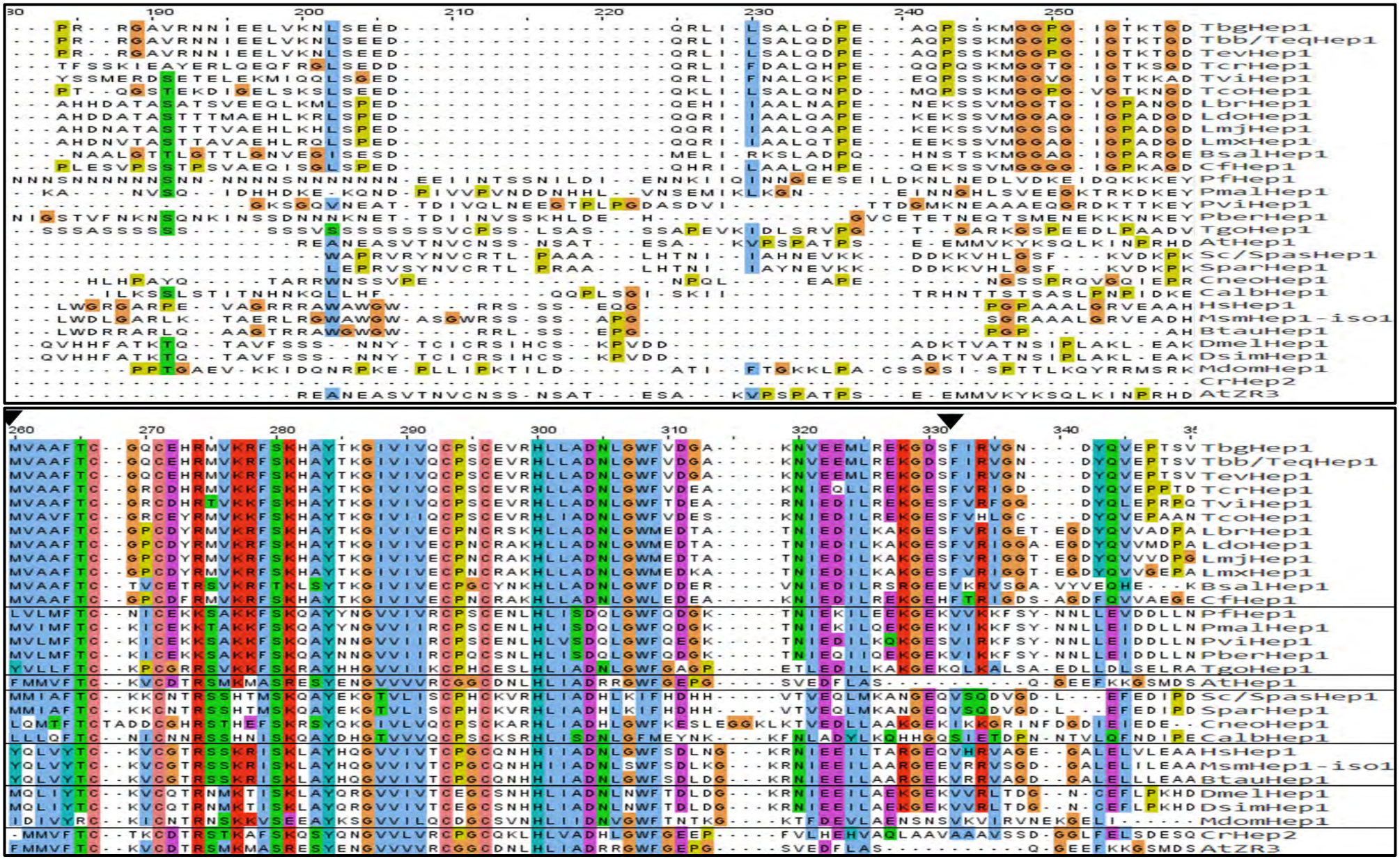

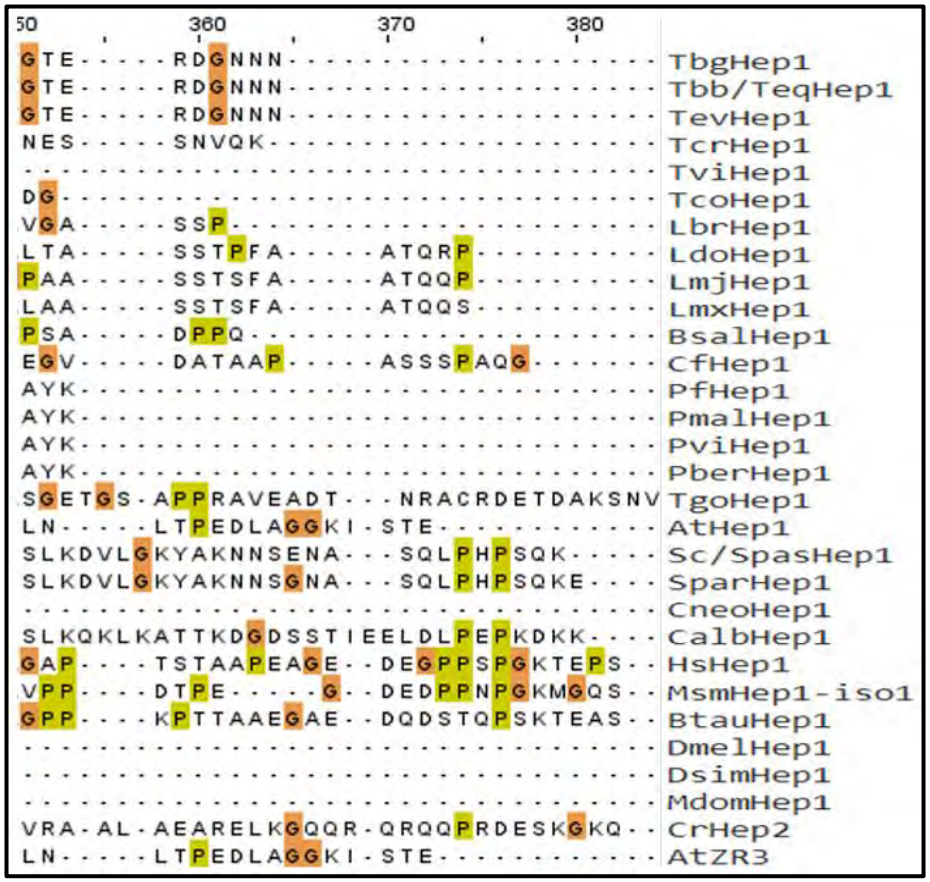

Figure A1: The Clustal Omega multiple sequence alignment (MSA) of the Hep1 orthologues and homologues. The sequences were aligned using the built in Clustal Omega MSA platform on the JalView web service. The annotation is based on the JalView Clustal colour option. The Hep1 sequences aligned were from: TbgHep1 (Tb972.3.2280), TbbHep1 (Tb927.3.2300), TeqHep1 (TEOVI_000221600), TevHep1 (TevSTIB805.3.2330), TcrHep1 (TcCLB.508479.274), TviHep1 (TvY486_0301660), TcoHep1 (TcIL3000_0_42310), LbrHep1 (LbrM.25.0680), LdoHep1 (LdBPK_250830.1), LmjHep1 (LmjF.25.0800), LmxHep1 (LmxM.25.0800), BsalHep1 (BSAL_79370), CfHep1 (CFAC1_220016500), PfHep1 (PF3D7_1420300), PmalHep1 (PmUG01_13038600), PviHep1 (PVP01_1328600), PberHep1 (PBANKA_1022900), TgoHep1 (TGME49_260340), AtHep1 (NP_974434.2), ScHep1 (NP_014089.2), SpasHep1 (QID81845.1), SparHep1 (XP_033768657.1), CneoHep1 (XP_024514386.1), CalbHep1 (KHC45981.1), HsHep1 (NP_001074318.1), MsmHep1-iso1 (NP_081104.1), BtauHep1 (XP_003586730.1), DmelHep1 (AAS15675.1), DsimHep1 (XP_016039443.1), MdomHep1 (XP_00518472.3), CrHep2 C-term (XP_001700157.1) and ATZR3 (AAO64784.1). The arrows serve to demarcate the conserved zinc finger regions. Tbb/TeqHep1 refers to the identical TbbHep1 and TeqHep1 orthologues, whilst Sc/SpasHep1 refers to the identical ScHep1 and SpasHep1 orthologues.

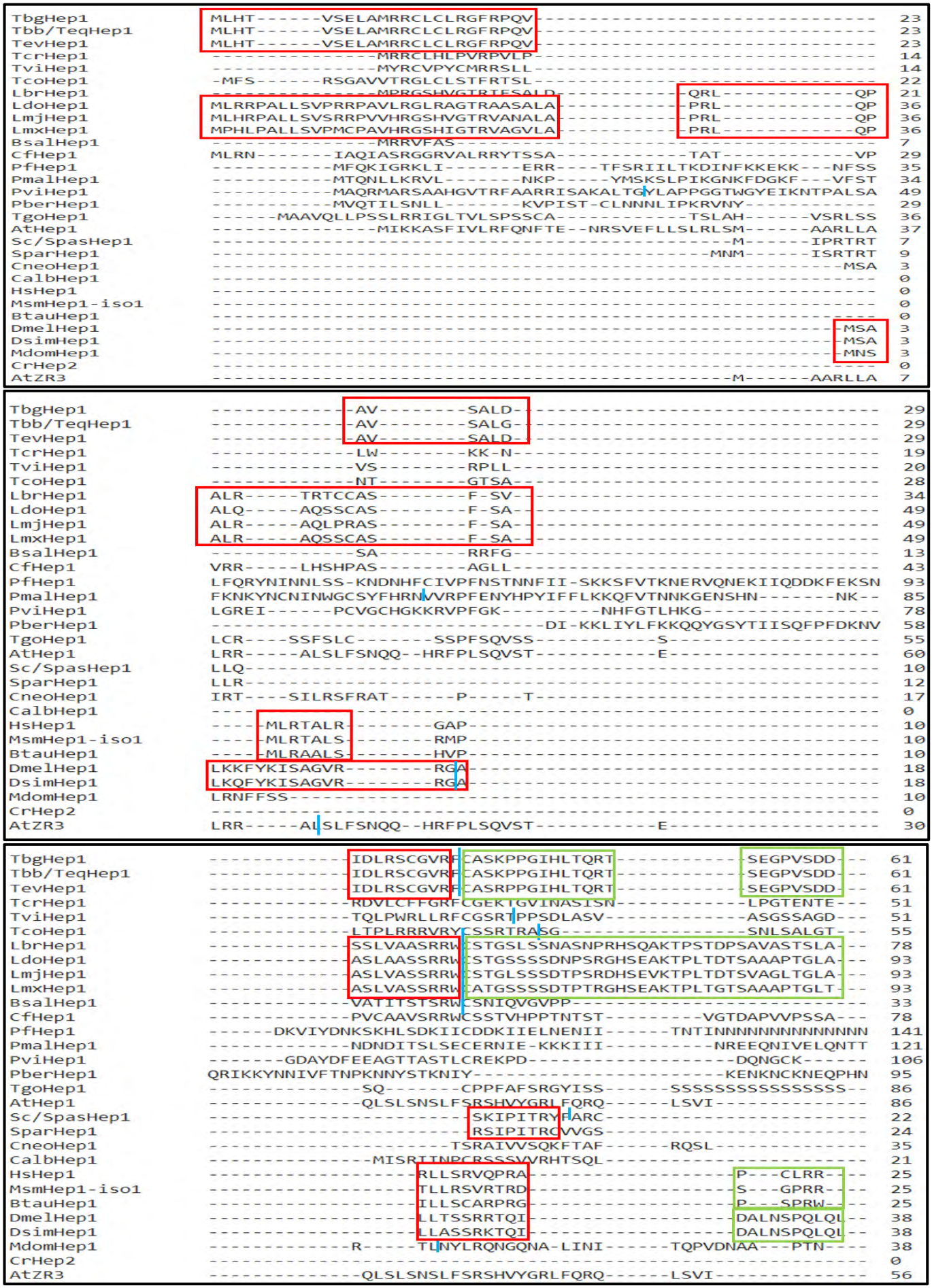

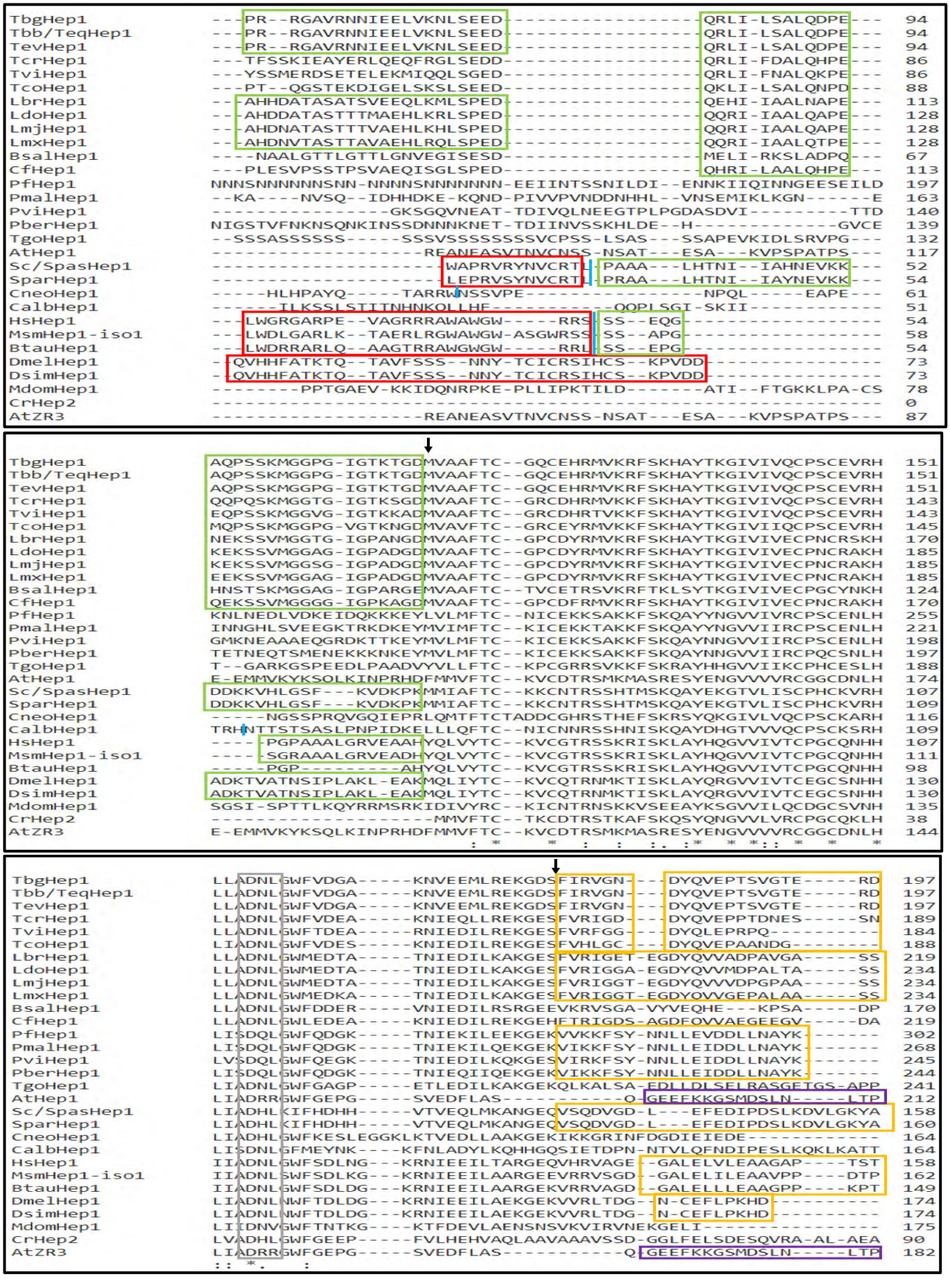
TbgHep1
Tbb/TeqHep1
TevHep1
TcrHep1
TviHep1
TcoHep1
LbrHep1
LdoHep1
LmjHep1
LmxHep1
BsalHep1
CfHep1
PfHep1
PmalHep1
PviHep1
PberHep1
TgoHep1
AtHep1
Sc/SpasHep1
SparHep1
CneoHep1
CalbHep1
HsHep1
MsmHep1-iso1
BtauHep1
DmelHep1
DsimHep1
MdomHep1
CrHep2
AtZR3

X

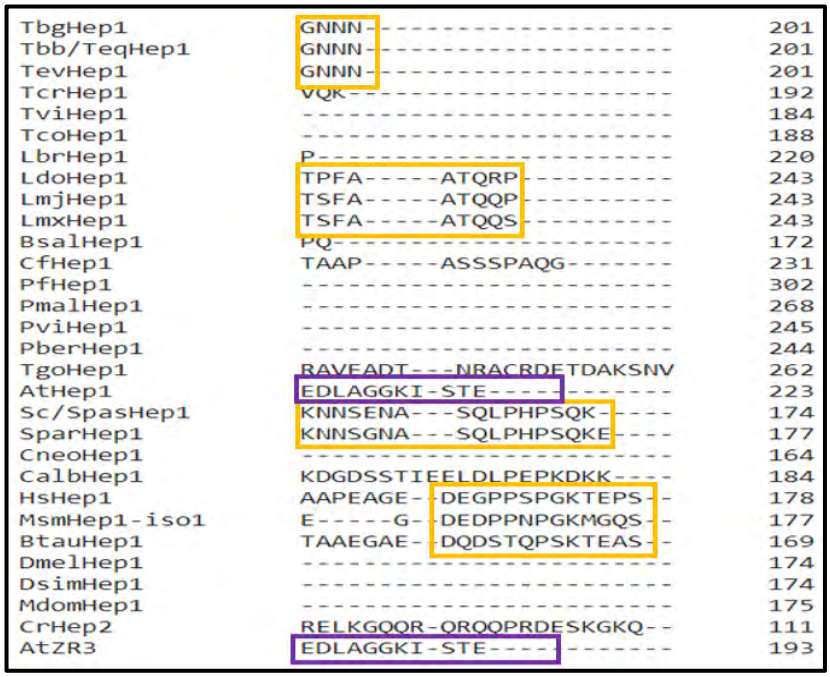

Figure A2: The colourless Clustal Omega multiple sequence alignment (MSA) of the Hep1 orthologues. The MSA was generated using Clustal Omega on the EMBL-EBI web server and annotated manually. The sequences aligned were from: TbgHep1 (Tb972.3.2280), TbbHep1 (Tb927.3.2300), TeqHep1 (TEOVI_000221600), TevHep1 (TevSTIB805.3.2330), TcrHep1 (TcCLB.508479.274), TviHep1 (TvY486_0301660), TcoHep1 (TcIL3000_0_42310), LbrHep1 (LbrM.25.0680), LdoHep1 (LdBPK_250830.1), LmjHep1 (LmjF.25.0800), LmxHep1 (LmxM.25.0800), BsalHep1 (BSAL_79370), CfHep1 (CFAC1_220016500), PfHep1 (PF3D7_1420300), PmalHep1 (PmUG01_13038600), PviHep1 (PVP01_1328600), PberHep1 (PBANKA_1022900), TgoHep1 (TGME49_260340), AtHep1 (NP_974434.2), ScHep1 (NP_014089.2), SpasHep1 (QID81845.1), SparHep1 (XP_033768657.1), CneoHep1 (XP_024514386.1), CalbHep1 (KHC45981.1), HsHep1 (NP_001074318.1), MsmHep1-iso1 (NP_081104.1), BtauHep1 (XP_003586730.1), DmelHep1 (AAS15675.1), DsimHep1 (XP_016039443.1), MdomHep1 (XP_00518472.3), CrHep2 C-term (XP_001700157.1) and ATZR3 (AAO64784.1). The turquoise vertical lines indicate the MitoProt and MitoFates predicted mitochondrial targeting sequence (MTS) cleavage sites of the proteins. In the red and green boxes, respectively, are the signature regions in the MTS and N-terminal regions. Signature sequences downstream of the zinc finger domain are enclosed in the purple and yellow boxes. In the grey box is the conserved DXX motif. The arrows serve demarcate the conserved zinc finger regions. Tbb/TeqHep1 refers to the identical TbbHep1 and TeqHep1 orthologues, whilst Sc/SpasHep1 refers to the identical ScHep1 and SpasHep1 orthologues.

		1	2	3	4	5	6	7	8	9	10	11	12	13	14	15	16	17	18	19	20	21	22
1	TbgHep1																						
2	Tbb/TeqHep1	0,0000																					
3	TevHep1	0,0000	0,0000																				
4	TcrHep1	0,2001	0,2001	0,2001																			
5	TviHep1	0,2807	0,2807	0,2807	0,1716																		
6	TcoHep1	0,2734	0,2734	0,2734	0,1935	0,2272																	
7	LbrHep1	0,4440	0,4440	0,4440	0,3961	0,3799	0,4427																
8	LdoHep1	0,4451	0,4451	0,4451	0,3972	0,3810	0,4439	0,0267															
9	LmjHep1	0,4501	0,4501	0,4501	0,3952	0,3846	0,4399	0,0396	0,0265														
10	LmxHep1	0,4444	0,4444	0,4444	0,3874	0,3710	0,4341	0,0535	0,0407	0,0542													
11	BsalHep1	0,7855	0,7855	0,7855	0,7888	0,6958	0,8024	0,6893	0,7057	0,7166	0,7138												
12	CfHep1	0,4235	0,4235	0,4235	0,3693	0,3914	0,4264	0,1992	0,2038	0,2000	0,1818	0,6378											
13	PfHep1	1,0452	1,0452	1,0452	1,0414	0,9803	0,9632	1,1373	1,1664	1,1415	1,2161	1,1319	1,2542										
14	PmalHep1	1,0160	1,0160	1,0160	1,0616	0,9891	0,9352	1,1852	1,1900	1,1953	1,2625	1,1721	1,2484	0,0955									
15	PviHep1	0,9792	0,9792	0,9792	1,0472	0,9228	0,8930	1,0468	1,0510	1,0557	1,1173	1,0688	1,2107	0,1764	0,1470								
16	PberHep1	1,1482	1,1482	1,1482	1,1685	1,1389	1,0702	1,2270	1,2320	1,2375	1,3068	1,1478	1,2922	0,1450	0,1007	0,1493							
17	AtHep1	1,6187	1,6187	1,6187	1,6380	1,5207	1,6496	1,6838	1,7501	1,7679	1,7401	1,1057	1,6555	1,1628	1,1926	1,1287	1,2147						
18	HsHep1	1,2011	1,2011	1,2011	1,2617	1,0831	1,1795	1,0490	1,0510	1,0988	1,0619	0,8003	1,0625	1,0861	1,1334	1,0911	1,1305	1,0573					
19	MsmHep1-iso1	1,2564	1,2564	1,2564	1,3178	1,1338	1,2333	1,1165	1,1181	1,1678	1,1311	0,7675	1,1465	1,0992	1,1610	1,1316	1,1584	0,9676	0,0781				
20	BtauHep1	1,2180	1,2180	1,2180	1,2779	1,0978	1,1951	1,0973	1,0990	1,1483	1,1115	0,8023	1,1266	1,0499	1,1105	1,1157	1,1072	1,0270	0,0524	0,0521			
21	CrHep2	1,5122	1,5122	1,5122	1,5050	1,3503	1,4391	1,6344	1,7184	1,7115	1,6632	1,1404	1,5976	1,2478	1,3430	1,2138	1,3234	0,9897	1,4289	1,5239	1,4756		
22	AtZR3	1,6187	1,6187	1,6187	1,6380	1,5207	1,6496	1,6838	1,7501	1,7679	1,7401	1,1057	1,6555	1,1628	1,1926	1,1287	1,2147	0,0000	1,0573	0,9676	1,0270	0,9897	

Figure A3: Distance matrix of the full-length Hep1 orthologues and homologues. The pairwise distance matrix was constructed in MEGAX using the Jones-Taylor-Thornton (JTT) amino acid substitution matrix-model (Gamma distribution: G) with a 1000 replicate bootstrap analysis. The Hep1 sequences aligned in the built in ClustalW multiple sequence alignment platform used to construct the matrix were from: TbgHep1 (Tb972.3.2280), TbbHep1 (Tb927.3.2300), TeqHep1 (TEOVI_000221600), TevHep1 (TevSTIB805.3.2330), TcrHep1 (TcCLB.508479.274), TviHep1 (TvY486_0301660), TcoHep1 (TcIL3000_0_42310), LbrHep1 (LbrM.25.0680), LdoHep1 (LdBPK_250830.1), LmjHep1 (LmjF.25.0800), LmxHep1 (LmxM.25.0800), BsalHep1 (BSAL_79370), CfHep1 (CFAC1_220016500), PfHep1 (PF3D7_1420300), PmalHep1 (PmUG01_13038600), PviHep1 (PVP01_1328600), PberHep1 (PBANKA_1022900), TgoHep1 (TGME49_260340), AtHep1 (NP_974434.2), ScHep1 (NP_014089.2), SpasHep1 (QID81845.1), SparHep1 (XP_033768657.1), CneoHep1 (XP_024514386.1), CalbHep1 (KHC45981.1), HsHep1 (NP_001074318.1), MsmHep1-iso1 (NP_081104.1), BtauHep1 (XP_003586730.1), DmelHep1 (AAS15675.1), DsimHep1 (XP_016039443.1), MdomHep1 (XP_00518472.3), CrHep2 C-term (XP_001700157.1) and ATZR3 (AAO64784.1). Tbb/TeqHep1 refers to the identical TbbHep1 and TeqHep1 orthologues.

		1	2	3	4	5	6	7	8	9	10	11	12	13	14	15	16	17	18	19	20	21
1	TbgHep1																					
2	Tbb/TeqHep1	0,0169																				
3	TevHep1	0,0000	0,0169																			
4	TcrHep1	1,3442	1,3797	1,3442																		
5	TvivHep1	1,4068	1,4037	1,4068	1,5454																	
6	TcoHep1	0,9112	0,9031	0,9112	1,2550	1,5353																
7	LbrHep1	1,7789	1,7546	1,7789	1,9339	1,8920	1,6795															
8	LdoHep1	1,8959	1,8722	1,8959	2,0256	1,7858	1,5649	0,3269														
9	LmjHep1	2,0528	2,0260	2,0528	1,9248	1,9795	1,6024	0,4267	0,1400													
10	LmxHep1	1,9443	1,9202	1,9443	1,9539	1,6793	1,5132	0,4221	0,1177	0,1952												
11	BsalHep1	2,3677	2,3652	2,3677	3,4792	3,6295	2,3728	2,3488	2,1340	2,2616	2,1870											
12	CfHep1	1,4218	1,4188	1,4218	1,5964	1,4745	1,6362	1,1888	1,0330	1,0453	0,9337	2,4224										
13	PfHep1	7,3055	7,7122	7,3055	5,3368	11,5240	10,1639	10,7114	10,4322	13,2582	11,4777	63,8935	10,2026									
14	Pmalhep1	41,4836	50,4445	41,4836	4,9218	9,5225	73,2779	5,1862	4,5160	4,4653	4,5274	9,2414	7,0525	5,6612								
15	PvivHep1	4,6334	4,9692	4,6334	5,2355	6,1951	5,8542	3,9012	4,0306	5,2617	4,2098	5,8937	5,6935	5,0634	12,7515							
16	PberHep1	4,6261	4,5779	4,6261	6,1347	7,3682	5,1240	11,2544	8,2575	9,7556	9,2425	7,7055	5,3023	2,1645	6,2564	5,7733						
17	AtHep1	6,4286	6,2527	6,4286	7,2922	3,5993	5,3752	7,4497	6,2131	7,4957	5,4385	8,4756	4,8884	93,3403	5,3650	58,7891	4,5419					
18	HsHep1	5,1483	5,1205	5,1483	4,7508	4,8320	4,3319	4,3210	3,6995	4,1257	3,7650	5,8445	5,2317	98,8772	7,2891	5,2430	8,0175	79,8677				
19	MsmHep1-iso1	5,1483	5,1205	5,1483	4,7508	4,8320	4,3319	4,3210	3,6995	4,1257	3,7650	5,8445	5,2317	98,8772	7,2891	5,2430	8,0175	79,8677	0,0000			
20	BtauHep1	5,1127	5,0904	5,1127	9,5861	5,7079	6,1643	4,6834	5,4176	7,3384	5,3160	4,9165	6,7477	97,8693	85,3559	5,9800	7,6267	87,4670	0,6147	0,6147		
21	AtZR3	6,4286	6,2527	6,4286	7,2922	3,5993	5,3752	7,4497	6,2131	7,4957	5,4385	8,4756	4,8884	93,3403	5,3650	58,7891	4,5419	0,0000	79,8677	79,8677	87,4670	

Figure A4: The distance matrix of the N-terminal regions of the Hep1 orthologues and homologues. The pairwise distance matrix was constructed in MEGAX using the Jones-Taylor-Thornton (JTT) amino acid substitution matrix-model (Gamma distribution: G) with a 1000 replicate bootstrap analysis. The Hep1 sequences aligned in the built in ClustalW multiple sequence alignment platform used to construct the matrix were from: TbgHep1 (Tb972.3.2280), TbbHep1 (Tb927.3.2300), TeqHep1 (TEOVI_000221600), TevHep1 (TevSTIB805.3.2330), TcrHep1 (TcCLB.508479.274), TviHep1 (TvY486_0301660), TcoHep1 (TcIL3000_0_42310), LbrHep1 (LbrM.25.0680), LdoHep1 (LdBPK_250830.1), LmjHep1 (LmjF.25.0800), LmxHep1 (LmxM.25.0800), BsalHep1 (BSAL_79370), CfHep1 (CFAC1_220016500), PfHep1 (PF3D7_1420300), PmalHep1 (PmUG01_13038600), PviHep1 (PVP01_1328600), PberHep1 (PBANKA_1022900), TgoHep1 (TGME49_260340), AtHep1 (NP_974434.2), ScHep1 (NP_014089.2), SpasHep1 (QID81845.1), SparHep1 (XP_033768657.1), CneoHep1 (XP_024514386.1), CalbHep1 (KHC45981.1), HsHep1 (NP_001074318.1), MsmHep1-iso1 (NP_081104.1), BtauHep1 (XP_003586730.1), DmelHep1 (AAS15675.1), DsimHep1 (XP_016039443.1), MdomHep1 (XP_00518472.3), and ATZR3 (AAO64784.1). Tbb/TeqHep1 refers to the identical TbbHep1 and TeqHep1 orthologues.

		1	2	3	4	5	6	7	8	9	10	11	12	13	14	15	16	17	18	19	20	21	22
1	TbgHep1																						
2	Tbb/TeqHep1	0,0000																					
3	TevHep1	0,0000	0,0000																				
4	TcrHep1	0,1227	0,1227	0,1227																			
5	TvivHep1	0,1811	0,1811	0,1811	0,0919																		
6	TcoHep1	0,1979	0,1979	0,1979	0,1468	0,1622																	
7	LbrHep1	0,3529	0,3529	0,3529	0,3243	0,2963	0,3583																
8	LdonHep1	0,3431	0,3431	0,3431	0,3148	0,2875	0,3483	0,0169															
9	LmjHep1	0,3431	0,3431	0,3431	0,3148	0,2875	0,3483	0,0169	0,0000														
10	LmxHep1	0,3431	0,3431	0,3431	0,3148	0,2875	0,3483	0,0169	0,0000	0,0000													
11	BSalHep1	0,5508	0,5508	0,5508	0,5738	0,4760	0,5522	0,4257	0,4397	0,4397	0,4397												
12	CfHep1	0,5508	0,5508	0,5508	0,5738	0,4760	0,5522	0,4257	0,4397	0,4397	0,4397	0,0000											
13	PfHep1	0,7857	0,7857	0,7857	0,7191	0,6694	0,6524	0,8376	0,8613	0,8613	0,8613	0,7993	0,7993										
14	PmalHep1	0,7817	0,7817	0,7817	0,7173	0,6551	0,5982	0,8492	0,8726	0,8726	0,8726	0,8460	0,8460	0,0871									
15	PviHep1	0,8323	0,8323	0,8323	0,7917	0,6743	0,6299	0,7972	0,8195	0,8195	0,8195	0,7597	0,7597	0,1487	0,1496								
16	PberHep1	0,9225	0,9225	0,9225	0,8200	0,8014	0,7272	0,8879	0,9122	0,9122	0,9122	0,8207	0,8207	0,1505	0,1316	0,1526							
17	AtHep1	1,3002	1,3002	1,3002	1,2630	1,1503	1,1834	1,3036	1,3368	1,3368	1,3368	0,8750	0,8750	0,9174	0,9514	0,8416	0,9737						
18	HsHep1	0,8798	0,8798	0,8798	0,8936	0,7613	0,8008	0,8412	0,8656	0,8656	0,8656	0,5779	0,5779	0,6311	0,6847	0,6686	0,6757	0,8495					
19	MsMHep1-iso1	0,9166	0,9166	0,9166	0,9313	0,7950	0,8358	0,8874	0,9127	0,9127	0,9127	0,6067	0,6067	0,6487	0,7132	0,7062	0,7045	0,8488	0,0327				
20	BtauHep1	0,8819	0,8819	0,8819	0,8958	0,7631	0,8028	0,8526	0,8772	0,8772	0,8772	0,5792	0,5792	0,6205	0,6839	0,6775	0,6749	0,8162	0,0163	0,0162			
21	CrHep2	1,2660	1,2660	1,2660	1,2489	1,2110	1,2650	1,4303	1,4365	1,4365	1,4365	1,0864	1,0864	1,0050	1,0902	0,9347	1,0624	0,7421	1,0259	1,0262	0,9873		
22	ATZR3	1,3002	1,3002	1,3002	1,2630	1,1503	1,1834	1,3036	1,3368	1,3368	1,3368	0,8750	0,8750	0,9174	0,9514	0,8416	0,9737	0,0000	0,8495	0,8488	0,8162	0,7421	

Figure A5: The distance matrix of the zinc finger domains of the Hep1 orthologues and homologues. The pairwise distance matrix was constructed in MEGAX using the Jones-Taylor-Thornton (JTT) amino acid substitution matrix-model (Gamma distribution: G) using a 1000 replicate bootstrap analysis. The Hep1 sequences aligned in the built in ClustalW multiple sequence alignment platform used to construct the matrix were from: TbgHep1 (Tb972.3.2280), TbbHep1 (Tb927.3.2300), TeqHep1 (TEOVI_000221600), TevHep1 (TevSTIB805.3.2330), TcrHep1 (TcCLB.508479.274), TviHep1 (TvY486_0301660), TcoHep1 (TcIL3000_0_42310), LbrHep1 (LbrM.25.0680), LdoHep1 (LdBPK_250830.1), LmjHep1 (LmjF.25.0800), LmxHep1 (LmxM.25.0800), BsalHep1 (BSAL_79370), CfHep1 (CFAC1_220016500), PfHep1 (PF3D7_1420300), PmalHep1 (PmUG01_13038600), PviHep1 (PVP01_1328600), PberHep1 (PBANKA_1022900), TgoHep1 (TGME49_260340), AtHep1 (NP_974434.2), ScHep1 (NP_014089.2), SpasHep1 (QID81845.1), SparHep1 (XP_033768657.1), CneoHep1 (XP_024514386.1), CalbHep1 (KHC45981.1), HsHep1 (NP_001074318.1), MsmHep1-iso1 (NP_081104.1), BtauHep1 (XP_003586730.1), DmelHep1 (AAS15675.1), DsimHep1 (XP_016039443.1), MdomHep1 (XP_00518472.3), CrHep2 C-term (XP_001700157.1) and ATZR3 (AAO64784.1). Tbb/TeqHep1 refers to the identical TbbHep1 and TeqHep1 orthologues.

Table A6: Details regarding the computational prediction of various physical properties of the Hep1 orthologues and homologues. The characteristics and parameters were computed on the Expasy ProtParam web server. The Hep1 sequences used in this assessment were from: TbgHep1 (Tb972.3.2280), TbbHep1 (Tb927.3.2300), TeqHep1 (TEOVI_000221600), TevHep1 (TevSTIB805.3.2330), TcrHep1 (TcCLB.508479.274), TviHep1 (TvY486_0301660), TcoHep1 (TcIL3000_0_42310), LbrHep1 (LbrM.25.0680), LdoHep1 (LdBPK_250830.1), LmjHep1 (LmjF.25.0800), LmxHep1 (LmxM.25.0800), BsalHep1 (BSAL_79370), CfHep1 (CFAC1_220016500), PfHep1 (PF3D7_1420300), PmalHep1 (PmUG01_13038600), PviHep1 (PVP01_1328600), PberHep1 (PBANKA_1022900), TgoHep1 (TGME49_260340), AtHep1 (NP_974434.2), ScHep1 (NP_014089.2), SpasHep1 (QID81845.1), SparHep1 (XP_033768657.1), CneoHep1 (XP_024514386.1), CalbHep1 (KHC45981.1), HsHep1 (NP_001074318.1), MsmHep1-iso1 (NP_081104.1), BtauHep1 (XP_003586730.1), DmelHep1 (AAS15675.1), DsimHep1 (XP_016039443.1), MdomHep1 (XP_00518472.3), CrHep2 C-term (XP_001700157.1) and ATZR3 (AAO64784.1).

	# AA residues	MW (Da)	pI	Ext-coefficient (oxi/red)	Instability index	Aliphatic index (GRAVY)	Localisation
Tbb/TeqHep1	201	22084.16	7.59	8980/8480	47.84	77.06 (-0.404)	Mitochondria
TbgHep1	201	22142.19	6.95	8980/8480	48.27	77.06 (-0.419)	Mitochondria
TevHep1	201	22170.21	6.95	8980/8480	50.56	77.06 (-0.422)	Mitochondria
TcrHep1	192	21763.75	6.95	15845/15470	51.77	72.55 (-0.547)	Mitochondria
TviHep1	184	20739.73	8.47	18825/18450	57.58	72.07 (-0.476)	Mitochondria
TcoHep1	188	20459.25	8.69	11835/11460	42.28	73.62 (-0.361)	Mitochondria
LbrHep1	220	23295.12	6.37	15845/15470	49.40	69.73 (-0.290)	Mitochondria
LdoHep1	243	25509.90	8.97	15845/15470	57.73	71.73 (-0.263)	Mitochondria
LmjHep1	243	25709.06	8.63	15720/15470	45.77	77.57 (-0.246)	Mitochondria
LmxHep1	243	25328.61	7.07	15845/15470	55.38	74.03 (-0.159)	Mitochondria
BsalHep1	172	18661.17	8.31	15720/15470	56.34	75.93 (-0.298)	Mitochondria
CfHep1	231	24273.37	6.70	14355/13980	65.19	76.49 (-0.230)	Mitochondria
PfHep1	302	35251.30	8.35	16305/15930	34.18	80.96 (-0.992)	Mitochondria
PmalHep1	268	31428.93	9.10	26275/25900	42.79	77.01 (-0.797)	Mitochondria
PviHep1	245	26813.41	8.54	21930/21430	30.39	68.16 (-0.560)	Mitochondria
PberHep1	244	28412.44	9.29	22265/21890	37.01	77.83 (-0.811)	Mitochondria
TgoHep1	262	27046.05	8.53	10595/9970	78.00	73.02 (-0.186)	Mitochondria
AtHep1	223	25003.56	9.04	10220/9970	45.46	77.80 (-0.287)	Mitochondria
ScHep1	174	19855.02	9.49	11835/11460	31.55	78.45 (-0.547)	Mitochondria
SpasHep1	174	19855.02	9.49	11835/11460	31.55	78.45 (-0.547)	Mitochondria
SparHep1	177	20035.20	9.42	6335/5960	31.34	80.90 (-0.514)	Mitochondria
CneoHep1	164	18451.93	9.16	14230/13980	65.54	72.01 (-0.601)	Mitochondria
CalbHep1	184	20723.49	8.97	4720/4470	59.46	83.70 (-0.624)	Mitochondria
HsHep1	178	19203.84	9.88	32220/31970	66.09	76.85 (-0.446)	Mitochondria
MsmHep1-iso1	177	19403.05	9.58	37720/37470	59.78	78.87 (-0.473)	Mitochondria
BtauHep1	169	18485.07	9.61	37720/37470	68.38	78.64 (-0.463)	Mitochondria
DmelHep1	174	19473.44	9.15	11960/11460	36.93	86.32 (-0.305)	Mitochondria
DsimHep1	174	19415.36	9.03	11960/11460	34.56	86.90 (-0.285)	Mitochondria
MdomHep1	175	19515.45	9.62	11710/11460	35.00	86.86 (-0.434)	Mitochondria
CrHep2 C-term	111	12273.91	7.72	7240/6990	41.79	72.07 (-0.442)	Chloroplast
ATZR3	193	21433.31	8.30	10220/9970	47.36	72.23 (-0.377)	Chloroplast

Table A7: Details regarding the computational prediction of molecular weights of the zinc finger domains and N-terminal regions of the Hep1 orthologues and homologues. The Hep1 sequences used in this assessment were from: TbgHep1 (Tb972.3.2280), TbbHep1 **(**Tb927.3.2300), TeqHep1 (TEOVI_000221600), TevHep1 (TevSTIB805.3.2330), TcrHep1 (TcCLB.508479.274), TviHep1 (TvY486_0301660), TcoHep1 (TcIL3000_0_42310), LbrHep1 (LbrM.25.0680), LdoHep1 (LdBPK_250830.1), LmjHep1 (LmjF.25.0800), LmxHep1 (LmxM.25.0800), BsalHep1 (BSAL_79370), CfHep1 (CFAC1_220016500), PfHep1 (PF3D7_1420300), PmalHep1 (PmUG01_13038600), PviHep1 (PVP01_1328600), PberHep1 (PBANKA_1022900), TgoHep1 (TGME49_260340), AtHep1 (NP_974434.2), ScHep1 (NP_014089.2), SpasHep1 (QID81845.1), SparHep1 (XP_033768657.1), CneoHep1 (XP_024514386.1), CalbHep1 (KHC45981.1), HsHep1 (NP_001074318.1), MsmHep1-iso1 (NP_081104.1), BtauHep1 (XP_003586730.1), DmelHep1 (AAS15675.1), DsimHep1 (XP_016039443.1), MdomHep1 (XP_00518472.3), CrHep2 C-term (XP_001700157.1) and ATZR3 (AAO64784.1).

	# AA residues (N-term/zinc finger)	MW (N-term/zinc finger) (Da)	Zinc finger domain (coverage)
Tbb/TeqHep1	113 / 64	12228.04 / 7210.33	114-177
TbgHep1	113 / 64	12286.08 / 7210.33	114-177
TevHep1	113 / 64	12314.09 / 7210.33	114-177
TcrHep1	105 / 64	11884.54 / 7277.45	106-169
TviHep1	105 / 64	11702.44 / 7264.30	106-169
TcoHep1	107 / 64	11297.75 / 7362.55	108-171
LbrHep1	132 / 64	13719.21 / 7147.27	133-196
LdoHep1	147 / 64	15060.91 / 7131.27	148-211
LmjHep1	147 / 64	15360.29 / 7131.27	148-211
LmxHep1	147 / 64	14960.80 / 7158.34	148-211
BsalHep1	86 / 64	8964.16 / 7311.35	87-150
CfHep1	132 / 64	13625.42 / 7311.35	133-196
PfHep1	217 / 64	25446.91 / 7354.56	218-281
PmalHep1	183 / 64	21555.34 / 7395.70	184-247
PviHep1	162 / 64	17242.32 / 7277.48	161-224
PberHep1	161 / 64	18812.28 / 7331.57	160-223
TgoHep1	152 / 64	15074.41 / 7147.46	151-214
AtHep1	137 / 63	15625.98 / 7005.96	137-199
ScHep1	69 / 64	8044.60 / 7332.56	70-133
SpasHep1	69 / 64	8044.60 / 7332.56	70-133
SparHep1	71 / 64	8167.72 / 7332.56	72-135
CneoHep1	77 / 71	8687.81 / 7937.10	77-147
CalbHep1	74 / 64	8245.55 / 7383.32	72-136
HsHep1	75 / 66	8378.56 / 7371.46	70-135
MsmHep1-iso1	75 / 66	8378.56 / 7386.51	74-139
BtauHep1	62 / 66	7084.22 / 7342.46	61-126
DmelHep1	94 / 66	10352.96 / 7554.72	98-163
DsimHep1	94 / 66	10294.88 / 7554.72	93-158
MdomHep1	99 / 65	11026.74 / 7256.18	98-162
CrHep2 C-term	N/A / 64	N/A / 7164.34	N/A
ATZR3	108 / 63	12186.91 / 7021.94	107-169

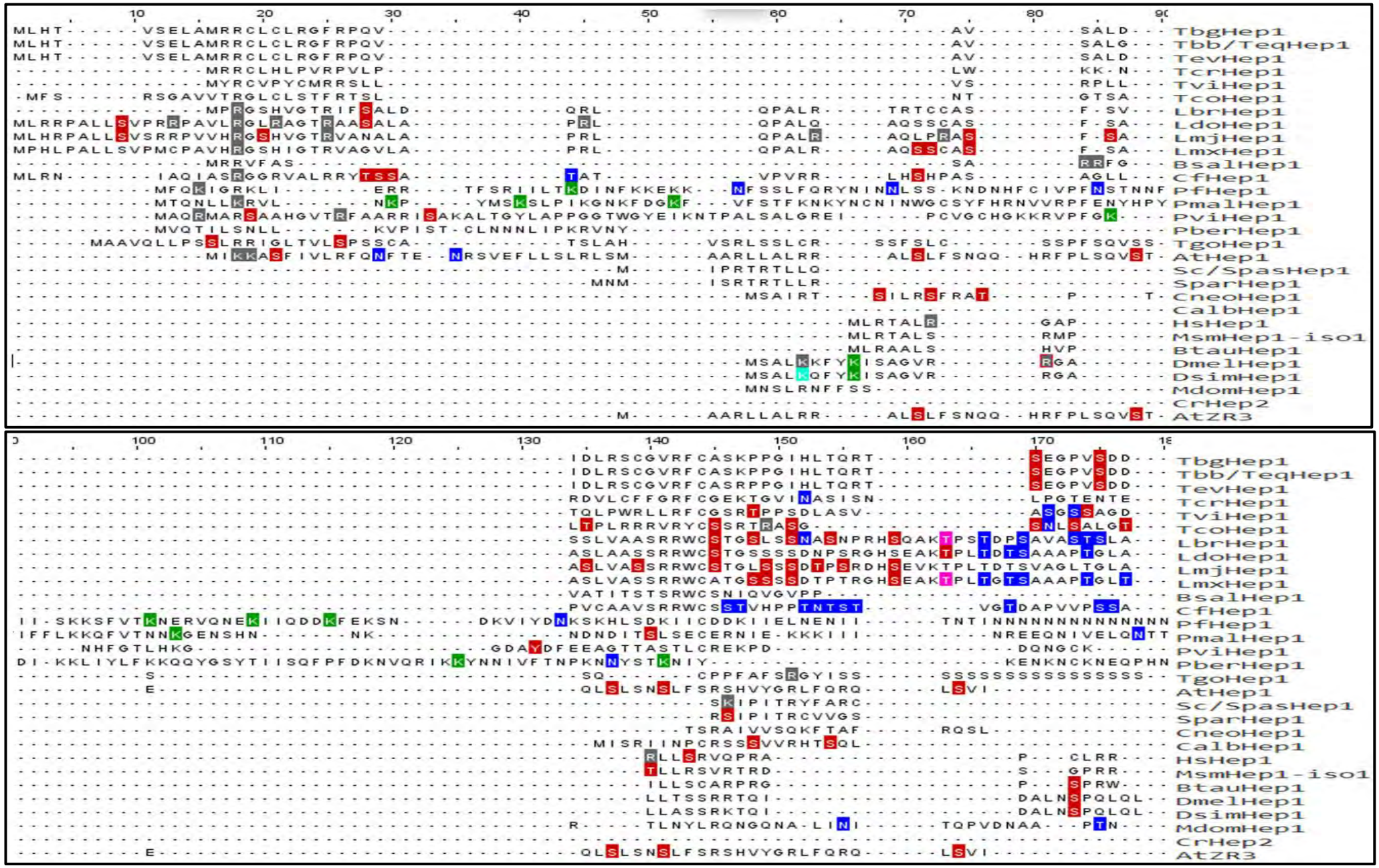
TbgHep1
Tbb/TeqHep1
TevHep1
TcrHep1
TviHep1
TcoHep1
LbrHep1
LdoHep1
LmjHep1
LmxHep1
BsalHep1
CfHep1
PfHep1
PmalHep1
PviHep1
PberHep1
TgoHep1
AtHep1
Sc/SpasHep1
SparHep1
CneoHep1
CalbHep1
HsHep1
MsmHep1-iso1
BtauHep1
DmelHep1
DsimHep1
MdomHep1
CrHep2
AtZR3

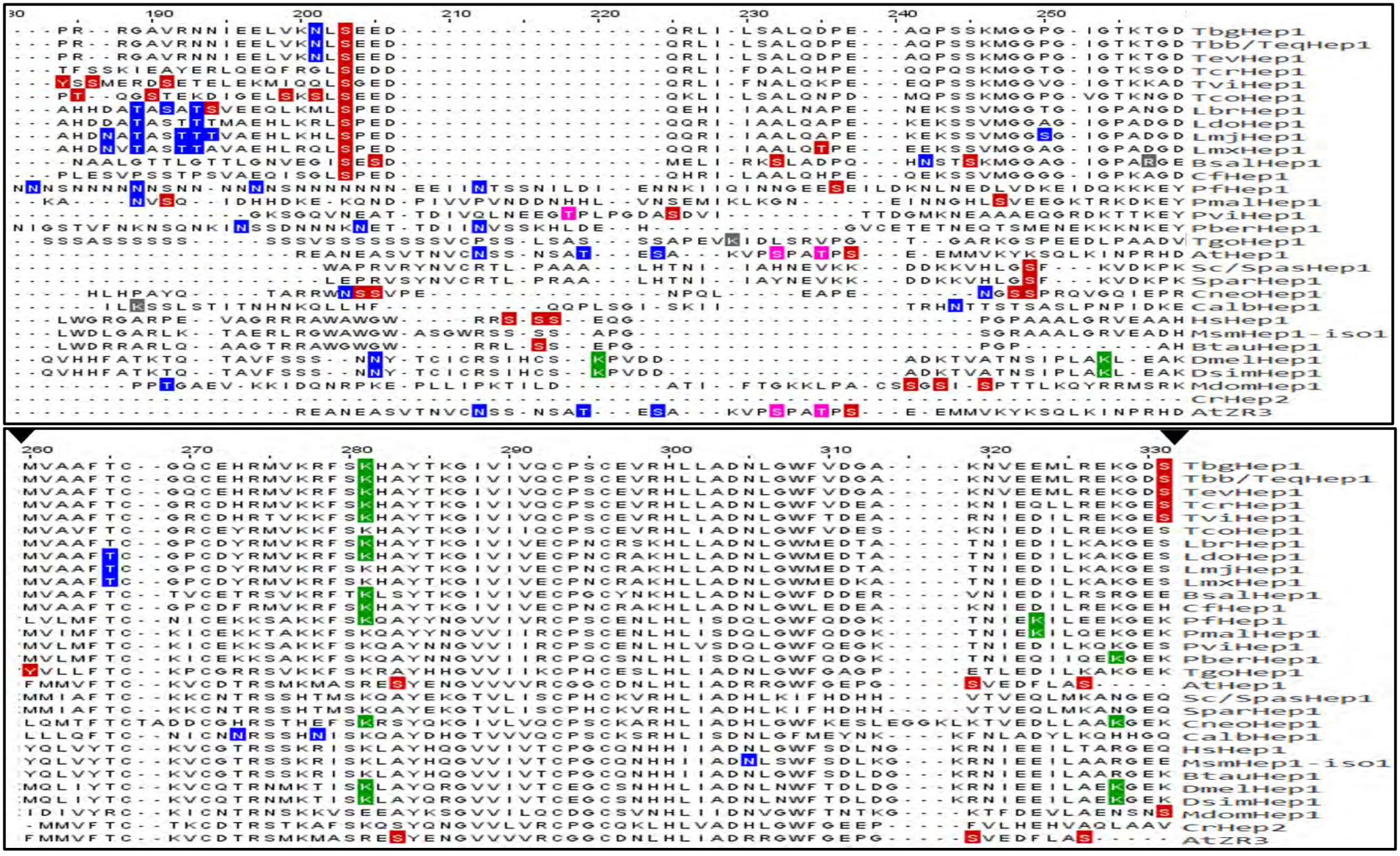
190 200 210 220 230 240 250
TbgHep1
Tbb/TeqHep1
TevHep1
TcrHep1
TviHep1
TcoHep1
LbrHep1
LdoHep1
LmjHep1
LmxHep1
BsalHep1
CfHep1
PfHep1
PmalHep1
PviHep1
PberHep1
TgoHep1
AtHep1
Sc/SpasHep1
SparHep1
CneoHep1
CalbHep1
HsHep1
MsmHep1-iso1
BtauHep1
DmelHep1
DsimHep1
MdomHep1
CrHep2
AtZR3
260 270 280 290 300 310 320 330
TbgHep1
Tbb/TeqHep1
TevHep1
TcrHep1
TviHep1
TcoHep1
LbrHep1
LdoHep1
LmjHep1
LmxHep1
BsalHep1
CfHep1
PfHep1
PmalHep1
PviHep1
PberHep1
TgoHep1
AtHep1
Sc/SpasHep1
SparHep1
CneoHep1
CalbHep1
HsHep1
MsmHep1-iso1
BtauHep1
DmelHep1
DsimHep1
MdomHep1
CrHep2
AtZR3

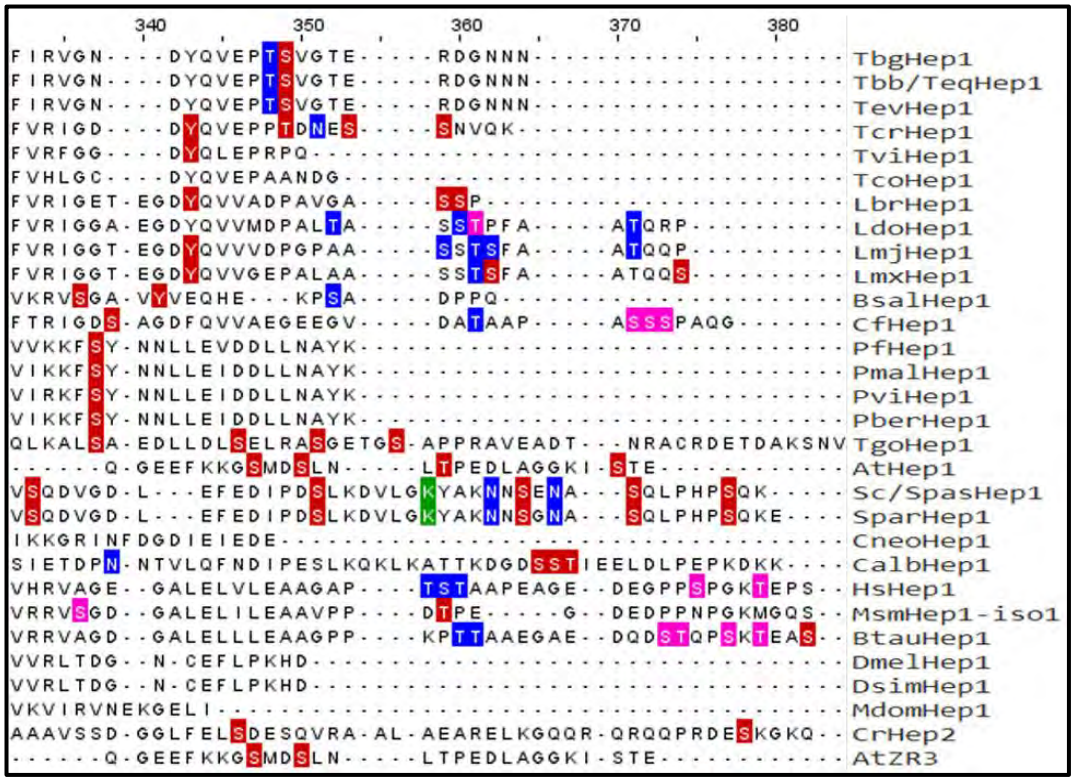

Figure A6: The predicted posttranslational modifications of the Hep1 orthologues. MusiteDeep was used to predict the posttranslational modifications using default settings and annotation was performed using JalView subsequent to conducting a Clustal Omega multiple sequence alignment on the web service. The Hep1 sequences used in this assessment were from: TbgHep1 (Tb972.3.2280), TbbHep1 (Tb927.3.2300), TeqHep1 (TEOVI_000221600), TevHep1 (TevSTIB805.3.2330), TcrHep1 (TcCLB.508479.274), TviHep1 (TvY486_0301660), TcoHep1 (TcIL3000_0_42310), LbrHep1 (LbrM.25.0680), LdoHep1 (LdBPK_250830.1), LmjHep1 (LmjF.25.0800), LmxHep1 (LmxM.25.0800), BsalHep1 (BSAL_79370), CfHep1 (CFAC1_220016500), PfHep1 (PF3D7_1420300), PmalHep1 (PmUG01_13038600), PviHep1 (PVP01_1328600), PberHep1 (PBANKA_1022900), TgoHep1 (TGME49_260340), AtHep1 (NP_974434.2), ScHep1 (NP_014089.2), SpasHep1 (QID81845.1), SparHep1 (XP_033768657.1), CneoHep1 (XP_024514386.1), CalbHep1 (KHC45981.1), HsHep1 (NP_001074318.1), MsmHep1-iso1 (NP_081104.1), BtauHep1 (XP_003586730.1), DmelHep1 (AAS15675.1), DsimHep1 (XP_016039443.1), MdomHep1 (XP_00518472.3), CrHep2 C-term (XP_001700157.1) and ATZR3 (AAO64784.1). Highlighted in red, blue, green and grey are amino acid residues predicted to be subject to phosphorylation, glycosylation, acetylation and methylation, respectively. Highlighted in pink are residues subject to both phosphorylation and glycosylation whilst in turquoise are residues subject to both acetylation and methylation. The arrows serve to demarcate the conserved zinc finger regions. Tbb/TeqHep1 refers to the identical TbbHep1 and TeqHep1 orthologues, whilst Sc/SpasHep1 refers to the identical ScHep1 and SpasHep1 orthologues.

1	Tb927.3.2270 Tb927.3.11280 Tb927.3.2290 Tb927.3.2300 Tb927.3.2310 Tb927.3.2320 Tb27.3.2330 Tb927.3.2340 Tb927.3.2350 Tb927.3.2360 Tb927.3.2370
2	TcCLB.508479.300 TcCLB.508479.290 TcCLB.508479.280 TcCLB.508479.274 TcCLB.508479.270 TcCLB.508479.260 TcCLB.508479.250 TcCLB.508479.240 TcCLB.508479.230 TcCLB.508479.224 TcCLB.508479.220 TcCLB.508479.216
3	Bsal_79355 Bsal_79360 Bsal_79365 Bsal_79370 Bsal_79375 Bsal_79380 Bsal_79385 Bsal_79390 Bsal_79395 Bsal_7979400 Bsal_79405 Bsal_79410
4	LmjF.25.0770 LmjF.25.0780 LmjF.25.0790 LmjF.25.0800 LmjF.25.0810 LmjF.25.0820 LmjF.25.0830 LmjF.25.0840
5	LbrM.25.0650 LbrM.25.0660 LbrM.25.0670 LbrM.25.0680 LbrM.25.0690 LbrM.25.0700 LbrM.25.0710 LbrM.25.0720
6	Cfac1_220016000 Cfac1_220016100 Cfac1_220016200 Cfac1_220016300 Cfac1_220016400 Cfac1_220016500 Cfac1_220016600 Cfac1_220016700 Cfac1_220016800 Cfac1_220016900 Cfac1_220017000
7	PF3D7_1420000 PF3D7_1420100 PF3D7_1420200 PF3D7_1420300 PF3D7_1420400 PF3D7_1420500 PF3D7_1420600 PF3D7_1420700 PF3D7_1420800
8	PBANKA_1023200 PBANKA_1023100 PBANKA_1023000 PBANKA_1022900 PBANKA_1022800 PBANKA_1022700 PBANKA_1022600 PBANKA_1022500 PBANKA_1022400
9	PmuG01_13038900 PmuG01_13038800 PmuG01_13008700 PmuG01_13038600 PmuG01_13038500 PmuG01_13038400 PmuG01_13038300 PmuG01_13038200 PmuG01_13038100
10	Tgme49_260390 Tgme49_260380 Tgme49_260375 Tgme49_260360 Tgme49_260340 Tgme49_260330 Tgme49_260325 Tgme49_260320
11	S000005257 S000005256 S000005255 S000005254 S000005253 S000005252 S000005251
12	FBgn0030674 FBgn0030675 FBpp0271786 FBgn0026666 FBgn0011741 FBgn0030678

Figure A7: The database accession IDs of the genes appearing in Figure 2.8 whereby the syntenic analysis of the various Hep1 orthologues is laid out. The accession numbers are listed from left to right as the respective genes they represent appear in Figure 2.8. **1)** *T. b. brucei*. **2)** *T. cruzi*, **3)** *B. saltans*, **4)** *L. major*, **5)** *L. braziliensis*, **6)** *C. fasciculata*, **7)** *P. falciparum*, **8)** *P.berghei*, **9)** *P. malariae* **10)** *T. gondii*, **11)** *S. cerevisiae* and **12)** *D. melanogaster*.

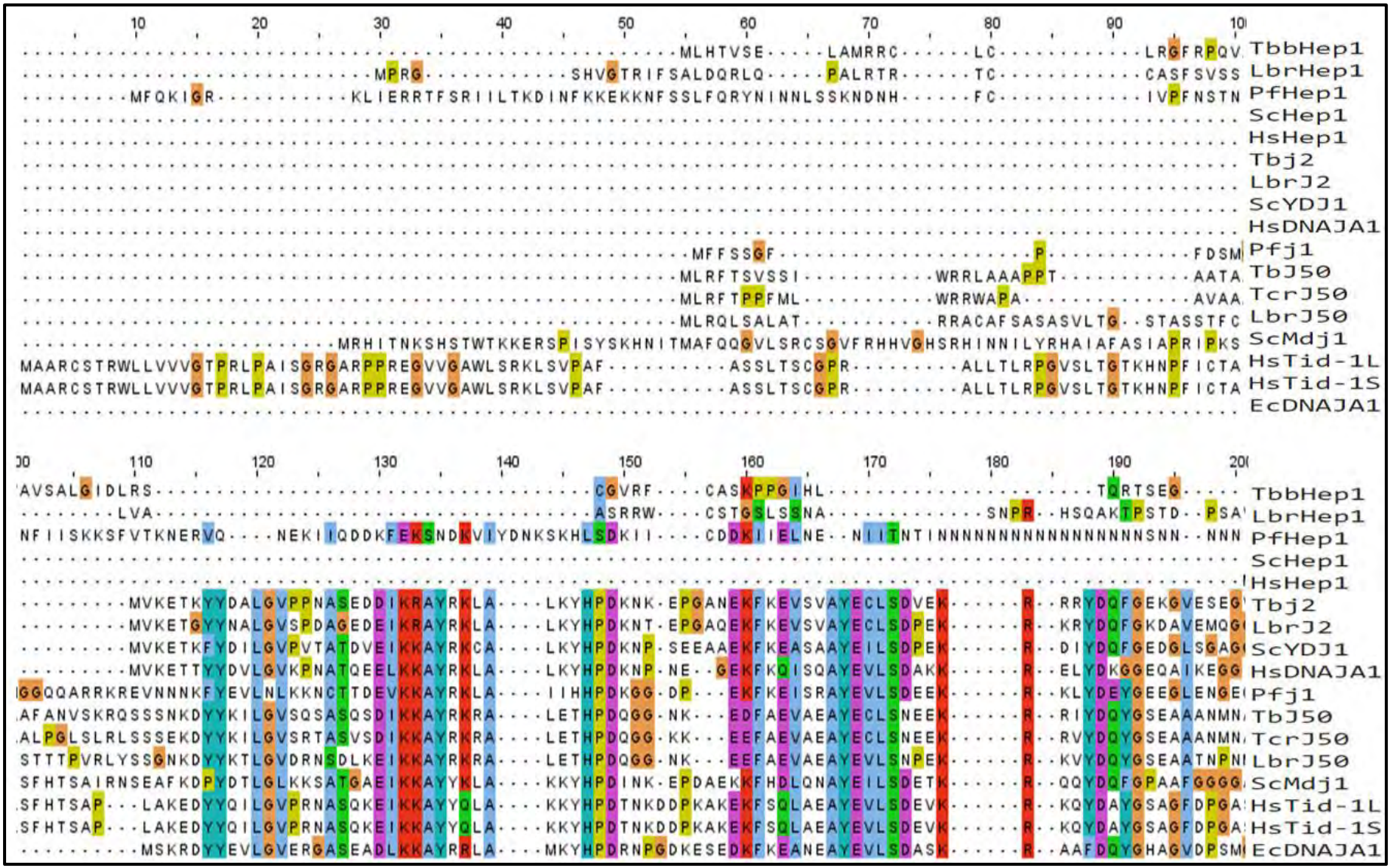
TbbHep1
LbrHep1
PfHep1
ScHep1
HsHep1
Tbj2
LbrJ2
ScYDJ1
HsDNAJA1
Pfj1
TbJ50
TcrJ50
LbrJ50
ScMdj1
HsTid-1L
HsTid-1S
EcDNAJA1

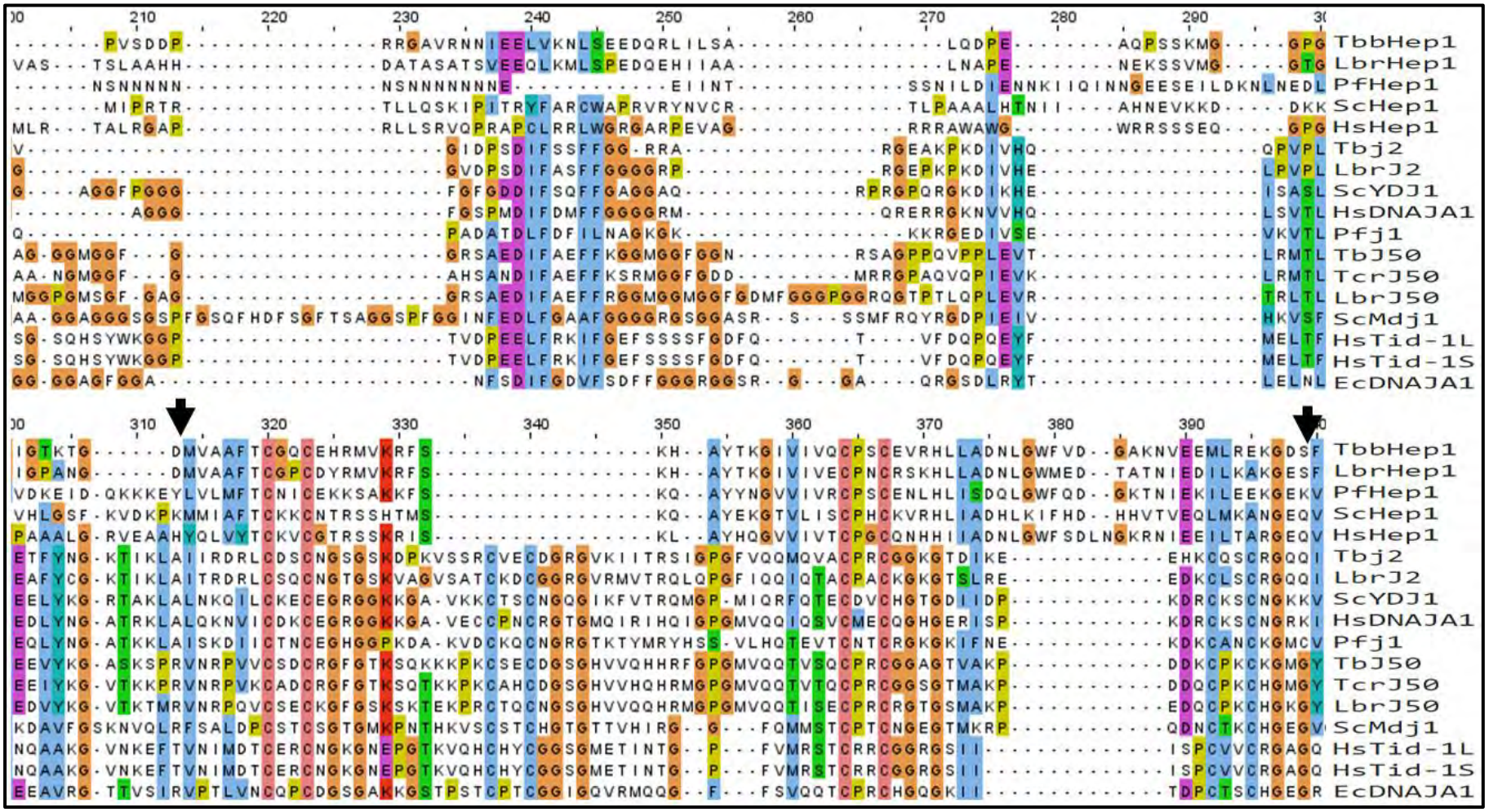
TbbHep1
LbrHep1
PfHep1
ScHep1
HsHep1
Tbj2
LbrJ2
ScYDJ1
HsDNAJA1
Pfj1
TbJ50
TcrJ50
LbrJ50
ScMdj1
HsTid-1L
HsTid-1S
EcDNAJA1

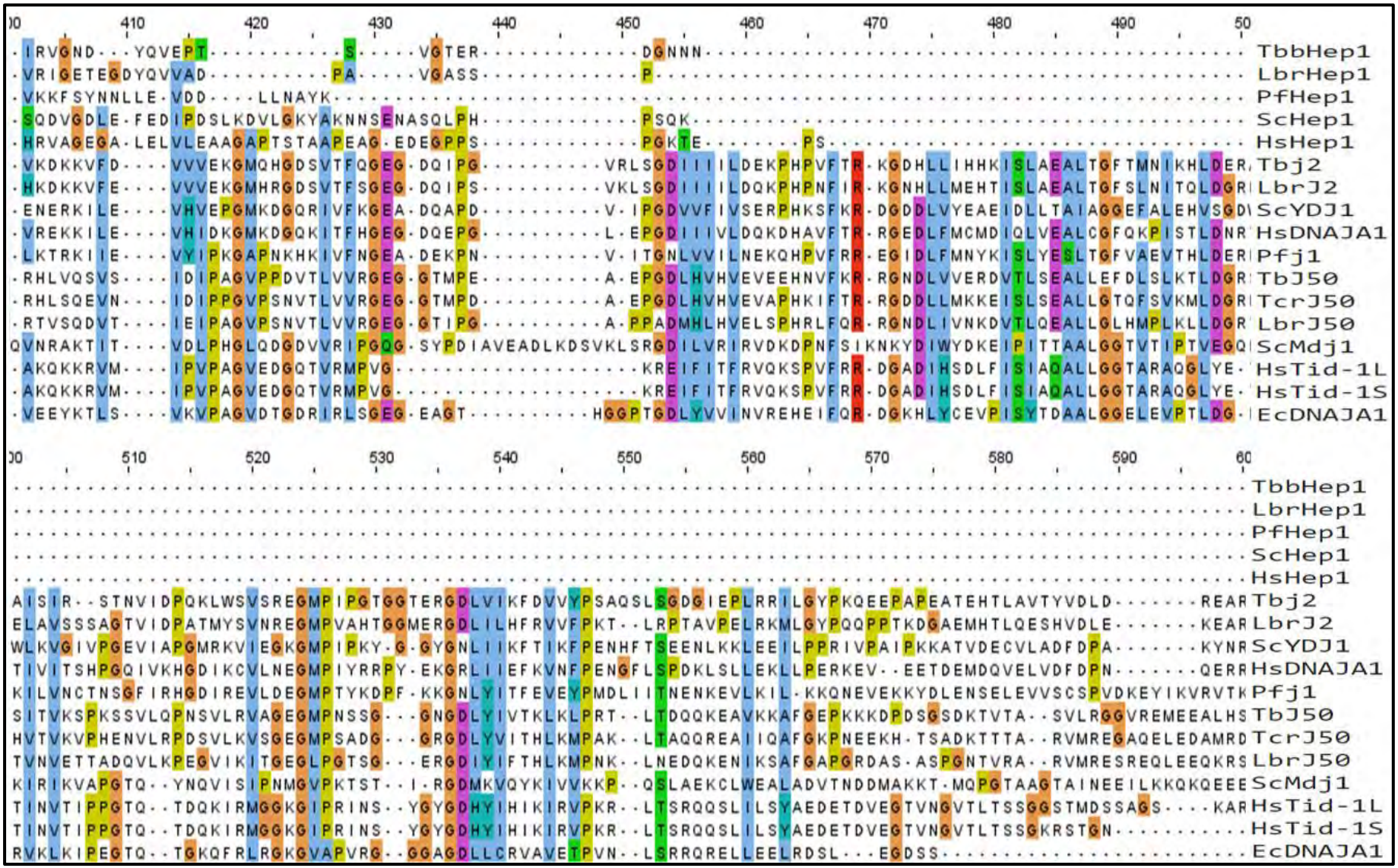
TbbHep1
LbrHep1
PfHep1
ScHep1
HsHep1
Tbj2
LbrJ2
ScYDJ1
HsDNAJA1
Pfj1
TbJ50
TcrJ50
LbrJ50
ScMdj1
HsTid-1L
HsTid-1S
EcDNAJA1

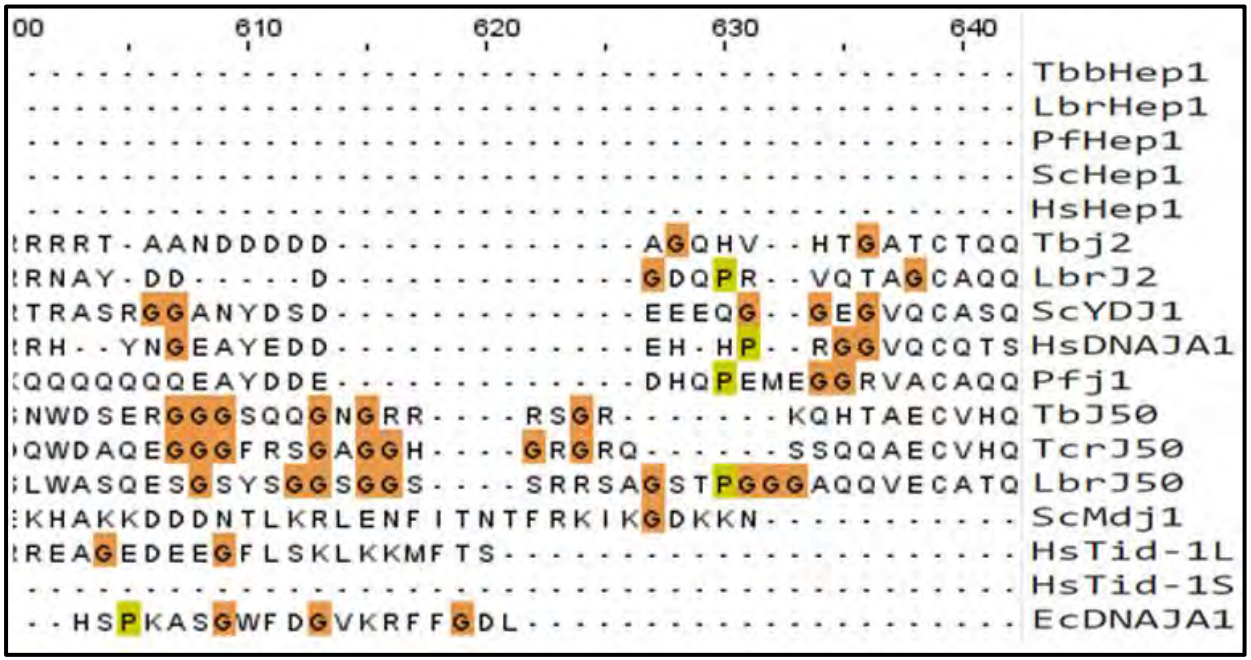

Figure A8: The Clustal Omega multiple sequence alignment (MSA) of the Hep1 and J-protein orthologues. The sequences were aligned using the built in Clustal Omega MSA platform on the JalView web service. The annotation is based on the JalView Clustal colour option. The sequences used for this MSA were from: TbbHep1 (Tb927.3.2300), LbrHep1 (LbrM.25.0680), PfHep1 (PF3D7_1420300), ScHep1 (NP_014089.2), HsHep1 (NP_001074318.1). The cytosolic and mitochondrial and prokaryotic type I J-protein sequences used for this assessment were from: Tbj2 (Tb927.2.5160), Lbrj2 (LbrM.27.2610), ScYdj1 (NP_014335.1), HsDNAJA1 (NP_001530.1), Tbj50 (Tb927.9.12730), Tcrj50 (TcCLB.510743.100), Lbrj50 (LbrM.34.2890), Pfj1 (PF3D7_1437900), ScMdj1 (QHB08320.1), HsTid-1L (NP_005138.3), HsTid-1S (NP_001128582.1) and EcDNAJA1 (MRF42610.1).

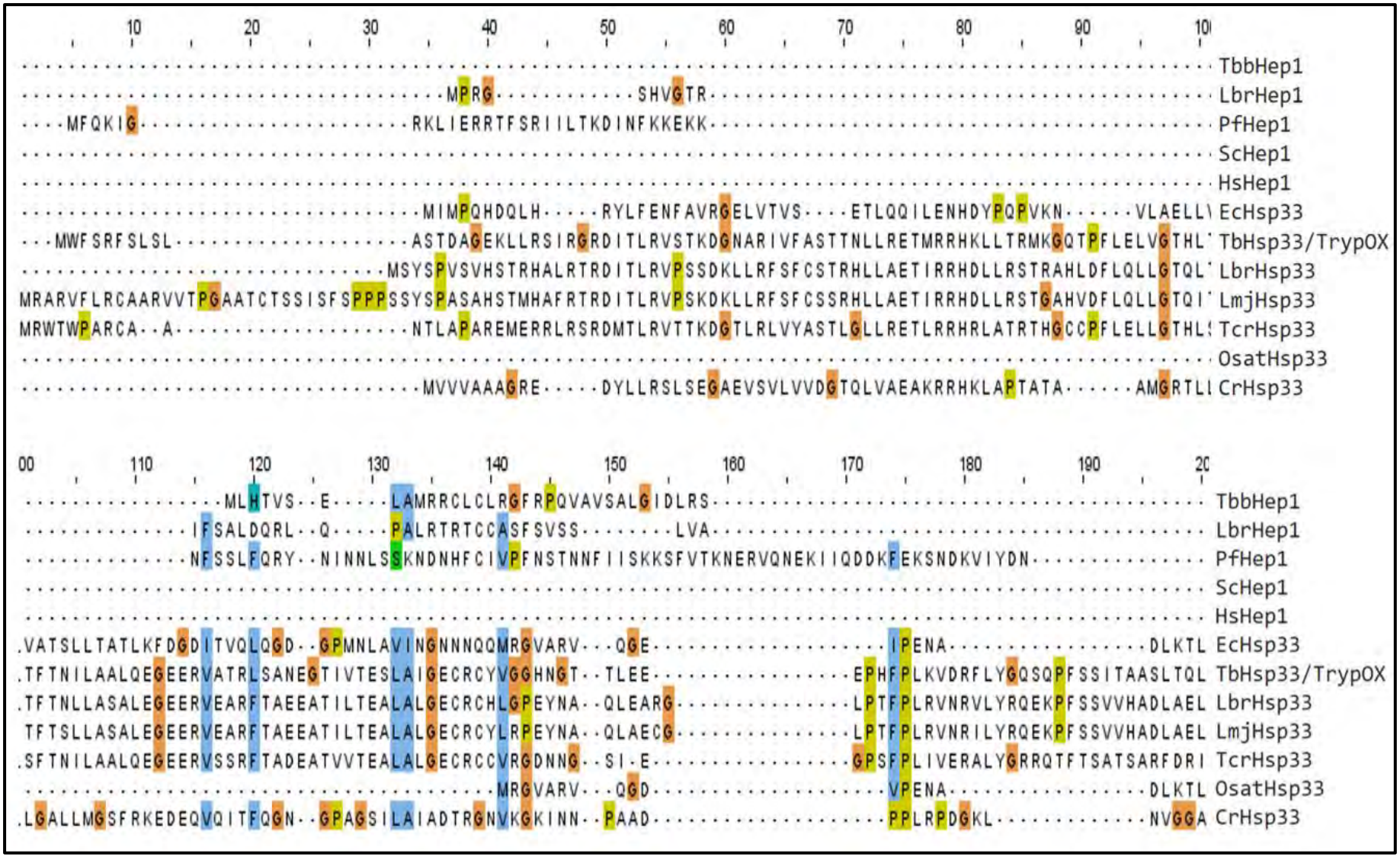
10 20 30 40 50 60 70 80 90 10
TbbHep1
LbrHep1
PfHep1
ScHep1
HsHep1
EcHsp33
TbHsp33/TrypOX
LbrHsp33
LmjHsp33
TcrHsp33
OsatHsp33
CrHsp33
00 110 120 130 140 150 160 170 180 190 20
TbbHep1
LbrHep1
PfHep1
ScHep1
HsHep1
EcHsp33
TbHsp33/TrypOX
LbrHsp33
LmjHsp33
TcrHsp33
OsatHsp33
CrHsp33

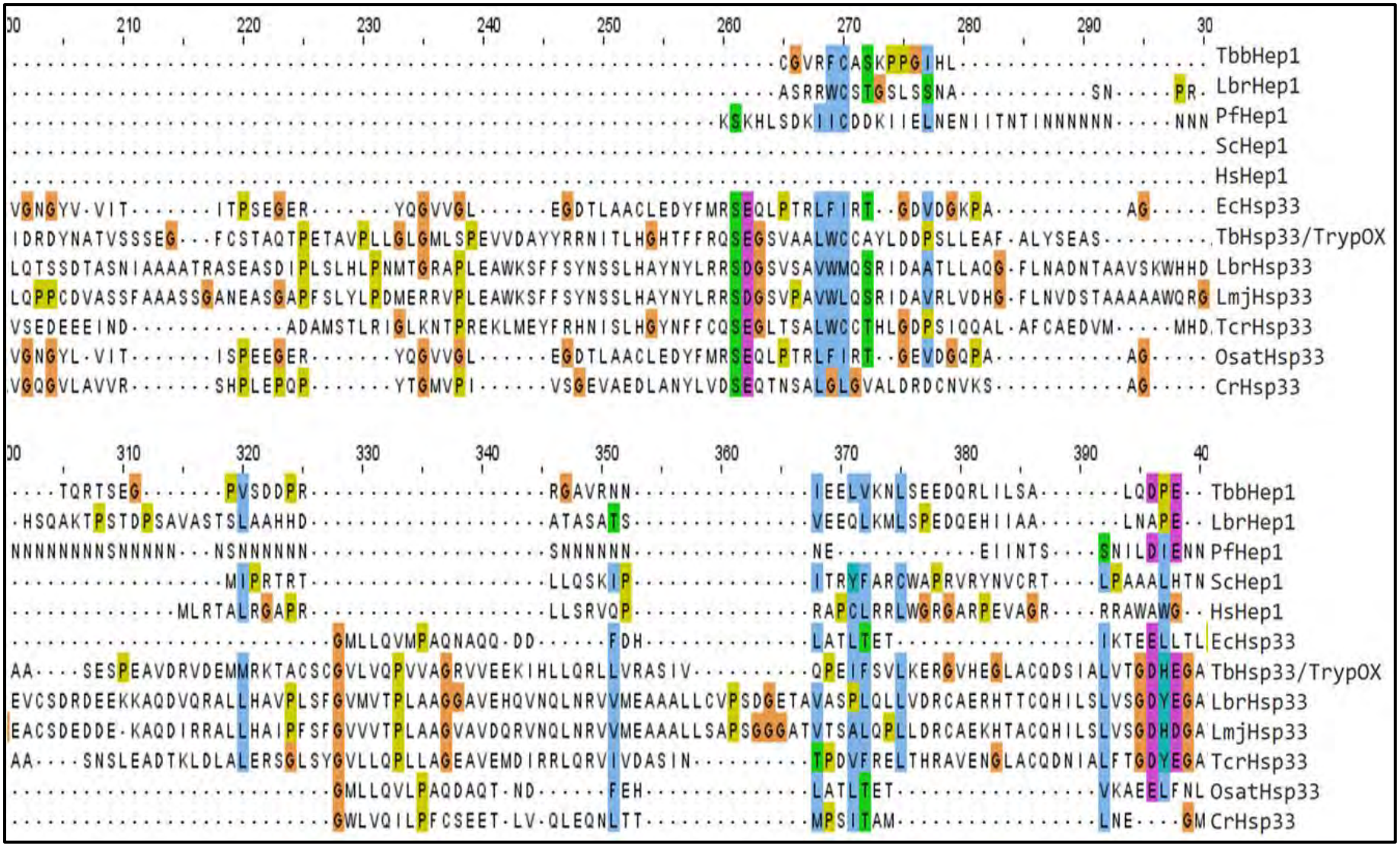
200 210 220 230 240 250 260 270 280 290 300
TbbHep1
LbrHep1
PfHep1
ScHep1
HsHep1
EcHsp33
TbHsp33/TrypOX
LbrHsp33
LmjHsp33
TcrHsp33
OsatHsp33
CrHsp33
300 310 320 330 340 350 360 370 380 390 400
TbbHep1
LbrHep1
PfHep1
ScHep1
HsHep1
EcHsp33
TbHsp33/TrypOX
LbrHsp33
LmjHsp33
TcrHsp33
OsatHsp33
CrHsp33

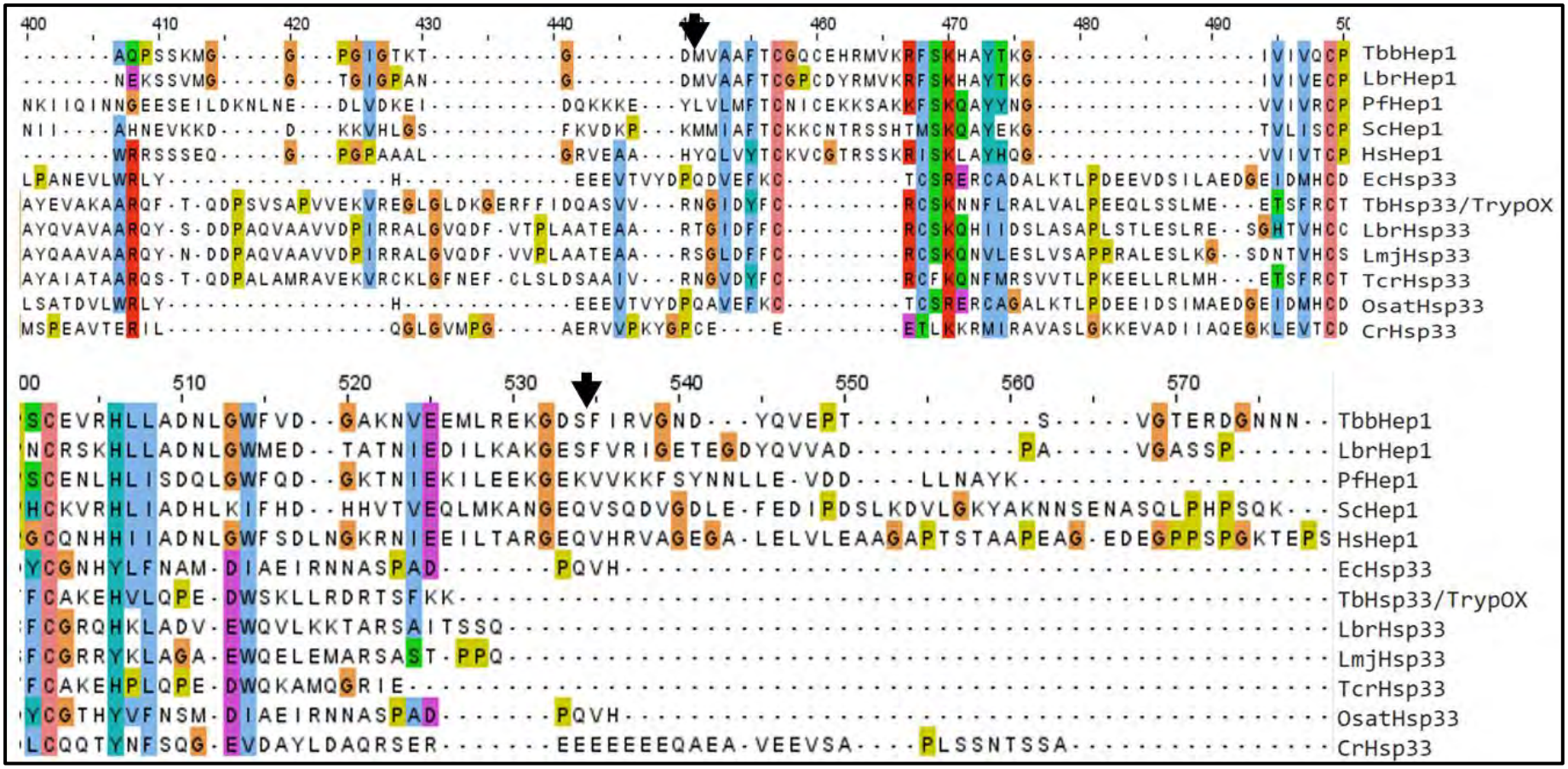

Figure A9: The Clustal Omega multiple sequence alignment (MSA) of the Hep1 and Hsp33 orthologues. The sequences were aligned using the built in Clustal Omega MSA platform on the JalView web service. The annotation is based on the JalView Clustal colour option. The sequences used for this MSA were from: TbbHep1 (Tb927.3.2300), LbrHep1 (LbrM.25.0680), PfHep1 (PF3D7_1420300), ScHep1 (NP_014089.2), HsHep1 (NP_001074318.1). The Hsp33 sequences used for this assessment were from: EcHsp33 (EDV67745.1), TbHsp33/TrypOX (Tb927.6.2630), LbrHsp33 (LBRM2903_300022900), LmjHsp33 (LmjF.30.1670), TcrHsp33 (TcCLB.509965.120), OsatHsp33 (EEC84194.1) and CrHsp33 (PNW70318.1).

A

		1	2	3	4	5	6	7	8	9	10	11	12	13	14	15	16
1	TbbHep1																
2	LbrHep1	0,7966															
3	PfHep1	2,1160	2,0587														
4	ScHep1	2,5834	2,2490	2,3023													
5	HsHep1	2,3879	2,2895	2,7016	2,0599												
6	Tbj2	3,4448	3,7331	5,0949	3,6321	3,7770											
7	LbrJ2	3,0794	3,6648	4,8551	3,1970	3,1504	0,3185										
8	ScYDJ1	3,7000	3,7734	4,4697	3,5796	4,0214	1,1769	1,1429									
9	HsDNAJA1	4,1630	4,0424	4,9278	4,4778	4,1216	0,9686	0,9815	0,7798								
10	Pfj1	4,2619	4,5536	4,9773	4,0478	4,4766	1,2527	1,1803	1,2863	1,1414							
11	TbJ50	4,0792	4,3648	5,4351	4,9854	5,0809	1,5274	1,6328	1,7473	1,8401	1,6297						
12	LbrJ50	4,2154	4,6545	6,4665	5,0499	5,5559	1,5156	1,5840	1,5683	1,6706	1,5326	0,3578					
13	ScMdj1	5,0162	5,0876	6,3352	4,1000	5,5482	1,8108	1,7289	2,0635	2,1125	2,2741	1,6322	1,5088				
14	HsTid-1L	4,6749	4,7509	4,6095	4,3449	4,3111	2,0526	2,1484	2,1076	2,0476	2,2067	1,7827	1,6672	1,4751			
15	HsTid-1S	4,6749	4,7509	4,6095	4,3449	4,3111	2,0526	2,1484	2,1076	2,0476	2,2067	1,7827	1,6672	1,4751	0,0000		
16	EcDNAJA1	3,5555	3,4493	4,8397	3,9980	3,6898	1,5450	1,4444	1,5175	1,5464	1,8955	1,5876	1,6711	1,3735	1,4335	1,4335	

B

		1	2	3	4	5	6	7	8	9	10	11	12
1	TbbHep1												
2	LbrHep1	0,6527											
3	PfHep1	1,5048	1,4397										
4	ScHep1	2,0043	1,6764	1,9243									
5	HsHep1	1,6153	1,7264	1,9924	1,8027								
6	EcHsp33	5,2249	6,6804	5,8620	7,9413	9,1286							
7	TbHsp33/TrypOX	5,1035	5,5475	5,9568	6,4145	5,8229	2,5336						
8	LbrHsp33	4,3087	4,3680	6,9231	5,1786	6,6288	3,0423	1,4896					
9	LmjHsp33	4,5220	4,4261	6,7082	5,0000	5,6649	3,1038	1,4294	0,2233				
10	TcrHsp33	4,5276	5,3343	6,3295	7,7065	4,8576	2,8677	0,8813	1,5115	1,4516			
11	OsatHsp33	5,3549	7,1345	6,5450	7,9093	8,7301	0,1602	2,4453	3,1343	3,1811	2,6898		
12	CrHsp33	5,7875	4,8139	5,4069	6,2432	5,9981	2,7881	3,8891	4,6655	4,3225	3,7203	2,9036	

Figure A10: The distance matrix of the of selected Hep1 orthologues with selected A) J-protein orthologues or B) Hsp33 orthologues. The pairwise distance matrix was constructed in MEGAX using the Jones-Taylor-Thornton (JTT) amino acid substitution matrix-model (Gamma distribution: G) with a 1000 replicate bootstrap analysis. The Hep1 sequences aligned in the built in ClustalW multiple sequence alignment platform used to construct the matrix were from: TbbHep1 **(**Tb927.3.2300), LbrHep1 (LbrM.25.0680), PfHep1 (PF3D7_1420300), ScHep1 (NP_014089.2), HsHep1 (NP_001074318.1). The cytosolic and mitochondrial and prokaryotic type I J-protein sequences used for this assessment were from: Tbj2 (Tb927.2.5160), Lbrj2 (LbrM.27.2610), ScYdj1 (NP_014335.1), HsDNAJA1 (NP_001530.1), Tbj50 (Tb927.9.12730), Lbrj50 (LbrM.34.2890), Pfj1 (PF3D7_1437900), ScMdj1 (QHB08320.1), HsTid-1L (NP_005138.3), HsTid-1S (NP_001128582.1) and EcDNAJA1 (MRF42610.1). The Hsp33 sequences used for this assessment were from: EcHsp33 (EDV67745.1), TbHsp33/TrypOX (Tb927.6.2630), LbrHsp33 (LBRM2903_300022900), LmjHsp33 (LmjF.30.1670), TcrHsp33 (TcCLB.509965.120), OsatHsp33 (EEC84194.1) and CrHsp33 (PNW70318.1).

A

		1	2	3	4	5	6	7	8	9	10	11	12	13	14	15	16
1	MsmHep1-iso1																
2	MpHep1-iso1	0,0251															
3	McarHep1-iso1	0,0083	0,0336														
4	McouHep1-iso1	0,0510	0,0698	0,0519													
5	GsurHep1-iso1	0,1050	0,1239	0,1141	0,1343												
6	AsylHep1-iso1	0,0784	0,1062	0,0874	0,1065	0,1654											
7	NgalHep1-iso1	0,2403	0,2630	0,2424	0,2881	0,2740	0,2713										
8	NgalHep1-iso2	0,2403	0,2630	0,2424	0,2881	0,2740	0,2713	0,0000									
9	HmolHep1-iso1	0,4040	0,4329	0,4168	0,4662	0,4319	0,4214	0,4000	0,4000								
10	HmolHep1-iso2	0,4069	0,4363	0,4199	0,4701	0,4393	0,4246	0,4028	0,4028	0,0558							
11	HmolHep1-iso3	0,4040	0,4329	0,4168	0,4662	0,4319	0,4214	0,4000	0,4000	0,0000	0,0558						
12	HmolHep1-iso4	0,3345	0,3607	0,3463	0,3908	0,3747	0,3489	0,3303	0,3303	0,0462	0,0462	0,0462					
13	CjacHep1-iso1	0,3281	0,3589	0,3399	0,3446	0,3702	0,3621	0,3789	0,3789	0,1996	0,2002	0,1996	0,1406				
14	CjacHep1-iso2	0,4199	0,4552	0,4329	0,4391	0,4669	0,4591	0,4776	0,4776	0,2405	0,2397	0,2405	0,2125	0,0640			
15	HsHep1	0,2999	0,3249	0,3114	0,3478	0,3586	0,3242	0,3261	0,3261	0,1030	0,1032	0,1030	0,0528	0,1375	0,2175		
16	BtauHep1	0,3112	0,3366	0,3227	0,3682	0,3830	0,3865	0,3466	0,3466	0,2936	0,3018	0,2936	0,2409	0,2743	0,3765	0,2495	

B

		1	2	3	4	5	6	7	8	9	10	11
1	MsmHep1-iso2											
2	MsmHep1-iso3	0,0284										
3	MpHep1-iso2	0,0724	0,0406									
4	MpHep1-iso3	0,0540	0,0714	0,0278								
5	McarHep1-iso2	0,0427	0,0133	0,0545	0,0861							
6	McouHep1-iso2	0,1334	0,0973	0,1305	0,1679	0,1000						
7	McouHep1-iso3	0,1109	0,1317	0,1679	0,1290	0,1352	0,0283					
8	GsurHep1-iso2	0,2507	0,2060	0,2403	0,2847	0,2220	0,2765	0,3234				
9	AsylHep1-iso2	0,1812	0,1598	0,2090	0,2299	0,1753	0,2259	0,2474	0,3549			
10	NgalHep1-iso3	0,4259	0,3867	0,4308	0,4679	0,3919	0,5010	0,5418	0,4765	0,4778		
11	NgalHep1-iso4	0,3825	0,4224	0,4690	0,4048	0,4280	0,5432	0,4726	0,5174	0,5012	0,0296	

Figure A11: Phylogenetic analysis of the mammalian Hep1 orthologues/isoforms possessing A) or lacking B) a zf-DNL domain. The maximum-likelihood tree was constructed using MEGAX with the Jones-Taylor (JTT) amino acid substitution model with Gamma distribution (G) from the built in ClustalW platform. The sequences used for the assessment presented in **A)** were from: MsmHep1-iso1 (NP_081104.1), MpHep1-iso1 (XP_021050144.1), McarHep1-iso1 (XP_021011688.1), McouHep1-iso1 (XP_031225303.1), GsurHep1-iso1 (XP_028628786.1), NgalHep1-iso1 (XP_029423617.1), NgalHep1-iso2 (XP_017655799.2), HmolHep1-iso1 (XP_032021543.1), HmolHep1-iso2 (XP_032021544.1), HmolHep1-iso3 (XP_032021545.1), HmolHep1-iso4 (XP_032021546.1), CjacHep1-iso1 (XP_035119009.1) and CjacHep1-iso2 (XP_035119020.1). The sequences used in the assessment presented in **B)** were from: MsmHep1-iso2 (NP_001132975.1), MsmHep1-iso3 (NP_001132976.1), MpHep1-iso2 (XP_021050145.1), MpHep1-iso3 (XP_021050146.1), McarHep1-iso2 (XP_021011689.1), McouHep1-iso2 (XP_031225305.1), McouHep1-iso3 (XP_031225306.1), GsurHep1-iso2 (XP_028628787.1), AsylHep1-iso2 (XP_052037846.1), NgalHep1-iso3 (XP_017655800.1) and NgalHep1-iso4 (XP_029423618.1).

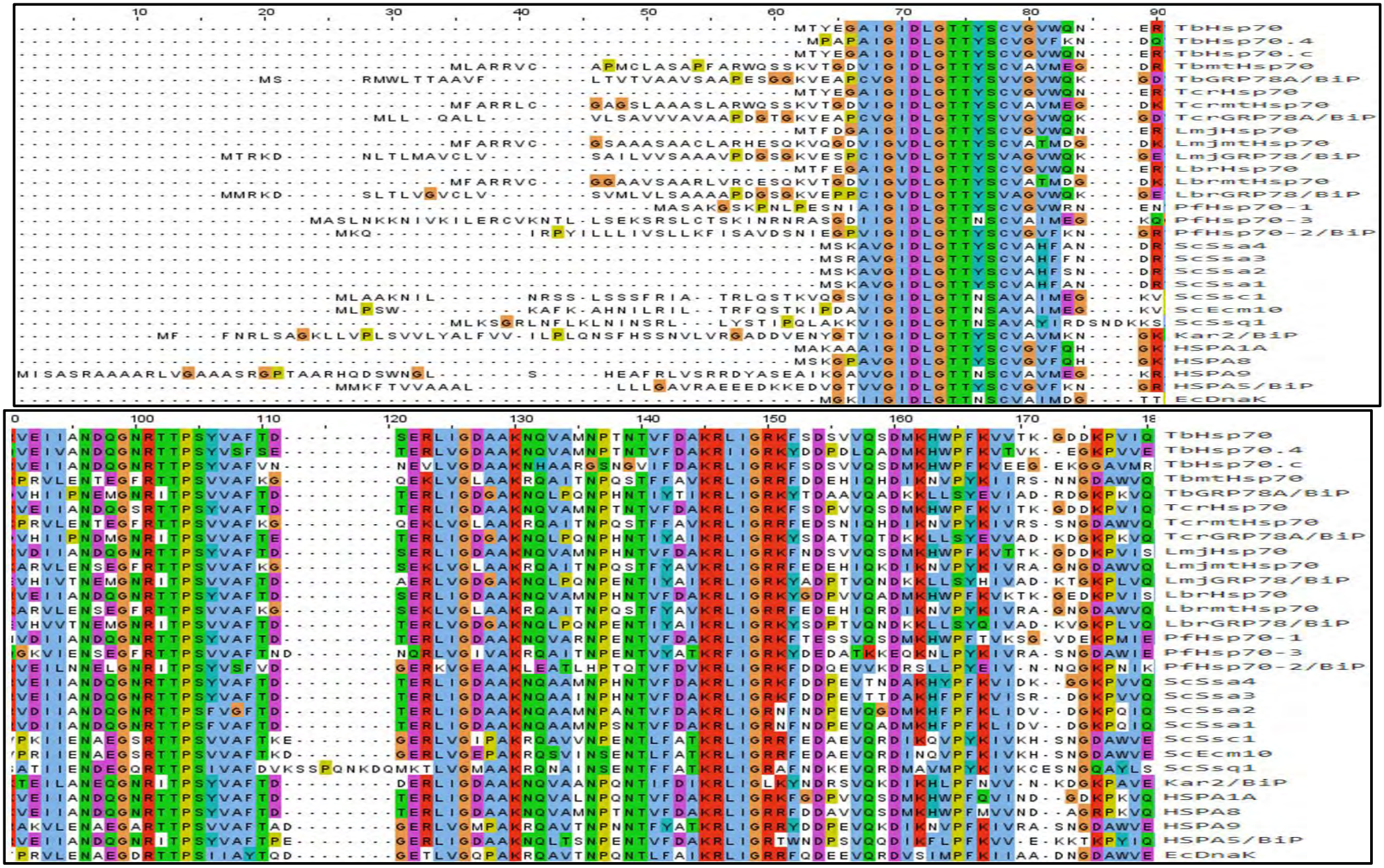

XXX

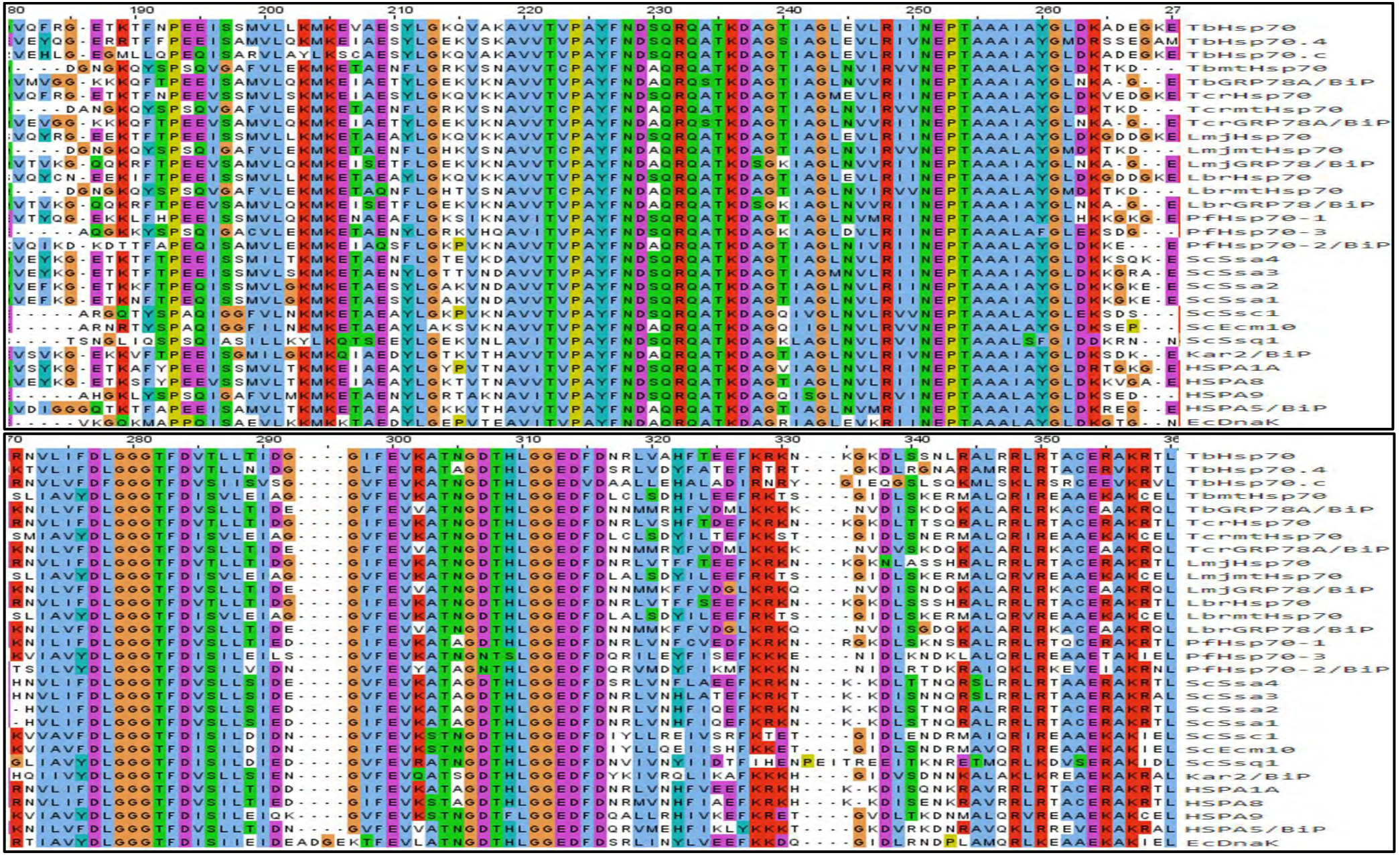
80 190 200 210 220 230 240 250 260 27
TbHsp70
TbHsp70.4
TbHsp70.c
TbmtHsp70
TbGRP78A/BiP
TcrHsp70
TcrmtHsp70
TcrGRP78A/BiP
LmjHsp70
LmjmtHsp70
LmjGRP78/BiP
LbrHsp70
LbrmtHsp70
LbrGRP78/BiP
PfHsp70-1
PfHsp70-3
PfHsp70-2/BiP
ScSsa4
ScSsa3
ScSsa2
ScSsa1
ScSsc1
ScEcm10
ScSsq1
Kar2/BiP
HSPA1A
HSPA8
HSPA9
HSPA5/BiP
EcDnaK
70 280 290 300 310 320 330 340 350 36
TbHsp70
TbHsp70.4
TbHsp70.c
TbmtHsp70
TbGRP78A/BiP
TcrHsp70
TcrmtHsp70
TcrGRP78A/BiP
LmjHsp70
LmjmtHsp70
LmjGRP78/BiP
LbrHsp70
LbrmtHsp70
LbrGRP78/BiP
PfHsp70-1
PfHsp70-3
PfHsp70-2/BiP
ScSsa4
ScSsa3
ScSsa2
ScSsa1
ScSsc1
ScEcm10
ScSsq1
Kar2/BiP
HSPA1A
HSPA8
HSPA9
HSPA5/BiP
EcDnaK

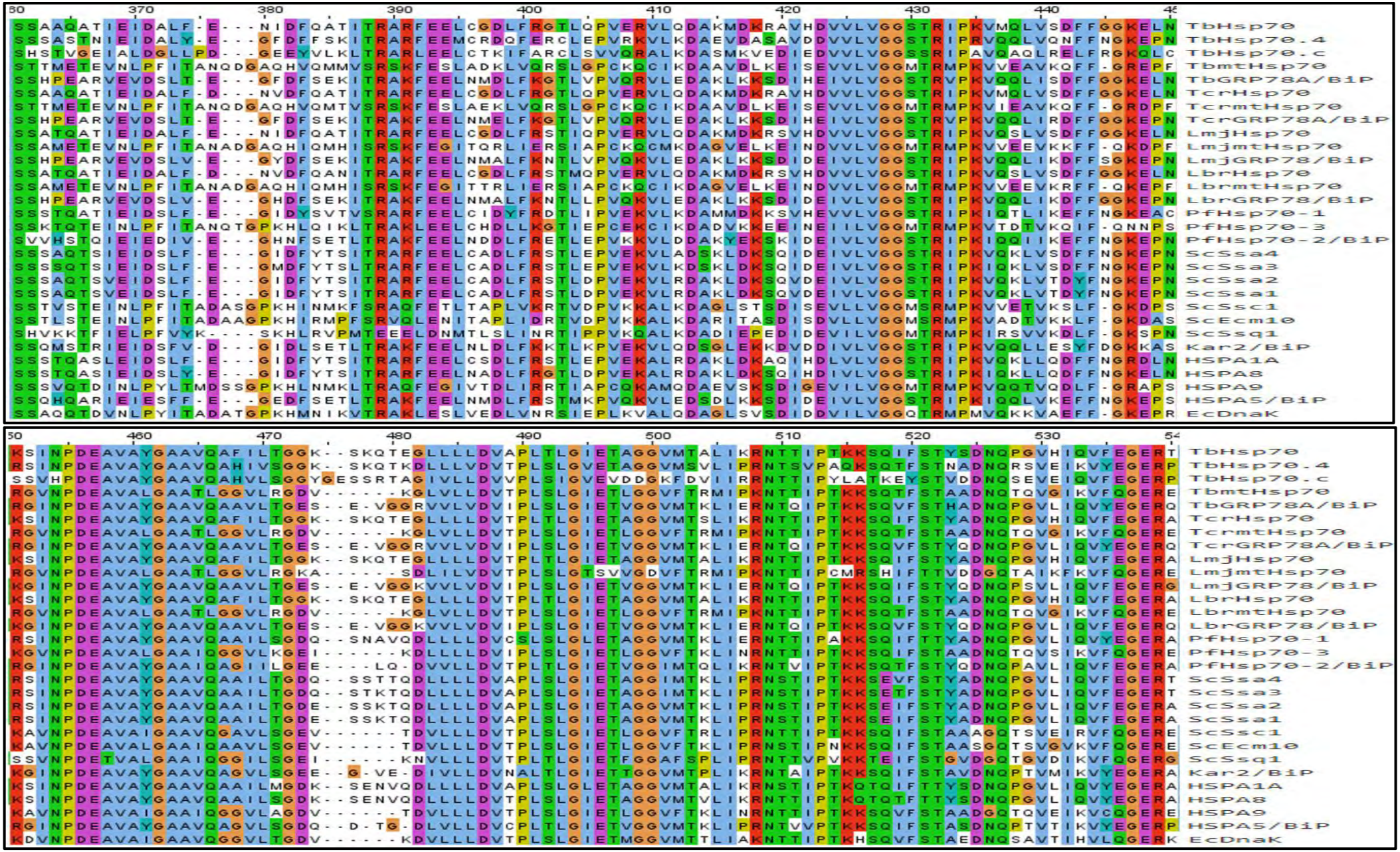
TbHsp70
TbHsp70.4
TbHsp70.c
TbmtHsp70
TbGRP78A/BiP
TcrHsp70
TcrmtHsp70
TcrGRP78A/BiP
LmjHsp70
LmjmtHsp70
LmjGRP78/BiP
LbrHsp70
LbrmtHsp70
LbrGRP78/BiP
PfHsp70-1
PfHsp70-3
PfHsp70-2/BiP
ScSsa4
ScSsa3
ScSsa2
ScSsa1
ScSsc1
ScEcm10
ScSsq1
Kar2/BiP
HSPA1A
HSPA8
HSPA9
HSPA5/BiP
EcDnaK

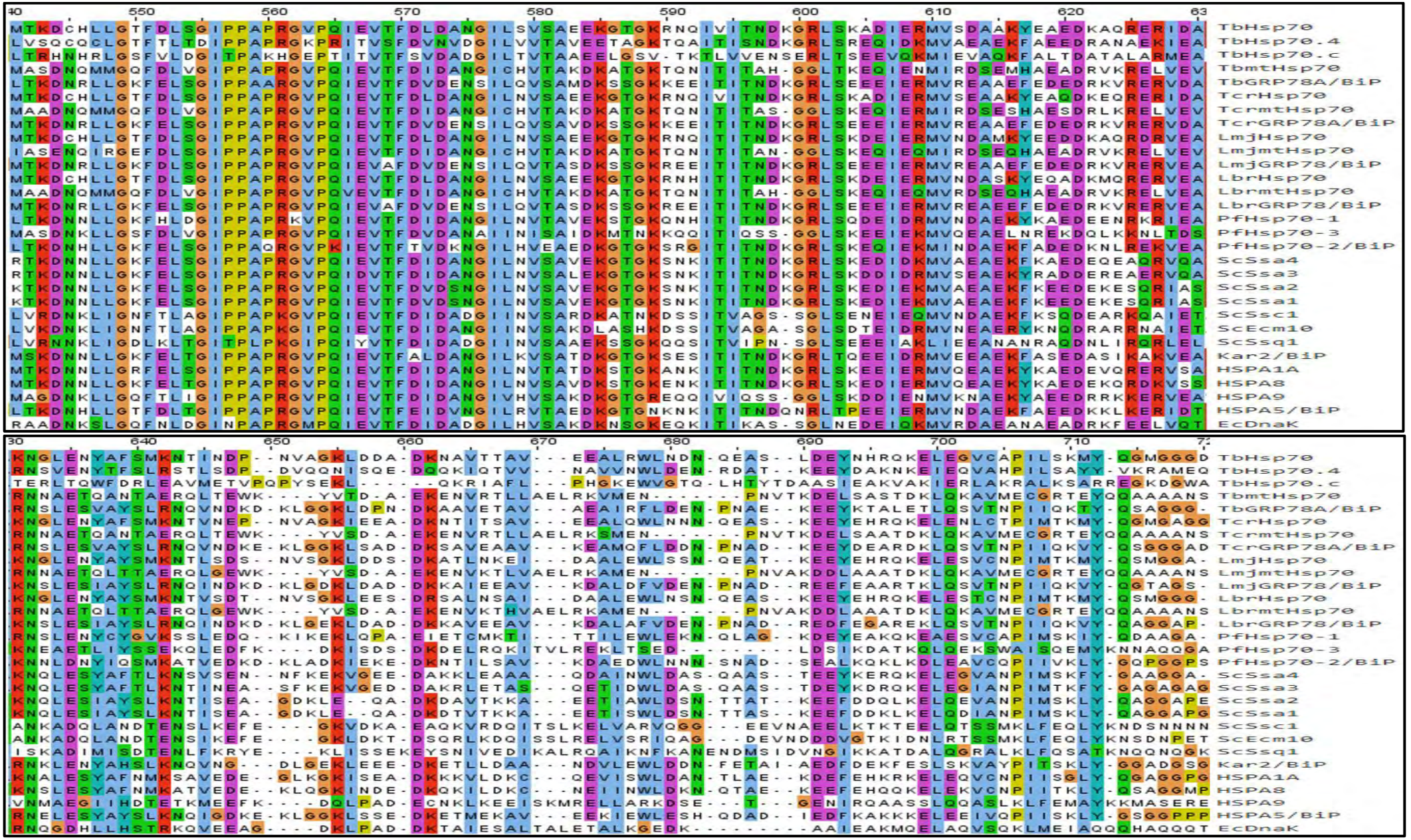
40 550 560 570 580 590 600 610 620 63
MTKDCHLLGTFDLSGIPPAPRGVPQIEVTFDLDANGILSVSAEEKGTGKRNQIVITNDKGRLSKADIERMVSDAAKYEAEDKAQRERIDA TbHsp70
LVSQCQCLGTFTLTDIPPAPRGKPRITVSFDVNVDGILVVTAVEETAGKTQAITISNDKGRLSREQIDKMVAEAEKFAEEDRANAEKIEA TbHsp70.4
LTRHNHRLGSFVLDGITPAKHGEPTITVTFSVDADGILTVTAAEELGSV-TKTLVVENSERLTSEEVQKMIEVAQKFALTDATALARMEA TbHsp70.c
MASDNQMMGQFDLVGIPPAPRGVPQIEVTFDIDANGICHVTAKDKATGKTQNITITAH-GGLTKEQIENMIRDSEMHAEADRVKRELVEV TbmtHsp70
LTKDNRLLGKFELSGIPPAARGVPQIEVTFDVDENSILQVSAMDKSSGKKEEITITNDKGRLSEEEIERMVREAAEFEDEDRKVRERVDA TbGRP78A/BiP
MTKDCHLLGTFDLSGIPPAPRGVPQIEVTFDLDANGILNVSAEEKGTGKRNQIVITNDKGRLSKADIERMVSEAAKYEAQDKEQRERIDA TcrHsp70
MAADNQMMGQFDLVGIPPAPRGVPQIEVTFDIDANGICHVTAKDKATGKTQNITITAS-GGLSKEQIERMIRDSESHAESDRLKRELVEV TcrmtHsp70
MTKDNRLLGKFELSGIPPAPRGVPQIEVTFDVDENSILQVSAVDKSSGKKEEITITNDKGRLSEEEIERMVREAAEFEDEDRKVRERVDA TcrGRP78A/BiP
MTKDCHLLGTFDLSGIPPAPRGVPQIEVTFDLDANGILNVSAEEKGTGKRNQITITNDKGRLSKDEIERMVNDAMKYEEDDKAQRDRVEA LmjHsp70
IASENQIRGEFDLSGIPPAPRGVPQIEVTFDIDANGICHVTAKDKATGKTQNITITAN-GGLSKEQIEQMIRDSEQHAEADRVKRELVEV LmjmtHsp70
MTKDNRLLGKFDLSGIPPAPRGVPQIEVAFDVDENSILQVTASDKSSGKREEITITNDKGRLSEEEIERMVREAAEFEDEDRKVRERVEA LmjGRP78/BiP
MTKDCHLLGTFDLSGIPPAPRGVPQIEVTFDLDANGILNVSAEEKGTGKRNHITITNDKGRLSKDEIERMVNDASKYEQADKMQRERVEA LbrHsp70
MAADNQMMGQFDLVGIPPAPRGVPQVEVTFDIDANGICHVTAKDKATGKTQNITITAH-GGLSKEQIEQMVRDSEQHAEADRVKRELVEA LbrmtHsp70
MTKDNRLLGKFELSGIPPAPRGVPQIEVAFDVDENSILQVTASDKSSGKREEITITNDKGRLSEEEIERMVREAEEFEDEDRKVRERVEA LbrGRP78/BiP
LTKDNNLLGKFHLDGIPPAPRKVPQIEVTFDIDANGILNVTAVEKSTGKQNHITITNDKGRLSQDEIDRMVNDAEKYKAEDEENRKRIEA PfHsp70-1
MASDNKLLGSFDLVGIPPAPRGVPQIEVTFDVDANAIINISAIDKMTNKKQQITIQSS-GGLSKEEIEKMVQEAELNREKDQLKKNLTDS PfHsp70-3
LTKDNHLLGKFELSGIPPAQRGVPKIEVTFTVDKNGILHVEAEDKGTGKSRGITITNDKGRLSKEQIEKMINDAEKFADEDKNLREKVEA PfHsp70-2/BiP
RTKDNNLLGKFELSGIPPAPRGVPQIEVTFDIDANGILNVSAVEKGTGKSNKITITNDKGRLSKEDIDKMVAEAEKFKAEDEQEAQRVQA ScSsa4
RTKDNNLLGKFELSGIPPAPRGVPQIDVTFDIDANGILNVSALEKGTGKSNKITITNDKGRLSKDDIDRMVSEAEKYRADDEREAERVQA ScSsa3
KTKDNNLLGKFELSGIPPAPRGVPQIEVTFDVDSNGILNVSAVEKGTGKSNKITITNDKGRLSKEDIEKMVAEAEKFKEEDEKESQRIAS ScSsa2
KTKDNNLLGKFELSGIPPAPRGVPQIEVTFDVDSNGILNVSAVEKGTGKSNKITITNDKGRLSKEDIEKMVAEAEKFKEEDEKESQRIAS ScSsa1
LVRDNKLIGNFTLAGIPPAPKGVPQIEVTFDIDADGIINVSARDKATNKDSSITVAGS-SGLSENEIEQMVNDAEKFKSQDEARKQAIET ScSsc1
LVKDNKLIGNFTLAGIPPAPKGIPQIEVTFDIDANGIINVSAKDLASHKDSSITVAGA-SGLSDTEIDRMVNEAERYKNQDRARRNAIET ScEcm10
LVRNNKLIGDLKLTGITPLPKGIPQIYVTFDIDADGIINVSAAEKSSGKQQSITVIPN-SGLSEEEIAKLIEEANANRAQDNLIRQRLEL ScSsq1
MSKDNNLLGKFELTGIPPAPRGVPQIEVTFALDANGILKVSATDKGTGKSESITITNDKGRLTQEEIDRMVEEAEKFASEDASIKAKVEA Kar2/BiP
MTKDNNLLGRFELSGIPPAPRGVPQIEVTFDIDANGILNVTATDKSTGKANKITITNDKGRLSKEEIERMVQEAEKYKAEDEVQRERVSA HSPA1A
MTKDNNLLGKFELTGIPPAPRGVPQIEVTFDIDANGILNVSAVDKSTGKENKITITNDKGRLSKEDIERMVQEAEKYKAEDEKQRDKVSS HSPA8
MAGDNKLLGQFTLIGIPPAPRGVPQIEVTFDIDANGIVHVSAKDKGTGREQQIVIQSS-GGLSKDDIENMVKNAEKYAEEDRRKKERVEA HSPA9
LTKDNHLLGTFDLTGIPPAPRGVPQIEVTFEIDVNGILRVTAEDKGTGNKNKITITNDQNRLTPEEIERMVNDAEKFAEEDKKLKERIDT HSPA5/BiP
RAADNKSLGQFNLDGINPAPRGMPQIEVTFDIDADGILHVSAKDKNSGKEQKITIKAS-SGLNEDEIQKMVRDAEANAEADRKFEELVQT EcDnaK
30 640 650 660 670 680 690 700 710 72
KNGLENYAFSMKNTINDP--NVAGKLDDA-DKNAVTTAV---EEALRWLNDN-QEAS--LDEYNHRQKELEGVCAPILSKMY-QGMGGGD TbHsp70
RNSVENYTFSLRSTLSDP--DVQQNISQE-DQQKIQTVV---NAVVNWLDEN-RDAT--KEEYDAKNKEIEQVAHPILSAYY-VKRAMEQ TbHsp70.4
TERLTQWFDRLEAVMETVPQPYSEKL------QKRIAFL---PHGKEWVGTQ-LHTYTDAASIEAKVAKIERLAKRALKSARREGKDGWA TbHsp70.c
RNNAETQANTAERQLTEWK----YVTD-A-EKENVRTLLAELRKVMEN-------PNVTKDELSASTDKLQKAVMECGRTEYQQAAAANS TbmtHsp70
RNSLESVAYSLRNQVNDKD-KLGGKLDPN-DKAAVETAV---AEAIRFLDEN-PNAE--KEEYKTALETLQSVTNPIIQKTY-QSAGGG- TbGRP78A/BiP
KNGLENYAFSMKNTVNEP--NVAGKIEEA-DKNTITSAV---EEALQWLNNN-QEAS--KEEYEHRQKELENLCTPIMTKMY-QGMGAGG TcrHsp70
RNNAETQANTAERQLTEWK----YVSD-A-EKENVRTLLAELRKSMEN-------PNVTKDELSAATDKLQKAVMECGRTEYQQAAAANS TcrmtHsp70
RNSLESVAYSLRNQVNDKE-KLGGKLSAD-DKSAVEAAV---KEAMQFLDDN-PNAD--KEEYDEARDKLQSVTNPIIQKVY-QSGGGAD TcrGRP78A/BiP
KNGLENYAYSMKNTLSDS--NVSGKLDDS-DKATLNKEI---DAALEWLSSN-QEAT--KEEYEHRQKELESVCNPIMTKMY-QSMGGA- LmjHsp70
RNNAETQLTTAERQLGEWK----YVSD-A-EKENVKTLVAELRKAMEN-------PNVAKDDLAAATDKLQKAVMECGRTEYQQAAAANS LmjmtHsp70
KNSLESIAYSLRNQINDKD-KLGEKLDAD-DKKAIEEAV---KDALDFVDEN-PNAD--REEFEAARTKLQSVTNPIIQKVY-QGTAGS- LmjGRP78/BiP
KNGLENYAYSMKNTVSDT--NVSGKLEES-DRSALNSAI---DAALEWLNSN-QEAS--KEEYEHRQKELESTCNPIMTKMY-QSMGGG- LbrHsp70
RNNAETQLTTAERQLGEWK----YVSD-A-EKENVKTHVAELRKAMEN-------PNVAKDDLAAATDKLQKAVMECGRTEYQQAAAANS LbrmtHsp70
KNSLESIAYSLRNQINDKD-KLGEKLDAD-DKKAVEEAV---KDALAFVDEN-PNAD--REDFEGARKKLQSVTNPIIQKVY-QAGGAP- LbrGRP78/BiP
RNSLENYCYGVKSSLEDQ--KIKEKLQPA-EIETCMKTI---TTILEWLEKN-QLAG--KDEYEAKQKEAESVCAPIMSKIY-QDAAGA- PfHsp70-1
KNEAETLIYSSEKQLEDFK----DKISDS-DKDELRQKITVLREKLTSED----------LDSIKDATKQLQEKSWAISQEMYKNNAQQGA PfHsp70-3
KNNLDNYIQSMKATVEDKD-KLADKIEKE-DKNTILSAV---KDAEDWLNNN-SNAD--SEALKQKLKDLEAVCQPIIVKLY-GQPGGPS PfHsp70-2/BiP
KNQLESYAFTLKNSVSEN--NFKEKVGEE-DAKKLEAAA---QDAINWLDAS-QAAS--TEEYKERQKELEGVANPIMSKFY-GAAGGA- ScSsa4
KNQLESYAFTLKNTINEA--SFKEKVGED-DAKRLETAS---QETIDWLDAS-QAAS--TDEYKDRQKELEGIANPIMTKFY-GAGAGAG ScSsa3
KNQLESIAYSLKNTISEA--GDKLE--QA-DKDAVTKKA---EETIAWLDSN-TTAT--KEEFDDQLKELQEVANPIMSKLY-QAGGAPE ScSsa2
KNQLESIAYSLKNTISEA--GDKLE--QA-DKDTVTKKA---EETISWLDSN-TTAS--KEEFDDKLKELQDIANPIMSKLY-QAGGAPG ScSsa1
ANKADQLANDTENSLKEFE----GKVDKA-EAQKVRDQITSLKELVARVQGG---EEVNAEELKTKTEELQTSSMKLFEQLYKNDSNNNN ScSsc1
ANKADQLANDTENSIKEFE----GKLDKT-DSQRLKDQISSLRELVSRIQAG---DEVNDDDVGTKIDNLRTSSMKLFEQLYKNSDNPET ScEcm10
ISKADIMISDTENLFKRYE----KLISSEKEYSNIVEDIKALRQAIKNFKANENDMSIDVNGIKKATDALQGRALKLFQSATKNQQNQGK ScSsq1
RNKLENYAHSLKNQVNG---DLGEKLEEE-DKETLLDAA---NDVLEWLDDN-FETAI-AEDFDEKFESLSKVAYPITSKLY-GGADGSG Kar2/BiP
KNALESYAFNMKSAVEDE--GLKGKISEA-DKKKVLDKC---QEVISWLDAN-TLAE--KDEFEHKRKELEQVCNPIISGLY-QGAGGPG HSPA1A
KNSLESYAFNMKATVEDE--KLQGKINDE-DKQKILDKC---NEIINWLDKN-QTAE--KEEFEHQQKELEKVCNPIITKLY-QSAGGMP HSPA8
VNMAEGIIHDTETKMEEFK----DQLPAD-ECNKLKEEISKMRELLARKDSE---T---GENIRQAASSLQQASLKLFEMAYKKMASERE HSPA9
RNELESYAYSLKNQIGDKE-KLGGKLSSE-DKETMEKAV---EEKIEWLESH-QDAD--IEDFKAKKKELEEIVQPIISKLY-GSGGPPP HSPA5/BiP
RNQGDHLLHSTRKQVEEAG----DKLPAD-DKTAIESALTALETALKGEDK---------AAIEAKMQELAQVSQKLMEIAQQQHAQQQT EcDnaK

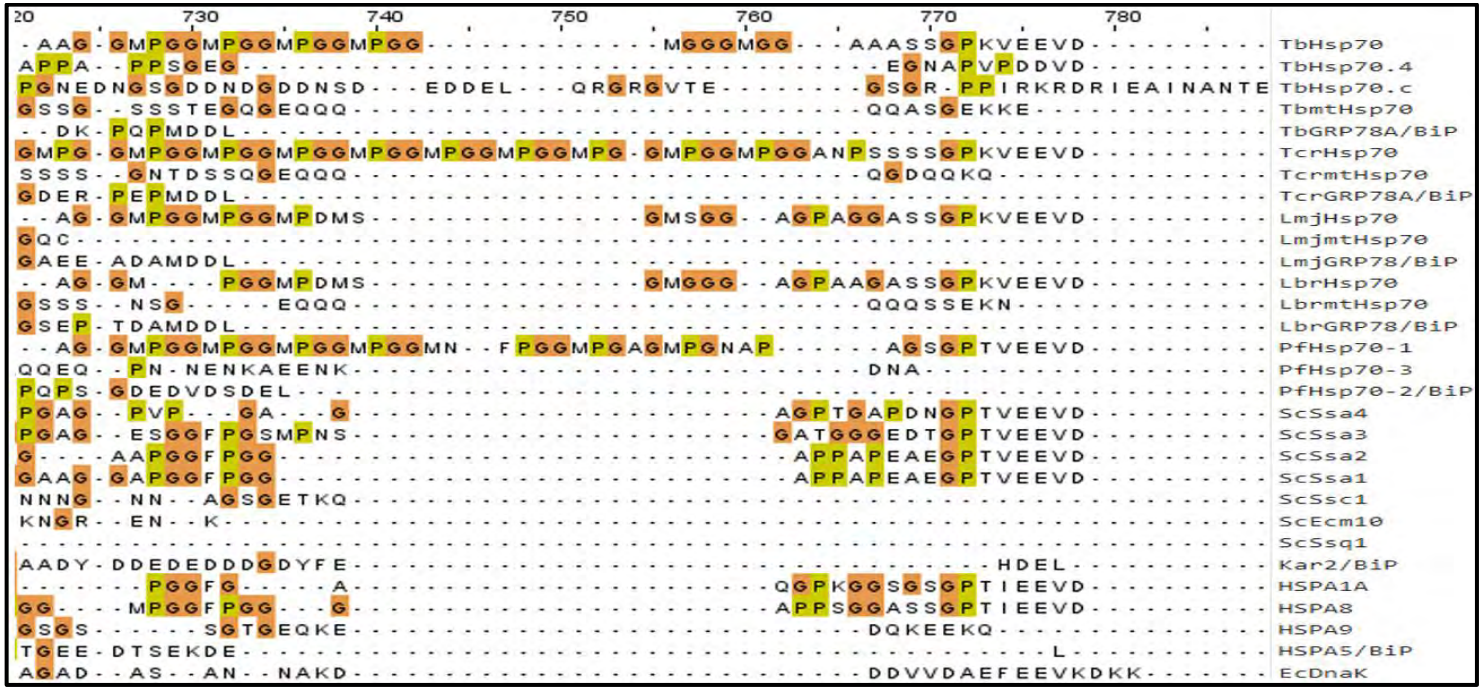

Figure A12: The Clustal Omega multiple sequence alignment of the Hsp70 orthologues. The sequences were aligned using the built in Clustal Omega platform on the JalView web service. The annotation is based on the JalView Clustal colour option. The sequences aligned were from: TbHsp70 (Tb927.11.11330), TbHsp70.4 (Tb927.7.710), TbHsp70.c (Tb927.11.11290), TbmtHsp70 (Tb927.6.3740), TbGRP78A/BiP (Tb927.11.7460), TcrHsp70 (TcCLB.511211.170), TcrmtHsp70 (TcCLB.507029.30), TcrGRP78A/BiP (TcCLB.506585.40), LmjHsp70 (LmjF.28.2770), LmjmtHsp70 (LmjF.30.2460), LmjGRP78/BiP (LmjF.28.1200), LbrHsp70 (LbrM.28.2990), LbrmtHsp70 (LbrM.30.2420), LbGRP78/BiP (LbrM.30.2420), PfHsp70-1 (PF3D7_0818900), PfHsp70-3 (PF3D7_1134000), PfHsp70-2/BiP (PF3D7_0917900), ScSsa4 (AJU50241.1), ScSsa3 (AJQ13321.1), ScSsa2 (AJV59097.1), ScSsa1 (AJO96864.1), ScSsc1 (AJV44330.1), ScEcm10 (AJU50104.1), ScSsq1 (AJV59432.1), ScKar2 (AJR59823.1), HSPA1A (NP_005336.3), HSPA8 (NP_006588.1), HSPA9 (AAH00478.1), HsHSPA5/BiP (AAI12964.1) and EcDnaK (WP_097477514.1).

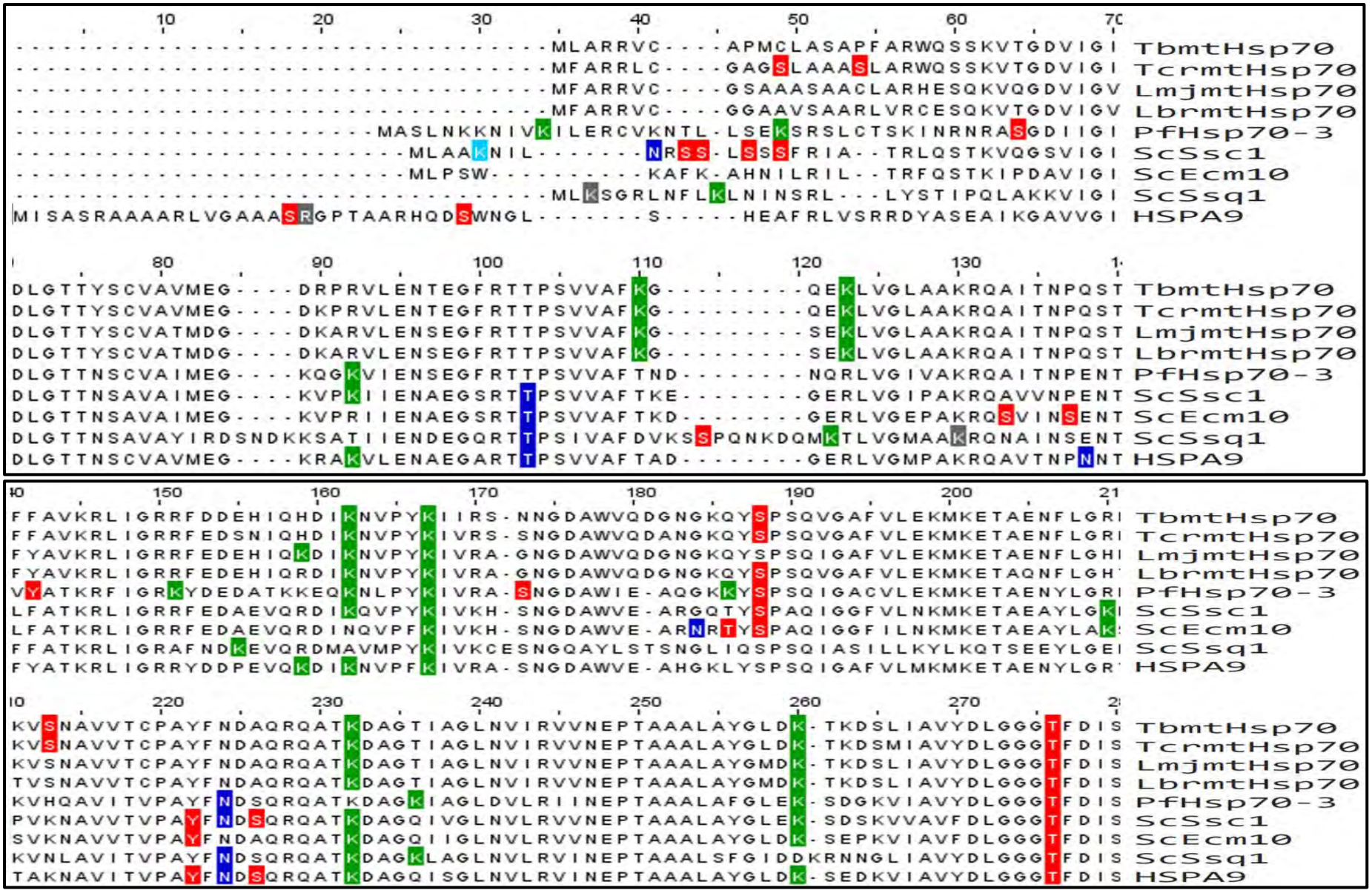
10 20 30 40 50 60 70
MLARRVC----APMCLASAPFARWQSSKVTGDVIGI TbmtHsp70
MFARRLC----GAGSLAAASLARWQSSKVTGDVIGI TcrmtHsp70
MFARRVC----GSAAASAACLARHESQKVQGDVIGV LmjmtHsp70
MFARRVC----GGAAVSAARLVRCESQKVTGDVIGV LbrmtHsp70
MASLNKKNIVKILERCVKNTL-LSEKSRSLCTSKINRNRASGDIIGI PfHsp70-3
MLAAKNIL-------NRSS-LSSSFRIA--TRLQSTKVQGSVIGI ScSsc1
MLPSW----------KAFK-AHNILRIL--TRFQSTKIPDAVIGI ScEcm10
ML KSGRLNFLKLNINSRL---LYSTIPQLAKKVIGI ScSsq1
MISASRAAAARLVGAAASRGPTAARHQDSWNGL-------S-----HEAFRLVSRRDYASEAIKGAVVGI HSPA9
80 90 100 110 120 130
DLGTTYSCVAVMEG----DRPRVLENTEGFRTTPSVVAFKG---------QEKLVGLAAKRQAITNPQST TbmtHsp70
DLGTTYSCVAVMEG----DKPRVLENTEGFRTTPSVVAFKG---------QEKLVGLAAKRQAITNPQST TcrmtHsp70
DLGTTYSCVATMDG----DKARVLENSEGFRTTPSVVAFKG---------SEKLVGLAAKRQAITNPQST LmjmtHsp70
DLGTTYSCVATMDG----DKARVLENSEGFRTTPSVVAFKG---------SEKLVGLAAKRQAITNPQST LbrmtHsp70
DLGTTNSCVAIMEG----KQGKVIENSEGFRTTPSVVAFTND--------NQRLVGIVAKRQAITNPENT PfHsp70-3
DLGTTNSAVAIMEG----KVPKIIENAEGSRTTPSVVAFTKE--------GERLVGIPAKRQAVVNPENT ScSsc1
DLGTTNSAVAIMEG----KVPRIIENAEGSRTTPSVVAFTKD--------GERLVGEPAKRQSVINSENT ScEcm10
DLGTTNSAVAYIRDSNDKKSATIIENDEGQRTTPSIVAFDVKSSPQNKDQMKTLVGMAAKRQNAINSENT ScSsq1
DLGTTNSCVAVMEG----KRAKVLENAEGARTTPSVVAFTAD--------GERLVGMPAKRQAVTNPNNT HSPA9
140 150 160 170 180 190 200 210
FFAVKRLIGRRFDDEHIQHDIKNVPYKIIRS-NNGDAWVQDGNGKQYSPSQVGAFVLEKMKETAENFLGRI TbmtHsp70
FFAVKRLIGRRFEDSNIQHDIKNVPYKIVRS-SNGDAWVQDANGKQYSPSQVGAFVLEKMKETAENFLGRI TcrmtHsp70
FYAVKRLIGRRFEDEHIQKDIKNVPYKIVRA-GNGDAWVQDGNGKQYSPSQIGAFVLEKMKETAENFLGHI LmjmtHsp70
FYAVKRLIGRRFEDEHIQRDIKNVPYKIVRA-GNGDAWVQDGNGKQYSPSQVGAFVLEKMKETAQNFLGHT LbrmtHsp70
VYATKRFIGRKYDEDATKKEQKNLPYKIVRA-SNGDAWIE-AQGKKYSPSQIGACVLEKMKETAENYLGRI PfHsp70-3
LFATKRLIGRRFEDAEVQRDIKQVPYKIVKH-SNGDAWVE-ARGQTYSPAQIGGFVLNKMKETAEAYLGKI ScSsc1
LFATKRLIGRRFEDAEVQRDINQVPFKIVKH-SNGDAWVE-ARNRTYSPAQIGGFILNKMKETAEAYLAK ScEcm10
FFATKRLIGRAFNDKEVQRDMAVMPYKIVKCESNGQAYLSTSNGLIQSPSQIASILLKYLKQTSEEYLGEI ScSsq1
FYATKRLIGRRYDDPEVQKDIKNVPFKIVRA-SNGDAWVE-AHGKLYSPSQIGAFVLMKMKETAENYLGRT HSPA9
210 220 230 240 250 260 270 28
KVSNAVVTCPAYFNDAQRQATKDAGTIAGLNVIRVVNEPTAAALAYGLDK-TKDSLIAVYDLGGGTFDIS TbmtHsp70
KVSNAVVTCPAYFNDAQRQATKDAGTIAGLNVIRVVNEPTAAALAYGLDK-TKDSMIAVYDLGGGTFDIS TcrmtHsp70
KVSNAVVTCPAYFNDAQRQATKDAGTIAGLNVIRVVNEPTAAALAYGMDK-TKDSLIAVYDLGGGTFDIS LmjmtHsp70
TVSNAVVTCPAYFNDAQRQATKDAGTIAGLNVIRVVNEPTAAALAYGMDK-TKDSLIAVYDLGGGTFDIS LbrmtHsp70
KVHQAVITVPAYFNDSQRQATKDAGKIAGLDVLRIINEPTAAALAFGLEK-SDGKVIAVYDLGGGTFDIS PfHsp70-3
PVKNAVVTVPAYFNDSQRQATKDAGQIVGLNVLRVVNEPTAAALAYGLEK-SDSKVVAVFDLGGGTFDIS ScSsc1
SVKNAVVTVPAYFNDAQRQATKDAGQIIGLNVLRVVNEPTAAALAYGLDK-SEPKVIAVFDLGGGTFDIS ScEcm10
KVNLAVITVPAYFNDSQRQATKDAGKLAGLNVLRVINEPTAAALSFGIDDKRNNGLIAVYDLGGGTFDIS ScSsq1
TAKNAVITVPAYFNDSQRQATKDAGQISGLNVLRVINEPTAAALAYGLDK-SEDKVIAVYDLGGGTFDIS HSPA9

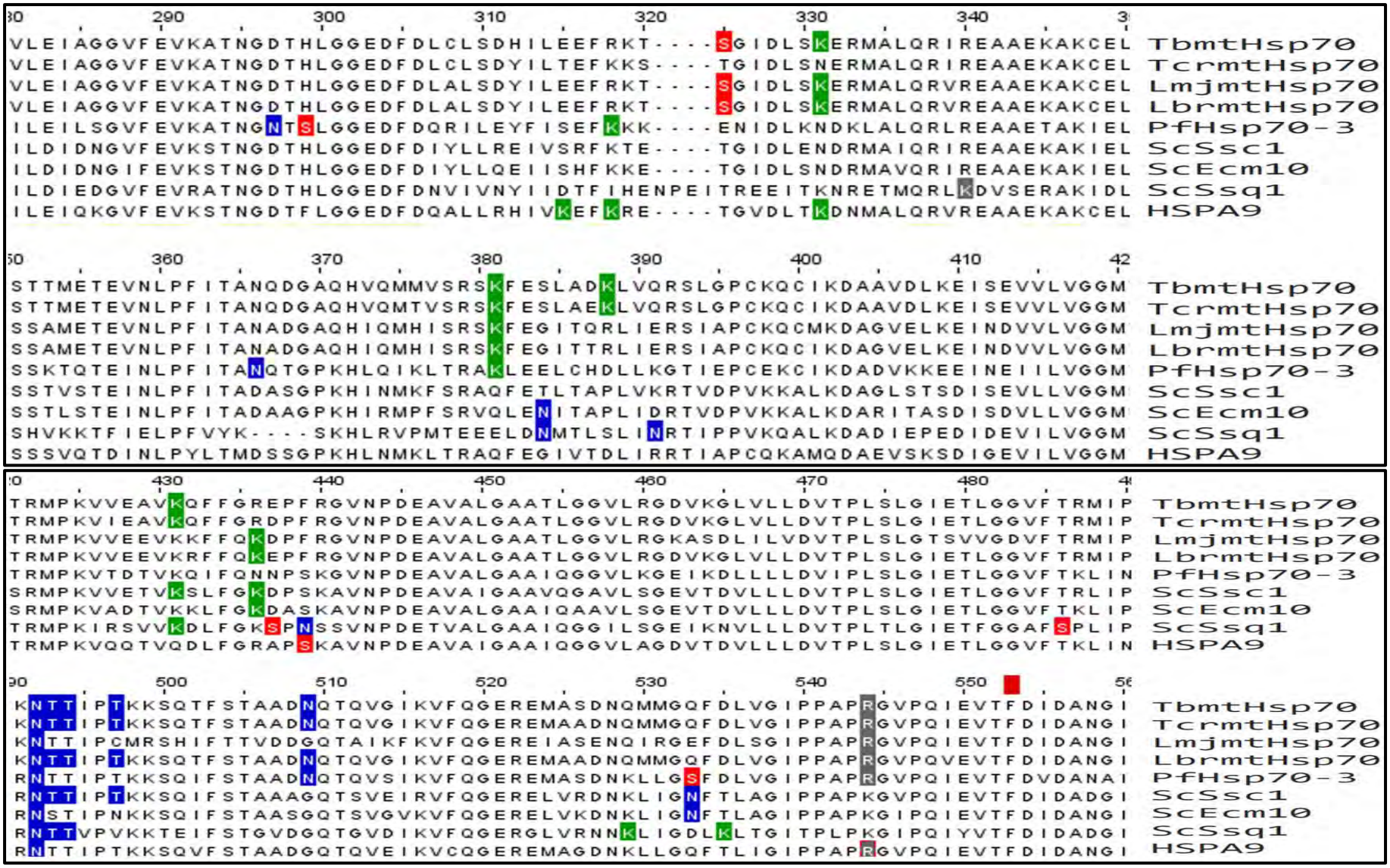
290 300 310 320 330 340
VLEIAGGVFEVKATNGDTHLGGEDFDLCLSDHILEEFRKT----SGIDLSKERMALQRIREAAEKAKCEL TbmtHsp70
VLEIAGGVFEVKATNGDTHLGGEDFDLCLSDYILTEFKKS----TGIDLSNERMALQRIREAAEKAKCEL TcrmtHsp70
VLEIAGGVFEVKATNGDTHLGGEDFDLALSDYILEEFRKT----SGIDLSKERMALQRVREAAEKAKCEL LmjmtHsp70
VLEIAGGVFEVKATNGDTHLGGEDFDLALSDYILEEFRKT----SGIDLSKERMALQRVREAAEKAKCEL LbrmtHsp70
ILEILSGVFEVKATNGNTSLGGEDFDQRILEYFISEFKKK----ENIDLKNDKLALQRLREAAETAKIEL PfHsp70-3
ILDIDNGVFEVKSTNGDTHLGGEDFDIYLLREIVSRFKTE----TGIDLENDRMAIQRIREAAEKAKIEL ScSsc1
ILDIDNGIFEVKSTNGDTHLGGEDFDIYLLQEIISHFKKE----TGIDLSNDRMAVQRIREAAEKAKIEL ScEcm10
ILDIEDGVFEVRATNGDTHLGGEDFDNVIVNYIIDTFIHENPEITREEITKNRETMQRLKDVSERAKIDL ScSsq1
ILEIQKGVFEVKSTNGDTFLGGEDFDQALLRHIVKEFKRE----TGVDLTKDNMALQRVREAAEKAKCEL HSPA9
360 370 380 390 400 410 420
STTMETEVNLPFITANQDGAQHVQMMVSRSKFESLADKLVQRSLGPCKQCIKDAAVDLKEISEVVLVGGM TbmtHsp70
STTMETEVNLPFITANQDGAQHVQMTVSRSKFESLAEKLVQRSLGPCKQCIKDAAVDLKEISEVVLVGGM TcrmtHsp70
SSAMETEVNLPFITANADGAQHIQMHISRSKFEGITQRLIERSIAPCKQCMKDAGVELKEINDVVLVGGM LmjmtHsp70
SSAMETEVNLPFITANADGAQHIQMHISRSKFEGITTRLIERSIAPCKQCIKDAGVELKEINDVVLVGGM LbrmtHsp70
SSKTQTEINLPFITANQTGPKHLQIKLTRAKLEELCHDLLKGTIEPCEKCIKDADVKKEEINEIILVGGM PfHsp70-3
SSTVSTEINLPFITADASGPKHINMKFSRAQFETLTAPLVKRTVDPVKKALKDAGLSTSDISEVLLVGGM ScSsc1
SSTLSTEINLPFITADAAGPKHIRMPFSRVQLENITAPLIDRTVDPVKKALKDARITASDISDVLLVGGM ScEcm10
SHVKKTFIELPFVYK----SKHLRVPMTEEELDNMTLSLINRTIPPVKQALKDADIEPEDIDEVILVGGM ScSsq1
SSSVQTDINLPYLTMDSSGPKHLNMKLTRAQFEGIVTDLIRRTIAPCQKAMQDAEVSKSDIGEVILVGGM HSPA9
430 440 450 460 470 480 490
TRMPKVVEAVKQFFGREPFRGVNPDEAVALGAATLGGVLRGDVKGLVLLDVTPLSLGIETLGGVFTRMIP TbmtHsp70
TRMPKVIEAVKQFFGRDPFRGVNPDEAVALGAATLGGVLRGDVKGLVLLDVTPLSLGIETLGGVFTRMIP TcrmtHsp70
TRMPKVVEEVKKFFQKDPFRGVNPDEAVALGAATLGGVLRGKASDLILVDVTPLSLGTSVVGDVFTRMIP LmjmtHsp70
TRMPKVVEEVKRFFQKEPFRGVNPDEAVALGAATLGGVLRGDVKGLVLLDVTPLSLGIETLGGVFTRMIP LbrmtHsp70
TRMPKVTDTVKQIFQNNPSKGVNPDEAVALGAAIQGGVLKGEIKDLLLLDVIPLSLGIETLGGVFTKLIN PfHsp70-3
SRMPKVVETVKSLFGKDPSKAVNPDEAVAIGAAVQGAVLSGEVTDVLLLDVTPLSLGIETLGGVFTRLIP ScSsc1
SRMPKVADTVKKLFGKDASKAVNPDEAVALGAAIQAAVLSGEVTDVLLLDVTPLSLGIETLGGVFTKLIP ScEcm10
TRMPKIRSVVKDLFGKSPNSSVNPDETVALGAAIQGGILSGEIKNVLLLDVTPLTLGIETFGGAFSPLIP ScSsq1
TRMPKVQQTVQDLFGRAPSKAVNPDEAVAIGAAIQGGVLAGDVTDVLLLDVTPLSLGIETLGGVFTKLIN HSPA9
500 510 520 530 540 550 560
KNTTIPTKKSQTFSTAADNQTQVGIKVFQGEREMASDNQMMGQFDLVGIPPAPRGVPQIEVTFDIDANGI TbmtHsp70
KNTTIPTKKSQTFSTAADNQTQVGIKVFQGEREMAADNQMMGQFDLVGIPPAPRGVPQIEVTFDIDANGI TcrmtHsp70
KNTTIPCMRSHIFTTVDDGQTAIKFKVFQGEREIASENQIRGEFDLSGIPPAPRGVPQIEVTFDIDANGI LmjmtHsp70
KNTTIPTKKSQTFSTAADNQTQVGIKVFQGEREMAADNQMMGQFDLVGIPPAPRGVPQVEVTFDIDANGI LbrmtHsp70
RNTTIPTKKSQIFSTAADNQTQVSIKVFQGEREMASDNKLLGSFDLVGIPPAPRGVPQIEVTFDVDANAI PfHsp70-3
RNTTIPTKKSQIFSTAAAGQTSVEIRVFQGERELVRDNKLIGNFTLAGIPPAPKGVPQIEVTFDIDADGI ScSsc1
RNSTIPNKKSQIFSTAASGQTSVGVKVFQGERELVKDNKLIGNFTLAGIPPAPKGIPQIEVTFDIDANGI ScEcm10
RNTTVPVKKTEIFSTGVDGQTGVDIKVFQGERGLVRNNKLIGDLKLTGITPLPKGIPQIYVTFDIDADGI ScSsq1
RNTTIPTKKSQVFSTAADGQTQVEIKVCQGEREMAGDNKLLGQFTLIGIPPAPRGVPQIEVTFDIDANGI HSPA9

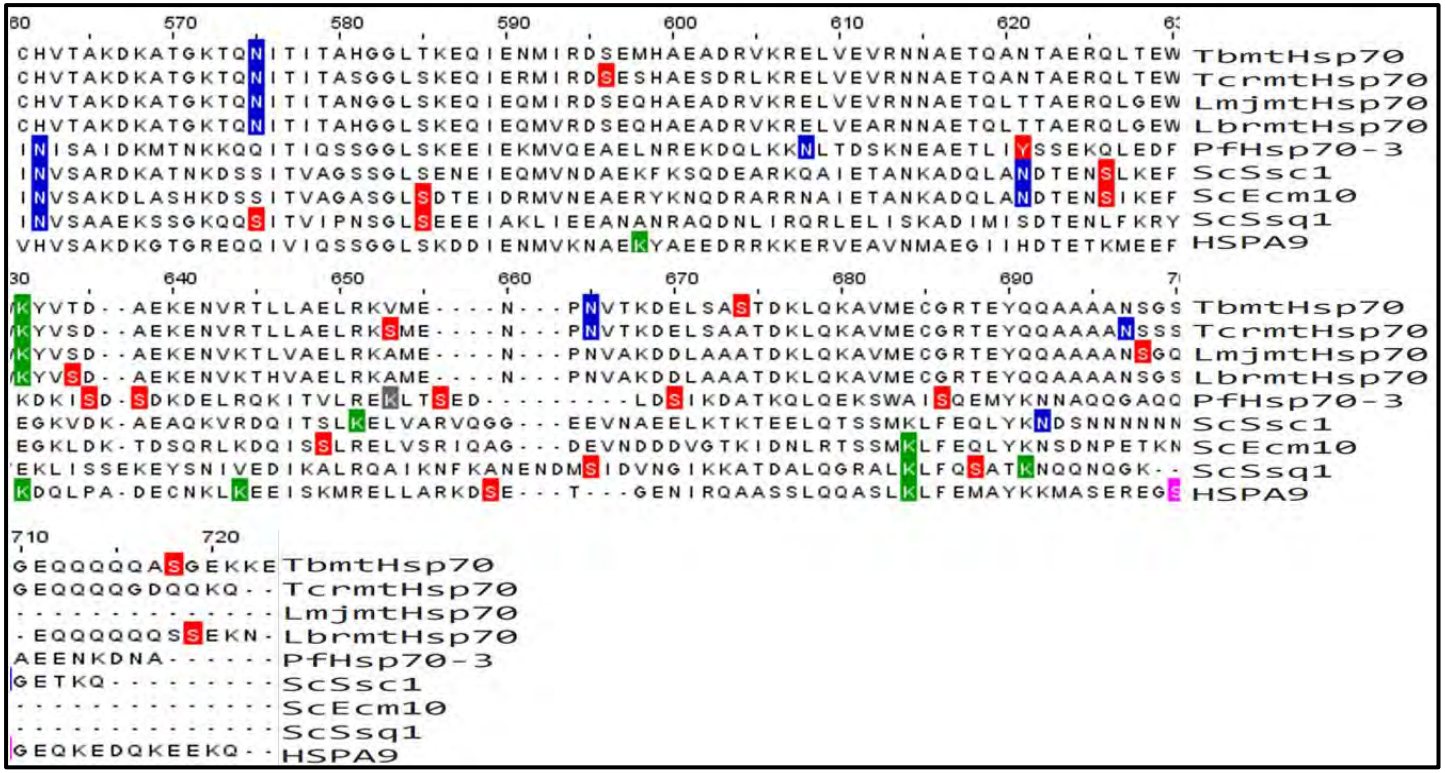

Figure A13: The predicted posttranslational modifications of the mtHsp70 orthologues. MusiteDeep was used to predict the posttranslational modifications using default settings and annotation was performed using JalView subsequent to conducting a Clustal Omega multiple sequence alignment on the web service. The mtHsp70 orthologues used in this assessment were: TbmtHsp70 (Tb927.6.3740), TcrmtHsp70 (TcCLB.507029.30), LmjmtHsp70 (LmjF.30.2460), LbrmtHsp70 (LbrM.30.2420), PfHsp70-3 (PF3D7_1134000), ScSsc1 (AJV44330.1), ScEcm10 (AJU50104.1), ScSsq1 (AJV59432.1) and HSPA9 (AAH00478.1). Highlighted in red, blue, green and grey are amino acid residues predicted to be subject to phosphorylation, glycosylation, acetylation and methylation, respectively. Highlighted in pink are residues subject to both phosphorylation and glycosylation whilst in turquoise are residues subject to both acetylation and methylation.

1	Tb927.6.3770	Tb927.6.3760	Tb927.6.3755	Tb927.6.3750	Tb927.6.3740	Tb927.6.3730	Tb927.6.3720
	Tb927.6.3710	Tb927.6.3700					
2	TcCLB432677.20	TcCLB511515.40	TcCLB511515.9	TcCLB507029.60	TcCLB507029.50	TcCLB507029.41	
	TcCLB507029.30	TcCLB507029.20	TcCLB507029.10				
3	LmjF.30.2490	LmjF.30.2480	LmjF.30.2470	LmjF.30.2460	LmjF.30.2450	LmjF.30.2440	LmjF.30.2430
4	LbrM.30.2450	LbrM.30.2440	LbrM.30.2430	LbrM.30.2420	LbrM.30.2410	LbrM.30.2400	LbrM.30.2390
5	PF3D7_1133800	PF3D7_1133900	PF3D7_1134000	PF3D7_1134100	PF3D7_1134200	PF3D7_1134300	

Figure A14: The database accession IDs of the genes appearing in Figure 2.22 whereby the syntenic analysis of the selected mtHsp70 orthologues is laid out. The accession numbers are listed from left to right as the respective genes they represent appear in Figure 2.22. **1)** *T. b. brucei*, **2)** *T. cruzi*, **3)** *L. major*, **4)** *L. braziliensis* and **5)** *P. falciparum.*

Appendix B

1.1 Yeast-Tryptone (2x YT) Media composition

In 1 L of water, 16 g of tryptone (pancreatic digest of casein), 10 g of yeast extract and 5 g of NaCl were dissolved and autoclaved for 30 minutes at 121 ℃ under 119 kPa of pressure. To make 2x YT agar, 15 g of bacteriological agar was added to freshly made 2x YT (unautoclaved) broth prior to autoclaving for 30 minutes at 121 °C under 119 kPa of pressure.

1.2 Chemical preparation of competent *E. coli* cloning and protein expression strains

The cells were inoculated to 5 mL of sterile 2x YT broth and incubated overnight at 37 °C overnight with agitation. After overnight growth at 37 °C, the resultant overnight (starter) culture was transferred to 45 mL of sterile 2x YT broth and incubated at 37 °C with agitation. Upon reaching the mid-log phase of growth as determined by measuring absorbance (turbidity) at 600 nm, the cells were transferred to sterile centrifuge tubes and pelleted by centrifugation at 5000 *g* at 4 °C. The supernatant was discarded, and the pelleted cells were resuspended in 10 mL of sterile refrigerated 0.1 M $MgCl_2$ and left on ice for 20 minutes. After incubation on ice, the cells were again pelleted by centrifugation at 5000 *g* at 4 °C under sterile conditions. The supernatant was subsequently discarded and the cell pellet resuspended in a sterile refrigerated mixture of $MgCl_2$ and glycerol (8.5 mL of 0.1 M $MgCl_2$, 1.5 mL of undiluted glycerol). The resultant competent cells were aliquoted into sterile microcentrifuge tubes (250 µL) and stored at -80 ℃ until required.

1.3 Transformations

The competent cells were thawed on ice and 50 µL aliquots prepared for transformation. To the 50 µL aliquots, 2 µL of plasmid DNA was added and mixed well before incubation on ice for 30 minutes. After incubation on ice, the cells were heat shocked at 42 ℃ for 45 seconds before being returned to ice for a 5-minute incubation. 950 µL of sterile 2x YT broth was then added to the 50 µL aliquots of competent cells, and then incubated for an hour at 37 ℃. After incubation the cells were centrifuged at 10000 *g* for 2 minutes. 900 µL of the supernatant broth was then discarded, and the pelleted cells resuspended in the remaining broth. The resuspended cells were then spread plated on 2x YT agar supplemented with the appropriate antibiotics, allowed to dry on the agar, and then incubated at 37 °C overnight. A negative control whereby no plasmid DNA was added to the 50 µL competent cells was also subjected to the same treatment and incubated at 37 °C overnight.

1.4 Miniprepping with The Zyppy™ plasmid miniprep kit

Cloning strains of the *E. coli* (DH5α and JM109) transformed with the desired plasmids were inoculated in 5 mL of 2x YT broth supplemented with the appropriate antibiotics and incubated overnight at 37 °C with agitation. After incubation the cells were pelleted and then subjected to Zyppy™ plasmid miniprep kit's protocol. However, in place of the Zyppy™ elution buffer, sterile tris-EDTA (TE) buffer (10 mM Tris-HCl pH 8.0, 1 mM EDTA) was used for the elution step.

1.5 Restriction enzyme digestions for plasmid confirmation

The plasmid restriction enzyme digestion reactions were set up as follows, and incubated at 37 °C overnight:

Table B1: Components of the restriction enzyme digestions.

	Undigested (µL)	Single digestion (µL)	Double digestion (µL)
Deionised water	13	12	13
Plasmid DNA	5	5	5
Restriction enzyme buffer	2	2	2
Restriction enzyme (RE)	-	1	1 of each RE

After incubation, samples of the reactions were prepared for agarose gel electrophoresis.

1.6 Agarose gel electrophoresis

To prepare agarose gels, 0.4 g or 0.5 g of agar was mixed with 50 mL of Tris-acetate-EDTA buffer (40 mM Tris, 20 mM acetic acid, 1 mM EDTA) to make a 0.8 % or 1.0 % agarose gel, respectively. The mixture was microwaved in order to completely dissolve the agarose. The solution was allowed to cool down, at room temperature, until it could be held by hand before ethidium bromide was added. The gel solution was then poured into the electrophoresis casting chamber and left to solidify (polymerize) at room temperature, with a comb inserted for well formation. Thereafter the gel was placed into the buffer tank and then submerged in TAE buffer. The gel was then loaded samples that were prepared as follows: 5 parts sample: 1 part 6x DNA loading buffer (0.25 % (w/v) bromophenol blue, 30 % (v/v) glycerol). Electrophoresis was carried out at 100 V or 80 v for 0.8 % and 1.0 % electrophoresis gels, respectively. Electrophoresis was cllowed to occur for 45 minutes, and then the gels were visualized under UV light on the ChemiDoc XRS$^+$ (Bio-Rad, U.S.A.). The DNA marker used in this study was the 1 kb DNA ladder (New England Biolabs, U.S.A.)

1.7 DNA extraction from the agarose gel

The DNA fragment of interest was cut out from the agarose gel with the aid of a UV transilluminator. Thereafter, the DNA was purified using the GeneJet gel extraction kit (ThermoFisher Scientific, U.S.A.), as per the manufacturer's protocol.

1.8 DNA ligation

500 ng of the DNA fragment purified from the gel cut out was ligated into the desired vector plasmid using T4 DNA ligase in the presence of ligation buffer. The ligation reaction was allowed to take place overnight at 4 °C. The resultant plasmid was propagated and miniprepped as outlines in A4.

1.9 Sodium dodecyl sulphate polyacrylamide gel electrophoresis (SDS-PAGE)

The SDS-PAGE samples were prepared by mixing the actual samples with 4x SDS-PAGE (250 mM Tris-HCl pH 6.8, 40 % glycerol, 8 % SDS, 5 % β-mercaptoethanol, 0.5 % bromophenol blue) sample buffer 3 parts to 1 part, respectively. The samples were then boiled at 100 °C for 10 minutes before being loaded onto the SDS-PAGE gel submerged in running buffer (25 mM Tris, 192 mM glycine, 0.1

% (w/v) SDS). Electrophoresis was carried out at 120 V for 90 minutes. The Bio-Rad Precision-Plus™ All Blue standards were used as the molecular weight marker.

Table B2: Table detailing the recipe for making poly acrylamide gels for SDS-PAGE.

Reagents (mL)	4 % stacking gel	10 % resolving gel	13.5 % resolving gel	15 % resolving gel
Water	3	4.15	2.95	2.5
1.5 M Tris-HCl (pH 8.8)	-	2.5	2.5	2.5
0.5 M Tris-HCl (pH 6.8)	1.25	-	-	-
10 % SDS	0.1	0.1	0.1	0.1
30 % acrylamide/bis	0.7	3.3	4.5	4.95
10 % APS	0.1	0.1	0.1	0.1
TEMED	.02	0.02	0.02	0.02

Subsequent to electrophoresis, the gel was stained in Coomassie (40 % (v/v) methanol, 2 % (v/v) acetic acid, 0.2 % (w/v) Comassie Brilliant Blue G-250) for 30 minutes before being destained in destaining buffer (40 % (v/v) methanol, 2 % (v/v) acetic acid) for as long as required. The SDS-PAGE gels were visualised using the ChemiDoc XRS$^+$ (Bio-Rad, U.S.A.). In some cases the gels were used for Western blotting instead of visualizing protein bands by means of Coomassie staining.

1.10 Western analysis

After SDS-PAGE, the gel was submerged in cold transfer buffer transfer buffer (25 mM Tris, 192 mM glycine, 20 % methanol (v/v)). Blotting pads and the 0.45 µM nitrocellulose membrane were also submerged in the cold transfer buffer. Thereafter, the blotting pads were wrung out until they were damp. The components were then stacked on the Trans-Blot® SD Semi-Dry Transfer cell (Bio-Rad, U.S.A.) from top to bottom in the following order: blotting pad, nitrocellulose 0.45 µM nitrocellulose membrane, SDS-PAGE gel, blotting pad. Transfer was then allowed to take plave at 15 V for an hour. Thereafter, the membrane was placed in 5 % blocking buffer (5 g skim milk powder in 100 mL TBS-T buffer (50 mM Tris-HCl, pH 7.5, 150 mM NaCl, 0.1 % (v/v) Tween® 20) for 2 hours. The membrane was then washed with TBS-T buffer 3 times before being incubated with the anti-his-tag primary antibody (H-3) (Santa Cruz Biotechnology, U.S.A.) in TBS-T buffer (2 µL in 5 mL). for 2 hours at room temperature. The membrane was then washes with TBS-T buffer 3 times before being incubated with m-IgGκ BP-HRP (Santa Cruz Biotechnology, U.S.A.) in TBS-T buffer (2 µL in 6 mL) for 2 hours at room temperature. The membrane was then washed 3 times in TBS-T buffer. Chemilluminescence protein detection was then carried out using the Clarity™ western ECL substrate (Bio-Rad, U.S.A.) as per the manufacturer's guide. To visualize the protein bands, the ChemiDoc XRS$^+$ (Bio-Rad, U.S.A.) was used.

1.11 Buffer exchange by means of dialysis

Eluted protein samples were transferred to SnakeSkin™ dialysis tubing 10 kDa MWCO (ThermoFisher Scientific, U.S.A.) and then the dialysis bags were sealed by tying with strings. The dialysis bags were placed in 1 L of cold dialysis buffer (10 mM Tris-HCl pH 7.5, 100 mM NaCl, 0.5 mM DTT, 50 mM KCl, 10 % glycerol (v/v)) in the cold room stirring overnight. The dialysis bags were then transferred to new 1 L of unused dialysis buffer for another round of dialysis in the cold room.

1.12 Protein concentration determination by means of the Bradford assay

Protein quantification was carried out by means of the Bradford's assay, utilizing Bradford reagent (100-1400 µg/mL) obtained from Sigma-Aldrich (U.S.A.). As a protein concentration standard, BSA (100-1000 µg/mL) diluted in the dialysis buffer was used. Thereafter, 5 µL aliquots of the standards and protein samples were pipetted into a 96-well plate. Bradford reagent, 150 µL, was then added to the standards and the protein samples. Absorbance was then measured at 595 nm using the Epoch2 multi-well plate reader (Agilent Scientific Instruments Biotek, U.S.A.).

1.13 Native PAGE protocol

Native PAGE was carried out using a continuous 12 % polyacrylamide resolving gel (3.48 mL H_20, 2.5 mL 1.5 M Tris-HCl pH 8.8, 3.96 mL acrylamide/bis, 100 µL 10 % APS, 20 µL TEMED). The buffer used is the same as the one used for SDS-PAGE, however void of the SDS. Electrophoresis was carried out at 60 V for 3 hours. Subsequent to electrophoresis, the gel was stained in Coomassie (40 % (v/v) methanol, 2 % (v/v) acetic acid, 0.2 % (w/v)) Comassie Brilliant Blue G-250) for 30 minutes before being destained in destaining buffer (40 % (v/v) methanol, 2 % (v/v) acetic acid) for as long as required. The SDS-PAGE gels were visualised using the ChemiDoc XRS^+ (Bio-Rad, U.S.A.).

1.14 Sonication of cell lysates

Cell lysates were thawed on ice. Thereafter, sonication was carried out in 3 pulses of 15 seconds at an amplitude of 60. In between the 15 second pulses, the lysates were cooled on ice for at least 45 seconds.

Appendix C

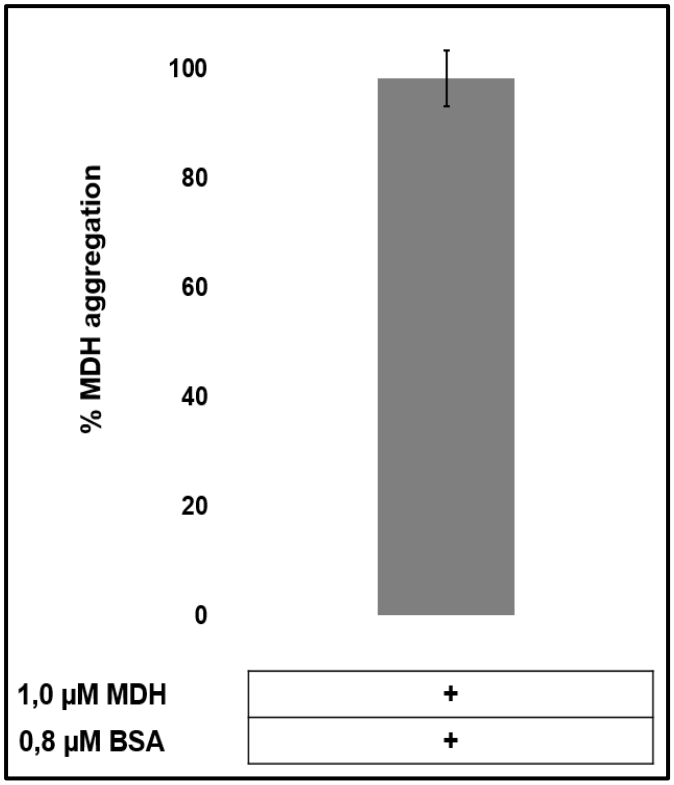

Figure C1: Control demonstrating that the suppression of MDH's aggregation observed in the assays is specifically due to the presence of the molecular chaperones in the reactions. The suppression of MDH's (1,0 µM) thermally induced aggregation was determined by measuring light scattering at 360 nm prior to and after incubation at 48 °C for 1 hour. The % aggregation was determined with the aggregation of the MDH alone set at 100 %. The concentration of BSA used on MDH was 0,8 µM. The assays were conducted in triplicate. The error bars represent standard deviation. Statistical significance was benchmarked at $P < 0,05$ using a student's T-test.

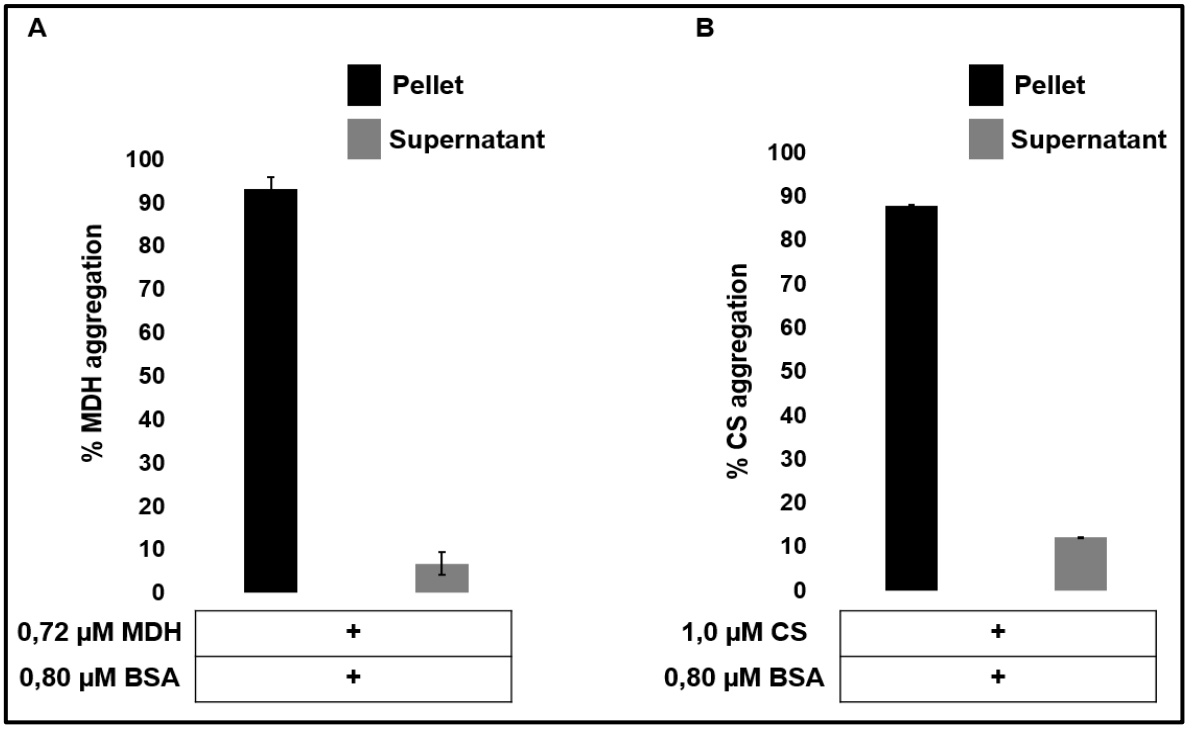

Figure C2; Control reactions demonstrating that the suppression of MDH and CS aggregation observed in the assays is specifically due to the presence of the molecular chaperones in the reactions. The suppression of **A)** MDH's (0,72 µM) and **B)** CS's (1 µM) thermally induced aggregation was determined by the densitometric quantification of the pellet (insoluble; black bars) and supernatant (soluble; grey bars) after incubation at 50 °C for 1 hour. The concentration of BSA used on MDH and CS was 0,8 µM. The assays were conducted in triplicate. The error bars represent standard deviation. Statistical significance was benchmarked at $P < 0,05$ using a student's T-test.

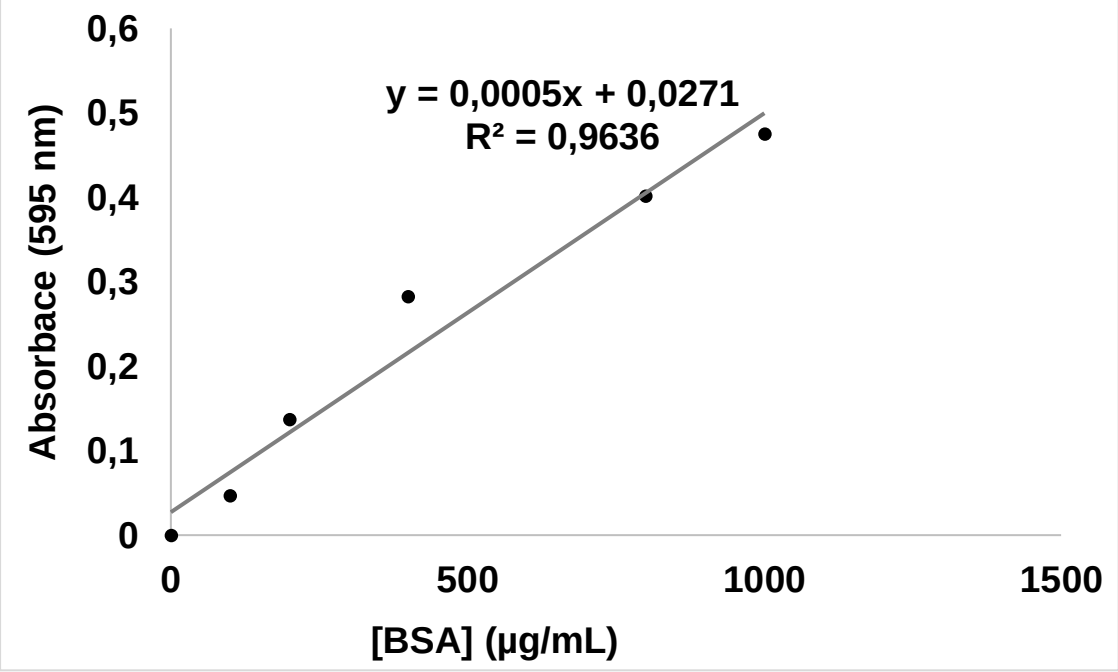

Figure C3: Bradford's assay protein concentration standard curve using BSA.

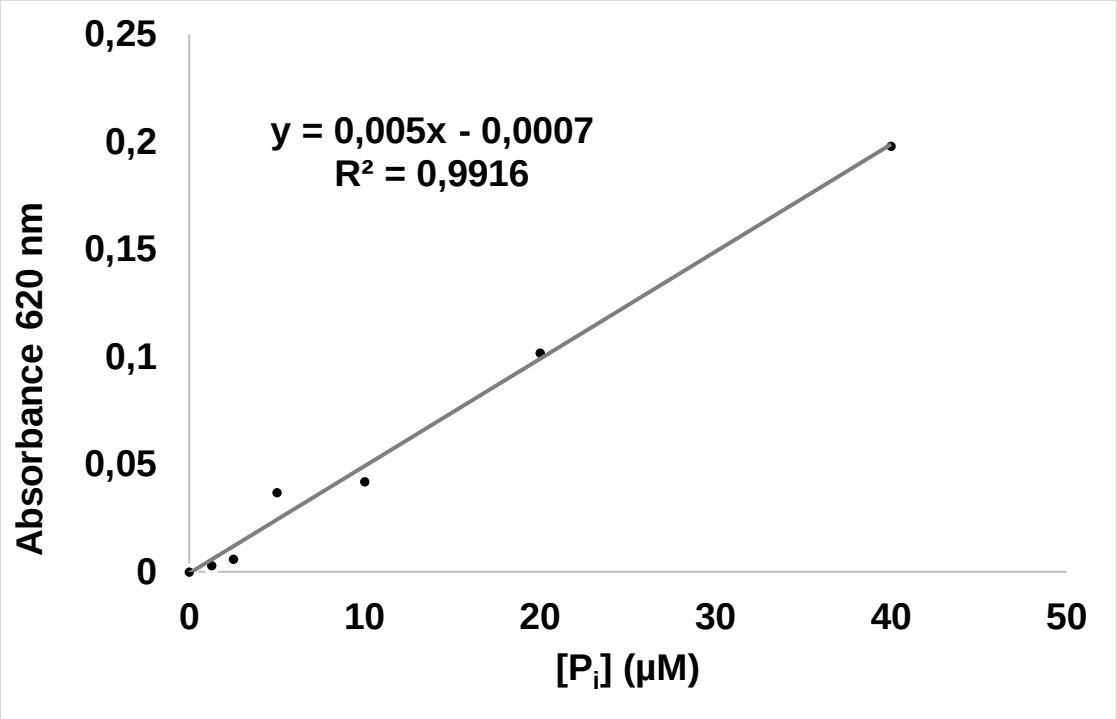

Figure C4: ATPase assay P_i standard curve using Na_2HPO_4.